THE JOURNAL OF

PHYSICAL CHEMISTRY

Volume 73, Number 3 March 1969

NOTES

COMMUNICATIONS TO THE EDITOR

AUTHOR INDEX

THE JOURNAL OF
PHYSICAL CHEMISTRY

VOLUME 73, NUMBER 3 MARCH 1969

Transference Number Measurements in Acetonitrile as Solvent

by Charles H. Springer,[1] J. F. Coetzee,[2]

Department of Chemistry, University of Pittsburgh, Pittsburgh, Pennsylvania 15213

and R. L. Kay

Mellon Institute, Carnegie-Mellon University, Pittsburgh, Pennsylvania 15213 *(Received September 23, 1968)*

The transference number of tetramethylammonium ion in tetramethylammonium perchlorate has been determined in anhydrous acetonitrile as solvent using a rising boundary sheared cell with tetraphenylarsonium perchlorate as indicator and with electrical monitoring of the boundary. A scale of single-ion conductivities based on the limiting value of this transference number (0.4768 ± 0.0002) differs by 0.35 conductivity unit from a scale based on the assumption that tetraisoamylammonium and tetraisoamylboride ions have equal mobilities.

Introduction

Reliable values of single-ion conductivities are useful for a variety of purposes, among them the investigation of ion–solvent interactions. The split of electrolyte conductivities into the ionic components ideally requires transference numbers, the accurate measurement of which presents serious experimental problems in many nonaqueous solvents. Transference numbers of high accuracy have been determined in few anhydrous solvents, with nitromethane[3] as the only example of the important class of dipolar aprotic solvents. For several other solvents, including acetonitrile,[4] provisional scales of single-ion conductivities have been based on the assumption that the constituent ions of certain reference electrolytes, such as tetraisoamylammonium tetraisoamylboride, have equal mobilities. However, the unambiguous evaluation of the validity of such scales still requires the direct measurement of transference numbers. We now report the results of such measurements in acetonitrile, which indicate that the error in the tentative scale based on the conductivity of tetraisoamylammonium tetraisoamylboride amounts to 0.35 conductivity unit.

Experimental Section

Transference number measurements were carried out using a moving boundary method with electrical monitoring of the boundary, as developed by Kay, Vidulich, and Fratiello.[5] A complete description of the apparatus can be found in ref 5 and can be compared to a similar method described by Lorimer, Graham, and Gordon.[6]

A rising boundary sheared cell with a cadmium anode and a silver–silver chloride cathode was employed to measure the transference number of the tetramethylammonium ion constituent in tetramethylammonium perchlorate. A stopcock was used to form the boundary. Tetraphenylarsonium perchlorate served as indicator. Measurements had to be restricted to tetramethylammonium ion since no other system could be found among 17 tried[1] that gave reproducible results.

The cell was calibrated at 25° using aqueous solutions of potassium chloride for which the transference numbers are known.[7] After each run the cell was cleaned

(1) From the Ph.D. thesis of this author, University of Pittsburgh, 1968.

(2) Please address all correspondence to this author.

(3) R. L. Kay, S. C. Blum, and H. I. Schiff, *J. Phys. Chem.*, **67**, 1223 (1963).

(4) J. F. Coetzee and G. P. Cunningham, *J. Amer. Chem. Soc.*, **87**, 2529 (1965).

(5) R. L. Kay, G. A. Vidulich, and A. Fratiello, *J. Chem. Instr.*, in press.

(6) J. W. Lorimer, J. R. Graham, and A. R. Gordon, *J. Amer. Chem. Soc.*, **79**, 2347 (1957).

(7) L. G. Longsworth, *ibid.*, **54**, 2741 (1932).

with acid dichromate solution and rinsed thoroughly with distilled and then conductivity water. Finally, the cell was filled with conductivity water and allowed to stand to leach out any dichromate that might still be present. Before a run was made, the cell was dried by passing dry filtered air through it. Before runs were made with acetonitrile, the cell was filled with dry solvent and allowed to stand overnight.

All measurements were carried out in a constant-temperature oil bath maintained at 25 ± 0.002° by means of a mercury-in-glass thermoregulator. The absolute temperature was determined with a calibrated resistance thermometer and a Mueller bridge.

All solutions were prepared by weight, vacuum corrected, and concentrations were converted to a volume basis by means of solution densities determined from the following relationship: $d = d_0 + A\bar{m}$ where d_0 is the density of the pure solvent and $\bar{m}$ is the concentration expressed in moles of solute per kilogram of solution. The parameter A was determined from the results of a number of density measurements.

Conductivity water was prepared by passing distilled water first through a commercial ion exchanger and then through a 1.2-m column of mixed-bed ion exchange resin. Conductivity water was collected from the column only after a thorough rinsing of the resin. In this way water with a conductivity of 1–2 × 10^{-7} ohm^{-1} cm^{-1} was obtained.

Technical grade (Matheson) acetonitrile was purified by the procedure described before[8] with the addition of a final fractional distillation under nitrogen from calcium hydride through a 1.22-m vacuum-jacketed Stedman column. The solvent was stored under nitrogen and had the following properties: density, 0.77663 g ml^{-1}; viscosity, 3.409 mp;[9] dielectric constant, 35.95;[9] conductivity, 1–2 × 10^{-8} ohm^{-1} cm^{-1}; water content, less than 1 mM as determined by Karl Fischer titration.

Tetramethylammonium perchlorate was precipitated by adding slowly an aqueous solution of tetramethylammonium chloride to an aqueous solution of sodium perchlorate. The salt was recrystallized four times from hot water and dried for 24 hr *in vacuo* at 70°.

Tetraphenylarsonium perchlorate was precipitated by mixing equivalent amounts of aqueous solutions of tetraphenylarsonium chloride and sodium perchlorate and was recrystallized from hot acetonitrile. Because of the low yield of this process, tetraphenylarsonium chloride first was recrystallized by adding anhydrous ether to its solution in acetonitrile. In order to remove hydrogen chloride, which was an impurity in some samples, and which forms a stable adduct with tetraphenylarsonium chloride, basic alumina (Brockman Activity 1, 80–200 mesh) was added to a solution of the salt in acetonitrile. After shaking overnight, the mixture was filtered and the salt regained by adding anhydrous ether.

Results

The transference number of the tetramethylammonium ion constituent of tetramethylammonium perchlorate was measured over the concentration range 6.25 × 10^{-4} to 1.25 × 10^{-2} M. The transference numbers were independent of current and of following solution (indicator) concentration, provided the latter was above the limiting Kohlrausch value given by the relationship: $T_L/C_L = T_F/C_F$, where T is the transference number, C is the concentration in moles per liter, and the subscripts refer to the leading and following solution, respectively.

No volume correction was applied because the details of the electrode reaction are not known sufficiently well. This omission probably is unimportant since the volume correction should be negligible at all but the highest concentrations. As has been the case in other transference number studies, both in aqueous[7] and in nonaqueous solutions,[10,11] internal consistency of the data required application of a solvent correction larger than the conductivity of the pure solvent, possibly because of contamination during handling or electrolysis of traces of water. The proper correction was taken to be that (single) value which produced optimum constancy of the limiting value of the transference number calculated as described below from the individual transference numbers measured over the entire concentration range. A solvent correction of 1.6 × 10^{-7} ohm^{-1} cm^{-1} was applied, which amounted to a maximum correction of 0.15%. Table I contains the corrected data averaged for each concentration; at least three runs were made at each concentration. The third column contains the average deviation.

Since the transference number is not a linear function of concentration, extrapolation to infinite dilution does not always give an unambiguous result. Following a suggestion of Longsworth,[7] a limiting value of the transference number was calculated from the measured value at each concentration using the equation[12]

$$T_0^+ = T^+ + \frac{(0.5 - T^+)}{\Lambda_0}\Lambda_e \qquad (1)$$

where Λ_e is the electrophoretic contribution to the conductivity. In the limiting Onsager equation, the electrophoretic term is given by

$$\Lambda_e = \beta C^{1/2} \qquad (2)$$

whereas consideration of the finite size of the ions leads

(8) J. F. Coetzee, G. P. Cunningham, D. K. McGuire, and G. R. Padmanabhan, *Anal. Chem.*, **34**, 1139 (1962).

(9) G. P. Cunningham, G. A. Vidulich, and R. L. Kay, *J. Chem. Eng. Data*, **12**, 336 (1967).

(10) A. Fratiello, Ph.D. Thesis, Brown University, 1962.

(11) G. A. Vidulich, Ph.D. Thesis, Brown University, 1964.

(12) R. L. Kay and J. L. Dye, *Proc. Nat. Acad. Sci. U. S.*, **49**, 5 (1963).

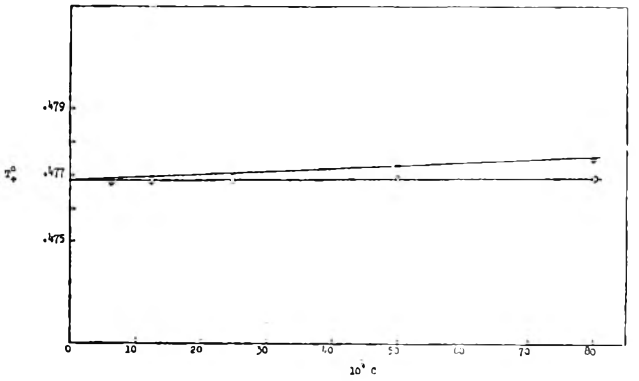

Figure 1. A plot of T_0^+ as given by eq 1 as a function of concentration for Me_4NClO_4 in acetonitrile: ● electrophoretic effect from limiting law, eq 2; ○ electrophoretic effect from extended Fuoss–Onsager eq 3 with $\mathring{a} = 8$.

to the expression

$$\Lambda_e = \beta C^{1/2}/(1 + \kappa\mathring{a}) \quad (3)$$

The values of Λ_0, β, κ, and $\mathring{a}$ used were 198.2, 233.5, $0.4858C^{1/2}$, and 8, respectively. Values of T_0^+ were calculated using both expressions for the electrophoretic effect, and were plotted as a function of concentration as shown in Figure 1. Both expressions lead to the same limiting value of 0.4768. Addition of small amounts of water (less than 0.01 M) had no measurable effect on the transference number. We estimate that the above value is accurate to 1 part in 2000.

In order to construct a scale of single ion mobilities, conductance measurements were made with tetramethylammonium and tetraphenylarsonium perchlorates. The measured equivalent conductivities in $ohm^{-1}\ cm^{-2}\ mol^{-1}$ at various molar concentrations are given in Table II along with the conductivity κ_0 of the pure solvent and the value of A used to calculate concentration.

The data were analyzed in terms of the Fuoss–Onsager theory,[13] according to which the following expression applies to nonassociated electrolytes

$$\Lambda = \Lambda_0 - SC^{1/2} + EC \log C + (J - F\Lambda_0)C \quad (4)$$

whereas for associated electrolytes it becomes

$$\Lambda = \Lambda_0 - S(C\gamma)^{1/2} + EC\gamma \log C\gamma + (J - F\Lambda_0)C\gamma - K_A C\gamma\Lambda f^2 \quad (5)$$

Table I: Summary of Corrected Transference Data Averaged for Each Concentration

10^4C	T^+ (cor)	Av dev
6.2833	0.4762	0.0003
12.488	0.4759	0.0003
24.950	0.4756	0.0001
49.268	0.4753	0.0002
79.845	0.4749	0.0002
124.80	0.4738	0.0001

Table II: Conductivity of Me_4NClO_4 and Ph_4AsClO_4 in Acetonitrile

Me_4NClO_4		Ph_4AsClO_4	
10^4C	Λ	10^4C	Λ
$\kappa_0 = 1.70 \times 10^{-8}$ $A = 0.071$		$\kappa_0 = 1.45 \times 10^{-8}$ $A = 0.181$	
8.7445	185.47	5.4094	151.32
17.0497	180.22	10.9002	148.16
25.2430	176.31	16.5933	145.82
33.6414	173.00	22.3367	143.95
43.6337	169.68	28.0988	142.33
52.0947	167.23	34.0167	140.89
61.3173	164.87	40.1667	139.56
$\kappa_0 = 1.63 \times 10^{-8}$		$\kappa_0 = 1.47 \times 10^{-8}$	
8.0006	186.07	5.2285	151.51
16.7803	180.40	10.4746	148.45
25.8105	176.13	15.9201	146.15
33.3053	173.20	21.3818	144.31
41.5158	170.44	26.9427	142.72
49.2200	168.15	32.7438	141.26
56.2015	166.23	38.5493	139.98

In eq 5, K_A is the association constant and all other symbols have their usual meaning.[13] The least-squares computer programs used for the analyses have been described elsewhere.[14–16] Although the equations include the viscosity correction $F\Lambda_0$ none was applied because it is not clear what value to use for F. In any case, the viscosity correction affects neither Λ_0 nor K_A and only results in small changes in J and the ion size parameter $\mathring{a}$ which is contained in J.

The parameters obtained from an analysis of the conductance data using both eq 4 and 5 are given in Table III. The standard deviations for each parameter have been included along with the standard deviation $\sigma\Lambda$ for the individual conductivity values. Only the

Table III: Conductance Parameters for Me_4NClO_4 and Ph_4AsClO_4 in Acetonitrile

Salt	Λ_0	$\mathring{a}$	K_A	$\sigma\Lambda$
Me_4NClO_4	197.58 ± 0.12	2.11 ± 0.04		0.10
	198.16 ± 0.007	3.13 ± 0.03	7.0 ± 0.2	0.01
	197.64 ± 0.11	2.11 ± 0.04		0.09
	198.14 ± 0.02	3.1 ± 0.1	6.5 ± 0.6	0.05
Ph_4AsClO_4	159.52 ± 0.06	4.51 ± 0.05		0.05
	159.58 ± 0.05	4.55 ± 0.05		0.04

(13) R. M. Fuoss and F. Accascina, "Electrolytic Conductance," Interscience Publishers, Inc., New York, N. Y., 1959.
(14) R. L. Kay, *J. Amer. Chem. Soc.*, **82**, 2099 (1960).
(15) J. L. Hawes and R. L. Kay, *J. Phys. Chem.*, **69**, 2420 (1965).
(16) G. P. Cunningham, Ph.D. Thesis, University of Pittsburgh, 1964.

Table IV: Limiting Equivalent Conductivities of Selected Salts in Acetonitrile at 25°

Salt	Λ_0	Ref	Salt	Λ_0	Ref
Me_4NBr	195.2	17	$LiClO_4$	173.0	20, 21
Et_4NBr	185.5	18	$KClO_4$	187.5	20
Pr_4NBr	171.0	17	$NaClO_4$	180.4	20
Bu_4NBr	162.1	17	Bu_4NClO_4	165.1	4
$(i\text{-Am})_3BuNBr$	158.5	18	$(i\text{-Am})_4NClO_4$	160.6	4
$(i\text{-Am})_4NBr$	157.4	18	Ph_4AsClO_4	159.5	a
Ph_4AsBr	156.6	18	$CsBPh_4$	145.4	20
Me_4NI	196.7	17	$RbBPh_4$	143.8	20
Pr_4NI	172.9	17	$KBPh_4$	141.8	20
$(EtOH)_4NI$	166.0	19	$NaBPh_4$	135.4	20
Bu_4NI	164.0	17	$(EtOH)_4NBPh_4$	122.3	19
Ph_4AsI	158.1	18	Bu_4NBPh_4	119.7	4
Me_4NClO_4	198.2	a	$(i\text{-Am})_4NBPh_4$	115.0	4
$CsClO_4$	191.0	20	Me_4NPi	171.8	17
$RbClO_4$	189.5	20	Bu_4NPi	139.4	17
			$(i\text{-Am}_4)NB(i\text{-Am})_4$	114.5	4

[a] This investigation.

parameters obtained from eq 4 are given for tetraphenylarsonium perchlorate, since eq 5 gave small negative association constants indicating that no significant association occurs.

From our data for tetramethylammonium perchlorate (Λ_0 = 198.2 and T_0^+ = 0.4768) it follows that $\lambda_0(Me_4N^+)$ = 94.5 and $\lambda_0(ClO_4^-)$ = 103.7.

A selected list of Λ_0 values for a variety of salts[4,17-21] is given in Table IV. All data were analyzed in terms of eq 4 and 5. From these numbers the list of best values of single-ion conductivities given in Table V was constructed, based on the above values for tetramethylammonium and perchlorate ions. The uncertainty in a given λ_0 value generally increases with increasing number of Λ_0 values required for its derivation. In Table V entries are in order of decreasing estimated reliability.

Discussion

Applicability of the Reference Electrolyte Tetraisoamylammonium Tetraisoamylboride. It is particularly interesting to compare the conductivities of the ions of the above reference electrolyte. Coetzee and Cunningham[4] have based a scale of single ion conductivities on the assumption that $(i\text{-Am})_4N^+$ and $(i\text{-Am})_4B^-$ have equal mobilities, because these ions have virtually the same size, and furthermore, solvation effects should be small since the ions are large and symmetrical and not very polarizable, and the single charge is reasonably well shielded. However, the results of the present investigation indicate that the mobility of the cation is 1.2% smaller than that of the anion. We have commented before[22] on differences in the interaction of acetonitrile with cations and anions. Recently, Pople and Gordon[23] have carried out an approximate molecular orbital calculation of the charge distribution in the acetonitrile molecule, with the following results (expressed in 10^{-3} electron unit)

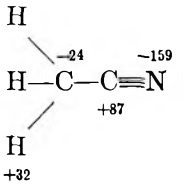

Table V: Limiting Equivalent Conductivities of Single Ions in Acetonitrile at 25° in Order of Decreasing Estimated Reliability

Cation	λ_0^+	Anion	λ_0^-
Me_4N^+	94.5	ClO_4^-	103.7
Bu_4N^+	61.4	Br^-	100.7
$(i\text{-Am})_4N^+$	56.9	I^-	102.4
Ph_4As^+	55.8	Ph_4B^-	58.3
Cs^+	87.3	$(i\text{-Am})_4B^-$	57.6
Rb^+	85.6	Pi^-	77.7
K^+	83.6		
Na^+	76.9		
$(EtOH)_4N^+$	64.0		
Et_4N^+	84.8		
Pr_4N^+	70.3		
Li^+	69.3		
$(i\text{-Am})_3BuN^+$	57.8		

(17) D. F. Evans, C. Zawoyski, and R. L. Kay, *J. Phys. Chem.*, 69, 3878 (1965).

(18) R. L. Kay, unpublished data.

(19) G. P. Cunningham, D. F. Evans, and R. L. Kay, *J. Phys. Chem.*, 70, 3998 (1966).

(20) R. L. Kay, B. J. Hales, and G. P. Cunningham, *ibid.*, 71, 3925 (1967).

(21) F. Accascina, *Rec. Sci. Rend.*, 7, 556 (1963).

(22) J. F. Coetzee and J. J. Campion, *J. Amer. Chem. Soc.*, 89, 2517 (1967).

(23) J. A. Pople and M. Gordon, *ibid.*, 89, 4253 (1967).

Although this charge distribution accounts only approximately for the measured dipole moment of acetonitrile, it nevertheless is clear that since considerable delocalization of positive charge occurs, the ion–dipole interaction of an anion with acetonitrile will be more diffuse and less energetic than that of a cation of equal size, numerical charge, and polarizability. However, rough calculations indicate that even for a cation, when it is as large as $(i\text{-Am})_4N^+$, the interaction with acetonitrile probably is too small to compete with solvent–solvent interactions.[24,25] Consequently, it probably would not be realistic to invoke differences in solvation in order to rationalize the difference in mobilities of these ions. However, it is likely that the two ions are unequally "wetted" by acetonitrile. It was pointed out by Lamb[26] that the coefficient 6π in the Stokes equation results from the assumption that the medium wets the moving particle. If the particle is not wetted but slips through the medium, the coefficient becomes 4π. One could speculate that the greater mobility of the anion results from a superior ability to slip through acetonitrile. It seems evident that no known reference electrolyte can be expected to provide highly accurate splits of conductivities in a variety of dissimilar solvents.

Applicability of the Conductance Theory. The measurement of conductivities and of the corresponding transference numbers as a function of concentration provides a means of evaluating the theory of conductance. The Fuoss–Onsager theory attributes the decrease in mobility with increasing concentration to the electrophoretic and the relaxation effects. In evaluating these effects a hard sphere, solvent continuum model has been used. An essential feature of this model is that for symmetrical electrolytes the relaxation and electrophoretic terms are the same for both ions. Kay and Dye[12] have shown that as a consequence the transference number should be independent of the relaxation

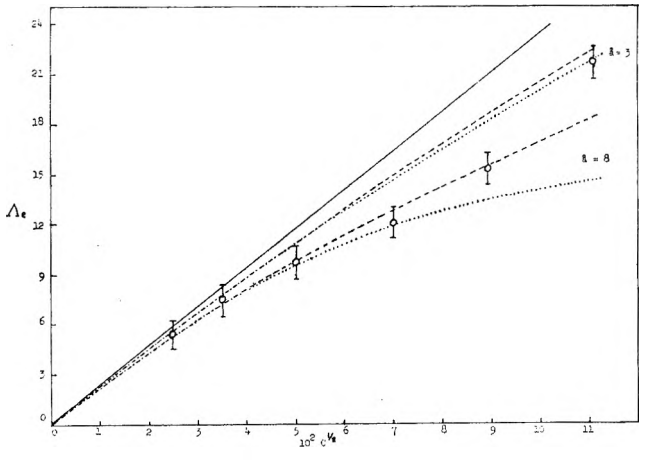

Figure 2. The electrophoretic effect calculated from eq 6: Φ, data; ——, limiting law; – – –, $\beta C^{1/2}/(1 + \kappa\mathring{a})$; • • •, $\beta C^{1/2} - [(\beta\kappa\mathring{a})/C]C$.

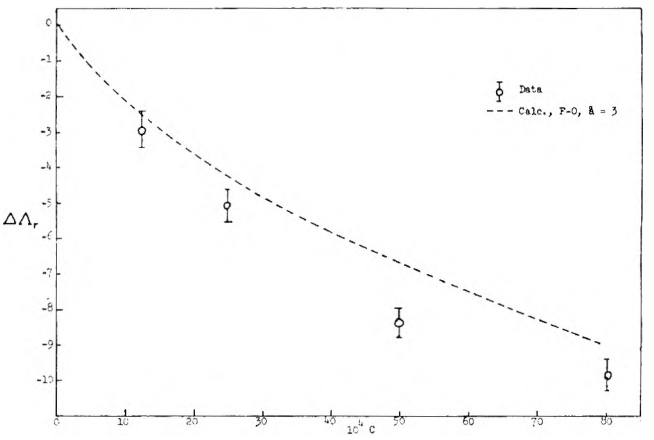

Figure 3. The points are a plot of the experimentally determined extended terms in the relaxation effect as given by eq 8. The dotted curve is a plot of eq 9 for $\mathring{a} = 3$.

effect and should be given by the expression

$$T^i = \frac{\lambda_0^i - \lambda_e^i}{\Lambda_0 - \Lambda_e} \qquad (6)$$

where the subscript e refers to the electrophoretic effect and other symbols have their usual meaning. For the special case of a symmetrical electrolyte, since $\lambda_e^{\pm} = \frac{1}{2}\Lambda_e$, eq 6 can be rearranged into eq 1. An experimental value for the electrophoretic effect, therefore, can be obtained from a combination of conductivity and transference data.

In Figure 2 experimental values of the electrophoretic effect for tetramethylammonium perchlorate in acetonitrile are compared with values predicted by the Fuoss–Onsager theory. It is evident that while the limiting equation (2) overestimates the electrophoretic effect, eq 3 with $\mathring{a} = 8$ Å gives good agreement with the experimental values. Thus, the transference data are consistent with a reasonable value for the ion size parameter. This should be contrasted with the value of 3 Å obtained from the conductance data. This unreasonably low value may be caused by the elimination of the viscosity correction $F\Lambda_0$ in eq 4 or by the fact that in the final conductance equation the electrophoretic effect has been written in an expanded form of which only two terms have been used. In order to be consistent in the elimination of terms of order $C^{3/2}$ or greater, eq 3 was expanded and used in the form

$$\Lambda_e = \beta C^{1/2} - \frac{\beta\kappa\mathring{a}}{C^{1/2}} C \qquad (7)$$

(24) Only ion–dipole and dipole–dipole interactions were considered, since these make the largest contribution to the total interaction energy. For these large ions, quadrupole, induced dipole, dispersion and other interactions, as treated in Buckingham's theory,[25] could be ignored, because of their high order dependence on distance.

(25) A. D. Buckingham, *Discussions Faraday Soc.*, 24, 151 (1957).

(26) H. Lamb, "Hydrodynamics," Dover Publishing Co., New York, N. Y., 1945, p 602.

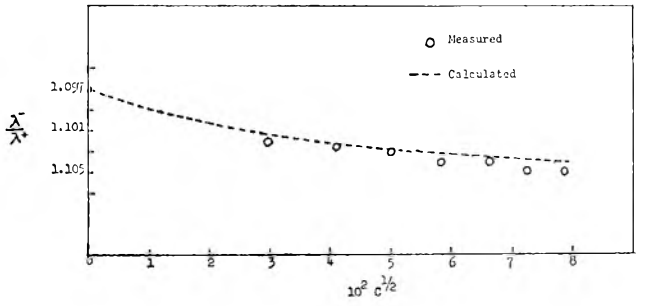

Figure 4. A plot of the ratio of cation to anion conductance as given by eq 12 for Me_4NClO_4 in acetonitrile.

The effect of this reduction can be seen in Figure 2. For $\mathring{a} = 8$, the electrophoretic effect calculated from eq 7 is too small at high concentrations but the lower value of $\mathring{a} = 3$ gives values of Λ_e that are higher than the experimentally determined values. Also, any reasonable estimate of F would result in an increase in $\mathring{a}$ of 0.3 at most. Consequently, it seems that the low $\mathring{a}$ value must be attributed to the approximations used in the evaluation of the relaxation effect.

A procedure has been described[12] whereby the measured contribution to the conductance from the relaxation effect can be compared with the theoretically predicted contribution. By introducing the quantity

$$\Delta\Lambda_r \equiv \Lambda - (\Lambda_0 - \Lambda_e)(1 - \alpha C^{1/2}) \qquad (8)$$

the terms for the experimental electrophoretic effect and the limiting relaxation effect are removed from the measured conductances, leaving only the extended terms for the relaxation effect, as well as the association term when applicable. In the Fuoss–Onsager theory, $\Delta\Lambda_r$ for an unassociated electrolyte is given by

$$\Delta\Lambda_r = EC \log C + J'C \qquad (9)$$

where

$$J' = J - \left(\alpha\beta + \frac{\beta\kappa\mathring{a}}{C^{1/2}}\right) \qquad (10)$$

If the electrolyte is associated, eq 9 becomes

$$\Delta\Lambda_r = EC\gamma \log C\gamma + J'C\gamma - K_A C\gamma\Lambda f^2 \qquad (11)$$

Experimental and theoretical values of $\Delta\Lambda_r$ are shown in Figure 3 from which it can be seen that a value of $\mathring{a}$ even lower than 3 is required to fit the experimental relaxation effect if the experimentally determined electrophoretic effect is used. The association constant is too small for its effect to be gauged.

Thus, it seems that the failure of the conductance data to give reasonable values of $\mathring{a}$ may be caused by approximations in the evaluation of the relaxation effect in the conductance equation.

An evaluation of the electrophoretic effect can also be obtained directly from single-ion conductivity data since it can be shown that the ratio λ^-/λ^+ is given by

$$\lambda^-/\lambda^+ = (\lambda_0^- - \lambda_e^-)/(\lambda_0^+ - \lambda_e^+) \qquad (12)$$

and therefore is independent of the relaxation effect, as is the case for the transference number. The hard sphere, solvent continuum model assumes that $\lambda_e^- = \lambda_e^+ = 0.5\Lambda_e$. If this assumption is correct, a plot of the ratio calculated from eq 12 *vs.* $C^{1/2}$ should have the same slope as a similar plot of the experimental ratio. Values of Λ_e were calculated from eq 3, and experimental values of $\lambda^\pm$ were obtained from transference numbers and corresponding equivalent conductivities for finite concentration. The results are illustrated by Figure 4. It seems that for tetraethylammonium perchlorate in acetonitrile the assumption that the electrophoretic effect is the same for both ions is valid.

Acknowledgments. We gratefully acknowledge financial support by the following agencies: National Aeronautics and Space Administration (for a Predoctoral Traineeship to C. H. S.), National Science Foundation (Grant No. GP-6478 X to J. F. C.), and the Office of Saline Water, U. S. Department of the Interior (Contract No. 14-01-0001-1729 to R. L. K.).

Kinetic Studies of Intramolecular Hydrogen Bonding in Methyl and Ethyl Salicylates and Salicylaldehyde by Means of Ultrasonic Absorption Measurement

by Tatsuya Yasunaga, Nobuhide Tatsumoto, Hiroshi Inoue, and Masaji Miura

Department of Chemistry, Faculty of Science, Hiroshima University, Hiroshima, Japan (*Received March 4, 1968*)

The Ultrasonic relaxational absorptions in methyl and ethyl salicylates and salicylaldehyde have been studied in the frequency range 2.5 to 95 Mc/sec at the various temperatures from 20 to 40°. The ultrasonic absorption measurements in derivatives of phenol and benzoic acid lead to the conclusion that the ultrasonic relaxations in methyl and ethyl salicylates and salicylaldehyde are associated with intramolecular hydrogen bonding between the phenolic hydroxyl group and an oxygen of adjacent carboxyl or carbonyl group. The kinetic values have been calculated for the reaction of intramolecular hydrogen bonding. The forward and backward rate constants at 30° are 1.2×10^6 and 3.1×10^7 sec^{-1} for methyl salicylate, 4.7×10^5 and 2.2×10^7 sec^{-1} for ethyl salicylate, and 4.0×10^5 and 2.6×10^7 sec^{-1} for salicylaldehyde, respectively. The heats of the hydrogen bonding at constant volume are 2.5, 2.5, and 3.5 kcal/mol for methyl and ethyl salicylates and salicylaldehyde, respectively.

Introduction

Relaxational techniques have extensively been applied to kinetic studies of rapid chemical reactions, such as intermolecular hydrogen bonding,[1,2] hydrolysis and protolysis of electrolyte,[3-5] and rotational isomerism.[5] Only a limited number of investigations have been made on kinetics of intramolecular hydrogen bonding by use of a temperature-jump method,[6] although the role of the hydrogen bond in biological systems has been the source of considerable speculation and numerous experimental studies.[7]

It has been well known by the ordinary spectroscopic methods that in methyl salicylate or salicylaldehyde a phenolic hydroxyl group forms a strong intramolecular hydrogen bond[8] with an oxygen of adjacent carboxyl or carbonyl group, but its kinetic study has not yet been done. The purpose of the present investigation is to decide the mechanisms of sound absorption in methyl and ethyl salicylates and salicylaldehyde and to calculate the kinetic values for the reaction associated with those.

Theoretical

The absorption spectrum of sound is presented in an expression for a single relaxation

$$\alpha'/f^2 = (\alpha/f^2) - B = \frac{A}{1 + (f/f_{max})^2} \qquad (1)$$

where α is an absorption coefficient of sound, α' is the relaxational absorption coefficient, A and B are the relaxational absorption and classical absorption, respectively, f is the frequency of sound, and f_{max} is the frequency at the maximum of the absorption per wavelength $\alpha'\lambda$. The values of absorption of sound are related to the values of dispersion of sound velocity by the equations

$$f_{inf}/f_{max} = V_\infty/V_0 \qquad (2)$$

$$V^2 = V_0^2 + \Delta V^2 \frac{(f/f_{inf})^2}{1 + (f/f_{inf})^2} \qquad (3)$$

$$\Delta V^2 = V_\infty^2 + V_0^2 \qquad (4)$$

$$(\alpha'\lambda)_{max} = \pi \Delta V^2 / 2 V_0 V_\infty \qquad (5)$$

where V is the velocity of sound, λ is the wavelength, and subscripts 0, ∞, inf refer to the frequencies of zero and infinite, and the point of the inflection of the velocity dispersion, respectively. Moreover, the relation between the heat capacity resulting from the reaction and the values of dispersion of sound velocity are represented as

$$C_p^r = C_p^0 - C_p^\infty \qquad (6)$$

$$C_v^r = C_v^0 - C_v^\infty \qquad (7)$$

(1) N. Tatsumoto, *J. Chem. Phys.*, **47**, 4561 (1967).

(2) B. Spakowski, *Compt. Rend. Acad. Sci. U.R.S.S.*, **18**, 169 (1938); J. Lamb and J. M. M. Pinkerton, *Proc. Roy. Soc.*, **A199**, 114 (1949); J. E. Piercy and J. Lamb, *Trans. Faraday Soc.*, **52**, 930 (1956); E. Freedman, *J. Chem. Phys.*, **21**, 1784 (1953); J. Lamb and D. H. A. Huddart, *Trans. Faraday Soc.*, **46**, 540 (1950); D. Tabuchi, *Z. Elektrochem.*, **64**, 141 (1960).

(3) T. Yasunaga, M. Tanoura, and M. Miura, *J. Chem. Phys.*, **43**, 3512 (1965).

(4) T. Yasunaga, N. Tatsumoto, and M. Miura, *ibid.*, **43**, 2735 (1965).

(5) S. L. Friess, E. S. Lewis, and A. Weissberger, "Investigation of Rates and Mechanisms of Reactions," Interscience Publishers, Inc., New York, N. Y., 1963.

(6) G. Porter, *Progr. Reaction Kinetics*, **2**, 300 (1964); M. H. Miles, E. M. Eyring, W. W. Epstein, and R. E. Ostlund, *J. Phys. Chem.*, **69**, 467 (1965).

(7) G. C. Pimentel and A. L. McClellan, "The Hydrogen Bond," Reinhold Publishing Corp., New York, N. Y., 1960.

(8) L. Pauling, "The Nature of the Chemical Bond," 3rd ed, Cornell University Press, Ithaca, N. Y., 1960.

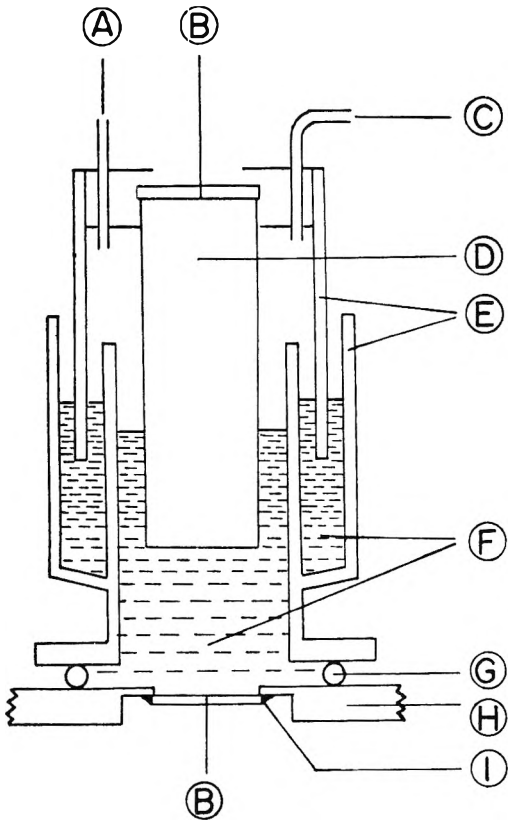

Figure 1. Sectional diagram of the cell for measuring ultrasonic absorption: A, N_2 gas outlet; B, X-cut quartz crystal; C, N_2 gas inlet; D, delay line (fused quartz); E, glass; F, sample liquid or solution; G, Teflon O-ring; H, stainless steel; I, epoxy resin.

$$C_p = C_v + (Tvl^2/\beta_T) \tag{8}$$

$$V_0^2 = (\rho\beta_T)^{-1}C_p^0/C_v^0 \tag{9}$$

$$V_\infty^2 = (\rho\beta_T)^{-1}C_p^\infty/C_v^\infty \tag{10}$$

$$2\pi f_{inf} = C_v^0/C_v^\infty\tau \tag{11}$$

where C_p and C_v are the heat capacities at constant pressure and constant volume, respectively, v is the volume, l is the thermal expansion coefficient, T is the absolute temperature, ρ is the density, β_T is the isothermal compressibility, τ is the relaxation time, and superscripts r, 0, and ∞ refer to the chemical reaction, the frequencies of zero and infinite, respectively.

In a chemical equilibrium such as

$$aA + bB + \ldots \rightleftharpoons qQ + rR + \ldots \tag{12}$$

one has Tabuchi's equations

$$C_p^r = W/\chi \tag{13}$$

$$W = E^2/RT^2 + [(\Delta v/R)(l/\beta_T) - \xi lT] + \xi C_v^\infty(\Delta v/v) \tag{14}$$

$$\xi = (a + b + \ldots) - (q + r + \ldots) \tag{15}$$

$$\chi = (a^2/n_A + b^2/n_B + \ldots) + (q^2/n_Q + r^2/n_R \ldots) \tag{16}$$

$$C_v^r = (E^2/RT^2)\chi^{-1} \tag{17}$$

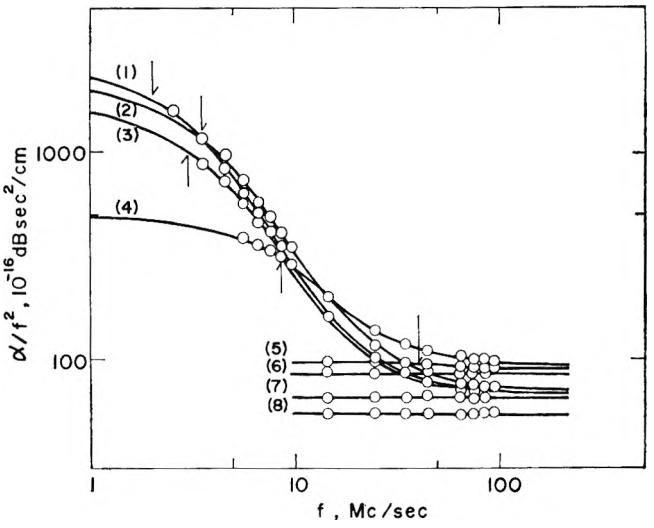

Figure 2. Ultrasonic absorption spectra: (1) salicylaldehyde (20°); (2) methyl salicylate (20°); (3) ethyl salicylate (25°); (4) 2.17 *M* salicylic acid in dioxane (15°); (5) 1.66 *M* benzoic acid in dioxane (16°); (6) 0.86 *M* ethyl *p*-hydroxybenzoate in dioxane (30°); (7) 0.5 mole fraction methyl benzoate in phenol (30°); (8) methyl benzoate (16°).

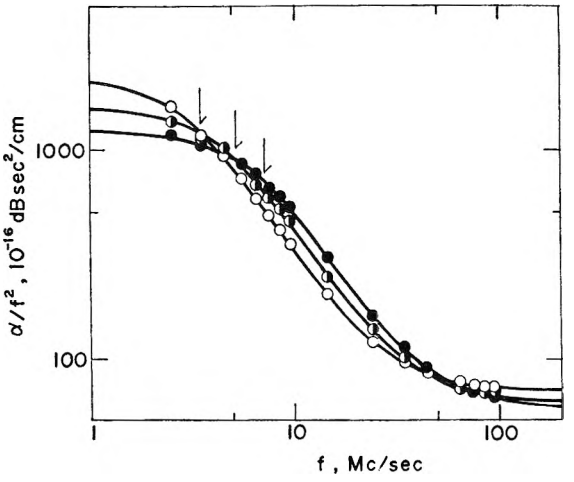

Figure 3. Ultrasonic absorption spectra in methyl salicylate: ○, 20°; ◑, 30°; ●, 40°.

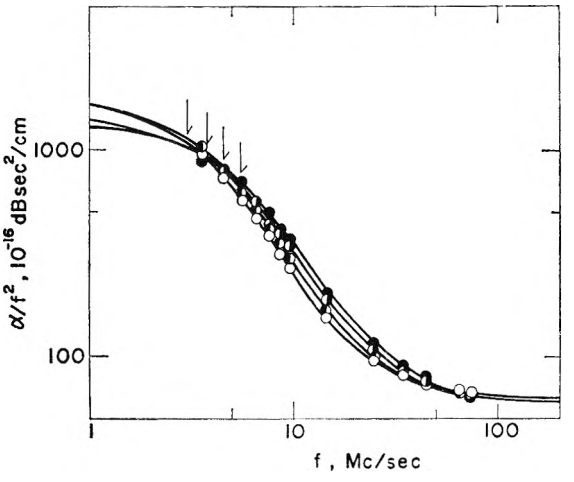

Figure 4. Ultrasonic absorption spectra in ethyl salicylate: ○, 25°; ◐, 30°; ◑, 35°; ●, 40°.

Table I: The Values Obtained from Ultrasonic Absorption Spectra and Other Measurements

Temp, °C	f_{max}, Mc/sec	α'_{max}, 10^{-1} cm^{-1}	V(3 Mc/sec), 10^5 cm/sec	ρ, g/cc	l, 10^{-4} deg^{-1}	C_p^0, 10^{-1} cal/g deg
			Methyl Salicylate			
20	3.5	1.643	1.4293	1.1846	7.07	3.910[a]
25	4.3	2.080	1.4106	1.1798	7.07	3.910
30	5.2	2.600	1.3923	1.1749	7.07	3.910
35	6.0	3.082	1.3747	1.1700	7.07	3.910
40	7.2	3.809	1.3565	1.1651	7.07	3.910
			Ethyl Salicylate			
25	3.0	1.128	1.3707	1.1259	8.56	3.74
30	3.7	1.435	1.3523	1.1210	8.56	3.74
35	4.5	1.805	1.3345	1.1161	8.56	3.74
40	5.5	2.268	1.3175	1.1113	8.56	3.74
			Salicylaldehyde			
20	3.0	1.364	1.4843	1.1653	7.38	3.825[b]
25	3.6	1.738	1.4659	1.1603	7.38	3.825
30	4.3	2.192	1.4471	1.1551	7.38	3.825
35	5.1	3.741	1.4281	1.1504	7.38	3.825
40	6.0	3.399	1.4104	1.1456	7.38	3.825

[a] H. H. Landolt and R. Börnstein, "Physikalische Chemische Tabellen," Vol. III, Part 3, Springer-Verlag, Berlin, 1936, p 2301. [b] E. W. Washburn, "International Critical Tables," Vol. V, McGraw-Hill Book Co., Inc., New York, N. Y., p 110.

where Δv is the volume change resulting from the reaction and E is the reaction heat per mole at constant volume.

Experimental Section

The measurements of sound absorption were made over the frequency range 2.5 to 95 Mc/sec at various temperatures, 15 to 40°. The techniques and apparatus were fully described in a previous paper.[1] The cell was designed as shown in Figure 1 for avoiding the air oxidation in the sample throughout the measurement of absorption. The velocity of sound was measured at 3 Mc/sec by an ultrasonic interferometer.[3] In the measurement of sound velocity the cell was also designed in the same way as in the measurement of absorption. The chemicals were all guaranteed reagents and were used throughout this study with purification.

Result and Discussion

The plots of the data are presented in Figures 2–7 along with their corresponding theoretical curves. The relaxational absorption can be seen in the frequencies

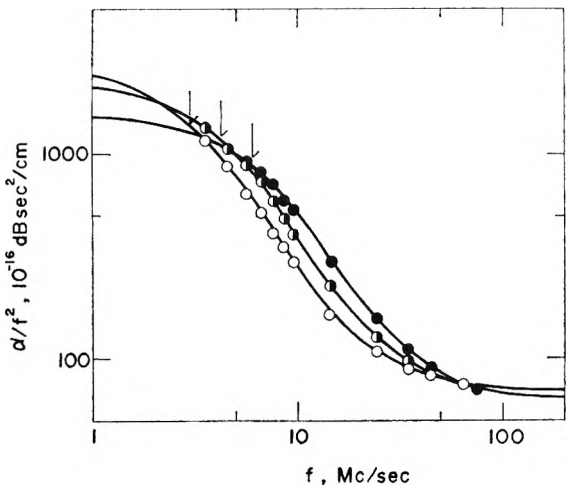

Figure 5. Ultrasonic absorption spectra in salicylaldehyde: ○, 20°; ◑, 30°; ●, 40°.

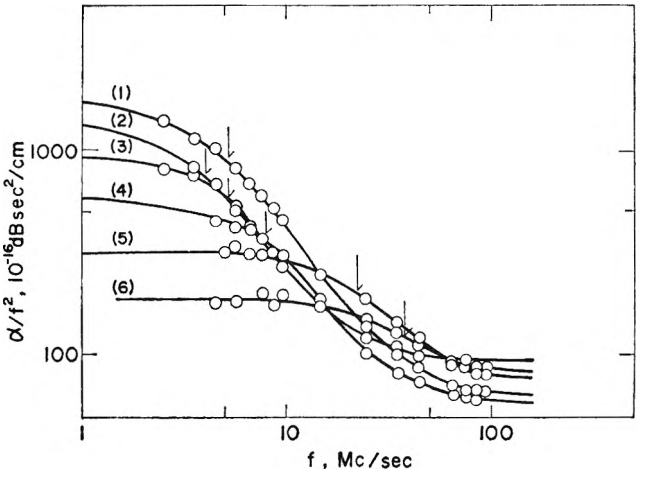

Figure 6. Ultrasonic absorption spectra in solutions of methyl salicylate at 30°: (1) 100% (7.8 M); (2) 3.2 M in benzene; (3) 4.8 M in n-hexane; (4) 4.8 M in methyl benzoate; (5) 3.3 M in dioxane; (6) 1.6 M in dioxane.

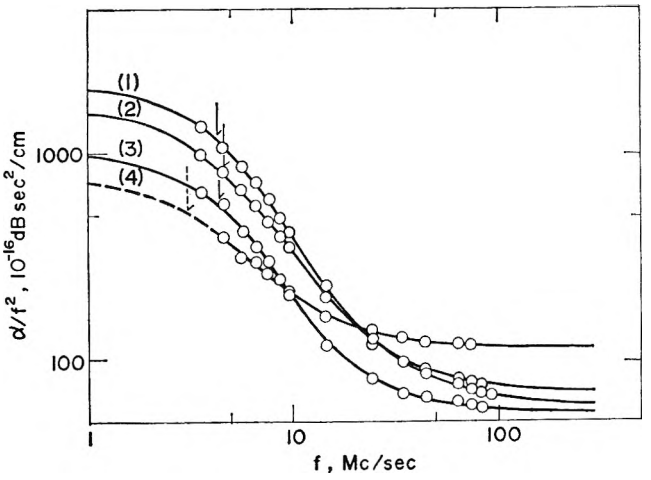

Figure 7. Ultrasonic absorption spectra in solutions of salicylaldehyde at 30°: (1) 100% (9.5 *M*); (2) 4.1 *M* in dioxane; (3) 4.2 *M* in methyl benzoate; (4) 4.2 *M* in benzene.

lower than 8 Mc/sec in methyl and ethyl salicylates and salicylaldehyde and at 8.5 Mc/sec in 2.17 *M* dioxane solution of salicylic acid, while the spectra in methyl benzoate, 1.66 *M* dioxane solution of benzoic acid, 0.86 *M* dioxane solution of ethyl *p*-hydroxybenzoate, and 0.5 mole fraction methyl benzoate in phenol do not show such an absorption although a very weak relaxational absorption can be seen at around 50 Mc/sec in dioxane solution of benzoic acid. The spectra in some solvent solutions of methyl salicylate and salicylaldehyde do not give the information on reaction order associated with the absorption because the effect of solvent on the relaxation frequency is great.

Table II: The Reaction Heat Capacities

Temp, °C	C_v^r, 10^{-3} cal/g deg	C_p^r, 10^{-3} cal/g deg
	Methyl Salicylate	
20	7.56	7.56
25	7.79	7.79
30	8.04	8.04
35	8.26	8.26
40	8.51	8.51
	Ethyl Salicylate	
25	4.11	4.11
30	4.24	4.24
35	4.39	4.39
40	4.52	4.52
	Salicylaldehyde	
20	6.31	6.31
25	6.69	6.69
30	7.07	7.07
35	7.45	7.45
40	7.84	7.84

The values for three constants, f_{max}, A, and B obtained from the absorption spectra were listed in Table I along with those from the other measurements. The reaction heat capacities, C_p^r and C_v^r, in Table II were calculated using eq 1–11 by the procedure of the previous paper.[1] The value for C_p^r is equal to that for C_v^r so that the volume change resulting from the reaction is absent as may be seen in eq 13 and 17. The absorption mechanism of this reaction, therefore, can be attributed to the thermal relaxation.

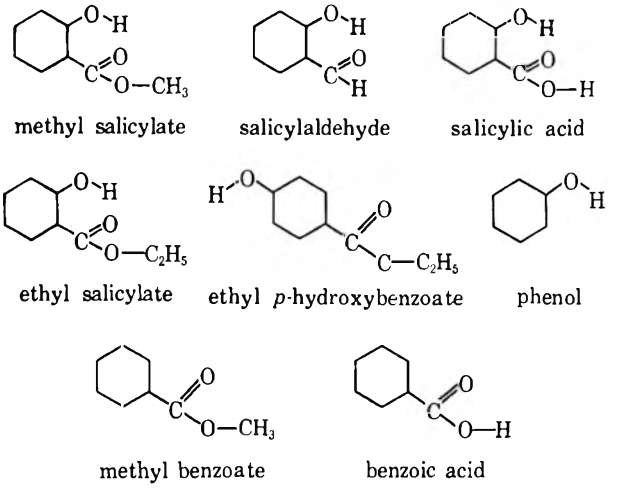

As the reaction is not accompanied with the volume change, the following ones may be considered to occur in these compounds.

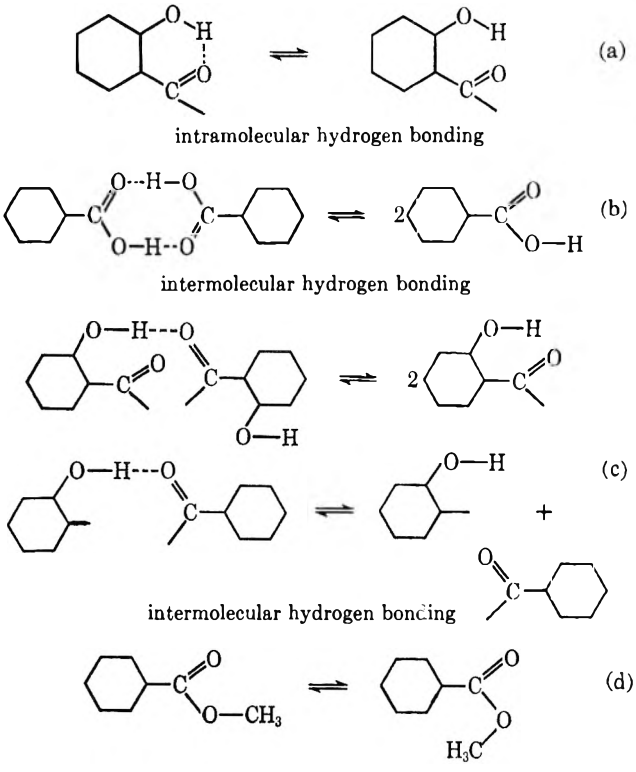

In methyl salicylate, reactions a, c, and d may be considered as the mechanism of the strong absorption in

Table III: The Kinetic Values for the Reaction of the Intramolecular Hydrogen Bonding

Temp, °C	E, kcal/mol	10^2K	k_f, 10^5 sec^{-1}	k_b, 10^7 sec^{-1}	$E_f^{\ddagger}$, kcal/mol	$E_b^{\ddagger}$, kcal/mol
			Methyl Salicylate			
20		3.4	7.1	2.1		
25		3.7	9.5	2.6		
30	2.5	4.0	12.	3.1	~8	5.8
35		4.2	15.	3.5		
40		4.5	19.	4.2		
			Ethyl Salicylate			
25		2.0	3.6	1.8		
30	2.5	2.1	4.7	2.2	~9	6.8
35		2.3	6.2	2.7		
40		2.4	8.0	3.3		
			Salicylaldehyde			
20		1.3	2.3	1.8		
25		1.4	3.0	2.2		
30	3.5	1.5	4.0	2.6	~9	5.6
35		1.7	5.1	3.1		
40		1.8	6.5	3.6		

the frequencies lower than 8 Mc/sec since this compound has the hydroxyl and carboxyl groups and forms the intramolecular hydrogen bond between them and is also an ester. However, the spectrum in methyl benzoate, in which reaction d may occur, does not show the absorption and then reaction d may be ruled out as the mechanism of absorption in methyl salicylate. In salicylaldehyde the absorption, which can be seen in the same frequency range as in methyl salicylate, is probably due to the relaxation of reactions a and c because this compound has the hydroxyl and carbonyl groups and forms the intramolecular hydrogen bond between them and is neither ester nor acid. However, the spectra in ethyl *p*-hydroxybenzoate and the mixture of methyl benzoate and phenol, in which reaction c may occur, do not show the absorption and then reaction c may be ruled out as the mechanism of absorption in methyl salicylate and salicylaldehyde. The absorptions in methyl salicylate and salicylaldehyde, therefore, are probably associated with reaction a. The mechanism of absorption in ethyl salicylate may be the same as that of methyl salicylate except for alkyl group in carboxyl group. In salicylic acid which forms intramolecular and intermolecular hydrogen bonds,[8] reactions a, b, and c can be considered as the absorption mechanism.

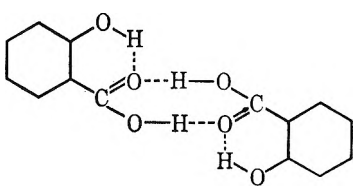

The absorption mechanism in salicylic acid, however, cannot be decided only by these experimental data because the absorption is in the middle frequency between the relaxation frequencies in benzoic acid and methyl or ethyl salicylate or salicylaldehyde. The weak absorption appearing in benzoic acid seems to be due to the relaxation of reaction b with regard to the relaxation frequency and the absorption intensity.[9]

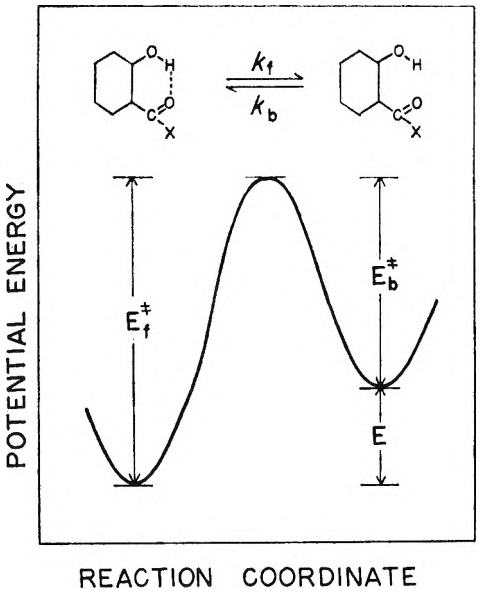

Figure 8. Internal molecular energy potential curve of methyl and ethyl salicylates or salicylaldehyde.

(9) J. Rassing, O. Østerberg, and T. A. Bak, *Acta Chem. Scand.*, 21, 1443 (1967).

For the intramolecular hydrogen bonding which is the uni-unimolecular reaction

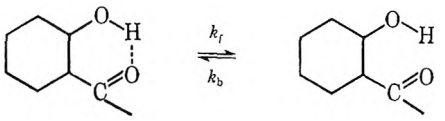

Equations 13 and 17 are represented by the equations

$$C_p' = \delta(1 - \delta)\left(\frac{E^2}{RT^2} + \frac{E\Delta vl}{RT^2/\beta_T}\right) \quad (18)$$

$$C_v' = \delta(1 - \delta)\frac{E^2}{RT^2} \quad (19)$$

where δ is the mole fraction of reactant. The integrated van't Hoff isochore is

$$\ln K_1 - \ln K_2 = (E/R)(T_2^{-1} - T_1^{-1}) \quad (20)$$

where K is the equilibrium constant which is given by

$$K = (1 - \delta)/\delta \quad (21)$$

Equations 18–21 are solved by the method of successive approximations in order to obtain E and K. The forward and backward rate constants of this reaction are calculated from f_{inf} and the equilibrium constant by the equation

$$2\pi f_{inf}(C_v^{\infty}/C_v^{0}) = k_b(1 + K) = k_f(1 + K^{-1}) \quad (22)$$

The heats of activation are given by the temperature dependence of the rate constant.

$$k/T = C\exp(-E^{\ddagger}/RT) \quad (23)$$

The energies and kinetic values for the intramolecular hydrogen bonding in methyl and ethyl salicylates and salicylaldehyde calculated from the experimental data are listed in Table III. The hydrogen-bonded molecules can be assumed to be more stable than the nonbonded ones in these compounds since these form the strong intramolecular hydrogen bonds. Energy states of the hydrogen-bonded and nonbonded molecules, therefore, can be represented by a curve in Figure 8. The difference of energies, E, E_f, and E_b for methyl and ethyl salicylates and salicylaldehyde may be considered to come from the difference of substituent.

Spectroscopic Studies of the Triethylamine–I_2 System in *n*-Heptane and in *p*-Dioxane

by Hari D. Bist[1] and Willis B. Person[2]

Departments of Chemistry, University of Iowa, Iowa City, Iowa 52240 and University of Florida, Gainesville, Florida 32601 *(Received March 11, 1968)*

Spectroscopic studies are reported of the triethylamine–I_2 complex in *n*-heptane and in *p*-dioxane solvents. In the *n*-heptane solution, we have verified results from earlier studies by Nagakura. In dioxane with excess triethylamine a rapid reaction occurs, passing through an intermediate, to form I^- quantitatively as an end product. This reaction has been followed spectroscopically, and the identity of the I^- product established. It is postulated that the intermediate iodine-containing species is $(Et_3N\text{–}I)^+$ {or $[(Et_3N)_2I]^+$}. Further characteristics of this reaction are reported, and a possible reaction sequence is suggested. Properties of the complex itself in dioxane are found to be quite similar to its properties in *n*-heptane, except for its instability with respect to this ion-producing reaction. Some observations are also reported of the properties of I_2 in dioxane.

Recently, we have begun the reinvestigation of a number of electron donor-acceptor complexes of iodine which have been well-studied by previous investigators, but whose importance as typical examples is so great that extra efforts to obtain accurate data are justified. One such complex is that formed between triethylamine and iodine, which is typical of strong complexes formed between amines, acting as an n-donor, and I_2, acting as an aσ-acceptor.[3]

This complex has been studied previously by Collin,[4] and very carefully by Nagakura.[5] Furthermore, its dipole moment has been measured,[6] so that this complex is one of the few systems for which that experimental

(1) Department of Physics, Indian Institute of Technology, Kanpur, U.P., India.

(2) To whom correspondence should be addressed, at the Department of Chemistry, University of Florida, Gainesville, Fla.

(3) The nomenclature follows (a) R. S. Mulliken, *J. Chim. Phys.*, 20 (1963); see also (b) R. S. Mulliken, *J. Phys. Chem.*, 56, 811 (1952), and (c) R. S. Mulliken and W. B. Person, "Physical Chemistry," H. Eyring, D. Henderson, and W. Jost, Ed., Vol. III, Academic Press, New York, N. Y., 1960, Chapter 19.

(4) J. Collin, *Bull. Soc. Roy. Sci. Liege*, 23, 395 (1954).

(5) S. Nagakura, *J. Amer. Chem. Soc.*, 80, 520 (1958).

(6) H. Tsubomura and S. Nagakura, *J. Chem. Phys.*, 27, 819 (1957).

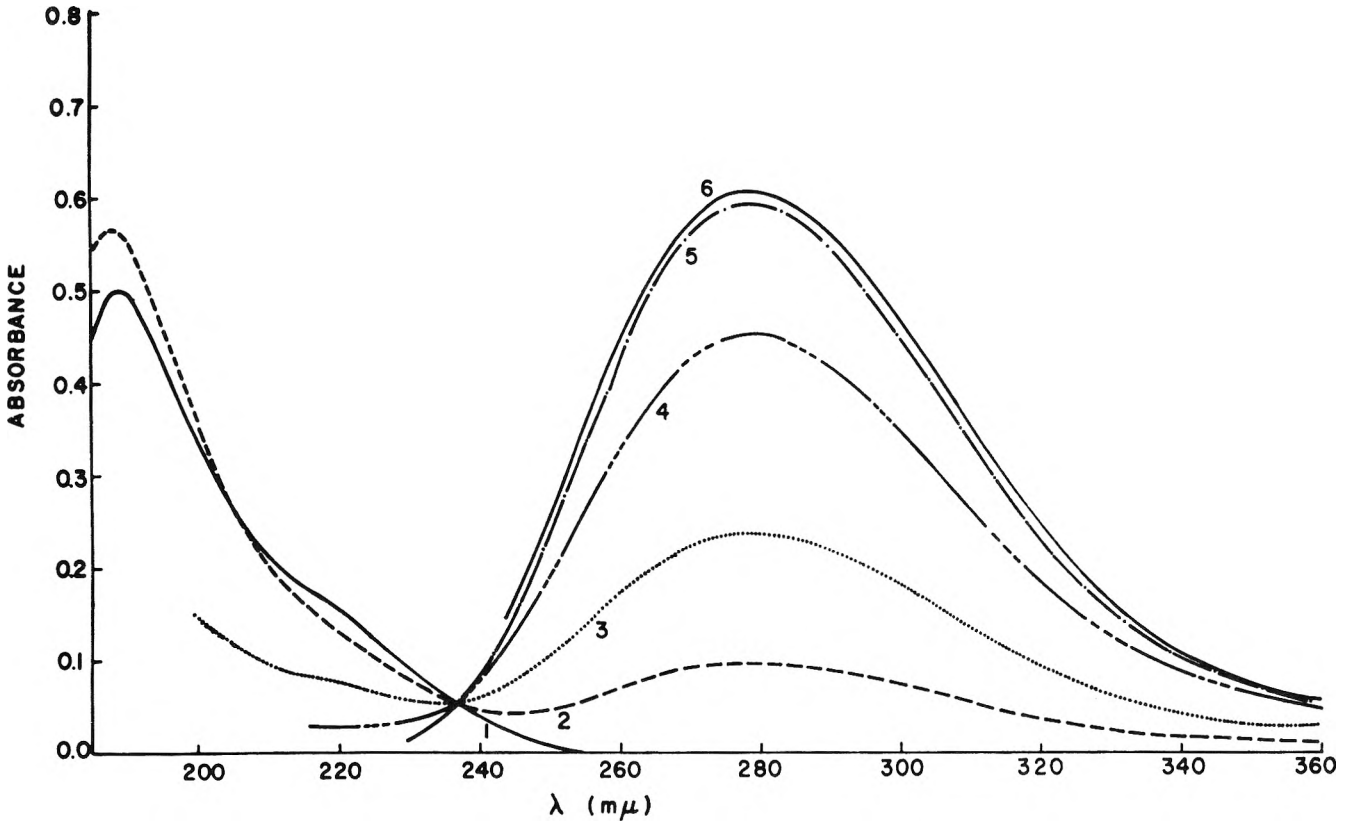

Figure 1. Ultraviolet absorption spectra at 24.5 ± 0.03° in a 1.0-cm path length cell, from mixed solutions in *n*-heptane having fixed I_2 concentration (2.8169×10^{-5} *M*) and varying TEA concentrations ($\times 10^{-5}$) as given here for curves (1) 0.000, (2) 3.513, (3) 10.536, (4) 42.144, (5) 168.578, and (6) 421.440 *M*. The lower wavelength limit is restricted due to limited transparency of TEA as its concentration increases.

value can be used to evaluate the contribution of the dative structure[7] to the ground structure.

The very high value found for the weight of the dative structure (59%) should, perhaps, have suggested earlier that this measurement should be questioned. At any rate, Toyoda and Person,[8] in attempts to repeat the dipole moment studies, raised the question of the nature of the species existing in solutions of triethylamine + I_2 in dioxane solution. Subsequently, Boule[9a] and independently, Hamilton and Sutton,[9b] have been able to measure the dipole moment of this complex in *n*-heptane, and have found a much lower value than that reported earlier.[6]

We have reinvestigated the ultraviolet spectrum of the triethylamine–I_2 complex in *n*-heptane and in dioxane. Our studies in *n*-heptane essentially confirm the earlier reports[4,5] of the properties of the complex; the studies in dioxane provide information about a short-lived complex, and verify a chemical reaction, by which the I_2 proceeds through an unidentified intermediate quantitatively to I^- in the presence of excess triethylamine (TEA). The details are given below.

Experimental Section

Chemicals. Triethylamine (Eastman, Red Label) was purified by the procedure given by Nagakura and Gouterman.[10] It was stored, briefly, under N_2 atmosphere in a desiccator before use. Purification of *p*-dioxane (Matheson Coleman and Bell, reagent grade) followed the procedure given by Weissberger, *et al.*[11] Fresh samples were distilled from sodium (under N_2) as needed. Iodine (Mallinckrodt reagent grade) was resublimed and stored in a dark bottle until use. *n*-Heptane (Phillips pure grade) was further purified by shaking with concentrated H_2SO_4 and washing until no coloration was observed, then shaking and washing with NaOH and water, drying over $CaCl_2$ and then distilling under N_2 from sodium. Special care was taken with the solutions studied in order to avoid interference from the O_2 contact charge-transfer absorption band.[12]

Stock solutions were prepared by weighing into

(7) (a) R. S. Mulliken, *J. Amer. Chem. Soc.*, **74**, 811 (1952); (b) see also G. Briegleb, "Electronen Donator–Acceptor Komplexe," Springer-Verlag, Berlin, 1961; (c) L. J. Andrews and R. M. Keefer, "Molecular Complexes in Organic Chemistry," (Holden-Day, Inc, San Francisco, Calif., 1964.

(8) K. Toyoda and W. B. Person, *J. Amer. Chem. Soc.*, **88**, 1629 (1966).

(9) (a) P. Boule, *ibid.*, **90**, 517 (1968); (b) A. J. Hamilton and L. E. Sutton, *Chem. Commun.*, 460 (1968).

(10) S. Nagakura and M. Gouterman, *J. Chem. Phys.*, **26**, 881 (1957).

(11) A. Weissberger, E. S. Proskauer, J. A. Riddick and E. E. Troops, Jr., "Technique of Organic Chemistry," Vol. VII, Interscience Publishers, New York, N. Y., 1963, p 372.

(12) D. F. Evans, *J. Chem. Soc.*, 345 (1953); 1315 (1951); 3885 (1957); H. Tsubomora and R. S. Mulliken, *J. Amer. Chem. Soc.*, **82**, 5966 (1960).

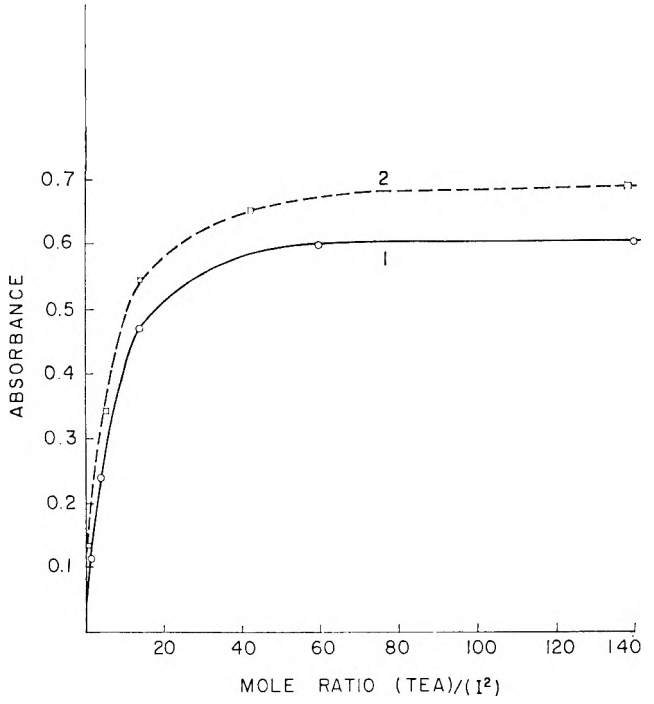

Figure 2. Absorbance values at 278 mμ at 24.5° against molar ratio TEA/I_2, keeping I_2 concentration constant: (1) $[I_2] = 2.817 \times 10^{-5}$ *M* in *n*-heptane; (2) $[I_2] = 3.151 \times 10^{-5}$ *M* in dioxane; the values have been extrapolated to zero time after mixing.

volumetric flasks. Dilutions were made volumetrically, with the aid of a microburet, to form the solutions for study. Spectra were measured with a Beckman DK-2A far-ultraviolet spectrometer, which was purged with N_2. The quartz cells (0.049, 1.0, and 10.0 cm) were used in the temperature-regulated cell holder which was kept at constant temperatures with the aid of a Haake circulator and Sargent water bath. The absorbance of the sample solutions were measured relative to a reference cell containing a matching TEA solution. Spectra of relative solutions were recorded as a function of time. The reactions appeared to be the same for solutions kept in the dark as for solutions kept out in the room light.

Results and Discussion

A. TEA–I_2 Complex in n-Heptane. Our spectra in this solvent are shown in Figure 1. We note there the following items.

(1) Curve 1 of Figure 1, for I_2 in pure *n*-heptane, verifies the results reported by Julien and Person,[13] particularly the contact charge transfer (CT) absorption band near 220 mμ. We note that the absorption in this region decreases as TEA is added to the system, which is to be expected if the I_2 in the complex is no longer available for a contact CT absorption with the solvent. We believe this spectrum is concrete evidence that such competition (between *n*-heptane and TEA for the I_2) does occur, and that the complexed I_2 does not then undergo contact CT absorption with the solvent but shows only the regular CT band of the complex at 278 mμ. Also, we note the apparent increase in the intensity of the 187-mμ I_2 band as the complex forms. This increase is probably real, since the reference beam contains TEA so that absorption by TEA is canceled. However, it is possible that the results here are not quantitatively correct.

(2) As the concentration of TEA increases, the CT band at 278 mμ increases in intensity at the expense of the contact CT band at 220 mμ. It is not possible to examine the spectra below about 220 mμ for these solutions more concentrated in TEA, because of the increased absorption in the reference beam. However, a clear isosbestic point is observed at 236 mμ.

(3) The absorbance at 278 mμ is plotted as a function of the mole ratio $[TEA]/[I_2]$ in Figure 2 (curve 1). We see that the absorbance does not increase appreciably as the TEA concentration increases above a mole ratio of 30, indicating that only a one-to-one complex forms. We found no indication of reaction (such as precipitation, as reported by Nagakura[5]) in these dilute solutions, even for TEA concentrations greater than 0.01 *M*.

In general, our results for this complex in this solvent are in complete agreement with those of Nagakura,[5] as indicated in the comparison summary of Table II, with the few additional observations listed above.

B. TEA–I_2 System in Dioxane. On the other hand, we found that this complex is very unstable in dioxane solution. As soon as the two components are mixed in solution a series of consecutive first-order reactions begin. These reactions occur in the absence of moisture. The nature of the intermediate product varies depending upon the initial concentrations of reactants. However, the main reaction path is apparently reproducible and convincing. Before describing these changes, we shall present here the results for the spectrum of the *complex* in dioxane solution.

The complex itself could be studied by recording spectra rapidly immediately after mixing solutions, and then later as a function of time. The spectrum of the

Table I: Spectral Properties of the Dioxane–I_2 Complex in Pure Dioxane

Our results				Ketelaar, *et al.*[a]	
λ_{max}, mμ	ϵ_{max}	$\Delta\nu_{1/2}$, cm^{-1}	f^e	λ_{max}, mμ	ϵ_{max}
450	812[b]	4240	0.015	450	...
264	4750[c,d]	7600	0.156	264	4450
212	12,500[d]	(6000)	0.32	...	...

[a] From ref 14. [b,c,d] Observations in 10-, 1.00-, and 0.049-cm cells, respectively. [e] Computed from $f \approx 4.32 \times 10^{-9} \epsilon_{max} \Delta\nu_{1/2}$.

(13) L. Julien and W. B. Person, *J. Phys. Chem.*, **72**, 3059 (1968).

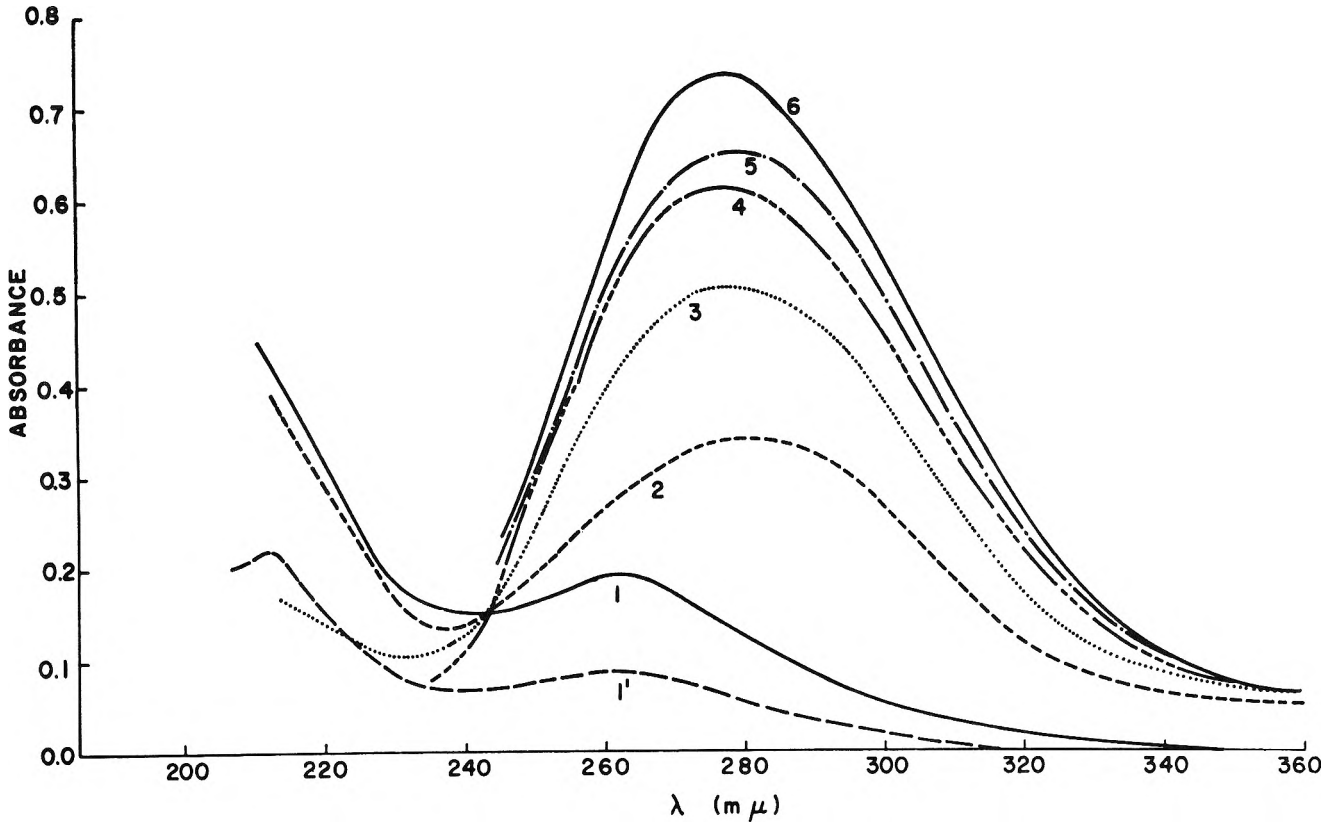

Figure 3. Ultraviolet absorption spectra (at about 24.0° in a 1-cm path length cell) of a mixed solution, having fixed I_2 concentration (3.151×10^{-5} *M*) and varying concentrations of TEA in dioxane. The concentrations ($\times 10^{-5}$) of TEA are 0.00, 14.73, 44.17, 132.82, 444.74, and 1325.22 *M*, respectively for curves 1, 2, 3, 4, 5, and 6, respectively. Curve 1′ represents absorbance of 3.151×10^{-4} *M* I_2 solution in dioxane using 0.049-cm cells.

complex is obtained by extrapolating the results to zero time.

a. Dioxane–I_2 Complex. In order to interpret our results, it was necessary for us to know the absorption of I_2 in the dioxane solution. We have, therefore, repeated the work of Ketelaar, *et al.*, on this system.[14] The results we have found for the spectrum of I_2 in pure dioxane may be seen in curves 1 and 1′ of Figure 3 and are summarized for all three regions of absorption in Table I. Our results for the blue-shifted visible I_2 band at 450 mμ and for the CT band of the dioxane–I_2 complex at 264 mμ agree well with those reported by Ketelaar, *et al.*[14]

The most interesting feature of these results for I_2 in dioxane is the absorption indicated in Figure 3 and Table I at 212 mμ. We must be most cautious about reporting new absorption bands occurring in the region, for the reasons discussed above. However, we cannot explain this absorbance near 212 mμ as O_2 absorption, and we have no reason to doubt its reality. If this absorption *is* due to a second CT band involving a second dative structure for this complex, it would suggest the need for further study of other ether–I_2 systems in order to investigate the possibility that the anomalously[15] low intensity for their CT band may be explained by failure to observe part of a doubled absorption band. However, it is also possible that this absorption band is some kind of contact CT band of I_2 with dioxane, although we do expect such a band for the complexed I_2, and we do not expect much of the I_2 in the pure dioxane to be uncomplexed.

b. TEA–I_2 Complex in Dioxane. The spectra of solutions of TEA and I_2 in dioxane, recorded within 2 min of mixing, are shown in Figure 3. These spectra, and others obtained by extrapolation, can be used in the usual way[16] to obtain the formation constant and molar absorptivities. The results are summarized in Table II. The formation constant has been evaluated for *n*-heptane using data at seven different wavelengths and six different solutions; for the *p*-dioxane solutions, we have evaluated K and ϵ_{max} from data at 278 mμ only.

The comparison between the results in Table II and the mole ratio plots in Figure 2 for the two different solutions is convincing evidence that we are studying

(14) J. A. A. Ketelaar, C. van de Stolpe, A. Goudsmit, and W. Dzcubas, *Rec. Trav. Chim.*, **71**, 1104 (1952); J. A. A. Ketelaar, *J. Phys. Radium*, **15**, 197 (1954).

(15) See R. S. Mulliken and W. B. Person, "Molecular Complexes: A Lecture and Reprint Volume," John Wiley and Sons, Inc., New York, N. Y., 1969.

(16) Using Nagakura's method [ref 5, and S. Nagakura, *J. Amer. Chem. Soc.*, **76**, 3070 (1954)], and using a computer program (L. Julien, Ph.D. thesis, University of Iowa, 1966) for Liptay's procedure [W. Liptay, *Z. Elektrochem.*, **65**, 375 (1961)].

Table II: Properties of the Triethylamine–I_2 Complex in *n*-Heptane and in Dioxane Solutions

Solvent	λ_{max}, mμ	ϵ_{max}	K_c,[a] l./mol
n-Heptane			
(ours)	278	22,600(±180)[b]	6000(±580)[b]
(Nagakura)[c]	278	25,600	4690
p-Dioxane	278	23,410(±120)[b]	4120(±560)[b]

[a] At 25° (24.5° for our studies). [b] Errors estimated from scatter of data in the Liptay analysis (see ref 15). [c] Nagakura, ref 5.

the same complex in both. The slight difference in properties of the complex in dioxane may not be significantly greater than the experimental error; however, it is not larger than solvent effects observed for other complexes.[17]

C. The Consecutive Reactions of TEA and I_2 in Dioxane. In Figure 4, we show the spectral changes occurring with time in a solution of TEA–I_2 in dioxane. The results in Figure 4a are for [TEA]/[I_2] ratio of 14; the results in Figure 4b are for a ratio of 140. These

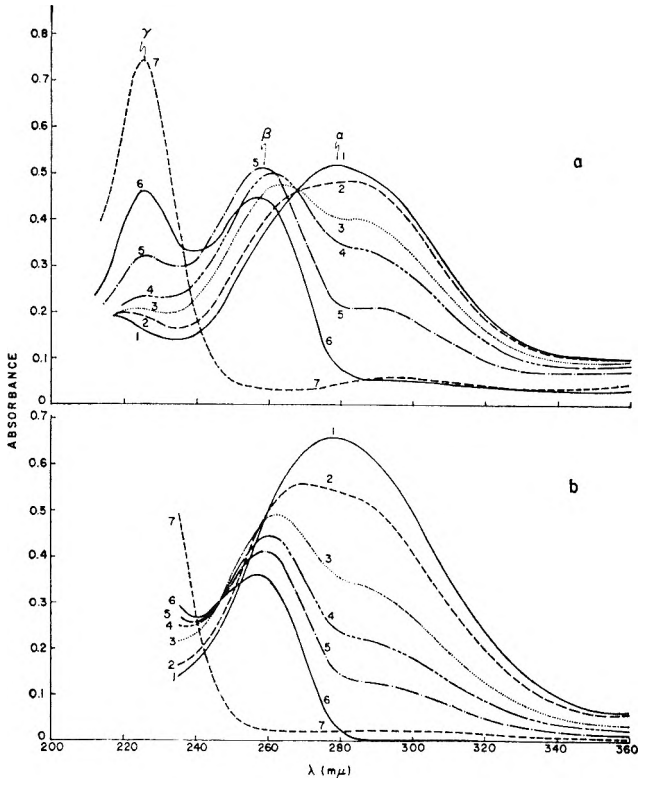

Figure 4. (a) Spectral changes with time in a dioxane solution having initial concentrations of TEA as 4.4 × 10^{-4} *M* and I_2 as 3.151 × 10^{-5} *M*. Mean scanning times in minutes (starting from mixing the solutions) are (1) <2, (2) 5, (3) 15, (4) 25, (5) 48, and (6) 150. Curve 7 was taken after 3 weeks (see text). (b) Spectral changes with time in a dioxane solution having the same I_2 concentration as in (a), but having higher TEA concentration (44.2 × 10^{-4} *M*). Mean scanning times in minutes for curves 1, 2, 3, 4, 5, and 6 are <2, 6, 16, 22, 28, and 50, respectively. Curve 7 is taken after 3 weeks.

results were obtained from the solutions corresponding to curves 3 and 5, respectively, of Figure 3 and the reaction takes place at 24.5°.

We note the following, in connection with Figure 4a. (1) Immediately after mixing, the band at 278 mμ, attributed above to the CT band of the complex, is observed. This band (labeled α in Figure 4a) decreases continuously in intensity with time, while two new bands (β at 258 mμ, and γ at 226 mμ) develop. The absorbance of these three bands is shown as a function of time in Figure 5 for a typical study. From these

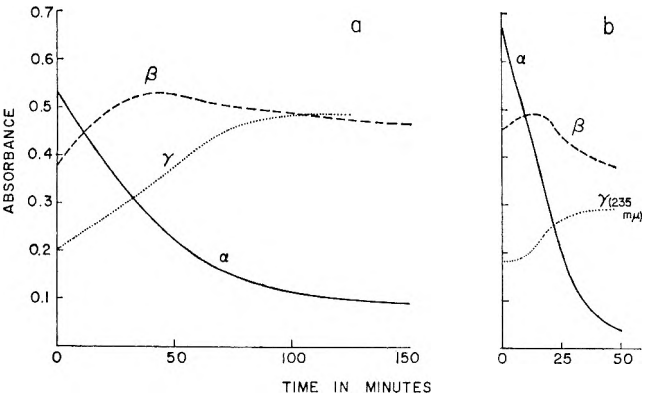

Figure 5. (a) Variation with time of the peak intensities of α, β, and γ bands in a dioxane solution having TEA and I_2 concentrations of 44.17 × 10^{-5} and 3.151 × 10^{-5} *M*. (b) Variations with time (for the solutions given in Figure 4b) of the intensities of the α and β bands and of the long wavelength end absorption at 235 mμ for the γ band. (The peak of γ bands could not be studied due to high absorption of TEA in 1-cm cell.)

two figures we can see that the absorption due to β increases rapidly to a maximum and then decreases, suggesting that the β band is due to an intermediate in the reaction formed first from the complex and then reacting further to yield the species responsible for the absorption at γ. Some of the initial absorption at γ is probably due to a species produced at the same rate as is the species responsible for β, although that is not clear. (2) Finally (after a few days), only the species responsible for the γ absorption remains in solution (see curve 7 of Figure 4a). This solution is stable. (3) The rates of the reactions are faster in solutions with higher concentrations of TEA. (See Figures 4b and 5b.) From the change in the half-life of the complex with TEA concentration, we may deduce that the reaction using up complex is first order in [TEA]. We note that the absorbance of the γ band at its peak (226 mμ) is so great for the solutions in Figure 4b that it cannot be studied in the 1-cm cells used for the other studies. Thus, in Figure 5b we present the absorbance at 235 mμ instead, as a measure of the concentration of the species

(17) For example, see C. C. Thompson, Jr., and P. A. D. de Maine, *J. Amer. Chem. Soc.*, **85**, 3096 (1963).

responsible for the γ absorption. Some studies were made using shorter path cells.

D. Identification of the Species Responsible for the Bands. The position of the γ band coincides remarkably well with the first "charge-transfer-to-solvent" (CTTS) band of the I^- ion in solution.[18-21] We attempted to verify this reasonable assignment by measuring the temperature dependence of ν_{max} for this band in our solutions, in order to compare it with the unusually high temperature dependence found for the CTTS band in I^- ion solutions. The results are shown in Figure 6, together with the temperature dependence

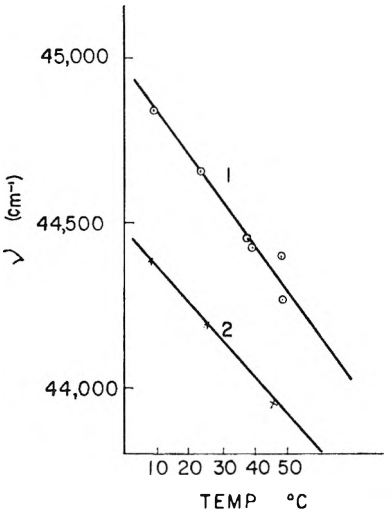

Figure 6. The temperature dependence of ν_m of the γ band and of the first long wavelength band of I^- ion at 226 mμ in water solution with temperature: (1) TEA–I_2 solution changed to give γ band; (2) TMAI solution in H_2O.

measured for a solution of tetramethylammonium iodide in water solution. We find for the slopes of these lines values of k_m ($= dE_m/dt$) of -13.5 cm^{-1}/deg for the γ band in dioxane solution and -11.7 cm^{-1}/deg for the I^- band in tetramethylammonium iodide in water. The latter value compares with other values reported for I^- ion in water of -11.6,[20] -11.8,[22] and -11.2[23] cm^{-1}/deg. We believe the close similarity found here for the temperature dependence of the γ band verifies its assignment to the I^- CTTS band in dioxane.

E. The Concentration of I^- in the Final Solution. Having identified the γ band, we may now use its absorbance, together with the known molar absorptivity of this band[2] [$\epsilon_{max} = 14{,}200$ at 226 mμ], to compute the concentration of I^- in the final solutions. As we shall show later, this solution also contains a small concentration of I_3^- ions, which must be computed. The results are shown in Table III. We see there that the I_2 initially present has been quantitatively accounted for in the final solution, most of it as I^-. In particular, we may be sure that there are no iodine atoms in the positive ion associated with the I^- in the final solution.

Table III: Calculation of the Concentration of Iodine in the Final Solution from a Reaction Mixture Containing an Initial I_2 Concentration of 3.151×10^{-5} M (1.00-cm Cell; Concentrations in 10^{-5} M)

Band at 226 mμ I^- ion[a]		Band at 295 mμ I_3^- ion[b]		Total [I] concn ($\times 10^5$) M	
Absorbance	[I^-]	Absorbance	[I_3^-]	Calcd	Initial
0.828	5.83	0.074	0.165	6.325	6.302

[a] Computed using $\epsilon_{I^-} = 14{,}200$ (ref 20). [b] Computed using $\epsilon_{I_3^-} = 44{,}670$ (ref 29).

F. The Molar Absorptivity of the β Band. The spectrum of a mixture of I_2 and TEA in dioxane at an intermediate stage in the reaction is shown in Figure 7. In this spectrum, the absorption due to the complex is almost zero; the absorbance due to I^- (γ band) is prominent, and there is still an appreciable absorption at β. In addition some I_3^- is present, as indicated.

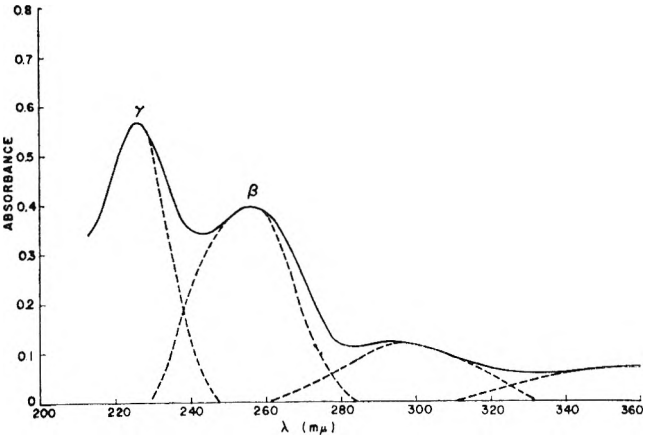

Figure 7. Ultraviolet absorption spectrum of a TEA–I_2 mixture in dioxane about 4 hr after preparation having initial TEA and I_2 concentration as 4.417×10^{-4} and 3.151×10^{-5} M, respectively.

From the molar absorptivity coefficients, we can compute the concentration of I^- and of I_3^- ions in this solution; from the difference between this calculation and the initial concentration of I_2, we can compute the concentration of I atoms contained in the intermediate responsible for the β band. We can be reasonably confident in this calculation that ultraviolet absorption by these missing I atoms should occur in this region, and so presumably in the β band. The results are summarized in Table IV.

(18) M. J. Blandamer, T. R. Griffiths, L. Shields, and M. C. R. Symons, *Trans. Faraday Soc.*, **60**, 1524 (1964).
(19) T. R. Griffiths and M. C. R. Symons, *ibid.*, **56**, 1125 (1960).
(20) J. Jortner, B. Raz, and G. Stein, *ibid.*, **56**, 1273 (1960).
(21) S. J. Strickler and M. Kasha, *J. Chem. Phys.*, **34**, 1077 (1961).
(22) G. Stein and A. Treinen, *Trans. Faraday Soc.*, **55**, 1091 (1959).
(23) M. Smith and M. C. R. Symons, *ibid.*, **54**, 338, 346 (1958).

Table IV: Calculation of the Concentration and Molar Absorptivity of the Intermediate Species Responsible for the β Band. (Initial $[I_2] = 3.151 \times 10^{-5}$ M; Concentration in 10^{-5} M)

I^- (226 mμ)		I_3^- (295 mμ)		Total I^-	Intermediate (258 mμ)		
Abs	$[I^-]^a$	Abs	$[I_3^-]^b$	$[I]^c$	Abs	$[B]^d$	ϵ_{max}
0.582	4.098	0.128	0.286	4.956	0.410	1.346	30,000

[a] Computed using $\epsilon_{I^-} = 14{,}200$ (ref 20). [b] Computed using $\epsilon_{I_3^-} = 44{,}670$ at 295 mμ (ref 29). [c] The sum of $[I^-] + 3[I_3^-]$. [d] Computed from $(6.302 - 4.956) \times 10^{-5}$, assuming only one I atom is contained in the intermediate, B.

We see there that the molar absorptivity of the intermediate responsible for β is quite high. The value quoted is based upon the calculated concentration of I *atoms*; if the intermediate contained two I atoms, then its molar absorptivity would be twice as large.

From a knowledge of λ_{max} and ϵ_{max} of the β band, one might hope to be able to identify the unknown intermediate responsible for this absorption. Unfortunately, this has not been easy for us. The wavelength corresponds quite closely to that found for the first absorption band in alkyl iodides;[24] for example, λ_{max} for C_2H_5I is 258 mμ. However, the molar absorptivities for the latter are smaller by a factor of about 70. We suspect that the species responsible for this absorption band is the $(Et_3N{-}I)^+$ ion (or perhaps $[(Et_3N)_2I]^+$). We think that the positive nature of the I atom in these ions might enhance the intensity of the transition from that found for the alkyl iodides. Analogous ions have been suggested by Lupinski[25] for the β-carotene–I_2 interaction [as $(\beta\text{-car–I})^+$] and by Slifkin[26] for the interaction of iodine with proteins, amines, and amino acids. However, for the former case it seems quite likely that the explanation for the strong absorption band reported by Lupinski may have nothing to do with the I atom.[27]

G. Summary of Reaction in Dioxane. Thus, we find the following reaction occurring between TEA and I_2 in dioxane solution

$$Et_3N + I_2 \rightleftarrows Et_3N{\cdot}I_2 \qquad \text{very rapid} \qquad (1)$$

$$Et_3N{-}I_2 \rightarrow B^+ + I^- \qquad \text{rapid} \qquad (2)$$

$$B^+(+Et_3N) \rightarrow X^+ + I^- \qquad \text{slow} \qquad (3)$$

We believe that B^+ is $(Et_3N{-}I)^+$ (or the diamine). We do not know the cation, X^+, in the final solution except that it contains no I atoms. However, Boule suggests that the $(Et_3NH)^+$ ion is formed even in anhydrous conditions from *n*-heptane solutions of Et_3N and I_2. We suspect that X^+ is $(Et_3NH)^+$, or perhaps

$$Et_3N^+{-}CH(CH_3){-}NEt_2,$$

by analogy with the results found for the γ-picoline system by Haque and Wood.[28]

We note (curve 7 of Figure 4) that there is no absorption observed in solutions of the final product which can be attributed to the cation X^+. We believe this observation is consistent with our postulated saturated cations, but that it rules out other possibilities containing double bonds. Unfortunately, we were not able to complete this experiment by identifying this cation.

The initial increase in the absorbance of I^- (γ band) in Figure 5 parallels the initial increase in the β band as B^+ is formed; hence it is reasonable to postulate the simultaneous formation of B^+ and I^- in step 2.

H. Side Reactions. If the $[TEA]/[I_2]$ ratio is smaller ($\sim$1) than in the studies reported above ($\sim$10 or more) then the I_3^- ion is found to form immediately after mixing the two solutions, even for solutions which are very dilute. The presence of this ion is revealed by the two characteristic strong bands[29] near 365 and 295

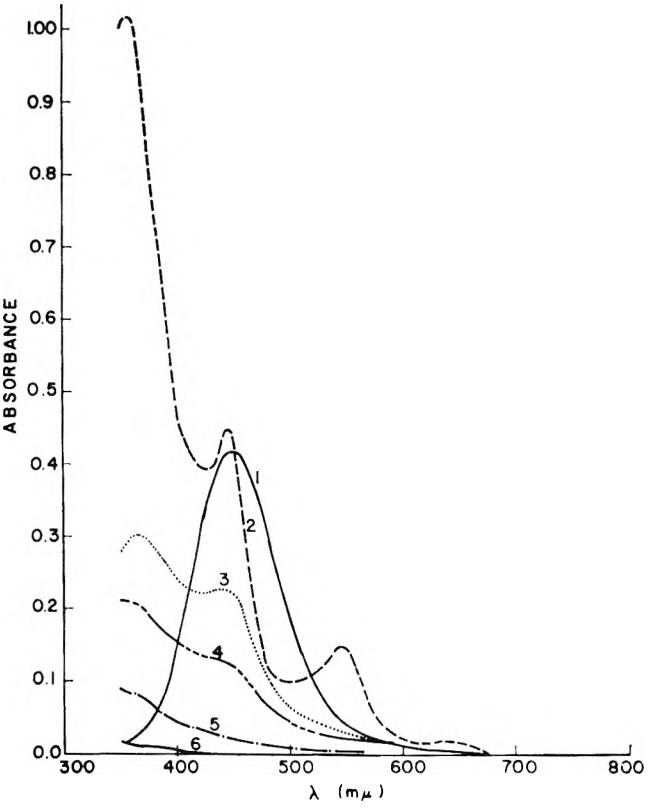

Figure 8. Visible bands of unknown origin in TEA–I_2 mixture in dioxane. The initial I_2 concentration was fixed (4.606×10^{-4} M) and the TEA concentrations ($\times 10^{-4}$) are (1) 0.000, (2) 9.961, (3) 29.88, (4) 89.65, (5) 298.84, and (6) 896.53 M. The spectra are taken approximately 30 hr after initial mixing.

(24) K. Kimura and S. Nagakura, *Spectrochim. Acta*, **17**, 166 (1961).
(25) J. H. Lupinski, *J. Phys. Chem.*, **67**, 2725 (1963).
(26) M. A. Slifkin, *Spectrochim. Acta*, **20**, 1543 (1964); **21**, 1391 (1965).
(27) T. G. Ebrey, *J. Phys. Chem.*, **71**, 1963 (1967).
(28) I. Haque and J. L. Wood, Paper C3, Anniversary Meeting of the Chemical Society, Exeter, England, April 3–6, 1967. See I. Haque and J. L. Wood, *Spectrochim. Acta*, **23A**, 2523 (1967).
(29) R. E. Buckles, J. P. Yuk, and A. I. Popov, *J. Amer. Chem. Soc.*, **74**, 4379 (1952).

mμ, with intensity ratios approximately 2:1. However, as excess TEA is added, the concentration of I_3^- ion formed decreases, presumably because the amine competes successfully with the I^- ion for the I_2. Thus in our studies with excess amines above the principal negative ion is I^-.

The dioxane solutions containing the lower [TEA]/[I_2] ratios form I_3^-; these I_3^--containing solutions are then unstable with respect to further decomposition to form I^- and to give changes in the visible spectrum reported below. The high absorption of the I_3^- ion prevents us from the same kind of detailed study as has been reported above for solutions with high [TEA]/[I_2] ratios. However, we have studied these puzzling changes in the visible region of the spectrum.

When the intermediate I_3^--containing species (which was formed in the dioxane solutions of low [TEA]/[I_2] ratio) decomposes to form I^-, three new bands appear in the visible region of the spectrum (at 450, 550, and 650 mμ) as shown in Figure 8. It is clear that these three bands decrease in intensity with increasing concentration of TEA. Furthermore, we have observed that the use of glass cells (rather than quartz) results in an increase in the intensity of these bands.

Although it is difficult to measure accurately the relative band intensities of these three bands, we believe our results clearly show that the three bands are not due to a single species. It may be worthwhile to point out that the 450-mμ band is not due to I_2 complexed with dioxane, since its band shape is quite different from that observed for the complex. We do not have any hypothesis concerning the nature of the unstable species causing this absorption in the samples with low [TEA]/[I_2] ratio.

Acknowledgment Financial assistance from Public Health Research Grants No. GM-10168 and GM-14648 is gratefully acknowledged. We are grateful to Professors R. E. Buckles (University of Iowa) and J. A. Deyrup (University of Florida) for discussions concerning the possible nature of the reaction between TEA and I_2.

The Contact Angle and the Depth of the Free-Energy Minimum in Thin Liquid Films. Their Measurement and Interpretation[1]

by Frits Huisman and Karol J. Mysels

Chemistry Department, University of Southern California, Los Angeles, California 90007 and Research Department, R. J. Reynolds Tobacco Company, Winston-Salem, North Carolina 27102

(Received March 11, 1968)

The depth of the energy minimum corresponding to an equilibrium thin liquid film is determined by measuring the contact angle between the film and bulk solution. The significance of this angle and its relation to conventional contact angles is discussed and an experimental method for measuring it described. Results for solutions of sodium dodecyl sulfate containing NaCl alone or with LiCl, KCl, or $(CH_3)_4NBr$ range up to 16° in contact angle and over 2 ergs/cm² in depth of the minimum. These provide excellent support for previous qualitative observations of kinetic and equilibrium relations. It is also shown that the minima should lie close to the attractive energy curve, but the disagreement between the simple theory of van der Waals forces and the experimental results is very large. Various possible reasons for this discrepancy are briefly discussed and an analogy between the second black films and compounds is pointed out.

Introduction

Medium-range intermolecular forces, those manifesting themselves between assemblages of molecules over distances of several tens to a few thousands angstroms, are the principal determinants of the behavior of thin liquid films and, particularly, of the stable ones formed by aqueous solutions in air which are generally called soap films.[2-10] As a direct consequence, the films are a valuable tool in the study of such forces. Figure 1 shows schematically how the partial specific surface free energy, ΔF, of a film must vary with its thickness as the net result of all the forces acting within it, in

(1) Presented at the Garvan Award Symposium honoring M. J. Vold during the 153rd National Meeting of the American Chemical Society, Miami Beach, Fla., April 1966.

(2) B. V. Deryagin and A. S. Titievskaya, *Discussions Faraday Soc.*, **18**, 27 (1954).

(3) A. Scheludko and D. Exerowa, *Kolloid-Z.*, **155**, 39 (1957).

(4) J. Th. G. Overbeek, *J. Phys. Chem.*, **64**, 1178 (1960).

(5) J. Lyklema, *Rec. Trav. Chim.*, **81**, 890 (1962).

(6) K. J. Mysels, *J. Phys. Chem.*, **68**, 3441 (1964).

(7) A. Scheludko, *Koninkl. Nederl. Akad. Wetenschapen, Amsterdam, Proc., Ser. B*, **65**, 76 (1962).

(8) J. Lyklema and K. J. Mysels, *J. Amer. Chem. Soc.*, **87**, 2539 (1965).

(9) A. Sheludko, *Advan. Colloid Interface Sci.*, **1**, 391 (1967).

(10) A. Sheludko, "Textbook of Colloids," Elsevier Publishing Co., Amsterdam, 1966.

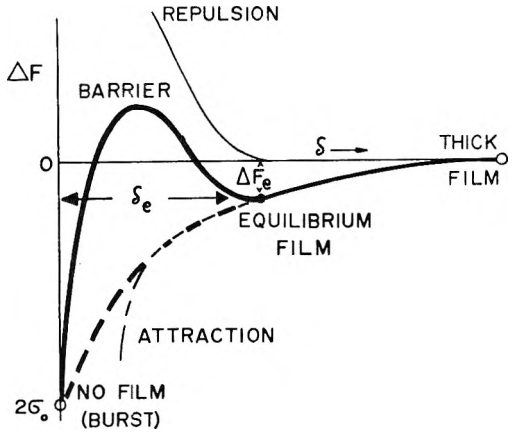

Figure 1. Changes in the partial specific surface free energy ΔF with film thickness δ. A (meta) stable film forms if a sufficient minimum results from a combination of attractive and repulsive potentials.

order to give a stable film. The experimental measurement of the parameters of such a curve can serve to test the theories and models attempting to explain the behavior of these systems and under proper conditions can help to disentangle the interaction of attractions and repulsions required to give the complex shape of this curve. In fact, it has been found that the shape can be more complicated than shown, having at least two minima of different depth.

Until recently only the abscissa of the minimum could be determined by measuring the thickness of the equilibrium film.[3,8] New approaches for determining the slope of the curve by light scattering[11,12] and for the descending branches by kinetics of thinning or bursting[13,14] have been proposed as well as a method for following the ascending branch by hydrostatic compression of the film.[15]

In the present paper we describe a method for measuring the depth, ΔF_e, of the minimum along with some results and a discussion of the theoretical problems they raise. The method itself has already been the subject of a brief preliminary communication with Razouk.[16]

It may be noted that soap films are related to two apparently very different fields of study. One is the stability of hydrophobic colloids where the structures are very different but the forces should be similar.[4,5] The other is that of lipid membranes where the structures are similar but the forces less so.[17,18] The main emphasis of research in these fields is also somewhat different. In the former field it is mainly on the height of the maximum rather than on the minimum of the free energy curve, and in the latter it is on transport properties[19] rather than on the forces determining the structure of the film itself.

The Pertinence of the Contact Angle. Experimentally, soap films and related thin films are always studied in contact with some bulk liquid, at least that of the Plateau border. In the present context we are concerned with equilibrium systems, more specifically metastable ones with respect to bursting of the film. The minimum of free energy shown in Figure 1 must therefore be that of the free energy, F, of the whole system and not Gibbs excess surface free energy. As F depends on the total surface of the system, it is convenient to consider only its increase per unit surface or the partial specific surface free energy of the system which is equal[20] to the surface tension, σ

$$(\partial F/\partial \Omega)_{T,V,n_i} = \sigma \qquad (1)$$

Ω denotes the surface area of the system. As Figure 1 indicates, we are concerned here with the fact that the partial specific surface free energy varies also with the thickness, δ, of the layer covered by the surface so that a more exact formulation requires the introduction of a thickness-dependent partial specific surface free energy of the system and a thickness-dependent surface tension.

$$(\partial F/\partial \Omega_\delta)_{T,V,n_i} = \sigma_\delta \qquad (2)$$

Since we are concerned primarily with variations of these quantities, it is convenient to take as a reference point the very thick surface, *i.e.*, bulk liquid, which we denote by subscript 0. As we are dealing with two-sided films, it is also better to use unit film area as a base. With these conventions we can define the partial specific surface free energy of a film ΔF, shown as the ordinate in Figure 1, by

$$\Delta F_\delta/2 = (\partial F/\partial \Omega_0)_{T,V,n_i} - (\partial F/\partial \Omega_\delta)_{T,V,n_i} = \sigma_0 - \sigma_\delta \qquad (3)$$

One value of ΔF is particularly important, the one corresponding to equilibrium films and denoted by ΔF_e. It is given by

$$\Delta F_e = 2(\sigma_0 - \sigma) \qquad (4)$$

where σ denotes the surface tension of the equilibrium film. For symmetrical films this quantity is defined operationally as half the tension of the film.

(11) A. Vrij, *J. Colloid Sci.*, **19**, 1, (1964); *Advan. Colloid Interface Sci.*, **2**, 39 (1968).

(12) J. A. Mann, Jr., *J. Colloid Interface Sci.*, **25**, 437 (1967).

(13) A. Scheludko, *Koninkl. Nederl. Akad. Wetenschapen, Amsterdam, Proc., Ser. B*, **65**, 87 (1962).

(14) A. Vrij, *Discussions Faraday Soc.*, **42**, 23 (1966).

(15) K. J. Mysels and M. N. Jones, *ibid.*, **42**, 42 (1967).

(16) K. J. Mysels, H. F. Huisman, and R. Razouk, *J. Phys. Chem.*, **70**, 1339 (1966). Note that the formula for θ is inverted and the calculation of disjoining pressure is in error (it refers to the pressure required to give the observed $\Delta\sigma$).

(17) J. Taylor and D. A. Haydon, *Discussions Faraday Soc.*, **42**, 51 (1966).

(18) J. F. Danielli, *J. Theor. Biol.*, **12**, 439 (1966).

(19) P. Mueller, O. D. Rudin, H. T. Tien, and W. C. Wescott in "Symposium on the Plasma Membrane," A. P. Fishman, Ed., American Heart Association, New York, N. Y., 1962; T. Hanai, D. A. Haydon and W. R. Redwood, *Ann. N. Y. Acad. Sci.*, **137**, Article 2, 731 (1966).

(20) R. E. Johnson, *J. Phys. Chem.*, **63**, 1955 (1959).

The point of the above argument is that the existence of an equilibrium film implies that it has a surface tension different from that of the bulk liquid with which it is in contact and in equilibrium. Because of this difference, a film having a thickness corresponding to the minimum must form a contact angle θ with bulk surface as shown in Figure 2. Examination of this

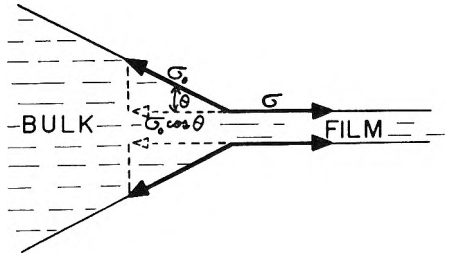

Figure 2. Bulk liquid and a thin film having a lesser surface tension can coexist in equilibrium only by forming the proper contact angle.

figure also shows that equilibrium requires that

$$\sigma = \sigma_0 \cos\theta \tag{5}$$

Hence

$$\Delta F_e = 2\sigma_0(1 - \cos\theta) \tag{6}$$

Thus, the problem of measuring the depth of the minimum reduces itself to that of measuring the contact angle between film and bulk surface since measurement of bulk surface tension is, in principle, trivial.

The Two Kinds of Contact Angle. The possibility of the existence of a contact angle between bulk liquid and a (mono) layer of it adsorbed upon another condensed phase was suggested at least 30 years ago[21] and is now well established.[22] On the other hand, the possibility of a bulk liquid forming a nonzero contact angle with a thin film of itself without any other condensed phase does not seem to have been considered until very recently. We are aware of two recent discussions, one by Deryagin and coworkers,[23] the other by Princen and Mason[24] of the theoretical significance of such a contact angle. Our preliminary publication[16] reported apparently the first observation and measurement of such a contact angle.

The contact angle of a liquid with its adsorbed monolayer on a condensed phase, and that of a liquid with its own thin film, display obvious similarities, particularly in the analysis of forces acting on the boundary and of the thermodynamics of the situation. There are also important differences between these two types of contact angles. As shown in Figure 3a, the ordinary contact angle involves three different phases and the junction of three monolayers, each at the boundary of a different pair of phases. The new contact angle situation, on the other hand, involves basically only two phases and the contact of two identical monolayers, separating the same pair of phases, with a bilayer

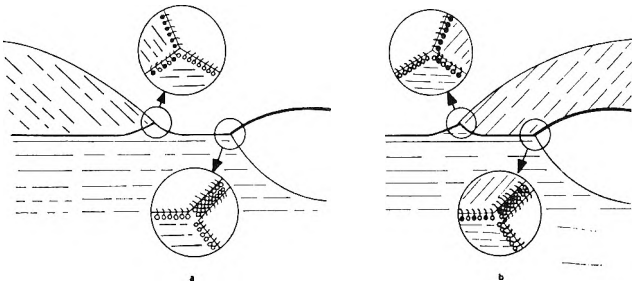

Figure 3. Schematic comparison of film contact angles and bulk contact angles. Left, the symmetrical film contact angle involves only two different phases. Right, an unsymmetrical film contact angle could involve three phases capable of having an ordinary contact angle also.

formed by the close approach of these monolayers and separating two parts of one of these phases.

It may be noted that the monolayers need not be monomolecular (*i.e.* one molecule thick) nor the bilayer needs to be bimolecular (*i.e.*, two molecules thick). The important factor is that due to the nature of phases that are being separated, the former is highly unsymmetrical, the latter two-faced and symmetrical.

The bilayer may be formed between two condensed phases, particularly two liquids, and a qualitative observation of the occurrence of such a contact angle has been reported already,[24,25] and now it also has been measured.[26]

Intermediate cases between the two extreme cases discussed above of a three-phase and a two-phase contact angle must also exist, particularly in the case of condensed phases. Thus, the composition of the fluid on one side of the bilayer may be changed gradually without affecting the essentials of the situation, although the bilayer must then also become somewhat unsymmetrical. Three different phases are then present, but as long as these changes in the fluid do not lead to immiscibility, a three-phase contact angle is not observable in the same system. At present there seems to be no intrinsic reason why this intermediate case should not be extended to two immiscible fluids separated by a correspondingly unsymmetrical bilayer. This would lead to the possibility of two different contact angles between three phases, as shown in

(21) D. H. Bangham and R. I. Razouk, *Trans. Faraday Soc.*, **33**, 1459 (1937); I. Langmuir, *J. Franklin Inst.*, **218**, 143 (1934); *Science*, **87**, 493 (1938).

(22) W. A. Zisman in "Contact Angle. Wettability and Adhesion," Advances in Chemistry Series, No. 43, American Chemical Society, Washington, D. C., 1964, p 1.

(23) B. V. Deryagin, G. A. Martynov, and Yu. V. Gutop, *Kolloid, Zh.*, **27**, 357 (1965); *Colloid J. (USSR)*, **27**, 298 (1965); in "Research in Surface Forces," Vol. 2, B. V. Deryagin, Ed., 1966, p 9; B. V. Deryagin, *Pure Appl. Chem.*, **10**, 375 (1965).

(24) H. M. Princen and S. G. Mason, *J. Colloid Sci.*, **20**, 156 (1965).

(25) G. D. M. MacKay, Ph.D. Thesis, McGill University, 1962.

(26) T. E. Thompson and R. Pagano, University of Virginia, personal communication; D. A. Haydon and J. L. Taylor, *Nature* **217**, 739 (1968).

Figure 3b, one metastable involving the bilayer, and the other stable and involving only monolayers.

Principle of the Method. Although the same contact angle exists whatever the configuration of the system, it is not always equally easy to observe or to measure. Several different approaches are possible.[26,27] Our method is based on the unique configuration (Figure 4)

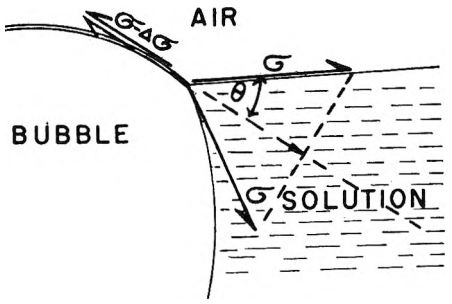

Figure 4. The special case of a contact angle between a flat surface and a bubble.

in which the surface of the bulk liquid is exactly plane and the film is part (the calotte) of a slightly protruding bubble. This bubble was formed on a Teflon tip to which it remained attached and by means of which it could be raised or lowered until the desired flatness of the bulk surface was realized. A simple schlieren system provided a very sensitive primary criterion of flatness. With some practice the aspect through a horizontal microscope provided an equally sensitive secondary one. Either defined the vertical position of the bubble to within 10 μ. The horizontal microscope also permitted the measurement of the diameter, d, and height, h, of the calotte by means of a filar micrometer. Simple geometry then shows that[16]

$$d/2h = \sin\theta/(1 - \cos\theta) = \cot\theta/2 \qquad (7)$$

In this method, the measurements of contact angle are made at equilibrium and with the pertinent part of the film at the same level as the bulk liquid. The liquid within the film is also subject to the capillary pressure of the outer bubble surface $2\sigma/R$ which is of the order of 300 dyn/cm^2. The negative of this is the disjoining pressure as defined by Deryagin.[28] The contact angle measurement provides a value of potential energy difference and no direct information about the disjoining pressure which is its derivative.[16] The finite value of this derivative in our experiments corresponds to a negligible departure from the true minimum.

Experimental Section

Contact Angle Apparatus. Figure 5 shows the principal features of the apparatus. The solution filled to overflow a square glass cell which was placed inside a larger one. This permitted observation of the profile of the calotte without interference from the meniscus

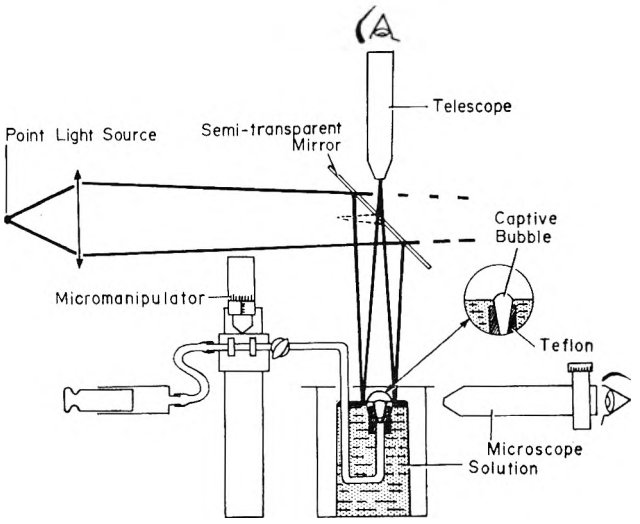

Figure 5. Apparatus for measuring the film contact angle.

yet permitted the use of a cover to reduce evaporation. The cover had a cutout permitting free movement of a gooseneck capillary tube at the end of which was a Teflon tip made by reaming a buret plug valve to provide a conical orifice. The capillary could be positioned and especially raised or lowered by a micromanipulator (Kulicke and Soffa Model 200MM) and was connected to a syringe for forming the air bubble. A stopcock permitted isolation of the bubble once it was formed. The schlieren system consisted of a 2-W concentrated (zirconium) arc lamp, a photographic lens, a semi-transparent mirror, and a low-power telescope focused on the solution surface through the mirror. A slight misalignment of the telescope acted as an effective knife edge. A low-power microscope equipped with a filar micrometer served to measure the calotte through the glass wall of the outer cell.

The measurements were limited mainly by the mechanical stability of the system. Vibrations caused ripples of the bulk surface which changed greatly the diameter of the calotte, especially at small contact angles when it is very flat. This disturbance could be greatly reduced by placing the cell on a vibration-absorbing support. Changes in the atmospheric pressure of the laboratory, which had a central air-conditioning system, affected the size of the bubble and thus its relation with the surface. With some practice it was possible, nevertheless, to measure the contact angle to some 5′ of arc. This corresponds to about 10^{-3} erg/cm^2 when the contact angle is 1° and to 2×10^{-2} when it is 10°. The corresponding ΔF_c values are about 10^2 and 0.7 erg/cm^2, respectively. The lowest contact angle observed was for a solution containing 0.009 M

(27) T. Kolarov, A. Scheludko, and D. Exerowa, *Trans. Faraday Soc.*, 64, 2864 (1968); H. M. Princen, *J. Phys. Chem.*, 72, 3342 (1968).

(28) B. V. Deryagin in "Research in Surface Forces," Vol. 1, B. V. Deryagin, Ed., Consultants Bureau, New York, N. Y., 1963, p 8; B. V. Deryagin and Yu. V. Gutop, *ibid.*, Vol. 2, 1966, p 17.

NaLS. The angle was clearly present in schlieren observation but could not be measured with the horizontal microscope and must have been less than 5′ corresponding to less than 6×10^{-5} erg/cm^2.

Surface tension measurements were made using the equilibrium Wilhelmy method with a sandpaper-depolished platinum foil attached to a commercial DuNouy apparatus.

Materials. The sodium dodecyl sulfate (NaLS) was a recently recrystallized portion of the preparation previously described[29] and was freed of lauryl alcohol by high-vacuum sublimation at 50°. Reagent grade salts were used, the LiCl being carefully dried before use and the KCl being further purified by heating for over an hour to 780° in a platinum dish.

Results and Comparison with Other Experiments

Figure 6 shows the results obtained on solutions containing 0.05% (1.7×10^{-3} *M*) NaLS and varying

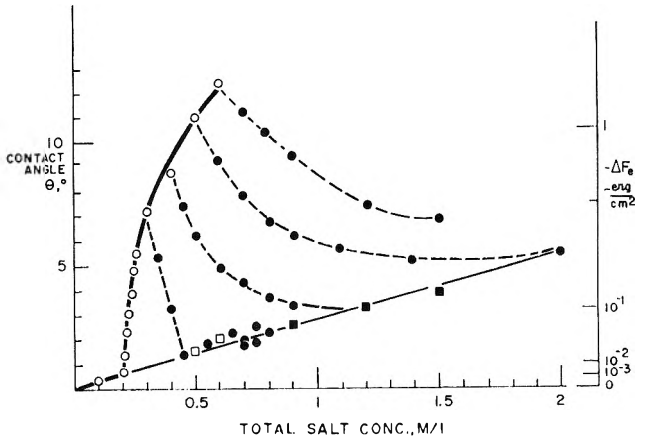

Figure 6. Variation of film contact angle (left scale) and of the depth of the minimum (right scale) in solutions of 0.05% NaLS as a function of ionic strength in the presence of NaCl alone, ○; of LiCl alone, ■; of over 90 mol % LiCl + NaCl, □; and of other mixtures of NaCl and LiCl, ●. Dashed lines connect points of equal NaCl content. All the points on the lowest line are first black films; those on the other lines above the lowest are second black. The nature of the film at 2.0 *M* is uncertain.

concentrations of NaCl, LiCl, or mixtures of these two salts. The directly measured contact angle is used as the ordinate and the approximate ΔF_e value is indicated on the right-hand side. As all our solutions had measured surface tensions within 5% of 30 dyn/cm (except one for which the uncertainty in the contact angle is larger), the two values correspond to each other closely, and the contact angle provides a more expanded scale at low values. All measurements were made in an air-conditioned room at a temperature of 23 ± 1°.

Total counterion concentration is used as the abscissa and systems having the same NaCl concentration are connected by dashed lines. For systems containing only NaCl there is a very slow increase in ΔF_e until 0.2 *M* is reached. This is followed by a rapid increase followed by a less rapid one above about 0.25 *M*. The first change of slope can be treated as a first-order transition since extrapolated lines correspond to less stable systems. The second change does not satisfy this condition and a smooth line has been drawn through the points.

Visual observations confirm that above 0.20 *M* there is an abrupt transition in the calotte in which a rapid thinning, change of curvature, and increase in contact angle occur simultaneously. This agrees perfectly with the work of Jones, Mysels, and Scholten[30] (JMS) who studied the transition between the "first" and "second" black films and found that the former had a thickness which varied with ionic strength but was always larger than the quite constant thickness of the latter, which is about 43 Å. The stability of the two states of the film depends on NaCl concentration and temperature, and their data also give 0.20 *M* NaCl at 23.5° for the equilibrium point. No visual or thickness peculiarity was observed by JMS at 0.25 *M* in agreement with the impossibility of a first-order transition from our data.

Visual observations of JMS showed clearly a rapid increase in the driving force for the formation of the second black film as the NaCl concentration increased. This can now be measured by the rapidly increasing difference between the extrapolated ΔF_e value for the first black film and the measured one for the second one.

This extrapolation is strengthened by measurements on films formed by systems containing either only LiCl or enough of this salt in addition to NaCl. In these systems the calottes show no abrupt transition, and the ΔF_e values lie on the same line as the first black film values for the NaCl systems. This is again in agreement with the visual observations and thickness measurement of JMS which showed that LiCl systems never formed a second black film and that addition of enough of this salt inhibited formation of second black in the presence of NaCl.

Further insight into this inhibitory effect is given by our measurements on the effect of gradual addition of LiCl to systems containing enough NaCl to form second blacks. As shown in Figure 6, this causes a reduction of ΔF_e despite the increase in ionic strength and a gradual approach to the value corresponding to the first black film at the relevant total counterion concentration.

The work of JMS also showed that addition of quaternary salts, such as tetramethylammonium bromide, also inhibited the formation of second black films and that this salt was considerably more effective than LiCl. On the other hand, KCl was found to be a promoter of the second black more effective than an

(29) K. J. Mysels and R. J. Otter, *J. Colloid Sci.*, 16, 462 (1961).
(30) M. N. Jones, K. J. Mysels, and P. C. Scholten, *Trans. Faraday Soc.*, 62, 1336 (1966).

equivalent concentration of NaCl. Our results for systems containing these ions are shown in Figure 7.

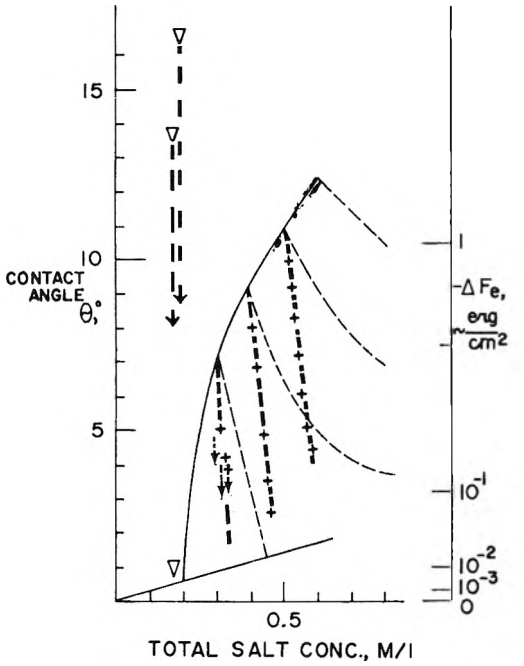

Figure 7. Effect of tetramethylammonium bromide, +, and of KCl, ▽, upon the film contact angle and the depth of the minimum of solutions containing 0.05% NaLS and NaCl. The pertinent lines of Figure 6 are reproduced for comparison. NaCl concentration is 0.15 *M* in the KCl experiments.

At higher NaCl concentration these measurements proceeded smoothly, but at lower ones, the contact angles decreased with time, the film appeared to be partially rigid in the KCl system, and in case of the tetramethyl system, the adhesion of the bubble to the Teflon sometimes became insufficient at higher ionic strengths. Purification of the KCl remedied the rigidity, increased the contact angles, and greatly reduced their drift with time but did not eliminate the latter completely. Thus, it seems that a significant surface active impurity inhibiting the second black film was still present and gradually became adsorbed on the surface and lowered the ΔF_e values. In view of the difficulty of surface purification in our apparatus, we report simply the highest values and indicate the observed drift by arrows. The uncertainty thus introduced is large but does not obscure the fact that the presence of KCl increases ΔF_e for the second black film very greatly, whereas that of tetramethyl salt reduces it more effectively than LiCl. This is again in agreement with visual observations. A less precise measurement suggests that the metastable first black film in the KCl system may also have a slightly higher ΔF_e than in the NaCl and LiCl systems.

Thus, our measurements of the contact angle fit very well with what has been learned previously about the effect of salts upon the formation of the second black film and upon the driving force involved in this transition. Hence, we see no reason to doubt the essential correctness of these measurements despite the fact that they are the first ones of this kind and that they raise serious problems with respect to theory as will now be discussed.

Comparison with Theory

Measurements of thicknesses of equilibrium films, particularly of the thicker "first black" ones, have been interpreted successfully heretofore[3,8] in terms of a balance between double-layer repulsion and van der Waals attraction due to dispersion forces as these theories have been developed in the Deryagin-Landau–Verwey–Overbeek theory of colloid stability.[31] Significant discrepancies in the more concentrated solutions did appear, however, and the constant thickness of the second black was very puzzling. The specific effect of cations was rationalized as due to the effect of specific adsorption upon the double-layer repulsion.[30]

The equilibrium thickness is the point at which the attractive and repulsive forces or, more exactly, pressures are equal. If these obey the theory, their contribution to the energy at this point is very unequal since the attractive dispersion forces increase with the inverse third (or fourth at larger distances) power of thickness whereas double-layer repulsion increases much more rapidly along an exponential path. Figure 5 of Lyklema and Mysels[8] shows typical theoretical curves of these pressures. As a result, the double-layer repulsion makes only a minor contribution to the total free energy of the system, and the depth of the minimum is very close to the position of the attractive energy curve. This is clearly shown by the families of theoretical potential energy curves for plates given by Verwey and Overbeek.[31,32]

A more quantitative evaluation of the contribution of the repulsive potential may be obtained as follows. Neglecting retardation effects, the compressive dispersion pressure is given[31] by

$$P_v = -A/6\pi\delta^3 \qquad (8)$$

where A is the Hamaker constant and δ the thickness of the film. The corresponding potential energy is

$$V_v = -A/12\pi\delta^2 \qquad (9)$$

It can therefore be written

$$V_v = P_v\delta/2 \qquad (10)$$

Similarly, the repulsive double-layer pressure is given by

$$P_r = 1.59 \times 10^9 c\gamma^2 e^{-\kappa d_2} \qquad (11)$$

(31) J. Th. G. Overbeek in "Colloid Science," Vol. 1, H. R. Kruyt, Ed., Elsevier Publishing Co., Amsterdam, 1952, Chapters IV and VI.

(32) E. J. W. Verwey and J. Th. G. Overbeek, "Theory of the Stability of Lyophobic Colloids," Elsevier Publishing Co., Amsterdam, 1948.

where κ is the inverse Debye length, γ^2 is a function of surface potential only, d_2 is the thickness of the aqueous core of the film, c is the molar concentration, and the numerical constant takes into account the temperature and dielectric constant. The corresponding repulsive potential is

$$V_r = 48.4\sqrt{c}\gamma^2 e^{-\kappa d_2} \quad (12)$$

Hence, this potential can be written in terms of the pressure as

$$V_r = P_r/3.28 \times 10^7\sqrt{c} \quad (13)$$

The ratio of the two potentials is therefore always

$$V_v/V_r = 1.64 \times 10^7\delta\sqrt{c}\,(P_v/P_r) \quad (14)$$

At equilibrium in the absence of hydrostatic pressures, $P_v = P_r$ by definition, hence

$$(V_v/V_r)_e = 1.64 \times 10^7\delta\sqrt{c} \quad (15)$$

The data of Lyklema and Mysels for film thicknesses as a function of ionic strength show that the product $\delta\sqrt{c}$ varies between 2 and 3×10^{-7} for films thicker than 150 Å and then increases to 8×10^{-7} as the film thins to 80 Å. Hence, within the framework of this theory the difference between the van der Waals contribution and ΔF_e is always less than 30% and very much less for the thinner films.

Our contact angle measurements give experimental ΔF_e values and these should be close to the curve calculated for dispersion forces if the above theory applies to the system. Figure 8 shows, therefore, our results as a function of thickness along with the calculated attractive energy curve. A more detailed presentation

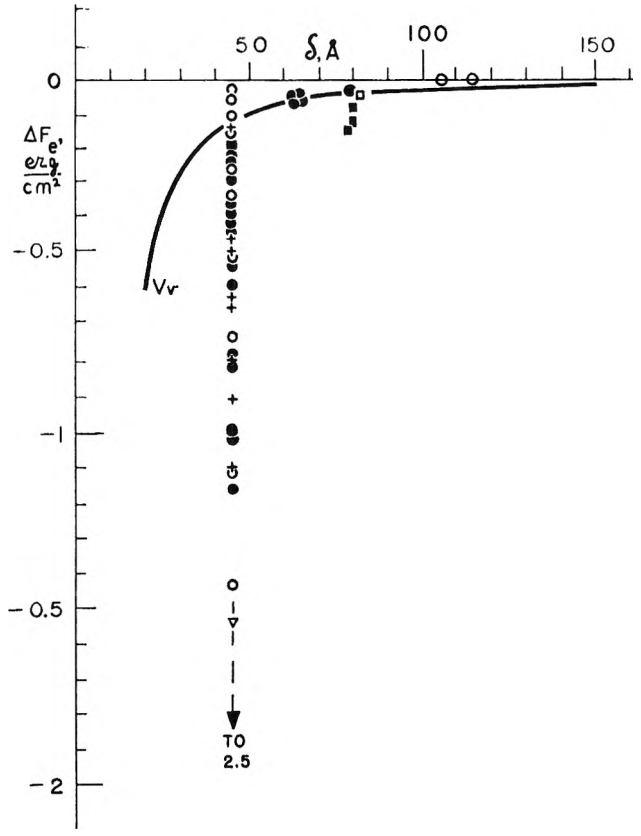

Figure 8. The relation between the depth of the minimum and film thickness omitting some points at low depths. Symbols and compositions same as in Figures 6 and 7.

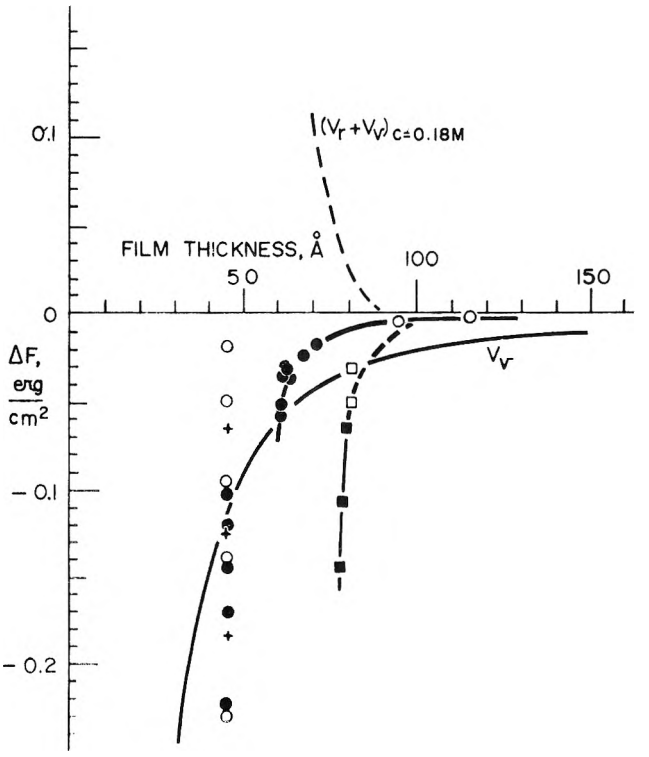

Figure 9. The relation between the depth of the minimum and film thickness for low ΔF_e values. Symbols and compositions same as in Figures 6 and 7. The dashed line is based on measurements of ref 15.

of the lower ΔF_e values is given in Figure 9. In both regions there seems to be little correlation between calculated and experimental values. This is particularly striking for the second black films, all located at about 43 Å, but is also true for the thicker first black films which we may consider first.

First Black Films. The data for these films is summarized in Table I. The above discussion assumes zero hydrostatic pressure difference between film and bulk, but the few hundred dyn cm^{-2} introduced by the bubble curvature are negligible at the higher ionic strengths with which we are concerned, as may be seen from Figure 6 of Lyklema and Mysels.[8]

Figures 8 and 9 involve not only the contact angle but also thickness values. Our apparatus was not suited for simultaneous measurements of both; hence plotted thicknesses are based on previous measurements, particularly those of JMS[30] with which our results correspond closely as discussed above. The JMS thickness measurements agree well with those previously obtained in this laboratory[8] and also with completely independent more recent ones of Lyklema

Table I: Properties of First Black Films in Equilibrium at 23° with Solutions Containing 0.05% Sodium Dodecyl Sulfate and the Indicated Concentration of Sodium and Lithium Chlorides

Concn, M NaCl	Concn, M LiCl	Contact angle	$\Delta F_e \times 10^3$ erg/cm	Thickness, Å
0.1	...	22′	1.3	115[a]
0.2	...	40′	4.4	96[b]
0.3	0.15	1°23′	18	71.5[a]
0.3	0.2	1°34′	25	68[b]
0.05	0.5	1°50′	32	82.5[c]
0.3	0.3	2°00′	37	65[b]
0.05	0.6	2°18′	52	82[c]
0.1	0.6	1°45′	30	63[b]
0.3	0.4	1°44′	31	63[b]
0.15	0.6	1°55′	36	62[b]
0.35	0.4	2°30′	59	62[a]
0.3	0.5	2°22′	53	61
...	0.9	2°35′	66	81[b]
...	1.2	3°20′	107	80[c]
...	1.5	3°55′	145	79[c]
0.5	1.5	5°30′	261	?

[a] From ref 30 corrected by −2 Å. [b] Interpolated as in *a*. [c] Extrapolated as in *a*.

and Bruil.[33] In using these measurements, interpolation and extrapolation was necessary and we assumed that the two systems containing over 90% LiCl had the thicknesses estimated for LiCl alone.

In the present work, the experimental optical data were recalculated on the assumption that the area per ion is 40 Å², which seems more realistic than the previously used 50 Å² in view of the work of Weil,[34] of Nilsson,[35] and of Wilson, *et al.*[36] Thus, we use

$$\delta = d_w - 9.3 \quad \text{and} \quad d_2 = \delta - 22 = d_w - 31.3$$

where δ is the total film thickness, d_2 is the thickness of the aqueous core, and d_w is the equivalent water thickness obtained from the optical measurements, all in ångström units. The difference from previous values[15,30,37] amounts to 2.1 Å in δ and 8 Å in d_2, which is not significant in the present context. The same computation has been applied to lithium compounds, although the measurements of Weil[34] suggest that these films may have higher areas per surfactant ion and therefore have thinner monolayers. Thus, these films might be thicker than shown by some 2 Å in relation to the sodium films, which again is not significant.

The theoretical line shown represents the equation

$$V_a = -\frac{Af}{12\pi\delta^2} \tag{16}$$

where Hamaker constant A was taken to be 6×10^{-13} and f takes into account retardation effects according to Casimir and Polder,[31,38] and we assumed that the pertinent wavelength for water is 10^3 Å.[8] Changes in these values would change the position of the curve or its curvature slightly but this would not improve the agreement with experimental values significantly.

This calculation assumes not only the applicability of the additivity of London forces but also homogeneity of the film. The sandwich structure of the film requires modifications which are not easy to estimate. One can expect, however, that the monolayers will exert compressive forces increasing as their separation becomes smaller. Thinner monolayers would be expected to exert less compression than thicker ones.

Figure 9 shows, however, that films containing only LiCl as the added electrolyte have deeper minima for the same total thickness than films containing only or largely NaCl. Yet, it is the former which presumably have thinner monolayers according to Weil's[34] measurements. Thus, the discrepancy is not likely to be due to the effect of monolayers alone. This is also confirmed by the analysis of Duyvis,[39] who calculated the potential energy of a three-layered film. His equation 18 may be written as

$$12\pi V_v = -\frac{A_{11}}{\delta^2} \times \left(1 - \frac{(A_{11} + A_{22} - 2A_{12})/A_{11}}{[1 - (2d_1/\delta)]^2} + \frac{2(A_{11} - A_{12})/A_{11}}{[1 - (d_1/\delta)]^2}\right) \tag{17}$$

where the subscript 1 refers to the outer layers and 2 to the central one. The first term represents the value for a homogeneous film of same total thickness but formed of the monolayer material. The correction terms should not vary rapidly with thickness until the film becomes quite thin since the numerators involve fractional differences between Hamaker constants and the denominators depart from unity only as the film becomes thin. On the other hand, our discrepancy is apparent also for relatively thick films.

Another assumption in the above treatment is that the same Hamaker constant is applied to all the films and its value based on an estimate for pure water. In fact, however, even the aqueous part of every film contains solutes which are present in varying concentrations. If these should have a significant effect upon the compressive forces, the large magnitude of deviations from the theoretical line for the more concentrated systems could be accounted for.

(33) J. Lyklema and H. Bruil, Wageningen University, personal communication.

(34) I. Weil, *J. Phys. Chem.*, **70**, 133 (1966).

(35) G. Nilsson, *ibid.*, **61**, 1135 (1957).

(36) A. Wilson, M. B. Epstein, and J. Ross, *J. Colloid Sci.*, **12**, 345 (1957).

(37) J. Lyklema, P. C. Scholten, and K. J. Mysels, *J. Phys. Chem.*, **69**, 116 (1965).

(38) H. B. G. Casimir and D. Polder, *Phys. Rev.*, **73**, 360 (1948).

(39) E. M. Duyvis, Thesis, Utrecht, 1962.

Under these conditions each composition would have a different theoretical ΔF *vs.* δ line and our experiments would only give a single point on each of these lines. Any line drawn through a series of points would then have a very different physical meaning, namely that of a locus of minima of a family of curves.

Second Black Films. The thickness of second black films is close to 43 Å and certainly varies over at most a 10 Å range as a function of ionic strength and ionic composition.[30] Figure 8 shows that their ΔF_e value can range from less than 0.02 erg/cm² to more than a hundred times this value. Hence, clearly these cannot be accounted for by forces varying smoothly with thickness only. On the other hand, our findings are in reasonable agreement with the suggestion, put forward earlier,[30] that the second black film is a well-defined organization capable of accommodating certain counterions, particularly those below a limiting size (*i.e.*, sodium but not lithium) and, of course, the surfactant ion, and having some structural similarity with liquid crystals. In this case, one would expect ΔF_e of second black films formed from solutions of constant surfactant concentration to vary linearly with the chemical potential of the sodium ion in these solutions by analogy with the properties of a precipitate. Figure 10, which replots the data for the second black films from Figures 6 and 7 on a logarithmic scale of counterion concentration, shows that this is indeed a good first approximation, although the deviations seem somewhat larger than experimental errors. Figure 10 shows also that on this scale the effect of lithium and tetramethyl ions is well represented by a set of almost parallel lines for each up to a certain concentration when a marked deviation occurs, perhaps along another straight line. Neglecting this last part, the results for the second black film can therefore be summarized by

$$\Delta F_e = A(\log [\mathrm{Na}] - \log B) - C(\log [\mathrm{Na} + \mathrm{Li}] - \log [\mathrm{Na}]) \quad (18)$$

For the NaCl–LiCl system, the values of the constants

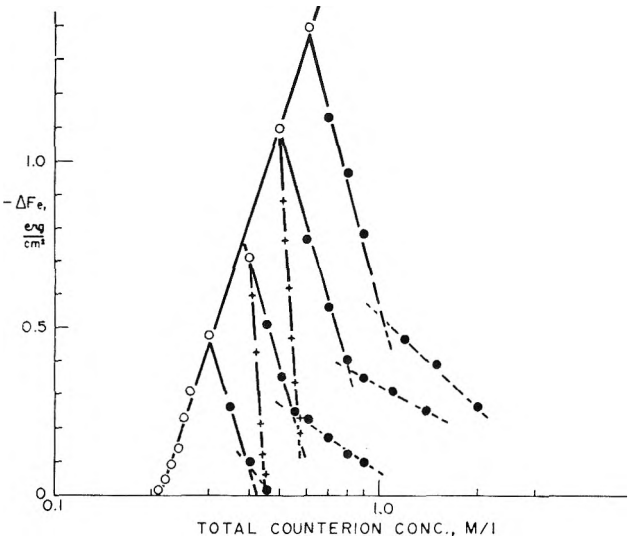

Figure 10. The specific free energy of formation of second black films as a function of the logarithm of the ionic concentration. Symbols and compositions same as in Figures 6 and 7.

are $A = 2.94$, $B = 0.21$, and $C \simeq 3.4$. The lines drawn in Figure 10 for the effect of LiCl upon each NaCl concentration give each a value for C which varies irregularly between 3.1 and 3.6. Expression 18 can be rewritten, using x for Li/(Na + Li), as

$$\Delta F_e = -A \log B + A \log [\mathrm{Na}] + C \log (1 - x) \quad (19)$$

which shows clearly that the effect of the lithium additive upon ΔF_e depends only on its mole fraction. The fewer available data for the tetramethyl ammonium ion can be treated in the same way with $C = 17.6 \pm 1.1$.

It is tempting to speculate that the same specific ionic effects which determine the structure of the second black film are also effective already in the thinner first blacks and influence their ΔF_e and thickness.

Acknowledgment. This work was supported in part by the National Science Foundation. We are grateful to Dr. H. M. Princen, Lever Research Center, for a helpful comment.

Solubility of Nonpolar Gases in Concentrated Electrolyte Solutions

by S. K. Shoor and K. E. Gubbins

Department of Chemical Engineering, University of Florida, Gainesville, Florida 32601 *(Received May 2, 1968)*

A theory of the solubility of gases in electrolytic solutions is presented which is based on the scaled particle theory. The resulting equation for the solute activity coefficient is compared with experimental data for seven nonpolar gases dissolved in potassium hydroxide solutions over a wide range of electrolyte concentration and temperature. The salting-out effect is well predicted by the theory. Calculated heats of solution agree well with experiment for small solute molecules, but are larger than observed values for the larger molecules. This is attributed to a temperature dependence of the molecular hard core diameter. The proposed theory is superior to electrostatic theories in its description of both the concentration and temperature dependence of the solute activity coefficients for these systems. It is found that the salting-out effect is largely due to changes in the cavity work term, which can be calculated with reasonable confidence. Such changes arise primarily from nonpolar solute–ion interactions, and not from the ionic charges themselves.

Introduction

Most of the theories proposed to explain the observed effect of salts on the solubility of nonelectrolytes are electrostatic in nature. The theory of Debye and McAulay[1] provided an expression for the salting coefficient in dilute electrolyte solutions. A variety of attempts to improve their theory have been made, and are discussed in reviews.[2-4] All of these theoretical approaches are closely similar and treat the solvent as a continuous dielectric medium containing ions and solute molecules. A quantitative test of these theories is difficult because the equations involved usually contain parameters which are not readily available. In addition, some qualitative aspects of salting effects are not satisfactorily explained by such theories even in dilute electrolyte solutions.[2,5] Internal pressure theories[2,6] adopt a different viewpoint to that of the electrostatic theories and succeed in explaining many of the observed experimental trends. However, predicted salting coefficients are often a factor of 2 or more larger than experimental values. At present none of the theories of salting phenomena can be regarded as fully satisfactory, and it is of interest to examine alternative approaches.

Pierotti[7,8] has recently proposed a theory of gas solubility in nonpolar solvents and in water which is based on the scaled-particle theory of Reiss, Frisch, Helfand, and Lebowitz.[9,10] The theory predicts solubilities within a factor of 2 of experiment for a wide variety of solutes and solvents, and gives a good representation of the effects of temperature and pressure. In this approach it is not necessary to propose any special models for the structure of the solvent (*e.g.*, hydrogen-bonding, "iceberg" models, etc.). However, the theory provides no information concerning the solution density, which must be available from experiment. As pointed out by Pierotti,[11] it is the use of experimental densities that allows the theory to avoid such structural concepts.

In this paper an approach similar to that used by Pierotti is adopted for the solubility of gases in electrolyte solutions. The solvent medium may be regarded as the electrolyte solution itself, and thus consists of a mixture of several species. It is assumed that the system contains m components, one of which is the solute gas (component 1),[12] whereas the remaining $(m - 1)$ components comprise the solvent species and may include water molecules, ions of different types, undissociated electrolyte, etc. The scaled-particle theory has been extended to mixtures by Lebowitz, Helfand, and Praestgaard.[13]

Theory

The Equation for Solubility. Assuming that the total potential energy is the sum of pair potentials, the following equation can be obtained for the partial molecular Gibbs free energy of the solute gas in the

(1) P. Debye and J. McAulay, *Physik. Z.*, **26**, 22 (1925).

(2) F. A. Long and W. F. McDevit, *Chem. Rev.*, **51**, 119 (1952).

(3) H. S. Harned and B. B. Owen, "The Physical Chemistry of Electrolytic Solutions," 3rd ed, Reinhold Publishing Corp., New York, N.Y., 1958, pp 80–88.

(4) B. E. Conway, *Ann. Rev. Phys. Chem.*, **17**, 481 (1966).

(5) Reference 3, p 534.

(6) W. F. McDevit and F. A. Long, *J. Amer. Chem. Soc.*, **74**, 1773 (1952).

(7) R. A. Pierotti, *J. Phys. Chem.*, **67**, 1840 (1963).

(8) R. A. Pierotti, *ibid.*, **69**, 281 (1965).

(9) H. Reiss, H. L. Frisch, and J. L. Lebowitz, *J. Chem. Phys.*, **31**, 369 (1959).

(10) H. Reiss, H. L. Frisch, E. Helfand, and J. L. Lebowitz, *ibid.*, **32**, 119 (1960).

(11) R. A. Pierotti, *J. Phys. Chem.*, **71**, 2366 (1967).

(12) The usual convention of labeling the solute as component 2 is not convenient here because the solvent medium contains several species.

(13) J. L. Lebowitz, E. Helfand, and E. Praestgaard, *J. Chem. Phys.*, **43**, 774 (1965).

liquid phase[14]

$$\mu_1^{L} = kT \ln \rho_1 \Lambda_1^3 + \sum_{j=1}^{m} \rho_j \int_0^{\infty} dr \int_{\xi} \frac{\partial u_{1j}(r, \xi)}{\partial \xi} \times g_{1j}(r, \xi) 4\pi r^2 \, d\xi \quad (1)$$

where

$$\Lambda_1 = \left(\frac{h^2}{2\pi m_1 kT}\right)^{1/2}$$

and ρ_j is number density of component j, u_{1j} is the pair potential between a solute gas molecule and a solvent molecule of species j at a distance r, and g_{1j} is the radial distribution function for $1 - j$ pairs. The term ξ is a coupling parameter[15] which allows the solute molecule to be coupled with the solvent. The lower and upper integration limits of ξ in eq 1 correspond to complete uncoupling and complete coupling of the solute molecule, respectively. The real molecules are assumed to possess hard cores of diameters $a_1, a_2 \ldots a_m$, so that the pair potential is of the form

$$u_{1j}(r, \xi) = u_{1j}^{h}(r, \xi_h) + u_{1j}^{s}(r, \xi_s) \quad (2)$$

where u_{1j}^{h} and u_{1j}^{s} are the hard-core and soft potential interactions, respectively, given by

$$\left.\begin{aligned} u_{1j}^{h}(r) &= \infty \qquad r \leq a_{1j} = \frac{a_1 + a_j}{2} \\ u_{1j}^{h}(r) &= 0 \\ u_{1j}^{s}(r, \xi_s) &= \xi_s u_{1j}(r) \end{aligned}\right\} \quad r > a_{1j} \quad (3)$$

In charging up the hard-core contribution the coupling parameter ξ_h varies from 0 to a_{1j}, and in charging the soft potential contribution ξ_s varies from 0 to 1. When the two coupling parameters are zero the solute molecule is decoupled from the system. If the two coupling processes are imagined to take place separately eq 1 becomes

$$\mu_1^{L} = kT \ln \rho_1 \Lambda_1^3 + \bar{g}_1^{h} + \bar{g}_1^{s} \quad (4)$$

where

$$\bar{g}_1^{h} = \sum_{j=1}^{m} \rho_j \int_{\xi_h=0}^{\xi_h=a_{1j}} d\xi_h \int_{r=0}^{\infty} \frac{\partial u_{1j}^{h}(r, \xi_h)}{\partial \xi_h} \times g_{1j}(r, \xi_h, \xi_s = 0) 4\pi r^2 \, dr \quad (5)$$

$$\bar{g}_1^{s} = \sum_{j=1}^{m} \rho_j \int_{\xi_s=0}^{\xi_s=1} d\xi_s \int_{r=a_{1j}}^{\infty} u_{1j}^{s}(r) \times g_{1j}(r, \xi_h = a_{1j}, \xi_s) 4\pi r^2 \, dr \quad (6)$$

For a vapor and liquid phase in equilibrium

$$\mu_1^{G} = \mu_1^{L} \quad (7)$$

and the chemical potential of the solute in the gas phase is given by[16]

$$\mu_1^{G} = kT \ln \left(\frac{\Lambda_1^3}{kT}\right) + kT \ln f_1^{G} \quad (8)$$

where f_1^{G} is the gas-phase fugacity of the solute.

Putting eq 4 and 8 in eq 7 and rearranging

$$\ln \left(\frac{f_1^{G}}{\rho_1}\right) = \frac{\bar{g}_1^{h}}{kT} + \frac{\bar{g}_1^{s}}{kT} + \ln kT \quad (9)$$

The mole fraction (solubility) of the solute gas in the solution is

$$x_1 = \frac{\rho_1}{\sum_j \rho_j} \quad (10)$$

so that eq 9 may be written

$$\ln \left(\frac{f_1^{G}}{x_1}\right) = \frac{\bar{g}_1^{h}}{kT} + \frac{\bar{g}_1^{s}}{kT} + \ln \left(kT \sum_j \rho_j\right) \quad (11)$$

At low pressures the fugacity in eq 11 may be replaced by partial pressure, and the last term on the right-hand side of this equation may be calculated if the density is known. It remains to evaluate the terms $\bar{g}_1^{h}$ and $\bar{g}_1^{s}$.

Evaluation of $\bar{g}_1^{h}$. This term represents the free energy of introducing a hard sphere of diameter a_1 into the solvent (electrolyte solution). Alternatively, it may be thought of as the work required to make a cavity of this size in the solvent.[9] Lebowitz, *et al.*,[13] have shown that this cavity work is given by

$$\frac{\bar{g}_1^{h}}{kT} = -\ln (1 - \zeta_3) + \left[\frac{6\zeta_2}{1 - \zeta_3}\right] \frac{a_1}{2} + \left[\frac{12\zeta_1}{1 - \zeta_3} + \frac{18\zeta_2^2}{(1 - \zeta_3)^2}\right] \left(\frac{a_1}{2}\right)^2 + \frac{4}{3}\pi \frac{P}{kT} \left(\frac{a_1}{2}\right)^3 \quad (12)$$

where

$$\zeta_n = \tfrac{1}{6}\pi \sum_{j=1}^{m} \rho_j (a_j)^n$$

and P is pressure.

Evaluation of $\bar{g}_1^{s}$. The term due to the soft part of the potential may be thought of as the free energy needed to introduce the solute molecule into the cavity, and may be written

$$\bar{g}_1^{s} = \bar{e}_1^{s} + P\bar{v}_1^{s} - T\bar{s}_1^{s}$$

where $\bar{e}_1^{s}$, $\bar{v}_1^{s}$, and $\bar{s}_1^{s}$ are partial molecular internal energy, volume, and entropy. Following Pierotti,[7] it is here assumed that the terms $P\bar{v}_1^{s}$ and $T\bar{s}_1^{s}$ are much smaller than the internal energy term and may be ignored. While the first of these terms is known to be small at low pressures, the approximation concerning $\bar{s}_1^{s}$ may lead to errors for some solutes. With

(14) N. Davidson, "Statistical Mechanics," McGraw-Hill Book Co., Inc., New York, N.Y., 1962, p 481.

(15) T. L. Hill, "Statistical Mechanics," McGraw-Hill Book Co., New York, N.Y., 1956, p 180.

(16) Reference 15, p 130.

these assumptions

$$\bar{g}_1^s \approx \bar{e}_1^s = \sum_{j=1}^{m} \int_{r=a_{1j}}^{\infty} u_{1j}(r) g_{1j}(r) \rho_j 4\pi r^2 \, dr \quad (13)$$

The radial distribution function is not readily evaluated. As an approximation we assume the solvent particles to be uniformly distributed about the solute molecule so that

$$g_{1j}(r) = 1 \qquad (r > a_{1j})$$

Equation 13 becomes

$$\bar{g}_1^s \approx \sum_{j=1}^{m} \rho_j \int_{a_{1j}}^{\infty} u_{1j}(r) 4\pi r^2 \, dr \quad (14)$$

The nonpolar part of the pair interaction between a solute molecule and a solvent molecule of type j is assumed to be given by the Lennard-Jones (6–12) potential

$$u_{1j}^{np} = 4\epsilon_{1j}\left[\left(\frac{\sigma_{1j}}{r}\right)^{12} - \left(\frac{\sigma_{1j}}{r}\right)^{6}\right] \quad (15)$$

where the mixture potential parameters ϵ_{1j} and σ_{1j} are related to the pure component parameters by the approximate mixing rules[17]

$$\sigma_{1j} = \tfrac{1}{2}(\sigma_1 + \sigma_j); \qquad \epsilon_{1j} = (\epsilon_1\epsilon_j)^{1/2} \quad (16)$$

It is now assumed that the electrolyte is completely dissociated, and the only species present in solution are solute molecules (1), water molecules (2), and positive and negative ions (3 and 4). In addition, the solute molecule is assumed nonpolar. The treatment for polar solutes, or of electrolyte solutions containing additional species (*e.g.*, undissociated electrolyte, various water structures, etc.) is an obvious extension of what follows. After averaging the interaction between the permanent dipole of the water molecule and the solute induced dipole over all orientations,[18] and ignoring terms due to higher multipole moments, the solute–water pair potential is

$$u_{12} = u_{12}^{np} - \frac{\mu_2^2\alpha_1}{r^6} \quad (17)$$

where u_{12}^{np} is given by eq 15, μ_2 is the dipole moment of a water molecule, and α_1 is the solute polarizability.

The total ion–induced dipole interaction of a solute molecule with all of the surrounding ions may be written[19]

$$u^{(C,ind\ \mu)} = -\int_0^E \boldsymbol{\mu}_1^{(ind)} \cdot d\mathbf{E}' = -\tfrac{1}{2}\alpha_1 E^2 \quad (18)$$

where $\mu_1^{(ind)}$ is the induced dipole for the solute and E is the electric field at the position of the solute molecule that is produced by all of the surrounding ions. The field E depends upon the distribution of ions about the neutral molecule. If, as above, the distribution is assumed uniform, there is on the average a spherically symmetrical charge distribution about the solute molecule. For such a distribution the field, and hence also the ion–induced dipole interaction of eq 18, is zero.[20] For the real solution it is clear that the solute molecule will experience some small fluctuating field E^f due to the surrounding ions, and since this term is squared in eq 18 there will be a finite ion–induced dipole interaction whose time average is not zero. This contribution is assumed small and is neglected here. Its inclusion would make the calculated $\bar{g}_1^s$ value more negative. The only ion–solute interactions included in eq 14 are therefore nonpolar contributions.

Substituting the above expressions for u_{1j} into eq 14 gives

$$\bar{g}_1^s \approx -16\pi \sum_{j=1}^{4} \rho_j \int_{a_{1j}}^{\infty} \epsilon_{1j}\left[\frac{\sigma_{1j}^6}{r^4} - \frac{\sigma_{1j}^{12}}{r^{10}}\right] dr - 4\pi\rho_2 \times \int_{a_{12}}^{\infty} \frac{\mu_2^2\alpha_1}{r^4} \, dr \quad (19)$$

On performing the integrations and following Pierotti[7,8] in taking $a_{1j} = \sigma_{1j}$

$$\bar{g}_1^s \approx -\frac{32\pi}{9} \sum_{j=1}^{4} \rho_j \epsilon_{1j}\sigma_{1j}^3 - \frac{4\pi\rho_2\mu_2^2\alpha_1}{3\sigma_{12}^3} \quad (20)$$

Comparison With Experiment

Shoor, Walker, and Gubbins[21] have reported experimental solubilities for a wide variety of nonpolar gases in postassium hydroxide solutions, and over a wide range of KOH concentration and temperatures. These values are compared below with those predicted by the scaled-particle theory. The experimental data were reported as activity coefficients (γ_1), the standard state being the hypothetical liquid state referred to the behavior of the solute at infinite dilution in water. Under these conditions

$$\frac{f_1^G}{x_1} = K_1^0\gamma_1 \quad (21)$$

where K_1^0 is the Henry constant for the gas in pure water. For a partial pressure of 1 atm and an ideal vapor phase, the solubility is $x_1 = 1/(K_1^0\gamma_1)$.

Molecular Parameters. Values of the Lennard-Jones σ and ϵ/k for solute gases were those obtained from second virial coefficient data and are shown together with polarizabilities in Table I. These parameters were taken from Hirschfelder, Curtiss, and

(17) J. O. Hirschfelder, C. F. Curtiss, and R. B. Bird, "Molecular Theory of Gases and Liquids," John Wiley & Sons, Inc., New York, N. Y., 1954, p 168.

(18) Reference 17, p 29.

(19) Reference 17, p 852.

(20) S. G. Starling and A. J. Woodall, "Physics," Longmans, Green and Co. Ltd., London, 1950, p 940.

(21) S. K. Shoor, R. D. Walker, Jr., and K. E. Gubbins, *J. Phys. Chem.*, **73**, 312 (1969).

Table I: Molecular Parameters for Solutes

Solute	σ_1, Å	ϵ_1/k, °K	$\alpha_1 \times 10^{24}$ cm³/molecule
He	2.63	6.03	0.204
H_2	2.87	29.2	0.802
Ar	3.40	122	1.63
O_2	3.46	118	1.57
CH_4	3.82	137	2.70
SF_6	5.51	200.9	6.21[a]
$C(CH_3)_4$	7.44[b]	232.5[b]	10.36[b]

[a] T. M. Reed, *J. Phys. Chem.*, 59, 428 (1955). [b] J. H. Bae, Ph.D. Thesis, University of Florida, Gainesville, Fla., 1966.

Bird[22] except where otherwise indicated, and are the same values as used by Pierotti[7,8] except in the cases of sulfur hexafluoride and neopentane. Values of σ, ϵ/k, and dipole moment μ for water were those used by Pierotti[8] (Table II).[23,24]

Table II: Molecular Parameters for Solvent Species

Solvent species	σ, Å	a, Å[c]	a, Å[d]	ϵ/k, °K	$\alpha \times 10^{24}$ cm³/molecule	μ, D
H_2O	2.75[a]	...	...	85.3[a]	...	1.84
K^+	2.60[b]	2.66	2.50	239[b]	0.835[e]	
OH^-	3.30[b]	3.52	0.92	137.2[b]	1.83[b]	

[a] Values from ref 8. [b] Calculated in this work. [c] Diameters from crystal radii, ref 23 and 24. [d] Diameters from ionic mobility, ref 24. [e] Reference 31.

Values of σ and ϵ/k do not seem to have been reported for ions. Although crystal radii should provide approximate values for σ, such radii are difficult to determine accurately, and considerable disagreement is shown between values reported by various workers. In view of the sensitivity of the calculated solubilities to the σ values, a procedure similar to that used by Pierotti[8] in determining σ for water was used. Experimental values of ln $(\gamma_1 K_1^0)$ were plotted against polarizability of the solute molecules at 25° for 10 and 20% by weight KOH solutions. The value of ln $(\gamma_1 K_1^0)$ extrapolated to zero polarizability is the experimental hard-sphere value. This may be compared with the theoretical hard-sphere value from eq 11 and 21

$$\lim_{\substack{\alpha_1 \to 0 \\ \sigma_1 \to 2.58 \text{ Å}}} \ln (\gamma_1 K_1^0) = \frac{\bar{g}_1^h}{kT} + \ln (kT \sum_j \rho_j) \quad (22)$$

where $\bar{g}_1^h$ is given by eq 12. As the other molecular parameters are known, the resulting two equations may be solved for the σ values for the two ions. The values are shown in Table II, and are seen to be in good agreement with crystal diameters. The abnormally low value of the diameter calculated from ionic mobility for the hydroxyl ion is due to the special mobility ("proton-jump") mechanism of these ions.[25]

Although experimental values of ϵ/k are not available for ions, several theories provide expressions for the potential interaction due to dispersion forces.[26,27] The Mavroyannis–Stephen theory[28] gives for the dispersion interaction

$$u_{ij}^{(dis)} = -\frac{3a_0^{1/2}e^2\bar{\alpha}_i\bar{\alpha}_j}{2r^6[(\bar{\alpha}_i/Z_i)^{1/2} + (\bar{\alpha}_j/Z_j)^{1/2}]} \quad (23)$$

where $a_0 = 0.5292$ Å is the Bohr radius, e is electronic charge, Z is the total number of electrons in the particle, and $\bar{\alpha}_i$ and $\bar{\alpha}_j$ are the polarizabilities for the two species in the mixture. Comparing with the dispersion term of the Lennard-Jones (6,12) potential

$$4\epsilon_{ij}\sigma_{ij}^6 = \frac{3a_0^{1/2}e^2\bar{\alpha}_i\bar{\alpha}_j}{2[(\bar{\alpha}_i/Z_i)^{1/2} + (\bar{\alpha}_j/Z_j)^{1/2}]} \quad (24)$$

For like-pair interactions, after substituting values for a_0 and e, this equation gives

$$\epsilon = 3.146 \times 10^{-24} \frac{\alpha^{3/2}Z^{1/2}}{\sigma^6} \text{ erg} \quad (25)$$

where α and σ are in cgs units. The Mavroyannis–Stephen theory gives ϵ values which are in considerably better agreement with values obtained from experimental data than those calculated from most previous theories.[29] Equation 25 was used to calculate the ϵ/k value for the K^+ ion shown in Table II. For OH^- no polarizability value could be found in the literature, and the value given in Table II was calculated from the relation between polarizability and mole refraction R[30]

$$\alpha = \frac{3}{4\pi}\left(\frac{V}{N}\right)\frac{n^2 - 1}{n^2 + 2} = \frac{3R}{4\pi N} \quad (26)$$

where V and N are volume and number of molecules and n is the index of refraction. Mole refraction data were obtained from the Landolt–Bornstein tables.[31]

Test of Theory. From eq 11 and 21

$$\ln (\gamma_1 K_1^0) = \frac{\bar{g}_1^h}{kT} + \frac{\bar{g}_1^s}{kT} + \ln (kT \sum_j \rho_j) \quad (27)$$

(22) Reference 17, p 1110.
(23) B. E. Conway, "Electrochemical Data," Elsevier Publishing Co., New York, N. Y., 1952.
(24) E. R. Nightingale, *J. Phys. Chem.*, 63, 138 (1959).
(25) J. D. Bernal and R. H. Fowler, *J. Chem. Phys.*, 1, 515 (1933).
(26) H. Margenau, *Philosophy of Science*, 8, 603 (1941).
(27) D. D. Fitts, *Ann Rev. Phys. Chem.*, 17, 59 (1966).
(28) C. Mavroyannis and M. J. Stephen, *Mol. Phys.*, 5, 629 (1962).
(29) T. M. Reed, III, University of Florida, personal communication, 1967.
(30) L. Pauling and E. B. Wilson, "Introduction to Quantum Mechanics," McGraw-Hill Book Co., Inc., New York, N. Y., 1935, p 227.
(31) Landolt–Bornstein, "Zahlenwerte und Funkion aus Physik-Chemie-Astronomie-Geophysik-Technik," Vol. I, Part 1, 1950.

Table III: Predicted and Experimental ln $(\gamma_1 K_1^0)$ Values for KOH Solutions

Solute	% KOH[a] 0% Exptl	0% Theor	10% Exptl	10% Theor	20% Exptl	20% Theor	30% Exptl	30% Theor	40% Exptl	40% Theor	50% Exptl	50% Theor
					25°							
He	11.86	11.62	12.25	11.98	13.10	12.85	14.05	13.62	...	...	...	...
H_2	11.17	11.10	11.85	11.85	12.41	12.53	13.17	13.42	14.13	14.63	15.2	16.15
Ar	10.62	10.27	11.38	11.04	12.30	11.98	13.40	13.13	14.63	14.47	...	...
O_2	10.66	10.47	11.50	11.28	12.46	12.25	13.54	13.43	14.73	14.82	16.07	16.59
CH_4	10.58	10.58	11.46	11.38	12.49	12.48	13.65	13.66	15.10	15.17	...	..
SF_6	12.38	10.75	13.88	12.38	15.58	14.10	17.52	16.25	...	...	...	...
$C(CH_3)_4$	11.51	11.80	12.99	13.55	14.81	16.43	16.85	19.87	...	...	...	...
					80°							
He	11.74	11.42	12.39	12.11	13.18	12.83	14.10	13.71	...	...	...	...
H_2	11.24	10.67	11.90	11.89	12.55	12.67	13.28	13.62	14.25	14.73	15.29	16.03
Ar	11.10	10.81	11.75	11.60	12.55	12.50	13.50	13.54	14.60	14.92	...	...
O_2	11.13	11.04	11.81	11.72	12.68	12.66	13.63	13.83	14.76	15.13	16.07	16.82
CH_4	11.14	11.18	11.86	12.05	12.70	13.10	13.69	14.35	14.80	15.79	...	...
SF_6	13.17	12.49	14.30	13.99	15.72	15.79	17.36	18.10	...	...	...	...
$C(CH_3)_4$	12.37	14.42	13.61	16.43	15.15	19.40	16.91	23.10	...	...	...	...

[a] Weight per cent KOH.

Predicted and experimental[21] values of ln $(\gamma_1 K_1^0)$ are compared in Table III for 7 nonpolar solutes in KOH solutions at two temperatures. The solute molecules considered exhibit a wide range of σ values, as seen from Table I. Hard and soft contributions to the chemical potential in eq 27 were calculated from eq 12 and 20 using the molecular parameters of Tables I and II together with experimental densities from the literature.[32]

For the solutes He, H_2, Ar, O_2, and CH_4 at 25° the agreement between theory and experiment is very good for all KOH concentrations. Values of $(\gamma_1 K_1^0)$ agree within a factor of about 2 or better even at the highest concentrations, and in most cases the discrepancies are substantially smaller than this. The agreement for these solutes at 80° is slightly poorer; however, it should be recalled that σ values for the ions were determined at 25°. Discrepancies between theory and experiment are larger in the cases of sulfur hexafluoride and neopentane. Because of the large hard-core diameters for these molecules, the calculated $(\gamma_1 K_1^0)$ are very sensitive to the value taken for σ of solute gas. Considerable uncertainty is involved in evaluating the Lennard-Jones σ parameter, and it is possible that the values used were in error. Similar considerations apply to the ϵ/k parameters for these molecules, although these have less effect on calculated $(\gamma_1 K_1^0)$ values. Because intermolecular interactions for sulfur hexafluoride and neopentane are both large and acentric, it also seems likely that the assumptions of $\bar{s}_1^s = 0$ and of a uniform molecular distribution around the solute are poor approximations in these cases.

The experimental and predicted temperature dependences of ln $(\gamma_1 K_1^0)$ are compared in Figure 1 for argon in 20% KOH solution. The partial molal heat of solution $\Delta\bar{H}_1$, provides a quantitative measure of the temperature dependence of solubility and is given by

$$\frac{\partial \ln (\gamma_1 K_1^0)}{\partial T} = -\frac{\Delta\bar{H}_1}{RT^2} \tag{28}$$

Observed and predicted $\Delta\bar{H}_1$ values are shown in Tables IV and V. From Table IV the predicted $\Delta\bar{H}_1$ values are seen to be too large, particularly for temper-

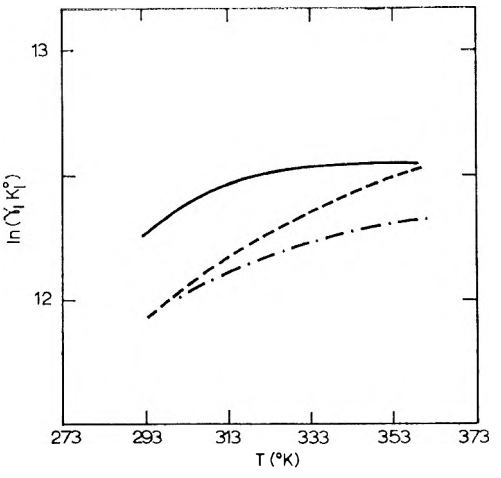

Figure 1. Effect of temperature on the activity coefficient of argon in 20% KOH solution: solid line, observed values; – – –, scaled-particle theory with constant σ; — · — ·, scaled-particle theory with temperature-dependent σ.

(32) M. K. Tham, K. E. Gubbins and R. D. Walker, *J. Chem. Eng. Data*, 12, 525 (1967); (b) Solvay Technical Bulletin No. 15, Allied Chemical Corp., New York, N. Y., 1960.

Table IV: Partial Molal Heats of Solution for Ar in 20% KOH Solution

Temp, °C	$\Delta\bar{H}_1$, cal/g mol Exptl	$\Delta\bar{H}_1$, cal/g mol Theory[a]
25	−2100	−2380
40	−1210	−2100
60	−400	−1780
80	−150	−1430

[a] Assuming σ independent of temperature.

Table V: Partial Molal Heats of Solution for Ar at 25°

Wt % KOH	$\Delta\bar{H}_1$, cal/g mol Exptl	$\Delta\bar{H}_1$, cal/g mol Theory[a]
0	−2800	−2750
10	−2700	−2640
20	−2100	−2380
30	−1700	−2110
40	−1240	−1770

[a] Assuming σ independent of temperature.

atures other than 25°. An examination of Table III indicates that for other solutes the predicted and observed temperature dependences are in agreement for helium and hydrogen, but discrepancies of the type shown in Figure 1 are found for the remaining solutes and become larger as the hard-sphere diameter increases. These errors appear to arise from the fundamental assumption that a pair potential of the form given by eq 2 may be used. In practice it is necessary to choose appropriate constant values for the hard-core diameter of each species. However, the real particles do not possess hard cores, and the effective core diameter may be expected to decrease with rising temperature because of both the increase in average particle kinetic energy and averaging over molecular orientations. This temperature dependence of the diameters has been discussed recently in connection with applications of scaled-particle theory to gas solubilities[11,33] and surface tension.[34] The predicted temperature dependence for both of these properties is improved if σ is allowed to decrease with rising temperature. In determining σ for water, Pierotti[8] found that the best value was 2.74 Å at 70° as opposed to 2.75 Å at 25°. To illustrate the effect of a small decrease with temperature of the σ values for the various species, calculations were performed for argon in 20% KOH using the following diameters (Å) at 25 and 80°

Temp, °C	σ_{Ar}	σ_{H_2O}	σ_K	σ_{OH}
25	3.40	2.75	2.60	3.30
80	3.39	2.74	2.59	3.29

Diameters at intermediate temperatures were obtained by linear interpolation. The resulting predicted temperature dependence of ln $(\gamma_1 K_1^0)$ is shown in Figure 1 and is seen to be much improved.

It is instructive to compare the relative magnitudes of the various terms in eq 27, and Table VI shows the contributions for argon at 25°. The free energy of cavity formation is seen to be the dominant term in eq 27 and is affected by the addition of ions to a much larger extent than is the $\bar{g}_1^s$ term. The success of the theory is probably due in large part to this fact, for the calculation to obtain $\bar{g}_1^h$ may be performed with considerably greater confidence than that needed to obtain $\bar{g}_1^s$. The last term on the right-hand side of eq 27, which corresponds to the free energy for the fixed solute molecule to wander within the solvent, is seen to vary little with KOH concentration. Of the various contributions to $\bar{g}_1^s$ the electrostatic interaction between solute and water molecules is a relatively small contribution, whereas that of the nonpolar interactions is large. Nonpolar interactions between solute and ions become appreciable at high concentrations. Similar trends are observed for the other solutes and temperatures. For sulfur hexafluoride and neopentane the relative magnitudes of the various terms are similar to those in Table VI, but because of the larger magnitudes of $\bar{g}_1^h$ and $\bar{g}_1^s$ together with their opposed signs the possibility of errors in the predicted values is increased.

Discussion

It is interesting to compare the scaled-particle theory with electrostatic theories of salt effects. As these theories are all quite similar,[2] only the theory of Debye and McAulay[1] and the more recent approach of Conway, Desnoyers, and Smith[35] will be considered. In the low (electrolyte) concentration limit the Debye–McAulay equation for the activity coefficient of solute is

$$\log \gamma_1 = k_s C_s \tag{29}$$

where C_s is the molar concentration of salt and k_s is the salting coefficient given by

$$k_s = \frac{\bar{\beta} N_0}{2.303 \times 1000 kTD_0} \sum_j \frac{\nu_j e_j^2}{a_j} \tag{30}$$

and N_0 is Avogadro's number, D_0 is the dielectric constant of water, ν_j is the number of ions of type j per mole of electrolyte, and e_j and a_j are ionic charge and diameter. The term $\bar{\beta}$ is related to the dielectric constant D of the nonelectrolyte solution by

$$D = D_0(1 - \bar{\beta}n)$$

(33) A. Ben-Naim and H. L. Friedman, *J. Phys. Chem.*, **71**, 448 (1967).

(34) S. W. Mayer, *J. Chem. Phys.*, **38**, 1803 (1963).

(35) B. E. Conway, J. E. Desnoyers, and A. C. Smith, *Phil. Trans. Roy. Soc. London*, **A256**, 389 (1964).

Table VI: Contributions to ln $(\gamma_1 K_1^0)$ for Argon in KOH Solutions at 25°

Wt % KOH	$\bar{g}_1^h/kT$	Soft contributions: Nonpolar interactions: Ar–H_2O	Ar–K^+	Ar–OH^-	Electrostatic term[a]	$\bar{g}_1^s/kT$	ln $(kT\Sigma_i\rho_i)$
0	7.41	−3.71	...	...	−0.64	−4.35	7.21
10	8.46	−3.64	−0.20	−0.21	−0.63	−4.68	7.26
20	9.71	−3.52	−0.44	−0.47	−0.61	−5.04	7.31
30	11.18	−3.34	−0.72	−0.76	−0.58	−5.40	7.35
40	12.85	−3.11	−1.03	−1.09	−0.54	−5.77	7.39

[a] Arising from the water dipole–solute induced dipole interaction term of eq 17.

where n is the number of molecules of nonelectrolyte solute per cubic centimeter of solution. Comparison of eq 29 with experiment is made difficult by the lack of experimental values for $\bar{\beta}$. However, following the method used by Conway,[35] it is possible to estimate this term from Kirkwood's theory of dielectrics. After some simplifying assumptions are made it can be shown that for a nonpolar solute and a highly polar solvent system[36]

$$\bar{\beta} = \frac{\bar{V}_1}{N_0} - \frac{6\pi\alpha_1}{D_0} \tag{31}$$

where $\bar{V}_1$ is partial molal volume of solute. Values of k_s calculated using eq 30 and 31 are compared with experiment in Table VII. Ionic diameters were calculated from crystal radii (Table II); no values of $\bar{V}_1$ could be found for sulfur hexafluoride and neopentane, so that a comparison was not possible for these solutes.

The more recent theory put forward by Conway, *et al.*,[35] is an improvement of Debye's theory,[37] and takes into account dielectric saturation effects. Each ion of type i is supposed to have a hydration shell of radius $r_h^{(i)}$ containing n_i water molecules, in which the dielectric constant is assumed very small. Outside of this shell the dielectric constant is assumed to be the value D_0 for pure water. Their equation for a nonpolar gas in a 1–1 electrolyte is

$$\frac{S_1^0 - S_1}{S_1^0 C_s} = \frac{18(n_3 + n_4)}{1000d - C_s M_s} + \frac{e^2(\bar{V}_1 D_0 - \frac{2}{3}P_1)}{2000kTD_0^2} \times \left[\frac{1}{r_h^{(3)}} + \frac{1}{r_h^{(4)}} - \frac{2}{R}\right] \tag{32}$$

where S_1, S_1^0 are the solubilities in electrolyte and pure water respectively, n_3 and n_4 are hydration numbers for the two ions, $r_h^{(3)}$ and $r_h^{(4)}$ are the corresponding radii of the primary hydration shells, d is density of solution, M_s is the molecular weight of electrolyte, e is electronic charge, P_1 is total molar polarization of solute, and R is a radius corresponding to the volume available per ion in the solution. In the infinite dilution limit

$$\lim_{C_s \to 0} \frac{S_1^0 - S_1}{S_1^0} = \ln \gamma_1 = 2.303 k_s C_s \tag{33}$$

where

$$k_s = \frac{1}{2.303}\left[\frac{18(n_3 + n_4)}{1000d} + \frac{e^2(\bar{V}_1 D_0 - \frac{2}{3}P_2)}{2000kTD_0^2} \times \left(\frac{1}{r_h^{(3)}} + \frac{1}{r_h^{(4)}}\right)\right] \tag{34}$$

This equation was used to calculate salting coefficients for the systems in Table VII using the values in Table VIII for the ionic parameters n and r_h. The hydration number for the OH^- ion was not available, and was

Table VII: Salting-Out Coefficients at Infinite Dilution, k_s, for KOH Solutions at 25°

Solute	$\bar{V}_1$, cm³/mole	k_s: Debye–McAulay eq 30	Conway eq 34	Expt'l
He	7.7[a]	0.0157	0.081	0.015
H_2	19.4[b]	0.039	0.094	0.129
Ar	24.2[a]	0.049	0.099	0.179
O_2	32.0[c]	0.065	0.108	0.180
CH_4	36.0[d]	0.073	0.112	0.197

[a] Reference 35. [b] R. Kobyashi and D. L. Katz, *Ind. Eng. Chem.*, **45**, 440 (1953). [c] T. Enns, P. F. Scholander, and E. D. Bradstreet, *J. Phys. Chem.*, **69**, 389 (1965). [d] W. L. Masterton and D. A. Robins, *J. Chem. Phys.*, **22**, 1830 (1954).

Table VIII

Ion	r_h, Å	n
K^+	2.72[a]	4.1[a]
OH^-	3.00[b]	5.3[c]

[a] Reference 35. [b] Reference 24. [c] Calculated.

(36) J. T. Edsall and J. Wyman, "Biophysical Chemistry," Vol. I, Academic Press Inc., New York, N. Y., pp 364, 370.
(37) P. Debye, *Z. Phys. Chem.* (Leipzig), **130**, 56 (1927).

calculated from the experimental partial molal entropy of hydration[23] using the method proposed by Ulich.[38]

It is apparent from Table VII that neither of the electrostatic theories predicts the observed salting-out coefficients satisfactorily. Figure 2 compares the

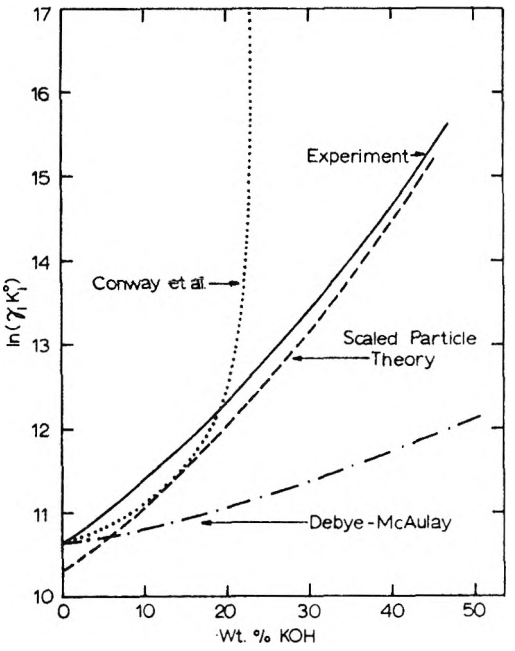

Figure 2. Theoretical and experimental activity coefficients of argon at 25°.

observed concentration dependence of the activity coefficient for oxygen at 25° with the predictions of the scaled-particle theory and the two electrostatic theories. The Debye–McAulay theory gives results much below experiment. While the theory of Conway, *et al.*, gives better results at low electrolyte concentrations, it predicts negative solubilities for higher KOH concentrations and is thus invalid in this region. The failure of the electrostatic theories to predict correctly either the effect of solute species or electrolyte concentration on the activity coefficient can be attributed to the assumptions made in these theories. It seems probable that it is an oversimplification to treat the solvent as a continuous dielectric medium, and that observed salt effects can be adequately accounted for only if the solute–solvent molecular interactions are explicitly introduced into the theory.

The scaled-particle theory has the advantage that the expression for solute chemical potential is derived from the equations of statistical mechanics by a series of well-defined approximations. Salting-out effects are accounted for within the framework of a more general theory that describes the solubility of gases in organic solvents and water[7,8] and provides a simple model of the solution process. The theory explains the effect of solute species and electrolyte concentration on salting-out in KOH solutions, where salt effects are large. In contrast to the electrostatic theories, it is possible to calculate the solubility of the gas in pure water. Furthermore, the molecular parameters needed are more readily obtained than those involved in electrostatic theories. From eq 27 it is seen that the scaled-particle theory predicts salting-in for systems in which the magnitude of $\bar{g}_1^s/kT$ exceeds the sum of the other two terms. Such behavior will occur if the "soft" interaction is very strong, and under such conditions the assumptions that $(P\bar{v}_1^s - T\bar{s}_1^s) \approx 0$ and that the molecular distribution is uniform may be poor approximations.

Of the approximations involved in the scaled-particle theory the basic assumption that molecules possess hard cores (eq 2) seems the most serious, and may lead to predicted heats of solution that are too high. In fairness to the scaled-particle theory, however, it should be pointed out that electrostatic theories cannot usually attempt such a calculation because the necessary parameters are not available. The validity of the approximations that $\bar{s}_1^s = 0$ and that the molecular distribution is uniform is difficult to evaluate because the change of $\bar{g}_1^s$ with electrolyte concentration is small compared to that for $\bar{g}_1^h$. It seems unlikely that these assumptions lead to large errors for small nonpolar molecules, but this may not be the case for larger nonpolar or polar solute molecules.

Unlike many of the electrostatic theories, the scaled-particle theory makes no appeal to assumptions concerning solvent structure, ionic hydration, etc. In addition, the ionic charge has little direct influence on salting-out. The most important effect of such charges appears to be in determining the density of the electrolyte solution.

(38) H. Ulich, *Z. Elektrochem.*, **36**, 497 (1930).

Electrolytic Hydrogen Evolution Reaction on Aluminum, Oxide-Covered Electrodes

by A. K. Vijh

Research & Development Laboratories, Sprague Electric Company, North Adams, Massachusetts
(Received June 3, 1968)

The electrolytic hydrogen evolution reaction (h.e.r.) on aluminum covered by thin "spontaneous" oxide has been examined in aqueous, buffered acetate solutions of pH $\simeq$5.5. Tafel parameters and their temperature dependence have been determined galvanostatically, with emphasis on the effect of time of polarization on these parameters. Galvanostatic cathodic charging curves and open-circuit decay of the electrode potential have also been examined. Tafel plots obtained by procedures involving short polarizations show slopes between $2.3 \times 3RT/F$ and $2.3 \times 4RT/F$, depending on the temperature. On long polarizations, some cathodic "activation" is manifested, which also reduces the values of b to $2.3 \times 2RT/F$ approximately. The initial discharge step is suggested as the probable rate-determining step (rds) in the overall reaction. This conclusion is based on the values of Tafel slopes and on the lack of appreciable electrode coverage by adsorbed hydrogen as deduced from transient studies. The values of "apparent" exchange current densities (*ca.* 10^{-8} A cm^{-2}, before surface activation) and apparent heat of activation (11 kcal mol^{-1}) have been concluded to be consistent with this mechanism. Relation of present studies to the mechanisms of rectification is briefly pointed out.

I. Introduction

In a previous report,[1] the mechanism of hydrogen evolution reaction (h.e.r.) was examined on aluminum electrodes which were essentially free of "spontaneous" surface oxide.[2] In the present investigation the mechanism of h.e.r. has been studied on aluminum electrodes covered by a "natural" surface oxide in solutions (pH $\simeq$5.5) in which the aluminum oxide is thermodynamically stable.[2] The oxide-covered aluminum has purposely not been called passive aluminum here, since oxide films on valve metals[3] are not passive in the sense of oxide films, *e.g.*, on Ni,[4] which are noninsulating.

There are few previous investigations on the mechanism of h.e.r. on oxide-covered electrodes,[5-8] probably because the difficulties involved in the determination of reliable kinetic parameters on these electrodes are considerable,[8] owing to rather pronounced irreproducibility from one electrode to another.[8-10] However, it is still possible to draw unambiguous mechanistic conclusions from the general magnitude of the various kinetic parameters, without conceding precise quantitative significance to the data, as will be attempted. An additional difficulty associated with the electrode processes on oxide-covered electrodes is the interpretation of anomalous transfer coefficients.[5-8,11]

II. Experimental Section

The electrochemical measurements were carried out in an aqueous solution which was 1 M in CH_3COOK and 0.22 M in CH_3COOH and had pH $\simeq$5.5. Preelectrolysis was purposely not carried out since it was observed in a previous study[1] that in acetate solutions, preelectrolysis tends to produce rather than remove impurities. All other experimental procedures were similar to those used in other modern work on electrode kinetics[12-16] and in our previous closely related study.[1] Preparation of the working electrode surface, however, was modified in the present investigation. After the chemipolishing, etching, washing, etc., sequence,[1] the electrodes were either exposed to air for a few days or were left in distilled water (which was not deaerated) for several days so that the electrode surface acquired a "spontaneous" oxide. The measurements to be reported here were obtained in descending direction of current density or temperature, unless stated otherwise, since it was observed that data in the descending direction were more reproducible than those in the ascending direction. This is probably because the electrode becomes rapidly "conditioned" at higher current densities or temperatures by achieving either a steady-state contamination[17] or a "steady-state" hydration which

(1) A. K. Vijh, *J. Phys. Chem.*, **72**, 1148 (1968).
(2) M. Pourbaix, "Atlas D'Equilibres Electrochimiques," Gauthier-Villars and Co., Paris, 1963, p 168.
(3) L. Young, "Anodic Oxide Films," Academic Press, New York, N. Y., 1961.
(4) K. J. Vetter, "Electrochemische Kinetik," Springer, Berlin, 1961; see English translation by Academic Press, New York, N. Y., 1967.
(5) A. C. Makrides, *J. Electrochem. Soc.*, **113**, 1158 (1966).
(6) A. N. Frumkin, *Discussions Faraday Soc.*, **1**, 57 (1947).
(7) J. Weiss, *ibid.*, **1**, 68 (1947); J. Kunze, *Corr. Sci.*, **7**, 273 (1967).
(8) R. E. Meyer, *J. Electrochem. Soc.*, **107**, 847 (1960).
(9) A. C. Makrides, *ibid.*, **109**, 977 (1962).
(10) J. N. Butler and M. Dienst, *ibid.*, **112**, 226 (1965).
(11) A. C. Makrides, *ibid.*, **113**, 1158 (1966).
(12) M. Salomon, Ph.D. Thesis, Ottawa, Canada, 1964.
(13) J. J. MacDonald and B. E. Conway, *Proc. Roy. Soc.*, **A269**, 419 (1962).
(14) B. E. Conway and M. Dzieciuch, *Can. J. Chem.*, **41**, 21, 38, 55 (1963).
(15) J. O'M. Bockris, H. Wroblowa, E. Gileadi, and B. J. Piersma, *Trans. Faraday Soc.*, **61**, 2531 (1965).
(16) A. K. Vijh and B. E. Conway, *Chem. Rev.*, **67**, 623 (1967).
(17) G. J. Hills, informal remarks in a session of the Electrochemical Society Symposium held in Toronto, Canada, 1964.

would tend to restrict it to a certain narrow range of catalytic activity.

III. Results

The "spontaneous" oxide exhibited a dc resistance in the anodic direction which gave rise to a voltage drop of *ca.* 0.5 V at an anodic current density of 7.95×10^{-5} A cm^{-2} (or *ca.* 0.63 V at 1 A cm^{-2}). This dc resistance would be equivalent to a thickness[18] of 6 Å if the "spontaneous" barrier oxide is assumed to be composed of amorphous Al_2O_3. When this electrode is immersed in the experimental solution at about 55°, it would acquire a layer of protective, nonbarrier, hydrated oxide, the thickness of which may, very roughly, be estimated to be less than[19] 2000 Å by ignoring any specific features that the hydration reaction may exhibit with respect to the anions in the solution.[20] This hydrated oxide probably consists of, by anology with the case of pure water, some ratio of amorphous oxide, bochmite and bayerite.[19]

1. Tafel Parameters. Since the values of the Tafel parameters were strongly dependent on the time of polarization at a given current density, as well as on the general procedure of obtaining the Tafel plots, four "different" methods were tried for obtaining the Tafel parameters and the results are given below.

(*a*) *Quasi Steady-State Method.* In this procedure, the value of electrode potential after approximately 5 sec was recorded. This time is rather arbitrary but is probably sufficient for charging processes to proceed to completion; this length of polarization, however, probably does not (?) result in any profound changes of the electrode surface. The results were reasonably reproducible on a given electrode; *e.g.*, the rate at a given potential could be reproduced within ±20%. The Tafel slopes thus obtained are comparable to ones obtained from the slow portion of an open-circuit emf decay curve.[21] Similar procedures have been used[22] in cases where drastic surface changes are produced by the polarization process. Tafel plots obtained on a given electrode at various temperatures are shown in Figure 1 and the data have been summarized in Table I.

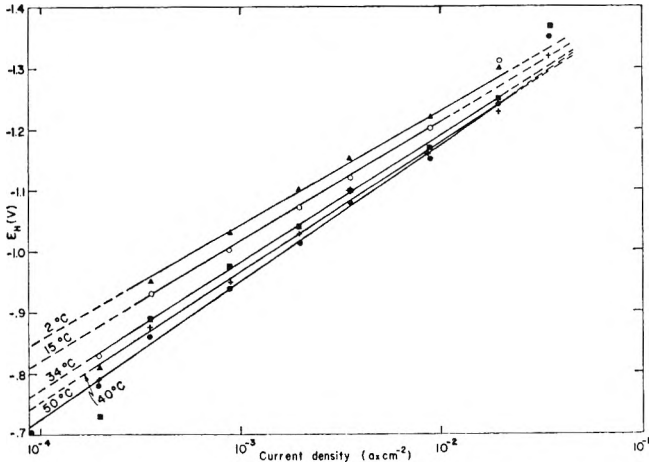

Figure 1. Galvanostatic Tafel plots for h.e.r. on oxide-covered aluminum electrodes obtained by quasi-steady-state procedure at the indicated temperatures.

Table I

Temp, °C	b, V	$-\log i_0$ (i_0, A cm^{-2})	a, V	α	H^*, kcal mol^{-1}
50	0.224	7.23	1.621	0.286	10.66
40	0.212	7.55	1.603	0.293	10.80
34	0.208	7.72	1.606	0.293	10.82
15	0.196	8.18	1.605	0.291	10.74
2	0.187	8.57	1.604	0.292	10.77

(*b*) *From Open-Circuit Emf Decay.* In Figure 2, electrode potential–log (time) relations obtained from the relevant portions[21] of open-circuit emf decay profiles have been presented. The data were obtained by following the emf decay on a recorder; they were also checked manually. In the absence of a significant pseudo-Faradaic process, the slopes of these lines, *i.e.*, $dE/d \log t$, have the same significance as the Tafel slopes[21] if the decays are triggered from high current densities (*ca.* $\geq 1 \times 10^{-3}$ A cm^{-2}). Tafel slopes are, again, higher than $2.3 \times 2RT/F$. Value of exchange current density, i_0, obtained by this method[21] is *ca.* 10^{-9}

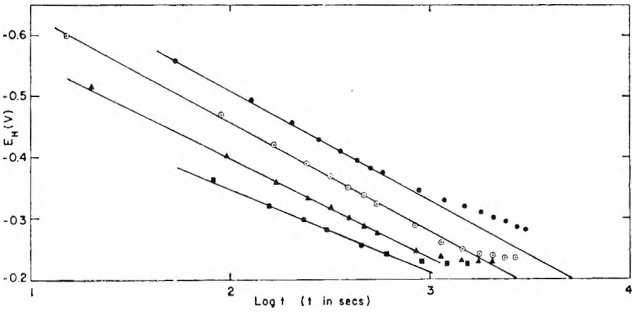

Figure 2. Plots of electrode potential E *vs.* log t (t in sec), obtained from slow portions of open circuit emf decay profiles (*e.g.*, Figure 9b at 23°). "Steady-state" polarization prior to the decay. Electrode potentials and corresponding current density prior to the decay and the b values on the subsequent decays are as follows: ■, $E = -1.305$ V, $i = 3.67 \times 10^{-2}$ A cm^{-2}, $b = 0.133$ V; ▲, $E = -1.227$ V, $i = 7.35 \times 10^{-3}$ A cm^{-2}, $b = 0.160$ V; ⊙, $E = -1.205$ V, $i = 3.67 \times 10^{-3}$ A cm^{-2}, $b = 0.176$ V; ●, $E = -1.188$ V, $i = 1.62 \times 10^{-3}$ A cm^{-2}, $b = 0.180$ V.

(18) W. J. Bernard and J. W. Cook, *J. Electrochem. Soc.*, **106**, 643 (1959); W. J. Bernard and J. J. Randall, Jr., *ibid.*, **107**, 483 (1960).

(19) R. K. Hart, *Trans. Faraday Soc.*, **53**, 1020 (1957).

(20) W. J. Bernard (Sprague Electric Co.), private communication.

(21) E. Gileadi and B. E. Conway in "Modern Aspects of Electrochemistry," Vol. 3, J. O'M. Bockris and B. E. Conway, Ed., Butterworth and Co. Ltd., London, 1964, Chapter V.

(22) G. Okamoto, M. Nagayama and N. Sato in Proceedings of the Eighth CITCE Meeting (Madrid, 1958), Butterworth and Co. Ltd., London, 1958, p 72; see also discussion of this paper.

A cm^{-2}. If the $dE/d \log t$ is plotted against the initial polarization potential (*i.e.*, potential before the commencement of the decay), a straight line is obtained (Figure 3). From Figure 3, it may be concluded that

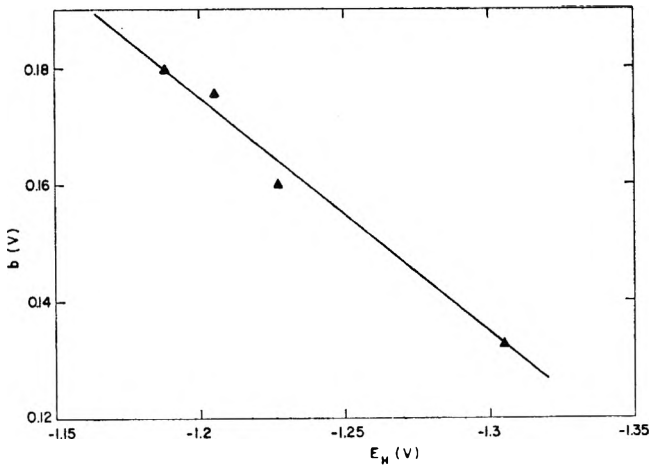

Figure 3. Plot of steady-state polarization potential (before the commencement of the open circuit decay) *vs.* b values obtained from the subsequent decay profiles; temperature 23°.

the higher the initial polarization potential, the lower the "Tafel" slope obtained from the emf decay curve, till a limitingly lower value, $2.3 \times 2RT/F$, is obtained, thus suggesting some "activation" of the electrode surface at higher cathodic potentials (*cf.* 4).

(*c*) *From Transient Potentials.* Tafel plots were also obtained by plotting the transient highest potential reached in the overshoot observed on galvanostatic cathodic charging against the logarithm of corresponding current density used in the transient. A typical plot is shown in Figure 4 (triangles). This procedure, though obviously questionable, has nonetheless one important advantage, namely, that it refers to the potential–log (rate) relation obtained on a "virgin" aluminum (oxide) electrode surface *before* it is modified by the very act of hydrogen evolution. The value of Tafel slope, b, obtained is $2.3 \times 3RT/F$ at room temperature and that of exchange current density, i_0, is *ca.* 10^{-10} A cm^{-2}.

(*d*) *"Steady-State" Tafel Parameters.* A typical "steady-state" Tafel plot (change of potential less 1 mV per 500 sec) has also been shown in Figure 4 (circles). The Tafel slope obtained is 0.11 ± 0.025 V and a typical value of the (apparent) exchange current density is *ca.* 10^{-15} A cm^{-2}. An *"activation"* (*i.e.*, increased rate at a given potential) of the initial electrode surface, after long polarizations required for the steady-state (*ca.* 30–60 min), may be noted in Figure 4.

Quantitative significance of b and i_0 obtained by this procedure is quite uncertain since the nature of electrode surface after long cathodic polarization is completely undefined.

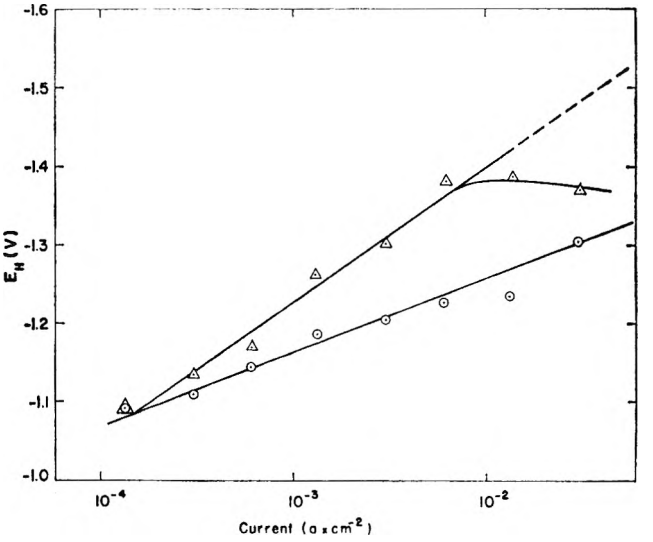

Figure 4. Typical galvanostatic Tafel plots (23°) obtained by "transient" method (△) and the steady-state method (⊙) on the same electrode: decreased electrode potential (at a given current density) and decreased Tafel slope caused by long cathodic polarization (30 to 60 min) may be noted.

2. Temperature Dependence of Tafel Parameters and Rest Potentials. A plot of $\log i_0$ *vs.* $1/T$, obtained from the data in Figure 1, has been presented in Figure 5. The slope of the straight line in Figure 5 gives an apparent heat of activation, ΔH^*, for the h.e.r. on oxide-covered aluminum in acetate solutions (pH 5.5). It may be noted that the *real* heat of activation cannot be calculated since the work functions of the oxide-covered aluminum is unknown.[23] The value of ΔH^* obtained from Figure 5 is 11 kcal mol^{-1}.

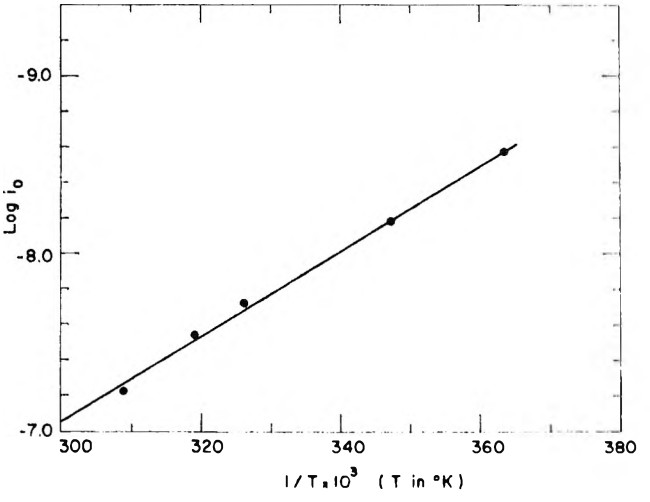

Figure 5. Plot of $\log i_0$ *vs.* $1/T$ (T in °K). The primary data from which this graph has been deduced are contained in Figure 1. The value of apparent heat of activation, ΔH^* obtained from this plot is 11 kcal mol^{-1}.

(23) B. E. Conway, "Theory and Principles of Electrode Processes," The Ronald Press Co., New York, N. Y., 1965.

The value of a in the equation, $\eta = a - b \log i$, is virtually constant (1.613 ± 0.009 V) at all temperatures (Table I). This implies that $(\Delta H^* - \alpha\eta)$ is equal to zero when the rate is 1 A cm^{-2}, in the temperature range 2–50°. This would offer an alternative way of calculating ΔH^* at a given temperature, for every one of the temperatures studied. The values obtained are shown in Table I. The value of ΔH^* is close to 11 kcal mol^{-1}, as would be expected since experimental α values have been used, and, like α values themselves (Table I), is *independent* of temperature. The independence of ΔH^* from temperature would also be suggested by lack of curvature in Figure 5. When α is independent of temperature, b must increase linearly with increasing temperature,[24] as indeed is observed and is shown in Table I.

In Figure 6, open-circuit rest potential values at various temperatures have been plotted against $1/T$, where T is in absolute degrees. The values of rest potential obtained in the descending direction of temperature fall on a straight line. Data obtained in the ascending direction of temperature, again, seem to be a bit erratic. An estimation of an apparent heat of activation from Figure 6 by an empirical procedure

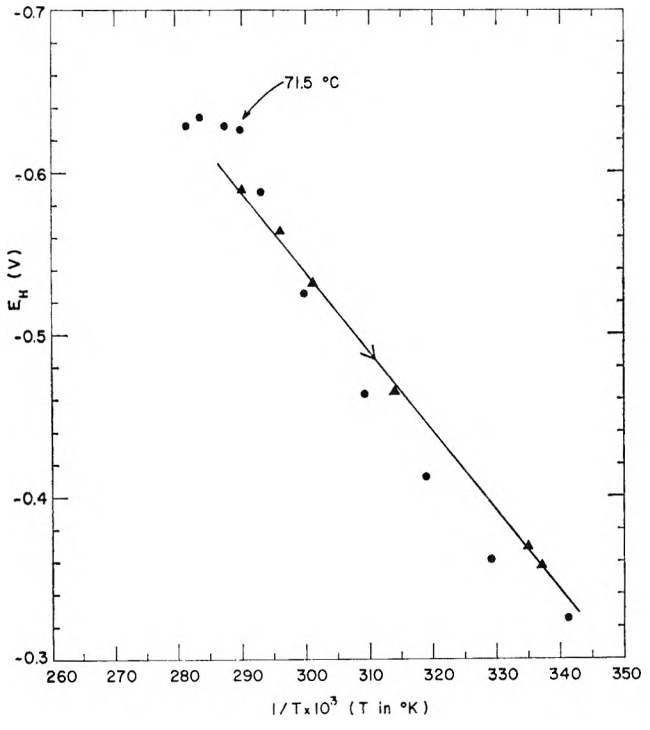

Figure 6. Plot of rest potentials (▲, descending direction of temperatures, T; ●, ascending direction temperatures, T) *vs.* $1/T$ (T in °K).

described previously,[1] again, yields a value close to 11 kcal mol^{-1}.

3. Galvanostatic Cathodic Charging Transients. Galvanostatic charging curves,[21] in the cathodic direction, were obtained for a wide range of $(i \times t)$, where i is the charging current density and t is the duration of the transient (Figure 7). No arrests or inflexions were observed, thus suggesting that h.e.r. probably proceeds on the aluminum (oxide) electrode *without significant steady-state coverage by adsorbed hydrogen.*

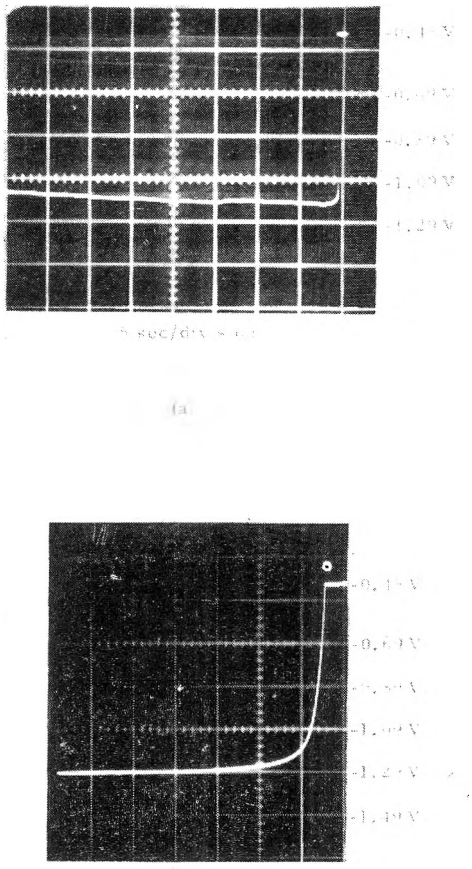

Figure 7. (a) Slow cathodic charging curve; charging current density = 3.2 × 10^{-4} A cm^{-2}; temperature = 50°; slight initial upsurge ("overshoot") of potential may be noted; this potential upsurge was much more pronounced at higher charging current densities and was followed, together with the subsequent relaxation curve, on a recorder. (b) A typical fast cathodic charging curve: charging current density = 1.44 × 10^{-3} A cm^{-2}; temperature 50°; C–V profile shown in Figure 8 was calculated from a charging curve of this type. An "overshoot" is observed on such a charging curve if the time scale is slower by about 1000 times (*cf.* Figure 7a). *Note*: No arrests or inflexions were observed over a wide range of (charging current density × time of full trace sweep) values.

In Figure 7b, a fast-charging curve has been depicted. A profile depicting the differential capacity (C)–electrode potential (V) relation, calculated from Figure 7b, has been shown in Figure 8. Absence of any pseudocapacity may be noted here.

(24) J. N. Agar, *Discussions Faraday Soc.*, 1, 81 (1947).

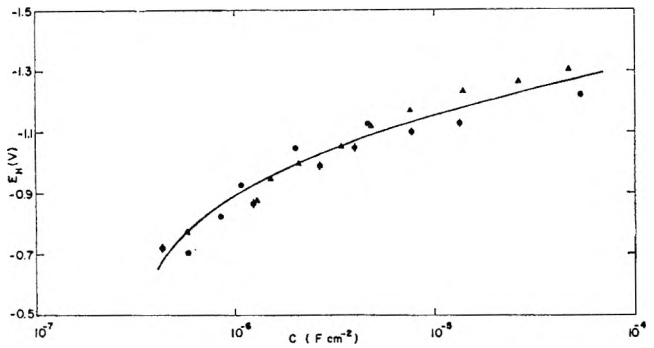

Figure 8. Differential capacity (C)–electrode potential (V) profile calculated from a fast, galvanostatic cathodic charging curve at 50° (*e.g.*, Figure 7b); different points refer to different values of charging current density.

4. Open-Circuit Emf Decay Profiles. If the "steady-state" (time of polarization = 2 min) electrode potential before the commencement of the open-circuit emf decay is fairly cathodic (*ca.* > −1.2 V), an arrest is observed in the subsequent profile (Figure 9a). This would preliminarily suggest an open-circuit desorption of possible adsorbed intermediates (*i.e.*, H in the present case). An attempt has been made to calculate a C–V curve (Figure 10) from Figure 9a, by combining it with the results[1,21,23] in Figure 1. In Figure 10, a capacity maximum is observed with C value equal to 465 μF cm^{-2} (*apparent* area). At this point it is important to mention[25] that the real surface area of hydrated aluminum oxide deposited on aluminum by dipping it in boiling water for 5 min is 40 times the real area of the substrate metal. In the present case, though such a drastic change in area is unlikely (since our temperature was below 55°), an appreciable increase (5 to 10 times) may, however, still be expected. From these considerations, it may be concluded that the differential capacity per cm^{-2} of *real* electrode area, associated with the capacity maximum in Figure 10, is of the order of double layer capacity. Hence absence of any pseudocapacity, at least any significant amounts of it, may again be concluded. It may be mentioned that the pseudocapacity corresponding to a complete electrode coverage by the adsorbed H, under Langmuir adsorption conditions (Temkin adsorption may be excluded from the fact that the capacity maximum in Figure 10 occurs over only a narrow range of potentials), would be expected[21] to be *ca.* 1×10^4 μF cm^{-2} assuming a roughness factor of about 6 for the hydrated oxide surface.

A numerical integration of the peak in Figure 10 would give charge, Q, associated with the arrest in Figure 9a. The value of Q thus obtained is 16 μC cm^{-2}. This value of Q is also obtained by numerical integration of the C–V profile (Figure 8) obtained from the charging curves, over the electrode potential range −0.9 to −1.3 V. This value of Q excludes the possibility of electrode being substantially covered by adsorbed H,

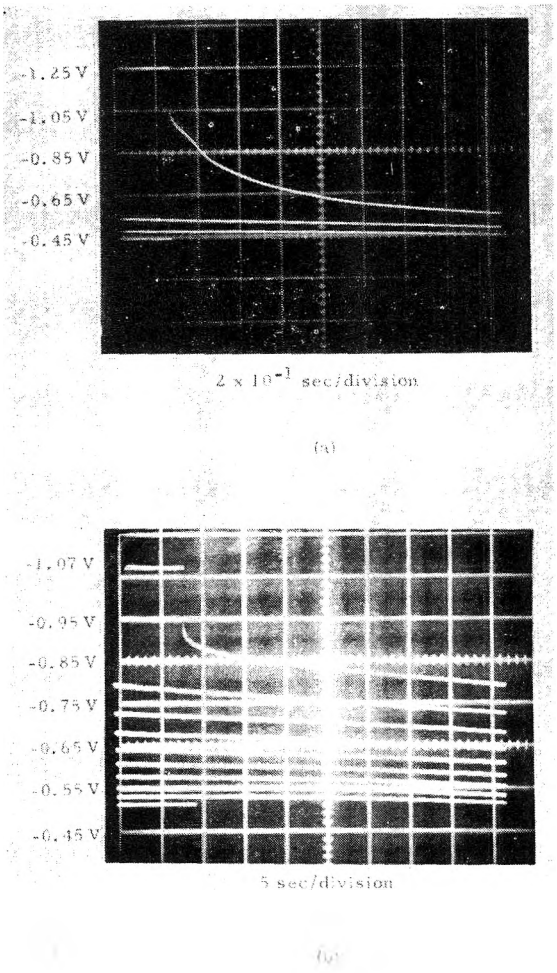

Figure 9. (a) An open-circuit profile triggered from high cathodic electrode potentials; an arrest may be noted; temperature is 50°; time of galvanostatic polarization prior to the commencement of the decay is equal to 2 min. (b) An open-circuit profile triggered from lower cathodic electrode potentials; temperature is 50°; time of galvanostatic polarization prior to the commencement of the decay is 2 min; the profile recorded on a slow time scale is purposely shown here to give some idea of the slow emf decays which were followed on a recorder and from which Figure 2 and thence Figure 3 were obtained.

during steady-state electrolysis. It may be of interest to note that the estimated value of Q for complete electrode coverage, by comparison with the case of smooth platinum,[26] would be 1260 μC cm^{-2} for an assumed roughness factor of 6. This method of obtaining Q is highly approximate. However, the observed Q is less than the Q estimated for complete coverage, by *two orders of magnitude.* Any errors in Q are not likely to change the conclusion that the electrode is not covered by significant amounts of adsorbed H during steady-state electrolysis.

Typical emf decay profiles obtained from a lower prior "steady-state" cathodic potential do not show any

(25) R. S. Alwitt, *J. Electrochem. Soc.*, 114, 843 (1967).
(26) P. Stonehart in "Power Sources," D. H. Collins, Ed., Pergamon Press, New York, N. Y., 1967, p 514.

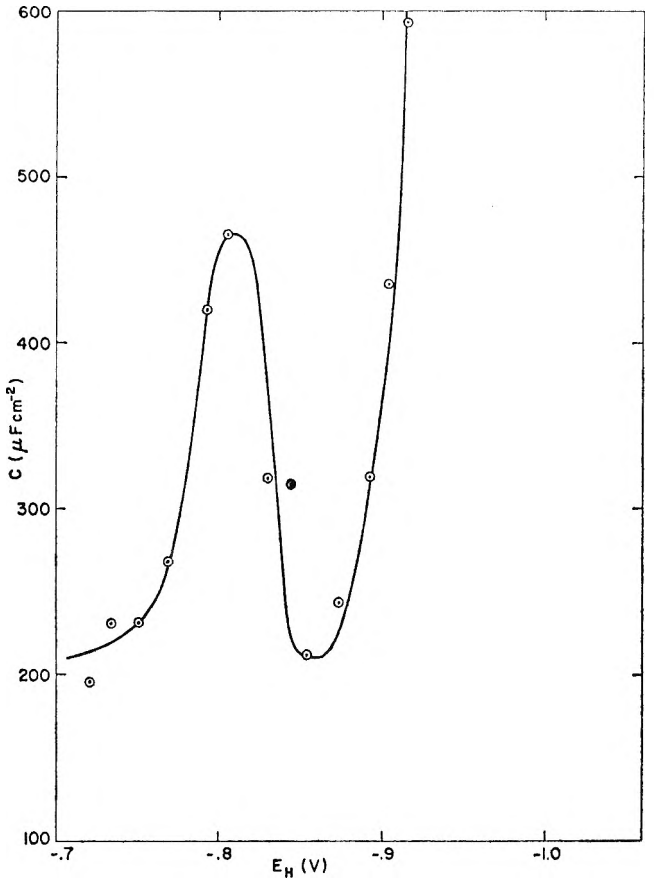

Figure 10. A C–V profile obtained from an open-circuit decay curve triggered at high cathodic potentials (*e.g.*, Figure 9a) by combining with the results reported in Figure 1.

arrests (Figure 9b), even on very fast time scales (*e.g.*, 500 μsec/cm) of the oscilloscope.

IV. Discussion

1. Anomalous Tafel Slopes. The values of Tafel slopes greater than $2.3 \times 2RT/F$ may be regarded as anomalous since the usual procedures (*i.e.*, quasiequilibrium or steady state) would always yield slopes equal to or less than $2.3 \times 2RT/F$. This statement is generally true both for Langmuir and Temkin conditions of adsorption,[12,21,23,27] except for a certain case[27] to be discussed below in the section on reaction mechanism. Experimentally, it has been observed that the presence of surface films, presumably semiconducting, increases the values of the Tafel slopes obtained before surface activation both for the anodic[11,13,14,16,22] and the cathodic reactions.[5–8,11]

Several theoretical attempts have been made to explain anomalously high Tafel slopes and have been discussed elsewhere.[16,28] Here the experimental values of Tafel slopes would be interpreted on lines somewhat similar to those of Meyer.[8] The complete rate equation for the h.e.r. in acidic solutions, relating current i to the total overpotential across metal–(oxide)–solution interface, η, may be written as[23]

$$i = \frac{kTZF}{h}(C_{H^+})_b(1-\theta) \times \exp -\frac{\Delta G^{0\ddagger}}{RT} \exp -\frac{\beta(\eta-\eta_f)}{RT} ZF$$

where concentrated solutions ($\geq 1\ N$) have been assumed. The various symbols have the usual significance;[23] η is the total overpotential and η_f is the overpotential across the film.

$$i = \text{constant} \times \exp -\frac{\beta(\eta-\eta_f)ZF}{RT}$$

In general, η_f, the potential drop across the film of given thickness and properties would be some function of the total overpotential.

$$\ln i = \text{constant}' - \frac{\beta(\eta-\eta_f)ZF}{RT}$$

or

$$(\eta-\eta_f) = \text{constant}'' - \frac{RT}{\beta ZF}\ln i$$

$$\partial\eta/\partial \log i = -\frac{2.3 \times RT}{\beta ZF(1-\partial\eta_f/\partial\eta)} = \text{Tafel slope}$$

In the absence of a film and assuming the usual values for β ($= 0.5$) and Z ($= 1$), the Tafel slope would be equal to 0.118 V at room temperature, as expected from theory. It is obvious that the present experimental value of α would be obtained if $\eta_f = 0.42\eta$. This presentation, in essence, is similar to that of Meyer. However, formally, this does not involve the premise of Meyer's that *two* processes, *i.e.*, transport of electrons in the film and protons across the double layer, simultaneously, control the overall kinetics. Meyer[8] tacitly implies two activation barriers of equal "height" (in series) for one act of the overall reaction; this, however, is quite unlikely. In the foregoing discussion, it has been assumed that the value of the *true* symmetry factor, β, is always 0.5. This assumption has been demonstrated to be valid in previous publications.[23,29–31]

2. Cathodic Activation. According to Vetter,[4] cathodic activation may be achieved at certain current densities on oxide-covered electrodes of some metals, including aluminum. This may be concluded to be true for the present case from Figure 4, which shows

(27) J. G. N. Thomas, *Trans. Faraday Soc.*, **57**, 1603 (1961).
(28) A. K. Vijh and B. E. Conway, *Z. Anal. Chem.* (Anniversary issue in honor of Prof. M. Von Stackelberg), **224**, 160 (1967).
(29) D. B. Matthews, Ph.D. Thesis, University of Pennsylvania, 1965.
(30) N. S. Hush, *J. Chem. Phys.*, **28**, 962 (1958).
(31) J. O'M. Bockris and D. B. Matthews, *Proc. Roy. Soc.*, **A292**, 479 (1966).

that activation results in lowering of Tafel slope, and the polarization values for a given rate of h.e.r.

It may be mentioned that the cathodic activation is also suggested by the fact that (Figures 2 and 3) the higher the initial polarization current density prior to the open circuit emf decay, the lower is the potential (even lower than the quasi-steady rest potential) to which the subsequent decay curve descends down. If the emf decay curve descends down to potentials lower than the quasi-steady rest potential, profound surface changes (activation?) must be inferred; in the limiting case, this activation would be expected to be so pronounced that the decay curve may even approach the reversible hydrogen potential, although only transiently.

3. Electrode Coverage. It has been shown in the section on Results [III (3) and III (4)] that the h.e.r. proceeds on oxide-covered electrodes *without* significant concentration of adsorbed H on the electrode. This would tend to exclude radical-ion and recombination as the possible rate-determining steps.[1,12,21,23,27,29,32]

4. Reaction Mechanism. The Tafel slopes observed on oxide-covered aluminum (Figures 1, 2, 4; Table I) are, most likely, values of $2.3 \times 2RT/F$ which have been modified by the presence of oxide. This observation, when combined with lack of significance concentration of adsorbed H, would uniquely give initial discharge step as the likely rds. Discussion of other possible mechanisms[33,34] and related theory has been given previously.[1]

The exchange current densities and apparent heats of activation observed in the present investigations are quite consistent with the initial discharge as the rds.[1] Independence of α from temperature (Table I) would exclude the importance of entropy and adsorption effects[24] thus suggesting initial discharge as the rds. The fact that Al_2O_3 is a poor catalyst for the gas phase chemisorption of H_2[35] would strongly emphasize that the overall reaction is controlled by the "slow" initial discharge. With the value of exchange current density, i_0, 10^{-8} A cm^{-2} approximately, Al (oxide) would have to be an *extremely* good catalyst for the adsorption of hydrogen (*e.g.*, W) for initial discharge to be excluded as the probable rds.[23,29,36]

The various electrocatalytic relations[23,29,36] cannot be applied to the present case since the work function of the oxide-covered aluminum is unknown.

It has been suggested by Thomas[27] that if a "fast" discharge step is followed by a "slow" recombination under conditions of moderate coverage (Temkin region) at high current densities, a Tafel slope equal to $2.3 \times 3RT/F$ may sometimes be obtained. This mechanism is unlikely in the present case since no Temkin behavior is observed in the C–V profiles (Figure 10). Furthermore, a significant, though not complete, electrode coverage by adsorbed H required by this mechanism is not observed. Finally, low exchange current densities and absence of a 30-mV slope or a limiting current excludes this mechanism for the present case.[37]

5. Relation to Rectification. In Figure 11, a values (of the constant in the empirical form of the Tafel equation, $\eta = a - b \log i$) obtained for the h.e.r. on aluminum in solutions of various pH values have been plotted against the corresponding pH. The experimental points at pH 0.37, 2.4, and 4.4 refer to aluminum electrodes in the absence of oxide.[1] The point at pH 5.5 refers to the electrode with oxide (*i.e.*, *ca.* 0.63 V oxide) (*cf.* 2). The dashed line joins the three points at lower pH and shows the value of a that would have been obtained at pH 5.5, if no barrier oxide were present. It is suggested that this increase in the a value is some indication of the potential drop across the film in the direction of *cathodic* polarization, when the rate of h.e.r. is 1 A cm^{-2}. It is important to note that the increased a value is *not* due to the decreased effective area of the electrode; *i.e.*, the h.e.r. is not proceeding only on flaws since the b value is *ca.* 0.2 V at room temperature. It seems that the h.e.r. is proceeding on the bulk of oxide in this particular case since the a value (at room temperature) has been deduced from Figure 1 (*i.e.*, *before* the activation of the surface). It may be concluded from Figure 11 that the potential drop across the thin

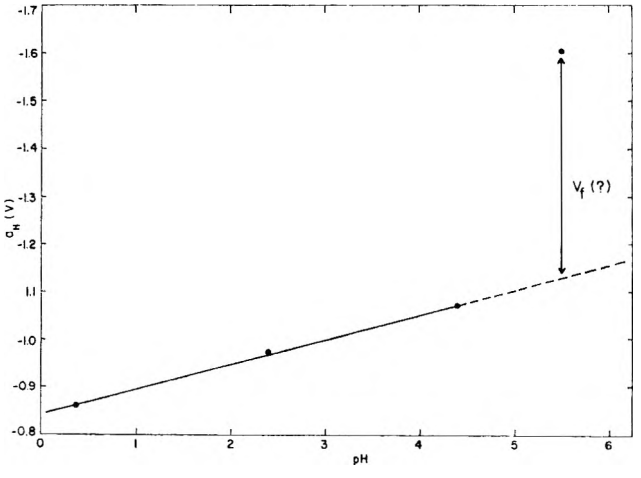

Figure 11. Plot of a values (in the Tafel equation, $\eta = a - b \log i$) for the h.e.r. on Al in solutions of various pH values; a values at pH 0.37, 2.4, and 4.4 have been obtained from ref 1 and refer to the electrode, which, presumably, has no oxide on it; a value at pH 5.5 refers, it is believed, to the electrode covered by "spontaneous" oxide. Here $(\partial a/\partial \mathrm{pH})_i$ has the significance of a reaction order derivative, $(\partial \eta/\partial \mathrm{pH})_i$, when the rate, i, is 1 A cm^{-2} (see ref 1).

(32) R. Parsons, *Trans. Faraday Soc.*, **47**, 1332 (1951); **54**, 1053 (1958).

(33). J. Horiuti in "Transactions of the Symposium on Electrode Processes," E. Yeager, Ed., John Wiley and Sons, Inc., New York, N. Y., 1961; see also discussion on this paper.

(34) G. J. Hills and D. R. Kinniburgh, *J. Electrochem. Soc.*, **113**, 1111 (1966); see also discussion on this paper.

(35) D. O. Hayward and V. T. M. Trapnell, "Chemisorption," Butterworth Inc., Washington, D. C., 1964.

(36) B. E. Conway and J. O'M. Bockris, *J. Chem. Phys.*, **26**, 632 (1957).

(37) S. Schuldiner, *J. Electrochem. Soc.*, **114**, 916 (1967).

barrier film is almost the same both in the anodic and cathodic direction of polarization. That would suggest that very thin films of oxide formed *spontaneously* probably do not rectify, at least, not before activation (flaw production?) of the surface has been achieved by some initial cathodic polarization. Here, it has been assumed that both Faradaic rectification (at film–solution interface)[38] and any possible rectification at the metal–oxide interface are negligible and do not enter into the argument. This behavior may be contrasted with that of anodically grown thicker films which are known to rectify when placed in metal–oxide–electrolyte configuration.[39] Here, an implied conclusion is that thin films which are probably continuous (*i.e.*, without flaws) before cathodic activation do not rectify whereas thicker films of the same oxide do rectify and hence[39] must have flaws at which the h.e.r. is sustained without developing an appreciable potential drop across the film in the cathodic direction of polarization. Most of these conclusions are, obviously, quite tentative and would need much more elaborate investigations of the matters mentioned above.

Acknowledgments. The author wishes to acknowledge helpful discussions with Drs. Robert S. Alwitt and Glenn M. Cook of these laboratories and Dr. M. Salomon of NASA, ERL, Cambridge, Massachusetts. Thanks are also due to Mr. W. Hilchey, of Sprague Test Equipment Department, for assistance in calibration of the instruments.

(38) K. S. G. Doss and H. P. Agarwal, *J. Sci. Ind. Res. India*, **9B**, 280 (1950); see also *Proc. Indian Acad. Sci.*, **34A**, 263 (1951); **35A**, 45 (1952); also see ref 23.

(39) Symposium on "Electrolytic Rectification and Conduction Mechanisms in Anodic Oxide Films," P. F. Schmidt and D. M. Smyth, Ed., The Electrochemical Society Inc., New York, N. Y., 1967.

Electronic Properties of Some TCNQ Complexes[1]

by A. Rembaum, A. M. Hermann, F. E. Stewart, and F. Gutmann

Polymer Research Section, Jet Propulsion Laboratory, California Institute of Technology, Pasadena, California 91103 *(Received June 13, 1968)*

A study of electrical properties of tetracyanoquinodimethane (TCNQ) complexes representing unit segments of nonconjugated as well as conjugated polymers is described. Corresponding studies with the analogous polymer complexes are presented. The model compounds chosen were a saturated donor 1,2-bis(4-pyridyl)-ethane and an unsaturated donor 1,2-bis(4-pyridyl)ethylene. Analyses are presented to substantiate the chemical structure. Spectrophotometric data are in agreement with previous results. Electron spin resonance studies show the triplet nature of the complexes, and rotational anisotropy in compressed pellets demonstrates orientation of molecules or crystallites during compression. Electronic transport properties including the first reported measurement of the Hall effect in TCNQ complexes are described. These measurements along with companion studies of conductivity and thermoelectric power indicate concentration of carriers of several orders of magnitude below that of the unpaired spins. The transport data presented are interpreted in terms of band theory.

I. Introduction

It was recently reported that certain heterocyclic salts exhibit an exceptionally high conductivity.[2,3] These compounds may be represented by the general formula $D^+(TCNQ^-)$ in which D is an aromatic molecule generally containing a nitrogen atom and $(TCNQ^-)$ symbolizes 7,7′,8,8′-tetracyanoquinodimethane in the form of a paramagnetic radical anion. Neutral TCNQ molecules may also take part in the complex in which case the electrical conductivity is increased by several orders of magnitude. A number of the TCNQ complexes exhibit room temperature conductivity varying from about 10^{-5} up to about 1 ohm^{-1} cm^{-1}, *i.e.*, the highest conductivity of organic crystals known to date. It was also shown recently[2b] that polymeric analogs of the TCNQ salts can be prepared. One such complex, copoly(styrene),1-butyl-2-vinylpyridinium $(TCNQ^-)$ TCNQ had a conductivity of 10^{-3} ohm^{-1} cm^{-1} and these polymeric

(1) This paper represents one phase of research performed by the Jet Propulsion Laboratory, California Institute of Technology, sponsored by the National Aeronautics and Space Administration, Contract NAS7-100.

(2) (a) R. G. Kepler, *J. Chem. Phys.*, **39**, 3528 (1963); (b) J. H. Lupinski and K. D. Kopple, *Science*, **146**, 1038 (1964).

(3) L. R. Melby, R. J. Harder, W. R. Hertler, W. Mahler, R. E. Benson, and W. E. Mochel, *J. Amer. Chem. Soc.*, **84**, 3374 (1962).

complexes could be cast from solution as homogeneous films. The mechanism of electronic transport in the above monomeric or polymeric salts is not well understood. In this report a study of the electrical properties of TCNQ complexes representing unit segments of nonconjugated as well as conjugated polymers is described.

The following two model compounds were chosen: a saturated donor 1,2-bis(4-pyridyl)ethane, and unsaturated donor 1,2-bis(4-pyridyl)ethylene. These two model compounds will be referred to as D_s and D_u, respectively.

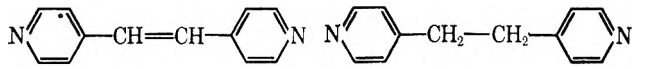

1,2-bis(4-pyridyl)ethylene D_u 1,2-bis(4-pyridyl)ethane D_s

Both D_s and D_u could be incorporated into a polymeric chain by means of the reaction[4]

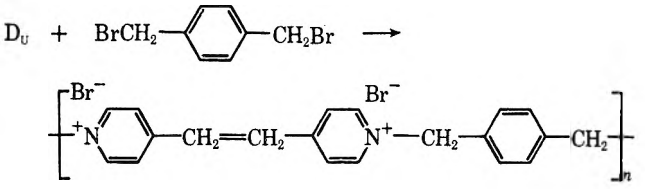

where n represents the number of unit segments. D_s reacted with p-dibromoxylene to yield an analogous polymer. These polymers when reacted with LiTCNQ will be designated by the symbols $D_u^{2+}(TCNQ^-)_2$ polymer and $D_s^{2+}(TCNQ^-)_2$ polymer, respectively. The polymers present the advantage of easier moldability and higher tensile strength than the corresponding monomeric analogs. Most of the electrical measurements were carried out on D_s or D_u mono- or diiodide salts after reaction of the latter with LiTCNQ or with a mixture of LiTCNQ and neutral TCNQ.

II. Experimental Section

1. Reagents. D_s was recrystallized from benzene (mp 122°). D_u was used as received (Aldrich) mp 153–155°. p-Dibromoxylene was recrystallized from benzene (mp 145–148°). All solvents were freshly distilled and TCNQ was used as received from the Dupont Co.

2. Preparation of Mono- and Bis-N-Methyl Pyridylium Derivatives of 1,2-Bis(4-Pyridyl)ethane. a. 1-(4-Pyridyl), 2-(4'-N-methylpyridylium iodide)ethane (D_sI). 1,2-Bis(4-pyridyl)ethane (0.01 mol = 1.84 g), dissolved in benzene (50 ml), was added dropwise to CH_3I (0.06 mol = 8.52 g) in benzene (10 ml). The mixture was heated while stirring to start the reaction, and the stirring continued for 1.5 hr at ambient temperature. It was then kept in the dark for approximately 4 hr. The light yellow microcrystals which had precipitated out were filtered off, washed with benzene, and dried *in vacuo*. *Anal.* Calcd for a monoiodide salt: I, 39.2. Found: I, 39.5.

b. 1-(4-Pyridyl), 2-(4'-N-methylpyridylium iodide)ethylene (D_uI). 1,2-Bis-(4-pyridyl)ethylene (0.01 mol = 1.82 g) was dissolved in benzene (50 ml) and added dropwise to CH_3I (0.06 mol = 8.52 g) in benzene (10 ml). The remaining procedure was identical with the previous example. *Anal.* Calcd for a monoiodide salt: I, 39.2. Found: I, 38.5.

c. 1,2-Bis(4-N-methylpyridylium iodide)ethane (D_sI_2). 1,2-Bis-(4-*N*-pyridyl)ethane (0.01 mol = 1.84 g) was dissolved in CH_3I (25 ml). The solution boiled for 8 hr while stirring and was kept in the dark at room temperature overnight. The white-yellow crystals were filtered off under suction, washed with ether, and dried *in vacuo*. *Anal.* Calcd for a diiodide salt: C, 35.91, H, 3.88, N, 5.98, I, 54.23. Found: C, 35.25, H, 3.6, N, 6.00, I, 53.1.

d. 1,2-Bis-(4-N-methylpyridylium iodide)ethylene (D_uI_2). 1,2-Bis-(4-pyridyl)ethylene (0.01 mol = 1.82 g) was dissolved in CH_3I (25 ml). The solution was boiled for 8 hr while stirring, then kept in the dark at room temperature overnight. The orange-yellow crystals were filtered off under suction, washed with ether, and dried *in vacuo*. *Anal.* Calcd for a diiodide salt: C, 36.04; H, 3.45; N, 6.02; I, 54.45. Found: C, 35.93; H, 3.45; N, 6.20; I, 53.9.

e. 1-(4-Pyridyl)2-(4'-N-methylpyridylium TCNQ⁻)-ethane ($D_s^+TCNQ^-$). 1-(4-Pyridyl),2-(4'-*N*-methylpyridylium iodide)ethane (0.00145 mol = 0.47 g) was dissolved by heating in 96% ethanol (10 ml) and dropwise added to a boiling solution of LiTCNQ (0.002 mol = 0.42 g) in ethanol (100 ml). LiTCNQ was prepared according to a described method.[3] The reaction was carried out under nitrogen. The mixture was cooled to room temperature in the dark, then kept at 0° for complete precipitation of the dark blue needles. The mixture was filtered under suction and the crystals were washed with ethanol and ether and dried *in vacuo*. *Anal.* Calcd: C, 74.41; H, 4.75; N, 20.83. Found: C, 73.55; H, 4.88; N, 20.43.

f. 1-(4-Pyridyl), 2-(4'-N-methylpyridylium TCNQ⁻)-ethylene ($D_u^+TCNQ^-$). 1-(4-Pyridyl), 2-(4'-methylpyridylium iodide)ethylene (0.0145 mol = 0.47 g) was dissolved in a mixture of 96% ethanol (10 ml) and H_2O (1 ml). The solution was added dropwise to a boiling solution of LiTCNQ (0.002 mol = 0.42 g) in ethanol (100 ml). This was followed by the procedure of the preceding sample. *Anal.* Calcd: C, 74.8; H, 4.27; N, 20.94. Found: C, 73.79; H, 4.52; N, 21.14.

g. 1,2-Bis(4-N-methylpyridylium TCNQ⁻)ethane ($D_s^{2+}(TCNQ^-)_2$. This was prepared by a procedure similar to that for the preceding sample and using

(4) A. Rembaum, W. Baumgartner, and A. Eisenberg, *J. Polymer Sci., B*, 6, 159 (1968).

an excess of LiTCNQ. *Anal.* Calcd: C, 73.29; H, 4.21; N, 22.50. Found: C, 74.63; H, 3.88; N, 23.32.

h. 1,2-Bis(4-N-methylpyridylium TCNQ⁻)ethylene $D_u^{2+}(TCNQ^-)_2$. The same procedure was used as for sample g. *Anal.* Calcd: C, 73.53; H, 3.90; N, 22.59. Found: C, 73.20; H, 4.33; N, 22.18.

i. Preparation of Complexes Containing Neutral TCNQ. Half a mole of neutral TCNQ was combined with 1 mol of each of the following: $D_s^+TCNQ^-$, $D_u^+TCNQ^-$, $D_s^{2+}(TCNQ^-)_2$, and $D_u^{2+}(TCNQ^-)_2$ by the procedure described below. To each of the iodides, D_sI, D_uI, D_sI_2, dissolved in hot ethanol were added simultaneously the calculated concentrations of LiTCNQ and neutral TCNQ dissolved by a mixture (1:1) of hot ethanol and acetonitrile. The operations were carried out in a nitrogen atmosphere. Precipitation began in each case while the mixture was still hot. After cooling, the products were filtered, washed with warm acetonitrile, ethanol, and ether, and dried *in vacuo*.

3. Preparation of Polymers and Their TCNQ Complexes. The polymers containing the model compounds in the chain have not been synthesized before. The kinetics of formation and properties of similar but aliphatic polymers, termed ionenes, are the subject of a separate publication.[4] The aromatic ionenes used in this study were prepared by reacting D_s or D_u with *p*-dibromoxylene in stoichiometric proportions in benzene or dimethylacetamide. Bromobenzene is also a convenient solvent for the polymerization reaction carried out at 100°. The precipitated polymers were filtered off, washed with benzene, and dried *in vacuo*, yield 98–99%. Analysis of polymer obtained by reaction of D_s with *p*-dibromoxylene: Calcd for a unit segment of $C_{20}H_{20}N_2$, Br_2: C, 54.0; H, 4.52; N, 6.25; Br, 35.61. Found: C, 53.10; H, 5.12; N, 6.32, Br, 32.31.

The polymer was soluble in water and decomposed on heating at 260–290°. Intrinsic viscosity in aqueous 0.1 *M* KBr = 0.21.

Analysis of Polymer Obtained by Reactions of D_u *with p-Dibromoxylene Calculated for a Unit Segment.* Calcd for $C_{20}H_{18}N_2Br_2$: C, 54.8; H, 4.05, N, 6.28; Br, 35.9. Found: C, 53.59; H, 4.73; N, 7.05; Br, 30.56. Intrinsic viscosity in aqueous 0.1 *M* KBr = 0.16. The TCNQ complexes were prepared by dissolving the polymers in 50% water–methanol mixtures, to which were added solutions of LiTCNQ in methanol. A mixed solvent, methanol–acetonitrile (20:80), was used for the preparation of polymeric salts with neutral TCNQ.

Analysis of Polymer Containing $D_s^{2+}(TCNQ^-)_2$ *Units.* Calcd for a unit segment of $C_{44}H_{28}N_{10}$; C, 75.80, H, 4.02, N, 20.1. Found: C, 75.01; H, 4.07; N, 19.45.

Analysis of Polymer Containing $D_u^{2+}(TCNQ^-)_2$ *Units.* Calcd for a unit segment of $C_{44}H_{26}N_{10}$: C, 76.1; H, 3.75; N, 20.2. Found: C, 76.25; H, 3.97; N, 19.5. The elemental analyses were carried out by means of a F & M model 185 CHN analyzer.

4. Spectrophotometric Data. Visible spectra of TCNQ complexes were determined by means of a Cary Model 14 Spectrophotometer in spectral grade acetonitrile as solvent. The analysis of the spectra yielded good agreement with previously published data.[3] As shown in Figure 1, the TCNQ radical anion absorbs

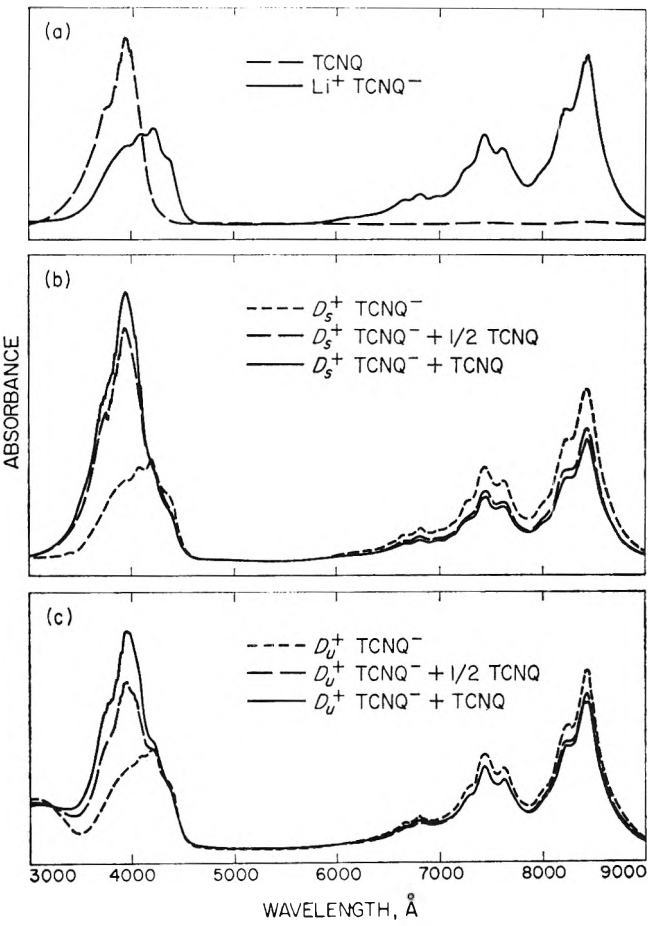

Figure 1. Visible absorption spectra (10^{-5} *M*) in acetonitrile.

strongly at 4200 Å (ϵ 24,300) and at 8420 Å (ϵ 43,300), while neutral TCNQ absorbs only at 3950 Å (ϵ 63,600). The intensity ratio of the 4200- and 8420-Å bands is approximately 0.57 for simple salts, and that of the 3950- and 8420-Å bands is approximately 2.0 for salts containing one neutral molecule of TCNQ per complex.

The spectrophotometric analysis agreed with the proposed radical anion-to-neutral acceptor ratio to within about 5%. However, the elemental analysis agreed, on the average, with the theoretical percentages of C, H, and N to about 1%.

5. Electrical Measurements. Conductivity measurements were made on 0.5-in. diameter cylindrical pellets in the absence of air. Pellets prepared under pressures between 20,000 and 100,000 psi had essenti-

ally identical conductivities. Electrical contact was made with vacuum-deposited gold electrodes. Using this technique, resistivity values could be reproduced within a factor of 2. Silver paste or platinum disk contact yielded much less reliable results. D_s^+-$(TCNQ^-)$ complexes were found to be unstable above 50°. However, complexes containing neutral TCNQ showed identical resistivity after heating at 90° for 24 hr.

In one case only, $(D_s^+TCNQ^-)$, was it possible to carry out measurements on a single crystal. The resulting activation energy, *viz.* 0.14 eV, was found to be the same (within experimental error) as that obtained with the compactions, *viz.* 0.13 eV.

The conductivity measurements were carried out in an evacuated glass cell containing a copper–constantan thermocouple. The glass cell was immersed in a dewar vessel containing the heat bath. Resistivity as a function of pressure was measured using vanadium alloy steel anvils of 0.25 in. contact diameter. The details of the apparatus were previously described.[5]

6. Electron Spin Resonance (Esr). Esr measurements were made by a previously reported procedure[6] on samples consisting of either small chips of compacted pellets, powdered complexes, or complexes dispersed in KCl. Pressure and grinding seemed to have no significant effect on the free spin concentration as derived from the esr intensity.

7. Seebeck Coefficient. The Seebeck coefficient was measured using a Keithley 610 BR electrometer. The sample temperature was varied by adjusting the flow of thermostatically controlled gaseous nitrogen past the sample. The thermal gradient ($\Delta T \sim 5°$) was achieved by variation of the currents through two heaters in physical contacts with the surfaces of the sample. Temperatures were measured by means of copper–constantan thermocouples connected to a Rubicon Model 2732 potentiometer.

8. Hall Effect. A schematic diagram of the Hall effect apparatus is shown in Figure 2. The bucking circuit allowed reduction of the misalignment voltage to the order of less than 0.5 mV. Resolution to some extent was dependent upon sample stability. In some cases, several days of waiting was required to achieve noise and drift levels low enough to measure mobilities of the order of 0.01 to 0.1 cm^2/V sec. The maximum magnetic field strength used was 6 kG. The VTVM employed was a Hewlett-Packard 412A or a Keithley Model 610A electrometer. An RC filter on the output of the VTVM decreased high frequency noise. The strip-chart recorder was a Varian Model G10. The accuracy of the apparatus was confirmed by the use of resistive mock-ups and an *n*-type germanium sample of known mobility as a reference.

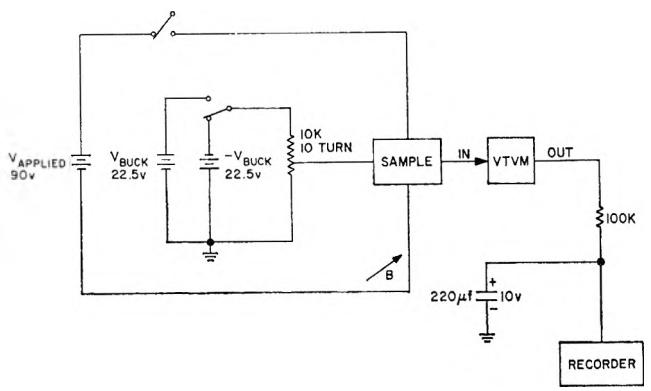

Figure 2. Schematic diagrams of the Hall apparatus.

III. Results

1. Resistivity (ρ) and Activation Energy (ϵ). The resistivities in ohm-centimeters and activation energies in electron volts of various TCNQ complexes (obtained from the equation $\rho = \rho_0 \exp(E/kT)$ over temperature intervals ranging from 77 to 300°K) are listed in Table I.

Table I: Resistivity (ρ) and Activation Energy (E) of TCNQ Complexes (E is Deduced from $\rho = \rho_0 \exp(E/kT)$)

	ρ at 25°, ohm cm	E, eV
$D_s^+TCNQ^-$	1.55×10^5	0.11
$D_s^{2+}(TCNQ^-)_2$	4×10^6	...
$D_s^{2+}(TCNQ^-)_2 \cdot \frac{1}{2}TCNQ$	4.7	0.04
$D_s^{2+}(TCNQ^-)_2TCNQ$	3.4	0.035
$D_s^{2+}(TCNQ^-)_2$ polymer	1.5×10^6	0.15
$D_s^{2+}(TCNQ^-)_2TCNQ$ polymer	92	...
$D_u^+TCNQ^-$ (polycrystalline)	1.1×10^4	0.13
$D_u^+TCNQ^-$ (single crystal)	...	0.14
$D_u^{2+}(TCNQ^-)_2$	2.1×10^5	...
$D_u^{2+}(TCNQ^-)_2TCNQ$	13	0.04
$D_u^{2+}(TCNQ^-)_2TCNQ$	3.8	0.035
$D_u^{2+}(TCNQ^-)_2$ polymer	5.2×10^5	0.15
$D_u^{2+}(TCNQ^-)_2TCNQ$ polymer	80	...

Average values are quoted with deviations being less than 30% for ρ and 10% for E. Such deviations are presumably due to variations in intergranular resistances.[7] The addition of neutral TCNQ dramatically lowers the resistivity and the activation energy presumably due to increased electron delocalization. The low activation energy of these latter complexes indicates the onset of metallic conduction.

The variation of resistivity with pressure of the $D_u^{2+}(TCNQ^-)_2TCNQ$ complex is shown in Figure 3. The curves were obtained on first increasing the pressure to 36 kbars then decreasing it to 1 kbar and repeating this procedure several times. Similar curves

(5) A. Rembaum, J. Moacanin, and H. A. Pohl, *Progr. Dielectrics*, 6, 41 (1965).

(6) F. E. Stewart and A. Rembaum, *J. Macrom. Sci.* (Chemistry) A1, 1143 (1967).

(7) R. G. Kepler in "Phonons and Phonon Interactions," T. A. Bak, Ed., W. A. Benjamin Inc., New York, N. Y., 1964, p 579.

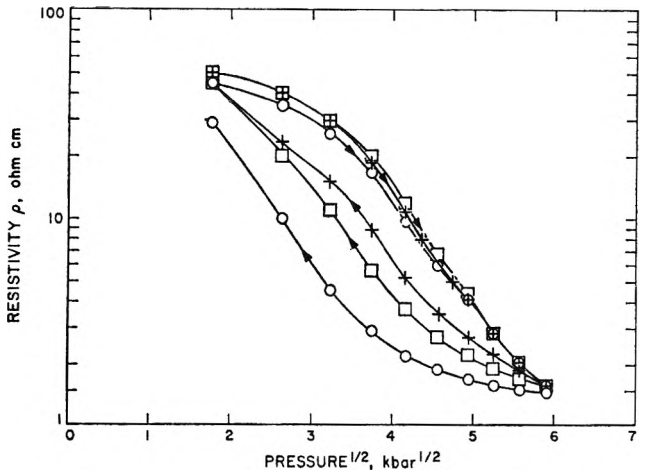

Figure 3. Resistivity *vs.* square root of pressure for $D_u^+(TCNQ^-)TCNQ$: ○, first cycle; □, second cycle; ×, third cycle.

were also obtained with all the other complexes described here.

It seems worth noting that there appears to be little difference between transport properties of the polymer complexes and complexes with the corresponding monomers. Thus the polymer complexes are only slightly less conductive than those of the monomer. Also the conjugation between the pyridine rings does not increase the conductivity to any significant extent. Furthermore, TCNQ polymers with a purely aliphatic backbone exhibit similar conductivity characteristics as those containing conjugated molecules.[4]

2. Electron Spin Resonance. The spin concentration of four representative samples and the singlet–triplet separation energy J estimated from the temperature variation of signal intensity is shown in Table II.

Table II: Temperature Dependence of Unpaired Spins

	Esr intensity at 25°, spins/mole × 10^{-23}	Singlet–triplet separation energy J, eV
$D_s^+TCNQ^-$	0.35	~0.03
$D_u^+TCNQ^-$	1.5	~0.045
$D_s^+TCNQ^- + TCNQ$	11.7	0
$D_u^+TCNQ^- + TCNQ$	8.0	0

Each of the four complexes studied here contains approximately Avogadro's number of unpaired electrons per mole at room temperature (Table II). Relative spin concentrations quoted are considered accurate to 30%; absolute values are known only to within a factor of 2.

Simple TCNQ salts follow a singlet–triplet model for paramagnetism[8] in which the esr intensity I is proportional to $T^{-1}[\exp(J/kT + 3)^{-1}]$. The singlet–triplet separation energy J may be calculated from the formula $J = 1.61kT_m$, where T_m is the temperature at which I is a maximum. We find for the $D_s^+TCNQ^-$ and $D_u^+TCNQ^-$ simple salts that T_m is considerably above ambient temperature and in the range in which these salts begin to decompose. Therefore an alternate procedure for determining J was attempted.

In the temperature range for which $J \gg kT$, the product $I \times T$ is proportional to $\exp(-J/kT)$, and a semilog plot of $1 \times T$ *vs.* T^{-1} will be a straight line the slope of which is (J/k) log e. From such a plot (Figure 4) the measured value of J was found to be not sufficiently large in comparison with kT to make the above approximation valid. We estimate that the measured value of J is too small by a factor of approximately 2. It can only be concluded that J is probably somewhat smaller than 0.1 eV.

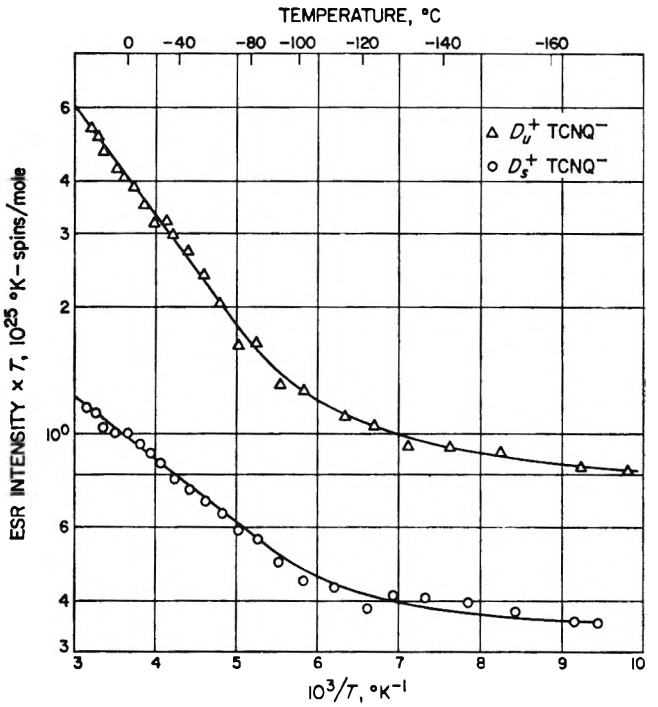

Figure 4. Temperature dependence of esr intensity for simple TCNQ salts.

In the low-temperature region of Figure 4 the triplet contribution to paramagnetism is small and the doublet impurity contribution predominates. In this region $I \times T$ is approaching a constant value independent of temperature.

Complex TCNQ salts containing neutral TCNQ exhibit a Pauli spin paramagnetism characteristic of a degenerate electron gas such as occurs in metals.[7] In this case the measured esr intensity is independent of temperature. Such a paramagnetism was found for some of our complex salts (Table II).

The shape of the esr signal of the complexed salts exhibits an interesting rotational anisotropy that to

(8) D. Bijl, H. Kainer, and A. C. Rose-Innes, *J. Chem. Phys.*, **30**, 765 (1959).

our knowledge has not been reported previously. If a pellet is rotated in the magnetic field in such a way that the direction in which the pressure was applied to it, $\hat{P}$, is kept perpendicular to the magnetic field H, no line-shape change results; however, a different spectrum is observed when the pellet is oriented with $\hat{P}$ parallel to $\hat{H}$ (Figure 5). This type of anisotropy

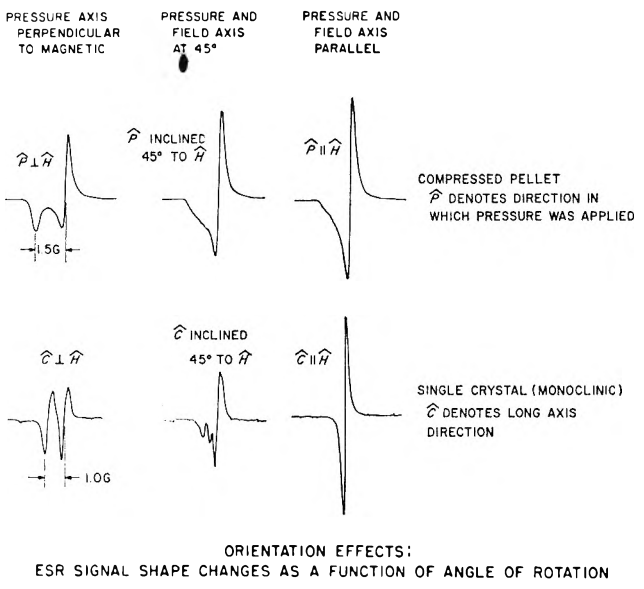

Figure 5. Rotational anisotropy of a compacted pellet compared to the anisotropy of a single crystal.

does not occur in the simple salts. The complex salts in a powdered form show a single line resonance. The esr signal shape for pellets with $\hat{P} \parallel \hat{H}$ (Figure 5) is similar to that of the same compound in the form of a single crystal, having axial symmetry. Compacted pellets, usually composed of many microcrystals randomly oriented, are not known to exhibit rotational anisotropy. It would appear that under pressure either the molecules of our complex salts or small crystallites assume a preferred orientation.

The spectral splittings in the case of the single crystals (or compressed pellets) are likely to be due to g-factor anisotropy. It is, however, somewhat difficult to rule out the possibility of zero-field splittings in the absence of measurements at different frequencies (which would check the dependence of the splittings on magnetic field strength), especially in view of the identification of zero-field splittings in other organic TCNQ complexes.[9] However, the splittings in the present case are of the order of 1 G, compared to splittings of $\sim$*100* G for other TCNQ complexes.[9] Furthermore, recent studies on the magnetic excitations in charge-transfer complexes of *p*-phenylenediamine–chloranil[10] (PDC) yielded esr spectra very similar to those shown in Figure 5. In the case of PDC, experiments at different frequencies firmly established the g-factor anisotropy (rather than zero-field splittings). In the latter case (PDC), the exciton was shown to be a Wannier exciton (as opposed to Frenkel excitons in TCNQ complexes[9]).

Assigning anisotropic g values to our spectra on the above basis, one obtains $g = 2.0033$, $g = 2.0024$ for $D_s^+TCNQ^- + TCNQ$ (Figure 5), and $g = 2.0036$, $g = 2.0028$ for $D_u^+TCNQ^- + TCNQ$. This g-factor anisotropy is thought to be due to inequivalent sites in the unit cell.[11] Attempts were made to observe anisotropy in the electronic conductivity of compressed pellets. However, no conductivity anisotropy was found.

3. Carrier Mobility Measurements. The Hall Effect and Magnetoresistance. In order to elucidate the conduction mechanism it was considered essential to determine the mobility of the electrical carriers. This was achieved directly by Hall effect measurements.

Table III: Electronic Properties of D_s and D_u Complexes

Sample	Sign of Hall coefficient at 25°	μ_{Hall} at 25° cm²/V sec	Q, Seebeck coeff, mV/°C at 25°	$Q \times T$, eV
$D_s^+(TCNQ^-)$	+	0.04	0.6	0.18
$D_u^+(TCNQ^-)$	±[a]	0.3	0.32 ± 07	0.1
$D_s^{2+}(TCNQ^-)_2$	...	...	1.0 ± 0.1	0.3
$D_u^{2+}(TCNQ^-)_2$	...	...	0.6 ± 0.08	0.18
$D_s^{2+}(TCNQ^-)_2$ polymer		<0.1	0.4	0.12
$D_u^{2+}(TCNQ^-)_2$ polymer		<0.1	0.2 ± 0.1	0.06

[a] Sign reversed upon standing 24 hr.

Table III contains the Hall mobility value for a compacted pellet of $D_s^+TCNQ^-$, the only sample for which a consistent signal was obtained. Figure 6 shows a strip-chart recording of the Hall signal. It is seen that the signal to noise ratio is sufficiently high

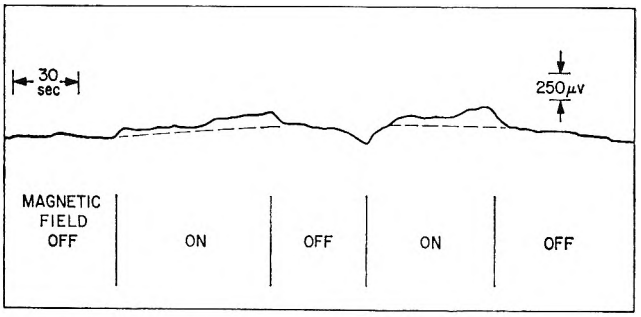

Figure 6. Strip chart recording of the Hall signal.

(9) D. B. Chestnut, H. Foster, and W. D. Phillips, *J. Chem. Phys.*, **34**, 684 (1961); D. B. Chestnut and W. D. Phillips, *ibid.*, **35**, 1002 (1961).
(10) R. C. Hughes and Z. G. Soos, *ibid.*, **48**, 1066 (1968).
(11) R. C. Hughes and Z. G. Soos, *ibid.*, **48**, 1066 (1968), and comment from anonymous referee.

to detect a Hall effect. The Hall mobility is 0.04 cm^2/V sec with a positive Hall coefficient corresponding to holes as the majority carriers. Table III shows the Hall effect results on other compacted pellets. For a sample of $D_u^+TCNQ^-$ the Hall coefficient was found to change signals upon standing for 24 hr. The positive signal of the Hall coefficient for $D_s^+TCNQ^-$ corresponds to the positive Seebeck coefficients also listed in Table III. Other samples showed no measurable Hall effect (see Table II).

While attempts at attaching Hall probes to tiny single crystals of $D_u^+TCNQ^-$ failed, an attempt was made to measure the magnetoresistance of these single crystals using a two-probe method. While a 2% change in resistance could have been detected in the presence of several kilogauss transverse magnetic field, none was observed. This puts an upper limit on the magnetoresistance mobility[12] of ~ 0.1 cm^2/V sec.

IV. Discussion

The dramatic increase observed here in conductivity by addition of neutral TCNQ to a paramagnetic TCNQ salt has been previously reported.[2,3,13] The increase in conductivity by about four orders of magnitude (Table I) is accompanied by an activation energy drop from about 0.15 to 0.03 eV. It should be noted that this drastic change in conductivity does not require stoichiometric proportions; thus increasing the ratio of TCNQ:$TCNQ^-$ from $\frac{1}{2}$ to 1 changes the conductivity values only slightly and has little effect on the activation energy.

These observations are consistent with the theoretical arguments of LeBlanc.[14] He accounts for the higher conductivity in the complex salts by creation of hole–electron pairs in the Heitler–London ground-state configuration without placing two electrons on the same TCNQ site (corresponding to the formation of a dianion), there being "neutral" molecules available to take the extra electron.

There are, however, some observations about the data which should be discussed. It should be pointed out that a single carrier model was used to estimate the Hall mobility because of lack of information about a two-carrier model. It is conceded on this basis that these calculated Hall mobilities may be smaller than the true electron or hole microscopic mobilities. Mention must also be made of the change with time in sign of the Hall constant for the $D_u^+(TCNQ)^-$ salt. Such behavior suggests oxygen doping as has been inferred for $Li^+(TCNQ)^-$ on the basis of a reversible change in the sign of the thermal emf upon oxygen treatment.[15]

Prescinding from these difficulties and taking the Hall mobility ($\mu = 0.04$ cm^2/V sec, Table III) as a measure of the true hole mobility in $D_s^+(TCNQ^-)$, one can calculate the concentration of holes from the single carrier relation

$$\sigma = ne\mu \tag{1}$$

where σ is the conductivity $= 6.5 \times 10^{-6}$ $(ohm\text{-}cm)^{-1}$ (see Table I), n is the concentration of holes, e is the electronic charge, and μ is the mobility.

A calculation of this type gives n of the order of 10^{14} cm^{-3}, *i.e.*, about 8 orders of magnitude below the concentration of unpaired spins as measured by the esr technique. It is clear, then, that the carriers are not the spin excitations themselves. This result is in agreement with previous findings[16] in studies with the poly-*n*-vinylcarbazole–iodine complex. In this TCNQ case, however, the evidence is more significant since, in paramagnetic TCNQ salts, the unpaired spins are not likely to arise from crystal defects or dislocations (as postulated for a number of π complexes[17]) because the concentration of free spins is approximately equal to the concentration of molecules.

As to the method of conduction of the carriers (once formed), one could possibly describe their motion in terms of band theory in view of the close agreement (in three of four cases) between the conductivity activation energies and the $Q \times T$ estimate of the Fermi level obtained from the thermal emf measurements. Furthermore, consider an estimate of the density of states N for the $D_s^+(TCNQ)^-$ sample (with measured Hall mobility = 0.04 cm^2/V sec). If one uses the relation[18]

$$n = N \exp[-(E_f - E_v)/kT] \tag{2}$$

where n is the concentration of holes $= \sigma/e\mu$ for σ, the measured conductivity (at 300°K), e is the electronic charge, and μ is the measured Hall mobility (at 300°K), and with $(E_f - E_v) = Q \times T = 0.18$ eV (see Table III), and $kT \sim 1/40$ eV, one finds a density of states N equal to 3×10^{18} cm^{-3}. Calculation of the density of states from the (wide) band theoretical expression

$$N = \frac{2\pi m^* kt^{3/2}}{\hbar^2} \tag{3}$$

where m^* is effective mass (taken here as the free electron mass) and the other symbols have their usual meaning, gives $N = 1.5 \times 10^{19}$ cm^{-3}. This is within

(12) A. C. Beer, "Galvanomagnetic Effects in Semiconductors," Academic Press, New York, N. Y., 1963, p 139.

(13) J. H. Lupinski, K. D. Kopple, and I. J. Hertz, *J. Polymer Sci., C*, 1561 (1967).

(14) O. H. LeBlanc, *J. Chem. Phys.*, 42, 4307 (1965).

(15) W. Simmons, Organic Crystal Symposium, National Research Council, Ottawa, 1962, p 195.

(16) A. M. Hermann and A. Rembaum, *J. Polymer Sci., C*, No. 17, 107 (1966).

(17) W. Slough, *Trans. Faraday Soc.*, 61, 408 (1965).

(18) See, for example, W. Shockley, "Electrons and Holes in Semiconductors," D. Van Nostrand Co., Inc., New York, N. Y., 1950.

order-of-magnitude agreement with the measured value (3×10^{18} cm^{-3}).

This description is, however, to a large extent unsatisfactory; the mobilities seem to be low enough as to be representative of mean free paths shorter than intermolecular spacings.[19] It is hoped that further measurements will pinpoint in greater detail the mechanism of carrier transport.

(19) A. F. Joffe, *Solid State Phys.* (USSR), **1**, 1 (1953).

Structure and Electrolyte Properties in Bolaform Electrolytes. III. The Hydrodynamics of Potassium Salts of Several Rigid Bolaform Disulfonic Acids in Dioxane–Water Mixtures at 25°

by Bert R. Staples[1] and Gordon Atkinson

Department of Chemistry, University of Maryland, College Park, Maryland 20740 *(Received June 17, 1968)*

The conductances of potassium benzenesulfonate, potassium *p*-benzenedisulfonate, potassium 4,4′-biphenyldisulfonate, and potassium 4,4″-terphenyldisulfonate in dioxane–water mixtures of 0 to 70% dioxane content were measured at 25°. The hydrodynamic properties of these elongated ions agree with the calculated properties based on a rigid ellipsoid model. The distance of closest approach in solution between the cation and anion is compared as calculated by five distinct methods. This distance was determined from thermodynamics of association, hydrodynamics, conductance *J* parameter, and the dielectric relaxation drag effects. This distance of closest approach agrees fairly well between all methods for each salt. The trend observed was generally in increasing distance of closest approach with increasing charge separation.

Introduction

The effects of ion structure on the conductance parameters of salts of rigid bolaform electrolytes have been investigated.[2] The present authors have presented the basic conductance behavior of the potassium salts of benzenesulfonic acid (KBS), *p*-benzenedisulfonic acid (K_2BDS), 4,4′-biphenyldisulfonic acid (K_2BPDS), and 4,4″-terphenyldisulfonic acid (K_2TPDS) in dioxane–water mixtures at 25°. This series of rigid bolaform electrolytes represents a unique, systematic increase in size and charge separation of the anion.

Rice[3] has examined models for a theoretical treatment of bolaform salts to obtain transport properties, and Atkinson and coworkers have applied these models to calculate the hydrodynamic parameters of bolaform salts in water[4] and dioxane–water[2] mixtures.

Assuming that the usual equations of viscous fluid motion describe the hydrodynamics of the model, Perrin[5] gives the expression for the frictional coefficient of a rigid ellipsoid as

$$\zeta = \frac{6\pi\eta_0(b'^2 - a'^2)^{1/2}}{\ln\left[(b'/a') + \sqrt{(b'/a')^2 - 1}\right]} \approx \frac{6\pi\eta_0 b'}{\ln(2b'/a')} \qquad (b' \gg a') \qquad (1)$$

All terms used are defined in the Appendix.

For the diquaternary ammonium bolaform ions investigated by Fuoss,[6] Rice found that the Peterlin[7] model of beads separated by massless rods was superior to the rigid ellipsoid model. Using the rigid bolaform ions such as the 4,4′-biphenyldisulfonate ion, $BPDS^{2-}$, Atkinson[4] found that the rigid ellipsoid model enabled one to accurately calculate the frictional coefficient of $BPDS^{2-}$ from the parameters of the benzenesulfonate ion, BS^-. Both of these results seem valid since, in the case of the diquaternary ammonium salts a nonrigid polymethylene chain separates the charge sites, but a rigid aryl framework lies between the charge sites of the $BPDS^{2-}$ ion.

Also, Rice, Thompson, and Nagasawa[8] have measured the diffusion coefficients of K_2BDS, K_2BPDS, and K_2TPDS and found that the Perrin rigid ellipsoid gave a very accurate description of that property.

In 1959, Fuoss[9] had proposed a method of getting a

(1) Taken in part from an M.S. thesis submitted to the Graduate School of the University of Maryland; National Bureau of Standards, Washington, D. C. 20234.
(2) B. R. Staples and G. Atkinson, *J. Phys. Chem.* **71**, 667 (1967).
(3) S. A. Rice, *J. Amer. Chem. Soc.*, **80**, 3207 (1958).
(4) G. Atkinson and S. Petrucci, *J. Phys. Chem.*, **67**, 1880 (1963).
(5) F. Perrin, *J. Phys. Rad.*, **7**, 1 (1936).
(6) Q. V. Brody and R. M. Fuoss, *J. Phys. Chem.*, **60**, 156 (1956).
(7) A Peterlin, *J. Chem. Phys.*, **47**, 6 and 669 (1950).
(8) G. Thomson, S. A. Rice, and M. Nagasawa, *J. Amer. Chem. Soc.*, **85**, 2537 (1963).
(9) R. M. Fuoss, *Proc. Nat. Acad. Sci. U. S.*, **45**, 807 (1959).

distance of closest approach from a semiempirical method utilizing the effect of dielectric relaxation drag on ions in polar solvents. This was demonstrated theoretically on a macroscopic basis consistent with Stokes' law by Boyd[10] in 1961. A year later Boyd's derivation was improved upon and refined by Zwanzig.[11]

This dielectric effect was described by Fuoss as the resultant effect of the motions of ions creating an electrostatic field in the surrounding polar medium which opposes that motion. More simply, it is an electrostatic coupling of ion with solvent causing an effective increase in viscosity, since there is extra work to orient the solvent dipoles as the ion passes among them.

The Fuoss[9] empirical equation

$$\lambda_i^0 = \frac{\mathfrak{F}^2}{6\pi N\eta(r_i + S/D)} \tag{2}$$

can be rearranged and then upon multiplying by D one obtains

$$F^* \equiv \frac{\mathfrak{F}^2 D}{6\pi N\eta\lambda_i^0} = S + (a_D)_i D \tag{3}$$

Thus a plot of $(\mathfrak{F}^2 D/6\pi N\eta\lambda_i^0)$ *vs.* D should yield a straight line with a slope of $(a_D)_i$. However, one may also use the Zwanzig[11] equation as tested by Atkinson and Mori[12]

$$\lambda_i^0 = \frac{\mathfrak{F}^2}{N\left[6\pi\eta r_i + \frac{2e^2\tau}{3r_i^3\eta}\left(\frac{\epsilon_0 - \epsilon_\infty}{\epsilon_0^2}\right)\right]} \tag{4}$$

rearranged to

$$L^* = \frac{\mathfrak{F}^2}{N\eta\lambda_i^0} = 6\pi r_i + \frac{2e^2}{3r_i^3}\left[\frac{\tau}{\eta}\left(\frac{\epsilon_0 - \epsilon_\infty}{\epsilon_0^2}\right)\right] \tag{5}$$

so that a plot of L^* *vs.* $\tau/\eta[(\epsilon_0 - \epsilon_\infty)/\epsilon_0^2]$ or R^* will give another distance of closest approach $(a_Z)_i \equiv r_i$ from the slope.

Thus a distance of closest approach determined by five methods may be compared: thermodynamics of association, conductance J parameter, dielectric relaxation [Fuoss empirical equation (2) and Zwanzig equation (5)], and hydrodynamics.

Results

Diffusion Coefficients. Reasonable agreement was found between the experimentally determined diffusion coefficients in water, made by Rice,[5] who based his measurements on the Perrin rigid ellipsoid model, and those calculated from conductance data. The calculated mutual diffusion coefficients were consistently about 10% higher than experiment, as shown in Table I. This seems satisfactory, since there is probably a few per cent experimental error in the determination of these mutual diffusion coefficients and these measurements are not in as dilute a range as the conductance measurements. The method for calculating the mutual diffusion coefficients from conductance data may be found in Robinson and Stokes[13] and is briefly outlined below.

Table I: Diffusion Coefficients

Salt	$\mathfrak{D}^0 \times 10^6$ (Rice[5] exptl.), cm² sec⁻¹	$\mathfrak{D}^0 \times 10^6$ (calcd from conductance), cm² sec⁻¹	% $\Delta\mathfrak{D}^0/\mathfrak{D}^0$ (cond.)
K_2(p)BDS	12.0	13.2	10.0
K_2BPDS	10.25	11.74	14.5
K_2TPDS	9.50	10.79	13.6

The Nernst–Hartley relation is

$$\mathfrak{D} = \frac{[\nu_1 + \nu_2]\lambda_1^0\lambda_2^0}{\nu_1|z_1|[\lambda_1^0 + \lambda_2^0]}\frac{RT}{\mathfrak{F}^2}\left[1 + \frac{d\ln y_\pm}{d\ln c}\right] \tag{6}$$

Then the limiting value at infinite dilution where $d\ln y_\pm/d\ln c \to 0$ is given by

$$\mathfrak{D}^0 = \frac{RT}{\mathfrak{F}^2}\frac{[\nu_1 + \nu_2]}{\nu_1|z_1|}\frac{\lambda_1^0\lambda_2^0}{[\lambda_1^0 + \lambda_2^0]} \tag{7}$$

Frictional Coefficients. Based on a rigid ellipsoid model the authors have calculated the ionic frictional coefficients (Table II) where a' has been taken to equal

Table II: Frictional Coefficients of Salts

		$\zeta \times 10^8$ sec cm⁻¹		
	% Dioxane	Calcd from Perrin model	Exptl	$\eta_0 \times 10^2$
KBS	0.0	...	0.442	0.895
	35.94	...	0.819	1.636
	49.68	...	0.956	1.908
	56.36	...	0.945	1.971
	66.52	...	1.13	1.952
K_2BDS	0.0	0.607	0.529	0.895
	35.94	1.11	1.22	1.636
	47.76	1.27	1.42	1.876
	54.79	1.33	1.74	1.962
	59.14	1.34	1.86	1.981
	65.59	1.33	2.67	1.958
K_2BPDS	0.0	0.797	0.631	0.895
	24.17	1.23	1.11	1.380
	46.83	1.66	1.47	1.861
	52.27	1.73	1.61	1.943
	59.14	1.77	1.84	1.981
	68.69	1.72	3.11	1.931
K_2TPDS	0.0	0.928	0.727	0.895
	41.94	1.83	1.67	1.766
	46.83	1.95	2.00	1.876
	52.27	2.01	1.83	1.943
	58.32	2.05	2.38	1.979

(10) R. H. Boyd, *J. Chem. Phys.*, **35**, 1281 (1961).
(11) R. Zwanzig, *ibid.*, **38**, 1603 (1963).
(12) G. Atkinson and Y. Mori, *J. Phys. Chem.*, **71**, 3523 (1967).
(13) R. A. Robinson and R. H. Stokes, "Electrolyte Solutions," Butterworth and Co. Ltd., London, 1955.

$0.5a_J$ value for KBS and b' has been measured from molecular models (Figure 1).

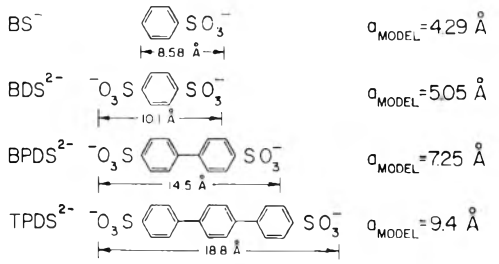

Figure 1. Dimensions of the molecular models.

Frictional coefficients calculated using the Perrin rigid ellipsoid model (eq 8) agree well with those calculated from experiment (Table II), thus demonstrating the probable validity of the rigid ellipsoid model proposed by Perrin.

$$\zeta = \frac{\mathfrak{F}\,|Z_i|\,e}{300\lambda_i^0} \qquad (8)$$

When one plots ζ *vs.* η_0, Figure 2 graphically illustrates the agreement between the theoretical slope using geometric dimensions of the Perrin model compared

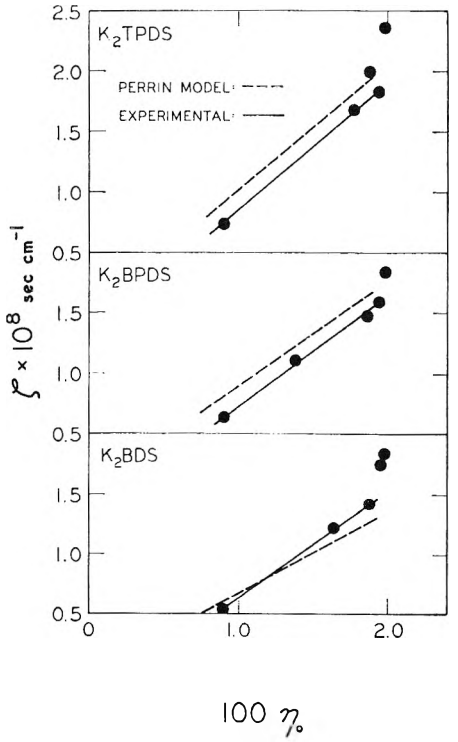

Figure 2. The frictional coefficient as a function of viscosity.

with the experimental slope. One can observe that the theoretical slope approaches that of the experimental slope as the size of the anion increases. That is, the description of the data by the model chosen closely approaches the experimental results as the anion increases its length and thereby appears more like an ellipsoid. This also indicates good agreement between Stokes' hydrodynamic radii from both the theoretical and experimental lines, as pictured in Figure 2. The random scattering above 50% dioxane can be explained by the failure of Stokes' law in this region where the local viscosity is no longer described by the bulk viscosity. The scattering is probably due to nonideality of the solvent mixture as shown by the parabolic curve of the η_0 *vs.* per cent dioxane in regions of high dioxane content as well as other properties.

Dielectric Relaxation. Based on eq 3, a plot of $(\mathfrak{F}^2D/6\pi N\eta\lambda_i^0)$ *vs.* D is shown in Figure 3 and another

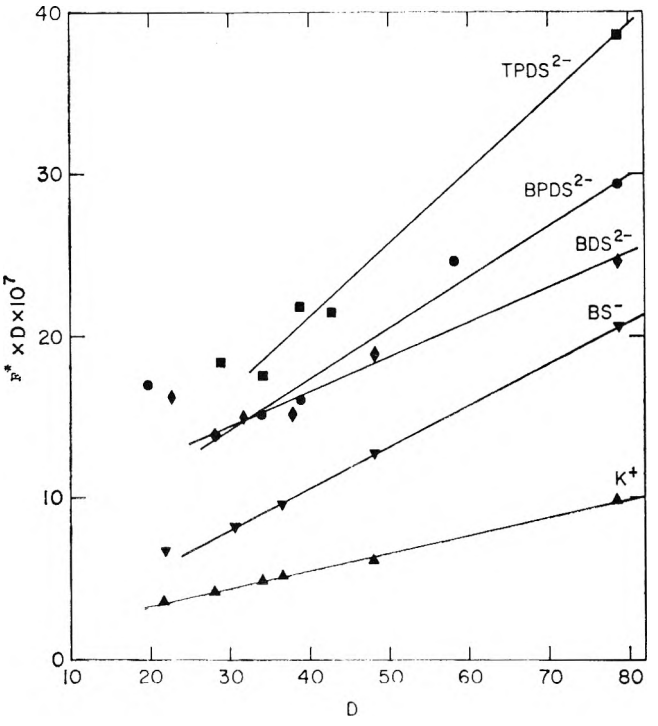

Figure 3. The ionic radius as a function of the dielectric constant.

plot, based on eq 5, is illustrated in Figure 4. The ionic radii in solution, derived from these two interpretations of dielectric friction are compared in Table III. These calculations demonstrate an increasing a_i distance with an increasing charge separation: $TPDS^{2-}$

Table III: Comparison of Ionic Distances Using the Dielectric Friction Approach

Ion	$(a_D)_i$, [a] Å	$(a_Z)_i$, [b] Å
K^+	1.10	1.9
BS^-	2.53	2.9
BDS^{2-}	2.55	1.3
$BPDS^{2-}$	3.33	1.5
$TPDS^{2-}$	4.18	2.4

[a] Fuoss interpretation. [b] Zwanzig derivation (from slope).

Table IV: Correlation of the Distance of Closest Approach

Salt	Distance of closest approach					
			Hydrodynamics			
	Thermodynamic[2] [Fuoss]a_K	Conductance[2] [Fuoss–Onsager]a_J	Dielectric relaxation [Fuoss]a_D	Dielectric relaxation [Zwanzig]a_Z (intercept)	Dielectric relaxation [Zwanzig]a_Z (slope)	Viscosity [Stokes]a_S
KBS	3.4	3.2[16]	3.6	3.7	4.7	4.0
K_2BDS	5.0	3.6	3.7	2.2	3.1	6.0
K_2BPDS	4.6	4.2	4.4	2.6	3.3	6.2
K_2TPDS	3.0	4.5	5.3	3.5	4.2	7.2

> $BPDS^{2-}$ > BDS^{2-}. It appears that the a_z obtained from the intercept is without solvation whereas the a_z derived from the slope includes solvation.

The Distance of Closest Approach. The comparison of the distances of closest approach, a_i, of the cation (K^+) and anion (Table IV) determined by five different approaches—thermodynamically, hydrodynamically, by conductance and through the effect of the dielectric relaxation drag—resulted in the following.

a. Thermodynamics. Fuoss' method of obtaining a_K from a plot of log K_{a_1} *vs.* $1/D$ yielded a trend opposite to all the other results.[2] The a_K decreased in size as the charge separation increased. This decrease might be attributed to the attempted interpretation of a spherical model, embodied in the theory, with an ellipsoidal anion, to the failure of the Fuoss-Edelson[2,14] technique for such a large ion, or to any combination of each. The possibility also exists that the cation might prefer to occupy an end position on the large terphenyldisulfonate anion. There probably is a particular distance of the separation of charges beyond which the cation will favor an ion pair where it is directly in contact with a single sulfonate group. This distance may have been reached with three benzene rings between the negative charges of the anion, but the following results seem to indicate that this is not the case. There appears to be no way of deciding which of these factors is or is not operating in this particular instance.

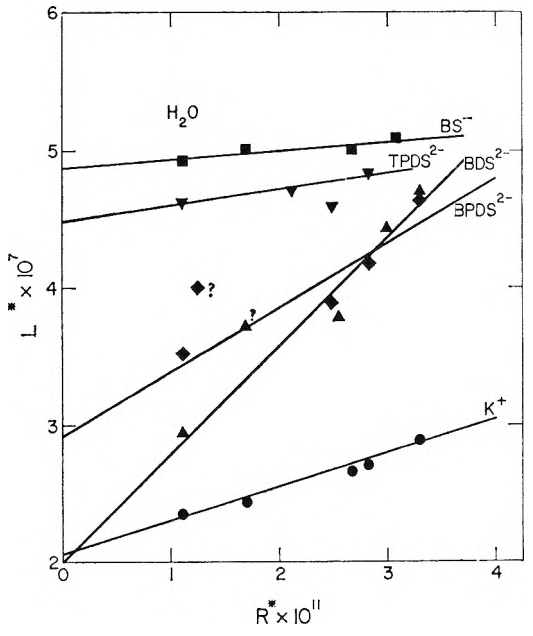

Figure 4. L^* *vs.* R^*. (Points marked "?" were not included in least-squares calculations. Omission of those points amounted to a change in r_i values of less than 0.1 Å.)

b. Conductance. A consistent increase in the a_J values was observed,[2] as the separation of charges increased.

c. Hydrodynamics. The Perrin rigid ellipsoid model seemed to give the best description and agreed with experimental results when diffusion coefficients (Table I) and hydrodynamic properties (Table II) were investigated. Some of the small differences (about 10% high) in the diffusion coefficients calculated from conductance parameters and those determined by Rice and coworkers[8] may well be due to slight association, that is, the presence of KA^- ion pairs in addition to single K^+ and A^{2-} ions, or to the dimensions of the ellipsoid assumed by Rice in his calculations. The a' value for the rigid ellipsoid was evaluated by Yokoi and Atkinson[15] who determined the a_J for KBS in water. The b' value for the rigid ellipsoid model was measured from end to end on molecular models to give a comparison between calculated and experimental frictional coefficients illustrated in Figure 2. The a_S values increased with increasing charge separation and it can be seen that this Stokes radius is generally larger than other a_i's since more solvation is probably included in this model.

d. Dielectric Relaxation. Once again an increasing a_D, determined by eq 3, was noted as charge separation increased, as was also indicated by the Zwanzig equation, eq 5 (a_Z).

Position of the Cation in an Ion Pair. Probably the most pertinent question to be decided is: "Can one determine what site the cation prefers to occupy in an ion pair with a charge-separated anion?" These investigators feel that a good educated guess can be advanced based on the determinations of the distance of closest approach, a_i. If a contact ion pair of KBS,

(14) R. M. Fuoss and D. Edelson, *J. Amer. Chem. Soc.*, **73**, 269 (1951).

(15) M. Yokoi and G. Atkinson, *ibid.*, **83**, 4367 (1961).

$C_6H_5SO_3^-K^+$ has an a_J of about 3.5 Å in dioxane–water mixtures,[2] then an increase in a_i with an increase in charge separation would indicate that the cation occupies an intermediate position between the two negatively charged sulfonate groups, as pictured in Figure 5. This is indicated since, if the cation was

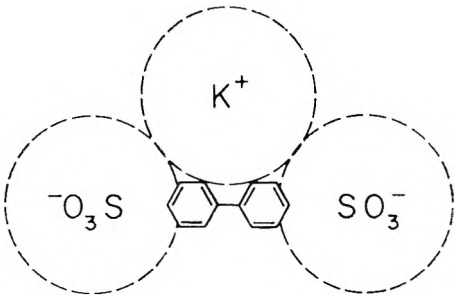

Figure 5. Probable position of the cation in an ion pair.

intimately associated with a single sulfonate group, a "contact" ion pair, the a_i should show no tendency to change with an increase in the separation of sulfonate charges. It is important to realize that all the distances of closest approach that have been determined are based on a distance, a_i, from charge *center* to charge *center*. Thus, if the cation was situated at one end of the charge separated anion, the a_i determined would be *constant*,

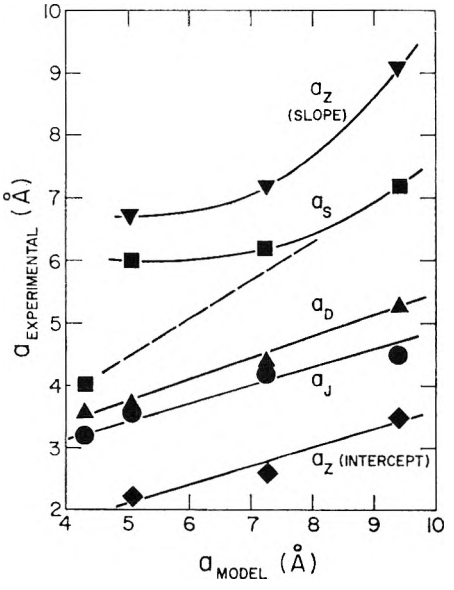

Figure 6. The experimental distance of closest approach as a function of the radius of the anion model. (Straight lines are used to show trends.)

within the experimental error, for all salts investigated. This is not the case as demonstrated by the results of the conductance a_J, the Stokes' hydrodynamic radius, a_S, and the a_D and a_Z determined from the dielectric relaxation friction (Table IV), where a definite change occurs in the distance of closest approach, beyond the limits of experimental error. The distances of closest approach (average values) experimentally determined by conductance (a_J), hydrodynamics (a_S) and the dielectric relaxation (a_D and a_Z) are shown in Figure 6 as a function of the anion radius measured from molecular models. It is therefore concluded that the cation assumes an intermediate position approximately equidistant between the two charges on the anion.

Acknowledgments. The authors wish to express their gratitude to the National Institutes of Health for their support under Grant GM 9232. The computer time used for this research project was supported by National Aeronautics and Space Administration Grant NsG-398 to the Computer Science Center of the University of Maryland.

Appendix. Symbols

a_D	$\sum[(a_D)_+ + (a_D)_-]$
a_Z	$\sum[(a_Z)_+ + (a_Z)_-]$
a_S	$\sum[(a_S)_+ + (a_S)_-]$
N	Avogadro's number
η	Bulk viscosity of solvent
$r_i = (a_D)_i$	"Stokes" radius of ith ion
S	Empirical constant of the Fuoss equation
$\epsilon_0 = D$	Static (low frequency) dielectric constant of solvent
ϵ_∞	Optical (infinite frequency) dielectric constant of solvent
τ	Dielectric relaxation time of solvent
e	Electronic charge
$\mathfrak{D}$	Mutual diffusion coefficient
$\mathfrak{F}$	Faraday
ζ	Frictional coefficient
ν_1	Number of ions which the cation produces
ν_2	Number of ions which the anion produces
λ_1^0	Equivalent ionic conductance of the cation at infinite dilution
λ_2^0	Equivalent ionic conductance of the anion at infinite dilution
λ_i^0	Equivalent ionic conductance of the ith ion at infinite dilution
$y_\pm$	Mean molar activity coefficient
R	Gas constant (8.314 J deg^{-1} mol^{-1})
c	Concentration of salt in moles/liter
R^*	$= \frac{\tau}{\eta}\left[\frac{\epsilon_0 - \epsilon_\infty}{\epsilon_0^2}\right]$
F^*	$= \frac{\mathfrak{F}^2 D}{6\pi N \eta \lambda_i^0}$

The Unit Compressibility Law for Mixtures

by Eugene M. Holleran and Gary J. Gerardi

Chemistry Department, St. John's University, Jamaica, New York 11432 *(Received June 21, 1968)*

The experimental data of Douslin, Harrison, and Moore on mixtures of methane and tetrafluoromethane are used to demonstrate that it is possible for mixtures as well as pure gases to obey the unit compressibility law, which relates the temperatures, T, and densities, d, at which $PV = RT$: $T/T_B + d/d_0 = 1$, where d_0 and the Boyle temperature T_B are characteristic constants for each substance or mixture. Thus this equation, which relates the states in which the effects of attractive and repulsive intermolecular forces on compressibility are balanced, can persist even in the presence of three separate intermolecular potentials, A–A, A–B, and B–B.

Introduction

The unit compressibility law (UCL) relates the temperatures, T, and the densities, d, at which the compressibility factor, $Z = P/dRT$, has the value unity. Thus, for $Z = 1$

$$T/T_B + d/d_0 = 1 \qquad (1)$$

where d_0 and the Boyle temperature T_B are constants characteristic of each substance. This relation was shown to hold[1] for 12 gases for which appropriate experimental data were available. However, a number of questions remained unanswered. For example, the law has as yet no theoretical foundation, and it was not certain whether small discrepancies with experimental data were due to inaccuracy of the law or of the data. Also, evidence was meager as to its validity for polar substances and for liquids. Finally, it was not known whether the law holds for mixtures.

The purpose of this paper is to present a partial answer to this last question by showing that the excellent experimental data on methane–tetrafluoromethane mixtures reported by Douslin, Harrison, and Moore[2] follow eq 1 within their experimental error.

Experimental Section

Procedure. In ref 2, the authors present PVT data for three CH_4–CF_4 mixtures containing approximately 25, 50, and 75% CH_4. They also include data for pure CH_4 and CF_4 reported earlier.[3,4] Measured pressures are tabulated for 25 densities up to 12.5 mol/l., and at temperatures ranging from 0 to 350° at the low densities and to 50° at the highest densities. Fortunately for the present purpose, the compressibility factor Z passes from less than unity to greater than unity within the experimental temperature range on every tabulated isochore, thus providing an excellent test of the unit compressibility law.

The procedure as employed in ref 1 is to interpolate on each isochore to the temperature at which $Z = 1$, and then to fit these temperatures and the densities to eq 1 by minimizing the sum of squares of $(T/T_B + d/d_0 - 1)$. Because of the very high precision of the CH_4–CF_4 mixture data, two refinements of the procedure were introduced here. First, instead of interpolating on the isochore by assuming Z to be linear in $1/T$, the unit-Z temperatures were obtained by fitting Z at each density to a quadratic in $(1/T)$ and solving this for T at $Z = 1$. Each least-squares quadratic was found to represent its entire isochore within experimental error, so that the unit-Z temperatures so obtained are as reliable as the data can provide. These temperatures (as listed in Table IV) are on the thermodynamic scale used in the experimental work.

The second procedural refinement involves an adjustment of the reported data. That this is legitimate is clear from the following discussion. In order to retain all possible experimental precision, the experimental authors listed their data to more significant figures than would be warranted by the probable absolute accuracy. In ref 3 the data are tabulated to six or seven figures although the maximum experimental error in the measurements is estimated to range from three parts in 10,000 at low temperatures and densities to 30 parts in 10,000 at the high temperatures and densities. Any systematic adjustment of the data that falls well within these limits is therefore justifiable. Such an adjustment was made by the experimenters[3] where a correction factor of 1.00023 was applied to eliminate an improbable behavior in a function of Z at low densities. In a similar way and for a similar reason, we have adjusted the compressibilities by a factor of $1 + \epsilon$ to provide the best fit of eq 1.

In ref 1 it was shown that relatively small errors in experimental data can produce large deviations from

(1) E. M. Holleran, *J. Chem. Phys.*, **47**, 5318 (1967).

(2) D. R. Douslin, R. H. Harrison, and R. T. Moore, *J. Phys. Chem.*, **71**, 3477 (1967).

(3) D. R. Douslin, R. H. Harrison, R. T. Moore, and J. P. McCullough, *J. Chem. Eng. Data*, **9**, 358 (1964).

(4) D. R. Douslin, R. H. Harrison, R. T. Moore, and J. P. McCullough, *J. Chem. Phys.*, **35**, 1357 (1961).

the linearity of eq 1 at low densities. Even very good experimental data usually yield unit-Z lines which exhibit a small low-density curvature in one direction or the other as could easily occur if precision exceeds accuracy. However, this curvature can be eliminated by adjusting all the Z values by a constant factor of $1 + \epsilon$. This procedure could be interpreted either as finding a straight T *vs.* d line for $Z = 1 + \epsilon$ (instead of for $Z = 1$), or as discovering and correcting a small systematic error in Z. As discussed in ref 1, the latter interpretation is preferred because the lines for $Z \neq 1$ are forced to curve sharply at low densities. The elimination of a low-density curvature in the unit-Z line thus appears to be sufficient justification for a systematic adjustment of PVT data, at least if the adjustment is within the limits of experimental error.

Such adjustments would be made without hesitation if the unit compressibility law were known theoretically to be exact at low densities. Some support for its low-density validity is afforded by the Lennard-Jones intermolecular potential, which appears to follow the UCL very closely.[5] Using literature values of the virial coefficients, which are known through the fifth coefficient E^*, as cited in ref 5, the densities, d^*, at which Z is unity were calculated from the truncated virial equation

$$Z = 1 + B^*d^* + C^*d^{*2} + D^*d^{*3} + E^*d^{*4} \quad (2)$$

and are listed in Table I. It can be seen that at low densities these results follow the UCL exactly with

Table I: The Unit Compressibility Law at Low Densities for a Lennard-Jones 12-6 Gas

T^*	d^* [a]
3.0	0.2936
3.1	0.2231
3.2	0.1528
3.3	0.0827
3.4	0.0126
3.5	−0.0576
3.6	−0.1277
3.7	−0.1978
3.8	−0.2677
3.9	−0.3371

[a] d^* is the density at which $Z = 1$ according to the five-term virial equation.

$T_B^* = 3.418$ and $d_0^* = 2.397$. The beginning curvature of d^* *vs.* T^* at the high and low tabulated T^*'s is consistent with the neglect of higher terms in the virial equation and in particular with a small positive F^*. The negative densities calculated for $T^* > T_B^*$, though not physically significant, serve to emphasize that the accurate linearity of the low-density unit-Z line for a Lennard-Jones gas extends all the way to zero density.

On the basis of the above discussions, and also because the resulting UCL constants will probably be more useful in subsequent applications to corresponding states and equations of state, it was decided to make the indicated small adjustments of the compressibility factor data.

Our procedure, therefore, consisted of finding a least-squares quadratic and thence a unit-Z temperature for each density, fitting these T's and d's to eq 1, repeating for a series of ϵ values, and selecting that ϵ which provided the best straight line for each mixture. The order of magnitude of ϵ used (10^{-4}) has only a small effect on the unit-Z temperatures at high densities, but as ϵ is varied, the systematic low density curvature switches from one direction to the other, and the sum of squares of the deviations, $\Delta = (T/T_B + d/d_0 - 1)$, passes through a minimum. This minimum was taken as the criterion for the selection of ϵ. This behavior is illustrated in Table II, where $\Sigma\Delta^2$ for the 50–50 mixture

Table II: The Effect of Varying ϵ on the Constants and the Linearity of Eq 1 for the 50–50 Mixture

$-\epsilon \times 10^5$	T_B, °K	d_0, mol/l.	$\Sigma\Delta^2 \times 10^7$ [a]
10	492.85	30.808	15.9
12	492.92	30.801	13.6
14	492.98	30.793	11.9
16	493.04	30.785	10.7
18	493.10	30.777	10.1
20	493.17	30.770	10.0
22	493.23	30.762	10.5
24	493.29	30.754	11.5
26	493.36	30.747	13.0
28	493.42	30.739	15.1

[a] $\Delta = T/T_B + d/d_0 - 1$.

is listed for $\epsilon \times 10^5$ from -10 to -28, with the minimum occurring at about -19. In this way, we minimize with respect to ϵ the sum of squares which was already minimized with respect to T_B and d_0 by the fit of eq 1. The considerable effect of this small data adjustment on the linearity of eq 1 and the values of its constants is evident in Table II.

This procedure was carried out for the three mixtures and also, because of the refinements, for the two pure gases which had already been treated in ref 1. During early calculations it was noted that the unit-Z temperatures for $d = 0.75$ (0.80 for CH_4) fell somewhat off-line, and so they were omitted from the determination of the best ϵ and eq 1 constants. These slight deviations could be eliminated, if desired, by a separate

(5) E. M. Holleran, *J. Chem. Phys.*, 49, 39 (1968).

Table III: Best Constants for the CH_4–CF_4 System

Mole % CH_4	$\epsilon \times 10^5$	$\bar{\Delta} \times 10^4$ [a]	d_0, mol/l.	T_B, °K	T_B, (B) [c]	$V_B \times 10^3$ [d]	ΔT_B [e]
100	8	3.1	35.729	509.22	509.3	54.3	1.1
75	−7	1.3	32.870	490.50	489.7	67.5	−0.7
50	−19	1.7	30.774	493.14	491.3	78.9	−1.8
25	−29	3.6	28.907	504.97	502.8	90.5	−2.4
0	−40	8.9[b]	27.702	520.99	518.1	104.1	−3.0

[a] $\bar{\Delta}$ is the average absolute value of $(T/T_B + d/d_0 - 1)$ for the 24 densities from 1 to 12.5 mol/l. [b] For the 18 points used in determining the constants for this gas, $\bar{\Delta}$ is 2.2×10^{-4}. [c] T_B found as T at which $B(T) = 0$; all $B(T)$ and the pure-gas T_B values are taken from ref 2. [d] The pure-gas values are from ref 2; the others were found from an empirical equation for B, quadratic in $(1/T)$. [e] Estimated as $1.5(T_B/V_B)\epsilon$.

correction at this d of the same order of magnitude as ϵ. Another difficulty was encountered with pure CF_4. The unit-Z T *vs.* d line for this gas exhibits a curvature at high densities which remains unaffected by the ϵ used to straighten the low density end. Accordingly, in order to find the most reliable constants for the unit compressibility law, the six highest density points were omitted, and the remaining 18 were used in the calculations for this gas.

Results and Discussion

Table III lists the best values of $\epsilon \times 10^5$ found for each of the five systems, together with the corresponding values of the constants T_B and d_0, and values of $\bar{\Delta}$, the average absolute deviation from linearity of the unit-Z T *vs.* d points (excluding the omitted points for $d < 1$). The increase of $|\epsilon|$ with increasing mole fraction of CF_4 suggests either an inaccuracy of the UCL for CF_4, or the possibility of a small error, such as a slight impurity, associated with this component.

T_B and d_0 are listed to five figures since these are the values which give the best linearity by the described procedure. However, they are sensitive to procedural variations and small experimental errors (Table II shows $\Delta T_B = 3 \times 10^3\epsilon$ and $\Delta d_0 = 4 \times 10^2\epsilon$ for the 50–50 mixture), and so are probably less reliable in an absolute sense by at least one figure.

Because of the modified procedure, the values of the constants given here for the pure gases differ somewhat from those given in ref 1. For CH_4 the old and new T_B's are 509.27 and 509.22, and the d_0's are 35.74 and 35.729. For CF_4 the corresponding values are 520.1, 520.99, and 27.6, 27.702, the larger discrepancies in this case being due to the inclusion of the high-density data in the determination of the old values.

Boyle temperatures determined independently *via* the second virial coefficient are listed in Table III for comparison with the unit compressibility law values. The agreement is only fair. With perfect data and analysis they should agree exactly. The discrepancies may be due to the data adjustment, as seen from the following. B is the zero density limit of $(Z - 1)/d = B + Cd^2 + \ldots$, and the ref 2 values were presumably found from the low density straight line plot of $(Z - 1)/d$ *vs.* d extrapolated to zero d. If Z is really $Z(1 + \epsilon)$, then the $(Z - 1)/d$ points are off by $\epsilon Z/d$. The deviation becomes infinite at zero density, but if the experimental points used to estimate the straight line are for example at 1 and 2 mol/l., then, since $Z \approx 1$, the $(Z - 1)/d$ points would be off by about ϵ and $\epsilon/2$, and the extrapolated B would be in error by about $3\epsilon/2$ l./mol. This leads to an error in T_B which is $\Delta T_B \approx 1.5(T_B/V_B)\epsilon$, where V_B is $T(dB/dT)$ at T_B. This dependence of T_B on ϵ is not greatly different from that seen in Table II. Estimates of V_B and ΔT_B are included in Table III. This very rough estimate accounts for most of the discrepancies in T_B, and so it may be anticipated that use of the adjusted data would provide slightly modified second virial coefficients which would in turn yield T_B values in better agreement with those of eq 1.

From the point of view of the unit compressibility law, the characteristic constants T_B and d_0 are determined for each mixture independently, as if each were a different substance. However, it is interesting to examine the dependence of these constants on composition. From Table III it is evident that the values for the mixtures are not simply average values, weighted by mole fraction. The T_B values are especially far below this and are not even intermediate between the values for the pure gases. This suggests a semiempirical correlation of the form[6] $T_B = X_1^2T_{B_1} + 2X_1X_2T_{B_{12}} + X_2^2T_{B_2}$, where $T_{B_{12}}$ would be T_B for a gas all of whose molecules interact like a CH_4–CF_4 pair, and X_1^2, $2X_1X_2$, X_2^2 are the fractions of binary interactions of the three possible types. However, the best T_{B12} of 469.6 does not reproduce the experimental $T_{B_{12}}$ very well, showing deviations up to 4.6°.

In Table IV are listed the unit-Z temperatures and the deviations $\Delta = (T/T_B + d/d_0 - 1)$ for the integer densities for the three mixtures and two pure gases. The high density curvature for the pure CF_4 is apparent. Once again, this indicates an inexactness of the UCL

(6) J. E. Lennard-Jones and W. R. Cook, *Proc. Roy. Soc.*, **A115**, 334 (1927).

Table IV: The Unit Compressibility Law for the CH_4–CF_4 System[a]

	Mole fraction of CH_4									
	1.00		0.75		0.50		0.25		0.00[c]	
d, M[b]	T	$\Delta \times 10^4$[d]	T	$\Delta \times 10^4$	T	$\Delta \times 10^4$	T	$\Delta \times 10^4$	T	$\Delta \times 10^4$
1	494.61	−7.0	475.34	−0.6	477.09	−0.5	487.69	3.8	502.15	3.8
2	480.85	2.6	460.67	2.2	461.07	−0.3	469.79	−4.9	483.13	−2.6
3	466.69	4.5	445.72	0.9	445.07	0.1	452.35	−4.3	464.35	−1.7
4	452.30	1.9	430.77	0.0	428.95	−1.8	434.93	−3.3	445.66	−0.3
5	437.88	−1.4	415.81	−0.9	412.93	−1.7	417.59	−0.8	426.93	+0.8
6	423.53	−3.4	400.88	−1.4	396.89	−2.1	400.20	+0.8	408.16	1.1
7	409.23	−4.4	385.91	−2.6	380.99	0.5	382.89	4.0	389.49	3.5
8	395.05	−2.9	371.14	0.5	365.06	2.3	365.49	5.4	370.61	2.0
9	380.88	−1.3	356.21	0.2	349.09	3.5	348.07	6.2	351.59	−2.1
10	366.66	−0.6	341.35	1.4	332.99	1.9	330.45	3.2	332.33	−11.3
11	352.49	1.0	326.38	0.5	316.88	0.2	312.75	−1.2	312.92	−23.0
12	338.44	4.9	311.46	0.4	300.72	−2.4	294.94	−8.0	293.22	−40.1

[a] The data are due to Douslin, Harrison, and Moore, ref 2. [b] Twenty-four points at half-integer density intervals were used in the calculations, except as noted below. [c] The six density points above 9.5 M were not used in determining the constants for this gas because of the large high-density deviations. [d] $\Delta = T/T_B + d/d_0 - 1$.

for CF_4, or an unsuspected high-density error in the measurements for this gas.

Considering the range of the data, the results shown in Table IV represent the most accurate adherence to the unit compressibility law that has yet been observed. For the three mixtures taken together, the average absolute deviation from linearity over the entire experimental density range is only about two parts in ten thousand. Results such as these strengthen the view that the unit compressibility law is an exact law of nature, and again raise the question of a theoretical explanation. The fact that the law can be obeyed by mixtures as well as pure gases provides the new information that the presence of three different pairwise molecular interaction potentials in one system does not interfere with its operation beyond affecting the constants. The T's and d's of the states for which the effects of the attractive and repulsive forces on Z are balanced continue to be related by eq 1. It would seem that behavior of this generality should follow rather directly from the fundamental laws of mechanics and known molecular interactions.

Corresponding States of CH_4, CF_4, and Their Mixtures

by Eugene M. Holleran and Gary J. Gerardi

Department of Chemistry, St. John's University, Jamaica, New York 11432 *(Received August 5, 1968)*

An excellent correlation of the compressibilities of CH_4, CF_4, and their mixtures is obtained in the three-constant system of corresponding states based on the unit compressibility law. The compressibility factors, $Z = PV/RT$, of the two pure gases and two mixtures are calculated from the data for the 50–50 mixture with an average discrepancy of about 5 parts in 10,000. The reduced equation of state is given in the form, $Z = 1 + k_B Y$, where Y is a function of reduced temperature, T/T_B, and reduced density, d/d_0. A table is given for Y, from which Z can be calculated from a knowledge of the three constants, T_B, d_0, and k_B.

Introduction

The purpose of this paper is to report the correspondence found for the compressibility factors of CH_4, CF_4, and their mixtures in the three-constant system of corresponding states based on the unit compressibility law (UCL). In this system the two UCL constants, T_B and d_0, are used to reduce temperature and density. The Boyle temperature, T_B, and the characteristic density, d_0, are defined by the unit compressibility law[1]

$$T_1/T_B + d_1/d_0 = 1 \qquad (1)$$

(1) E. M. Holleran, *J. Chem. Phys.*, **47**, 5318 (1967).

where T_1 and d_1 are the temperatures and densities of the states of the fluid in which the compressibility factor, $Z = PV/RT$, equals unity.

A good correspondence was found[2] between the compressibility factors of Ar and Xe at equal temperatures, θ, and reduced densities, δ, where

$$\theta = T/T_B; \quad \delta = d/d_0 \tag{2}$$

However, the extent of the agreement was made somewhat unclear by small uncertainties in the constants and the data. In a more tractable temperature range, and with more reliable constants, the attainment of a good correlation of the compressibilities of Ar and CH_4 was found to require the introduction of a third constant.[3] This constant was defined as the ratio of the deviations from ideality, $(Z - 1)$, of the two gases at equal θ's and δ's. With this additional constant, the compressibility factor for CH_4 was calculated from the data for Ar with an average deviation of only four parts in ten thousand.

The characteristic density d_0 is related to the second and third virial coefficients, B and C, by the equation[4]

$$d_0 = V_B/C_B \tag{3}$$

in which C_B is C at T_B, and V_B is the Boyle volume, $T_B(dB/dT)_{T_B}$. Using this relationship, the third constant mentioned above was identified[5] as the ratio for the two gases of their constants k_B defined as

$$k_B = d_0V_B = d_0^2C_B = V_B^2/C_B \tag{4}$$

Thus, the $(Z - 1)$ ratio equals the k_B ratio, and according to this three-constant system of corresponding states, $(Z - 1)/k_B$ is taken as a universal function of θ and δ. With this assumption, the compressibilities and related properties of fluids can be correlated accurately in terms of their three characteristic constants, T_B, d_0, and k_B, with the effect of k_B given analytically.

In order to obtain a correspondence as accurate as that found in ref 3, it is necessary to have reliable experimental values of these constants (at least T_B and d_0; k_B can be found from the correlation). Unfortunately such information is presently not yet available for most substances. However, the precise experimental data of Douslin, Harrison, and Moore[6] for CH_4, CF_4, and three of their mixtures have provided accurate constants[6,7] (Table I), and these gases and mixtures therefore represent an excellent opportunity to apply this three-constant system of corresponding states.

Table I: Constants for the Five Gases

%CH_4	T_B, °K	d_0, mol/l.	k_B[a]	k[b]	k_B ratio
100	509.2	35.73	1.94	0.7924	0.80
75	490.5	32.87	2.22	0.9038	0.91
50	493.1	30.77	2.43	1.0000	1.00
25	505.0	28.91	2.62	1.0903	1.08
0	521.0	27.70	2.88	1.2085	1.19

[a] Values found as V_Bd_0 in ref 5. [b] Optimum ratio of $(Z - 1)$'s of given gas and 50–50 mixture at equal θ's and δ's.

Compressibility Correlation. The basic correlation for two gases, 1 and 2, is given by

$$\frac{(Z - 1)_2}{(Z - 1)_1} = \frac{(k_B)_2}{(k_B)_1} = k \tag{5}$$

at equal θ's and δ's, with the relative deviations from ideality determined by the k_B ratio, k. From eq 5 the compressibility factors of four of the gases (the two pure gases, and the 75% and 25% CH_4 mixtures) were calculated from that of the 50–50 mixture taken as a reference standard. Assuming equal experimental accuracies for Z, and equally reliable constants, it can be seen from eq 5 that the best reference standard would be the gas with the largest k_B. In this way, the $(Z - 1)$'s calculated for other gases from the reference would always be smaller than those of the reference, and experimental uncertainties would be minimized. The reverse calculation would magnify any errors in the data or in their empirical representation. For this reason argon, with its small k_B, is not well suited as a reference standard, particularly for mixtures containing CF_4, which has a very large k_B. For the present calculations, the 50–50 mixture with its intermediate k_B was a compromise choice as the reference gas because its data fit the unit-compressibility law better[7] than 75% or 100% CF_4, and its UCL constants are therefore more reliably known.

The compressibility data used in the present correlation are those of ref 6 adjusted as in ref 7. The adjustment consisted of multiplying Z by a factor of $(1 + \epsilon)$, with the values of $\epsilon \times 10^6$ used being 8, −7, −19, −29, −40 for the gases containing 100, 75, 50, 25, 0% CH_4, respectively. These constant overall adjustments for each gas were made in order to provide the best fit of the unit compressibility law and hence the most reliable T_B and d_0 values. For the most part, the adjustments are well within experimental error. They modify Z by a few parts in ten thousand at most and so do not change the order of magnitude of the correlation found here.

The compressibility factor for each gas (2) was calculated from the reference gas (1) by

$$Z_2 = (1 - k) + kZ_1 \tag{6}$$

in the region of θ and δ in which the two sets of data overlap. Z_1 for the 50–50 reference mixture was interpolated from its tabulated data by the following two steps. First, for the density interpolation, the Z_1 data at each constant experimental temperature were fit by

(2) E. M. Holleran, *J. Phys. Chem.*, **72**, 1230 (1968).
(3) E. M. Holleran and G. J. Gerardi, *ibid.*, **72**, 3559 (1968).
(4) E. M. Holleran, *J. Chem. Phys.*, **49**, 39 (1968).
(5) E. M. Holleran, *J. Phys. Chem.*, **73**, 167 (1969).
(6) D. R. Douslin, R. H. Harrison, and R. T. Moore, *ibid.*, **71**, 3477 (1967).
(7) E. M. Holleran and G. J. Gerardi, *ibid.*, **73**, 525 (1969).

least squares to a polynomial in the density. It was found that polynomials of the fourth to seventh degree, depending on the temperature, were sufficient to reproduce the data points to within two or three parts per ten thousand. The coefficients of these polynomials are listed in Table II which has been deposited with NAPS.[8] Because they were not intended for extrapolation below the smallest experimental density of 0.75 mol/l., the first coefficients, c_0, were not constrained to unity, and the c_1 values are not very good representations of the second virial coefficient, B. On each of these isotherms, Z_1 was interpolated at the densities for which $\delta_1 = \delta_2$, that is, at the densities given by $d_1 = d_2(d_{01}/d_{02})$, where the d_2 values are the tabulated experimental densities for gas (2).

Second, for the temperature interpolation, these isochoric compressibilities were then fit to an empirical equation quadratic in $1/T$. At every density these equations reproduced the input values with a maximum deviation of two or three parts per ten thousand. On each of these isochores, Z_1 was calculated at the temperatures for which $\theta_1 = \theta_2$, that is, at the temperatures given by $T_1 = T_2(T_{B1}/T_{B2})$, where T_2 are the experimental temperatures.

In calculating Z_2 from Z_1 by eq 6, the values of k used finally were those which gave the smallest sum of absolute deviations, $\Delta = Z_2 - Z_1$. The values of k_B for these gases found in ref 5 as d_0V_B and listed in Table I are probably accurate to within 1%, and their ratios were taken as the first estimates of k. Then by varying k slightly the optimum value was easily found for each gas. These k's are also listed in Table I along with the ratio of the k_B's, and the agreement is seen to be good. The k_B values and their ratios are approximately linear in mole fraction, and in fact the ratios for the five gases are not far from the simple series, 0.8, 0.9, 1.0, 1.1, 1.2.

The experimental compressibilities, Z, (adjusted by the factor $(1 + \epsilon)$, as noted earlier), and the differences between these and the calculated values, $(Z - Z_2) \times 10^4$, are listed in Tables III to VI for the 100, 75, 25, and 0% CH_4 systems. (Tables IV, V, VI have been deposited with NAPS.)[8] The data for all these gases cover the same range of T and d, but because of the differences in T_B and d_0, the ranges of θ and δ do not exactly overlap with the 50% reference. The data points outside the overlap region were not included in Tables III to VI because the calculated Z_2 would require extrapolation rather than interpolation with the empirical equations.

The compressibility correlation obtained in this way is seen in the tables to be excellent. The average absolute differences are 4.9, 3.2, 4.4, and 8.4 units in the fourth decimal place (roughly parts per ten thousand) for the 100, 75, 25, and 0% systems, respectively. Pure CF_4 correlates least well, and this is consistent with the fact that its data also give the poorest fit of the unit compressibility law.[7] For all the gases, the worst agreement occurs generally at the highest densities and temperatures, that is, near the limiting experimental conditions. Omission of some of these peripheral values would permit an improved overall correlation, and would also change the k values slightly. The four decimals given for k in Table I therefore simply represent the values used in the present calculations and do not indicate the absolute accuracy of the k_B ratios, which is still probably not better than ±0.5%.

It should also be noted that since CH_4 and Ar correlate very well,[3] we can expect that the compressibility of Ar can also be calculated accurately from the 50–50 (or other) CH_4–CF_4 mixture, although the reverse would be somewhat less accurate as discussed earlier.

Generalized Equation of State. The above results demonstrate the correspondence of the quantity $(Z - 1)/k_B$ for these five gases at equal reduced temperatures and densities. As shown in ref 3, this implies a similar correspondence of the reduced residual thermodynamic properties divided by k_B. It also implies the correspondence of B/V_B and C/C_B at equal reduced temperatures, and these implications appear to be borne out at ordinary temperatures by both experimental measurements and theoretical calculations, as discussed in ref 5.

If this behavior proves to be general, then the properties of any gas can be found from a knowledge of its three constants, T_B, d_0, k_B, and a tabulation of the reduced properties as functions of θ and δ. In particular, the equation of state can be given in generalized form by

$$Z = 1 + k_B \times Y(\theta, \delta) \qquad (7)$$

where $Y(\theta, \delta)$ can be tabulated from accurately known measurements of $(Z - 1)/k_B$ for one or several reference gases. In Table VII are listed the values of Y as derived from the 50–50 mixture data at small enough intervals of θ (0.02) and δ (0.01) to permit easy interpolation. The value of k_B was taken as 2.430, and if this should later prove to be in error, Y will have to be corrected accordingly. The unit-Z line can be seen running diagonally through Table VII.

Given T_B, d_0, and k_B, the compressibility factor can be found from Table VII for (as we assume) any gas at any temperature and density in this range by interpolating Y at $\theta = T/T_B$ and $\delta = d/d_0$, and applying eq 7. For example, spot checks with CH_4, CF_4, and the three mixtures show that this procedure will quickly give Z accurate to the third decimal in most cases, (*i.e.*, within about 0.1%). Calculations for Ar also give good results, as might be expected. For N_2, using the constants given in ref 5 and 7, a few test calculations show somewhat greater discrepancies, but this could

(8) For Tables II, IV, V, and VI, order NAPS Document 00164 from ASIS, National Auxiliary Publications Service c/o CCM Information Sciences, Inc., 22 West 34th Street, New York, N. Y. 10001, remitting $1.00 for microfiche or $3.00 for photocopies.

Table III: Correspondence of Pure CH_4 with the 50% Mixture[a]

	Density, mol/l.						
t, °C	1.0	1.5	2.0	2.5	3.0	3.5	4.0
25	0.9596	0.9412	0.9240	0.9079	0.8932	0.8796	0.8673
	0	−1	−2	−3	−4	−5	−6
30	0.9615	0.9439	0.9275	0.9124	0.8986	0.8859	0.8743
	0	−1	−2	−3	−2	−2	−3
50	0.9680	0.9536	0.9404	0.9282	0.9172	0.9074	0.8988
	−1	−3	−3	−5	−6	−6	−6
75	0.9750	0.9640	0.9540	0.9451	0.9373	0.9307	0.9250
	−1	−3	−5	−5	−6	−6	−7
100	0.9809	0.9728	0.9657	0.9596	0.9545	0.9505	0.9475
	−1	−3	−3	−3	−4	−4	−4
125	0.9859	0.9803	0.9755	0.9717	0.9690	0.9673	0.9667
	−2	−2	−4	−5	−4	−3	−2
150	0.9903	0.9868	0.9842	0.9825	0.9817	0.9821	0.9833
	−1	−1	−2	−2	−2	−1	−2
175	0.9941	0.9924	0.9916	0.9917	0.9927	0.9948	0.9980
	0	−1	−1	−1	−1	−1	1
200	0.9974	0.9974	0.9982	0.9999	1.0026	1.0061	1.0106
	0	0	0	1	1	0	1
225	1.0004	1.0017	1.0040	1.0071	1.0111	1.0161	1.0220
	0	0	1	1	1	2	2
250	1.0031	1.0057	1.0092	1.0135	1.0187	1.0250	1.0322
	1	1	2	2	2	3	3
275	1.0054	1.0091	1.0139	1.0193	1.0257	1.0329	1.0413
	1	1	3	3	3	3	4
300	1.0075	1.0122	1.0179	1.0243	1.0317	1.0401	1.0494
	1	1	2	2	2	3	3
325	1.0094	1.0151	1.0217	1.0290	1.0375	1.0466	1.0568
	2	1	3	3	4	4	4
350	1.0112	1.0177	1.0252	1.0335	1.0425	1.0528	1.0638
	2	3	4	6	5	7	6

	Density, mol/l.						
t, °C	4.5	5.0	5.5	6.0	6.5	7.0	7.5
25	0.8563	0.8465	0.8381	0.8310	0.8251	0.8208	0.8179
	−6	−6	−4	−3	−3	−1	2
30	0.8641	0.8550	0.8473	0.8409	0.8358	0.8322	0.8295
	−3	−3	−3	−2	−1	1	−1
50	0.8915	0.8853	0.8800	0.8764	0.8744	0.8732	0.8733
	−4	−4	−6	−4	1	1	1
75	0.9207	0.9175	0.9156	0.9150	0.9153	0.9174	0.9204
	−5	−4	−2	0	−1	4	4
100	0.9456	0.9450	0.9455	0.9472	0.9501	0.9548	0.9603
	−4	−3	−3	−2	−2	3	3
125	0.9673	0.9688	0.9716	0.9753	0.9807	0.9870	0.9951
	−1	0	1	0	3	2	5
150	0.9856	0.9891	0.9937	0.9996	1.0067	1.0151	1.0248
	−2	−1	−1	0	0	1	0
175	1.0021	1.0070	1.0136	1.0211	1.0299	1.0399	1.0515
	1	−1	2	2	3	1	0
200	1.0163	1.0229	1.0309	1.0397	1.0503	1.0617	1.0747
	1	0	2	0	3	0	−4
225	1.0291	1.0373	1.0464	1.0567	1.0683	1.0814	1.0956
	3	5	3	3	1	0	−5
250	1.0404	1.0499	1.0602	1.0719	1.0846	1.0988	1.1142
	4	5	4	4	1	−2	−7
275	1.0508	1.0611	1.0726	1.0855	1.0992	1.1145	1.1309
	5	5	4	5	1	−3	−11
300	1.0597	1.0712	1.0836	1.0975	1.1123	1.1282	
	3	4	2	2	−1	−10	
325	1.0680	1.0803	1.0937	1.1083	1.1239	1.1404	
	3	2	1	−1	−6	−19	
350	1.0759	1.0891	1.1033	1.1186	1.1352		
	6	5	3	0	−3		

	Density, mol/l.						
t, °C	8.0	8.5	9.0	9.5	10.0	10.5	11.0
25	0.8163	0.8163	0.8179	0.8214	0.8263	0.8335	0.8424
	4	6	10	14	15	19	18
30	0.8290	0.8297	0.8321	0.8358	0.8416	0.8495	0.8596
	4	7	10	10	12	16	19
50	0.8754	0.8789	0.8841	0.8909	0.8991	0.9096	0.9222
	6	8	14	16	15	16	16
75	0.9252	0.9316	0.9396	0.9493	0.9607	0.9740	0.9895
	6	10	12	13	12	10	6
100	0.9674	0.9762	0.9865	0.9992	1.0130	1.0287	1.0470
	2	4	3	7	2	−4	−5
125	1.0046	1.0156	1.0278	1.0426	1.0588	1.0769	1.0972
	6	6	1	3	−2	−11	−14
150	1.0362	1.0488	1.0633	1.0794	1.0977		
	0	−4	−8	−13	−21		
175	1.0647	1.0791	1.0952	1.1134			
	0	−3	−9	−12			
200	1.0895	1.1050	1.1229				
	−4	−13	−17				
225	1.1114	1.1285					
	−10	−17					
250	1.1311						
	−14						

	Density, mol/l.		
t, °C	11.5	12.0	12.5
25	0.8541	0.8672	0.8837
	22	19	19
30	0.8712	0.8858	0.9023
	15	17	9
50	0.9372	0.9540	0.9737
	15	6	−2
75	1.0068	1.0269	1.0503
	−3	−23	−26
100	1.0676	1.0904	
	−11	−45	

[a] The compressibility Z, and $[Z - Z(\text{calcd})] \times 10^4$.

easily be due to the present uncertainties in the values of the constants.

As far as can be seen at the present time, this three-constant system of corresponding states is very promising. It has the advantage of requiring only one graph or table (such as Table VII) to represent the compressibilities of substances with different values of the third constant, k_B. In this respect it is superior to the sys-

Table VII: Generalized Compressibility. The Quantity $10^4(Z-1)/k_B$ as a Function of Reduced Temperature and Density

	θ									
δ	0.55	0.57	0.59	0.61	0.63	0.65	0.67	0.69	0.71	0.73
0.03	−264	−241	−219	−199	−180	−163	−148	−133	−119	−106
0.04	−345	−314	−285	−259	−235	−212	−191	−172	−154	−137
0.05	−423	−384	−349	−316	−286	−258	−232	−208	−185	−164
0.06	−497	−451	−409	−370	−334	−301	−270	−241	−215	−189
0.07	−568	−515	−466	−421	−379	−341	−305	−272	−241	−212
0.08	−635	−575	−520	−469	−422	−378	−338	−300	−265	−232
0.09	−699	−632	−570	−513	−461	−412	−367	−325	−286	−249
0.10	−759	−685	−618	−555	−497	−444	−394	−347	−304	−263
0.11	−816	−735	−662	−593	−530	−472	−417	−367	−319	−275
0.12	−869	−782	−703	−629	−560	−497	−438	−383	−331	−283
0.13	−919	−826	−740	−661	−587	−519	−456	−396	−341	−289
0.14	−966	−866	−774	−690	−611	−538	−470	−407	−347	−291
0.15	−1009	−903	−805	−715	−632	−554	−482	−414	−350	−291
0.16	−1048	−936	−833	−738	−649	−566	−490	−418	−351	−287
0.17	−1084	−966	−857	−756	−663	−576	−494	−418	−347	−280
0.18	−1117	−993	−878	−772	−673	−581	−496	−416	−341	−270
0.19	−1116	−1015	−895	−784	−680	−584	−494	−409	−330	−256
0.20	−1171	−1035	−909	−792	−683	−582	−488	−400	−317	−239
0.21	−1192	−1050	−918	−797	−683	−578	−479	−386	−300	−218
0.22	−1209	−1061	−924	−797	−679	−569	−466	−369	−278	−193
0.23	−1223	−1069	−927	−794	−671	−556	−448	−348	−253	−164
0.24	−1232	−1073	−925	−787	−659	−539	−427	−322	−223	−131
0.25	−1238	−1072	−918	−775	−642	−518	−401	−292	−189	−92
0.26	−1239	−1067	−908	−759	−621	−492	−371	−257	−150	−49
0.27	−1236	−1057	−892	−738	−595	−461	−335	−217	−106	0
0.28	−1228	−1043	−872	−712	−564	−425	−294	−172	−56	52
0.29	−1215	−1024	−846	−681	−527	−383	−248	−121	0	111
0.30	−1196	−999	−816	−645	−486	−336	−196	−64	60	176
0.31	−1172	−968	−779	−602	−437	−283	−138	0	126	247
0.32	−1142	−931	−736	−553	−383	−223	−72	68	200	325
0.33	−1105	−888	−686	−498	−322	−157	0	144	281	410
0.34	−1062	−838	−629	−434	−253	−83	78	227	368	501
0.35	−1012	−780	−565	−364	−176	0	164	318	464	
0.36	−953	−714	−492	−285	−92	89	259	418	569	
0.37	−886	−641	−413	−200	0	189	366	533	692	
0.38	−810	−558	−323	−105	103	297	479	651		
0.39	−725	−466	−223	0	215	414	601	778		

	θ												
δ	0.75	0.77	0.79	0.81	0.83	.085	0.87	0.89	0.91	0.93	0.95	0.97	0.99
0.03	−94	−83	−72	−62	−53	−44	−36	−28	−20	−13	−6	0	6
0.04	−121	−106	−92	−79	−66	−54	−43	−33	−23	−13	−4	4	12
0.05	−145	−126	−109	−92	−77	−62	−49	−35	−23	−11	0	11	21
0.06	−166	−144	−123	−104	−85	−68	−51	−36	−21	−7	6	19	31
0.07	−185	−159	−135	−113	−91	−71	−52	−34	−16	0	15	30	44
0.08	−201	−172	−145	−119	−94	−71	−50	−29	−10	9	27	44	60
0.09	−214	−182	−151	−122	−95	−69	−45	−22	0	21	41	60	78
0.10	−225	−189	−155	−123	−93	−65	−38	−12	12	35	57	78	98
0.11	−233	−194	−157	−122	−89	−57	−28	0	27	52	76	99	121
0.12	−238	−195	−155	−117	−81	−47	−15	15	44	72	98	123	147
0.13	−240	−194	−151	−110	−71	−34	0	33	65	94	123	150	176
0.14	−239	−190	−143	−99	−58	−19	19	54	88	120	151	180	208
0.15	−235	−183	−133	−86	−42	0	40	78	114	148	181	212	242
0.16	−228	−172	−119	−69	−22	22	65	105	144	180	215	248	280
0.17	−218	−158	−102	−50	0	48	93	136	176	215	252	288	321
0.18	−204	−141	−82	−26	26	77	124	169	213	254	293	330	366
0.19	−186	−121	−58	0	56	109	159	207	252	296	337	376	414
0.20	−165	−96	−31	31	89	145	198	248	296	341	385	426	466
0.21	−141	−69	0	65	126	185	240	293	343	391	437	481	523
0.22	−113	−37	35	103	168	229	287	342	395	446	494	540	584
0.23	−80	0	74	146	213	277	338	396	451	504	554	602	648

Table VII (*Continued*)

0.24	−43	40	118	192	263	330	393	454	512	567	620	670	719
0.25	0	85	167	244	318	387	454	517	577	635	690	743	793
0.26	45	135	220	301	377	450	519	585	648	708	765	820	873
0.27	97	191	279	363	442	518	590	659	724				
0.28	154	251	343	430	513	591							
0.29	217	318	413	503	589	670							
0.30	287	391	490	584	674	759							
0.31	362	470	573	670	762	851							
0.32	444	556	662	763									
0.33	533												
0.34	627												

	θ											
δ	1.01	1.03	1.05	1.07	1.09	1.11	1.13	1.15	1.17	1.19	1.21	1.23
0.03	12	18	23	28	33	38	42	47	51	55	59	63
0.04	20	28	35	42	48	54	60	66	72	77	82	87
0.05	30	40	49	57	65	73	80	88	95	101	108	114
0.06	43	54	65	75	85	94	103	111	120	128	135	143
0.07	58	71	83	95	106	117	127	137	147	156	165	174
0.08	75	90	104	117	130	143	144	166	177	188	198	207
0.09	95	111	127	142	157	171	184	197	209	221	233	244
0.10	117	136	153	170	186	201	216	231	244	257	270	282
0.11	142	162	182	200	218	235	251	267	282	296	310	324
0.12	170	192	213	233	252	271	289	306	322	338	353	368
0.13	201	224	247	269	290	310	329	348	365	383	399	415
0.14	234	260	284	308	330	352	372	392	412	430	448	465
0.15	271	298	324	349	374	397	419	440	461	481	500	518
0.16	311	340	368	394	420	445	469	491	513	535	555	574
0.17	354	385	414	443	470	496	522	546	569	592	614	635
0.18	400	433	464	495	523	551	578	604	629	653	676	
0.19	450	485	518	550	581	610						
0.20	504	541	576	609	641							
0.21	563	601	638	674	708							
0.22	626	666	705	743	778							
0.23	693	735	776									
0.24	765	809	852									
0.25	842											
0.26	923											

tems which use as the third constant the critical compressibility factor,[9,10] or the acentricity factor of Pitzer.[11–15] However, because of experimental limitations on the range of the data used, Table VII does not represent extreme deviations from ideality. For CF_4, with the relatively large k_B of 2.88, the Z values extend from 0.69 to 1.21. Also, the system has not been tested for greatly dissimilar compounds. Although CF_4 and CH_4 differ considerably in k_B, so that $(Z - 1)$ for CF_4 is always about 50% greater than for CH_4, the difference appears to be due mainly to molecular size. It would be interesting to test polar compounds, but unfortunately their Boyle temperatures are relatively high, and good quality PVT data are usually in a region of θ and δ which does not permit direct evaluation of the constants T_B and d_0 by eq 1, and in large part does not overlap Table VII.

Further application of this system will depend on (a) its general validity, (b) the accurate determination of characteristic constants for additional gases, (c) the extension of Table VII to wider ranges of θ and δ, and (d) the preparation of similar tables for other properties.

Acknowledgment. Although the experimental data are cited in the text, the authors wish to acknowledge a special indebtedness to D. R. Douslin, R. H. Harrison, and R. T. Moore, without whose careful measurements the present work would have been impossible.

(9) H. P. Meissner and R. Seferian, *Chem. Eng. Progr.*, **47**, 579 (1951).

(10) A. L. Lydersen, R. A. Greenkorn, and O. A. Hougen, College of Engineering, University of Wisconsin, Engineering Experimental Station Report 4, Madison, Wis., Oct 1955.

(11) K. S. Pitzer, *J. Amer. Chem. Soc.*, **77**, 3427 (1955).

(12) K. S. Pitzer, D. Z. Lippmann, R. F. Curl, C. M. Huggins, and D. E. Petersen, *ibid.*, **77**, 3433 (1955).

(13) K. S. Pitzer and R. F. Curl, Conference on Thermodynamics and Transport Properties of Fluids, London, July 1957.

(14) W. C. Edmister, *Petrol. Refiner*, **37**, 173 (1958).

(15) N. Satter, N. Abdus, and J. M. Campbell, *Soc. Petrol. Eng. J.*, 333 (1963).

Physical Properties and Chemical Reactivity of Alternant Hydrocarbons and Related Compounds. XVII.[1] Electronic Spectra of Amino and Hydroxy Derivatives of Benzenoid Hydrocarbons

by M. Tichý

Institute of Industrial Hygiene and Occupational Diseases, Prague, Czechoslovakia

and R. Zahradník

Institute of Physical Chemistry, Czechoslovak Academy of Sciences, Prague, Czechoslovakia *(Received June 24, 1968)*

The electronic absorption spectra of the monoamino and monohydroxy derivatives of benzene, naphthalene, and of derivatives of phenanthrene, pyrene, and benzo[*c*]phenanthrene were recorded in 50% aqueous methanol and in alkaline (0.2 *M* NaOH) 50% aqueous methanol. For 11 representatives, the position of the first $S \rightarrow T_1$ transitions were estimated from phosphorescence spectra. It was found that several first bands of the absorption curves ($S_0 \rightarrow S_x$ transitions) can be reasonably interpreted by means of the unmodified method of Pariser, Parr, and Pople, using the Mataga–Nishimoto approximation for the electron repulsion integrals.

In recent years, semiempirical methods have been widely employed in the study of the properties of an extensive series of conjugated hydrocarbons and their derivatives.[2] The shortcomings of these calculations are mainly the following: (i) the theory is usually checked on a relatively small series of substances, (ii) insufficient attention is paid to the structural homogeneity of the individual groups, and (iii) higher degrees of accuracy are attempted with an increase in the numbers of empirical parameters, without achieving an essential improvement in the agreement between experimental and theoretical data. Of course, the old disadvantage encountered in the application of the HMO method is also manifested. Only in a few cases is it possible to find papers of different authors whose results are safely comparable. The nonuniformity involved in the use of the HMO method is far less consequential; the most serious source of nonuniformity is not due to the use of different numerical values for the monocentric and bicentric core integrals (α_μ^c, $\beta_{\mu\nu}^c$) but rather (i) to the possibility of expressing α_μ^c (*cf.* ref 3) and $\beta_{\mu\nu}^c$ (*cf.* ref 4) as functions of q_μ (π-electron density on an atom μ) and $p_{\mu\nu}$ (a bond order between atoms μ and ν), which is utilized only by some authors (moreover, the shape of the functional dependence usually varies), and (ii) to the use of several types of expressions for the approximation of the mono-[5] and the bicentric electron repulsion integrals.[6–11]

We believe that until it is possible to suggest a generally applicable version of a semiempirical method based upon systematic studies, it is appropriate to utilize the *simplest possible* version of the LCI–SCF method. For this reason we employed the original method of Pariser, Parr, and Pople (here referred to as PPP), in which bicentric electron repulsion integrals were approximated according to Mataga and Nishimoto;[8] for the monocentric integrals, the approximation of Pariser was used.[5]

The applicability of the PPP method has already been studied for numerous alternant[2,12–17] as well as nonalternant[18–20] hydrocarbons, of heteroanalogs of the pyridine type,[21–22] and of various sulfur-containing heterocyclic systems.[23] (For a review see ref 2, 24).

(1) Part XVI: C. Párkányi, E. J. Baum, J. Wyatt, and J. N. Pitts, Jr., *J. Phys. Chem.*, in press.

(2) R. G. Parr, "The Quantum Theory of Molecular Electronic Structure," W. A. Benjamin, Inc., New York, N. Y., 1963.

(3) R. D. Brown and M. L. Heffernan, *Aust. J. Chem.*, **13**, 38 (1960).

(4) C. A. Coulson and A. Gołebiewski, *Proc. Phys. Soc.* (London), **78**, 1310 (1961).

(5) R. Pariser, *J. Chem. Phys.*, **21**, 568 (1953); **24**, 250 (1956).

(6) J. A. Pople, *Trans. Faraday Soc.*, **49**, 1375 (1953).

(7) R. Pariser and R. G. Parr, *J. Chem. Phys.*, **21**, 466, 767 (1953).

(8) N. Mataga and K. Nishimoto, *Z. Physik. Chem.* (Frankfurt), **13**, 140 (1957).

(9) K. Ohno, *Advan. Quantum Chem.*, **3**, 239 (1967).

(10) K. Ohno, *Theoret. Chim. Acta*, **2**, 219 (1964).

(11) K. Nishimoto, *ibid.*, **5**, 74 (1966).

(12) J. Koutecký, J. Paldus, and R. Zahradník, *J. Chem. Phys.*, **36**, 3129 (1962).

(13) N. S. Ham and K. Ruedenberg, *ibid.*, **25**, 13 (1956).

(14) R. L. Hummel and K. Ruedenberg, *J. Phys. Chem.*, **66**, 2334 (1962).

(15) R. S. Becker, I. S. Singh, and E. A. Jackson, *J. Chem. Phys.*, **38**, 2144 (1963).

(16) J. E. Bloor, B. R. Gilson, and N. Brearley, *Theoret. Chim. Acta*, **8**, 35 (1967).

(17) N. L. Allinger, M. A. Miller, L. W. Chow, R. A. Ford, and J. C. Graham, *J. Amer. Chem. Soc.*, **87**, 3430 (1965).

(18) E. Heilbronner and J. N. Murrell, *Mol. Phys.*, **6**, 1 (1963).

(19) J. Koutecký, P. Hochman, and J. Michl, *J. Chem. Phys.*, **40**, 2439 (1964).

(20) N. L. Allinger, J. Chow Tai, and T. W. Stuart, *Theoret. Chim. Acta*, **8**, 101 (1967).

(21) G. Favini, I. Vandoni, and M. Simonetta, *ibid.*, **3**, 45 (1965).

(22) J. Koutecký, unpublished results, 1966.

(23) J. Fabian, A. Mehlhorn, and R. Zahradník, *J. Phys. Chem.*, **72**, 3975 (1968).

(24) R. Zahradník, *Fortschr. Chem. Forsch.*, **10**, 1 (1968).

A suitable extension of this work appeared to be a study of derivatives of aromatic hydrocarbons in which the heteroatom is an exocyclic atom. PPP studies of derivatives were the subject of a number of papers, the majority of which, however, was only concerned with aniline, phenol, and benzene derivatives with several substituents. Only a few papers deal with naphthalene derivatives[25-31] (in this connection we quote only papers on derivatives of benzenoid hydrocarbons formed by the attachment of substituents that carry only one p_zAO contributing two π-electrons to conjugation).[32] Simultaneously with our work, initial studies were undertaken of larger groups of derivatives of polynuclear hydrocarbons (amino and hydroxy derivatives,[33-36] thiophenols[37]). Recently, we have been concerned with arylmethyl cations[38] and with derivatives of odd alternant systems, perinaphthenones.[39]

In view of the importance of the hydroxy and amino derivatives of benzenoid hydrocarbons, we considered it desirable to measure the spectra of all systems in question in the region 50–20 kK under uniform conditions. The comparison of theoretical excitation energies and oscillator strengths with experimental data is the main subject of the present paper.

Calculations

The original version of the PPP method was employed (details are given in ref 40). The values of the empirical parameters employed are summarized in Table I.

Table I: Empirical Parameters for LCI–SCF Calculations (Description in the Text)

Atom, μ	I_μ, eV	A_μ, eV	$\gamma_{\mu\mu}$, eV	$\beta_{\mu C^6}$, eV
C	11.22	0.69	10.53	−2.388
N	27.3	9.3	18.0	−1.910
O	32.9	10.0	22.9	−2.388
O^-	21.0	9.5	11.5	−2.388

In Table I, I_μ, A_μ, $\gamma_{\mu\mu}$, and $\beta_{\mu C^6}$ stand for the valence-state ionization potential, the electronic affinity, the monocentric electronic repulsion integral, and the core resonance integral, respectively. The bicentric repulsion integrals have been calculated from the Mataga–Nishimoto formula[8]

$$\gamma_{\mu\nu} = \frac{14.399}{R_{\mu\nu} + a_{\mu\nu}} \text{ eV}$$

where $R_{\mu\nu}$ (Å) is the distance between atoms μ and ν and $a_{\mu\nu}$ is a constant, the value of which equals 1.382 Å for both carbon–carbon and carbon–heteroatom pairs. In a parameter study, we have found (the results of a calculation are not shown here because of lack of space) that changes in $a_{\mu\nu}$ values used for carbon–heteroatom pairs have an insignificant effect on the results.[41] For this reason, we prefer to use the constant value of $a_{\mu\nu}$ for all pairs.

The values given for the empirical parameters (Table I) are based upon a parameter study in which we considered separately changes of I_μ (10–30 eV), $\gamma_{\mu\nu}$ (10–30 eV), and $\beta_{\mu\nu}$ (0.5–2.0 eV).[42] The selection of the parameters was carried out by comparison of the calculated excitation energies and oscillator strengths with the experimental absorption curves of naphthylamines, naphthols, and naphtholates.

Generally 16 monoexcited configurations, formed by excitation of an electron from the four highest occupied into the four lowest free molecular orbitals, were included in our calculations. In the case of benzene derivatives, all monoexcitated configurations were taken into consideration.

In the calculations we assumed the same length for all bonds in the molecule, including the carbon–heteroatom bond (1.4 Å), and an idealized geometry ($\sphericalangle$CCC 120°). From our previous work,[40,42] it is relatively certain that the use of an idealized geometry and the consideration of the same length for a carbon–heteroatom exocyclic bond as for a carbon–carbon bond in a molecule have only a negligible effect on the values of energetic characteristics with which we are concerned. Until there are more extensive experimental data (measurements at low temperature, of $S_0 \rightarrow T_1$ transitions, of $T_1 \rightarrow T_x$ transitions, polarization of bands, etc.), any serious attempt at analysis of discrepancies between theoretical calculations and experimental data will be hardly possible.

We abandoned our original intention to present a tabulated survey of the parameters so far employed in the literature, first, in view of the considerable non-

(25) H. Baba and S. Suzuki, *Bull. Chem. Soc. Jap.* **34**, 76 (1961).
(26) H. Baba and S. Suzuki, *ibid.*, **35**, 683 (1962).
(27) K. Nishimoto and R. Fujishiro, *J. Chem. Phys.*, **36**, 3494 (1962).
(28) K. Nishimoto, *J. Phys. Chem.*, **67**, 1443 (1963).
(29) S. Suzuki and H. Baba, *J. Chem. Phys.*, **38**, 349 (1963).
(30) K. Nishimoto and R. Fujishiro, *Bull. Chem. Soc. Jap.* **37**, 1660 (1964).
(31) L. S. Forster and K. Nishimoto, *J. Amer. Chem. Soc.*, **87**, 1459 (1965).
(32) A more detailed literature survey is available on request to the authors.
(33) K. Nishimoto and L. S. Forster, *Theoret. Chim. Acta*, **4**, 155 (1966).
(34) G. W. Pukanic, D. R. Forshey, Br. J. D. Wegener, and J. B. Greenshields, *ibid.*, **9**, 38 (1967).
(35) D. R. Forshey, G. W. Pukanic, Br. J. D. Wegener, and J. B. Greenshields, *ibid.*, **9**, 288 (1968).
(36) J. Michl, R. S. Becker, and C. A. Earhart, in preparation.
(37) J. Fabian, A. Mehlhorn, and G. Tröger, *Theoret. Chim. Acta*, **9**, 140 (1967).
(38) R. Zahradník, A. Krohn, J. Pancíř, and D. Šnobl, *Collection Czech. Chem. Commun.*, in press.
(39) R. Zahradník, M. Tichý, and D. H. Reid, *Tetrahedron*, **24**, 3001 (1968).
(40) P. Hochmann, R. Zahradník, and V. Kvasnička, *Collection Czech. Chem. Commun.*, in press.
(41) R. Zahradnik, J. Fabian, and A. Mehlhorn, unpublished results.
(42) M. Tichý, Thesis, Institute of Physical Chemistry, Czechoslovak Academy of Sciences, Prague, 1966.

uniformity of the data and, secondly, because such a comparison would be of value only if it offered the possibility of selecting the optimum series of parameters. The published data, however, do not permit such an analysis.

Experimental Section

The electronic absorption spectra were recorded by means of a recording double-beam spectrophotometer (UNICAM SP 700), in a 50% aqueous methanol solution and in an alkaline (0.2 *M* NaOH) 50% aqueous methanol solution. The absorption curves in cyclohexane were also recorded; they will be published in another paper.[43] In our present work we have employed only spectra recorded in aqueous methanol solutions in order to preserve uniform experimental conditions, since the solubility of phenolate anions in nonpolar solvents is insufficient. The phosphorescence of amines was recorded in a solid EPA solution at 77°K by means of Aminco–Bowman spectrofluorimeter equipped with phosphorescence attachment. The phosphorescence in frozen ethanol solutions was measured at 77°K in an apparatus constructed in the laboratory. The results were corrected for the variable sensitivity of the detectors at different wavelengths.[44]

The hydroxy derivatives of anthracene[45,46] and phenanthrene[47,48] were prepared by methods already described. The samples of amino and hydroxy derivatives of benzo[*c*]phenanthrene were obtained from Professor M. S. Newman.[49,50] The other compounds were commercial. Their purity was checked by means of the melting points and also by a comparison of the electronic spectra with data from the literature when these were available. The samples were kept under nitrogen and the measurements were carried out in solutions which had been purged with oxygen-free N_2. The samples were purified by column chromatography on alumina, by repeated crystallization, by distillation under reduced pressure, or by zone melting. The parent skeletons of the compounds studied in the present work are given in Table II. The numbers of positions bearing the substituents are indicated.

Table II: Survey of the Investigated Substances. The Roman Figures I–VII in Tables II, III, and IV Indicate the Parent Hydrocarbon; the Arabic Figures 1–9 Denote the Position in which the Hydrocarbon is Substituted by a Functional Group (NH_2, OH or O^-)

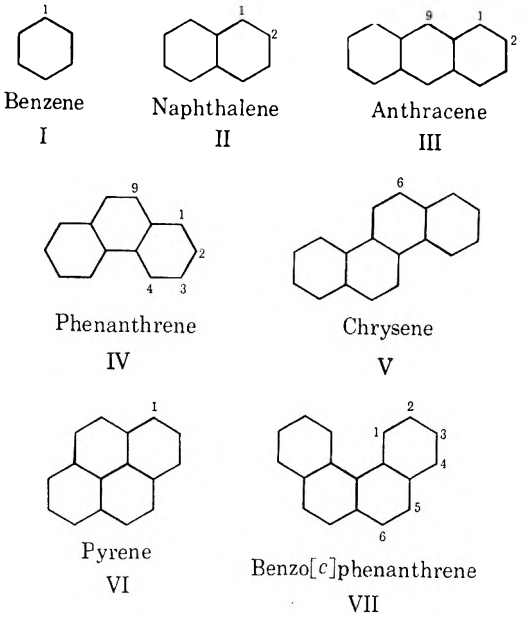

Results and Discussion

The results of the measurements and calculations for 15 amines, 14 phenols, and 14 phenolates are presented in Figures 1–3. The absorption curves were recorded in the region 50–20 kK and are given for the values of log ϵ beginning approximately at 1.7. Figures 1–3 show the absorption curves of the parent hydrocarbons[51] for the sake of comparison (dotted lines). For several compounds, the positions of the maxima of fluorescence[52] and phosphorescence are also presented. Figure 1 does not include the absorption curve of 9-aminoanthracene. The measured experimental curve[53] is in satisfactory agreement with the theoretical spectral data obtained by means of the LCI–SCF method.

The values of the theoretical excitation energies are indicated by the positions of abscissas whose lengths are proportional to the logarithms of the oscillator strength. Because the strong overlap of bands in the electronic spectra of the derivatives does not allow an accurate determination of the experimental oscillator strengths of the individual transitions, a comparison between the theoretical and experimental intensities is less reliable than a comparison of the excitation energies. For this reason, we limit ourselves to an empirical comparison of log f_{th} with log ϵ_{exp} (ϵ being the molar extinction coefficient), and we perform this comparison according to the well established relationship[19]

$$\log \epsilon_{exp} = \log f_{th} + 4$$

The positions of forbidden transitions are indicated by

(43) "UV Atlas of Organic Compounds," Vol. 5, H.-H. Perkampus, Ed., Verlag Chemie, Weinheim; Butterworth and Co. Ltd., London.

(44) E. Lippert, W. Nägele, I. Seibold-Blankenstein, U. Staiger, and W. Voss, *Z. Anal. Chem.*, **170**, 1 (1959).

(45) R. E. Schmidt, *Ber.*, **37**, 66 (1904).

(46) C. Liebermann and A. Bollert, *Ann.*, **212**, 57 (1882).

(47) L. F. Frieser, "Organic Syntheses," Coll. Vol. II, John Wiley and Sons Inc., New York, N. Y., 1943, p 482.

(48) N. O. Foye, M. Weitzenhoff, and A. M. Stranz, *J. Amer. Pharm. Assoc.*, **41**, 312 (1952).

(49) M. S. Newman and J. Blum, *J. Amer. Chem. Soc.*, **86**, 503 (1964).

(50) M. S. Newman and J. Blum, *ibid.*, **86**, 1835 (1964).

(51) E. Clar, "Polycyclic Hydrocarbons," Academic Press, Springer-Verlag, 1964.

(52) I. B. Berlman, Ed., "Handbook of Fluorescence Spectra of Aromatic Molecules," Academic Press, New York, N. Y., 1965.

(53) R. A. Friedel and M. Orchin, "Ultraviolet Spectra of Aromatic Compounds," Bureau of Mines Bulletin, Pittsburgh, Pa., 1951.

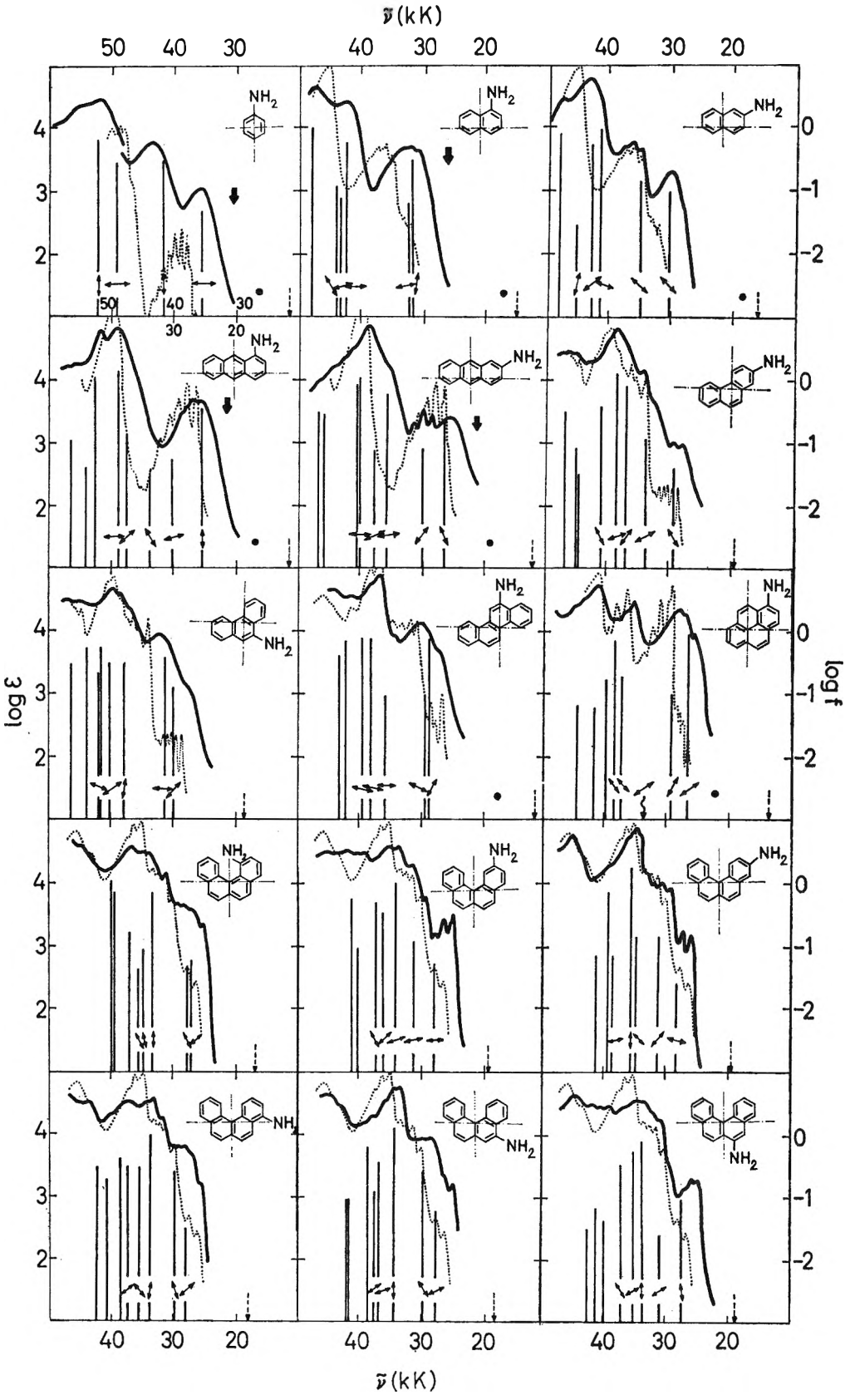

Figure 1. Absorption curves of amines (full thick lines) (50% aqueous methanol) and of parent hydrocarbons[61] (thin dotted lines). Experimental data on the maximum of fluorescence[52] and phosphorescence are indicated by an arrow (↓) and a circle (•), respectively. The results of the LCI–SCF calculations for the excitation energies and oscillator strengths are indicated by vertical straight lines; the directions of polarization are marked by short both-sided arrows. The theoretical position of the $S \rightarrow T_1$ transition is indicated by a short vertical dashed arrow. The formula of the compound with the axes of orientation is given in the upper right corner.

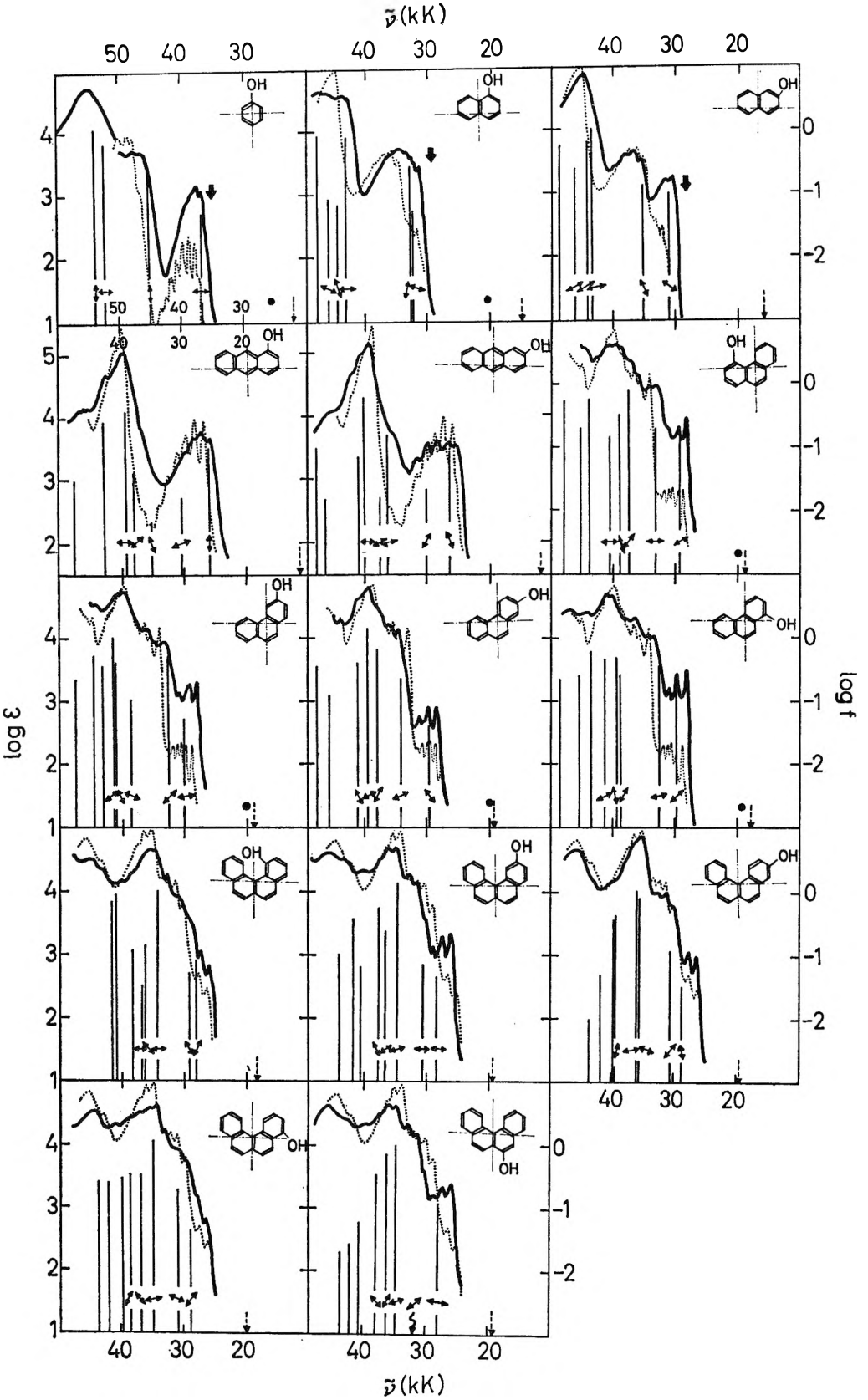

Figure 2. Absorption curves of phenols (50% aqueous methanol) and parent hydrocarbons. For details see the caption to Figure 1.

a wavy line with an arrow. Figures 1–3 also present the theoretical directions of polarization of the individual transitions; these data relate to molecules oriented in the way given in the right upper corners of the figures. Short dashed arrows indicate the theoretical positions of the $S \rightarrow T_1$ transitions.

Excitation Energies. Figures 1–3 present the excitation energies for the first eight $S_0 \rightarrow S_x$ transitions.

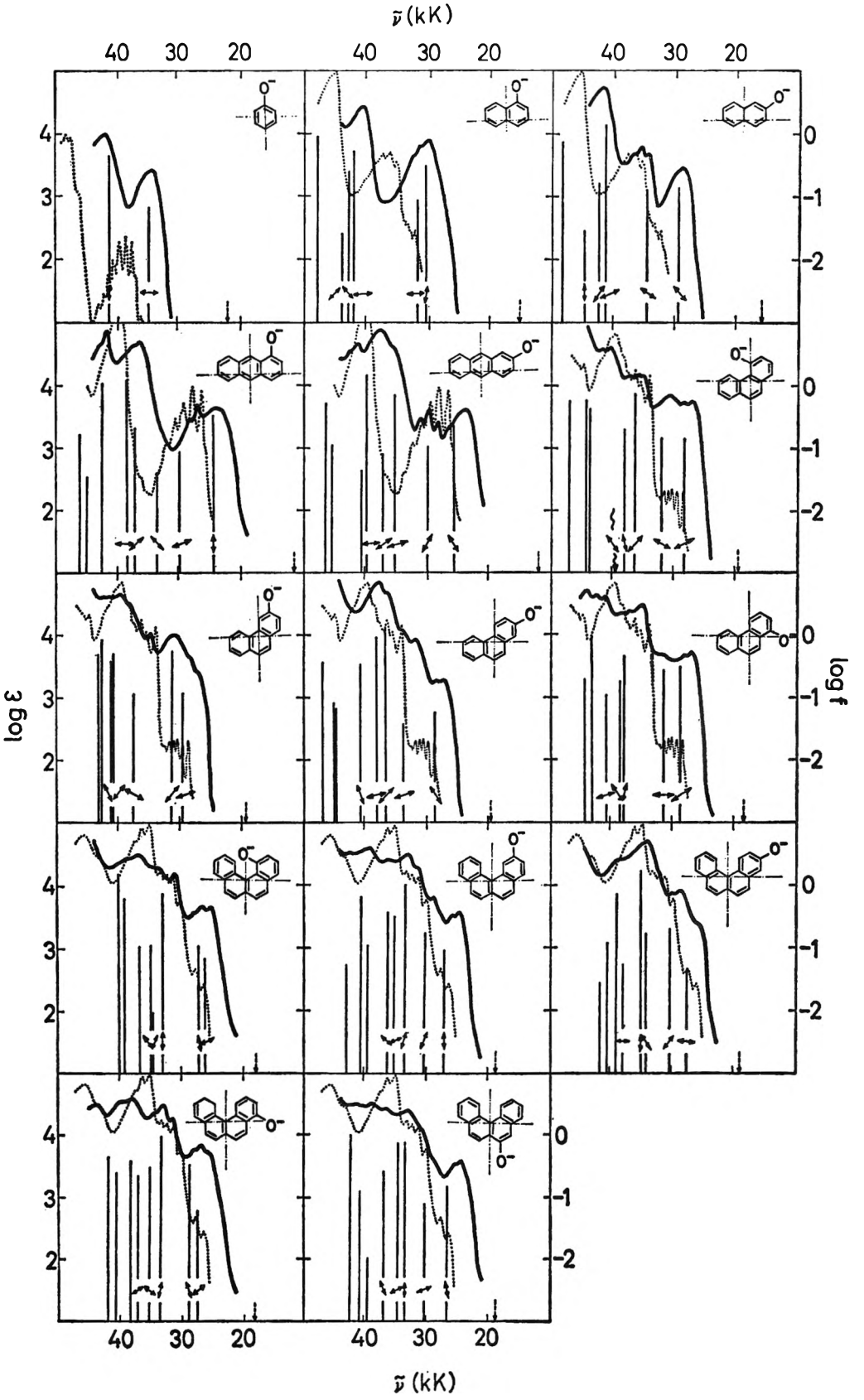

Figure 3. Absorption curves of phenols (0.2 *M* NaOH in 50% aqueous methanol) and of parent hydrocarbons. For detailed explanation see the caption to Figure 1.

Table III: LCI–SCF Spectral Characteristics of Aromatic Amines (See Parameters in Table I)[a]

Compd	ΔE^{LCI} eV	ΔE^{LCI} kK	log f	cos θ	Predominant configurations i, j (wt)
I-1	4.378	35.32	−1.30	0.000	1,1′(79.7); 2,2′(19.5)
	5.161	41.64	−0.43	1.000	1,2′(92.2)
	6.092	49.15	−0.54	0.000	2,2′(56.3); 3,1′(26.1); 1,1′(17.6)
	6.475	52.24	−0.19	1.000	2,1′(85.8)
	7.305	58.93	−0.11	0.000	2,3′(20.0); 3,1′(74.9)
II-1	3.902	31.48	−0.51	0.994	1,1′(94.3)
	3.978	32.09	−1.21	0.203	1,2′(68.6); 2,1′(28.0)
	5.231	42.20	−0.24	0.009	2,1′(35.2); 3,1′(18.2); 1,2′(17.8); 2,2′(16.7)
	5.338	43.07	−1.12	0.293	3,1′(74.0)
	5.421	43.74	−0.93	−0.853	1,3′(91.4)
II-2	3.736	30.14	−1.00	−0.715	1,1′(63.4); 1,2′(13.5); 2,1′(13.5)
	4.304	34.73	−0.87	−0.746	1,2′(33.3); 2,1′(32.0); 1,1′(30.5)
	5.121	41.32	−0.02	0.334	2,1′(40.3); 1,2′(23.6); 3,1′(16.8)
	5.277	42.58	−0.26	0.598	2,2′(24.6); 1,2′(21.4); 3,1′(12.7)
	5.602	45.20	−1.54	0.964	1,3′(66.6); 3,1′(11.4)
III-1	3.167	25.55	−0.46	0.995	1,1′(95.8)
	3.754	30.28	−1.27	0.343	1,2′(60.5); 3,1′(34.2)
	4.187	33.78	−1.51	−0.767	1,2′(93.7)
	4.662	37.61	−0.87	0.656	1,3′(88.2)
	4.818	38.87	0.12	0.013	3,1′(43.0); 1,2′(26.2); 2,2′(12.3)
III-2	3.254	26.25	−0.55	−0.897	1,1′(90.4)
	3.687	29.75	−1.10	0.879	2,1′(50.8); 1,2′(32.5)
	4.388	35.40	−0.22	0.239	3,1′(34.5); 2,1′(32.4); 1,2′(20.5)
	4.647	37.49	−1.14	0.398	1,3′(83.0)
	4.929	39.77	0.02	0.022	3,1′(49.0); 1,2′(20.7); 4,1′(13.7)
III-9	3.185	25.70	−0.36	1.000	1,1′(97.0)
	3.666	29.58	−0.98	0.000	1,2′(69.9); 2,1′(26.8)
	4.155	33.52	−1.28	0.000	1,3′(97.3)
	4.853	39.16	F		4,1′(87.5)
	4.918	39.68	0.20	0.000	2,1′(61.5); 1,2′(22.9); 3,1′(13.2)
IV-2	3.616	29.18	−1.41	−0.890	1,1′(70.1); 2,2′(21.9)
	4.197	33.86	−0.94	0.415	2,1′(69.6); 1,2′(26.8)
	4.573	36.90	−0.11	0.827	1,2′(32.0); 2,1′(15.1); 2,2′(13.7)
	4.757	38.38	0.09	0.312	1,2′(35.9); 2,2′(19.0)
	5.070	40.90	−0.41	−0.898	2,2′(35.7); 1,3′(23.6); 1,1′(12.9)
IV-3	3.695	29.81	−1.18	0.242	2,1′(56.6); 1,2′(26.4); 1,1′(11.4)
	3.973	32.05	−0.26	0.714	1,1′(82.3)
	4.658	37.58	−0.99	−0.340	3,2′(29.1); 2,1′(16.9)
	5.066	40.87	−0.28	0.716	2,2′(51.0); 3,1′(25.9)
	5.100	41.15	−0.29	−0.935	2,1′(38.3); 1,2′(21.5); 3,2′(11.8)
IV-4	3.569	28.80	−0.95	0.468	1,1′(62.4); 1,2′(16.1)
	4.031	32.52	−0.78	−0.194	1,2′(51.7); 1,1′(25.7); 2,1′(17.6)
	4.502	36.32	−0.17	0.773	2,2′(41.2); 2,1′(23.7); 1,2′(13.2)
	4.701	37.93	−0.60	−0.993	2,1′(42.3); 3,1′(25.4); 2,2′(18.0)
	4.959	40.01	−1.71	−0.233	3,2′(26.5); 2,3′(21.6); 4,1′(18.2)
IV-9	3.717	29.99	−0.89	0.745	1,2′(50.6); 1,1′(22.9); 2,1′(21.1)
	3.876	31.27	−0.41	0.029	1,1′(70.1); 1,2′(21.3)
	4.702	37.93	−0.52	0.984	2,1′(48.6); 1,2′(23.6); 1,3′(14.7)
	4.993	40.28	−0.52	0.578	2,2′(54.6); 1,2′(26.8)
	5.168	41.69	−0.27	−0.306	1,3′(36.9); 2,2′(24.3)
V-6	3.542	28.58	−0.13	0.847	1,1′(94.5)
	3.633	29.31	−1.04	−0.315	1,2′(69.4); 2,1′(27.0)
	4.411	35.59	−1.06	0.042	1,3′(92.5)
	4.700	37.92	−0.14	−0.038	2,1′(40.5); 3,2′(16.6); 1,2′(15.8); 1,4′(13.7)
	4.872	39.30	−0.13	−0.061	2,1′(22.8); 1,4′(21.0); 2,3′(15.3); 3,2′(14.0)

Table III (*Continued*)

Compd	ΔE^{LCI} eV	ΔE^{LCI} kK	log f	cos θ	Predominant configurations i, j (wt)
VI-1	3.286	26.51	−0.07	0.577	1,1′(88.7)
	3.604	29.08	−1.00	0.865	1,2′(59.3); 2,1′(28.8)
	4.191	33.81	F		1,3′(96.2)
	4.605	37.15	−0.74	−0.731	4,1′(62.4); 2,1′(20.3)
	4.747	38.30	−0.15	−0.814	2,1′(42.5); 4,1′(30.5); 1,2′(20.8)
VII-1	3.359	27.10	−1.23	0.605	1,1′(74.5); 1,2′(12.8)
	3.430	27.67	−1.29	−0.918	1,2′(53.1); 1,1′(15.3); 2,1′(14.0)
	4.113	33.18	−0.15	0.996	2,1′(42.7); 1,2′(26.3); 3,1′(11.0)
	4.307	34.75	−1.04	−0.980	3,1′(40.6); 2,1′(26.2); 2,2′(23.6)
	4.402	35.51	−1.36	−0.896	1,3′(68.6); 3,1′(12.2)
VII-2	3.498	28.22	−1.29	−0.027	1,1′(62.1); 2,2′(18.8)
	3.894	31.42	−0.93	0.193	1,2′(50.7); 2,1′(26.1); 1,1′(17.7)
	4.260	34.37	0.00	0.278	2,1′(46.2); 2,2′(24.3); 1,2′(13.5)
	4.495	36.27	−0.47	0.725	3,1′(37.8); 1,2′(17.5)
	4.644	37.47	−0.30	−0.869	2,2′(31.9); 1,3′(23.2); 1,1′(15.2); 1,2′(12.2)
VII-3	3.446	27.80	−1.60	−0.225	1,2′(39.8); 2,1′(26.6); 1,1′(22.3)
	3.814	30.77	−0.85	0.703	1,1′(61.6); 1,2′(16.1)
	4.249	34.28	−0.85	−0.736	3,1′(26.1); 3,2′(12.9); 2,2′(12.5); 1,4′(11.0)
	4.347	35.07	0.25	0.999	2,1′(52.0); 1,2′(28.3)
	4.718	38.07	−1.16	0.160	3,1′(32.5); 4,1′(19.4); 3,2′(15.9); 1,4′(14.2)
VII-4	3.466	27.96	−1.50	0.663	1,2′(40.9); 1,1′(19.7); 2,1′(16.3)
	3.697	29.83	−0.60	−0.949	1,1′(59.0); 1,2′(30.7)
	4.178	33.71	−0.02	0.976	2,1′(66.3); 1,2′(15.9)
	4.403	35.52	−0.53	−0.699	2,2′(25.7); 3,1′(20.3)
	4.641	37.44	−0.46	0.540	2,2′(21.2); 1,4′(19.6); 3,2′(14.0)
VII-5	3.431	27.68	−1.23	0.883	1,1′(38.4); 1,2′(32.9); 2,1′(11.8)
	3.694	29.80	−0.61	−0.503	1,1′(46.6); 1,2′(41.5)
	4.266	34.42	0.10	0.066	2,1′(73.9); 1,2′(14.7)
	4.572	36.88	−0.46	0.936	2,2′(47.1); 1,4′(17.5)
	4.660	37.59	−0.92	0.779	1,3′(76.1)
VII-6	3.372	27.20	−1.04	−0.987	1,1′(72.9); 2,2′(16.9)
	3.812	30.76	−1.60	0.536	1,2′(53.2); 2,1′(41.7)
	4.163	33.59	−0.09	0.000	2,2′(52.7); 1,1′(14.5)
	4.334	34.96	−0.25	0.465	2,1′(43.1); 1,2′(36.0)
	4.586	37.00	−0.46	−0.858	1,3′(23.0); 3,1′(15.7); 1,4′(14.8); 2,2′(13.2); 2,4′(11.8)

[a] F means forbidden transition; ΔE^{LCI} are $S_0 \rightarrow S_x$ excitation energies (of the first five states); log f is the logarithm of the oscillator strength; θ is the angle between the vector of the transition moment and the y axis of the molecule (ordinate) (see designation in Figures 1–3); wt is the weight of the $i \rightarrow j$ configuration in the respective CI-wave function.

However, only the data for the first three to four transitions are usually suitable for interpretation. In the presentation we prefer to use the method of comparing theory and experiment as employed in Figures 1–3 for absorption curves with well developed absorption bands. Nevertheless it is noteworthy that the correlation of the energies of the maxima of the first three bands with the theoretical energies of the electron transitions from the ground state to the first three excited states is significant. (The choice of bands is difficult due to their overlapping. Therefore, only well resolved spectra have been chosen). Much less conclusive is the analogous dependence for the $S \rightarrow T_1$ transitions. This is not surprising, for it is known that the approximation of the γ integrals according to Mataga and Nishimoto, though satisfactory for $S_0 \rightarrow S_x$ transitions, is unsatisfactory for $S \rightarrow T$ transitions.[11] One should note that the energies of the maxima of phosphorescence correlate satisfactorily with the HMO energies of the $N \rightarrow V_1$ transitions. This is not surprising, because we have recently found a close correlation for an extensive set of data of this kind for substances of different structural types.[54]

Intensities. As already pointed out, although the comparison of theoretical and experimental data is a rough method, it can be stated that the calculated values indicate semiquantitatively the differences in the experimental data (for the first three to four bands).

Directions of Polarization. No studies have as yet

(54) R. Zahradník, and J. Pancíř, unpublished results.

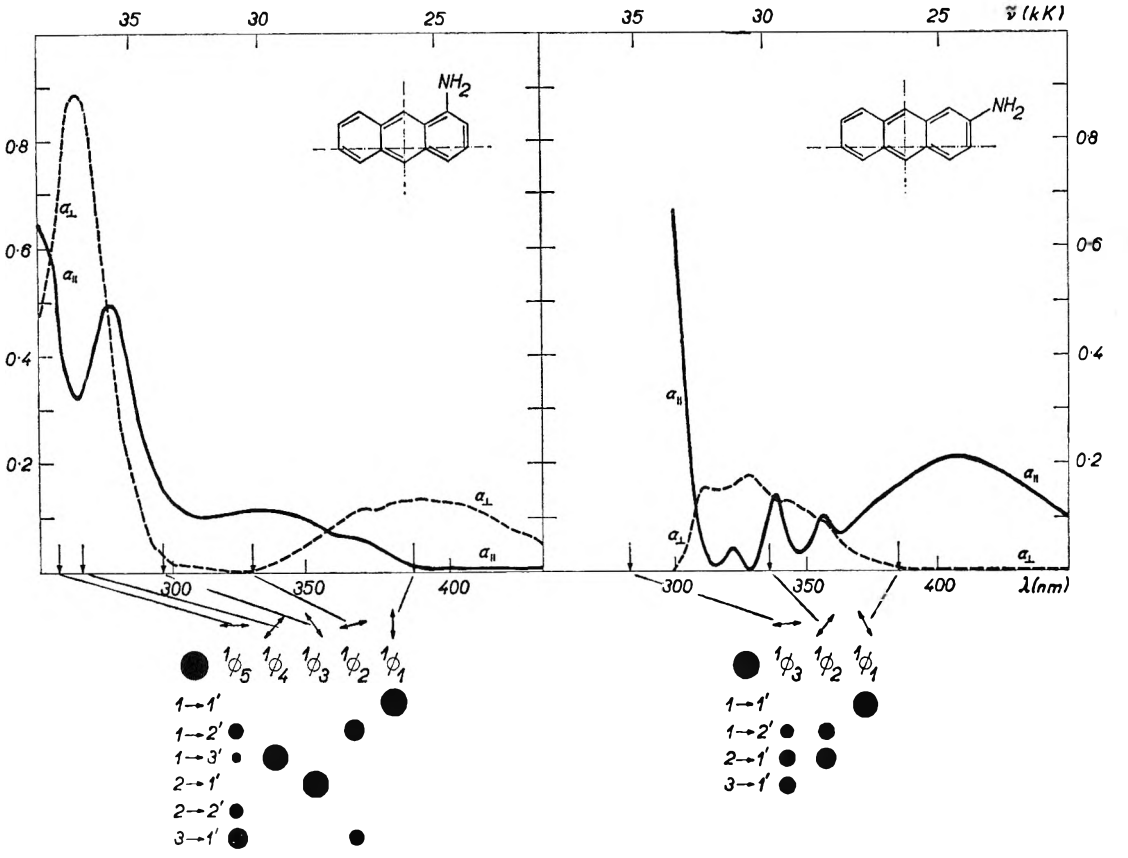

Figure 4. Measurement of the dichroism of 1-amino- and 2-aminoanthracene adsorbed on a stretched polyvinyl alcohol foil. Dichroic reduced curves[56] related to the absorption of light polarized perpendicularly ($a_\perp$) or parallel ($a_\parallel$) to the stretching direction are indicated by a dashed and by a full line, respectively. The position of the theoretical $S_0 \rightarrow S_x$ excitation energies are indicated by short vertical arrows, the theoretical directions of polarization by short both-sided arrows; the corresponding CI-wave functions are in the lower part of the figure. The representation of the $i \rightarrow i'$ configuration by weight in the CI-wave function is indicated by a full circle: the amount of 100% is shown by the area on the left side above the designation of the configurations.

been published which could confirm the correctness of the semiempirically calculated directions of polarization. The measurement of the dichroism of substances adsorbed on stretched foils is very attractive, since this offers information about the absolute directions of polarization; this method has already been successfully employed for symmetrical molecules.[55] None of the derivatives experimentally investigated in our work has more than one plane of symmetry; for this reason, we selected 1- and 2-substituted amino and hydroxy derivatives of anthracene for dichroic examination because these molecules are at least rod-shaped. Figure 4 presents the results of measurements for amino derivatives. The comparison of the theoretical and the experimental directions of polarization of these unsymmetric molecules is difficult; however, the measurement of the dichroism even of these systems offers a valuable help in revealing less intense bands which, in conventional measurement, are overlapped by bands of higher intensity. The theoretical directions of polarization of the first two bands of 1-aminoanthracene are in agreement with experiment. In the case of the 2-isomer one can hardly say more than that the polarizations of the first and the second band, in both theory and experiment, are not the same. For the 1-isomer it was possible to carry out measurements from 250 nm upwards; in the region from this wavelength to the long-wave region, two groups of bands are visible on the conventional curve; polarization measurements and calculations have revealed that five transitions exist in this region.

Configuration Interaction and Composition of the CI-Wave Functions. Although in some cases the influence of configuration interaction upon the SCF-excitation energies is similar to that observed on the parent benzenoid hydrocarbons [the first two bands have the character of a p band and, roughly speaking, of α band (Table III, see *e.g.*, III-1, III-2, III-9) or the appearance of an α band followed by a p band (IV-3)], in the majority of cases the situation is rather complicated and vague. Nevertheless it can be said that the contribution of the $1 \rightarrow 1'$ configuration in the first excited state is nearly

(55) (a) J. H. Eggers and E. W. Thulstrup, 8th European Spectroscopic Congress on Molecular Spectroscopy, Copenhagen, 1965; (b) E. W. Thulstrup and J. H. Eggers, *Chem. Phys. Letters*, 1, 690 (1968).

Table IV: Comparison of the LCI–SCF Spectral Characteristics of Naphthalene, 1-Aminonaphthalene, 1-Hydroxynaphthalene, and 1-Naphtholate[a]

Compound	ΔE^{LCI} eV	ΔE^{LCI} kK	log f	cos θ	Predominant configurations i, j (wt)
Naphthalene	4.036	32.56	F		1,2′(48.8); 2,1′(48.8)
	4.370	35.26	−0.61	1.000	1,1′(93.4)
	5.673	45.77	0.31	0.000	1,2′(50.0); 2,1′(50.0)
	5.686	45.87	F		2,3′(36.8); 3,2′(36.8); 1,4′(13.2); 4,1′(13.2)
	5.709	46.06	F		3,1′(50.1); 1,3′(49.7)
1-Hydroxynaphthalene	3.998	32.26	−1.26	−0.331	1,2′(64.5); 2,1′(29.5)
	4.028	32.49	−0.54	0.979	1,1′(91.4)
	5.350	43.16	−0.08	0.012	2,1′(42.8); 1,2′(20.8); 3,1′(18.3)
	5.504	44.40	−1.16	−0.986	1,3′(62.9); 3,1′(29.7)
	5.689	45.90	−1.05	−0.477	3,1′(60.4); 1,3′(32.3)
1-Aminonaphthalene	3.902	31.48	−0.51	0.994	1,1′(94.3)
	3.978	32.09	−1.21	0.203	1,2′(68.6); 2,1′(28.0)
	5.231	42.20	−0.24	0.009	2,1′(35.2); 3,1′(18.2); 1,2′(17.8); 2,2′(16.7)
	5.338	43.07	−1.12	0.293	3,1′(74.0)
	5.421	43.74	−0.93	−0.853	1,3′(91.4)
1-Hydroxynaphthalene anion	3.757	30.31	−0.52	0.984	1,1′(95.3)
	3.916	31.60	−1.06	0.019	1,2′(72.9); 2,1′(23.4)
	5.201	41.96	−0.28	0.112	2,1′(40.3); 3,2′(16.0); 1,2′(14.4)
	5.318	42.91	−0.60	−0.667	1,3′(81.4)
	5.439	43.88	−1.59	0.820	3,1′(82.1)

[a] See Table III.

always the greatest, although in some cases it amounts to only 50%. This is illustrated in Table III which contains data on the percentile representation of the individual configurations in the CI-wave functions in the excited singlet states of amines. These data must be viewed with a certain caution, because the composition of the CI-wave functions is sensitively dependent upon the numerical values of the empirical parameters. This is obvious from Table IV which presents a comparison of the spectral characteristics and the CI-wave functions of naphthalene and of models of its 1-amino and 1-hydroxy derivatives and of the respective naphtholate. It is obvious that the parameter change on going from the amino to the hydroxy derivative is accompanied by an increase in energy of the state in which the $1 \rightarrow 1'$ configuration predominates above the energy of the state formed by the $1 \rightarrow 2'$ and $2 \rightarrow 1'$ configurations. The parameter change also leads to a considerable change in the logarithms of the oscillator strengths and the directions of polarization of the first two successive transitions. The reduction of the theoretical $S_0 \rightarrow S_1$ energy in the transition from naphthalene to naphtholate (Table IV, columns 2 and 3) due to the change of the parameters is clearly indicated by a bathochromic shift of the first band in the electronic absorption spectra of these compounds.

Parameters. Although the results so far obtained do not permit us to suggest a widely applicable optimum set of parameters, it seems advisable to summarize the values that have given satisfactory results in the study of electronic spectra by the unmodified PPP method with the use of the Mataga–Nishimoto approximation for $\gamma_{\mu\nu}$ in work with an idealized geometry (see Table V).[56] These values differ somewhat from those em-

Table V: Suggestion of Empirical Parameters for the Unmodified PPP Method (Approximation of the γ Integrals According to Nishimoto and Mataga, Idealized Geometry). For a Detailed Explanation See Description in the Text of Table I

Atom, μ	Example	I_μ, eV	A_μ, eV	$\gamma_{\mu\mu}$, eV	$\beta_{\mu C}{}^c$, eV
C	...	11.42	0.58	10.84	−2.318
—N=[22]	Pyridine	14.1	1.8	12.3	−2.318
—NH_2	Aniline	27.5	9.2	18.3	−2.318
=O[39]	Phenalenone	13.8	2.2	11.6	−2.318
—OH	Phenol	33.1	9.9	23.2	−2.318
—O^-	Phenolate	21.2	9.4	11.8	−2.318
=S[56]	Thiofluorenone	12.86	2.92	9.9	−1.623
—SH[37]	Thiophenol	21.0	10.16	10.84	−1.159
—S—[56]	Thiophene	20.0	9.16	10.84	−1.623

ployed for the calculations in the present study (see Table I), because we have recently adjusted our values to those used for C in several laboratories with which we are in contact. The values for the heteroatoms were changed accordingly. Since the increase of the value $\beta_{CN}{}^c$ from −1.910 to −2.318 eV does not lead to

(56) J. Fabian, A. Mehlhorn, and R. Zahradník, unpublished results.

a significant change of the LCI excitation energy, we recommend the use of the same value as for β_{CO}[c]. These values will undoubtedly change in the course of further studies, especially if we attempt to achieve a more general applicability.

Acknowledgment. We are indebted to Professor M. S. Newman of the Ohio State University, Columbus, Ohio, for samples of the amino and hydroxy derivatives benzo[*c*]phenanthrene, to Professor Z. R. Grabowski of Academy of Science, Warsaw, Poland, and to Dr. M. J. Janssen of the University, Groningen, the Netherlands, for phosphorescence measurements, and to Dr. M. Nepraš of Research Institute of Organic Synthesis, Rybitví, Czechoslovakia for measurements of the dichroic curves.

Ultrasonic Absorption in Aqueous Salts of the Lanthanides

by Douglas P. Fay, Daniel Litchinsky, and Neil Purdie[1]

Department of Chemistry, Oklahoma State University, Stillwater, Oklahoma 74074 *(Received June 26, 1968)*

The rates of formation of the complexes MSO_4^+ have been measured using the ultrasonic pulse technique for the trivalent ions of praseodymium, neodymium, samarium, terbium, holmium, erbium, thulium, and lutetium. These results complete the series of trivalent lanthanide sulfates. To test the independence of the rate-controlling step from the identity of the entering ligand, the nitrates of trivalent lanthanum, cerium, praseodymium, samarium, and erbium have been studied. The spectra are more complex than those of the corresponding sulfates but a qualitative interpretation is presented which suggests that the third step in the overall complex formation mechanism is observed.

Introduction

In the continuation of previous work on the kinetics of complexation of the lanthanide ions in solution,[2] the sulfate series has been concluded and a number of the nitrates have been examined. The three-step complex formation mechanism of Eigen[3] was adopted in the earlier treatment of the data, the chemical relaxation having been attributed to the third step of the mechanism, that of substitution into the hydration sphere of the cation. Because of the limitations in identifying a relaxation with a specific step in the mechanism by this technique, some valid arguments were presented to reinforce the somewhat intuitive assumption made. If the absorption could be shown to be independent of the anion, experimental justification for the assumption would be obtained. To this end a number of the lanthanide nitrates have been studied. Although the sound absorption spectra are not typical of a single relaxation, a qualitative interpretation is presented which suggests that the original interpretation is correct.

In one respect the treatment of the data in the original presentation for the sulfates was inconsistent. This has been remedied in this work and the results for La(III), Ce(III), Sm(III), Eu(III), Gd(III), Dy(III), and Yb(III) have been recalculated and are included for comparison with those for the remaining ions in the series. The results are discussed in the light of other available data.

Experimental Section

Measurements of the absorption of ultrasonic energy were made at selected frequencies between 5 and 75 MHz using the pulse method.[4] The system is similar to that described previously[2] for the low-frequency range. A temperature of $25 \pm 0.05°$ was maintained for all measurements reported.

Solutions. Rare earth nitrates and oxides with a purity of 99.9% were obtained from the American Potash and Chemical Corp. The nitrates were used without further purification. The hydrated rare earth sulfates were prepared from the corresponding oxide. The oxides were dissolved in 6 *N* hydrochloric acid and 6 *N* sulfuric acid added to yield a quantitative amount of the sulfate which was precipitated by the addition of a large excess of absolute ethyl alcohol. Stock solutions were prepared and analyzed for cation concentration by the titration with standard sodium hydroxide of the sulfuric acid or nitric acid produced by ion exchange on Dowex 50W-X8, 20–50 mesh resin. Sulfate was estimated gravimetrically as barium sulfate. Dilutions

(1) To whom communications should be directed.

(2) N. Purdie and C. A. Vincent, *Trans. Faraday Soc.*, **63**, 2745 (1967).

(3) M. Eigen and K. Tamm, *Z. Elektrochem.*, **66**, 93, 107 (1962).

(4) M. Eigen and L. DeMaeyer, "Technique of Organic Chemistry," Interscience Publishers Inc., New York, N. Y., Vol. VIII, Part 2, Chapter 18.

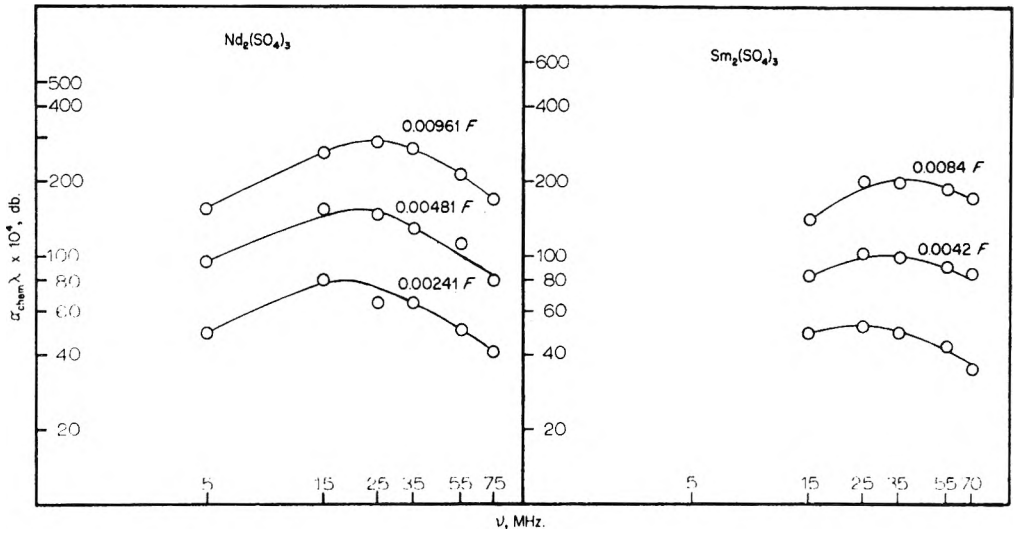

Figure 1. Excess sound absorption *vs.* frequency as a function of concentration for neodymium and samarium sulfates. Samarium data from ref 2. (Concentration for lower curve is 0.0021 *F*.)

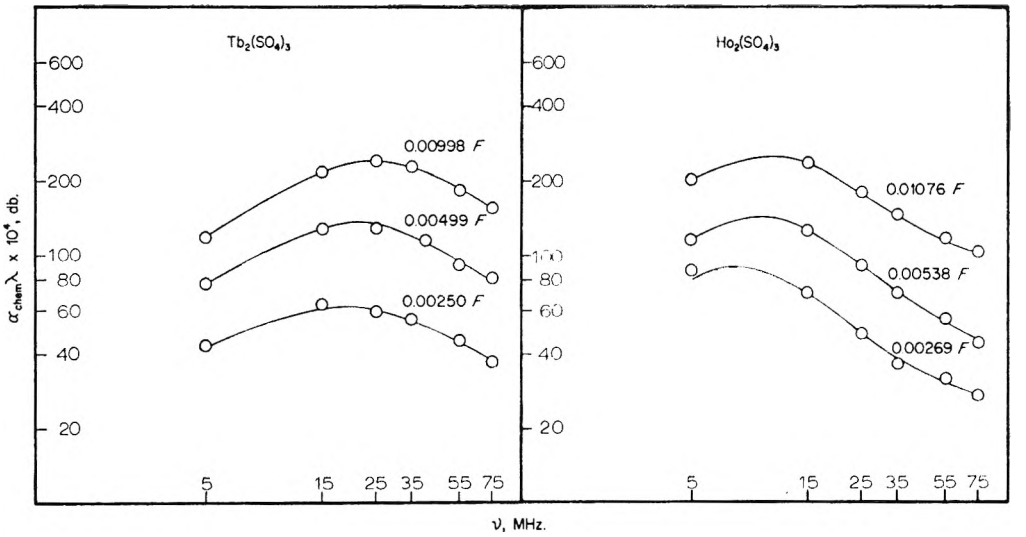

Figure 2. Excess sound absorption *vs.* frequency as a function of concentration for terbium and holmium sulfates.

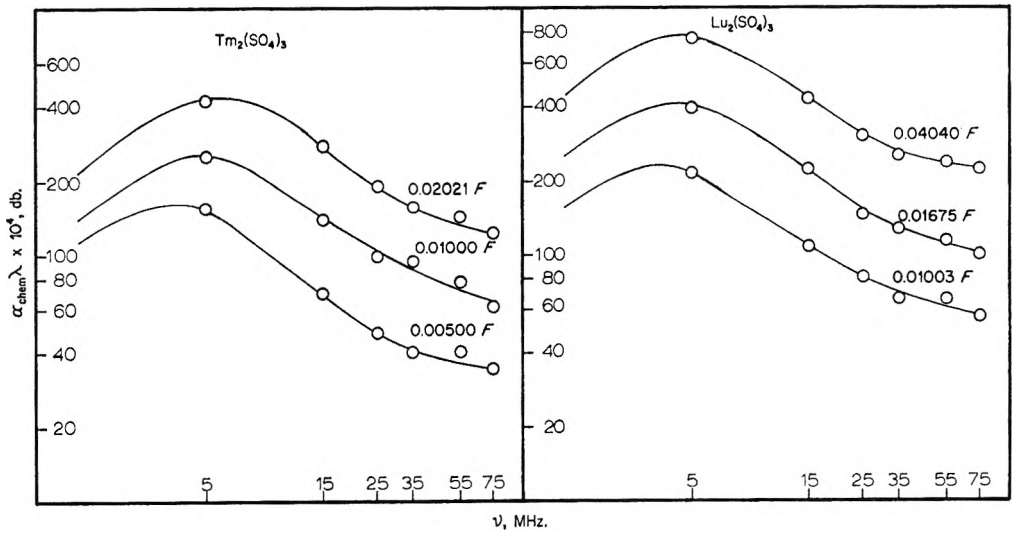

Figure 3. Excess sound absorption *vs.* frequency as a function of concentration for thulium and lutetium sulfates.

of the stock solutions were made with deionized water, at least three concentrations being examined for each salt.

Results

I. The Lanthanide Sulfates. The relaxation spectra of the sulfates of Pr(III), Nd(III), Sm(III), Tb(III), Ho(III), Er(III), Tm(III), and Lu(III) at various concentrations are given in Figures 1–3 and 4a–8a. The solid lines are calculated from the equation for a single relaxation. The excess sound absorption produced by the chemical process is expressed as $\alpha_{chem}\lambda$. The attenuation of a plane progressive sound wave traversing a solution is given by the expression

$$I = I_0 \exp(-2\alpha\chi) \quad (1)$$

where I is the sound intensity at distance χ, I_0 is the sound intensity at distance zero, and α is the absorption coefficient for the solution. The experimentally measured absorption is α, and α_{chem} is obtained by subtracting the solvent contribution α_{H_2O}. The units of α_{chem} in eq 1 are nepers/cm.

Only one maximum is observed in the frequency range examined, and the magnitude of the excess absorption is concentration dependent. Reasons for believing that the absorption is due to substitution into the inner hydration sphere of the cation have been enumerated in the first paper of this series.[2] This is the third step in the overall mechanism for complex formation proposed by Eigen[3]

$$M^{3+}(aq) + SO_4^{2-}(aq) \underset{k_{21}}{\overset{k_{12}}{\rightleftharpoons}} [M^{3+}(H_2O)_2SO_4^{2-}]$$

(I)

$$k_{23}\downarrow \quad \uparrow k_{32}$$

(II)

$$[M{\cdot}SO_4^{+}] \underset{k_{43}}{\overset{k_{34}}{\rightleftharpoons}} [M^{3+}(H_2O)SO_4^{2-}]$$

(III)

The relaxation time for the rate-controlling step is given by the equation[2]

$$\tau_{III}^{-1} = 2\pi\nu_{mIII} = k_{43} + k'_{34} \quad (2)$$

where ν_{mIII} is the frequency of the maximum absorption. Because of the coupling of the successive equilibrium reactions, the correction for the activities of the ions in the first step is transmitted to k_{34}[4]. k'_{34} in eq 2 includes this correction. The rate expression for step III can be rewritten in terms of concentration and equilibrium constants

$$2\pi\nu_{mIII} = k_{43} + \Phi(C)k_{34} \quad (3)$$

$$= k_{43} + \left[\frac{\theta(C)}{K_{12}K_{23} + (1 + K_{23})[\theta(C)]}\right]k_{34} \quad (4)$$

where K_{12}, K_{23}, and K_{34} are the thermodynamic dissociation constants for steps I, II, and III, respectively.[2] $\theta(C)$ is given by the expression

$$\theta(C) = \Pi_f C\left\{(5 - 4\beta) + \left[(3 - 2\beta)\frac{\partial \ln \Pi_f}{\partial \ln \beta}\right]_C\right\} \quad (5)$$

where C is the concentration of solute in moles per liter of $M_2(SO_4)_3$, β is the degree of association at equilibrium, and Π_f is the activity quotient $f_{3+}f_{2-}/f_{\pm}$. β was calculated for each value of C by standard iteration procedure using the total thermodynamic equilibrium constants, where available, derived from conductivity measurements.[5] The activity coefficients f_{3+}, f_{2-}, $f_{\pm}$ were evaluated using a modified form of the Davies equation.[6]

$$-\log f_i = 0.509 Z_i^2\left\{\frac{\mu^{1/2}}{1 + B\mathring{a}\mu^{1/2}} - 0.3\,\mu\right\} \quad (6)$$

where f_i and z_i are the activity coefficient and charge of the ion i, respectively, μ is the ionic strength $= 3C + 12(1 - \beta)C$, $B = 0.33 \times 10^8$, and $\mathring{a}$ is the distance of closest approach of the ions. As a rule $\mathring{a}$ is taken to be equal to 3 Å which is too small for a 2:3 electrolyte. To be consistent with the theoretical calculation of K_{12}, required in the solution of eq 8, a value of 8.86 Å, equal to the sum of the ionic radii plus two water molecule diameters, was used. This represents a major departure from the original treatment.[2] The solution of the derivative in the expression for $\theta(C)$ was evaluated according to[7]

$$\frac{\partial \ln \Pi_f}{\partial \ln \beta} = \frac{\partial \ln \Pi_f}{\partial \mu}\frac{\partial \mu}{\partial \ln \beta}$$

$$= 0.509(Z_{M^{3+}}{}^2 + Z_{SO_4^{2-}}{}^2 - Z_{MSO_4^{+}}{}^2)^2 \times \left[\frac{1}{2\mu^{1/2}(1 + B\mathring{a}\mu^{1/2})^2} - 0.3\right](1 - \beta)C \quad (7)$$

If it can be argued that the chemical relaxation is a result of step III, the rate constants, and hence K_{34}, can be obtained from a graphical solution of eq 3. The unknowns in this equation are K_{12} and K_{23}. K_{12} was calculated to be 2.3×10^{-3} M using the Bjerrum equation[8]

$$K_{12}^{-1} = \frac{4\pi N\mathring{a}^3}{1000} b^3 Q(b) \quad (8)$$

and was essentially independent of the small changes in $\mathring{a}$ for the series. Previously,[2] K_{23} was taken to be 0.51, the value for $MgSO_4$.[9] Additional calculations showed

(5) A. E. Martell and L. G. Sillén, "Stability Constants," Special Publication No. 17, The Chemical Society, London, 1964, p 237.

(6) C. W. Davies, "Ion Association," Butterworth and Co. Ltd., London, 1962.

(7) J. Steuhr and E. Yeager, "Physical Acoustics," W. P. Mason, Ed., Academic Press, New York, N.Y., 1965 Vol. II, Part A, p 388.

(8) R. A. Robinson and R. H. Stokes, "Electrolyte Solutions," 2nd ed, Butterworth and Co. Ltd., London, 1959, p 392.

(9) G. Atkinson and S. K. Kor, *J. Phys. Chem.*, 69, 128 (1965).

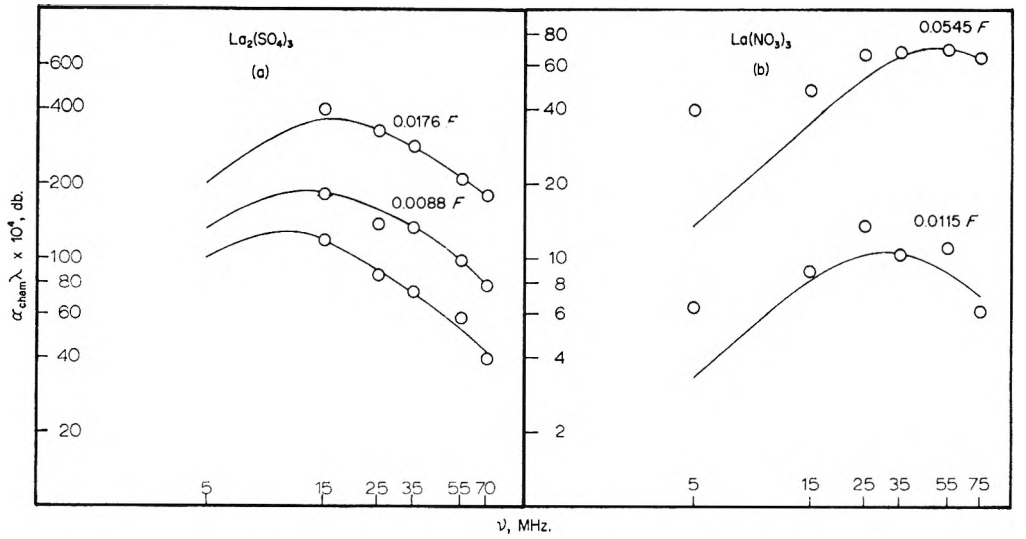

Figure 4. Excess sound absorption *vs.* frequency as a function of concentration for (a) lanthanum sulfate (lower curve, 0.0044 *F*) and (b) lanthanum nitrate. Sulfate data from ref 2. Single relaxations for nitrate calculated from τ_{max} values for samarium nitrate.

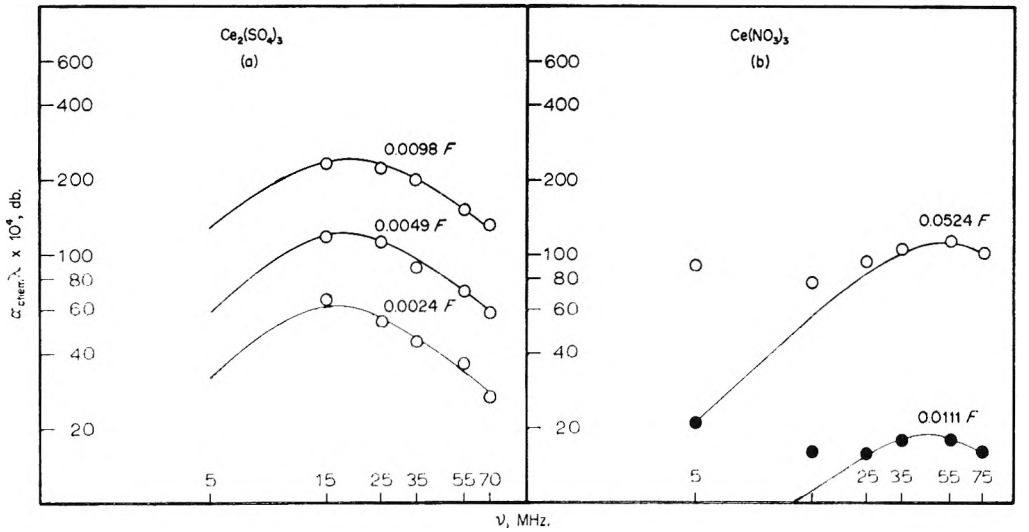

Figure 5. Excess sound absorption *vs.* frequency as a function of concentration for (a) cerium sulfate and (b) cerium nitrate. Sulfate data from ref 2. Single relaxations for nitrate calculated from τ_{max} values for samarium nitrate.

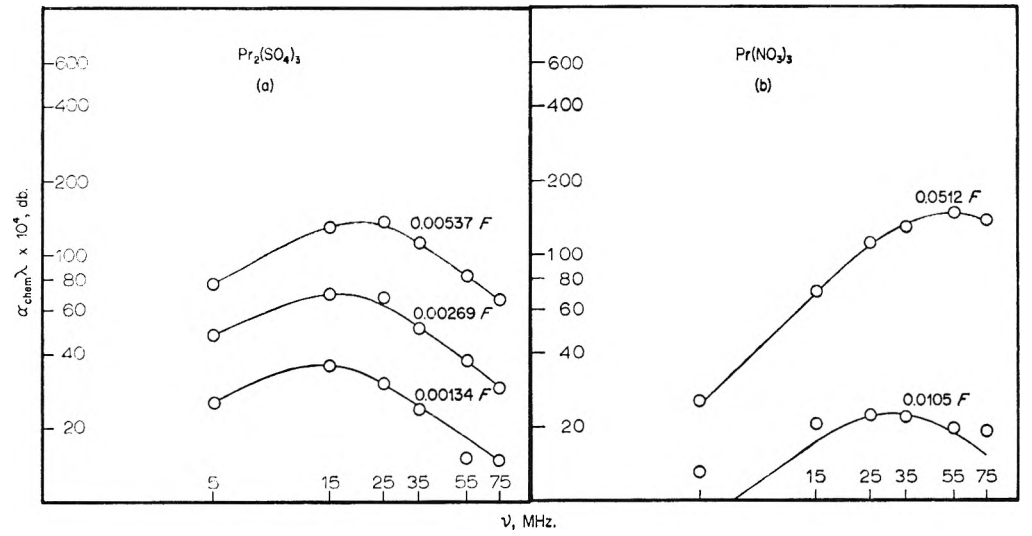

Figure 6. Excess sound absorption *vs.* frequency as a function of concentration for (a) praseodymium sulfate and (b) praseodymium nitrate. Single relaxations for nitrate calculated from τ_{max} values for samarium nitrate.

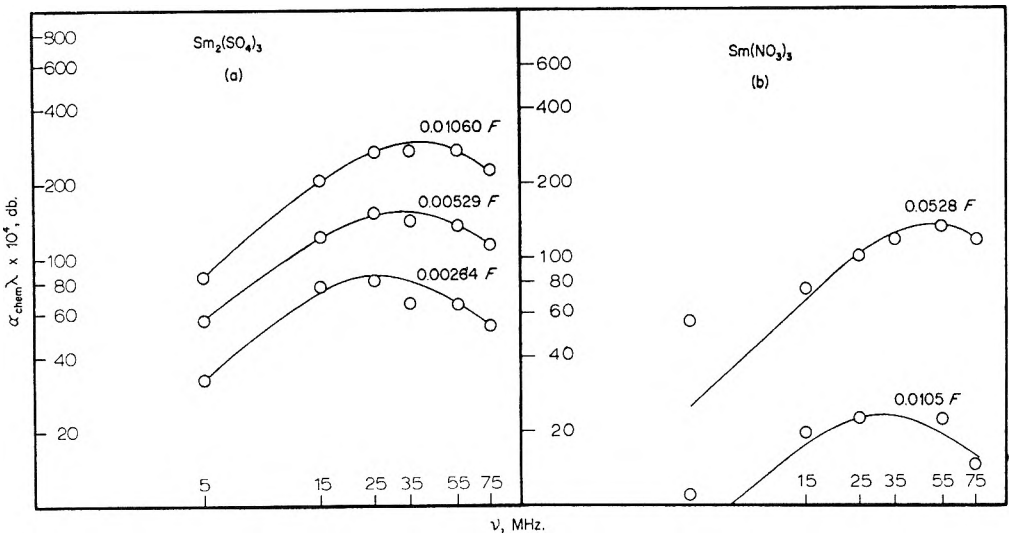

Figure 7. Excess sound absorption *vs.* frequency as a function of concentration for (a) samarium sulfate (this work) and (b) samarium nitrate.

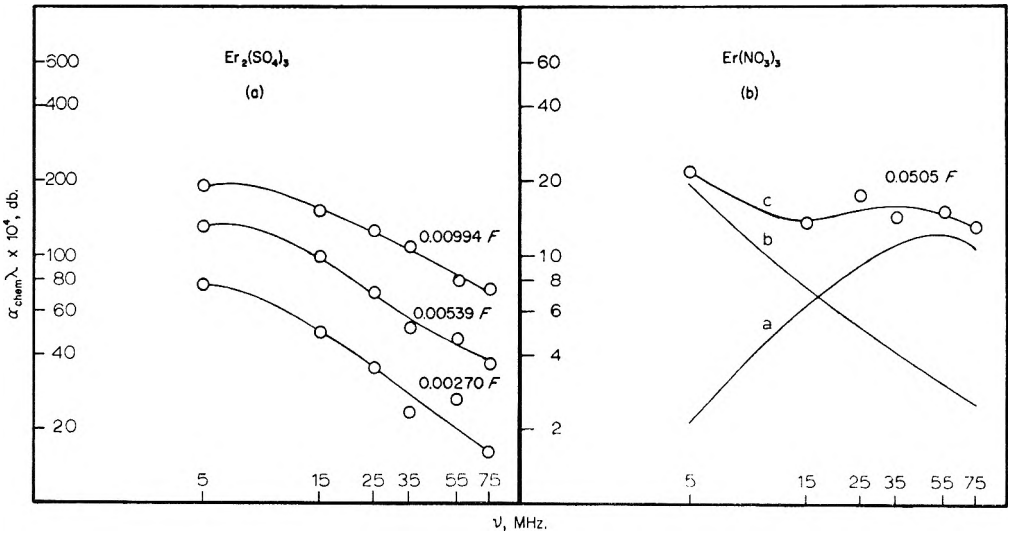

Figure 8. Excess sound absorption *vs.* frequency as a function of concentration for (a) erbium sulfate and (b) erbium nitrate. In Figure 8(b) curve a is the theoretical single relaxation for outer substitution using τ_{max} for samarium nitrate; curve b is the theoretical single relaxation for inner substitution which added to curve a would give the experimentally observed chemical absorption curve c. ν_{mIII} is outside the frequency range.

that k_{43} was insensitive to K_{23} within the range 0.1 to 1.0, but that the value of k_{34} increased proportionately. The overall thermodynamic association constants K_T, as determined by conductometric techniques, are related to the equilibrium constants for the individual steps by the expression

$$K_T = \frac{1 + K_{34} + K_{23}K_{34}}{K_{12}K_{23}K_{34}} \qquad (9)$$

By a reiterative procedure, using eq 4 and 9, a value of K_{23} was calculated for samarium to give the best agreement between K_T obtained kinetically with that obtained conductometrically. This value, $K_{23} = 0.72$, was subsequently used in the determination of k_{34} and k_{43} for the remaining ions. The agreement between the overall kinetic constants and the literature conductometric values[5] was good in all cases. Typical magnitudes for the terms in eq 5 are shown for samarium in Table I.

The characteristic relaxation frequency ν_{mIII} was determined graphically from the linear plots of α_{chem}/ν^2 *vs.* α_{chem} according to the equation[10]

$$\alpha_{chem}/\nu^2 = -\alpha_{chem}/\nu_m{}^2{}_{III} + A \qquad (10)$$

where the slope is $-1/\nu_m{}^2{}_{III}$ and A is the amplitude of the absorption.

Concentrations and relaxation frequencies are given in Table II. The values of k_{34} (sec^{-1}) and k_{43} (sec^{-1}) are given in Table III for all the lanthanide(III) ions.

(10) J. H. Andreae, P. L. Joyce, and R. J. Oliver, *Proc. Phys. Soc.*, **82**, 75 (1960).

Table I: Samarium Sulfate (δ = 8.86 Å; K_{12} = 2.3 × mol l.$^{-1}$; K_{23} = 0.72)

$10^3 \times C$	β^{-1}	Πf	$10^2 \times \mu$	$\partial \ln \Pi f / \partial \ln \beta$	$10^3 \times \theta(C)$	$\Phi(C)$
10.60	0.0822	0.1967	4.21	−0.095	2.53	0.507
5.29	0.1173	0.2503	2.33	−0.132	1.73	0.457
2.64	0.1636	0.3162	1.31	−0.157	1.21	0.403

The values are in some cases 40% lower than in the original work. This is in part due to the more exact solution of the derivative term in $\theta(C)$ but more so to the use of the modified Davies equation in the calculation of activity coefficients.

II. The Lanthanide Nitrates. The sound absorption spectra for the nitrates of La(III), Ce(III), Pr(III), Sm(III), and Er(III) are shown in Figures 4b–8b. Again the solid lines are theoretical single relaxation curves. The solution concentrations had to be much higher for a relaxation to be observed. Quantitative interpretation of the data is complicated by the existence of more than one relaxation. However, the differences in the spectra from each other and from the corresponding lanthanide sulfates allow a qualitative description to be made. The curves differ in three respects. (1) Whereas the sulfate solutions of equal concentration absorb to the same order of magnitude, a comparison among the nitrates shows an order of magnitude difference, Table IV. (2) The low-frequency maximum of the sulfates has been shifted to a higher value in all cases except erbium. (3) In the nitrates, the relaxations are considerably broadened with respect to those of the corresponding sulfates. These observations are indicative of multiple relaxations.

Table II: Relaxation Frequency Data

Ion	Formal concn × 10^2	$2\pi\nu_{mIII}$, MHz	$1/K_T$, mol l.$^{-1}$
Pr	0.54	120	2.38 × 10^{-4}
	0.27	97	
	0.13	76	
Nd	0.96	141	2.29 × 10^{-4}
	0.48	117	
	0.24	92	
Sm	1.06	229	2.17 × 10^{-4}
	0.53	195	
	0.26	158	
Tb[a]	1.00	153	2.56 × 10^{-4}
	0.50	136	
	0.25	108	
Ho	1.08	69	2.57 × 10^{-4}
	0.54	57	
	0.27	43	
Er	0.99	51	2.56 × 10^{-4}
	0.54	43	
	0.27	34	
Tm[a]	2.02	35	2.36 × 10^{-4}
	1.00	30	
	0.50	22	
Lu[a]	4.04	30	2.56 × 10^{-4}
	1.68	27	
	1.00	25	

[a] Stability constants obtained by interpolation from a plot of K_T *vs.* atomic number.

Table III: Rate Constants

Ion	$10^{-8} \times k_{34}$, sec^{-1}	$10^{-7} \times k_{43}$, sec^{-1}	$1/r$, Å^{-1}
La[a]	2.1	5.6	0.870
Ce[a]	3.3	7.0	0.902
Pr	4.4	6.4	0.918
Nd	5.2	8.8	0.926
Sm	7.4	14.0	0.962
Eu[a]	6.6	14.6	0.970
Gd[a]	6.7	12.8	0.981
Tb	5.2	9.6	1.000
Dy[a]	4.2	5.2	1.010
Ho	2.8	3.5	1.030
Er	1.9	3.0	1.043
Tm	1.4	1.0	1.053
Yb[a]	~0.8	~3.7	1.065
Lu	~0.6	~1.8	1.077

[a] Recalculated from data of Purdie and Vincent.[2]

Discussion

The most serious limitation of the sound absorption technique in studying kinetics of chemical reactions is the uncertainty in assigning a relaxation to a specific step in a multistep mechanism. It is essential to the present discussion that the characteristic frequency for substitution into the sulfate hydration sphere be identified. If step III is rate controlling, the relaxation for step II should occur at a higher frequency. The independence of an observed 200-MHz relaxation on the cation, in a number of divalent transition metal sulfates, led to its identification with step II in the overall mechanism.[3] In the earlier work on the lanthanide

Table IV: Absorption Peak Maxima

Ion	Sulfate[a] $(\alpha_{chem}\lambda)_{max}$, db	Nitrate[b] $(\alpha_{chem}\lambda)_{max}$, db
La	0.0120[c,d]	0.0070
Ce	0.0120[c,d]	0.0115
Pr	0.0190	0.0145
Sm	0.0155	0.0130
Er	0.0140[c]	0.0022

[a] Solutions are approx 5 × 10^{-3} *F*. [b] Solutions are approx 5 × 10^{-2} *F*. [c] Peaks are not complete. [d] Data from ref 2.

sulfates, where data were available up to 230 MHz, this appeared as a broadening of the observed relaxation on the high-frequency side, an observation confirmed by Atkinson.[11] The amplitude of this high-frequency relaxation was at least one order of magnitude smaller than those absorptions assigned to cation inner-sphere substitution. From the point of view of relaxation amplitudes, therefore, the low absorptions observed in the nitrates of lanthanum and erbium, around 35–55 MHz, might be interpreted as due to the equilibrium involving substitution into the nitrate ion, that is step II. This relaxation manifests itself because the lanthanide nitrates are known to form predominantly outer-sphere complexes with some inner-sphere substitution occurring only at high concentrations.[12] A similar small relaxation has been observed in preliminary studies of calcium nitrate and uranyl nitrate, but, as expected, is absent in potassium nitrate. Lanthanide sulfates on the other hand are predominantly inner-sphere complexes consistent with another trivalent metal sulfate, $Cr_2(SO_4)_3$.[13] The relaxation amplitude is correspondingly higher. Since in aqueous solution the effect of the pressure wave on the volume change in the equilibrium reaction is more important than the temperature effect on ΔH, more energy is absorbed in the process with the largest volume change. That process would be inner complex formation where the resultant reorganization of the solvent is greater.

The amplitude of the absorption in the sulfates increases with increasing concentration of inner complex. To produce an appreciable concentration of inner complex in the nitrate solutions, that a similar relaxation might be observed, higher concentrations of the nitrates had to be used. For the most part a tenfold increase in cation concentration was sufficient. The magnitude of the absorption for lanthanum nitrate, for example, is much smaller than that of a more dilute lanthanum sulfate solution, consistent with a lower concentration of inner complex. If then the assignment of the relaxations in the sulfates to cation substitution is correct, the characteristic frequencies for inner substitution in the nitrates would be expected to occur in approximately the same frequency range, 4–40 MHz. From the sulfate data the relaxation frequency for inner-sphere substitution increases from Er(III) through La(III), Ce(III), Pr(III), and Sm(III). For the nitrates the absorption amplitude increases in the same order. If the low absorption observed for erbium nitrate can be interpreted as due to substitution into the outer-sphere complex with the minimum of interference from the inner-sphere substitution process, then as the relaxation frequency for inner-substitution for the other cations increases, the extent of interaction and the absorption also increases. This model satisfactorily describes the differences in the spectra described before and provides qualitative experimental proof that *the original assignment of relaxations to step III is correct.*[2]

Using this interpretation, it should be possible to obtain quantitative confirmation by determining the rate constants for steps II and III; the values of k_{34} should be the same for both anions if the mechanism is Sn1. To determine these rate constants the relaxation times for both processes must be separated from the complex sound absorption spectrum, and the quantity $\theta(C)$ (see eq 13) must be evaluated. $\theta(C)$ is related to τ_{II} by the expression

$$\tau_{II}^{-1} = k_{32} + \left[\frac{\theta(C)}{K_{12} + \theta(C)}\right] k_{23} \qquad (11)$$

Let us consider these in turn.

It is theoretically possible to analyze a complex spectrum for multiple processes if the conditions are satisfactory. Accurate experimental data is a necessity and τ_n should at least be equal to $2\tau_{n-1}$. For cerium, praseodymium, and samarium nitrates, however, $\tau_{III} \simeq \tau_{II}$ and the spectra are almost typical of a single relaxation. Describing the absorption in terms of α/ν^2 rather than as $\alpha\lambda$, the simplest general equation for multiple relaxations will become

$$\alpha/\nu^2 = A + \frac{B_{II}}{[1 + (\nu/\nu_{mII})^2]} + \frac{B_{III}}{[1 + (\nu/\nu_{mIII})^2]} \qquad (12)$$

for two steps, where A is the classical solvent absorption and the sum of the remaining two terms is the excess absorption due to chemical processes. From erbium nitrate the magnitude of the second term on the right-hand side is very small and the measurements cannot be too accurate. To partition the total excess absorption, for samarium say, into a sum of two contributions when one is very small, cannot be done with confidence and the relaxation times therefore may not be considered unique solutions. The validity of this argument assumes the additivity of terms in the multiple relaxation equation which is the case only in the limit when the individual relaxations are independent. If, however, as a first approximation, the value of B_{II} for erbium nitrate is assumed to be constant for all of the nitrates, B_{III} for samarium is a very large quantity, almost equal in magnitude to B_{III} for samarium sulfate. This is unreasonable because the molar concentration of inner $SmNO_3^{2+}$ complex is much less than the molar concentration of inner $SmSO_4^+$ complex. The total observed excess absorption α_{chem}/ν^2, therefore, is much greater than the simple sum of the individual contributions. General equations have been derived which account for this effect[14] but the large number of undetermined constants involved makes it very difficult to interpret, except in extreme cases of simplification. The relaxa-

(11) G. Atkinson, private communication.

(12) I. Abrahamer and Y. Marcus, *Inorg. Chem.*, **6**, 2103 (1967).

(13) N. Fogel, J. M. J. Tai, and J. Yarborough, *J. Amer. Chem. Soc.*, **84**, 1145 (1962).

(14) R. T. Beyer, *J. Acoust. Soc. Amer.*, **29**, 243 (1957).

tion frequency, however, approximates to that of the slower step. Since the curve, as far as it is possible to tell, is symmetrical, an estimate of τ_{II} equal to τ_{III} for samarium cannot be far from the real value. The τ_{II} values for samarium could then be used for the remaining salts at equal concentrations. This estimate is probably as good as would be obtained by a more protracted analysis.

To evaluate $\theta(C)$, the degree of association β must be calculated from the overall association constants. The thermodynamic

$$\theta(C) = \Pi_f C\left\{4 - 2\beta + (3 - \beta)C\left(\frac{\partial \ln \Pi_f}{\partial \ln \beta}\right)_c\right\} \quad (13)$$

association constants for the rare earth nitrates are not available. A study of the reactions at high ionic strength, for which stability constants are available for a few of the rare earth nitrates, might be more advantageous at this time rather than attempting to measure the thermodynamic constants. It is conceivable that the relaxations may be separated under these conditions although there is no precedent for making this observation. Such a study is at present in progress. Quantitative proof of the assignment of relaxations is therefore beyond our reach at present. Nevertheless, based upon the intuitive arguments outlined in previous work[2] and the qualitative evidence described here, the interpretation of the results as indicative of inner substitution of the cation will be considered correct for the following discussion.

Rate constants for step III, k_{34} and k_{43}, are given in Table III for the monosulfates. The estimated error is $\pm 15\%$, but for the slower rates, which approach the experimental limits of the instrument, the error is probably greater than this. In the graphical solution of eq 3, the intercept at $\Phi(C) = 0$ is negative. However, when A (from eq 10) is plotted as a function of $\Phi(C)$ a zero value of A is obtained at a finite value of $\Phi(C)$, which means that a certain limiting concentration of inner complex must be present in solution before absorption in excess of the solvent is observed. This limiting value of $\Phi(C)$ was used to determine k_{43}.

The rates of complex formation are 40% lower than the original estimate,[2] but are still an order of magnitude greater than those observed by Geier[15] for the rates of formation of murexide complexes, by Swinehart[16] for a number of lanthanide anthranilate complexes, and by Reuben and Fiat,[17] in proton magnetic resonance studies of dysprosium. However, good agreement was found with results by Grecsek[18] for Pr(III), Nd(III), and Dy(III) from sound absorption and by Marianelli[19] for Gd(III) by oxygen-17 nmr line broadening studies of the rate of water exchange. This controversy can only be resolved when results are available for the lanthanide ions with a certain ligand by more than one technique, and under similar conditions of ionic strength. If this fails then a possible explanation may transpire from further consideration of the mechanism. It is possible that the complexity of the entering ligand, or its ability to chelate with the cations, would preclude a simple SN1 mechanism.

From Figure 9, the rate constants k_{34} are seen to reach a maximum around samarium as before[2] and to

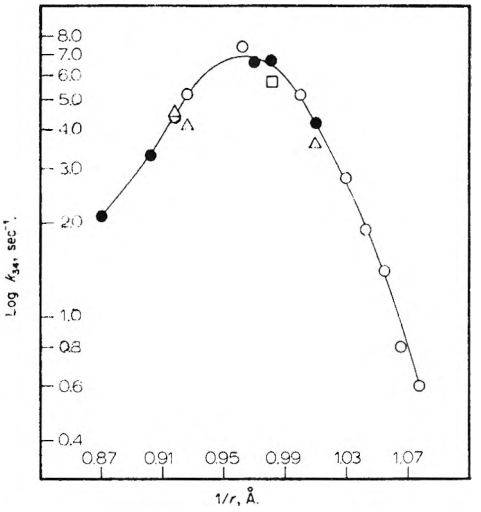

Figure 9. Dependence of logarithm of the rate constant for the rate-controlling step on the reciprocal cation radius. Data from: ●, ref 2; ○, this work; △, ref 18; □, ref 19. (Values in ordinate × 10^{-8}.)

fall on a smooth curve when plotted as a function of the reciprocal cation radius. The dependence is quite different from the linear behavior for log k_{34} *vs.* $1/r_{\text{cation}}$ for the alkali metal and the alkaline earth metal series,[20] but resembles somewhat the rather complicated trends in ΔG, ΔH, and ΔS for complex formation for a number of ligands with the rare earth cations.[21] These trends have been interpreted as a consequence of a change in coordination number as the radius of the cation decreases across the series. If the mechanism is SN1 so that the participation of sulfate anion in forming the transition state is small, trends in the rates of substitution may be expected to reflect changes in the intimate structure of the cations, namely a change in coordination number. Based upon this observation a feasible kinetic model was described in the first paper on the lanthanide sulfates.[2] Unlike the murexide results, no minimum is observed around erbium. There is, perhaps, more error in the calculated k_{34} values for the

(15) G. Geier, *Ber. Bunsenges. Phys. Chem.* **69**, 617 (1965).
(16) J. H. Swinehart, private communication.
(17) J. Reuben and D. Fiat, *Chem. Commun.*, 729 (1967).
(18) J. J. Grecsek, M.S. Thesis, University of Maryland, 1966.
(19) R. Marianelli, Ph.D. Thesis, University of California, Berkeley, 1966.
(20) M. Eigen, *Ber. Bunsenges. Phys. Chem.*, **67**, 753 (1963).
(21) G. H. Nancollas, "Interactions in Electrolyte Solutions," Elsevier Publishing Co., New York, N. Y., 1966, p 108.

slower reactions at the end of the series, but some credibility is given to the observation if, from Table II, the characteristic frequencies are compared for solutions of equal concentration. The dependence of the rates of formation on the reciprocal cationic radius follows, to some extent, that of the heats of hydration of the trivalent lanthanide ions,[22] which might indeed suggest an SN1 mechanism.

Acknowledgment. We wish to acknowledge the financial assistance of the Research Corporation and the Research Foundation, Oklahoma State University, which made it possible to construct the equipment; Dr. A. J. Barlow, Department of Electrical Engineering, University of Glasgow for its assembly; and Mr. H. Hall of this department for his help in the design and fabrication of the mechanical arrangement. We are also grateful to NASA for providing a fellowship to D. P. F.

(22) G. Choppin, unpublished results.

Radiolysis of Cyclic Fluorocarbons. II. Perfluoroaromatics at Elevated Temperatures[1]

by F. W. Bloch and D. R. MacKenzie

Brookhaven National Laboratory, Upton, New York 11973 *(Received July 15, 1968)*

Aromatic fluorocarbons are known to have high thermal stability but only moderate stability to radiation at or slightly above room temperature. In the present study of perfluorobenzene, perfluoronaphthalene, perfluorobiphenyl, and perfluoro-*o*-terphenyl, we find that this moderate radiation stability is maintained at elevated temperatures where most organic compounds undergo rapid decomposition by heat alone. For example, perfluorobiphenyl at 500° is several orders of magnitude more stable thermally and many times more stable to γ radiation than are the hydrocarbons biphenyl and *o*-terphenyl. At 100° polymerization is almost the only process occurring and G values range from 1.5 to 3. At 450° it is still the most important process, with G values from 2 to 6, but formation of F_2-addition products has become appreciable. Fragmentation is insignificant. Although the temperature coefficient of overall radiolytic decomposition is small, quite large changes occur in the product distributions in going from 100 to 450°. This is particularly apparent in the case of C_6F_6 where products have been characterized to the greatest extent. The implications regarding mechanism and changes in mechanism with temperature are discussed.

I. Introduction

It has been known for some time that the commoner cyclic fluorocarbons, both alicyclic and aromatic, are extremely stable thermally.[2,3] Our own work[4] has shown that at temperatures from room to 100° the aromatic and alicyclic fluorocarbons have similar G values for radiation decomposition, and their resistance to radiation is intermediate between aromatic and alicyclic hydrocarbons. Because of their known thermal stability, it was of interest to find out whether these compounds retained their reasonably good radiation stability up to temperatures as high as those at which hydrocarbons undergo severe degradation. Thus we extended our irradiation experiments to elevated temperatures (up to 500°).

II. Experimental Section

The compounds studied were perfluorobenzene (C_6F_6), perfluorobiphenyl ($C_{12}F_{10}$), perfluoronaphthalene ($C_{10}F_8$), and perfluoro-*o*-terphenyl ($C_{18}F_{14}$). The perfluoroterphenyl was synthesized by J. W. Dale and G. J. O'Neil of Monsanto Research Corp., Everett, Mass. It was available in only very limited amounts and was irradiated as received (98% pure). The other compounds, obtained from Imperial Smelting Corp., Ltd., Bristol, England, were highly purified by preparative scale gas–liquid partition chromatography (glpc).[4]

A Karl Fischer spectrophotometric analysis showed a water content of <40 ppm for all the purified compounds. This small amount of water and probably

(1) This work was performed under the auspices of the U. S. Atomic Energy Commission.

(2) I. B. Johns, E. A. McElhill, and J. O. Smith, *Ind. Eng. Chem., Prod. Res. Develop.*, **1**, 2 (1962).

(3) L. A. Wall, R. E. Donadio, and W. J. Pummer, *J. Amer. Chem. Soc.* **82**, 4846 (1960).

(4) D. R. MacKenzie, F. W. Bloch, and R. H. Wiswall, Jr., *J. Phys. Chem.*, **69**, 2526 (1965). Paper I of this series.

traces of other hydrogen-containing impurities[5] were shown to yield very small amounts of HF but no other hydrogen-containing compounds in detectable amounts. Thus the laborious drying procedure followed in our low-temperature work[4] was omitted. Otherwise preparation of samples for irradiation was essentially the same as in that investigation.

All compounds were irradiated at 450° and perfluorobiphenyl radiolyses were carried out also at 200, 300, 350, 400, and 500°. Dose rates in the ^{60}Co γ field were of the order of 10^6 to 10^7 rads/hr and total absorbed doses were around 80 Mrads. In all experiments, except those with C_6F_6, the amount of material and size of cell were adjusted so that the bulk of the material in the radiation zone was in the liquid state.[6] C_6F_6 was irradiated as a gas at a pressure of approximately 300 atm (calculated on the basis of the unmodified gas law). Pyrolyses were carried out in parallel experiments for all compounds except the perfluoroterphenyl so that G values could be adjusted for thermal decomposition.

Prefluorinated nickel was chosen as the container material because of its inertness to fluorine attack at moderate temperatures. A Hoke 411 Monel valve with Inconel X spring and silver soldered diaphragm was connected to each cell so that the whole cell system could be irradiated and the volatile products subjected to analysis. Cells were wound with Amperex sheathed heating wire and insulated with Kaylo (Owens-Corning). Cells were brought up to temperature as quickly as possible before being lowered into the γ field. Temperature was maintained with a Minneapolis Honeywell proportional controller to within $\pm 1°$ of the stated value throughout an experiment.

Product analysis was performed by glpc and mass spectrometer after fractional vacuum distillation of the cell contents, using the same procedure as in the low-temperature work.[4] The material remaining in the cell after the last vacuum transfer constituted the polymer residue. A correction for residual starting material, based on glpc analysis, was applied to the polymer yields. A corresponding correction was made, where necessary, for polymeric material in the vacuum distillates.

III. Results

Our results are summarized in Tables I–III and in Figure 1. Some results from low-temperature irradiations are included.

Overall destruction of starting compound is reported as G_{total}, where G has the usual meaning of molecules converted per 100 eV absorbed in the sample. G values are also recorded for formation of polymer (compounds of carbon number greater than that of the starting compound) and formation of addition products (molecules having two F atoms more than the starting compound). $G_{polymer}$ is given in terms of molecules of starting compound consumed. Fluorocarbon gas yields are not given in the tables. They were determined in each experiment in the manner described previously[4] and were very low (≤ 0.01). We do not attach significance to such small yields of fluorocarbon gases, particularly since we are unable to state to what extent they may have been due to impurities. For example, enough hydrogen-containing material was always present[7] to form HF, which produced SiF_4 by reaction with glass in the gas-handling apparatus with a G value of ≈ 0.05.

The principal products in the experiments reported here were polymers, although addition products were formed in significant amounts, particularly with the fused ring compound perfluoronaphthalene. In the

Table I: Results of ^{60}Co γ Irradiation of Aromatic Fluorocarbons at Elevated Temperatures

Compound	Temp, °C	Dose, Mrads	G_{total}	$G_{polymer}$	$G_{addition}$
C_6F_6	67	107	3.0	2.9	≈ 0.04
	450	78	6.3	5.9	0.4
$C_{10}F_8$	108	860[a]	1.30	1.27	≈ 0.03
	450	80	4.6	3.1	1.5
o-$C_{18}F_{14}$	450	79	≤ 3.5[b]	≤ 3.3[b]	≤ 0.2[b]
$C_{12}F_{10}$	100	77	1.8	1.8	≈ 0.01
	200	79	1.9	1.8	0.1
	300	79	2.35	2.05	0.3
	350	79	2.4	2.1	0.3
	400	77	2.3	2.0	0.3
	450	79	2.5	2.2	0.3
	500	79	3.7	3.2	0.5

[a] 1.5-MeV electrons. [b] No pyrolysis correction applied.

Table II: Comparison of Polymeric Product Yields From C_6F_6 Radiolysis at 67 and 450°

Temp, °C	Phase	G values in terms of $G_{-C_6F_6}$: $C_{12}F_{10}$	Partially saturated C_{12}'s[a]	Higher polymer	Total polymer
67	Liquid	0.05	0.15	2.7	2.9
450	Gas at 300 atm	2.3	1.2	2.4	5.9

[a] Assuming same detector sensitivity (glpc) as for $C_{12}F_{10}$.

The principal products in the experiments reported here were polymers, although addition products were formed in significant amounts, particularly with the fused ring compound perfluoronaphthalene. In the

(5) An obvious source of such contamination is bleeding from the preparative scale glpc columns. For example, well conditioned polypropylene glycol columns appeared not to be bleeding at 150° when collections were made for 10 min. However, collections of 30 min or more showed that bleeding was occurring at the rate of about 0.2 mg/hr. Since samples were collected for about 10 min and column temperature was usually <150°, the amount of contaminant introduced in this way was ≤ 0.01 wt %.

(6) Information obtained since the experiments were done indicates that the critical temperatures of $C_{12}F_{10}$ and $C_{10}F_8$ are slightly less than 400° so that the $C_{10}F_8$ irradiation at 450° and the $C_{12}F_{10}$ irradiation at 400° and above were carried out in the gas phase at pressures higher than critical.

(7) See Experimental Section.

Table III: Comparison of Thermal and Low LET Radiation Decomposition of Aromatic Hydrocarbons and Fluorocarbons

	Biphenyl		*o*-Terphenyl	
	Hydrocarbon	Fluorocarbon	Hydrocarbon	Fluorocarbon
Thermal decomposition, weight fraction per hour at 500°	0.048[a]	0.00016	(0.18)[d]	...
G_{total} at 260°	0.5[b]	2.15	...	...
G_{total} at 450°	...	2.5	6.4[c]	≤ 3.5
G_{total} at 500°	...	3.7	(17)[d]	...
Apparent activation energy of radiolysis in kcal/mol				
Temperature range 80–260°	1.2[b]	0.5	0.3[e]	...
Temperature range 450–500°	...	$\gtrsim 5$	22[c]	...

[a] D. A. Scola, unpublished results reported in IDO-11 055, May 10, 1963, and confirmed by present authors. [b] Reference 11. [c] Reference 8. [d] Extrapolated from data in ref 8. [e] Results of A. W. Boyd, quoted in Report IDO-11401, Dec 1964, p 51.

perfluoro-*o*-terphenyl experiment, only traces of product other than polymer were formed, so identification of addition products was based only on glpc retention times. In the other experiments identification was by mass spectrometry of individual components collected as glpc fractions. There were two or more such components for each starting compound. In the perfluorobiphenyl experiments, only 2 out of 6 components of appropriate glpc retention time were definitely identified because of the small samples available, but it seems virtually certain that the other four were also addition products. Fragmentation products were minor in experiments with $C_{12}F_{10}$ at the higher temperatures, and barely detectable at the lower temperatures and with C_6F_6. No fragmentation was observed with $C_{10}F_8$ and *o*-$C_{18}F_{14}$.

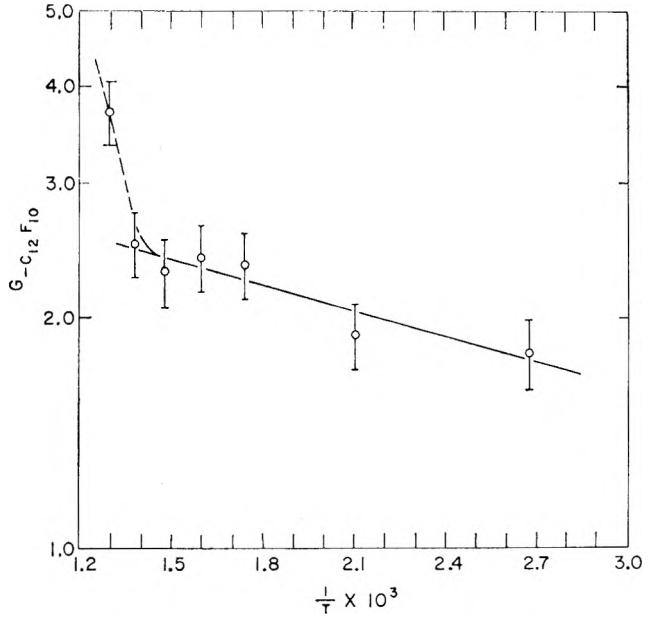

Figure 1. Temperature dependence of radiolytic decomposition rate of $C_{12}F_{10}$.

G values given in Tables I and II are the results of two or more experiments except in the case of *o*-$C_{18}F_{14}$ and $C_{12}F_{10}$ at 500°. Several sets of triplicate experiments with $C_{12}F_{10}$ showed a total spread in G_{total} of 12 to 16%, with an average deviation about the mean of ±5 to 7%. Spreads almost as large were obtained in carefully controlled experiments at room temperature with Fricke dosimeter solution in place of fluorocarbon in our experimental arrangement. Thus, it was concluded that our imprecision was caused almost entirely by inability to reproduce the sample cell position in the irradiation tubes.

We feel that the absolute yield values are good to ±10%. The Fricke dosimeter dose rate in standard glass container at the center of each irradiation facility was known to ±2% and was converted to dose rate in our materials using the appropriate electron densities. Correction for energy absorption in the nickel cells and insulating material was approximately 11% and was determined experimentally.

IV. Discussion

Radiation Stability. From the data in the tables it is evident that the perfluoroaromatics as a class are reasonably stable to irradiation at 450° and even higher. At 500°, perfluorobiphenyl is several orders of magnitude more stable thermally than the hydrocarbons biphenyl and *o*-terphenyl and is many times more stable to γ radiation than *o*-terphenyl. The value of G_{total} of 17 for *o*-terphenyl at 500° (Table III) is an extrapolation from 480° and may well be a lower limit. In fact a *G* value in the normally accepted sense probably cannot be assigned to the system at this temperature in view of the very high thermal decomposition rate of nearly 20% per hour.[8]

The value of G_{total} given for perfluoro-*o*-terphenyl at 450°, on the other hand, is an upper limit. Since the irradiation time was 3 days, a certain amount of pyrolysis undoubtedly occurred, and to the extent that it did an adjustment should be applied to decrease the *G* value below 3.5. Thus perfluoro-*o*-terphenyl has a stability more like that of perfluorobiphenyl than that of perfluoronaphthalene. The latter still has a *G* value less than that of the hydrocarbon *o*-terphenyl at 450°, and even C_6F_6 at this temperature shows no greater decomposition.

Temperature Coefficients of Radiolytic Decomposition Rates. The data in Table I show that for all the compounds studied there is a comparatively small change in G_{total} (or any of the *G* values listed) in going from

(8) J. M. Scarborough and R. B. Ingalls, *J. Phys. Chem.*, **71**, 486 (1967).

around 100 to 450°. This is in marked contrast with aromatic hydrocarbons whose behavior is known.[9,10] Even the terphenyls, whose radiolytic decomposition rates are very low at moderate temperatures (G = 0.18 for *o*-terphenyl at 300°),[11] show a 30-fold increase in this rate in going to 450°.

Although G_{total} for the fluorocarbons does not change much in going from 100 to 450°, there is a rather large change in the product distribution. For one thing the yield of F_2-addition products increases by a factor of 10 or more (Table I), indicating an appreciable temperature coefficient for the rates of reactions leading to these products. For C_6F_6 the distribution of polymeric products also changes markedly between 67 and 450° (Table II). At the lower temperature, over 90% of the polymer is a product of relatively high molecular weight and only about 2% is the dimer, perfluorobiphenyl. At 450°, however, 60% is dimeric, made up of 20% partially saturated dimers and 40% perfluorobiphenyl. The marked increase in yield of dimers is accompanied by a significant decrease in yield of higher polymers. This situation is not simply explained, for example, in terms of positive and negative temperature coefficients, and will be discussed further in the section entitled Radiolysis Mechanism.

The least-squares plot of the perfluorobiphenyl results up to 450° (Figure 1) yields an apparent Arrhenius activation energy of 0.5 kcal/mol. As shown in Table III, this is of the same order as, though even lower than, the apparent activation energy for radiolysis of the hydrocarbon biphenyl in the temperature range 80 to 260°. The hydrocarbon polyphenyls in general show two activation energies, one for low temperature, and a considerably larger one for high temperatures.[10,12] Thus the high-temperature activation energy for *o*-terphenyl radiolysis (400 to 480°) is 22 kcal/mol.[8] Tomlinson, *et al.*,[13] have confirmed that for *m*-terphenyl 350° is the transition temperature above which a high apparent activation energy is observed.

Somewhere between 450 and 500° the radiolytic decomposition rate for perfluorobiphenyl obviously begins to increase quite rapidly. The dashed line in Figure 1 merely indicates this; no precise activation energy can be determined without more points above 450°, but the slope of the dashed line, probably a minimum, would yield a value of 5 kcal/mol. Thus apparently perfluorobiphenyl, and likely the other aromatic fluorocarbons, also show two activation energies for radiolysis. For the fluorocarbons, however, this high temperature region must begin at a considerably higher temperature than for the hydrocarbons. For perfluorobiphenyl our results cover the temperature range sufficiently closely to leave no doubt of this. For C_6F_6 and $C_{10}F_8$ the changes in G_{total} from 100 to 450° are so small that clearly a region of high activation energy has not yet, or has only just, been entered at 450°. The change from low to high apparent activation energy has nothing to do with change of state since the critical temperatures of all the compounds studied (except for the perfluoroterphenyl) are below 400°.

Tomlinson[13] points out that the radiation decomposition of hydrocarbon terphenyls at elevated temperatures requires a more complex description than heretofore proposed (*e.g.*, in the radiopyrolysis model[14] and thermal spike model[8]). This situation undoubtedly applies to other aromatic hydrocarbons and also to aromatic fluorocarbons. In the case of hexafluorobenzene, for example, as already pointed out, rather large changes in yields of important products take place even in the region of low apparent activation energy.

Radiolysis Mechanism. One of the important differences in radiolysis mechanism between fluorocarbons and hydrocarbons arises from the types of reactions available to H atoms and F atoms, respectively. Both can undergo addition to the aromatic molecule. However, while the H atom can abstract H from a hydrocarbon molecule, the F atom cannot abstract F from a fluorocarbon molecule because of the very large difference in C–F and F–F bond strengths (80 to 90 kcal/mol). Also because of this large difference, even if a significant amount of molecular fluorine could form by some other mechanism, such as molecular elimination, the reaction

$$F_2 + R\cdot \longrightarrow RF + F\cdot$$

will be particularly favored, whereas the corresponding reaction with H_2 is endothermic. Thus molecular hydrogen can build up as a product in hydrocarbon radiolysis, while molecular fluorine is not likely to do so in fluorocarbon radiolysis. In fact, experimentally it has not been observed in either aromatic or alicyclic systems.[4]

There seems to be no doubt that excitation of aromatic fluorocarbons by γ rays will lead to a significant proportion of radical species, as already shown for the aromatic hydrocarbons benzene[9] and biphenyl.[10] Whether or not the bulk of the reactions involve these radicals, it is useful to consider them as constituting a reasonable fraction of the overall mechanism.

In order to account for the observed products, reactions 1 to 9 are postulated, where M represents a molecule of starting compound and Ar· the radical formed by loss of one F atom from that compound.

(9) See, for example, J. Hoigné and T. Gaumann, *Helv. Chim. Acta*, 44, 1337 (1961).

(10) M. A. Sweeney, K. L. Hall, and R. O. Bolt, *J. Phys. Chem.*, 71, 1564 (1967).

(11) R. O. Bolt and J. G. Carroll, "Radiation Effects on Organic Materials," Academic Press, New York, N. Y., 1963, p 307.

(12) R. O. Bolt and J. G. Carroll, "Radiation Effects on Organic Materials," Academic Press, New York, N. Y., 1963, p 324.

(13) D. Wuschke and M. Tomlinson, *Nucl. Sci. Eng.*, 31, 521 (1968).

(14) E. A. Mason, T. H. Timmins, D. T. Morgan, and W. N. Bley, unpublished report, MIT-334-70, MITNE-78, Massachusetts Institute of Technology, 1966.

$$M^* \longrightarrow Ar\cdot + F\cdot \quad (1)$$

$$F\cdot + M \longrightarrow FM\cdot \quad (2)$$

$$FM\cdot + F\cdot \longrightarrow MF_2 \quad (3)$$

$$FM\cdot + M \longrightarrow MF_2 + Ar\cdot \quad (4)$$

$$FM\cdot + FM\cdot \longrightarrow M + MF_2 \quad (5)$$

$$Ar\cdot + Ar\cdot \longrightarrow Ar{-}Ar \quad (6)$$

$$FM\cdot + FM\cdot \longrightarrow FM{-}MF \quad (7)$$

$$FM\cdot + Ar\cdot \longrightarrow FM{-}Ar \quad (8)$$

$$\left.\begin{matrix} Ar\cdot + M \\ FM\cdot + M \end{matrix}\right\} \longrightarrow \longrightarrow \longrightarrow \text{polymers} \quad (9a), (9b)$$

Although valence isomers play a significant role in γ radiolysis of C_6F_6 at room temperature,[15] we had no way of determining their effect as transient species in high-temperature systems and so do not consider them in the present paper.

We have no direct evidence regarding the relative importance of reactions 4 and 5 in formation of addition products, MF_2, although there is indirect evidence that the disproportionation reaction (5) may become appreciable at elevated temperatures. Perfluoroalkyl radicals are reported not to disproportionate at room temperature,[16,17] nor at considerably higher temperatures,[18] but we have found that at elevated temperatures (350 to 400°) certain cyclic fluorocarbon radicals disproportionate readily.[19] Also in aromatic hydrocarbon systems evidence has been obtained[20] for disproportionation of substituted phenyl radicals formed in pulse radiolysis. The fact that F_2 addition product yields in each of the compounds perfluorobenzene, -naphthalene, and -biphenyl increase at least an order of magnitude in going from $\approx$100 to 450° indicates that one or both of reactions 4 and 5 increase greatly in importance, since reaction 3 is expected to be very efficient at any temperature.

Reactions 6 to 9 lead to dimeric products or higher polymers and are relatively more important. It is clear that competition between the various reactions for the radicals FM· and Ar· determines the product distribution, and that the products at 450°, insofar as we have been able to observe them, can be explained by different rate constant ratios in the different systems. Thus reactions 7, 8, and particularly 9 predominate over reactions 3, 4, and 5 in the case of C_6F_6, $C_{12}F_{10}$, and perfluoro-*o*-terphenyl whereas in the case of $C_{10}F_8$ they are more nearly equal. However, in the naphthalene system polymers still outweigh addition products because of the contributions of reactions involving Ar· radicals—(6), (8), and (9a).

High-Temperature Reactions in C_6F_6. In view of the relatively small effect of temperature on over-all radiolytic decomposition of the perfluoroaromatics, it is of considerable interest to know the nature of the reactions at high temperature. In the case of C_6F_6, the change in distribution of products, especially polymeric, between ambient and 450° (Tables I and II) gives us some idea, though no direct proof, of the relative importance of the reactions in our scheme and of others so far not touched on. The complexity indicated in this system is probably also present in the other perfluoroaromatics.

At low temperature, reactions 9a and 9b (combined as reaction 9 below) predominate over reactions 6, 7, and 8.

$$R\cdot + C_6F_6 \longrightarrow R{-}C_6F_6\cdot \quad (9)$$

$$R{-}C_6F_6\cdot + C_6F_6 \longrightarrow R{-}C_6F_6{-}C_6F_6\cdot$$

$$\text{etc. to } R{-}(C_6F_6)_n\cdot \quad (10)$$

where R· represents either $C_6F_5\cdot$ or $C_6F_7\cdot$. Chain termination would be by combination with R· (or F atom) and/or disproportionation

$$R{-}(C_6F_6)_n{-}R \quad (11)$$

$$R{-}(C_6F_6)_n\cdot + R\cdot$$

$$R{-}(C_6F_6)_{n-1}{-}R + RF \quad (12)$$

Reactions 6, 7, and 8 are expected to have essentially zero activation energy so that their rates should increase only modestly in going to 450°. Thus they cannot likely account for the marked increase in yield of dimers. Reactions 9 and 10, on the other hand, should show a moderate activation energy and therefore still predominate over reactions 6, 7, and 8 at high temperature. The fact that higher polymer actually decreases at high temperature while dimers increase markedly must mean that reactions 10 are somehow greatly reduced in effectiveness, and chain termination steps occur right at the beginning of the chain-forming process. For example, dimers occur when $n = 1$ in reactions 11 and 12 and R· = F atom in reaction 11.

Reduction in the effectiveness of (10) seems most reasonably explained by depolymerization reactions, such as the reverse of (10) and (11), whose rates have become competitive with the rates of the forward reactions. This is consistent as well with the fact that overall loss of C_6F_6 has not increased greatly in spite of the increased rates of the forward reactions.

(15) (a) J. Fajer and D. R. MacKenzie, *J. Phys. Chem.*, **71**, 784 (1967); (b) J. Fajer and D. R. MacKenzie, "Radiation Chemistry," Vol. II, Advances in Chemistry Series, American Chemical Society, Washington, D.C., 1968, p 469.

(16) L. Kevan, *J. Chem. Phys.*, **44**, 683 (1966); A. Sokolowska and L. Kevan, *J. Phys. Chem.*, **71**, 2220 (1967).

(17) G. O. Pritchard, G. H. Miller, and J. R. Dacey, *Can. J. Chem.*, **39**, 1968 (1961).

(18) G. H. Miller, G. O. Pritchard, and E. W. R. Steacie, *Z. Physik. Chem.*, **15**, 262 (1958).

(19) D. R. MacKenzie, V. H. Wilson, and E. W. Anderson, *J. Chem. Soc. B*, 762 (1968).

(20) K. D. Asmus, B. Cercok, M. Ebert, A. Henglein, and A. Wigger, *Trans. Faraday Soc.*, **63**, 2435 (1967).

It is also likely that at high temperature an appreciable amount of higher polymer arises from radical scavenging by C_6F_8 and partially saturated dimers, *e.g.*

$$C_6F_8 + R\cdot \longrightarrow R{-}C_6F_8. \qquad (13)$$

or some other type of olefin polymerization. Otherwise one might expect a greater buildup of C_6F_8 and a much higher ratio of partially saturated dimers to perfluorobiphenyl. It does not seem unusual that the cyclic dienes would have more of a tendency to polymerize than the perfluorobiphenyl. Indeed, in view of the latter's performance under high-temperature radiolysis it might be expected that, once formed in the C_6F_6 radiolysis, it would take little part in further reactions.

Acknowledgments. We are grateful to R. H. Wiswall, Jr., for helpful discussions, and to Robert Smol and William J. Brown for skillful experimental assistance.

Infrared Intensities as a Quantitative Measure of Intramolecular Interaction. VII.[1] The ν_{13} Band near 1500 Cm^{-1} in Monosubstituted and *para*-Disubstituted Benzenes

by R. T. C. Brownlee, P. J. Q. English, A. R. Katritzky, and R. D. Topsom

School of Chemical Sciences, University of East Anglia, Norwich, England, and the School of Physical Sciences, La Trobe University, Melbourne, Australia *(Received July 18, 1968)*

The integrated intensity is reported for the 1500-cm^{-1} band for many monosubstituted and *para*-disubstituted benzenes. The values in monosubstituted benzenes are linearly related to σ_R^0 but the accuracy of this identity is lower than with the 1600-cm^{-1} intensities previously reported. The values obtained suggest the polarization $C^-{-}H^+$ in the aromatic C–H bonds. The values obtained for the *para*-disubstituted benzenes can be explained in terms of the intensities of the corresponding monosubstituted compounds and give further evidence for the participation of d orbitals in bonding halogen atoms to the aromatic nucleus.

We have recently shown[2] that the infrared intensities of the ν_{16} ring-stretching bands of monosubstituted benzenes give a quantitative measure of the distortion of the π-system of the ring along the main axis. This integrated area, A, of the bands near 1600 and 1585 cm^{-1} is related to σ_R^0 for the substituent. $A = 17{,}600(\sigma_R^0)^2 + 100$.

The small constant term in the equation is required since an overtone band also occurs in this frequency range. In later papers, we explained the intensities of the corresponding bands in *para*-[3] and *ortho* and *meta*-disubstituted[4] benzenes in terms of their values for the related monosubstituted compounds. This allowed various conclusions to be drawn about electronic and steric effects on substituent interactions.

In one of these papers[2b] we also listed some extinction coefficients for the 1500-cm^{-1} vibration in monosubstituted benzenes and showed their square roots to be linearly related to σ_R^0 although the precision of the correlation was much less than with the 1600-cm^{-1} values. We suggested[2b] that this probably reflected the deviation from Lorentzian shape of some of the bands for compounds containing asymmetric substituents and also the greater experimental difficulties in obtaining accurate intensity values. We considered it worthwhile to try to obtain rather more accurate intensity values for the 1500-cm^{-1} absorptions of mono- and disubstituted benzenes both as a support for our previous work and to gain information on the nature of the vibration.

The 1600-cm^{-1} (ν_{16a}) and 1585-cm^{-1} (ν_{16b}) bands in monosubstituted benzenes arise from the infrared-forbidden in-plane ν_{16} benzene vibration at 1585 cm^{-1}. The direction and amplitudes of the atomic displacements in the degenerate pair in benzene itself are shown below.

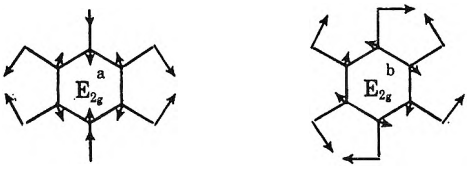

(1) Part VI; A. R. Katritzky, C. R. Palmer, F. J. Swinbourne, T. T. Tidwell, and R. D. Topsom, *J. Amer. Chem. Soc.*, **91**, 636 (1969).

(2) (a) R. T. C. Brownlee, A. R. Katritzky, and R. D. Topsom, *ibid.*, **87**, 3260 (1965); (b) *ibid.*, **88**, 1413 (1966); (c) R. T. C. Brownlee, R. E. J. Hutchinson, A. R. Katritzky, T. T. Tidwell, and R. D. Topsom, *ibid.*, **90**, 1757 (1968).

(3) P. J. Q. English, A. R. Katritzky, T. T. Tidwell, and R. D. Topsom, *ibid.*, **90**, 1767 (1968).

(4) A. R. Katritzky, M. V. Sinnott, T. T. Tidwell, and R. D. Topsom, *ibid.*, in press.

Such diagrams of the forms of the normal modes are the result of force-field calculations on benzene and a comparison of the calculated and observed frequencies in its halogenated and deuterated analogs.[5]

The degeneracy is lifted when the symmetry is reduced from D_{6h} to C_{2v} by attaching one symmetrical substituent to the ring and two infrared-active vibrations are obtained. Calculations[5] show that the forms of the normal coordinates are very similar to benzene itself.

A considerable amount of the potential energy of the vibration of these modes is involved in C–H bending. Scherer[6] has calculated the actual potential energy distribution and showed that the contribution from C–H bend is about 30%. Most of the intensity arises from the ν_{16a} vibration, however, and it can be seen that the C–H bending modes are symmetrical and any contributions to the dipole moment from them will cancel out. The intensity thus derives from C–C stretch modes. The contribution to the potential energy from the C–H stretching mode has been shown[6] to be negligible.

If the substituent is not symmetrical the ν_{16a} and ν_{16b} vibrations have A′ symmetry and thus intensity can be shared. Because of this mixing and the closeness of the two absorption frequencies, the combined intensities were always used for correlations.

The situation is rather more complex for the ν_{13} bands. These arise from the infrared allowed degenerate in-plane vibration of benzene which occurs at 1479 cm^{-1}. The form of the vibration is shown[5] below.

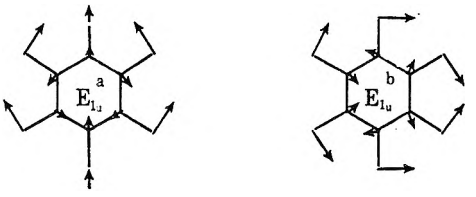

We can consider this mode to be made up of contributions from various symmetry coordinates in the E_{1u} class of benzene. These are shown[7] for E_{1u}^{a} below.

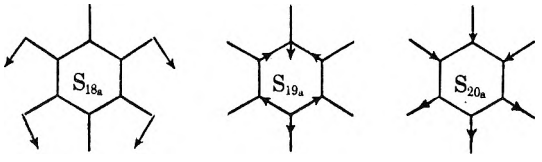

The intensity of the vibration, A, can be expressed as $A^{1/2} = (\text{constant})\partial\mu/\partial Q$ where $\partial\mu/\partial Q$ is the change of dipole moment with respect to the normal coordinate at the equilibrium position. This can be expressed[7] in terms of the symmetry coordinates for the 1500-cm^{-1} vibration.

$$A^{1/2} = (\text{constant})\left(\frac{\partial\mu}{\partial S_{18}} S'_{18} + \frac{\partial\mu}{\partial S_{19}} S'_{19} + \frac{\partial\mu}{\partial S_{20}} S'_{20}\right)$$

where $S'_{18} = \partial S_{18}/\partial Q$ etc.

The constants S in this equation have been calculated by various workers[6-9] from force-field calculations. The values disagree slightly, but it is clear that the potential energy is distributed about 70% in S_{18} and 30% in S_{19}, S_{20} making little contribution. The calculated normal coordinates arising in the E_{1u}^{a} class are shown below.

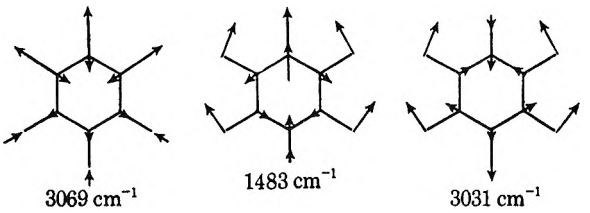

Whiffen[7] has shown that the whole of the dipole change in the 1489-cm^{-1} vibration in benzene is caused by the bending movements of the C–H dipoles. The replacement of one hydrogen by a symmetrical substituent lifts the degeneracy and two bands ν_{13a} and ν_{13b}, are observed. The normal modes have the form

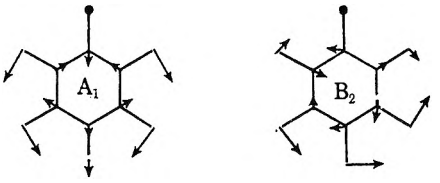

These modes are very similar to those in benzene itself although the contribution of C–H bend to the potential energy diagram falls with substitution. The intensity now derives both from C–H bend and from C–C stretch as influenced by the electronic nature of the substituent. The corresponding normal modes of *para*-disubstituted benzenes[8] are fairly similar.

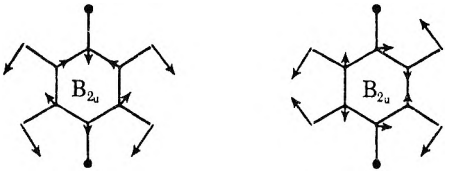

An analysis[8] has shown that the strength of the CCl bond is not high enough in monochloro or *p*-dichlorobenzene to make CCl stretching terms important. Substituent ring stretching terms would be somewhat more important in fluorobenzenes and this is shown by the increase in wavelength at which the ν_{13a} vibration is observed (Table I). The other compounds investigated have substituent-ring bond strength similar to chlorobenzene. Contributions from CCl bending modes to the potential energy distribution of this vibration have also been shown to be small but these will not, in any case, cause a change in the dipole transition moment.

(5) J. R. Scherer, "Planar Vibrations of Chlorinated Benzenes," The Dow Chemical Co., Midland, Mich.

(6) J. R. Scherer, *Spectrochim. Acta.*, **21**, 321 (1965).

(7) D. H. Whiffen, *Phil. Trans. Roy. Soc. London*, **A248**, 131 (1955).

(8) J. R. Scherer, *Spectrochim. Acta.*, **19**, 601 (1963).

(9) N. Neto, M. Scrocco, and S. Califana, *ibid.*, **22**, 1981 (1966).

Table I: Spectral Data for the ν_{13a} Bands in Monosubstituted Benzenes

Compound	Infrared solvent	ν, cm^{-1}	$A^{1/2}$ [a]	$\epsilon^{1/2}$ [b]	$\pm\sigma_R^0$ [c]	Compound	Infrared solvent	ν, cm^{-1}	$A^{1/2}$ [a]	$\epsilon^{1/2}$ [b]	$\pm\sigma_R^0$ [c]
PhH	CCl_4	1480	28.9	17.7	0.00	PhNCS	CCl_4	1491	...	31.9	0.355
PhD	CCl_4	1478	...	18.8	0.00	PhNSO	CCl_4	1484	...	21.2	0.085
PhF	CCl_4	1497	54.1	32.3	0.34	PhNCNPh	CCl_4	1489	...	58.3	0.46
PhCl	CCl_4	1489	38.0	33.7	0.215	$PhND_3^+Cl^-$	D_2O	1500	...	30.2	0.185
PhBr	CCl_4	1476	36.5	43.2	0.23	$PhNMe_3^+Cl^-$	D_2O	1495	...	51.5	0.15
PhI	CCl_4	1474	29.4	27.7	0.22	Ph_3P	CCl_4	1480	21.15	23.3	0.06[d]
$PhICl_2$	$CHCl_3$	1469	...	30.9	0.12	Ph_5P	$CHCl_3$	1481	18.86	19.0	0.03[d]
Ph_2I^+	DMSO	1474	...	36.8	0.28	Ph_3As	$CHCl_3$	1483	19.18	21.8	0.07[d]
PhOH	CCl_4	1499	...	38.5	0.40	Ph_5As	$CHCl_3$	1482	18.83	19.3	0.04[d]
PhOMe	CCl_4	1498	57.5	44.4	0.43	Ph_3Sb	$CHCl_3$	1479	15.66	14.0	0.07[d]
PhOEt	CCl_4	1499	...	48.4	0.44	Ph_5Sb	$CHCl_3$	1479	17.63	18.8	0.06[d]
$PhOPr^i$	CCl_4	1495	...	50.5	0.43	Ph_3Bi	$CHCl_3$	1475	16.66	16.8	0.11[d]
Ph_2O	CCl_4	1488	...	47.9	0.36	PhMe	CCl_4	1496	22.4	19.6	0.10
PhOCOMe	CCl_4	1493	...	37.6	0.235	PhEt	CCl_4	1496	...	19.5	0.105
$PhOCOCF_3$	CCl_4	1493	...	34.8	0.235	$PhPr^n$	CCl_4	1497	...	20.2	0.11
$PhOSO_2Me$	CCl_4	1489	...	40.0	0.265	$PhPr^i$	CCl_4	1494	...	20.0	0.115
$PhOCF_3$	CCl_4	1492	...	39.1	0.25	$PhBu^s$	CCl_4	1494	...	19.7	0.115
PhOH	D_2O	1493	...	41.9	0.425	$PhCH_2CHO$	CCl_4	1499	...	20.5	0.11
PhO^-Na^+	D_2O	1482	...	79.6	0.595	$PhCH_2CN$	CCl_4	1498	...	18.4	0.09
PhSH	CCl_4	1481	...	27.6	0.195	Ph_2CH_2	CCl_4	1496	...	31.2	0.115
PhSMe	CCl_4	1482	...	26.8	0.25	$PhCH_2OH$	CCl_4	1497	...	14.0	0.00
PhSEt	CCl_4	1482	...	26.8	0.19	$PhCH_2OMe$	CCl_4	1487	...	15.3	0.055
Ph_2S	CCl_4	1476	31.4	20.9	0.19	$PhCH_2Br$	CCl_4	1487	...	15.5	0.00
PhSCOMe	CCl_4	1499	...	22.4	0.08	$PhCH_2Cl$	CCl_4	1487	...	14.3	0.00
$PhSCF_3$	CCl_4	1477	...	15.7	0.00	$PhCHBr_2$	CCl_4	1486	...	13.8	0.00
PhS^-Na^+	D_2O	1474	...	26.7	0.335	$PhCHCl_2$	CCl_4	1486	...	13.1	0.00
$PhSO_3^-Na^+$	D_2O	1482	...	15.4	0.00	$PhCBr_3$	CCl_4	1484	...	15.1	0.00
Ph_2SO_2	$CHCl_3$	1480	...	7.4	0.065	PhC_2F_5	CCl_4	1502	...	9.5	0.08
$PhSO_2Me$	$CHCl_3$	1482	...	11.2	0.07	Ph_3CH	CCl_4	1496	...	32.8	0.115
$PhSO_3Me$	CCl_4	1481	...	10.9	0.085	Ph_2	CCl_4	1484	...	20.4	0.095
$PhSO_2Cl$	CCl_4	1479	9.0	12.0	0.11	$PhCHCH_2$	CCl_4	1496	...	16.2	0.05
$PhSO_2^-Na^+$	D_2O	1478	...	14.1	0.00	PhCHCHCOOEt	CCl_4	1498	...	17.2	0.10
Ph_2SO	CCl_4	1478	...	12.6	0.065	PhCHO	CCl_4	1480	0	3.0	0.245
$PhSF_5$	CCl_4	1488	...	19.8	0.07	PhCOMe	CCl_4	1491	0	5.1	0.22
Ph_2Se	$CHCl_3$	1477	31.1	31.9	0.195[d]	Ph_2CO	CCl_4	1488	...	0	0.19
$PhND_2$	CCl_4	1501	48.8	46.7	0.52	PhCOOH	CCl_4	1496	...	11.6	0.29
PhNDMe	CCl_4	1505	...	51.0	0.525	PhCOOMe	CCl_4	1493	...	21.4	0.155
$PhNMe_2$	CCl_4	1508	70.8	50.0	0.535	PhCOOEt	CCl_4	1491	9.7	8.1	0.18
PhNHEt	CCl_4	1506	...	60.6	0.52	PhCOCl	CCl_4	1487	...	6.6	0.215
$PhNHBu^n$	CCl_4	1506	...	65.7	0.535	Ph_2C_2	CCl_4	1501	...	25.0	0.15
$PhNHPr^i$	CCl_4	1505	...	59.2	0.535	PhCCH	CCl_4	1489	...	20.3	0.07
$PhNEt_2$	CCl_4	1513	...	63.9	0.57	PhCN	CCl_4	1492	20.8	17.7	0.085
Ph_3N	CCl_4	1495	...	32.2	0.44	$PhCF(CF_3)_2$	CCl_4	1502	...	18.3	0.03
$PhN(CF_3)_2$	CCl_4	1492	...	31.8	0.13	$PhCOH(CF_3)_2$	CCl_4	1504	...	18.6	0.11
$PhNHNH_2$	C_6H_{12}	1497	...	50.6	0.485	Ph_4Si	$CHCl_3$	1481	8.77	7.8	0.0[d]
PhNHOH	$CHCl_3$	1494	...	23.1	0.22	Ph_4Ge	$CHCl_3$	1486	13.27	17.5	0.0[d]
PhNMeOH	$CHCl_3$	1499	...	42.3	0.41	Ph_4Sn	$CHCl_3$	1481	12.72	12.1	0.0[d]
Ph_2N_2	CCl_4	1485	...	23.1	0.055	Ph_4Pb	$CHCl_3$	1477	13.87	12.5	0.0[d]
PhNCO	CCl_4	1513	...	42.4	0.40	Ph_2Hg	C_4H_8O	1481	12.0	13.1	0.03[d]

[a] A in l. mol^{-1} cm^{-2}. Values corrected for number of phenyl groups where necessary. [b] ϵ is an estimate of the integrated intensity given by $\epsilon = A_{max}\Delta\nu_{1/2}/cl$. [c] Calculated from 1600-cm^{-1} intensities. [d] Calculated in the same way from unpublished intensity measurements, A. R. Katritzky, R. D. Topsom, and L. N. Yakhontov.

We now report integrated intensity values for the ν_{13a} and a few ν_{13b} vibrations of monosubstituted and *para*-disubstituted benzenes and discuss them in terms of the theory developed above.

Experimental and Results Section

Compounds were obtained commercially or prepared by known methods. Purities were checked by gas chromatography or melting point. Spectra were obtained on a Perkin-Elmer 125 spectrophotometer under conditions similar to those previously specified. Solvents were purified as before. Intensity area A values quoted are averages of four readings, usually on two separate solutions; reproducibility of $A^{1/2}$ was ± 2 units. The extinction coefficients ϵ were determined from the formula $\epsilon = a_{max}\Delta\nu_{1/2}/cl$. These are less accurate

Table II: Spectral Data[a] for the ν_{13a} Bands in *para*-Disubstituted Benzenes

Substituents	$\Sigma A_{mono}^{1/2}$	ν cm^{-1} (obsd)	$A_{obsd}^{1/2}$	$\Sigma A_{mono}^{1/2} - 15.8$
NMe_2, Br	107.3	1490	86.1	91.5
NMe_2, I	100.2	1497	89.7	84.4
NMe_2, Cl	108.8	1503	95.6	93.0
NMe_2, CN	91.6	1524	84.2	75.8
NMe_2, COOR	81.5	1524	64.7	65.7
NH_2, NH_2	97.6	1517[b]	89.3	81.8
NH_2, OMe	106.3	1511	93.7	90.5
NH_2, F	102.9	1512	91.4	87.1
NH_2, Br	85.3	1491	69.2	69.5
NH_2, I	78.2	1488	62.0	62.4
NH_2, Cl	86.8	1506	70.8	71.0
NH_2, Me	71.2	1519	62.3	55.4
NH_2, COOR	58.5	1518[b]	35.1	42.7
NH_2, COMe	48.8	1516[b]	19.7	33.0
OMe, OMe	115.0	1510	98.5	99.2
OMe, F	111.6	1508	98.1	95.8
OMe, Br	94.0	1480	73.1	78.2
OMe, I	86.9	1488	69.7	71.1
OMe, Cl	95.5	1494	77.3	79.7
OMe, Me	79.9	1511	66.1	64.1
OMe, CN	78.3	1501	69.3	62.5
OMe, COOR	67.2	1513	49.4	51.4
OMe, COMe	57.5	1511	41.9	41.7
OMe, CHO	57.5	1512	50.7	41.7
F, F	108.2	1518	97.1	92.4
F, Br	90.6	1486	72.3	74.8
F, I	83.5	1484	69.7	67.7
F, Cl	92.1	1493	73.6	76.3
F, Me	76.5	1506, 1499	67.1	60.7
F, CN	74.9	1509	65.7	59.1
F, SO_2Cl	63.1	1494	49.5	47.3
F, COOR	63.8	1510	44.6	48.0
F, COMe	54.1	1507	36.7	38.3
F, CHO	54.1	1507	42.2	38.3
Br, CN	57.3	1482	42.4	41.5
Cl, Cl	76.0	1477	56.6	60.2
Cl, Me	60.4	1492	47.0	44.6
Cl, CN	58.8	1494, 1485	47.2	43.0
Cl, SO_2Cl	47.0	1477	32.4	31.2
Cl, COOR	47.7	1488	25.6	31.9
Cl, COMe	38.0	1488	20.8	22.2
Cl, CHO	38.0	1487	25.0	22.2
Me, Me	44.8	1517	32.1	29.0
Me, CN	43.2	1510	25.1	27.4
Me, SO_2Cl	31.4	1493	13.7	15.6
Me, COMe	22.4	...	0	6.6
CN, CN	41.6	1502[b]	21.0	25.8
CN, COOR	30.5	1502	6.3	14.7
COOR, COOR	19.4	1506[b]	16.6	3.6
COMe, COMe	0	1501[b]	25.0	(−)15.8
CHO, CHO	0	1503[b]	27.5	(−)15.8

[a] Determined in carbon tetrachloride solution unless otherwise specified. [b] Determined in chloroform solution because of low solubility in carbon tetrachloride.

because of the relatively wide slit width employed and since not all the peaks have Lorentzian shape. The A values also contained the entire absorption within the principal band as nearby combination bands may share intensity with the ring vibration.

The values given in Tables I and II relate to the ν_{13a} bands for the monosubstituted and *para*-disubstituted benzenes and occur between 1480 and 1525 cm^{-1}. Most of the compounds investigated had interfering substituent absorptions in the 1440-cm^{-1} regions but $A^{1/2}$ values for the ν_{13b} band in a few compounds where measurements were possible are given in Table III.

Table III: Spectral Data[a] for the ν_{13b} Bands in Some Mono- and *para*-Disubstituted Benzenes

Substituents	ν, cm^{-1}	$A_{obsd}^{1/2}$
NH_2	1467	13.4
Cl	1446	20.2
CN	1448	18.4
F, F	1430	11.7
F, Cl	1426	11.6
F, Br	1426	11.6
F, I	1426	12.1
Cl, Cl	1418	11.6

[a] Determined in carbon tetrachloride solution.

No extensive published values for integrated intensities are available for comparison although approximate extinction coefficients have been measured[10] and integrated intensities reported[11] for some monosubstituted alkyl benzenes. Carbon tetrachloride was employed as the solvent except where low solubility of the aromatic compound necessitated otherwise. Most of the common solvents used earlier absorb strongly in the 1500-cm^{-1} region and it was not possible to examine solvent effects on the vibration.

Discussion

Monosubstituted Benzenes. Table I lists the spectral data for the ν_{13a} bands in monosubstituted benzenes. The integrated intensities were measured for a representative selection of substituents, but otherwise the more readily obtainable extinction coefficient is reported. Unfortunately, interfering substituent vibrations made it impossible to measure the ν_{13b} intensities of all but a few of the compounds (Table III). Monosubstituted benzenes containing one symmetrical substituent are of C_{2v} symmetry overall and the ν_{13a} and ν_{13b} modes are of A_1 and B_2 character, respectively. They are therefore not expected to share intensity and discussion of the ν_{13a} intensities should be meaningful. With less symmetrical substituents, the overall symmetry of the molecule drops to C_s and the vibrations now have A' symmetry and can share intensity. Mixing is less likely than with the ν_{16} bands since the frequency separation is much greater. The analysis below is developed for symmetrical substituents.

(10) A. R. Katritzky and J. M. Lagouski, *J. Chem. Soc.*, 4155 (1958); A. R. Katritzky and P. Simmons, *ibid.*, 2051, 2058 (1959).
(11) A. S. Wexler, *Spectrochim. Acta*, **21**, 1725 (1965).

It has previously been observed[10] that electron-donating substituents increase the intensity of the 1500-cm^{-1} (ν_{13a}) band, while electron acceptors weaken it. Assuming that the dipole change due to the C–H bending component is constant, we can explain the effect of the substituent as generating an additional dipole change with respect to the C–C stretch symmetry coordinate as postulated[2] for the 1600-cm^{-1} mode. The dipole changes generated in the vibration of a mono-donor-substituted compound will be as shown below. It is important to remember that S'_{18} and S'_{19} are of opposite sign, that is the C and H atoms move out of phase. The C–H dipole has been taken[12,13] to be in the direction of C^-–H^+.

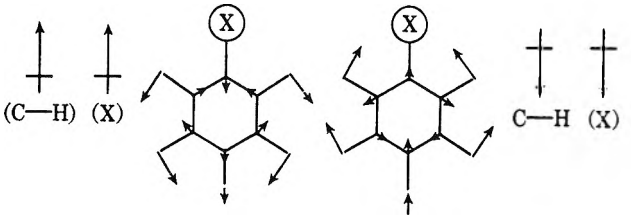

Then the intensity can be considered to arise as

$$A_{\text{monodonor}}^{1/2} = (\text{C–H contribution}) + (\text{X})$$

where (X) is the contribution from the C–C stretch coordinate as affected by the electronic nature of the substituent.

Similarly, for an electron-accepting substituent $A_{\text{mono,acc}}^{1/2} = (\text{C–H}) - (\text{Y})$. The magnitude of the (C–H) contribution can be estimated from the intensity of the degenerate ν_{13} vibration in benzene itself. The intensity is 835 l. mol^{-1} cm^{-2} but since it arises from ν_{13a} and ν_{13b}, half can ascribed to ν_{13a}. The $A^{1/2}$ value is thus 20.5 units. This is the contribution from $\partial\mu/\partial S_{18a} S'_{18a}$ and should approximate to the value of the C–H contribution for monosubstituted benzenes although the latter will be somewhat smaller since S'_{18} will decrease relative to S'_{19} as the benzene is substituted.

If the C–H contribution is constant, then a graph of $A^{1/2}$ against σ_R^0 should be linear and give the former contribution as its intercept on the $\sigma_R^0 = 0$ axis. Figure 1 shows the $A^{1/2}$ values for symmetrical substituents plotted against σ_R^0 values derived from our earlier work.[2c] A fair linear plot is obtained, the value for aniline being the only one to deviate considerably. It is possible to write an equation to relate $A^{1/2}$ to the σ_R^0 value but this would be far more approximate than the equation used for the ν_{16} vibrations. The intercept suggests a contribution of some 19.5 $A^{1/2}$ units from C–H bend in agreement with our arguments above.

The nature of the contributions to the intensity suggests that the assumption of C^-–H^+ polarity in the C–H bonds was correct. This is the usually accepted polarity but Schmid[14] has recently argued that the intensities of aromatic C–H stretching vibrations indicate polarity in the reverse direction. However the "dipoles" discussed by Schmid are apparently not directly comparable[15] with the ones that we have discussed.

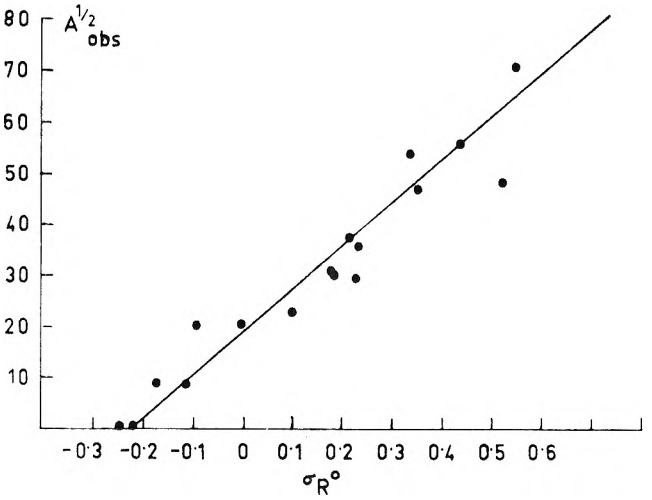

Figure 1. Plot of $A^{1/2}$ for ν_{13a} band of monosubstituted benzenes against σ_R^0 values.

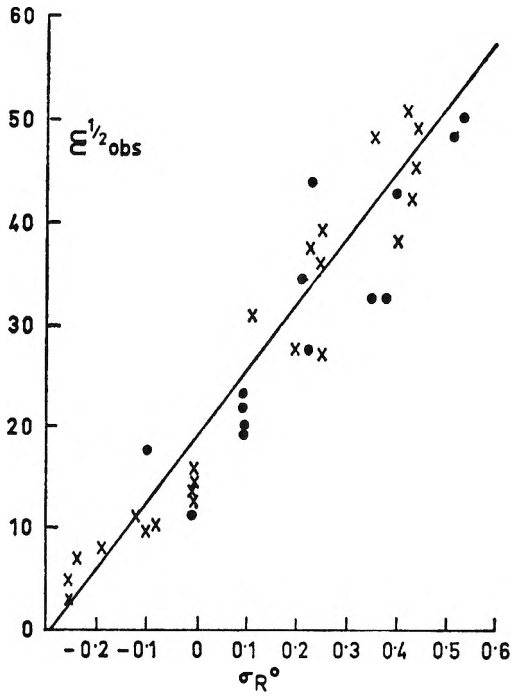

Figure 2. Plot of $\epsilon^{1/2}$ for ν_{13a} band of monosubstituted benzenes against σ_R^0 values.

Figure 2 shows a plot of $\epsilon^{1/2}$ values for a representative selection of substituents against σ_R^0. The general relationship is not of high precision but seems to be equally well followed by substituents of high or low symmetry.

Para-Disubstituted Benzenes. If we assume, as in the

(12) A. R. H. Cole and A. J. Mitchell, *Spectrochim. Acta*, **20**, 739 (1964).

(13) G. J. Boobyer, *ibid.*, **23A**, 335 (1967).

(14) E. D. Schmid, *ibid.*, **22**, 1659 (1966).

(15) V. Hoffmann, and E. D. Schmid, *Z. Naturforsch.*, **22A**, 2048 (1967); E. D. Schmid, private communication.

case of the 1600-cm^{-1} band, that the dipoles induced in the ring by two noninteracting *para*-substituents are additive, and further, that the composition of the normal mode does not change appreciably between compounds, we can deduce the $A^{1/2}$ value for a *para*-disubstituted compound. In the case of *para* C_6H_4XX' where X and X′ are both electron donating substituents, the dipoles are shown below.

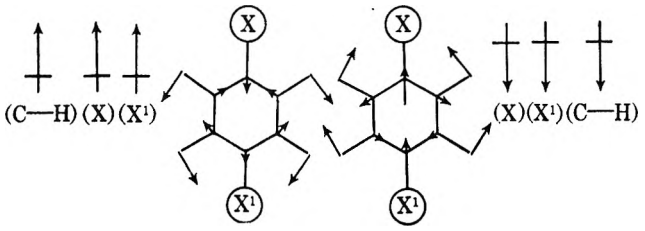

In contrast to the case of the ν_{16} vibration, the dipoles reinforce one another for a "di-donor" since the vibration is antisymmetric with respect to the two ends of the molecule. Expressed in terms of various components

$$A^{1/2} = (\text{C–H}) + (\text{X}) + (\text{X}')$$
$$= [(\text{C–H}) + (\text{X})] + [(\text{C–H}) + (\text{X}')] - (\text{C–H})$$
$$= A_x^{1/2} + A_{x'}^{1/2} - (\text{C–H}) \quad (1)$$

This can also be illustrated in terms of the valence-bond treatment developed[2,3] earlier. In a monosubstituted benzene, during the vibration ν_{13a} there is a distortion of the molecule in the same sense of I $\rightleftharpoons$ II (where the effect is much exaggerated).

In a *para*-disubstituted benzene where both substituents are electron-donating, the situation can be visualized as III $\rightleftharpoons$ IV leading to an oscillating dipole of the type found in the carbon dioxide active stretching mode. The dipole contributions of the substituents are thus additive.

Similarly for *para* C_6H_4XY where X is a donor and Y an acceptor

$$A_{xy}^{1/2} = (\text{C–H}) + (\text{X}) - (\text{Y})$$
$$= [(\text{C–H}) + (\text{X})] + [(\text{C–H}) - (\text{Y})] - (\text{C–H})$$
$$= A_x^{1/2} + A_y^{1/2} - (\text{C–H})$$

Thus we get eq 1 as above and this equation can similarly be shown also to apply to *para*-disubstituted benzenes containing two electron-accepting groups. One therefore expects that a plot of $A^{1/2}$ values for the ν_{13a} vibrations of *para*-disubstituted benzenes with substituents of high symmetry, against the sums of the $A^{1/2}$ values for the corresponding monosubstituted compounds, should give a straight line of slope 1. The C–H contribution should be obtained from the intercept and this would be expected to be of somewhat lower magnitude than 19.5 units since increased substitution causes[6,8] a decreased C–H bending contribution to the vibration.

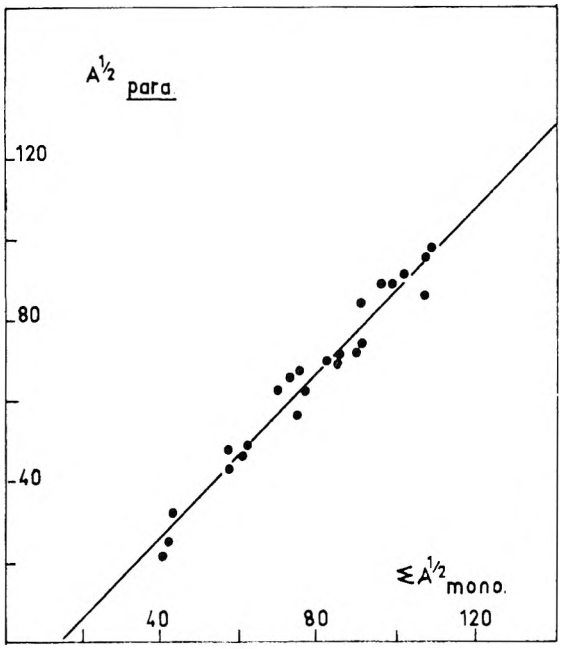

Figure 3. Plot of $A^{1/2}$ for ν_{13a} band of *para*-disubstituted benzenes against the sums of the $A^{1/2}$ values for the corresponding monosubstituted derivatives (substituents of C_{2v} or greater symmetry).

Figure 3 shows the results (Table II) for compounds with substituents of high symmetry plotted against the sum of the $A^{1/2}$ values of the corresponding monosubstituted compounds (Table I). The agreement with the simple theory outlined above is remarkably good and the line fitted by the least-squares procedure is given by

$$A_{x,y}^{1/2} = 1.02(A_x^{1/2} + A_y^{1/2}) - 15.8 \quad (2)$$

The slope and intercept are in excellent agreement with the prediction above.

Substituents of Low Symmetry. It was pointed out above that when benzene was substituted with a group of lower than C_{2v} symmetry, the ν_{13a} and ν_{13b} bands became of the same symmetry class and could mix to share intensities. Such mixing should not be great here because of the frequency separation of the two bands. If there is no mixing, the effect of a substituent on the two modes

can be thought of as the sum of two vectors, one parallel to the C–X bond affecting only the ν_{13a} intensity, and one perpendicular to this affecting only the ν_{13b} band. This is illustrated below for acetophenone.

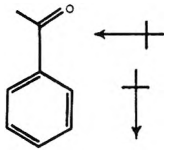

In this case we expect the ν_{13a} mode for all *para*-disubstituted benzenes to follow the equation already developed. Figure 4 shows the results for *para*-disubstituted compounds containing substituents of less than C_{2v} symmetry plotted against the sum of the $A^{1/2}$ values for the corresponding monosubstituted compounds. The line superimposed is the same as that in Figure 3. The line is closely followed indicating little or no mixing taking place between ν_{13a} and ν_{13b} vibrations.

"Through-Conjugation" and d-Orbital Participation. The intensity values for the ν_{16} vibrations of *para*-disubstituted benzenes were found to be greater than calculated from the values for the corresponding monosubstituted compounds where one substituent was a strong donor and the other a strong acceptor. This can readily be explained in terms of contributions to the structure of the type below. This phenomenon is sometimes described as "through conjugation."

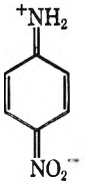

Similar results were found for *para*-substituted chloro-, bromo- and iodobenzenes when the *para*-substituent was a powerful electron donor. The enhancement also increased in the series Cl < Br < I. This was explained in terms of electron acceptance into the d orbitals of the halogen atoms. This d-orbital participation by elements having unfilled d orbitals has been fairly widely accepted[16] on the basis of corresponding results obtained in the ultraviolet region. Some workers[17] had earlier explained the ultraviolet results as arising because the increasing polarizability of the C–halogen bond allowed the other substituent to donate additional charge to the ring.

Our results show no general enhancement of the ν_{13a} intensities for either of the groups of compounds mentioned above. Thus the values for compounds such as *p*-methoxybenzophenone and *p*-iododimethylaniline are close to those calculated on the basis of formula 1. This can be shown to be expected for a *para*-disubstituted compound containing a donor and an acceptor substituent. If Δ is taken as the additional effect of one substituent on the dipole transition moment over that expected, then it should also represent the additional effect of the other substituent. Thus modifying eq 1

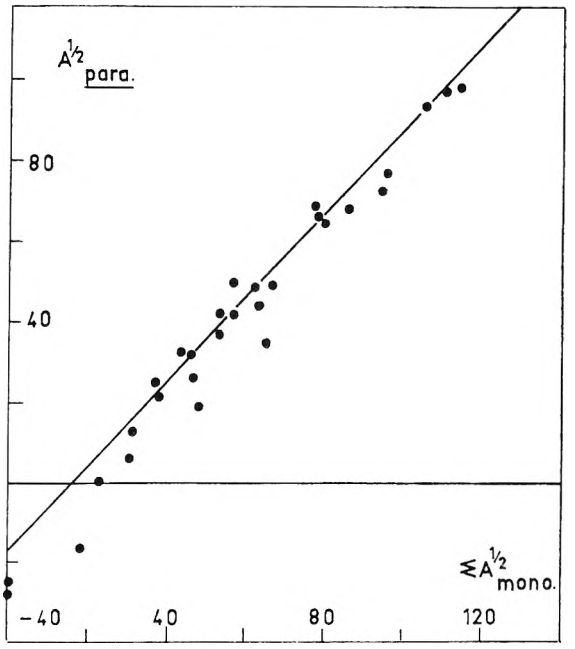

Figure 4. Plot of $A^{1/2}$ for ν_{13a} band of *para*-disubstituted benzenes against the sums of the $A^{1/2}$ values for the corresponding monosubstituted derivatives (at least one substituent of less than C_{2v} symmetry).

$$A_{\text{donor,acc}}{}^{1/2} = (\text{C–H}) + (\text{X} + \Delta) - (\text{Y} + \Delta)$$
$$= (\text{C–H}) + (\text{X}) - (\text{Y})$$
$$= A_x{}^{1/2} + A_y{}^{1/2} - (\text{C–H}) \text{ as before}$$

A similar result follows for a *para*-donor-substituted halobenzene if the d-orbital explanation is correct. If the enhancement in this case, however, was due to the polarization of the C–halogen σ bond allowing the donor to delocalize more change into the ring, the equation would be as below where X is the donor and Y the halogen.

$$A_{\text{donor,hal}}{}^{1/2} = (\text{C–H}) + (\text{X} + \Delta) - (\text{Y})$$
$$= A_x{}^{1/2} + A_y{}^{1/2} - (\text{C–H}) + \Delta \quad (3)$$

and enhancement would be expected.

ν_{13b} *Vibration.* Only a few intensity values for the ν_{13b} band could be obtained for monosubstituted and *para*-disubstituted benzenes and these are shown in Table III. The intensity attributable to the ν_{13b} absorption in benzene itself will be 20.4 $A^{1/2}$ units since the ν_{13a} and ν_{13b} are degenerate. The intensity of the ν_{13b} band

(16) J. R. Hoyland and L. Goodman, *J. Phys. Chem.*, **64**, 1816 (1960); L. Goodman and R. W. Taft, *J. Amer. Chem. Soc.*, **87**, 4385 (1965); W. K. Musker and G. B. Savitsky, *J. Phys Chem.*, **71**, 431 (1967).

(17) W. M. Schubert, H. Steadly, and J. M. Craven, *J. Amer. Chem. Soc.*, **82**, 1353 (1960); W. M. Schubert and H. Steadly, *ibid.*, **82**, 1357 (1960); but see amplification of Schubert's views in W. M. Schubert, R. B. Murphy, and J. Robins, *Tetrahedron*, **17**, 199 (1962).

arising from the C–H bend coordinate in monosubstituted and *para*-disubstituted benzenes should be less since the 1- and 4-hydrogen atoms which contribute to the normal mode are replaced.

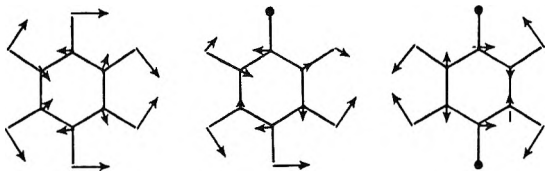

No C–C stretch contribution is expected to this band for substituents of C_{2v} or higher symmetry and so a constant value of $A^{1/2}$ of less than 20.4 units is expected for monosubstituted benzenes and a constant but lower still value is expected for *para*-disubstituted benzenes. These predictions seem substantiated by the results. Unfortunately, it was not possible to obtain corresponding values for asymmetric substituents because substituent vibration interfered in the available compounds.

Spectroscopic Aspects. The results above clearly provide valuable support for the normal coordinate analyses made for chloro and deuteriobenzenes being valid for other substituents. We intend to measure the intensities of a series of deuterated mono- and disubstituted benzenes to further this aspect of the work.

Acknowledgment. R. D. Topsom is grateful for a grant from the Australian Research Grants Committee.

Counterion Complexing and Sol Stability. I. Coagulation Effects of Aluminum Salts in the Presence of Fluoride Ions[1]

by Egon Matijević, Stanka Kratohvil, and Jon Stickels

Institute of Colloid and Surface Science and Department of Chemistry, Clarkson College of Technology, Potsdam, New York 13676 *(Received July 22, 1968)*

The coagulation and the reversal of charge of silver halide sols by aluminum ions in the presence of fluoride ions have been studied as a function of pH. Using known stability constants, the composition of the electrolyte environment was calculated. This included all aluminum fluoride complexes as well as the aluminum hydrolyzed species. With the increasing addition of fluoride ions larger amounts of aluminum perchlorate are required to coagulate the sol. The calculations show that at pH <4 the unhydrolyzed aluminum ion acts as the counterion while at pH >4 the hydrolyzed aluminum ion is the coagulant. The complexing of aluminum ions by fluoride produces lower charged species which have no effect upon the stability over the critical coagulation concentration range of the aluminum salt. The charge of the sols can be reversed by the hydrolyzed aluminum ions, but not by the fluoride complexes.

Introduction

The effects of complexing of counterions upon the stability of lyophobic colloids have received considerable attention in recent years. The interactions of hydrolyzed metal ions with lyophobic sol particles have been particularly thoroughly investigated. Owing to hydrolysis, the charge of the counterion is most frequently changed causing great variations in the coagulation concentrations. In addition, the hydrolyzed species adsorb appreciably more strongly than the corresponding unhydrolyzed ions. Depending on the conditions, this adsorption may either enhance the coagulation or restabilize the sol, due to charge reversal.[2,3]

Much less attention was accorded to complexing with ligands other than hydroxyl. Recently, it was shown that chelation of metal counterions affects the sol stability[4] in a most striking way.

This study deals with the interactions of aluminum salts with silver halide sols in the presence of various amounts of fluoride ions. It was attempted to carefully evaluate the effect of an inorganic complexing ligand (other than hydroxyl) upon the coagulation and reversal of charge ability of a metal counterion. The aluminum fluoride system was chosen for theoretical and practical reasons. The counterion behavior of aluminum and of its hydrolyzed species has been extensively studied and it is rather well understood.[5,6]

(1) Supported by the Federal Water Pollution Control Administration Grant WP-00815.

(2) E. Matijević, S. Kratohvil, and L. J. Stryker, *Discussions Faraday Soc.*, **42**, 187 (1966).

(3) E. Matijević, "Charge Reversal of Lyophobic Colloids" in "Principles and Applications of Water Chemistry," John Wiley and Sons, Inc., New York, N. Y., 1967.

(4) E. Matijević and N. Kolak, *J. Colloid Interface Sci.*, **24**, 441 (1967).

(5) E. Matijević, K. G. Mathai, R. H. Ottewill, and M. Kerker, *J. Phys. Chem.*, **65**, 826 (1961).

(6) E. Matijević, G. E. Janauer, and M. Kerker, *J. Colloid Sci.*, **19**, 333 (1964).

Also, good thermodynamic data are available for the aluminum fluoride complexes[7-10] which make feasible a quantitative analysis of the interactions between the sol particles and the electrolyte environment.

One of the practical aspects of this work is related to water chemistry. Many natural waters contain small amounts of fluorides and a number of communities fluoridize their waters. Since aluminum salts are still the most frequently used coagulants, the interactions of fluoride with aluminum ions may significantly influence the purification procedures and the effectiveness of fluoridation. This is particularly true because of the great stability of aluminum fluoride complexes.

Silver halide sols were employed because extensive studies of their stability are available and therefore a comparison of the coagulation and reversal of charge data by aluminum in the absence of fluoride is possible. In addition fluoride ion alone will have little effect upon sol stability since silver fluoride is a rather soluble salt.

Experimental Section

A. Materials. Aluminum perchlorate (K and K Laboratories) was used without further purification. The concentration of the stock solution was determined gravimetrically using the 8-hydroxy-quinoline reagent. To avoid aging effects,[6] the necessary dilutions were made frequently. All other chemicals were of the highest commercial purity grade. Solutions were prepared with doubly distilled water from an all-Pyrex still.

Silver bromide and silver iodide sols *in statu nascendi* served as colloidal systems. In all experiments the concentration of the sols was 1×10^{-4} *M* with an excess halide concentration of 1.9×10^{-3} *M*. Aged negative silver halide sols, used in some of the electrophoresis experiments, were prepared according to the procedure by Ottewill, *et al.*[11,12]

B. Methods. (*a*) *Precipitation of Aluminum Fluoride.* To determine the conditions which lead to the formation of precipitates when solutions of aluminum and fluoride salts are mixed, the entire solubility diagram was established. This was accomplished by observing the appearance of the first trace of precipitate in a series of systems in which the fluoride (or aluminum) concentration was kept constant while the concentration of aluminum (or fluoride) was gradually changed. The total volume of each system in a series was 10 ml. At first an attempt was made to detect the first appearance of the precipitate by turbidity or light scattering, but this failed to give reliable results. It was found that visual observation of the first trace of precipitate at the bottom of the test tube, 24 hr after mixing the precipitating components, could be used to reproducibly establish the limiting concentrations at which the precipitate still occurs. No further changes could be detected after 24 hr. The pH of the systems was controlled and measured at various periods of time. The results obtained by using fluoride as the variable component were in very good agreement with data obtained when the concentration of the aluminum salt was varied.

(*b*) *Coagulation and Reversal of Charge of Silver Halide Sols.* Scattering intensities were measured on a series of systems prepared by mixing solutions containing the two precipitation components and other electrolytes as needed. As a rule in one series either the concentration of the aluminum salt was varied and the pH kept constant or vice versa. In the first case constant amounts of silver nitrate and potassium fluoride and varying amounts of aluminum perchlorate were in one series of test tubes while the other series contained potassium bromide and acid ($HClO_4$) or base (NaOH) as needed to keep the pH at a desired value. In the second case the concentrations of aluminum perchlorate were kept constant while the addition of the acid or the base was varied gradually in order to change pH in rather small increments. Usually each test tube contained 5 ml of the solution to give 10 ml after mixing. All reported concentrations refer to this final volume of 10 ml. It was found that identical results were obtained if the reaction components were contained in different volumes, such as 9 ml + 1 ml.

Table I: Cumulative Formation Constants for Aluminum Fluoride Complexes

$$\beta_n = [AlF_n^{(3-n)+}]/[Al^{3+}][F^-]^n$$

	a	*b*	*c*	*d*
$\log \beta_1$	6.13	6.61	7.01	6.32
$\log \beta_2$	11.15	11.97	12.75	11.63
$\log \beta_3$	15.00	16.03	17.02	15.45
$\log \beta_4$	17.74	18.71	19.72	17.60
$\log \beta_5$	19.37	20.04	20.91	18.03
$\log \beta_6$	(19.84)		20.86	

[a] Ionic strength 0.53, ref 7. [b] Ionic strength 0.07 (calcd), ref 9. [c] Ionic strength zero (calcd), ref 10. [d] Ionic strength 0.1, ref 18.

The rate of coagulation of silver halide sols *in statu nascendi* was followed by measuring the scattering intensities with an Aminco light scattering photometer. The procedure for the determination of the *critical coagulation concentration* (ccc) and the *critical*

(7) C. Brosset and J. Orring, *Svensk Kemisk Tidskr.*, **55**, 101 (1943).
(8) W. M. Latimer and W. L. Jolly, *J. Amer. Chem. Soc.*, **75**, 1548 (1953).
(9) E. L. King and P. K. Gallagher, *J. Phys. Chem.*, **63**, 1073 (1959).
(10) J. D. Hem, Geological Survey Water-Supply Paper 1827-B, 1968, pp B1–B33.
(11) R. H. Ottewill and M. S. Rastogi, *Trans. Faraday Soc.*, **56**, 866 (1960).
(12) R. W. Horne and R. H. Ottewill, *J. Phot. Sci.*, **6**, 39 (1958).

stabilization concentration (csc) was described in detail earlier.[13,14]

Electrophoretic mobilities were measured in a microelectrophoresis cell of the Mattson type[15] as described earlier.[6] All determinations were made ten minutes after the mixing of the reaction components.

A Beckman Model G pH meter with glass electrodes was used to adjust and control the pH. The instrument was calibrated regularly with appropriate buffer solutions.

Computations

In order to interpret the results it was necessary to compute the composition of the electrolyte environment for various experimental values of the ccc and csc of aluminum perchlorate in the presence of different amounts of potassium fluoride as a function of pH. In the calculations, carried out by means of an IBM 360 digital computer, the existence of all aluminum fluoride complexes $AlF_n^{(3-n)+}$ for $n = 1$–6, the dissociation of HF, and the hydrolysis of aluminum ion were considered. It was assumed that only one hydrolyzed complex ion exists at room temperature. Two different but very similar formulations have been suggested for the composition of the hydrolyzed aluminum species:[5,6,16] $Al_8(OH)_{20}^{4+}$ and $Al_7(OH)_{17}^{4+}$. While we believe that the octamer is the more likely species, in calculations in this work the heptamer has been assumed for which the formation constant is available,[16] $\log \beta_{17,7} = -48.8$. It should be noted that both suggested species are of the same charge (+4) which is essential in the discussion of sol stability.

The composition of the various species was computed from the following two equations

$$[Al]_{tot} = [Al^{3+}] + \beta_1[Al^{3+}][F^-] + \beta_2[Al^{3+}][F^-]^2 + \beta_3[Al^{3+}][F^-]^3 + \beta_4[Al^{3+}][F^-]^4 + \beta_5[Al^{3+}][F^-]^5 + \beta_6[Al^{3+}][F^-]^6 + \beta_{17,7}[Al^{3+}]^7[H^+]^{17} \quad (1)$$

$$[F]_{tot} = [F^-] + \beta_1[F^-][Al^{3+}] + 2\beta_2[F^-]^2[Al^{3+}] + 3\beta_3[F^-]^3[Al^{3+}] + 4\beta_4[F^-]^4[Al^{3+}] + 5\beta_5[F^-]^5[Al^{3+}] + 6\beta_6[F^-]^6[Al^{3+}] + [H^+][F^-]\,1/K \quad (2)$$

The value for the ionization constant of the hydrofluoric acid $K = 6.7 \times 10^{-4}$.[17] Table I contains several sets of values[18] for the cumulative formation of aluminum fluoride complex constants

$$\beta_n = [AlF_n^{(3-n)+}]/[Al^{3+}][F^-]^n$$

where $\beta_n = k_1 \cdot k_2 \ldots k_n$, and k_n is the complex constant

$$k_n = [AlF_n^{(3-n)+}]/[AlF_{n-1}^{(4-n)+}][F^-]$$

The values for similar ionic strength as obtained by two different laboratories are in rather good agreement (Table Ia,d). Larger differences are observed only in the case of β_5 and β_6. The value of the last constant is the least reliable. However, it turns out that the concentrations of AlF_5^{2-} and AlF_6^{3-} were negligible in the systems under investigation.

Since it is impractical in the coagulation work to adjust and keep constant the ionic strength, calculations were carried out using formation constants for ionic strengths 0.53 and 0.07. No significant differences resulted in the computed concentration of various complex species. Therefore only data as calculated using the values for β_n by Brosset and Orring[7] will be reported.

The Newton–Raphson iteration procedure was used to obtain the roots of the polynomial equations written for $[Al]_{total}$ and $[F]_{total}$. Equation 1 was used to solve for $[Al^{+3}]$ and eq 2 was used to solve for $[F^-]$. Since a polynomial equation will have as many roots as the degree of the equation (real or imaginary and possibly degenerate), a verification procedure was used to see that the most physically logical root was calculated. Initial estimates of the values of $[Al^{3+}]$ and $[F^-]$, which are required for the Newton–Raphson method, were chosen so that the following ranges were checked: $10^{-9}\ M < [F^-] < [F]_{total}$ and $10^{-9}\ M < [Al^{+3}] < [Al]_{total}$. In all cases considered in this paper, only one root existed for $[Al^{+3}]$ and $[F^-]$ in these ranges of concentration.

Finally, recently, considerable effort was made in presenting the composition of solutions containing complex fluorides by means of various graphical plots.[10,19] While such graphical presentations may serve to give an approximate idea of the solution composition, they are inadequate for such an analysis as is being carried out in this work.

Results

Figure 1 represents the solubility diagrams of aluminum fluoride when potassium fluoride was mixed with aluminum nitrate and aluminum perchlorate, respectively. The two solubility curves are similar except over the range of the highest aluminum salt concentrations. Solubility data obtained by using a concentration gradient of the aluminum salt keeping the fluoride concentration constant and vice versa gave the same results. The shape of the solubility curves is typical of systems which exhibit complex solubility. In principle, it is possible to detect the composition of the predominant complex solute species from an analysis of the solubility dia-

(13) B. Težak, E. Matijević, and K. Schulz, *J. Phys. Chem.*, **55**, 1557 (1951).
(14) E. Matijević and M. Kerker, *ibid.*, **62**, 1271 (1958).
(15) S. Mattson, *ibid.*, **32**, 1532 (1938); **37**, 223 (1933).
(16) G. Biedermann, *Svensk Kemisk Tidskr.*, **76**, 362 (1964).
(17) H. H. Broene and T. De Vries, *J. Amer. Chem. Soc.*, **69**, 1644 (1947).
(18) K. E. Kleiner, *Zh. Obshch. Khim.*, **20**, 1747 (1950).
(19) G. Goldstein, *Anal. Chem.*, **36**, 244 (1964).

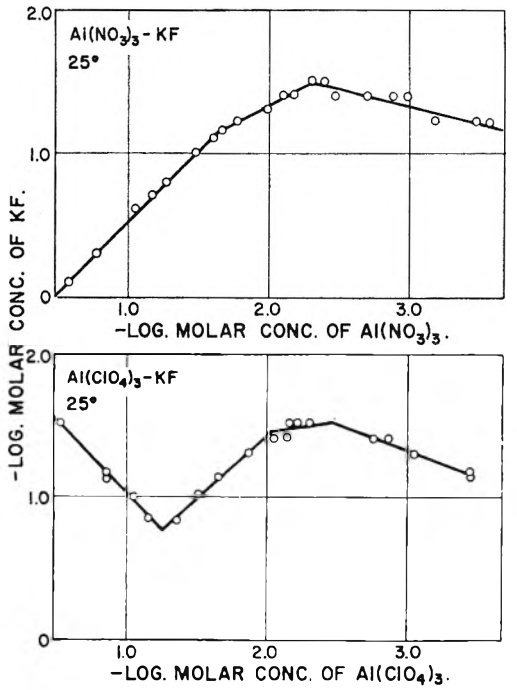

Figure 1. Solubility curves of aluminum fluoride at 25°. The upper curve was obtained by mixing $Al(NO_3)_3$ with KF, and the lower curve by mixing $Al(ClO_4)_3$ with KF. Precipitate is formed below these curves.

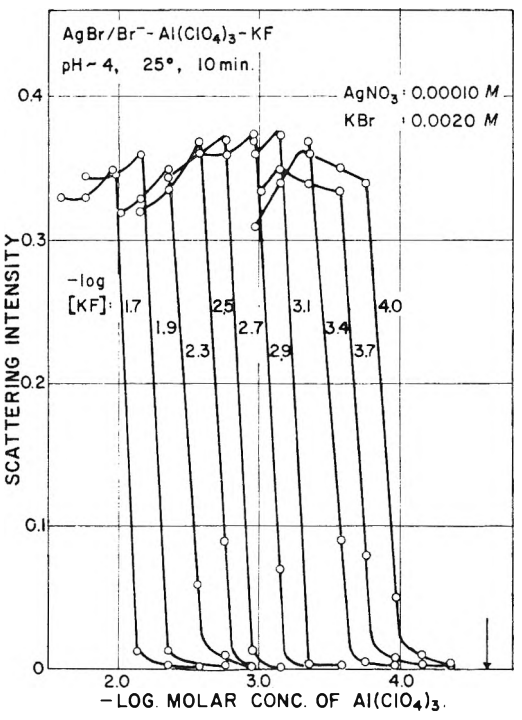

Figure 2. Scattering intensities of a silver bromide sol *in statu nascendi* coagulated by aluminum perchlorate in the presence of various amounts of potassium fluoride, 10 min after mixing the reacting components. Concentrations: $AgNO_3$, 1.0×10^{-4} *M*; KBr, 2×10^{-3} *M*; pH ~4, KF: as indicated next to each curve. Wavelength, 546 mμ; temperature, 25°.

grams.[20,21] In order to do so the chemical composition of the solid phase has to be known. In the case of aluminum fluoride this composition varies depending on the concentrations of the precipitating components.[22,23] No attempt was made to analyze the composition of the solid phase in order to detect the soluble complexes. The primary purpose of establishing the solubility diagrams was to ensure that no solid aluminum fluoride precipitates under the conditions of the coagulation experiments.

Figure 2 gives a number of curves for a negatively charged silver bromide sol coagulated by aluminum perchlorate in the presence of various amounts of potassium fluoride. High scattering intensity indicates coagulated sols. The ccc is obtained by extrapolating the steep part of the curve to zero scattering intensity. All data are for 10 min after mixing the reacting components. This time was found to be critical for silver bromide sols *in statu nascendi*.[13] It is quite apparent that with an increasing amount of fluoride ions the coagulation concentration of the aluminum salt also increases. The arrow indicates the ccc for the same sol using $Al(ClO_4)_3$ in the absence of potassium fluoride. All experiments were carried out at a pH close to 4.0. Similar series of systems were studied at lower and higher pH values.

Figure 3 is a plot of ccc of $Al(ClO_4)_3$ as a function of the added potassium fluoride. A linear relationship (solid line) is obtained at several pH values investigated. All points refer to the silver bromide sol. The dashed line is for a silver iodide sol *in statu nascendi*. Obviously both sols behave quite similarly. Above these lines the sols are coagulated and below the sols are stable.

It is to be expected that pH would have a great effect upon the coagulation of silver halide sols by aluminum salts in the presence of fluoride ions. In addition to fluoride complexes, hydrolysis products are formed at higher pH. Figure 4 gives as an example two curves where the scattering intensity is plotted against the pH. Both curves are for the same sol and identical fluoride concentration. The only difference is that each curve represents systems containing somewhat different but constant concentrations of $Al(ClO_4)_3$. The effect is quite striking.

The "log $[Al(ClO_4)_3]$–pH" domain for a silver bromide sol in the presence of a constant concentration of KF (3×10^{-4} *M*) is given in Figure 5. Open circles are for experiments in which the aluminum perchlorate concentration was kept constant and the pH changed gradually while black circles were obtained when pH was kept constant and the concentra-

(20) V. B. Vouk, J. P. Kratohvil, and B. Težak, *Arhiv kem.*, **25**, 219 (1953).

(21) K. F. Schulz, E. Matijević, and M. Kerker, *J. Chem. Eng. Data*, **6**, 333 (1961).

(22) C. Brosset and U. Wahlberg, *Svensk Kemsk Tidskr.*, **55**, 335 (1943).

(23) C. Brosset, Separate, Stockholm, 1942, 120 pp.

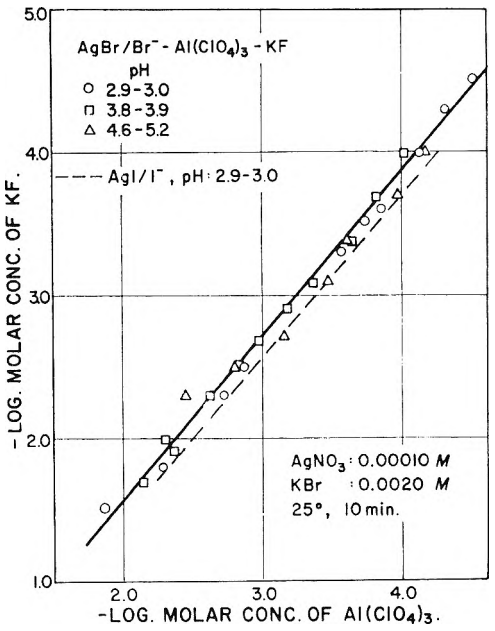

Figure 3. The dependence of the ccc of $Al(ClO_4)_3$ for a silver bromide sol *in statu nascendi* as a function of the concentration of added KF (solid line) for three different pH ranges: 2.9–30 (○), 3.8–3.9 (□), and 4.6–5.2 (△). The dashed line is for a silver iodide sol *in statu nascendi* at pH 2.9–3.0.

tion of $Al(ClO_4)_3$ varied. The two blackened squares represent points of zero charge as measured electrophoretically. For the same concentration of $Al(ClO_4)_3$ the sols are negatively charged below the pH value indicated by the square and positively charged above this value. The latter is due to charge reversal. The sols are coagulated over the range indicated by hatching. Below the shaded region the electrolyte concentration is too low to affect the sol stability. Above this region the sols are stable due to charge reversal.

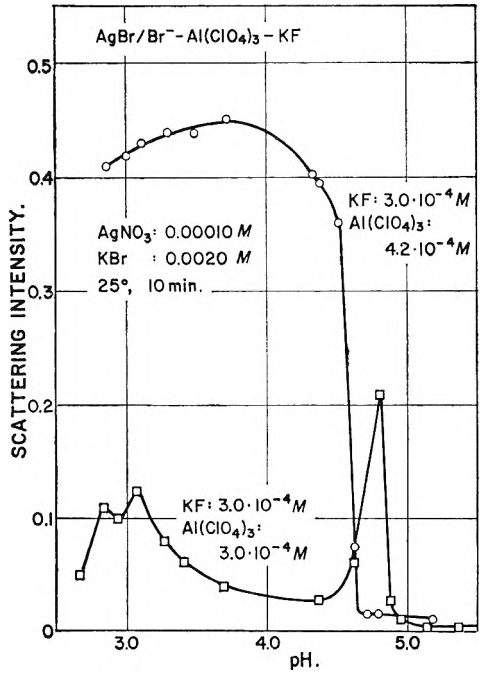

Figure 4. Scattering intensities of a silver bromide sol *in statu nascendi* in the presence of the same concentration of KF (3.0×10^{-4}) and two different concentrations of $Al(ClO_4)_3$ (3.0×10^{-4} *M*, □; 4.2×10^{-4} *M*, ○) as a function of pH.

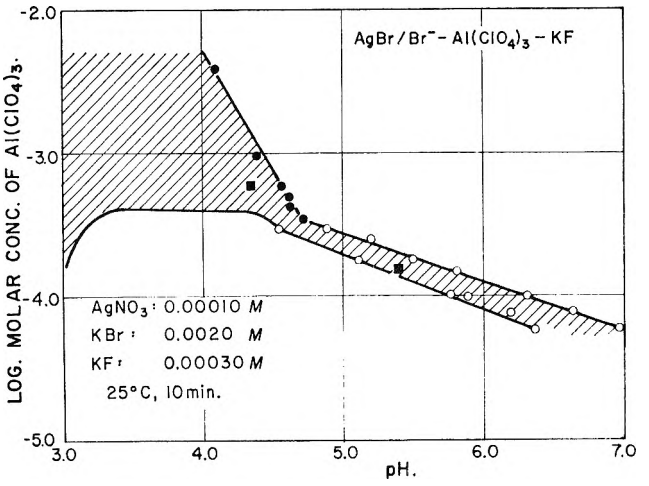

Figure 5. The "log $[Al(ClO_4)_3]$-pH" domain for a silver bromide sol *in statu nascendi* in the presence of a constant amount of KF. Concentrations $AgNO_3$: 1.0×10^{-4} *M*, KBr: 2.0×10^{-3} *M*, KF: 3.0×10^{-4} *M*. The coagulation region is indicated by hatching. Open circles give data obtained at constant pH, and the blackened circles at constant concentration of $Al(ClO_4)_3$. Blackened squares indicate points of zero charge.

Finally, Figure 6 gives a series of such domains for various concentrations of KF. The heavy lines indicate the ccc and csc in the absence of fluoride as determined before.[5] The dashed line gives the pre-

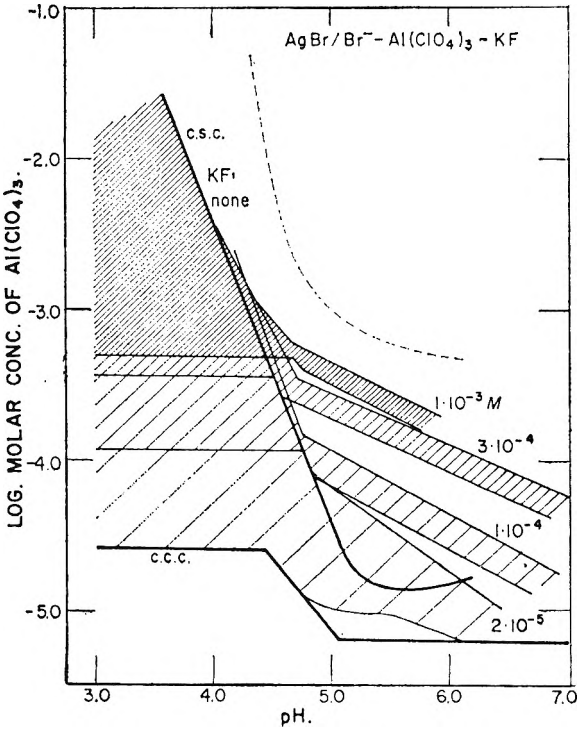

Figure 6. The entire "log $[Al(ClO_4)_3]$-pH" domain for a silver bromide sol *in statu nascendi* in the presence of various amounts of KF. The heavy solid line gives the ccc and the csc in the absence of KF. Hatched areas represent coagulation regions for various concentrations of KF, as indicated in the diagrams. Dashed line gives the precipitation boundary of $Al(OH)_3$ in absence of AgBr.

cipitation boundary of aluminum hydroxide. Again, the shaded area in each case represents the conditions at which the silver bromide is coagulated.

Discussion

A comparison of the coagulation concentrations (Figure 3) and of the "log $[Al(ClO_4)_3]$–pH" domains (Figure 6) in the absence and the presence of fluoride ions best illustrates the large effects due to counterion complexing. Here an attempt will be made to interpret these results in terms of aluminum–fluoride interactions. At pH >4 the hydrolysis of aluminum ions will also be considered. No such analysis of metal ions complexing by anions other than hydroxyl has been applied to stability data heretofore.

Table II contains the concentrations of all the species for a number of systems corresponding to the ccc of aluminum perchlorate in the presence of various fluoride concentrations for three different pH values. These refer to the conditions along the straight line in Figure 3. An inspection of Table II reveals a very interesting fact. When hydrolysis is negligible (pH 3 and 4) all complex counterions are in concentrations much too low to exhibit any coagulation effects.[24,25] The calculations indicate that at pH 3 and 4 the concentration of the unhydrolyzed aluminum ion along the ccc line in Figure 3 is reasonably constant. The variations in values are small if one considers the complexity of the system. More importantly, the average value $[Al^{3+}] = 3 \times 10^{-6}$ M is in excellent agreement with the ccc for trivalent counterions as determined for the same silver bromide sol.[24] Specifically, the coagulation concentration for $Al(NO_3)_3$ in the absence of complexing anions is 2.5×10^{-6} M.[5] It would seem then that the unhydrolyzed aluminum ion is the only effective coagulating species in the presence of fluoride ions at pH <4. The higher concentrations of the aluminum salt needed to coagulate the sol when fluoride is added are due to tying up of the aluminum ion in the form of lower charged complexes which exhibit no coagulation effect in the available concentrations.

At pH ~5 the amount of free Al^{3+} is in all cases considerably below the ccc and so is the concentration of all other complex species, except the *hydrolyzed* aluminum ion. The calculated concentrations of $Al_7(OH)_{17}^{4+}$ are somewhat higher than the experimentally determined values in the absence of fluoride[5,6] but there is no doubt that the hydrolyzed ions are the only species present in concentrations sufficiently high to coagulate the silver bromide sol. It is not surprising that in this case the agreement is not as quantitative as it is at lower pH values. As mentioned before, there is still some doubt regarding the formulation of the hydrolyzed complex and certainly the value of the hydrolysis constant could be somewhat different. Also the coagulation data at these

Table II: Calculated Concentrations of Various Ionic Species in Solution along the Coagulation Curve (Figure 3) for the Electrolyte Mixture $Al(ClO_4)_3$–KF

pH	$[Al]_{tot}$	$[F]_{tot}$	$[Al^{3+}]$	$[F^-]$	$[AlF^{2+}]$	$[AlF_2^+]$	$[AlF_3]$	$[AlF_4^-]$	$[AlF_5^{2-}]$	$[AlF_6^{3-}]$	[HF]	$[Al_7(OH)_{17}^{4+}]$
3	1.25×10^{-4}	1.00×10^{-4}	3.9×10^{-5}	1.4×10^{-6}	7.5×10^{-6}	1.1×10^{-5}	...	...	...	...	2.1×10^{-6}	...
3	3.00×10^{-4}	3.00×10^{-4}	5.7×10^{-5}	3.0×10^{-6}	1.9×10^{-4}	4.9×10^{-5}	...	...	...	...	3.7×10^{-6}	...
3	1.00×10^{-3}	1.60×10^{-3}	2.6×10^{-5}	1.2×10^{-5}	4.2×10^{-4}	5.1×10^{-4}	4.3×10^{-5}	...	...	...	1.7×10^{-5}	...
3	3.00×10^{-3}	5.00×10^{-3}	5.6×10^{-5}	1.5×10^{-5}	1.1×10^{-3}	1.7×10^{-3}	1.7×10^{-4}	1.4×10^{-6}	...	...	2.2×10^{-5}	...
4	1.25×10^{-4}	1.00×10^{-4}	3.8×10^{-5}	1.4×10^{-6}	7.5×10^{-6}	1.1×10^{-5}	...	...	...	...	2.1×10^{-3}	...
4	3.00×10^{-4}	3.00×10^{-4}	5.6×10^{-5}	2.5×10^{-6}	1.9×10^{-4}	5.1×10^{-5}	...	...	...	...	3.8×10^{-7}	...
4	1.00×10^{-3}	1.60×10^{-3}	2.5×10^{-5}	1.2×10^{-5}	4.1×10^{-4}	5.2×10^{-4}	4.5×10^{-5}	...	...	...	1.8×10^{-6}	...
4	3.00×10^{-3}	5.00×10^{-3}	5.5×10^{-5}	1.5×10^{-5}	1.1×10^{-3}	1.7×10^{-3}	1.8×10^{-4}	1.5×10^{-6}	...	...	2.2×10^{-6}	...
5	1.25×10^{-4}	1.00×10^{-4}	1.3×10^{-6}	1.3×10^{-5}	2.2×10^{-5}	2.9×10^{-5}	2.6×10^{-6}	...	...	...	1.9×10^{-7}	1.0×10^{-5}
5	3.00×10^{-4}	3.00×10^{-4}	1.4×10^{-6}	2.2×10^{-5}	4.2×10^{-5}	9.5×10^{-5}	1.5×10^{-5}	...	...	...	3.2×10^{-7}	2.1×10^{-5}
5	5.00×10^{-4}	4.00×10^{-4}	1.6×10^{-6}	2.4×10^{-5}	5.2×10^{-5}	1.3×10^{-4}	2.2×10^{-5}	...	...	...	3.5×10^{-7}	4.2×10^{-5}
5	1.00×10^{-3}	1.60×10^{-3}	1.6×10^{-6}	4.7×10^{-5}	9.9×10^{-5}	4.8×10^{-4}	1.6×10^{-4}	4.1×10^{-6}	...	...	6.9×10^{-7}	3.7×10^{-5}

Table III: Calculated Concentrations of Various Ionic Species in Solution of $Al(ClO_4)_3$–KF for Several Regions of the Domains in Figure 6

pH	$[Al]_{tot}$	$[F]_{tot}$	$[Al^{3+}]$	$[F^-]$	$[AlF^{2+}]$	$[AlF_2^+]$	$[AlF_3]$	$[AlF_4^-]$	$[AlF_5^{2-}]$	$[AlF_6^{3-}]$	$[Al_7(OH)_{17}^{4+}]$
3.5	2.4×10^{-5}	2.0×10^{-5}	7.5×10^{-6}	1.4×10^{-6}	1.4×10^{-5}	2.1×10^{-6}	2.1×10^{-8}	...	...	...	...
6.0	2.4×10^{-5}	2.0×10^{-5}	4.2×10^{-9}	1.9×10^{-5}	1.1×10^{-7}	2.2×10^{-7}	...	...	...	...	...
5.0	2.0×10^{-4}	3.0×10^{-4}	1.2×10^{-6}	2.3×10^{-5}	3.9×10^{-5}	9.5×10^{-5}	1.6×10^{-5}	2.0×10^{-7}	...	...	3.4×10^{-6}
5.5	2.0×10^{-4}	3.0×10^{-4}	8.3×10^{-5}	7.2×10^{-5}	8.1×10^{-5}	6.1×10^{-5}	3.1×10^{-5}	1.2×10^{-6}	...	...	1.0×10^{-5}
											1.4×10^{-5}

higher pH values in the presence of KF are less reproducible. Therefore the best we can expect is to draw qualitative conclusions in this instance.

An attempt was also made to correlate various regions of the "log $[Al(ClO_4)_3]$–pH" domains in the presence of KF with the composition of the electrolyte environment. Only a few samples will be given here. The first line in Table III is for conditions at which no coagulation is observed (see Figure 6). Indeed all of the charged species are in concentrations well below the corresponding ccc. The second line is for a point within the coagulation range. The concentration of the hydrolyzed species is in this case sufficient to coagulate the sol. Similarly, the hydrolyzed aluminum species is the coagulant in the last two cases in which a different amount of KF was added. Both points are within the coagulation range.

It was established that charge reversal only takes place when hydrolyzed aluminum ions are present in sufficiently high concentrations. This is in agreement with our earlier observation.[2,3] Regardless of their concentration, aluminum fluoride complex ions do not reverse the charge of the silver halide sols. This is to be expected since these complexes should still be strongly hydrated and as such could not adsorb on lyophobic sol particles.

In conclusion, it can be stated that the stability of silver halide sols in the presence of aluminum and fluoride ions can be interpreted in terms of complexing of counterions. At pH <4 the *unhydrolyzed* aluminum ion coagulates the sol, although its concentration may represent only a small fraction of the total aluminum salt required. At pH >5 the hydrolyzed aluminum ions coagulate the sols and also reverse the charge if present in sufficient concentration. Complexing of aluminum ions by fluoride essentially removes the coagulating aluminum species in the form of lower charged complexes which have no effect upon the coagulation of the silver halides. It is therefore possible to explain the stability data of lyophobic colloids in the presence of aluminum and fluoride species. It is also possible to quantitatively predict the behavior of solutions containing aluminum and fluoride ions with regard to their coagulation ability at pH <4. Due to complexity of the system only qualitative predictions can be made for pH >4.

Acknowledgment. The authors are indebted to Mr. Gordon H. Fricke for his assistance in the computations presented in this work.

(24) E. Matijević, D. Broadhurst, and M. Kerker, *J. Phys. Chem.*, **63**, 1552 (1959).

(25) E. Matijević, K. F. Schulz, and B. Težak, *Croat. Chem. Acta*, **28**, 81 (1956); B. Težak, E. Matijević, and K. F. Schulz, *J. Phys. Chem.*, **59**, 769 (1955).

Charge-Transfer Interactions of Chlorophylls a and b and Pheophytins a and b with *sym*-Trinitrobenzene[1]

by J. R. Larry[2] and Q. VanWinkle

Department of Chemistry, The Ohio State University, Columbus, Ohio 43210 *(Received July 29, 1968)*

Chlorophylls a and b and pheophytins a and b form strong 1:1 molecular complexes with *sym*-trinitrobenzene. These interactions are interpreted to be of the charge-transfer type. Equilibrium constants and thermodynamic constants for complex formation were determined from spectroscopic data. Electron-donating abilities increase in the order pheophytin b < chlorophyll b < pheophytin a < chlorophyll a. Complexation leads to vibrational frequency increases for the ring V carbonyl of chlorophyll a and chlorophyll b and the aldehyde carbonyl of chlorophyll b. Nuclear magnetic resonance spectra of the equilibrium systems reveal that only certain protons of the chlorophyll molecule shift from their normal positions. These observations give some insight into the orientation of the two molecules in the complex.

Introduction

Charge-transfer phenomena have been considered to have important biological significance. Calvin[3] has incorporated these concepts into a theory of photosynthesis. More recently, Evstigneev[4] has proposed a mechanism whereby primary energy transfer processes

(1) Taken from the Ph.D. dissertation of J. R. Larry, The Ohio State University, 1966. This investigation was supported in part by a Public Health Service fellowship, 5-F1-GM-24, 532-02, from the National Institutes of General Medical Sciences.

(2) National Institutes of Health Predoctoral Fellow (1964–1966). Electrochemicals Department, E. I. DuPont de Nemours and Co., Wilmington, Del.

(3) M. Calvin, *J. Theoret. Biol.*, **1**, 258 (1961).

(4) V. B. Evstigneev, *Photochem. Photobiol.*, **4**, 171 (1965).

are initiated by chlorophyll molecules which are adjacent to either electron donors or electron acceptors.

Various studies have shown that the central magnesium atom is the most important site for electron acceptance. It is currently believed that the cyclopentanone region (ring V) of the chlorophyll molecule is primarily responsible for the electron donation ability. Support for this stems from the fact that oxidation of this ring occurs with considerable ease. In addition, the interaction of the ring V carbonyl with the magnesium of another chlorophyll molecule to promote dimerization[5] may also be taken as evidence for this view.

In general, few detailed investigations have been made for situations where chlorophyll assumes the role of an electron donor. This research effort was directed toward a study of the interactions of chlorophylls a and b and their derivatives with an electron acceptor. A major objective was to elucidate the mode and site of interaction between the donor and acceptor molecules so that additional knowledge of the properties and functions of the chlorophylls might be gained.

Experimental Section

Preparation of Chlorophylls. Approximately 10 lb of fresh spinach leaves were used for a single preparation. All operations beginning with the extraction and ending with the final purified chlorophylls were performed at 5° under green lighting. The plant pigments were extracted in reagent grade acetone by means of a Waring blender. This homogenate was filtered through a previously prepared pad of Hy-flo Super Cell to remove all insoluble material. The acetone extract was transferred to 2 l. of petroleum ether (30–60° boiling range). From this point in the procedure two completely different methods were used to obtain the final pure chlorophylls.

The petroleum ether solution was evaporated to near dryness and redissolved in a solvent system containing 90% petroleum ether and 10% ethyl ether. This solution was directly adsorbed on a column of magnesium sulfate–Hy-flo Super Cell 1:1 by weight. The columns were prepared by packing the adsorbent in acetone and then rinsing with petroleum ether to remove the acetone. After adsorption the pigments were developed with a solvent system containing a v/v ratio of 60–40 petroleum ether–ethyl ether with 2% acetone. The middle fractions of the chlorophyll a and b bands were collected. These fractions were separately chromatographed and the middle fraction of the second chromatography was collected for crystallization.

The second procedure used was similar to that of Jacobs, Vatter, and Holt[6] except that final purification was done on a magnesium sulfate–Hy-flo Super Cell column instead of a sugar column.

The spectroscopic parameters for the chlorophylls agree by both methods of preparation and also with the values reported for the better preparations in the literature.

Preparation of Solutions. For visible spectra equilibrium studies, chlorophyll solutions were prepared by weighing out a desired amount of sample, usually 0.8 to 1.0 mg, on a Sartorious microbalance to an accuracy of ±0.000002 g. This material was subsequently stored in a 100-ml volumetric flask which was later desiccated and degassed with a liquid nitrogen trap under vacuum. This was taken into a controlled atmosphere box (O_2, CO_2, H_2O content less than 50 ppm) where the solution was prepared using anhydrous ethyl ether (Mallinkrodt analytical reagent) which was previously degassed by evaporation and agitation under vacuum. No attempt was made to remove traces of water from this solvent.

Trinitrobenzene (Will Scientific Inc.) was purified by crystallization from ethyl ether before use. Samples of this material were weighed out in 10-ml volumetric flasks on a Sartorious microbalance, desiccated and degassed, and taken into the controlled atmosphere box.

To prepare chlorophyll–trinitrobenzene solutions, 10 ml of the prepared stock of chlorophyll was delivered volumetrically to the previously weighed trinitrobenzene samples. In this manner the initial chlorophyll concentration was kept constant for all solutions. Solutions were prepared at 20°. Pyrex absorption cells of 1-cm path length having a ground-glass joint and fitted with Teflon stoppers were filled under nitrogen for subsequent spectral analysis. Visible spectra were recorded on a Cary 14 spectrophotometer which was equipped with a device to control temperatures to ±0.1° for equilibrium studies.

Infrared studies on the chlorophyll–trinitrobenzene system were done under ordinary atmospheric conditions but under green lighting. Ethyl ether (Merck anhydrous reagent) and spectroquality reagent grade chloroform (Matheson Coleman and Bell) were used for solution preparation. Infrared spectra were recorded on a Beckman IR-9 spectrophotometer using a fixed path length cell having CaF_2 windows and counterbalancing with a Beckman variable path length cell.

The nmr studies were conducted using a Varian A 60 spectrometer. The solvents employed were 99% deuterated chloroform (Merck Sharp and Dohme of Canada) and methanol-d_1. Tetramethylsilane was used as an internal standard.

Results

Visible Absorption Spectra. Figure 1 illustrates changes which occur in the visible spectra of chlorophyll a upon the addition of increasing amounts of 1,3,5-trinitrobenzene. All bands experience a considerable

(5) J. J. Katz, G. L. Closs, F. C. Pennington, M. R. Thomas, and H. H. Strain, *J. Amer. Chem. Soc.*, **85**, 3801 (1963).

(6) E. E. Jacobs, A. E. Vatter, and A. S. Holt, *Arch. Biochem. Biophys.*, **53**, 228 (1954).

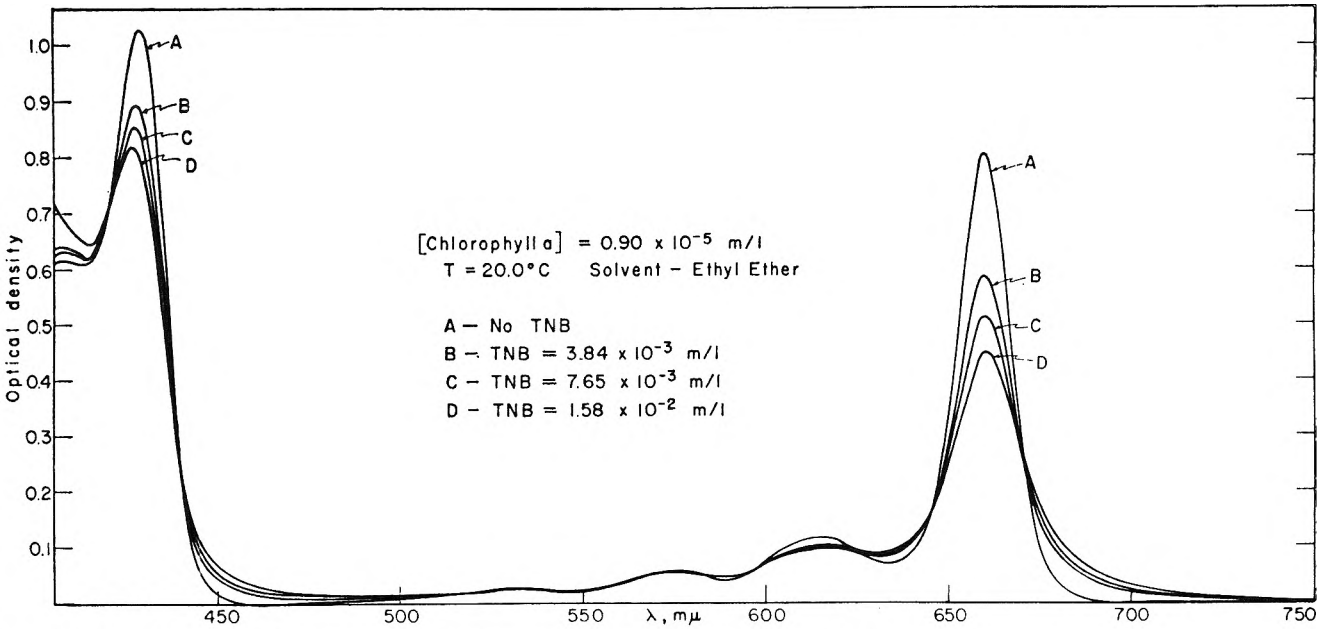

Figure 1. Spectral changes observed upon interaction of trinitrobenzene with chlorophyll a.

decrease in optical density and decided broadening of the band structure. In general only small changes in actual band positions occur. Present throughout the spectra are a number of isosbestic points. The existence of these points is interpreted in terms of a general reaction

$$nD + mA \rightleftharpoons D_nA_m \qquad (1)$$

Assuming that $m = n = 1$, the equilibrium reaction between electron donor (D) and electron acceptor (A) in forming the donor–acceptor complex (DA) becomes

$$D + A \rightleftharpoons DA \qquad (2)$$

Only D and DA, which represent in this case chlorophyll and the chlorophyll–trinitrobenzene complex, absorb in the wavelength region of interest and $[A] \gg [D]$. By definition the equilibrium constant, K, may be expressed

$$K = \frac{C_{DA}}{C_D C_A} \qquad (3)$$

where C_{DA}, C_D, and C_A represent the concentrations of the complex, donor, and acceptor, respectively. The activity coefficients are assumed to be unity.

For the equilibrium involved in eq 2, Nash[7] has shown that eq 4

$$\frac{1}{C_A} = \frac{d^0}{d^0 - d}[K - K\epsilon_{DA}/\epsilon_D] - K \qquad (4)$$

applies at a particular wavelength, where C_A is the molar concentration of free acceptor, ϵ_{DA} and ϵ_D are the molar extinction coefficients of complex and donor, d^0 is the optical density of pure donor, and d is the total optical density of donor and complex.

In most instances only the red absorption band was used to determine equilibrium constants. The results obtained by applying eq 4 to the chlorophyll *a*–trinitrobenzene system at 660.0 mμ are presented in Figure 2 where the reciprocal of acceptor concentration is plotted

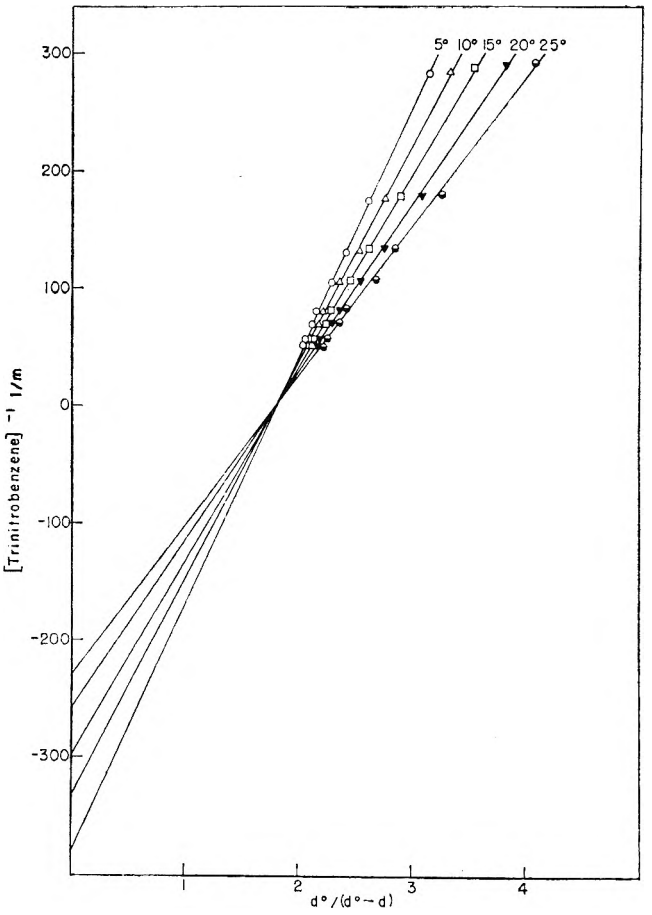

Figure 2. Determination of K at various temperatures for chlorophyll a–trinitrobenzene at λ 660.0 mμ.

(7) C. Nash, *J. Phys. Chem.*, **64**, 950 (1960).

against $d^0/(d^0 - d)$. The initial concentration of trinitrobenzene was corrected at the various temperatures due to changes in solvent volume. The data fit very nicely to a straight line which supports the choice of 1:1 stoichiometry.

In order to obtain the most accurate value of K as the data warranted, values of the slope and intercept were determined by a least-squares treatment in which errors occurring in both the ordinate and abscissa were considered. Thus errors resulting from long extrapolations to find the intercept are eliminated. The details of this treatment are presented in a text by Worthing and Geffner.[8] Table I shows the variation of equilibrium constants with temperature for 660.0 and 662.5 mμ.

Table I: Chlorophyll a–Trinitrobenzene. Variation of K with Temperature (Solvent, Ethyl Ether)

t, °C	$K_{660.0}$, l./mol	$K_{662.5}$, l./mol	K_{av}, l./mol
5.0	380 ± 4	381 ± 5	381 ± 3
10.0	332 ± 6	332 ± 4	332 ± 3
15.0	301 ± 4	292 ± 3	295 ± 2
20.0	259 ± 3	258 ± 3	259 ± 2
25.0	231 ± 4	226 ± 4	228 ± 3[a]

[a] An independent investigation of this system at 25° by vapor pressure osmometry using a Mechrolab osmometer yielded an average equilibrium constant of 284 ± 24. Although this method is quite suitable for detecting complexation, it is not sufficiently accurate for good quantitative results.

The value of ΔH was determined in the usual manner from the slope of a log K *vs.* $1/T$ plot. This plot is presented in Figure 3. Once again the line drawn is the line of least squares. The value of ΔH was found to be -4.08 ± 0.01 kcal/mol. A table presenting all thermodynamic values for the complexes studied will appear at the end of this section.

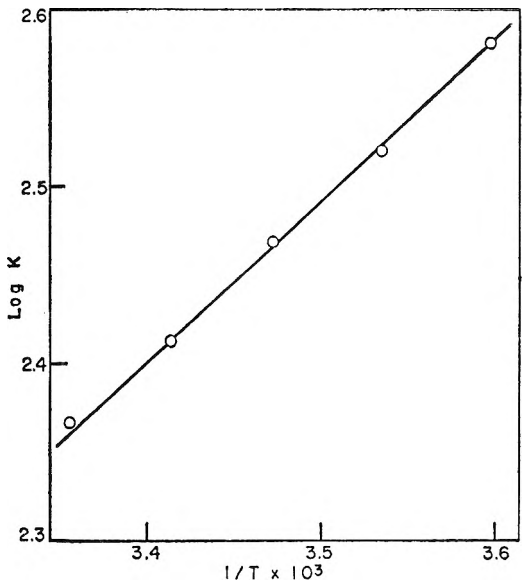

Figure 3. Temperature dependence of log K for chlorophyll a-trinitrobenzene.

Figure 4 illustrates changes which result from the interaction of trinitrobenzene with pheophytin a. Similar spectral changes occur with chlorophyll b or pheophytin b and trinitrobenzene (not shown here). The same type of analysis was applied for these systems as described previously for chlorophyll a. Application of eq 4 to the data yields a linear plot in each case.

Table II: Pheophytin a–Trinitrobenzene. Variation of K with Temperature (Solvent, Ethyl Ether)

t, °C	$K_{667.5}$, l./mol	$K_{665.0}$, l./mol	K_{av}, l./mol
5.0	133 ± 3	130 ± 7	133 ± 3
10.0	115 ± 4	123 ± 4	119 ± 3
15.0	100 ± 3	98 ± 5	100 ± 2
20.0	86 ± 4	85 ± 6	86 ± 3
25.0	80 ± 4	81 ± 4	81 ± 3

Table III: Chlorophyll b–Trinitrobenzene. Variation of K with Temperature (Solvent, Ethyl Ether)

t, °C	$K_{642.5}$, l./mol	$K_{645.0}$, l./mol	K_{av}, l./mol
5.0	91 ± 3	83 ± 5	89 ± 2
10.0	79 ± 3	76 ± 4	79 ± 2
15.0	73 ± 3	69 ± 4	71 ± 2
20.0	61 ± 3	57 ± 5	60 ± 3
25.0	52 ± 4	51 ± 5	52 ± 3

Table IV: Pheophytin b–Trinitrobenzene. Variation of K with Temperature (Solvent, Ethyl Ether)

t, °C	$K_{652.5}$, l./mol	$K_{655.0}$, l./mol	K_{av}, l./mol
4.0	49 ± 4	47 ± 4	48 ± 3
9.4	44 ± 4	38 ± 4	41 ± 3
15.0	36 ± 4	34 ± 4	35 ± 3
20.0	32 ± 4	31 ± 4	32 ± 3
25.0	29 ± 4	28 ± 4	29 ± 3

Table V: Thermodynamic Constants for Complexation of Trinitrobenzene with Chl a, Chl b, Pheo a, and Pheo b

System	$-\Delta H°$, kcal/mol	$-\Delta G°_{298}$, kcal/mol	$-\Delta S°_{298}$, cal/mol deg
Chl a–TNB	4.08 ± 0.01	3.23 ± 0.01	2.85 ± 0.01
Pheo a–TNB	4.47 ± 0.24	2.60 ± 0.03	6.28 ± 0.70
Chl b–TNB	4.45 ± 0.18	2.34 ± 0.04	7.08 ± 0.47
Pheo b–TNB	3.85 ± 0.08	1.99 ± 0.04	6.24 ± 0.13

This of course indicated a 1:1 complex formation for all systems. These results are summarized in Tables II, III, and IV. For comparative purposes, values of

(8) A. Worthing and J. Geffner, "Treatment of Experimental Data," John Wiley and Sons, Inc., New York, N. Y., 1942.

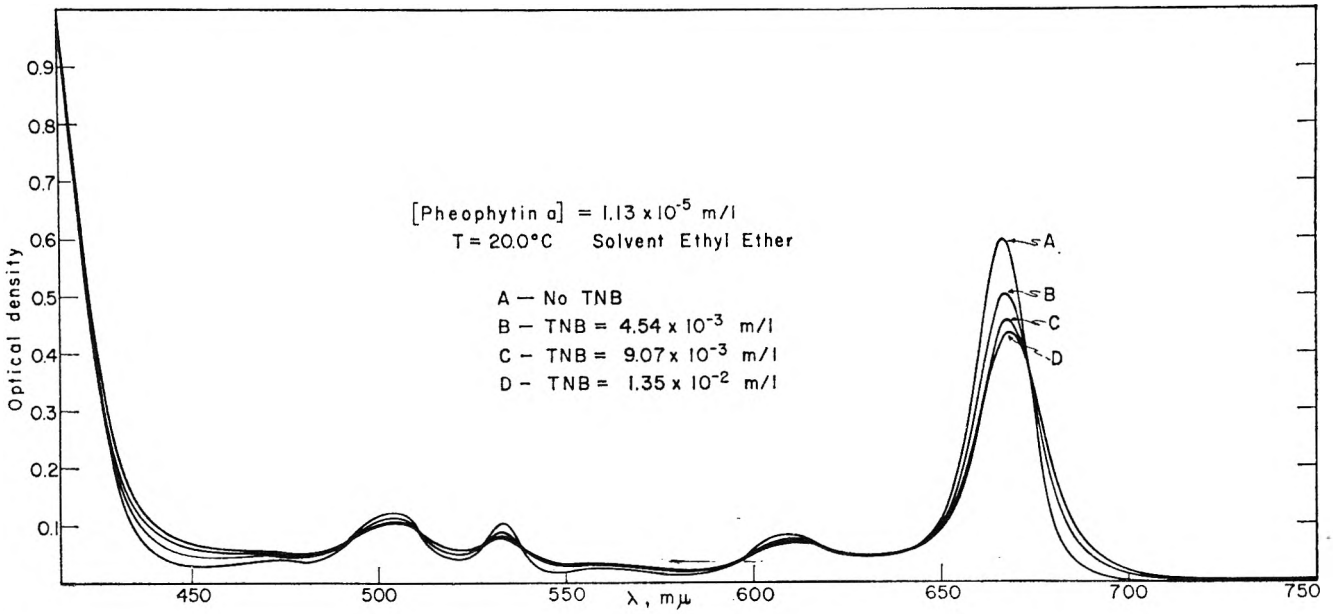

Figure 4. Spectral changes observed upon interaction of trinitrobenzene with pheophytin a.

the thermodynamic constants for the systems investigated are summarized in Table V.

The molar extinction coefficients of the complexes were determined from the slopes of the lines obtained by plotting eq 4. For each system the value obtained from each of the plots at various temperatures was constant within experimental error. (See Table VI.)

Table VI: Molar Extinction Coefficients of Trinitrobenzene with Chl a, Chl b, Pheo a, and Pheo b (Solvent, Ethyl Ether)

System[a]	λ, mμ	ε × 10⁻⁴
Chl a–TNB	660.0	3.67
	662.5	3.74
Pheo a–TNB	665.0	2.31
	667.5	2.72
Chl b–TNB	642.5	2.13
	645.0	2.23
Pheo b–TNB	652.5	1.68
	655.0	2.06

[a] Under the conditions used here, chlorophyll and pheophytin are present in ether solutions as monomeric solvated species. One or two ether molecules are bound by the magnesium atom of the chlorophyll. The pheophytins with protons in place of magnesium probably also bind ether at the center of the porphyrin ring. The interaction of TNB with chlorophyll and pheophytin in ether is not expected to displace ether from the center of the porphyrin ring since ether is a nucleophilic agent whereas TNB is well known for its electrophilic character.

Infrared Spectra

Chlorophyll a–Trinitrobenzene. The most accessible region in the infrared spectrum of chlorophyll is the carbonyl region, 1600–1800 cm^{-1}. Two ester carbonyl and one ketone carbonyl are present in chlorophyll a. In polar solvents these give rise to two bands.[9] Figure 5 presents the infrared spectrum of pure chlorophyll a in ethyl ether and illustrates the changes which occur in the carbonyl region in the presence of trinitrobenzene.

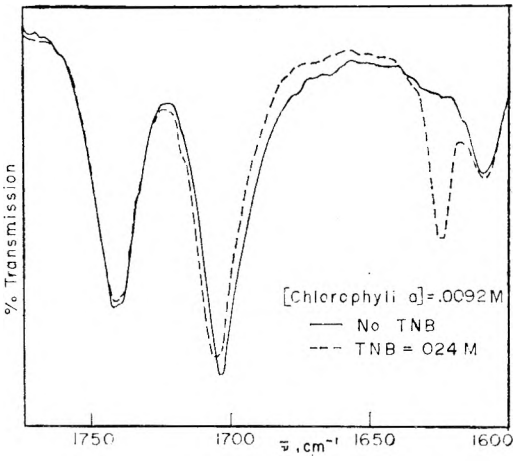

Figure 5. Infrared spectral changes observed on interaction of chlorophyll a and trinitrobenzene in ethyl ether.

The spectra were recorded on an expanded wavelength scale. The normal positions for the ester and ketone frequencies in ethyl ether occur at 1742 and 1704 cm^{-1}, respectively. It can be seen that the presence of trinitrobenzene causes an overall shift in the ketone band of approximately 3 cm^{-1} to higher frequencies. No change occurs in the position of the ester carbonyl band. In addition, it appears that the ketone band is somewhat broadened in the process. This indicates that the peak is a composite one.

(9) For discussion on the interpretation of the absorptions in the region of 1600–1750 cm^{-1}, see ref 5.

In order to determine the approximate position of the component of this band which is due to the complexed species, a difference spectrum was recorded in which a solution of chlorophyll a and trinitrobenzene was placed in the sample beam and an equimolar chlorophyll a solution in the reference beam of the spectrophotometer.

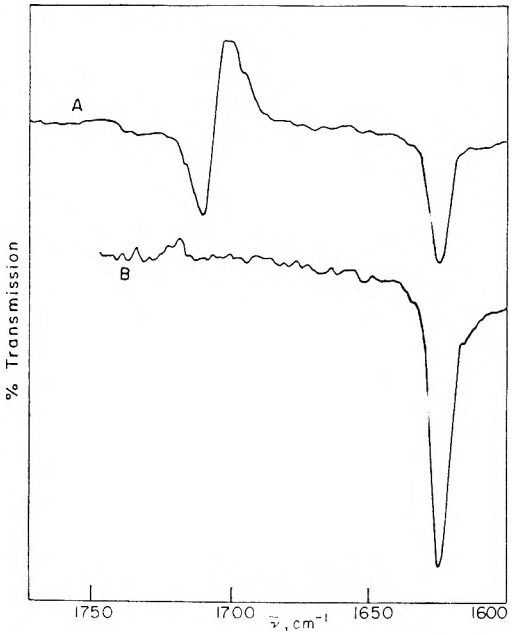

Figure 6. A. Difference spectrum of chlorophyll a–trinitrobenzene *vs.* chlorophyll a in ethyl ether. B. Trinitrobenzene in ethyl ether, 0.03 *M*.

A typical difference spectrum is shown in Figure 6 in which the trinitrobenzene–chlorophyll a ratio was approximately 3:1. Also presented is a spectrum of pure trinitrobenzene in order to indicate absorptions of this compound in this region. Two absorption bands characterize the difference spectrum. The band at 1625 cm^{-1} is due to the trinitrobenzene in the solution. The band occurring at 1712 cm^{-1} is due to the ketone carbonyl band of the chlorophyll complex which appears at slightly higher frequencies than the ketone of free chlorophyll a. In agreement with the previously observed finding that the ester carbonyl is unaffected during interaction, it can be seen that there is no absorption in this region. Since there is more free ketone carbonyl present in the reference than in the sample, negative absorption occurs in the region of 1704 cm^{-1}. This, of course, has some effect on the position and intensity of the ketone carbonyl band of the complex due to some overlap.

In addition, the infrared spectrum of this system was recorded in Spectrograde chloroform. Although no special drying of this solvent was done, there is still enough dimer present in the solution of pure chlorophyll to give rise to the carbonyl band at 1640 cm^{-1}. The changes occurring in the infrared spectrum of chlorophyll a in chloroform upon interaction with trinitrobenzene are shown in Figure 7. It can be seen that there is a very slight shift occurring in the overall position of the ketone carbonyl at 1680 cm^{-1}. What is more noticeable, however, is the dramatic broadening of this band and increased intensity on the high-frequency side as the ratio of trinitrobenzene to chlorophyll a is increased. The observed broadening is evidence that two bands are present in this region. Again no change is observed in the ester carbonyl at 1730 cm^{-1}. The effect of complexation upon the carbonyl bond at about 1640 cm^{-1} due to dimer formation is not readily discernible because of contribution to absorption in this region from small peaks of trinitrobenzene as well as overlap resulting from the more intense band at about 1625 cm^{-1}.

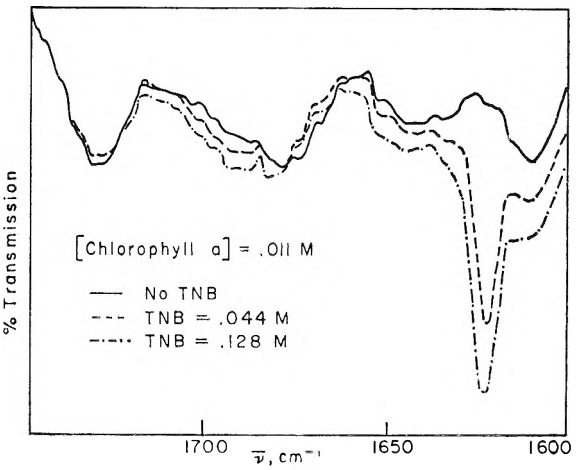

Figure 7. Infrared spectral changes observed on interaction of chlorophyll a and trinitrobenzene in chloroform.

The difference spectrum for a solution in which there is a 9:1 trinitrobenzene–chlorophyll a ratio was examined (not shown here). The difference spectrum showed two main bands—one occurring at about 1625 cm^{-1} (belongs to trinitrobenzene), and a second band occurring at 1695 cm^{-1} (belongs to the keto carbonyl with a shift from 1680 cm^{-1} to 1695 cm^{-1}). Base line optical density readings of the 1695-cm^{-1} band for three difference spectra in which the trinitrobenzene–chlorophyll a ratios were about 1.5:1, 9:1, and 12:1 were 0.044, 0.066, and 0.080, respectively. This is in agreement with the equilibrium concept since increasing the trinitrobenzene concentration while keeping the chlorophyll a concentration constant should result in more complex formation.

Chlorophyll b–Trinitrobenzene. Since chlorophyll b has two ester carbonyls, one ketone carbonyl, and one aldehyde carbonyl, three bands occur in the carbonyl region of the infrared spectrum. The positions of these bands in ethyl ether are 1742, 1707, and 1670 cm^{-1}, respectively, for the ester, ketone, and aldehyde carbonyls. The effects on these bands arising from

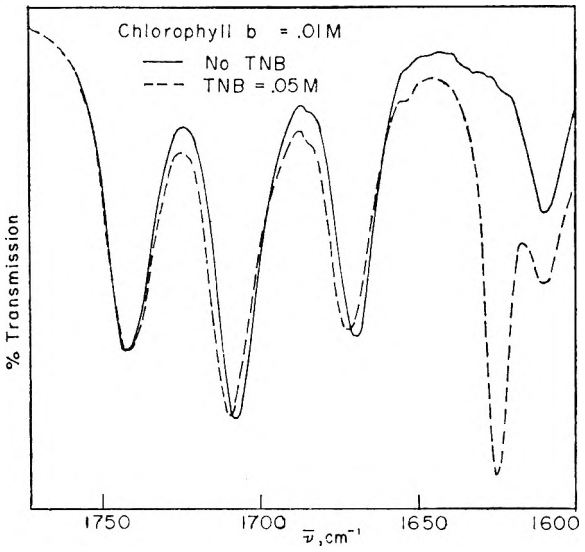

Figure 8. Infrared spectral change observed on interaction of chlorophyll b and trinitrobenzene in ethyl ether.

chlorophyll b interaction with trinitrobenzene in ethyl ether are shown in Figure 8. It can be seen that both the aldehyde carbonyl and the ketone carbonyl experience an overall shift of about 3 cm^{-1} to higher frequencies. In addition, an overall broadening occurs in both peaks. No change is observed in the ester carbonyl band.

Figure 9 shows the difference spectrum for a solution in which there is a 5:1 trinitrobenzene–chlorophyll b ratio. As expected, two bands belonging to the complexed chlorophyll b appear on the high-frequency side of the normal aldehyde and carbonyl bands at approximately 1676 and 1715 cm^{-1}. Thus a shift of about 6 cm^{-1} and 8 cm^{-1} occurs for the aldehyde and ketone carbonyls, respectively.

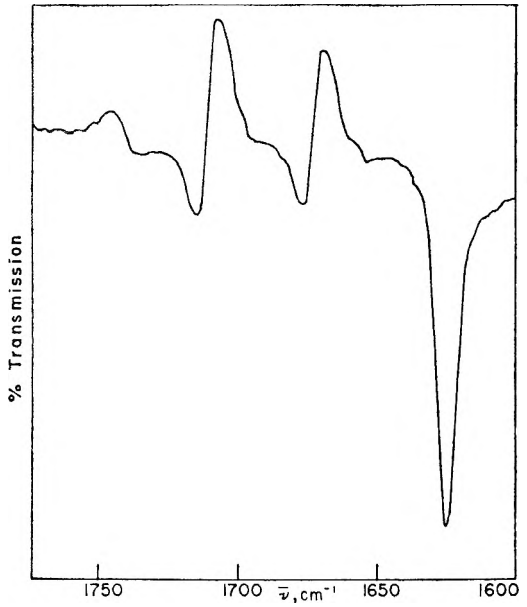

Figure 9. Difference spectrum of chlorophyll b–trinitrobenzene *vs.* chlorophyll b in ethyl ether.

Nuclear Magnetic Resonance

Chlorophyll a–Trinitrobenzene. The nuclear magnetic resonance spectra of chlorophylls and derivatives have been studied and completely interpreted by Closs, *et al.*[10] Their interpretations have been used as a guide for observing the effects of trinitrobenzene on the nmr spectra of chlorophylls.

Since it is apparent that all visible and nearly all infrared spectral results were obtained with monomeric chlorophyll, correlations with any results from nmr could only be accomplished if chlorophyll existed in the same state. Closs, *et al.*, had previously shown in their work the dependence of the chlorophyll spectral positions with methanol-d_4. Since methanol-d_1 was used in this research, the methyl resonances coincide with a few chlorophyll resonances at high ratios. However, it was possible to use a maximum of about an 8:1 ratio of methanol to chlorophyll before this occurs. The titration curves of Closs, *et al.*, show that most of the chlorophyll resonances change very little with methanol concentration in this range, thus indicating that most of the chlorophyll should be in a monomeric state. Even so, it is apparent that for any intercomparison of nmr results the methanol concentration must be the same in order to make peak positions meaningful.

Since references will be made from time to time to specific protons on the chlorophyll molecule, Figure 10

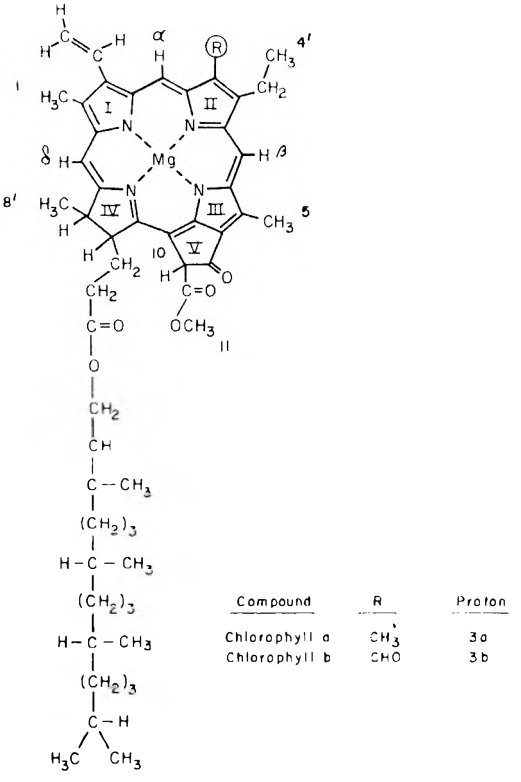

Figure 10. Proton nomenclature for chlorophylls.

(10) G. Closs, J. Katz, F. Pennington, M. Thomas, and H. Strain, *J. Amer. Chem. Soc.*, **85**, 3809 (1963).

shows the chlorophyll structure with the protons of interest labeled for easy correlation. A typical nmr spectrum of chlorophyll a in deuteriochloroform containing 0.7 M methanol-d_1 is presented in Figure 11.

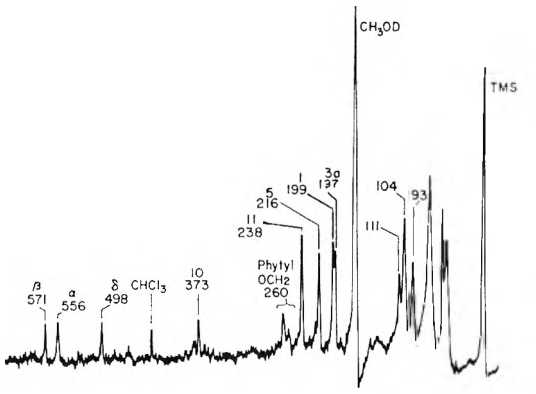

Figure 11. Nmr spectrum of chlorophyll a (0.1 M) in $CDCl_3$ with 0.7 M CH_3OD.

The spectral effects produced through the interaction of trinitrobenzene on chlorophyll a in the same solvent system are shown in Figure 12 in which the ratio of trinitrobenzene to chlorophyll a is 3:1. The peak positions, as measured in cycles per second away from the internal standard tetramethylsilane, are indicated.

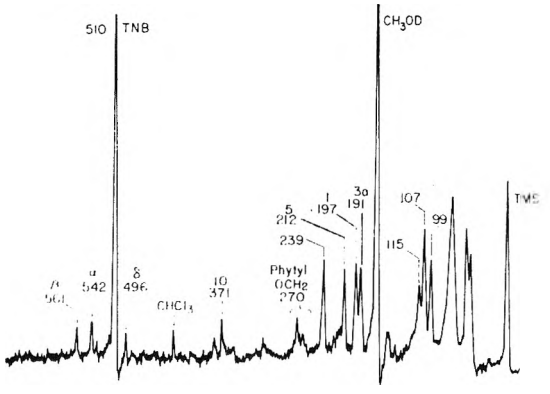

Figure 12. Nmr spectrum of chlorophyll a (0.1 M) and trinitrobenzene (0.3 M) in $CDCl_3$ with 0.7 M CH_3OD.

Also, the specific proton which is responsible for the resonance is shown. Table VII lists a more complete description of how peak position varied as the mole ratio of trinitrobenzene to chlorophyll a was increased. The position of the resonance for the hydrogens of trinitrobenzene is also indicated. The peak positions are probably accurate to within 1 cps.

It can be seen from this table that most of the major changes occur when the mole ratio is 1:1. Only small changes, if any, occur afterwards. The largest changes are observed for the phytyl oxygen bonded methylene protons and for the α- and β-methine bridge protons.

Table VII: Shifts in the Proton Resonances of Chlorophyll a–Methanol on Interaction with Trinitrobenzene

Proton	No TNB	1:1	2:1	3:1
3a	197	192	191	191
1	199	198	197	197
5	216	212	212	212
11	238	238	238	239
Phytyl OCH_2	260	267	269	270
10	373	372	371	371
δ	498	496	496	496
α	556	545	542	542
β	571	562	560	560
TNB		461	488	510

The first experiences a paramagnetic shift while the latter two show a diamagnetic shift. Other notable changes occur for hydrogens 3a and 5, both of which show diamagnetic shifts. Little or no change occurs for protons 1, 11, 10, and δ. Since the protons of trinitrobenzene are equivalent, they give rise to a single peak. The position of this peak for the pure compound in the same solvent system is 560 cycles from tetramethylsilane. It can be seen from the table that a very large diamagnetic shift is observed for these protons. At a 1:1 mole ratio the shift from its normal position is nearly 100 cycles. The position of the trinitrobenzene proton resonance for the pure compound is constant throughout this concentration range.

Although not noted in this table, some changes also occur in the peaks located between 90 and 115 cycles. Even though only three main peaks appear in this region, Closs, *et al.*,[10] have shown these to contain a doublet and triplet structure and by double-resonance techniques were able to assign the actual position of the doublet and triplet which are specifically due to protons 8′ and 4′, respectively. The peak occurring at 93 cycles is part of the triplet structure of 4′. The other two peaks at about 104 and 111 cycles in the pure chlorophyll a spectrum comprise the doublet of 8′ as well as the two other peaks of the 4′ triplet structure. Although it is not certain if both hydrogens are affected, the fact that the outer peak of the 4′ triplet structure at 93 has shifted to 99 cycles definitely indicates that the 4′ hydrogens are being affected. Although the detailed results are not tabulated, practically identical shifts are observed as above when the methanol to chlorophyll ratio is 1:1 and 2:1.

Another result of interest concerned an experiment performed with no methanol added. In pure deuteriochloroform the chlorophyll is almost completely dimerized (see ref 10). Table VIII shows the change for those protons which appear in the spectra and are readily interpretable. It is not possible to observe proton 10 and the protons belonging to the first methylene group of the phytyl ester. A comparison with Table VII indicates that the same pattern of proton

Table VIII: Shifts in the Proton Resonances of Dimeric Chlorophyll a on Interaction with Trinitrobenzene

Proton	No TNB	TNB:Chl a (2:1)
5	171	168
3a	191	188
1	196	196
11	198	201
δ	491	490
α	550	537
β	562	551
TNB		505

shifts occurs in both the monomeric and dimeric states of chlorophyll.

Chlorophyll b–Trinitrobenzene. The nmr spectrum of 0.1 *M* chlorophyll b in deuteriochloroform containing 0.7 *M* methanol-d_1 is shown in Figure 13. The spectrum is quite similar in appearance to chlorophyll a.

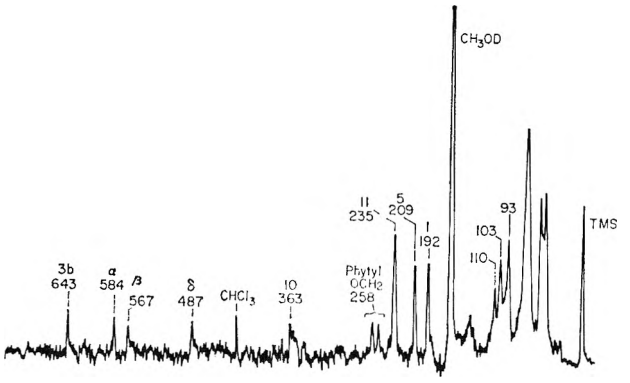

Figure 13. Nmr spectrum of chlorophyll b (0.1 *M*) in $CDCl_3$ with 0.7 *M* CH_3OD.

An overall view of the spectral changes occurring from the interaction of trinitrobenzene with chlorophyll b is shown in Figure 14. The ratio of trinitrobenzene to chlorophyll b is 5:1. As indicated by the designated peak positions, very few marked changes occur between this spectrum and pure chlorophyll b of Figure 13.

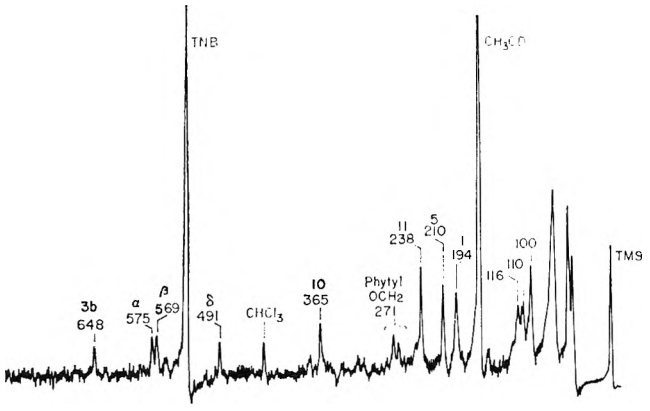

Figure 14. Nmr spectrum of chlorophyll b (0.1 *M*) and trinitrobenzene (0.5 *M*) in $CDCl_3$ with 0.7 *M* CH_3OD.

Table IX lists a more accurate account of how peak positions are altered as the mole ratio of trinitrobenzene to chlorophyll b is increased.

It can be seen from Table IX that only the α proton and the phytyl oxygen bonded methylene protons show relatively large shifts. The first experiences a diamagnetic shift while the latter shows a paramagnetic shift.

Table IX: Shifts in the Proton Resonances of Chlorophyll b–Methanol on Interaction with Trinitrobenzene

Proton	No TNB	1:1	2:1	3:1	5:1
1	192	194	194	194	194
5	209	210	210	210	210
11	235	237	238	238	238
Phytyl OCH_2	258	267	269	270	271
10	363	366	366	366	366
δ	487	490	490	490	491
β	567	570	570	570	570
α	584	581	580	578	575
3b	643	646	647	648	648
TNB		502	511	521	534

All other protons listed show small paramagnetic shifts. Not too much change if any occurs for hydrogen 5. Again the proton resonance for trinitrobenzene shows a large diamagnetic shift from the interaction. A shift of nearly 60 cycles is observed when the two components are equimolar.

Discussion

The manner in which chlorophyll interacts with other molecules is fundamentally important since additional knowledge of the electronic distribution of the chlorophyll molecule can be obtained. Equilibrium studies have indicated that, in the case of the strong electron acceptor molecule, *sym*-trinitrobenzene, very strong 1:1 molecular complexes with the chlorophylls and derivatives are formed. The strength of these complexes depends upon the porphyrin ring substituents; the equilibrium constants for the "a" complexes are 3–4 times larger than the "b" complexes. The infrared and nmr results allow us to describe in more detail the nature of the interaction.

The complexation of trinitrobenzene with chlorophylls a and b caused shifts in the carbonyl region to higher frequencies. Difference spectra revealed that the frequency of the cyclopentanone C=O for chlorophyll a was increased by about 8 and 15 cm^{-1} in ethyl ether and chloroform, respectively. In the case of chlorophyll b in ethyl ether the cyclopentanone C=O and the aldehyde C=O were shifted 6 and 8 cm^{-1}, respectively, to higher frequencies.

The fact that these shifts are all to higher wave numbers indicates that the interaction with trinitrobenzene is not directly linked to the carbonyl groups even though this group does have the ability to act as a

center for electron donation. Numerous eaxmples of this type occur in the literature.[11,12] Localized interactions of this type tend to significantly lower the carbonyl vibrational frequency. In addition, the nmr results to be discussed subsequently do not support this mode of interaction.

The shifts of the carbonyl bands must result from inductive effects. Assume that the interaction of trinitrobenzene occurs within the π-electron system of chlorophyll. (Nmr results support this view.) The importance of donor–acceptor interaction in stabilizing the ground state of the molecular compound implies partial removal of an electron from a bonding orbital of chlorophyll to an antibonding orbital of trinitrobenzene.

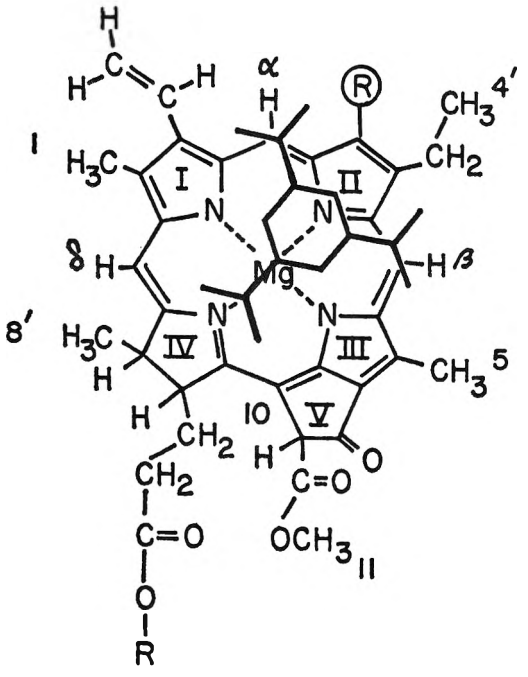

Figure 15. Proposed structure of the chlorophyll–trinitrobenzene complex.

The electron deficiency which is created in the π-electron system of chlorophyll is minimized through the conjugation of the porphyrin system of chlorophyll to electron rich centers such as the carbonyl groups. The decrease in the polar character of the carbonyl bond results in an increase in the vibrational frequency. Since the aldehyde and ring V ketone carbonyls of chlorophyll b and the ring V ketone carbonyl of chlorophyll a are in conjugation with the ring each should experience this effect. This does occur. In addition, since the ester carbonyl is not in conjugation with the π-electron system no change should occur in this frequency. This is exactly what is observed. Furthermore, it would seem apparent that the overall effects experienced in any specific part of the molecule would be small. In agreement, only small shifts (6–15 cm^{-1}) are observed in the carbonyls.

Nuclear magnetic resonance results for the system chlorophyll a–trinitrobenzene indicate that major changes occur only in the resonances of α-, β-, and phytyl oxygen bonded methylene. The direction of the shifts for the α and β protons (13 and 11 cycles to higher fields) implies that in the overall process these protons are positioned near the diamagnetic part of the induced field of the ring current of trinitrobenzene. Small but significant changes were also noted for the 4′ and 3a protons. The large upfield shift of 100 cycles for trinitrobenzene indicates that it too must be in a highly shielded region such as is provided within the porphyrin ring system.

These proton shifts, together with the evidence from the infrared, allow us to visualize a model which best represents the complex. From the structures of the individual components it is inferred that the two molecules are planar to each other in the complex. On the basis of the nmr results the most logical choice is to place the benzene ring of the trinitrobenzene molecule in the vicinity of the nitrogen atom of ring II. The bulky nitro groups can then lie in the region of the α and β protons. It is not evident whether the upfield shifts of these protons are due to the proximity of the nitro groups or to the alteration of electron density in this area. A general representation of the complex as presented here is illustrated in Figure 15.

The shifting of the phytyl oxygen-bonded methylene to lower fields upon complexation indicates that the hydrocarbon tail was initially oriented in such a manner as to be within the diamagnetic shielding zone of the chlorophyll ring. Molecular models show that there is enough latitude in tail length so that this methylene group can extend into the region of the porphyrin head. The interaction with trinitrobenzene can displace the tail from its preferred arrangement so that now these hydrogens are outside the ring and experience more normal shielding values. The displacement probably occurs as a result of steric considerations.

It was also noted in the results that similar changes in the nmr spectra occurred when chlorophyll was in essentially a dimeric state. Thus it appears that a similar complex is formed between dimer and trinitrobenzene.

The observed nmr shifts resulting from chlorophyll b–trinitrobenzene interaction were quite small in most cases. This is undoubtedly due to the fact that the concentration of complex was small as a consequence of a low equilibrium constant. Visible spectra indicated that the equilibrium constant for chlorophyll b and trinitrobenzene in ethyl ether was only about one-fifth as much as the equilibrium constant for the corresponding chlorophyll a system. Although the equilibrium value in chloroform was not determined, there is reason to believe that it is much smaller than in ethyl

(11) G. Dallinga, *Acta Cryst.*, **7**, 665 (1954).

(12) H. G. Taufen, M. J. Murray, and F. F. Cleveland, *J. Amer. Chem. Soc.*, **63**, 3500 (1941).

ether. This is based on the fact that the changes observed in the infrared for chlorophyll b in ethyl ether did not occur in chloroform even when the mole ratio of trinitrobenzene to chlorophyll b was 18:1. Consequently, a sufficient amount of complex is not present for the nmr runs of chlorophyll b in order to gain much information about the system. There obviously is some complexing since the proton resonance of trinitrobenzene is shifted about 60 cycles to higher fields indicating it is within the diamagnetic shielding zone of the chlorophyll ring. Also there is a considerable paramagnetic shift of the phytyl oxygen bonded methylene group. The only proton which experiences a diamagnetic shift is the α proton. It seems likely that the system here would be quite similar to the chlorophyll a complex. The shift of methylene protons is again interpreted as arising from displacement of the hydrocarbon tail from the region of the ring by trinitrobenzene

The conclusion that charge-transfer interaction occurs in the vicinity of the α and β protons of the chlorophyll molecule is in disagreement with some of the current opinions which regard the cyclopentanone region (ring V) an important center of high electron density. However, it seems quite logical that the area of the chlorophyll molecule which will be involved in electron donation will depend on the environment in which the molecule is placed. It is very likely that solvent perturbations will be a major factor in determining this region. Furthermore, steric considerations with the acceptor molecule must not be neglected. This may be a contributing factor in the present situation. If the hydrocarbon tail is preferentially oriented in such a way that it is within the vicinity of the porphyrin head as nmr results imply, then perhaps large molecules, such as trinitrobenzene, must interact with the upper part of the chlorophyll molecule where steric interactions with the tail are minimized. Obviously it would be of interest to investigate systems like the one presented here or else similar ones in various solvent systems. A systematic study of this type could reveal what role solvent plays in influencing the site of electron donation.

Nelson[13] has investigated the electronic energy levels in chlorophyll derivatives. He found values of 4.93 eV for ethyl chlorophyllide a and 5.16 eV for ethylchlorophyllide b. This means that ethyl chlorophyllide a is a better electron donor than ethyl chlorophyllide b in the solid film. If solvent effects are small, the binding constants for TNB in ether should be larger for chlorophyll a than for chlorophyll b. This is what is observed here. A quantitative correlation has not been made.

Acknowledgments. This research has been generously supported by grants from the National Science Foundation (GB2254) and the National Institutes of Health (5R01 GM10856-06).

(13) R. C. Nelson, *Photochem. Photobiol.*, 8 (5), 441 (1968).

Equilibria in Pyridine. II. Behavior of Some Monovalent Silver Salts in Pyridine

by L. M. Mukherjee, J. J. Kelly, McDonald Richards, and J. M. Lukacs, Jr.

Chemistry Department, Polytechnic Institute of Brooklyn, Brooklyn, New York 11201 *(Received August 1, 1968)*

The cell $Zn(Hg)|ZnCl_2(s)||AgX$ in pyridine$|Ag(s)$ has been used to study the behavior of the nitrate, picrate, chloride, cyanide, and thiocyanate of silver(I). Correlating the potentiometric behavior with the conductance data for these different silver salts eventually made possible the evaluation of the standard potential of the reaction $Ag(solv)^+ + e \rightleftharpoons Ag(s)$ in pyridine. The value of $E^\circ_{Ag^+|Ag}$ so obtained is 0.551 V *vs.* a normal hydrogen electrode at 25°.

Introduction

In this work a silver indicator electrode has been used to study the behavior of silver nitrate, picrate, chloride, cyanide, and thiocyanate in pyridine, in conjunction with a $Zn(Hg)|ZnCl_2(s)$ reference electrode[1] which has previously been standardized against a normal hydrogen electrode (nhe). Correlation of these potentiometric results with earlier conductance studies[2,3] eventually provided the value of the standard potential of the reaction

$$Ag(solv)^+ + e \rightleftharpoons Ag(s) \qquad (1)$$

in pyridine. In the case of silver nitrate and picrate,

(1) (a) L. M. Mukherjee and J. J. Kelly, *J. Phys. Chem.*, 71, 2348 (1967); (b) L. M. Mukherjee, J. J. Kelly, W. Baranetzky, and J. Sica, *ibid.*, 72, 3410 (1968).

(2) (a) W. F. Luder and C. A. Kraus, *J. Am. Chem. Soc.*, 69, 2481 (1947); (b) D. S. Burgess and C. A. Kraus, *ibid.*, 70, 706 (1948).

(3) J. H. Mathews and A. J. Johnson, *J. Phys. Chem.*, 21, 294 (1916–1917).

use has been made of the dissociation constants reported by Kraus, *et al.*[2] However, although the previously reported conductance studies for the chloride, cyanide, and thiocyanate strongly suggest the possible existence of a substantial degree of ion association, no quantitative estimates of the equilibrium constants for these systems are available. Therefore, before any correlation with the potentiometric results in these cases could be attempted, it became necessary to explain their conductance data[3] on the basis of typical equilibria involving simple ions and triple ions as well as quadrupoles ("dimers"). We used a simple trial and error procedure in this connection until a satisfactory agreement with the observed conductances was obtained. The trial values of these different parameters which yielded the best fit have subsequently been incorporated in the potentiometric results.

Theory

Conductance of AgCl, AgCN, and AgCNS. The conductance data of AgCl, AgCN, and AgCNS do not suggest any simple relationship. On the contrary, it is strongly indicated that these systems involve considerable ion association. The following equilibria are postulated to account for their observed behavior

$$Ag^+X^- \overset{K_1}{\rightleftharpoons} AgX; \quad K_1 = [AgX]/[Ag^+][X^-] \tag{2}$$

$$AgX + Ag^+ \overset{K_{2a}}{\rightleftharpoons} Ag_2X^+;$$

$$K_{2a} = [Ag_2X^+]/[AgX][Ag^+] \tag{3a}$$

$$AgX + X^- \overset{K_{2b}}{\rightleftharpoons} AgX_2^-;$$

$$K_{2b} = [AgX_2^-]/[AgX][X^-] \tag{3b}$$

$$Ag_2X^+ + X^- \overset{K_{3a}}{\rightleftharpoons} Ag_2X_2;$$

$$K_{3a} = [Ag_2X_2]/[Ag_2X^+][X^-] \tag{4a}$$

$$AgX_2^- + Ag^+ \overset{K_{3b}}{\rightleftharpoons} Ag_2X_2;$$

$$K_{3b} = [Ag_2X_2]/[AgX_2^-][Ag^+] \tag{4b}$$

From the charge-neutrality rule

$$[Ag^+] + [Ag_2X^+] = [X^-] + [AgX_2^-] \tag{5}$$

Assuming $K_{2a} = K_{2b} = K_2$, we obtain

$$[Ag^+](1 + K_2[AgX]) = [X^-](1 + K_2[AgX]) \tag{6}$$

Thus

$$[Ag^+] = [X^-] \tag{7a}$$

and

$$[Ag_2X^+] = [AgX_2^-] \tag{7b}$$

From mass balance, the total concentration C_{AgX} can be expressed as

$$C_{AgX} = [Ag^+] + [AgX] + 2[Ag_2X^+] + [AgX_2^-] + 2[Ag_2X_2] \tag{8}$$

Combining eq 8 with eq 7b, one obtains

$$C_{AgX} = [Ag^+] + [AgX] + 3[Ag_2X^+] + 2[Ag_2X_2] \tag{9}$$

Now, expressing [AgX], $[Ag_2X^+]$, and $[Ag_2X_2]$ in terms of $[Ag^+]$ according to eq 2, 3a, 3b, 4a, and 4b and equating K_{2a}, K_{2b}, and K_2 as before and setting $K_{3a} = K_{3b} = K_3$, we obtain

$$C_{AgX} = [Ag^+] + K_1[Ag^+]^2 + 3K_1K_2[Ag^+]^3 + 2K_1K_2K_3[Ag^+]^4 \tag{10}$$

According to eq 10, for any assumed values of $[Ag^+]$, K_1, K_2, and K_3, the corresponding value of C_{AgX} can be calculated.

Calculation of Λ_c. The equivalent conductance Λ_c can be obtained from the relationship

$$\Lambda_c = \frac{\lambda_{Ag^+}[Ag^+] + \lambda_{X^-}[X^-] + \lambda_{Ag_2X^+}[Ag_2X^+] + \lambda_{AgX_2^-}[AgX_2^-]}{C_{AgX}} \tag{11}$$

where the λ's indicate the respective ion conductances. On the basis of eq 7a and 7b, eq 11 can be simplified to give

$$\Lambda_c = \frac{(\lambda_{Ag^+} + \lambda_{X^-})[Ag^+] + (\lambda_{Ag_2X^+} + \lambda_{AgX_2^-}) \times [Ag_2X^+]}{C_{AgX}} \tag{12}$$

Equation 12 has been used to calculate the conductance of AgCl, AgCN, and AgCNS assuming different trial values of K_1, K_2, and K_3 for each system until a satisfactory agreement with the observed conductance was obtained. In all cases, variation of the ion conductances with concentration has been ignored, and the sums $\lambda_{Ag^+} + \lambda_{X^-}$ and $\lambda_{Ag_2X^+} + \lambda_{AgX_2^-}$ have been set equal to 80 and 40, respectively. The assumed value of 80 for $\lambda_{Ag^+} + \lambda_{X^-}$ seems fairly reasonable and compares favorably with the estimates of limiting conductances[4] reported for these electrolytes in pyridine.

Potentiometry. For a silver salt AgX which as a monomer dissociates according to

$$AgX \text{ (or } Ag^+X^-) \rightleftharpoons Ag^+ + X^- \tag{13}$$

the (over-all) dissociation constant, K_{AgX}, can be expressed as

$$K_{AgX} = a_{Ag^+}a_{X^-}/a_{AgX} \tag{14}$$

where a_{Ag^+} and a_{X^-} denote the activities of Ag^+ and X^- and a_{AgX} represents the activity of the uncharged species.

If it is assumed that the ionic activity coefficients are equal and the activity coefficient of the uncharged species is unity, eq 14 can be rearranged to give

$$a_{Ag^+} = \sqrt{K_{AgX}[AgX]} \tag{15}$$

on the basis of the electroneutrality rule.

(4) P. Walden, L. F. Audrieth, and E. J. Birr, *Z. Physik. Chem.*, **A160**, 337 (1932).

Furthermore, if K_{AgX} is sufficiently small, the equilibrium concentration [AgX] may be replaced by the corresponding analytical concentration C_{AgX} to permit the rewriting of eq 15 in the form

$$a_{Ag^+} = \sqrt{K_{AgX}C_{AgX}} \quad (16)$$

The expression for the emf of the cell I at 25° [cell I: Zn(Hg)|$ZnCl_2$(s) reference electrode||AgX|Ag(s)] is given by

$$E = E^\circ_{Ag^+|Ag} - E_{ref} + 0.05916 \log a_{Ag^+} \quad (17)$$

Substituting eq 16 into eq 17 gives

$$E = E^\circ_{Ag^+|Ag} - E_{ref} + 0.02958 \log K_{AgX} + 0.02958 \log C_{AgX} \quad (18)$$

It is evident from eq 18 that in the case of a silver salt which dissociates in the manner shown by eq 13 and which has a relatively small value of K_{AgX} (*cf.* eq 14) a plot of E *vs.* log C_{AgX} will be a straight line with a slope of 0.02958 V at 25°.

Calculation of $E^\circ_{Ag^+|Ag}$. In order to calculate $E^\circ_{Ag^+|Ag}$ from the emf data using eq 17, knowledge of the activity of silver ion for a given concentration of a silver salt is required. Estimates of the equilibrium constants as obtained from conductance measurements are useful in this respect. The total salt concentration corresponding to an arbitrary value of free silver ion concentration can be calculated from eq 10 for the chloride, cyanide, and thiocyanate. In order to obtain similar relationship for the silver nitrate and picrate the (thermodynamic) dissociation constants of 9.3×10^{-4} and 3.06×10^{-3}, respectively, derived from the Fuoss–Kraus treatment,[2] on the basis of simple monomeric dissociation, have been used in the expression

$$C_{AgX} = [Ag^+] + [Ag^+]^2 f_i^2 / K_{AgX} \quad (19)$$

where f_i denotes the ionic activity coefficient. Thus, using, when appropriate, eq 10 or 19, together with the Debye–Hückel limiting law in the form

$$-\log f_i = 8.191\sqrt{\mu}$$

it is possible to generate values of a_{Ag^+} corresponding to different values of the total concentrations for each of the silver salts studied. Plots of 0.05916 log a_{Ag^+} *vs.* log C_{AgX} can then be constructed for comparison with the E *vs.* log C_{AgX} plot of interest. In the regions where the slopes are the same and preferably at concentrations low enough to permit the use of the Debye–Hückel limiting law, the difference between the observed emf, E, for cell I and the calculated value of 0.05916 log a_{Ag^+} for a given total concentration would be a measure of $E^\circ_{Ag^+|Ag} - E_{ref}$ (*cf.* eq 17). From a knowledge of E_{ref} it is therefore possible finally to calculate $E^\circ_{Ag^+|Ag}$.

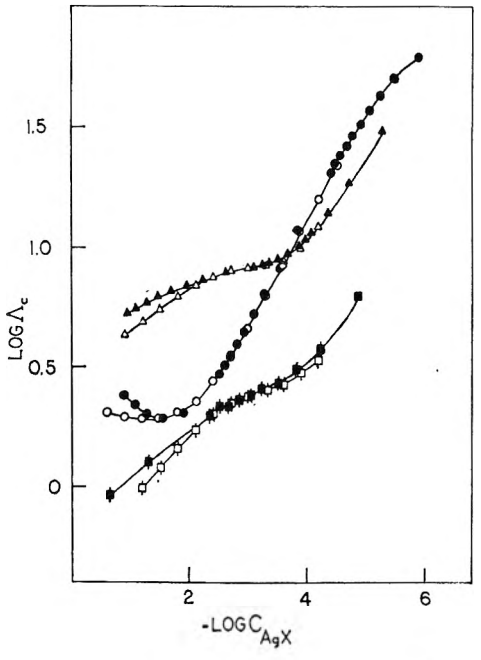

Figure 1. Plot of log Λ_c *vs.* $-\log C_{AgX}$. AgCl: ⊡ (exptl), ■ (calcd $K_1 = 1.2 \times 10^7$; $K_2 = 1.6 \times 10^4$; $K_3 = 6.5 \times 10^6$); AgCNS: ○ (exptl), ● (calcd $K_1 = 2.9 \times 10^5$; $K_2 = 1.0 \times 10^2$; $K_3 = 0$); AgCN: △ (exptl), ▲ (calcd $K_1 = 7.5 \times 10^6$; $K_2 = 2.0 \times 10^4$; $K_3 = 2.0 \times 10^4$).

Experimental Section

Chemicals. Pyridine was purified, stored, and dispensed according to the procedure described previously.[1b] Silver nitrate used was of reagent grade. The chloride, cyanide, and thiocyanate were prepared by metathesis using excess silver nitrate and the appropriate potassium salts. Silver picrate was obtained by the reaction of silver nitrate with picric acid and subsequently recrystallization twice from ethanol.

Potentiometric Techniques. These have been described elsewhere.[1,5] Both Hg|$HgCl_2$(s), LiCl(s), and Zn(Hg)|$ZnCl_2$(s) reference electrodes proved suitable for use in pyridine solutions. The general procedures for preparing these electrodes have been discussed previously.[1,5] The emf values reported in this study are considered reliable to within ±2 mV. All measurements were made in an air bath maintained at 25 ± 0.5°.

Results and Discussions

Plots of log Λ_c *vs.* $-\log C_{AgX}$ for AgCl, AgCN, and AgCNS based on the conductance data of Mathews and Johnson[3] are shown in Figure 1. The theoretical plot for each system based on calculations according to eq 12 is also given for comparison. The values of K_1, K_2, and K_3 which yielded the best fit in individual cases have been given in the legend.

The results of potentiometric measurements for the different silver salts are summarized in Figure 2 in the form of E *vs.* $-\log C_{AgX}$ plots. As is evident, in all of

(5) S. Bruckenstein and L. M. Mukherjee, *J. Phys. Chem.*, **64**, 1601 (1960).

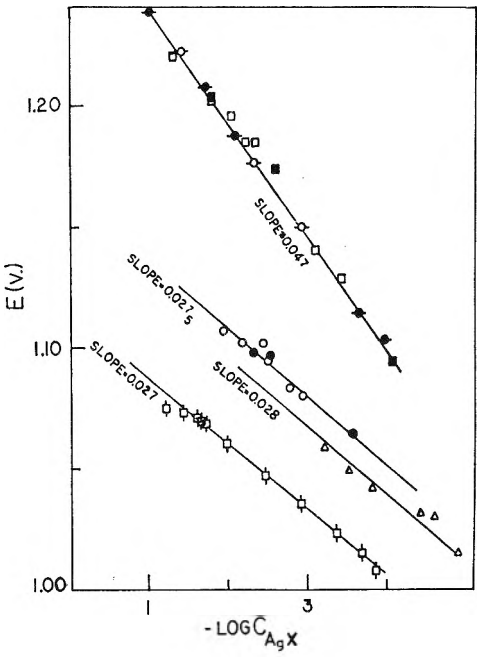

Figure 2. Plot of E *vs.* $-\log C_{AgX}$: ⊕, AgCl; △, AgCN; ○, AgCNS; □, $AgNO_3$; -○-, Ag(pic) (*vs.* Zn(Hg)|$ZnCl_2$ (s) reference electrode); ●, AgCNS; ■, $AgNO_3$; -●-, Ag(pic) (*vs.* Hg|$HgCl_2$ (s), LiCl (s) reference electrode). All emf's shown in the figure are referred to the Zn(Hg)|$ZnCl_2$ (s) reference electrode. (The emf of the cell Zn(Hg)|$ZnCl_2$ (s) reference electrode||LiCl (s), $HgCl_2$ (s)|Hg reference electrode is 1.2245 V.)

the present cases the plots are linear over the concentration ranges studied; the average slopes are in the vicinity of 0.02958 V as required by eq 18 except in the case of the nitrate and picrate. The slightly higher slope (~0.047 V) observed in these last two cases is conceivably due to their relatively greater degree of dissociation which would invalidate the simplifying assumption made in deriving eq 16 from eq 15.

In all cases, the plots of the calculated values of 0.05916 log a_{Ag^+} *vs.* $-\log C_{AgX}$ (Figure 3) are more or

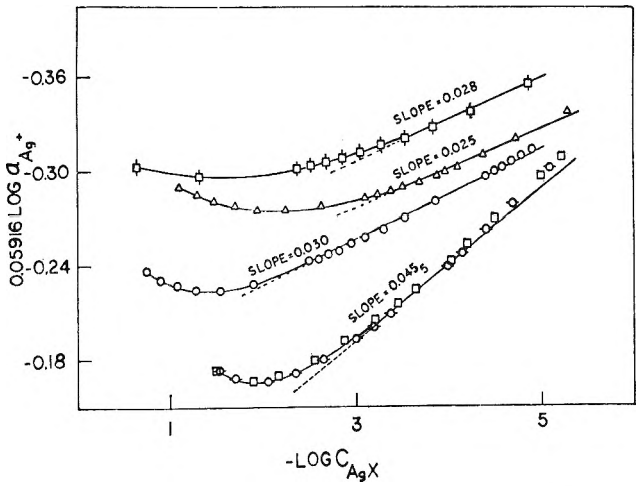

Figure 3. Plot of 0.05916 log a_{Ag^+} *vs.* $-\log C_{AgX}$: ⊕, AgCl; △, AgCN; ○, AgCNS; □, $AgNO_3$; -○-, Ag(pic).

less linear below ~10^{-3} M with curvature developing at high concentrations. Possibly, the curvature may indicate deviation caused by the inapplicability of the Debye–Hückel limiting law in calculating activity coefficients at high concentrations. Table I summarizes

Table I: Standard Potential of the Reaction $Ag^+ + e \rightleftharpoons Ag(s)$ in Pyridine

AgX	$-\log C_{AgX}$[a]	$E°_{Ag^+\|Ag}$,[b] V
AgCl	3.00	1.340
	3.50	1.341
	3.75	1.340
	Av	1.340 ± 0.0003
AgCN	3.50	1.345
	4.00	1.343
	Av	1.344 ± 0.001
AgCNS	2.50	1.338
	3.00	1.336
	3.50	1.338
	Av	1.337 ± 0.001
$AgNO_3$	3.25	1.339
	4.00	1.338
	Av	1.338 ± 0.0005
Ag(pic)	3.25	1.338
	4.00	1.338
	Av	1.338 ± 0

[a] Interpolated values used in comparing plots given in Figures 2 and 3. [b] *Vs.* the Zn(Hg)|$ZnCl_2$(s) reference electrode.

the average values of $E°_{Ag^+|Ag}$ calculated with reference to the different silver salts. The grand average value of $E°_{Ag^+|Ag}$ is found to be 1.339 ± 0.002 V *vs.* Zn(Hg)|$ZnCl_2$(s) reference electrode. Using the value of −0.788 V[1] for the potential of the Zn(Hg)|$ZnCl_2$(s) reference electrode *vs.* nhe, the value of $E°_{Ag^+|Ag}$ is found to be 0.551 V.

It may be remarked at this point that, although the procedure adopted for the treatment of the conductance data of AgCl, AgCN, and AgCNS is indeed approximate, the generally consistent agreement obtained in the present correlation is significant and provides a verification of the over-all reliability of the trial values of the various parameters, such as K_1, K_2, etc., and the ion conductances used in the calculations. Furthermore, it should be recognized that, in spite of the fact that all K's as introduced in the treatment of the conductance data are formal constants, the activity coefficient correction for the monomer dissociation into simple ions—the predominant process at low concentrations—is relatively unimportant. Thus, the values of K_1 for AgCl, AgCN, and AgCNS should closely compare with the corresponding thermodynamic values. Based on the present value of K_1 our estimate of the monomeric dissociation constant, K_{AgX} (*cf.* eq 14), for AgCl is 8.3 × 10^{-8}. Earlier spectrophotometric

studies[6] of silver chloride solutions in pyridine which yielded a value of 8.4×10^{-5} for K_{AgCl}, on the assumption of simple dissociation only, are not corroborated in the present work.

Acknowledgment. Acknowledgment is made to the donors of the Petroleum Research Fund, administered by the American Chemical Society, for partial support of this research.

(6) S. Bruckenstein and J. Osugi, *J. Phys. Chem.*, **65**, 1868 (1961).

Application of the Polanyi Adsorption Potential Theory to Adsorption from Solution on Activated Carbon

by Milton Manes[1a] and L. J. E. Hofer[1b]

Mellon Institute, Pittsburgh, Pennsylvania 15213 *(Received August 2, 1968)*

Liquid-phase adsorption isotherms at 25° on an activated carbon have been determined, over a wide range of concentrations, for the following systems: Sudan III (benzeneazo-*p*-benzeneazo-*β*-naphthol) in acetone, cyclohexane, carbon tetrachloride, benzene, and carbon disulfide, and Butter Yellow (*p*-dimethylaminoazobenzene) in methanol, acetonitrile, acetone, 2-propanol, cyclohexane, heptane, benzene, and carbon disulfide. Except for the high capacity range, most of the data can be fitted to a correlation curve determined for the same carbon from gas-phase adsorption measurements, as predicted by the Polanyi adsorption potential theory. The experimental link between liquid and gas-phase adsorption and the relative constancy of the solvent effect on adsorption (measured in appropriate units) appear to introduce a measure of predictability to at least some liquid-phase adsorption isotherms. Adsorption tends to be weakest in solvents of highest refractive index.

Introduction

The Polanyi adsorption potential theory[2] and modifications thereof have been widely applied to gas-phase adsorption.[3-7] By contrast, application of the theory to liquid-phase adsorption has been used only in modified form for adsorption of binary liquids[8] and apparently not at all for solutes. Since the nature of the forces on adsorbed molecules may be expected to be independent of their state of aggregation, it seemed reasonable to expect that the adsorption isotherms of at least properly chosen solute–solvent systems should conform to a significant degree to the Polanyi theory. Such conformation has been found for the adsorption isotherms of two solutes (Sudan III and *p*-dimethylaminoazobenzene) in a wide variety of solvents. The results provide the expected experimental link between gas-phase and liquid-phase adsorption on activated carbon and, to the extent that they will be confirmed by continuing work, introduce the possibility of predicting adsorption isotherms on activated carbons for a wide variety of systems from minimal data.

Theoretical Section

The Polanyi adsorption potential theory for gases may be summarized as follows: within the range of the attractive forces of the solid surface (the "adsorption space") the potential energy of a given gas is reduced, relative to its value at infinity, by an amount ϵ (the adsorption potential) that for a given gas depends on proximity to the solid surface. One can imagine points of equal ϵ to be joined to form equipotential surfaces that together with the solid surface enclose a volume $v(\epsilon)$. The plot of $v(\epsilon)$ against ϵ (the "characteristic curve") depends on the structure of the adsorbent, and no attempt is made to derive it from theory; it is independent of temperature. When the adsorbent, initially under vacuum, is exposed to increasing pressures of gas,

(1) (a) Professor, Department of Chemistry, Kent State University, Kent, Ohio; (b) Head, Adsorption Fellowship (Sponsored by Pittsburgh Activated Carbon Division of the Calgon Corporation) Mellon Institute, Carnegie-Mellon University, Pittsburgh, Pa.

(2) (a) M. Polanyi, *Verh. Deut. Physik. Ges.*, **16**, 1012 (1914); **18**, 55 (1916); *Z. Elektrochem.*, **26**, 370 (1920); (b) M. Polanyi, *Z. Physik*, **2**, 111 (1920).

(3) M. M. Dubinin, *Chem. Rev.*, **60**, 235 (1960).

(4) W. K. Lewis, E. R. Gilliland, B. Chertow, and W. P. Cadogan, *Ind. Eng. Chem.*, **42**, 1319 (1950).

(5) R. J. Grant, M. Manes, and S. B. Smith, *A.I.Ch.E. J.*, **8**, 403 (1962).

(6) R. J. Grant and M. Manes, *Ind. Eng. Chem. Fundamentals*, **3**, 221 (1964).

(7) R. J. Grant and M. Manes, *ibid.*, **5**, 490 (1966).

(8) R. S. Hansen and W. V. Fackler, *J. Phys. Chem.*, **57**, 634 (1953).

the attractive forces of the solid for the gas molecules reinforce their attraction for each other, with the result that the gas liquefies between the solid surface and that equipotential surface for which

$$\epsilon(v) = RT \ln p_s/p \qquad (1)$$

where p is the (equilibrium) pressure of the gas and p_s the vapor pressure of the corresponding liquid at the equilibrium temperature. Given an adsorption isotherm over some capacity range, one can calculate the characteristic curve over the same capacity range by use of eq 1 and an estimate of the density of the presumed liquid adsorbate. Having determined the characteristic curves one can now calculate adsorption isotherms at other temperatures.

If the adsorptive forces for different gases are of the same nature, then one may expect that the characteristic curves for different gases on a single adsorbate should all be the same except for a constant factor multiplying the adsorption potential. Dubinin[3] expressed this in the equation

$$v = f\left(\frac{\epsilon}{\beta}\right) \qquad (2)$$

where β is his "affinity coefficient." Dubinin and Timofeev[9] have compared the experimental affinity coefficients of a set of gases with the corresponding molar volumes (V) and with several different estimates of the molar polarizabilities, and have concluded that the affinity ratios of different pairs of gases are best approximated by the ratio of their molar volumes. Lewis, Gilliland, Chertow, and Cadogan[4] and Grant Manes, and Smith[5] found that within the homologous series of saturated hydrocarbons on activated carbon, the plots of volume adsorbed *vs.* ϵ/V collapsed to a single curve (the "generalized correlation curve") with considerable accuracy. However, Dubinin and Timofeev found that the discrepancy between molar volume ratios and affinity coefficient ratios could be as much as 20% (some of which could have been due to specific chemical effects). Similarly, Grant, Manes, and Smith[5] found that at equal adsorbate volumes ϵ/V was some 10% higher for carbon disulfide than for the hydrocarbon series. Anticipating that these differences turn out to be quite significant, we now consider adsorption from solution.

Polanyi[2a] originally supposed that adsorption of solid solutes from solution would be analogous to the adsorption of gases with precipitation of solid taking the place of liquefaction of gas, and with the adsorption potential now estimated as

$$\epsilon_s(v) = RT \ln c_s/c \qquad (3)$$

where c_s and c are the saturated and the equilibrium concentrations and ϵ_s is the adsorption potential of the pure solute adsorbing as a vapor. However, in a subsequent paper,[2b] he noted that the adsorption of a solid solute would have to be accompanied by the desorption of an equal volume of solvent. As a result, eq 1 would have to be modified to read (with a slight change in notation)

$$RT \ln \frac{c_s}{c} \equiv \epsilon_{sl} = \epsilon_s - \epsilon_l \frac{V_s}{V_l} \qquad (4)$$

where ϵ_l is the adsorption potential of the solvent and V_s and V_l, the molar volumes of (solid) solute and solvent.

Polanyi concluded from eq 4 that adsorption of a solute would be weakest from solvents with the highest values of $\epsilon_l V_s/V_l$ (or ϵ_l/V_l for constant V_s). He then drew attention to an observation of Freundlich to the effect that adsorption tends to be weakest in those solvents that are themselves most strongly adsorbed from solution. He noted further that since the various solvents would differ only slightly in their values of $\epsilon_l V_s/V_l$, one would expect that the equilibrium concentrations at equal capacities for various solvents would differ largely because of differences in solubilities, as had been found by Davis[10] in studies on the adsorption of iodine on carbon. We shall return to these points later.

Let us now consider some of the consequences of the Polanyi adsorption potential theory for solutions in terms of plots of volume adsorbed *vs.* the adsorption potential per unit volume, *i.e.*, in terms of "generalized correlation curves." We can rewrite eq 4 as

$$\frac{\epsilon_{sl}(V)}{V_s} = \frac{\epsilon_s(V)}{V_s} - \frac{\epsilon_l(V)}{V_l} \qquad (5)$$

which we can again rewrite somewhat more compactly as

$$\alpha_{sl} = \alpha_s - \alpha_l \qquad (6)$$

where each α is the corresponding ϵ/V. If we assume, with Polanyi, that the characteristic curves for the solvent and the solute have the same functional form (except for a constant factor in the adsorption potential), then the α's are directly proportional to the affinity coefficients of Dubinin.[3] Consider now some of the consequence of eq 6 by reference to Figure 1, which shows schematic plots of volume adsorbed *vs.* adsorption potential on a scale that corresponds roughly to some experimental observations on activated carbon. All of the curves in Figure 1 are drawn so that they can be collapsed to a single curve by application of a single abscissa scale factor. The deviation from unity of the scale factor required to make two such curves coincide is a measure of the extent to which the adsorption potential deviates from proportionality to the molar volume. We assume that the scale factor α (or the affinity coefficient β) of the solute is signif-

(9) M. M. Dubinin and D. P. Timofeev, *Compt. Rend. Acad. Sci. URSS*, **54**, 701 (1946).

(10) O. C. M. Davis, *Trans. Chem. Soc.*, **91**, 1966 (1907).

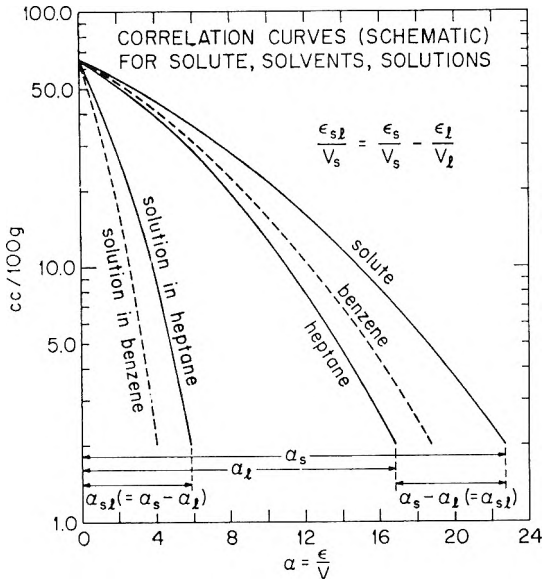

Figure 1. Schematic plot of the volume of adsorbate adsorbed (cm^3) per unit weight of carbon (100 g) *vs.* the adsorption potential per unit volume of the solvent (l), the solute (s), and the solute from solution (sl) illustrating the relation $\alpha_{sl} = \alpha_s - \alpha_l$.

icantly higher than that of any of the solvents (otherwise the Polanyi theory would predict stronger adsorption of the solvent). The correlation curves for the gas-phase adsorption of two solvents and the corresponding correlation curves for adsorption of solute in the liquid solvents are also shown. The larger the α_l for the solvent, the smaller the α_{sl} for the solution. Now Polanyi[2b] pointed out that one could verify eq 4 for volatile solutes (such as iodine) by separately determining α_s and α_l by gas-phase adsorption followed by the determination of α_{sl} in liquid-phase experiments. However, most solutes of interest are not volatile, and one cannot therefore determine α_s independently. A somewhat less direct check on the theory would be to determine the differences between the α_{sl} for a single solute in different solvents and to see whether these differences would correspond to the differences in α_l as determined from vapor-phase measurements. Moreover, in the absence of the requisite vapor-phase data (which might be impossible to determine for solvents of low volatility), one could determine α_{sl} for a number of solutes in a set of solvents and observe whether the differences in α_{sl} between solvents (for a given solute) would remain constant for all solutes.

Instead of expressing the relative values of the α's at some stated adsorption volume, we can consider the ratios between the α's and α_h, where α_h is the scale factor for some standard reference substance (or substances, if they all have the same α), in which case we can rewrite eq 6 as

$$\frac{\alpha_{sl}}{\alpha_h} = \frac{\alpha_s - \alpha_l}{\alpha_h} \tag{7}$$

or

$$\gamma_{sl} = \gamma_s - \gamma_l \tag{8}$$

where $\gamma_{sl} = \alpha_{sl}/\alpha_h$, etc. If the reference substance is the solvent, then $\gamma_s = \gamma_{sl} + 1$.

Experimental Section

Since, as noted earlier, all of the foregoing discussion is based on the assumption that the expected link between liquid-phase and gas-phase adsorption in fact exists, an initial objective was to gather sufficient liquid-phase and gas-phase adsorption data on an activated carbon for comparing the resulting correlation curves. The principal problem was to find systems for which one could determine the liquid-phase adsorption isotherms down to the low capacity range, in order to permit a critical comparison of the resulting correlation curves. Oil-soluble dyes of relatively low molecular weight were originally sought as candidate solutes because of ease of spectrophotometric analysis over a wide range of concentrations (typically five decades), solubility in a wide variety of solvents, and expected relative ease of purification. The work reported here is based on the liquid-phase adsorption data for two azo dyes, Sudan III (benzene-azo-*p*-benzene-azo-β-naphthol) and Butter Yellow (*p*-dimethylamino-azobenzene).

Materials. Commercial Sudan III was recrystallized from acetone–toluene. Butter Yellow was recrystallized from ethanol; treatment of the concentrate with activated carbon was necessary to achieve the desired spectral purity. Successive recrystallizations did not significantly change the optical extinction coefficients. The largest experimental error due to impurities was expected to be in the possible change in composition of the equilibrium solution on adsorption; therefore, initial experiments were carried out in which the optical absorption curve for the solution remaining after adsorption of 99% of a sample on activated carbon was indistinguishable from a similar curve determined on a 100:1 dilution of a similar sample.

The adsorbent in all cases came from a single batch of Pittsburgh Activated Carbon grade CAL activated carbon, which was pulverized to pass 200 mesh. This carbon is normally used for removal of color bodies from solutions (*e.g.*, cane and invert sugar); it was chosen for maximum availability of its surface area to the solute dyes. Except for oven drying before weighing, the carbon was used as received. The surface area (BET) was 1140 m^2/g.

The solvents used, methanol, acetonitrile, acetone, 2-propanol, *n*-heptane, cyclohexane, benzene, carbon tetrachloride, and carbon disulfide, were in every case Fisher Spectranalyzed reagents.

Procedures. Equilibration took place in 125-ml screw-capped erlenmeyer flasks, the screw caps being sealed with Teflon gaskets. The flasks were shaken at

least 16 hr at 25° in a thermostated shaker bath; check experiments at longer shaking times established that the shaking time sufficed for equilibration. After equilibration the carbon was allowed to settle out and a portion of the supernatant liquid was cleared by centrifuging. The cleared equilibrium solution, after suitable dilution, was analyzed in a Cary spectrophotometer. The sample size and initial concentration of solution were so adjusted that no more than 99% of the original sample was adsorbed. The relative amounts of carbon, dye, and solvent were so chosen that the adsorption of solvent did not introduce a significant error into the calculations.

Solubilities of the dyes in the individual solvents were determined by spectrophotometric analysis of saturated solutions. Addition of a small amount of activated carbon to the equilibrium mixture improved the reproducibility of the solubility measurements.

The densities of the pure dyes (necessary for calculating correlation curves) as determined at 25° by helium displacement were: Sudan III, 1.302 g/cc; Butter Yellow, 1.208 g/cc. The gas-phase correlation curve was determined from adsorption isotherm data for ethane, propane, and butane on a McBain balance, using the methods described by Grant and Manes.[6]

Data and Results

Figures 2 and 3 give the adsorption data for Sudan III and Butter Yellow, plotted on a log–log plot as g of dye/100 g of carbon *vs.* the relative concentration c/c_s.

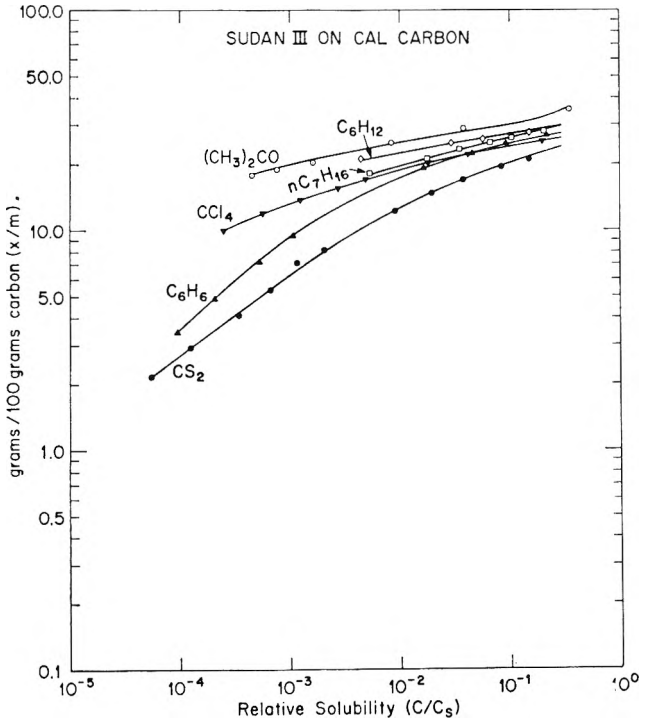

Figure 2. Isotherms of Sudan III on CAL carbon from various solutions. (C_s is the solubility and C is the concentration of dye in equilibrium with the carbon for the loading indicated.)

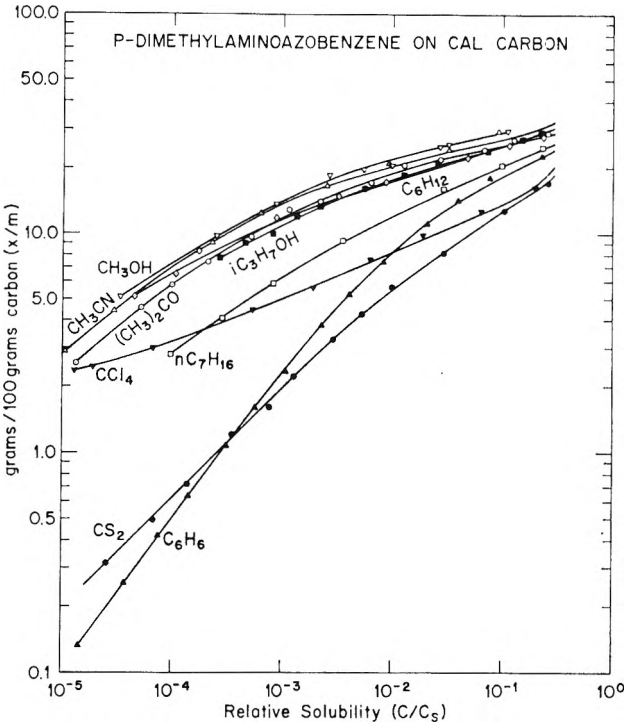

Figure 3. Isotherms of Butter Yellow on CAL carbon from various solutions. (C_s is the solubility and C is the concentration of dye in equilibrium with the carbon for the loading indicated.)

(The ordinate scales have been expanded to increase the spread between the isotherms.) The original data may be reconstructed from the solubilities, which are here listed (in grams per liter). Sudan III: acetone, 1.5; heptane, 0.078; cyclohexane, 0.16; carbon disulfide, 8.7; benzene, 6.0; carbon tetrachloride, 2.5. Butter Yellow: methanol, 9.0; acetonitrile, 32; acetone, 94; 2-propanol, 7.0; heptane, 6.1; cyclohexane, 11.5; benzene, 20; carbon tetrachloride, 15; and carbon disulfide, 235.

Since a plot of weight adsorbed *vs.* relative concentration at a single temperature may be regarded as a characteristic curve (except for constant factors in both ordinate and abscissa), one would expect that the adsorption isotherms should be superimposable by application of an abscissa scale factor and that they should not cross. This is approximately the case for Sudan III, although the carbon disulfide line shows a tendency to cross the benzene line at low concentrations. It is also approximately the case for the data on Butter Yellow, with the exception of a highly anomalous curve for carbon tetrachloride and the crossover of the benzene and carbon disulfide lines in the relatively low capacity range.

Figures 4, 5, and 6 relate the liquid-phase adsorption data to gas-phase adsorption on the same carbon. The abscissa scale gives $(1/2.303R)(\epsilon/V)$ rather than ϵ/V, following the notation of earlier publications.[5–7] The solid line in all cases is the hydrocarbon correlation line, similar to the one shown in Figure 7 of ref 6 for a

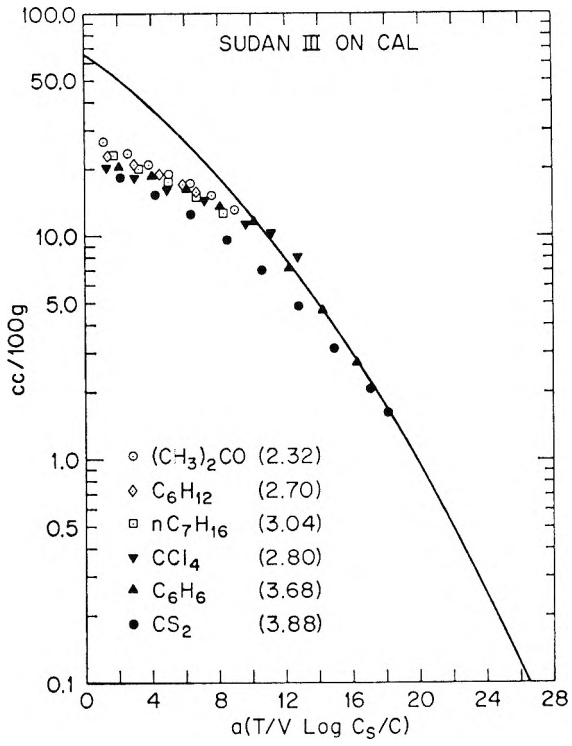

Figure 4. Relation of the adsorption potential per unit volume of Sudan III from various solvents to that of heptane (determined in the gas phase).

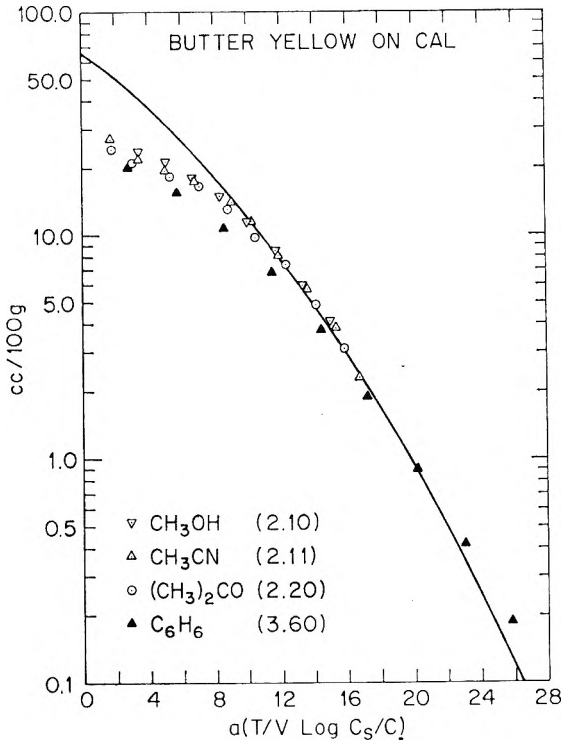

Figure 5. Relation of the adsorption potential per unit volume of Butter Yellow from various solvents to that of heptane (determined in the gas phase).

different carbon. For clarity in presentation, points in each case were taken at equal intervals from the corresponding isotherms rather than plotting entire curves; the points are therefore not experimental points. Corresponding to the x/m of each such point on the isotherm, the value v/m (cc/100 g) was calculated, using the solid density of the dye. The corresponding value of $(T/V_s) \log c_s/c$ was then calculated. The resulting points in all cases fell on curves well to the left of the hydrocarbon gas-phase correlation curve. Each abscissa value was then multiplied by a single constant $(1/\gamma_{sl})$ that was chosen to give optimum fit to the gas-phase correlation curve in the low-capacity range; it was obvious that the fit would be poor at the highest capacities. The factors required to bring about the shown coincidence are listed for each solvent. In all cases, the low capacity limit was set by the sensitivity of the analytical measurements.

It is immediately apparent that in the high capacity limit the gas-phase correlation curve does not apply for either solute, the extrapolated limits of the solid-phase capacities being about half of the gas-phase capacity limit. This is in keeping with Polanyi's suggestion[2b] that eq 4 should not necessarily hold in the region of maximum adsorption. However, many of the data appear to follow a single correlation curve to a fair approximation. The convergence of the data on Sudan III to the gas-phase correlation curve is better shown by the calculations than by Figure 4, in which the data run out just as they begin to coincide with the gas-phase correlation curve. The data on Butter Yellow, on the other hand, fit quite nicely over a wide range of capacities, with the obvious exception of the data for carbon tetrachloride and carbon disulfide.

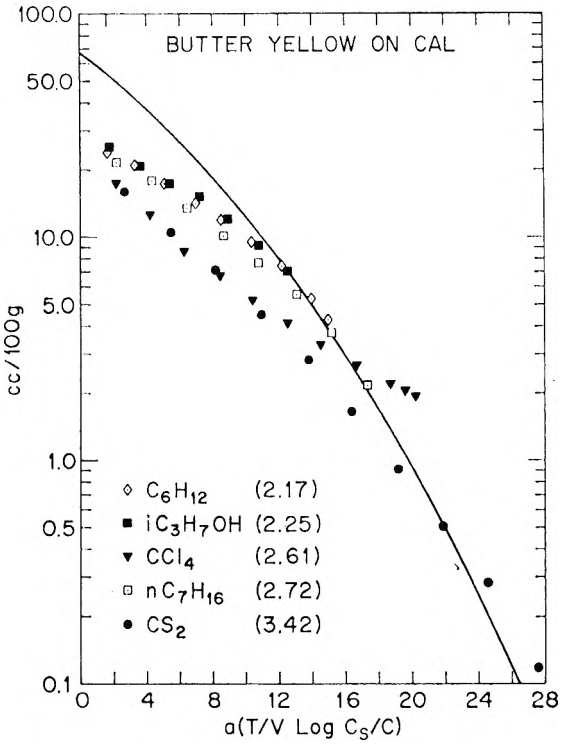

Figure 6. Relation of the adsorption potential per unit volume of Butter Yellow (from additional solvents) to that of heptane (determined in the gas phase).

These data have the (perhaps dubious) advantage of demonstrating that all data cannot be made to superimpose on the gas-phase correlation curve by application of a single abscissa scale factor. An initial speculation is that the anomalous behavior of carbon tetrachloride is associated with steric hindrance to closest approach to the carbon surface, which would be expected to be most pronounced at low capacities.

Consider now the constancy of the differences in the factors γ_{sl} between the different solvents. Table I lists

Table I: Comparison of γ_{sl} Values for Two Solutes in Different Solvents

	Sudan III		Butter Yellow	
	γ_{sl}	Difference	γ_{sl}	Difference
Acetone	0.43	0.17	0.45	0.16
Heptane	0.33	0.07	0.37	0.08
Cyclohexane	0.37	0.11	0.46	0.17
CCl_4	0.36	0.09	0.38	0.09
Benzene	0.27	0.01	0.28	−0.01
CS_2	0.26		0.29	

these factors for those solvents common to both dyes, together with the difference between each value and the corresponding value for carbon disulfide (which was chosen as an arbitrary reference point). The data show reasonable constancy, with cyclohexane showing the highest deviation.

In order to check the extent to which the adsorption isotherms fit the correlation, the correlated data for Sudan and for Butter Yellow were combined and a best correlation curve was drawn by eye. This correlation curve, together with the (empirical) value of γ_{sl} was used to back-calculate adsorption isotherms for individual solvent–solute systems. Three typical resulting curves are shown in Figure 7. The agreement, while not exact, extends over a very wide concentration range.

Finally, an attempt was made to estimate the γ_{sl} values without any recourse to adsorption measurements. The relatively crude estimate was made as follows: it was assumed that the adsorption potential per unit volume, α, is proportional to the polarizability per unit volume,[11] and that this, in turn, is proportional to refractivity per unit volume, p, by the Lorentz–Lorenz equation

$$p \equiv \frac{[R]}{V} = \frac{n^2 - 1}{n^2 + 2} \qquad (9)$$

where $[R]$ is the molar refraction. The value of p was calculated for each solvent from its refractive index and for each solute from its molecular structure and density and a table of atomic refractivities.[12] To express α_h (from the gas-phase hydrocarbon correlation) in terms of a liquid refractive index, heptane was picked as a

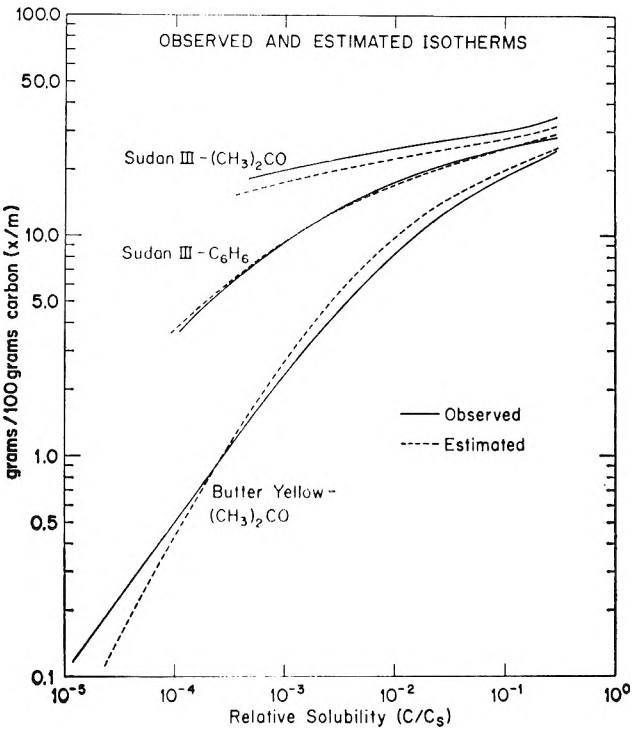

Figure 7. Comparison of observed and estimated isotherms.

standard liquid hydrocarbon, since its α should follow the generalized hydrocarbon correlation. The calculation is, therefore

$$\gamma_{sl} = \frac{p_s - p_l}{p_7} \qquad (10)$$

where p_7 is the refractivity per unit volume of heptane.

Table II: Comparison between Experimental and Calculated Values of γ_{sl}

	Sudan III		Butter Yellow	
	Obsd	Calcd	Obsd	Calcd
Methanol	...	...	0.48	0.58
Acetonitrile	...	...	0.47	0.54
Acetone	0.43	0.47	0.45	0.51
2-Propanol	...	...	0.44	0.47
Heptane	0.33	0.40	0.37	0.44
Cyclohexane	0.37	0.32	0.46	0.36
Benzene	0.27	0.15	0.28	0.19
CS_2	0.26	<0	0.29	<0

The thus calculated values of γ_{sl} are shown in Table II. Although the calculation breaks down badly for carbon disulfide and is poor for benzene, it does show

(11) F. London and M. Polanyi, *Naturwissenschaften*, **18**, 1099 (1930).

(12) N. A. Lange, Ed., "Handbook of Chemistry," McGraw-Hill Book Co., New York, N. Y., 1961, p 1391. The data are taken from Smiles, "The Relation between Chemical Constitution and Some Physical Properties," Longmans, Green and Co., London, 1910.

the trend of the observed results. The principal source of error is that the adsorption potentials per unit volumes are, in fact, somewhat less than proportional to p. Therefore, the calculated values of γ_{sl} tend to exaggerate the higher values and underestimate the lower ones. The calculation is likely to be useful, nevertheless, in bracketing the behavior of a nonvolatile solvent according to its refractive index.

Although refractive index appears to contain a good deal of predictive value for ϵ_1/V_1, it is almost certainly not the only factor. The anomalous behavior of CCl_4 and cyclohexane is probably associated with their bulky structures, as a result of which a significant part of the solvent molecule cannot achieve as close an approach to the carbon surface as can other relatively unhindered molecules. This supposed steric effect requires further investigation.

There are a number of factors that have been omitted from this initial report. For example, the effect of nonideality of the solutions has not been considered. In all likelihood, most of the nonideality effects are comprehended in the solubilities. The fact that the adsorption of the solids does not quite approach the gas-phase adsorbate volumes may be rationalized in terms of the problem of packing a solid into pores or interstices. We are as yet without specific confirmation on this point.

Moreover, it should be noted that the choice of solutes has probably been a fortunate one for showing the desired relationships and that other solutes may not do quite as well. The determined γ_s values for Sudan III and Butter Yellow are, respectively, 1.33 and 1.37. These are very high values, consistent with flat aromatic molecules; solutes with lower γ_s values may show more complex behavior.

Let us now return to Polanyi's expectation that the relative concentrations in different solvents at the same loading would be largely due to solubility differences. We note that the effect of the displacing power of the solvent $\epsilon_1 V_s/V_1$ depends on the molar volume of the adsorbate and on the amount adsorbed, being most pronounced at the highest adsorption potentials, or lowest loadings. Polanyi cited relatively small displacement effects[10] in iodine solutions. However, iodine has a molar volume of only 51.4; the solvent displacement effect on the isotherm would therefore be relatively small. By contrast, with Butter Yellow (molar volume = 186.5) and Sudan III (molar volume = 270.6), the effect of solvent on relative concentration can be as high as two orders of magnitude (and greater with lower capacities). As noted elsewhere,[13] the displacement effect can become quite significant in choosing a solvent for extraction of an adsorbate.

Finally, we consider the rule of Freundlich,[14] *i.e.*, "If in one substance as solvent another substance is strongly adsorbed, the solvent itself, when in solution, will be weakly adsorbed, and vice versa." If one follows Hansen and Fackler's[8] application of the Polanyi theory to adsorption from mixed liquids, one would expect the strength of adsorption of an individual liquid (*i.e.*, the energy of adsorption per mole) to depend not only on its α (or γ) value but also on its molecular weight. On the other hand, the molecular weight of the solvent should be quite irrelevant to the strength of adsorption of a solid solute from it. Therefore, the criteria derived from Polanyi theory may be expected to be better predictors of strength of adsorption than the Freundlich rule, particularly for solvents of high molecular weight.

Conclusions

1. For the two solutes thus far investigated, the adsorption isotherms for a wide variety of solvents can fit over a wide range (but not the entire range) to a correlation curve derived from gas-phase adsorption. These data provide the expected link between liquid-phase and gas-phase adsorption.

2. Although the data do not fit the gas-phase correlation curve in the high-capacity range, they appear to fit a somewhat different correlation curve, which can be used to calculate adsorption isotherms.

3. Refractive index is a good (but not infallible) predictor of the displacing power of solvents.

4. Anomalies, such as adsorption from carbon tetrachloride, and to a lesser extent from cyclohexane and carbon disulfide, remain to be explained. Steric effects are suggested as an initial speculation for the anomalies in carbon tetrachloride and cyclohexane.

Acknowledgments. This work was part of the research program of the Adsorption Fellowship at Mellon Institute, sponsored by the Pittsburgh Activated Carbon Division of Calgon Corporation. We wish to thank Jonathan C. Cooper, General Manager of Pittsburgh Activated, and George Tobias, its Technical Director, for their active interest and support. We are indebted to Richard J. Grant for many helpful discussions. Most of the experimental work was carried out by E. V. Conley and W. E. Baker. The surface area was determined by the Physical Measurement Group at Mellon Institute. We also wish to thank Mr. John H. Jones (U. S. Food and Drug Administration, Washington 25, D. C.) for advice on the relative purity of dyes.

(13) M. Manes and L. J. E. Hofer, submitted to *Ind. Eng. Chem. Process Design Develop.*

(14) H. Freundlich, "Colloid and Capillary Chemistry," Methuen & Co., Ltd., London, 1926 (English translation) p 194.

Anion Exchange of Metal Complexes. XVII.[1] The Selective Swelling of the Exchanger in Mixed Aqueous-Organic Solvents

by Y. Marcus

Department of Inorganic and Analytical Chemistry, The Hebrew University, Jerusalem, Israel

and J. Naveh

Israel Atomic Energy Commission, Nuclear Research Center, Negev, Israel *(Received August 5, 1968)*

The swelling of Dowex-1 anion exchangers of cross-linking 4, 8, and 16% DVB was measured in several organic solvents and their aqueous mixtures for the chloride and perchlorate ionic forms. For the pure solvents and chloride form resins swelling decreases in the order water > formamide > methanol > ethanol > acetonitrile > 1-propanol > 2-propanol > acetone > dioxane. The perchlorate form shows altogether less swelling, and relatively high swelling by formamide and dimethylformamide. In mixed aqueous-organic solvents preferential swelling by the alcohols is found at the lowest mole fractions and by water over most of the composition range. The amides and methanol show rather little preference for swelling by either water or the organic solvent. Most of the observed phenomena can be explained by the effects of the organic solvent on the structure of water outside the resin, and by preferential ion-solvation effects.

Introduction

The selective sorption and elution of metal complexes on anion exchangers from mixed aqueous–organic solvents has been shown in recent years to be an extremely powerful tool for metal–ion separations,[2] even more than the now classical separation in aqueous solutions.[3] In an earlier publication in this series[1] it was pointed out that, whereas in aqueous solutions the net reaction occurring, whatever the actual mechanism, is the exchange of complex metal anions for the counter anions in the resin, in anhydrous organic solvents of low dielectric constant the net reaction is the distribution of the uncharged metal complex species between the two phases. These two extreme types of behavior give rise to the experimentally useful method of "combined ion exchange and solvent extraction" based on the use of mixed aqueous–organic solvents.[4] In order to understand the reactions occurring in such mixtures, and hence to be able to predict the behavior of yet untested systems, it is important to have full information on the swelling behavior of the resin and its selectivity for water and the solvent, on the manner in which these properties are affected by electrolytes, and on their invasion into the resin from mixed solvents. These factors are subject to study in our laboratories now, and this paper reports on systems with no added electrolytes.

Whereas selectivities of cation exchangers for both ions and solvents have been reported by numerous authors,[5] the behavior of anion exchangers has been the subject of only a few reports.[6] As will be shown later in the Discussion, there are great similarities between the modes of behavior shown by these two kinds of resin, and the information available for cation exchangers is therefore relevant for understanding the behavior of the anion-exchange resins.

In the following, the swelling properties of polystyrene methylene trimethyl ammonium type anion exchange resins, cross-linked by 4, 8, and 16% divinylbenzene, and in the chloride and perchlorate forms will be reported for several water-miscible solvents. The parameters studied for each system are the uptake of each solvent as a function of the composition, so that the variation of the total swelling and the selectivity of the resin for the solvent and water can be calculated.

Experimental Section

Materials. The resins used were commercial samples of polystyrene methylene trimethylammonium type, Dowex-1 X4, X8, and X16, *i.e.*, with nominal cross-linking of 4, 8, and 16% divinylbenzene, of 20 to 50 mesh size. In order to characterize the resin samples,

(1) Previous paper in series: J. Penciner, I. Eliezer, and Y. Marcus, *J. Phys. Chem.*, **69**, 2955 (1965).

(2) J. Korkisch in "Progress in Nuclear Energy, Series IX, Analytical Chemistry," S. C. Stewart and H. A. Elion, Ed., Vol. 6, Pergamon Press, Oxford, 1966, pp 1–94.

(3) K. A. Kraus and F. Nelson, *Proc. Intern. Conf. Peaceful Uses At. Energy, Geneva, 1955*, **7**, 113 (1956).

(4) J. Korkisch, *Sep. Sci.*, **1**, 159 (1966).

(5) (a) O. D. Bonner and J. C. Moorefield, *J. Phys. Chem.*, **58**, 555 (1954); (b) H. P. Gregor, D. Noble, and M. H. Gottlieb, *ibid.*, **59**, 10 (1955); (c) C. W. Davies and B. D. R. Owen, *J. Chem. Soc.*, 1676 (1956); (d) D. Reichenberg and W. F. Wall, *ibid.*, 3364 (1956); (e) R. W. Gable and H. A. Strobel, *J. Phys. Chem.*, **60**, 513 (1956); (f) C. W. Davies and A. Narebska, *J. Chem. Soc.*, 4169 (1964); (g) R. Arnold and S. C. Churns, *ibid.*, 325 (1965); (h) H. Ohtaki, H. Kakihana, and K. Yamasaki, *Z. Phys. Chem.* (Frankfurt), **21**, 224 (1959); (i) H. Ohtaki, *ibid.*, **27**, 209 (1961).

(6) (a) G. W. Bodamer and R. Kunin, *Ind. Eng. Chem.*, **45**, 2577 (1953); (b) H. Rückert and O. Samuelson, *Acta Chem. Scand.*, **11**, 703 (1957); (c) E. Sjostrom, L. Nykänen, and P. Laitinen, *ibid.*, **16**, 392 (1962).

their density, water content in the air-dried state, and anion exchange capacity were determined.

The density was determined at 22° in 25 ml pycnometers, by displacement of *n*-dodecane, for samples dried over phosphoric anhydride in a vacuum desiccator. The density found for the dry resin in chloride form was 1.1281 g/ml for the X4 sample and 1.1273 g/ml for the X8 sample, reliable to 0.3 mg/ml.

The water content of the air-dried free-flowing chloride-form resin samples was determined by drying in a vacuum desiccator over phosphoric anhydride to constant weight. Six samples of X4 resin and seven samples of X8 resin were tested. After 1 day of drying, 2.0 ± 1.0% excess of the final weight remained, after 2 days 0.8 ± 0.6%, and the value after 4 days represents the equilibrium dry weight of the resin (the deviations are one standard deviation from the mean). The water content of the air-dried resin is 98.6 ± 0.4 for X4 resin, 69.1 ± 0.4 for the X8 resin, and 33.3 ± 0.6 for the X16 resin, in g of water/100 g of completely dried resin.

The capacity of the phosphoric anhydride-dried chloride-form resin samples was determined by exchanging the chloride for perchlorate with an excess of the latter and titrating the chloride liberated. For six samples of X4 resin the value 4.04 ± 0.01 was obtained, for eight samples of X8 resin 3.63 ± 0.03, and for seven samples of X16 resin 2.32 ± 0.02, all in mequiv/g of completely dried resin. Recalculated to the air-dried form, the numbers were 2.02, 2.15, and 1.74 mequiv/g, respectively.

The perchlorate form of the resin was prepared from the chloride form by the standard method of displacement in a column, until no chloride could be detected in the effluent.

The solvents used were all of analytical reagent grade, in the usual anhydrous or "absolute" form. The actual water content was determined in each case by Karl Fischer titration and taken into account.

Procedures. The resin underwent the following treatment before the determination of the swelling behavior. Through a column of the resin were passed in order 2 *M* aqueous solutions of sodium hydroxide, water, hydrochloric or perchloric acid, water, sodium hydroxide, water, ethanol (to remove nonpolymerized impurities), water, hydrochloric or perchloric acid, and water. The resin was then centrifuged at 3700 rpm for 15 min in a standard procedure to obtain free-flowing air-dried resin. Weighed portions of these resin samples were then dried overnight in a vacuum desiccator over phosphoric anhydride. The weight of the dried perchlorate resin was nearly $(1 + 0.064\bar{C})$ times the weight of the dried chloride resin, $\bar{C}$ being the capacity of the dry resin in chloride form, as expected from the increase in the equivalent weight. The deviations from this ratio were − 2.2 ± 0.7% for six samples; *i.e.*, the drying of the chloride was slightly less efficient than the drying of the perchlorate. Taking the latter to be absolute, the dried chloride resin retains 0.3 ± 0.1 mol of water per equivalent of resin.

To a weighed dry resin sample was added a *ca.* 40-fold excess by weight of a given solvent or aqueous solvent of known composition, and the mixture was equilibrated in a closed vessel at room temperature (*ca.* 22°) for several hours. The results obtained after 1 week of equilibration were the same as those obtained after 2 hr, so that time allowed was in every case sufficient for reaching equilibrium. The resin was then quantitatively transferred into a tube with a sintered glass bottom, placed in a centrifuge tube, which was then tightly closed, to prevent evaporation of solvent. After centrifugation by the standard procedure, the resin was weighed and the water content determined by a Karl Fischer titration. Separate experiments showed that water in the resin can be determined with 99.5% accuracy compared with results obtained by complete drying, with an excess of Karl Fischer reagent being back-titrated. With the X4 resin the end point was sharp; with the X8 resin a small amount of reagent was strongly sorbed by the resin and had to be removed with a known excess of water to complete the titration.

The overall precision (one standard deviation) of the total swelling, obtained by weighing of multiplicate samples, was *ca.* ± 3%, and so the precision of solvent in the swollen resin, obtained by difference, was *ca.* ± 4%. The extreme difference between determinations was 5%. The equilibrium composition of the solvent in which the resin was swollen was also obtained by difference. Since the liquid was at a *ca.* 40 times excess by weight, its composition changed only slightly by removal of solvent by the dry resin, and was obtained with good precision, *ca.* ± 1%. The concentration of the solvent in the mixture was obtained from the amounts weighed in. The volume concentration could be calculated by measuring the contraction on mixing.

Results

Total Swelling. The total weight swelling of the resin samples of X4, X8, and X16 cross-linking has been measured in several solvents, with results shown in Table I, as moles of solvent taken up per equivalent of dry resin. The water content of the solvents was sufficiently small to avoid appreciable errors in the figures, within a precision of ± 3%.

The total specific swelling $\bar{n} = \bar{n}_S + \bar{n}_W$ has been measured as a function of composition for X4 and X8 resin for several water–solvent mixtures, and the results are shown in Figures 1 and 2, for chloride and perchlorate resins, respectively. In order to avoid a loss of accuracy by referring the results to imprecisely known equivalents of resin (*i.e.*, $\bar{n}/\bar{C}$), the primary

Table I: Total Swelling of Dowex-1 Anion Exchangers in Several Solvents in Moles per Equivalent of Dry Resin

Solvent	Resin types: X4 Cl^-	X8 Cl^-	X16 Cl^-	X4 ClO_4^-	X8 ClO_4^-
Water	18.8	14.1	8.1	3.4	3.6
Methanol	8.5	6.8	4.8	1.68	1.92
Allyl alcohol		3.7			
Ethanol	5.2	2.90	3.30	1.07	1.16
1-Propanol	3.5	2.35	2.52	0.34	0.20
2-Propanol	3.1				
Formamide	11.0	8.2	4.8	6.5	4.2
Dimethylformamide			0.8	4.2	3.2
Ethylene glycol			3.25		
Acetonitrile	2.03	2.45	2.73		
Acetone	0.69	0.54	1.0		
Dioxane	0.29	0.23	0.5		

data, moles of solvent per kg of dry resin, are given. Data have usually been obtained up to *ca.* 98 mole % of the solvent in the equilibrium solution. In most cases 0.5–1.0 mol of water/kg of resin in perchlorate form and 1.0–2.0 mol of water/kg of resin in chloride

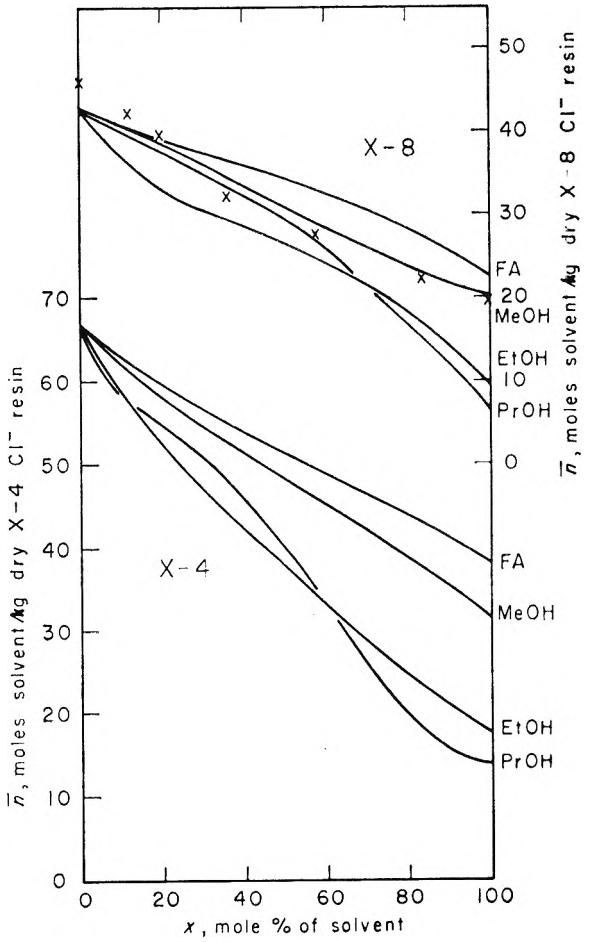

Figure 1. The total swelling $\bar{n}$ in mol of solvent/kg of dry resin in chloride form. Upper set of curves X8 resin, right-hand ordinate, lower set X4 resin, left-hand ordinate. Solvents: FA, formamide; MeOH, methanol; EtOH, ethanol; and PrOH, 1-propanol. Crosses, data for X7.5 resin from ref 6c.

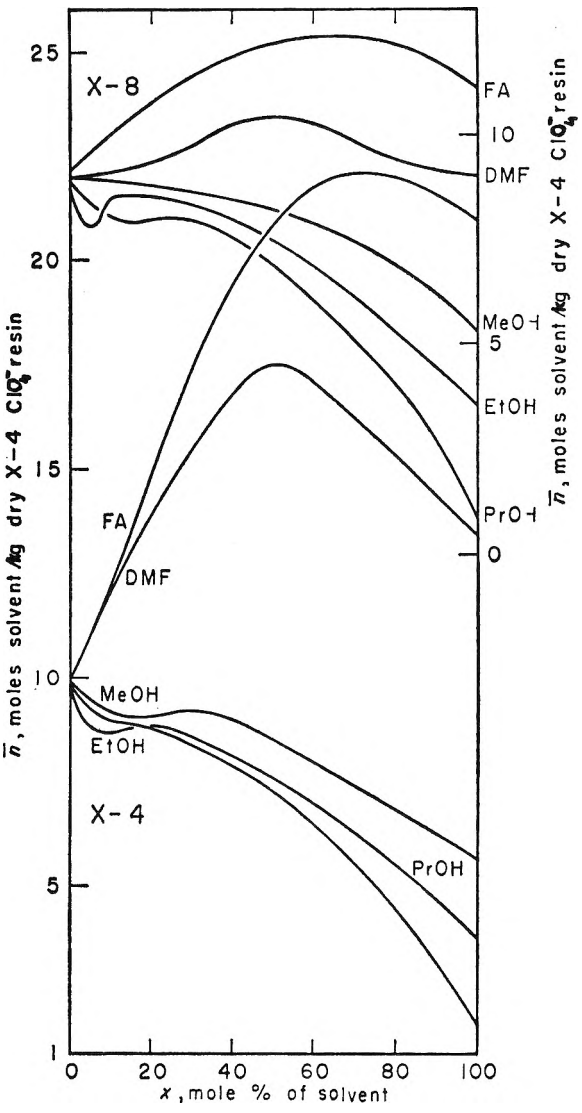

Figure 2. The total swelling $\bar{n}$ in mol of solvent/kg of dry resin in perchlorate form. Upper set of curves, X8 resin, right-hand ordinate; lower set, X4 resin, left-hand ordinate. Symbols for solvents same as Figure 1, with addition of DMF, dimethylformamide.

form were retained on the resin and are included in the values shown. No attempt to remove the last traces of water was made. The only comparable data in the literature are those obtained for methanol and Dowex-1 X7.5 in chloride form,[6c] shown as crosses in Figure 1. Their agreement with our X8 data is quite good. The data available for ethanol[6b] are for Dowex-2, which contains a 2-hydroxyethyl group instead of one methyl group in the quaternary ammonium exchange site. Because of the extra hydrogen bonding this permits, the results are not comparable with the present data.

Solvent Selectivity. The data used to construct Figures 1 and 2 also permitted the evaluation of the solvent selectivity, *i.e.*, the mole fraction of the solvent in the resin, $\bar{x}_S = \bar{n}_S/\bar{n}$ as a function of its mole fraction in the equilibrium solution, x_S. Some additional data have been obtained for a few solvents at given

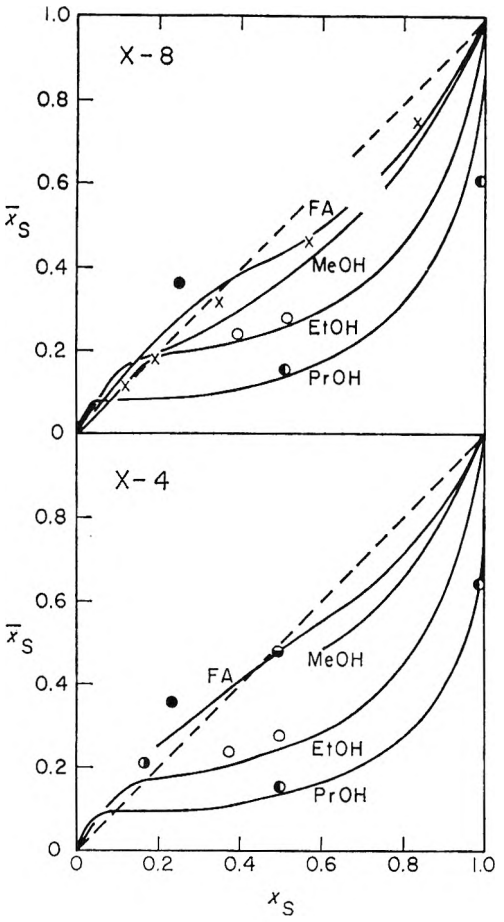

Figure 3. The solvent selectivity, $\bar{x}_S$ as a function of x_S, for chloride form resin: X8, upper part; X4, lower part. Symbols for the solvents same as Figure 1, with addition of ○, dimethylformamide; ◐, acetonitrile; ◑, urea; ◒, ethylene glycol; ●, formaldehyde.

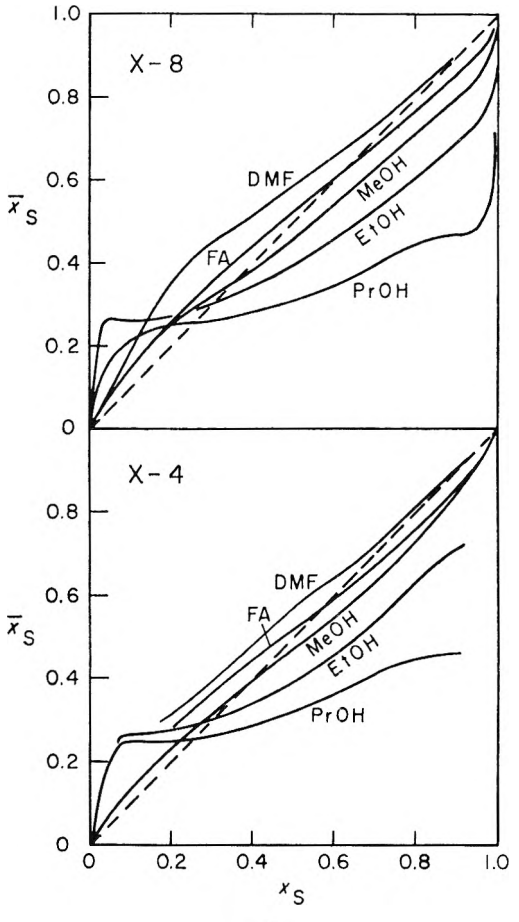

Figure 4. The solvent selectivity, $\bar{x}_S$ as a function of x_S, for perchlorate form resin; X8, upper part; X4, lower part. Symbols for the solvents same as in Figure 1.

mole fractions, *i.e.*, not over the whole composition range, and these have been shown in Figure 3 along with the other data for chloride form resin, while the data for the perchlorate form resin are shown in Figure 4. Again, the data for methanol and Dowex-1 X7.5 chloride in the literature[6c] are shown as crosses in Figure 3, in reasonable agreement with our data.

For further correlation with published data, the selectivity results for the intermediate x_S region, *i.e.*, $0.2 < x_S < 0.8$, were treated according to the empirical equation suggested by Rückert and Samuelson[6b]

$$\log ((1 - \bar{x}_S)/\bar{x}_S) = p \log ((1 - x_S)/x_S) + \log k \quad (1)$$

and the values of the parameters p and $\log k$ shown in Table II were obtained by a least-squares calculation. The values of p and $\log k$ are, of course, not independent,[6b] but the logarithmic data fit fairly well straight lines with the slopes p having the figures shown in the table, within the standard deviations shown. This procedure was used also by Rückert and Samuelson, who found for several resins (Dowex-50 and Dowex-2) and counterions (Li^+, Na^+, K^+, Cl^-, ClO_4^-, and SO_4^{2-}) with ethanol the value $p = 0.6$, nearly the same as we found for Dowex-1 X4 and X8 for chloride and perchlorate. The table shows that p is *not* sensitive to the cross-linking and the anion also for the other solvents within the stated precision, but it *is* sensitive to the solvent.

On the other hand, $\log k$, while not appreciably sensitive to the cross-linking, is sensitive to both the anion and the solvent. For all the systems $\log k$ (Cl^-) is larger than $\log k$ (ClO_4^-), for ethanol the difference being 0.28 ± 0.06. The corresponding difference for Dowex-2[6b] is 0.19, which is somewhat smaller, but nearly within the precision limits, and is certainly in the same direction.

Discussion

The behavior of several aqueous–organic solvent mixtures has been presented, but the most complete data were obtained for the alcohols, methanol, ethanol, and 1-propanol, and these will therefore be discussed first. It is expedient to discuss three composition ranges of aqueous alcohols separately: the water-rich region, up to *ca.* $x_S = 0.2$, the intermediate region, from $x_S = 0.2$ to $x_S = 0.8$, and the alcohol-rich region, above *ca.* $x_S = 0.8$.

Table II: Parameters for the Empirical Equation (1)

Solvent	Resin −X	Chloride		Perchlorate	
		p	log k	p	log k
Formamide	4	0.80 ± 0.04	0.11 ± 0.02	0.80 ± 0.04	−0.03 ± 0.03
	8	0.80 ± 0.04	0.09 ± 0.05	0.80 ± 0.04	−0.05 ± 0.01
Dimethylformamide	4			0.75 ± 0.04	−0.10 ± 0.04
	8			0.75 ± 0.04	−0.16 ± 0.01
Methanol	4	0.75 ± 0.03	0.16 ± 0.04	0.75 ± 0.03	0.09 ± 0.04
	8	0.75 ± 0.03	0.21 ± 0.04	0.75 ± 0.03	0.06 ± 0.04
Ethanol	4	0.55 ± 0.02	0.44 ± 0.04	0.55 ± 0.02	0.20 ± 0.02
	8	0.55 ± 0.02	0.46 ± 0.03	0.55 ± 0.02	0.14 ± 0.04
1-Propanol	4	0.25 ± 0.02	0.76 ± 0.05	0.25 ± 0.02	0.36 ± 0.05
	8	0.25 ± 0.02	0.74 ± 0.03	0.25 ± 0.02	0.27 ± 0.05

In the water-rich region, the unexpected result that the alcohol is preferred in the resin over water is observed (Figures 3 and 4). The phenomenon is more pronounced for the perchlorate form of the resin than for the chloride form, but resins of X4 or X8 cross-linking yield approximately the same results. The preferred sorption decreases from propanol through ethanol to methanol at the lowest alcohol concentrations, but reverses at the higher concentrations. Some results for 2-propanol and allyl alcohol with chloride-form resin show the same phenomenon of preferred sorption, even more than does 1-propanol.

The explanation for these results should lie in the structure of water and the effect of low concentrations of alcohol on it, recently discussed in detail by Franks and Ives (ref 7, p 14). Water is much less structured in the resin than in the solution, and is less structured in the tight perchlorate form resins than in the swollen chloride form resins. There is then less water–water bond breaking, and more opportunities for alcohol–water bond formation, with overall decrease in enthalpy in the less structured situations. Furthermore, the larger the hydrocarbon portion of the alcohol, the more hydrophobic bonding it causes, and the more entropy is lost in the more highly structured phase. Therefore, again, an increase in entropy results if the alcohol is transferred into the resin phase. This behavior is similar to that exhibited by large ions with negligible specific affinity to the resin fixed ions, which are pushed from the structured external solution into the resin, according to the concepts of Diamond and Whitney.[8]

The $x < 0.2$ range is, however, not a simple one to understand, and although predominantly aqueous in character, "may be structurally very wide indeed."[7] The present work does not include results at such low alcohol concentrations or temperatures that anomalous (negative) deviations from Raoult's and Henry's laws and enhancement of the water structure[9] are observed for the alcohols. It would be interesting to obtain data for the very lowest concentrations, where also the water-immiscible but partly soluble butanols could be used.

Effects other than water structure could also be supposed to cause the observed behavior. However, hydration of the ions, small as it is for the large chloride, perchlorate, and trimethylmethylene ammonium ions, need not be more important than alcoholic solvation. The alcohols have similar dipole moments and should thus have similar solvation enthalpies,[10] and a compensation between the effects on the cation, the anion, and the dispersion forces with the resin skeleton may occur. Thus, in spite of the meager knowledge of the quantitative aspects of structure in the water-rich region, it is concluded that this, rather than other effects, is primarily responsible for the observed behavior in this region.

In the intermediate composition region, where the normal structure of the water has been largely broken and replaced by small units of alcohol–water associates, the concept of solvent sorting by ions is useful,[11] superimposed on a direct interaction of the hydrocarbon parts of the solvents with the resin skeleton by dispersion forces. The resin phase can be taken to constitute the "vicinity of the ions," while the external phase is, of course, free from ions. Using our symbols in Padova's[11] eq 1, it becomes

$$[(1 - \bar{x}_S)/\bar{x}_S]/[(1 - x_S)/x_S] = 10^{\alpha} \qquad (2)$$

This is the same as our eq 1, with $\alpha = \log k$, except that our denominator has the power $p < 1$. No explanation can be offered for the values of p, although it is significant that they are independent of the resin and the ions, so that they probably are not due to selective solvation effects. Thus, the ratio of alcohol to water is lower in the resin over and beyond the ratio predicted from selective solvation. This may be due to steric effects, a point discussed further below. The α values (Table II), however, are qualitatively as expected: the span of selective solvation is larger for

(7) F. Franks and D. J. G. Ives, *Quart. Rev.*, **20**, 1 (1966).
(8) R. M. Diamond and D. C. Whitney, in "Ion Exchange," Vol. 1, J. A. Marinsky, Ed., M. Dekker, New York, N. Y., p 297.
(9) G. L. Bertrand, F. J. Millero, C. Wu, and L. G. Hepler, *J. Phys. Chem.*, **70**, 699 (1966).
(10) B. Case and R. Parsons, *Trans. Faraday Soc.*, **63**, 1224 (1967).
(11) J. Padova, *J. Phys. Chem.*, **72**, 796 (1968).

the smaller anion chloride than the larger perchlorate, and water is the more preferred the larger the alcohol.[11]

In this respect it is important to note that the rejection of the alcohol is correlated with the low total swelling in this region. Thus, plots of $\bar{n}_S$ *vs.* x_S (not shown) for ethanol, 1-propanol, 2-propanol, and allyl alcohol show plateaus in the region $0.2 < x_S < 0.8$ or even slight maxima (for the perchlorate forms of the resins). In other words, as the mole fraction of water in the external solution decreases, $\bar{n}_W$ decreases approximately linearly, while $\bar{n}_S$ remains constant. This behavior, as well as a maximum in the organic solvent content, was found also for the sorption of acetone on cation exchangers,[5c] and is shown only with solvents containing a substantial aliphatic portion, *i.e.*, not with methanol, formamide, or dimethylformamide. It is conceivable that the solvents ethanol, propanol, and allyl alcohol saturate the resin by dispersion interactions with the organic skeleton, irrespective of solvent composition. This does not explain why there are 2–3 mol of solvent per benzene ring in the chloride form of the resin, and only *ca.* 1 mol per ring for the perchlorate form, since the dispersion interactions should be the same. Again, steric effects may be responsible for this.

In the alcohol-rich region, the selectivity for water over alcohol becomes extreme. Other workers too have noted that certain solvents are not sorbed by ion exchangers unless some water is present. Thus no dioxane is sorbed on a cation exchanger unless it contains at least one mole of water per equivalent of resin.[5f] Thus, in the chloride form of the resin, where the residual water at the highest solvent concentration was still 0.3–0.6 mol/equiv, the $\bar{n}_S$ *vs.* x_S curves turned up again at the end of the plateau, whereas with the perchlorate form, where the residual water was only 0.1–0.3 mol/equiv, the curves turned downward. In this region also, the differences between the various alcohols are very pronounced (Table I). Steric effects among the isomeric alcohols may explain the lower swelling by 2-propanol, in particular if association of the alcohols is taken into account.[7] Interaction of the π electrons of the allyl alcohol with the aromatic rings may explain its relatively high swelling power.

The two amides studied, formamide and dimethylformamide, also show interesting behavior in that their total swelling curves with the perchlorate form of the resin show maxima (Figure 2), while they show only slight deviations from nonselective swelling in their mixtures with water (Figures 3 and 4 and Table II). Finally, the higher swelling of the perchlorate form of the resin by dimethylformamide than by the alcohols, compared with the opposite behavior of the chloride form of the resin, is significant. It is known[12] that aprotic dipolar solvents solvate anions the better the larger they are, so the stronger swelling of the perchlorate resin than of the chloride resin by dimethylformamide can be explained by this solvation effect. Formamide, although protic, forms weaker hydrogen bonds than do methanol and alcohols in general, and so shows the same effect. As for their aqueous solutions, they too break the structure of water and form strong associates.[13] With the chloride form of the resin, formamide behaves regularly, in a manner very similar to methanol. It probably fits into the hydrogen-bonded structure of the water, while modifying it, and competes with the water for the solvation of the chloride ion through hydrogen bonding, of which it is capable. There is thus little selectivity for either water or formamide (and even methanol) over the whole composition range. For the perchlorate form of the resin, the situation is different. Both amides solvate the perchlorate ion strongly, even more so than does water, probably by virtue of their larger dipole moment (3.86 D for dimethylformamide, 3.68 D for formamide, compared with 1.85 for water and 1.67 for methanol). As x_S increases, the quantity $\bar{n}_S$ increases more rapidly than $\bar{n}_W$ decreases, causing the maxima in the $\bar{n}$ curves in Figure 4. These are more pronounced in the altogether more highly swollen X4 resin, possibly because of the prevalence of heteromolecular associates in the intermediate composition range, which are more stable than the homomolecular associates,[13,14] and constitute the "free" solvent in the highly swollen resin. The tighter X8 resin contains only "solvating" solvent, with little "free" solvent, and in this role the molecules of the solvents act singly.

There are, of course, some subtle features in the data for total swelling (Figures 1 and 2) and selective swelling (Figures 3 and 4), which cannot be explained with the above crude factors. No quantitative theory for predicting the swelling behavior can yet be proposed. However, the data presented are consistent with our present knowledge of mixed aqueous organic solvents, their structure, and solvation properties. Further insight should be gained from the volumetric behavior of the systems studied, and experiments along this line are now in progress.

Acknowledgment. The authors wish to thank Mr. Mayo Nissim for technical help in carrying out the experiments.

(12) J. Miller and A. J. Parker, *J. Amer. Chem. Soc.*, **83**, 117 (1961); A. J. Parker, *Quart. Rev.*, **16**, 163 (1962); A. J. Parker, *J. Chem. Soc., A*, 220 (1966).

(13) B. E. Geller, *Zh. Fiz. Khim.*, **35**, 1105 (1961); T. M. Ivanova and B. E. Geller, *ibid.*, **35**, 1221 (1961); W. Kangro, *Z. Physik. Chem.*, **32**, 273 (1962); J. A. Rupley, *J. Phys. Chem.*, **68**, 2002 (1964)

(14) E. N. Vasenko, *Dokl. Lvovsk. Politekh. Inst.*, **1**, 84 (1955).

Low-Temperature Oxygen Atom Addition to Olefins. III. Transition State and the Reaction with *cis*- and *trans*-2-Butenes[1]

by Milton D. Scheer and Ralph Klein

National Bureau of Standards, Washington, D. C. 20234 *(Received August 5, 1968)*

The reaction of ground-state oxygen atoms O(^{3}P), with either *cis*- or *trans*-2-butene at cryogenic temperatures produces *cis*- and *trans*-2,3-epoxybutane, 2-butanone, and isobutyraldehyde. Product ratios are different for the two 2-butenes. Two precursor states, one leading to the *trans* epoxide and 2-butanone, and the other to the *cis* epoxide and isobutyraldehyde, are implied by the constancy of the ratios *trans*-2,3-epoxybutane/2-butanone and *cis*-2,3-epoxybutane/isobutyraldehyde. A new transition state for the O atom–olefin reaction is proposed. A prediction based on the new transition state for the O atom reaction with 2-methyl-2-butene was consistent with the experimental finding.

Results of observations on the reaction of O atoms with condensed olefins at low temperatures were given in the two previous papers of this series.[2,3] Products of the low-temperature reaction with propene, butene-1, and *cis*- and *trans*-2-butene were shown to be the same as those of the higher temperature gas phase results obtained by Cvetanovic[4] exclusive of degradation products. Under the higher temperature conditions they arise from fragmentation of "hot" oxygen adducts and at lower temperatures from ozonolysis when ozone is present. Cracking products can be eliminated under either condition of operation. In the present work, the reactions of O atoms with *cis*- and *trans*-2-butene are examined in considerable detail. Some of the previously developed concepts, particularly those relating to the transition state intermediate, require modification to be consistent with the results. Using a new model, prediction of the course of the reaction with 2-methyl-2-butene was made and verified experimentally.

The products of the O atom–2-butene reaction are *trans*- and *cis*-2,3-epoxybutane, 2-butanone, and isobutyraldehyde. The ratios are different for *trans*-2-butene as compared to the *cis*-2-butene. There is also a temperature dependence and from its analysis the equilibrium constant for the transformation *cis*-2,3-epoxybutane $\rightleftharpoons$ *trans*-2,3-epoxybutane can be calculated.

Experimental Section

The apparatus used to obtain these results has been described previously.[2,3] The olefins were diluted with propane for the 77 and 90°K experiments and with 2-methylbutane and *n*-butane at 113°K. Boiling liquid nitrogen (77°K), oxygen (90°K), and melting isopentane (113°K) were used as the cryogenic baths for maintaining isothermal conditions in the vessel and at the reactant film. Gas chromatographic product analyses were obtained using a 2 m long, 6 mm diameter column, containing 2,4-dimethylsulfolane on chromosorb W.

The reaction rates of films containing the 2-butenes were found to be zero order in olefin concentration. This is the same as the previously reported results[3] for propene and 1-butene. Such observations suggest that the oxygen atoms easily penetrate hydrocarbon films. We are concerned here with the chemical reactions rather than the diffusion processes, however.

Table I gives the fractional yields of the four products obtained with *trans*- and *cis*-2-butene at several temperatures. It is noteworthy that starting with *trans*-2-butene, over 90% of the products from the 77°K reaction are *trans*-2,3-epoxybutane and 2-butanone. Even at 113°K they constitute about 85% of the products. It is of considerable interest that the ratio of *trans*-2,3-epoxybutene to 2-butanone is about 0.8 independent of whether the reactant olefin is *cis*- or *trans*-2-butene. The gas phase result of about 1.0 is not sufficiently different to cast doubt on the conclusion that *trans-2,3-epoxybutane and 2-butanone originate from the same precursor state.* The data also imply that *cis*-2,3-epoxybutane and isobutyraldehyde have a common origin. Therefore, in the reaction of O with 2-butene, *two precursor states are formed, one leading to trans-2,3-epoxybutane and 2-butanone, and the other to cis-2,3-epoxybutane and isobutyraldehyde.* A pictorial representation embodying these criteria is shown in Figure 1a and b for *cis*- and *trans*-2-butene reactants.

Representation of the Precursor State. The representation of the precursor or transition state in the O atom reaction with olefins has previously been given as a triplet free radical with localized spins.[5] For *trans*-2-

(1) Supported by the U. S. Public Health Service.

(2) A. N. Hughes, M. D. Scheer, and R. Klein, *J. Phys. Chem.*, **70**, 798 (1966).

(3) R. Klein and M. D. Scheer, *ibid.*, **72**, 616 (1968).

(4) R. J. Cvetanović, *Advan. Photochem.*, **1**, 115 (1963).

(5) R. J. Cvetanović, *J. Chem. Phys.*, **25**, 376 (1956).

Table I: Fractional Product Yields for the Reaction between $O(^3P)$ and *cis*- and *trans*-C_4H_8-2 in the 77–300°K Temperature Range

Reactant	T, °K	*trans*-2,3-Epoxybutane	*cis*-2,3-Epoxybutane	Isobutyraldehyde	2-Butanone
trans-C_4H_8-2	77	0.51	0.03	0.04	0.42
trans-C_4H_8-2	90	0.50	0.06	0.07	0.37
trans-C_4H_8-2	113	0.50	0.09	0.07	0.34
trans-C_4H_8-2	300[a]	0.33	0.15	0.21	0.31
cis-C_4H_8-2	77	0.29	0.26	0.20	0.25
cis-C_4H_8-2	90	0.30	0.24	0.21	0.25
cis-C_4H_8-2	113	0.35	0.23	0.15	0.27
cis-C_4H_8-2	300[a]	0.26	0.25	0.23	0.26

[a] Gas phase. These results are from R. J. Cvetanović, *Advan. Photochem.*, **1**, 115 (1963).

butene this would be

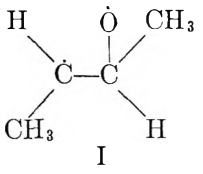

I

The O atom, it is assumed, has added to one of the two carbons of the double bond. It was postulated that in unsymmetrical double bonds, the addition is favored on the least-substituted carbon. This is, of course, not relevant to the 2-butenes. The triplet intermediate then transforms to ground state compounds by ring closure to form the epoxide, or by migration of one of the groups on the O bearing carbon to the carbon with the free electron. On the basis of the data previously at hand, the precursor state (I) provided an adequate rationale for the products observed in the O atom–olefin reaction. At 300°K, the differences between the *cis*- and *trans*-2-butene with O atom reactions were not striking. It did not appear to require any significant modifications of the intermediate state from I in the *cis*-2-butene reaction. There was only weak maintenance of configuration as deduced from product analysis. The intermediate formed might also be shown in the *cis* form

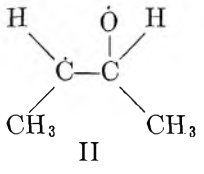

II

as opposed to I with the *trans* representation. Ring closure and migration must be postulated as competitive with the transformation I ⇋ II involving rotation about the 2,3 C–C bond since there is a difference in the *cis*-2,3-epoxybutane/*trans*-2,3-epoxybutane ratios for the two 2-butene isomers.

The low-temperature results, indicating emphatically that *trans*-2,3-epoxybutane and 2-butanone have one precursor and *cis*-2,3-epoxybutane and isobutyraldehyde another, require a reformulation of the precursor states. The 2-butene molecule has a planar skeletal structure with orbitals perpendicular to the plane. It has been suggested that in the initial act, the approach of the O atom is in a direction perpendicular to the plane. The olefinic bond is transformed to a single bond type. A triplet radical with a completed C–O bond and unpaired electrons localized as shown in I or II results. This model presents several difficulties. Transformation to final products requires a spin-forbidden transition. Compared to rotation about the central C–C pair, changes such as the processes of ring closure or H or CH_3 migration, with their change of multiplicity, would be expected to be considerably slower. On this basis identical products would be obtained regardless of whether the 2-butene reactant was *cis* or *trans*. That this is not the case for the O atom addition to the condensed olefins in the cryogenic temperature region is readily seen from Table I. The gas-phase results at 300°K do not show the striking difference in the products of the *cis* compared with *trans*; nevertheless, there is still a distinction. In all cases it is found that rotation about the C–C axis to give a configurational change does occur. The process of ring closure and group migration particularly in the low-temperature ranges are at least as efficient as the rotation.

Assuming I to be the precursor to the *trans*-2,3-epoxybutane and II to *cis*-2,3-epoxybutane, it could not be inferred from the appropriate three-dimensional models why I should be the precursor for 2-butanone and II should be the precursor for isobutyraldehyde, as the experimental evidence demands. It would appear that the transition state (or precursor) in the O atom

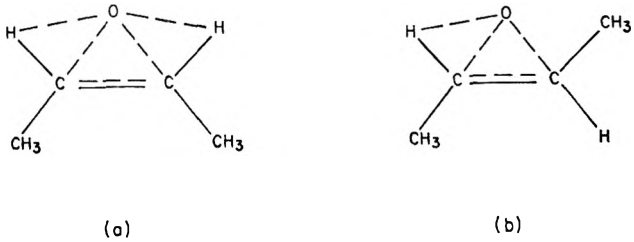

(a) (b)

Figure 1. Transition states in the reaction of $O(^3P)$ with: (a) *cis*-2-butene; (b) *trans*-2-butene.

addition to an olefin as represented by I or II need be abandoned. The formulation of a structure which satisfactorily accounts for the low as well as the higher temperature observations follows.

(1) The initial approach of the O atom to the olefinic bond is considered to be in the plane of the molecule rather than perpendicular to it. A reorganization of the electronic structure commences, but there appears to be no *a priori* reason why the uncoupled electrons need be localized.

(2) An interaction between the O atom and any neighboring H atoms bonded to an olefinic carbon occurs. This is to be interpreted as not hydrogen bonding in the usual sense, but a loosely bound structure involving O and H. A pictorial representation embodying these criteria is shown in Figure 1a and b for *cis*- and *trans*-2-butene reactants. Two additional "rules" have to be postulated. (I) Interconversion between (a) and (b) must occur to a limited extent; that is rotation in the complex about C···C is allowed. (II) in the case of a migrating group, if there is a choice between H and CH_3, the H rather than CH_3 migrates. This requirement arises from the fact that in the low-temperature reaction with *trans*-2-butene, the principal products are *trans*-2,3-epoxybutane and 2-butanone. It is tempting to generalize with the specification that the ease of migration is inversely related to the mass of the migrating group, but this awaits the development of observations on other molecules.

The passage from the precursor state to final products, apart from interconversion between precursor states, requires electronic and spatial rearrangements. The four carbons and the two secondary C–H group hydrogens are coplanar in 2-butene. This is not the case for either 2-butanone or isobutyraldehyde. In 2,3-epoxybutane, the COC ring is in a plane perpendicular to the original 2-butene skeletal moiety. The concept of two precursor states, one for the epoxide and the other for the aldehyde or ketone, is interesting since correlation could be made with the geometry of the approach of the O atom. That perpendicular to the 2-butene plane could be associated with epoxide formation, and parallel with aldehyde or ketone formation. Because the *cis*-2-butene results show that *trans*-2,3-epoxybutane is formed, together with its associated 2-butanone in a constant ratio for the temperature employed, regardless of starting isomer, the concept of one precursor for the epoxide and another for the carbonyl is not tenable.

Consideration of the rotation about the central C–C bond in the precursor state whereby (a) and (b) are interconverted (Figure 1) is of considerable interest insofar as reaction enthalpy release rate is concerned. Clearly equilibrium among the isomeric forms is not established, for the *cis* and *trans* epoxide are formed in comparable quantities from the *cis*-2-butene whereas the *trans* oxide is formed preponderantly from *trans*-2-butene. Increase of initial temperature from 77 to 300°K changes the ratio of the *cis* to the *trans* isomers, as derived from either of the 2-butenes. The enthalpy release in the process $O + C_4H_8 \rightarrow C_4H_8O$ is about 4×10^5 J. Any effects of ambient temperature should be quite negligible if the isomer ratio were dictated by this heat. The conclusion is that the rotation about the C–C bond leading to isomerization occurs either before any appreciable enthalpy is released, or the heat transfer from the molecule to its matrix is rapid compared to the rotational process. The latter is considered unlikely. On the other hand, formation of the aldehyde or ketone requires breaking of a C–C or a C–H bond, an energetically costly process. The inference is strong that these processes occur during the period of the change from precursor to final products, while rotation is associated solely with the precursor state.

The reaction between an oxygen atom and 2-butene is represented by eq 1 and 2. The mechanism below includes the provision of interconversion of intermediates. Starting with *trans*-2-butene and the as-

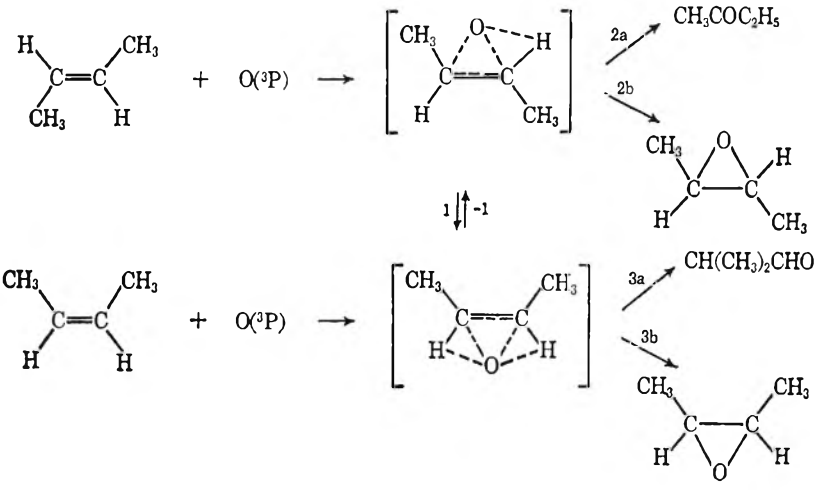

(1)

(2)

sumption of a steady state for the intermediates, there is obtained

$$\left(\frac{trans\ \text{epoxide}}{cis\ \text{epoxide}}\right)_{trans\text{-2-butene}} = \frac{k_{2b}}{k_1}\left(1 + \frac{k_{-1} + k_{3a}}{k_{3b}}\right) \quad (3)$$

The *cis*-2-butene as reactant yields

$$\left(\frac{cis\ \text{epoxide}}{trans\ \text{epoxide}}\right)_{cis\text{-2-butene}} = \frac{k_{3b}}{k_{-1}}\left(1 + \frac{k_1 + k_{2a}}{k_{2b}}\right) \quad (4)$$

The ratio of rates of isomerization of the precursor to ring closure, that is the formation of the epoxide, is readily calculated from (3) and (4). If the left side of (3) is designated as A and of (4) as B, then k_1/k_{2b}, the ratio of the rate of isomerization of the *trans* intermediate to the rate of formation of the *trans*-2,3-epoxybutane, is

$$\frac{B(1 + D) + C + 1}{AB - 1}$$

where C and D are k_{2a}/k_{2b} and k_{3a}/k_{3b}, respectively. A, B, C, and D are experimentally determined quantities. The corresponding expression for k_{-1}/k_{3b} is

$$\frac{A(1 + C) + D + 1}{AB - 1}$$

Figures 2 and 3 give the Arrhenius plots for these rate

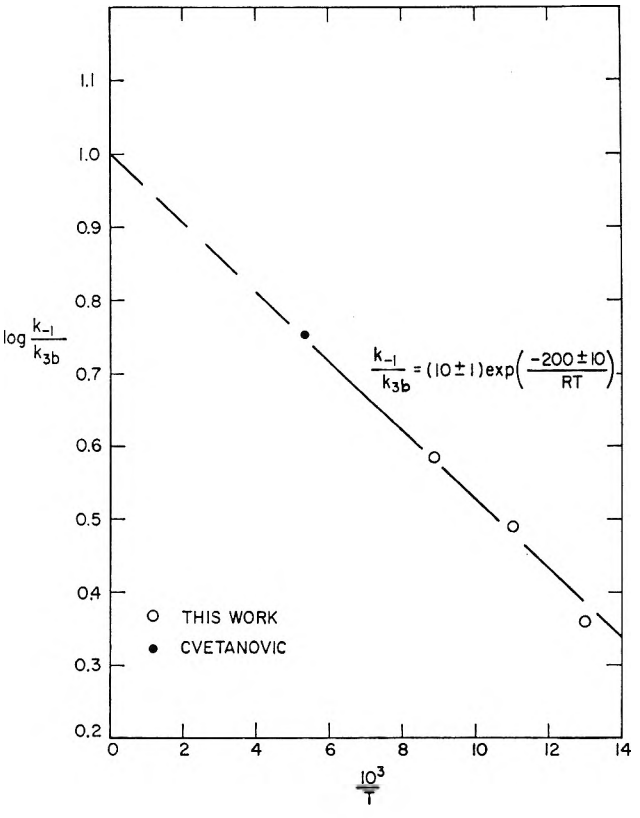

Figure 2. Arrhenius plot for relative rates of rotation to epoxide formation from the *trans* complex.

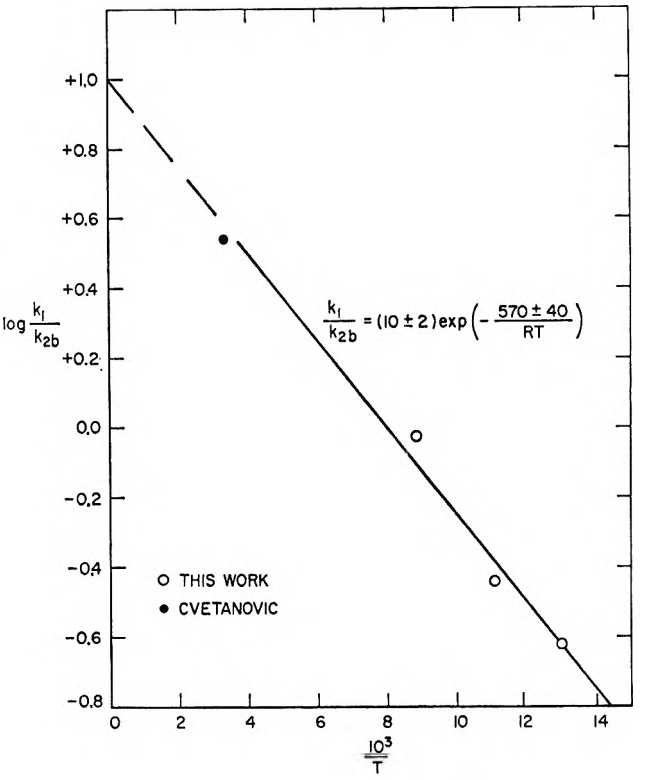

Figure 3. Arrhenius plot for relative rates of rotation to epoxide formation from the *cis* complex.

constant ratios. The results are represented by

$$\frac{k_{-1}}{k_{3b}} = (10 \pm 1)\ \exp\left[\frac{-200 \pm 10}{RT}\right] \quad (5)$$

$$\frac{k_1}{k_{2b}} = (10 \pm 1)\ \exp\left[\frac{-570 \pm 40}{RT}\right] \quad (6)$$

Uncertainties are standard errors of the reported values based on a least-squares treatment of the data. Both ratios approach 10 at high temperatures. An estimate can be made of the equilibrium *trans*-2,3-epoxybutane $\rightleftharpoons$ *cis*-2,3-epoxybutane. This is $k_1k_{3b}/k_{2b}k_{-1}$ if it is assumed that k_{2b} and k_{3b} are approximately equal. Thus

$$k_{eq} = \exp\left[\frac{-370}{RT}\right]$$

with an indicated zero entropy change and an endothermic enthalpy of 1549 J/mol[6] for the process *trans*- to *cis*-epoxide. The *trans*-2,3-epoxybutane is slightly more stable than its *cis* analog.

The transition state model for the O atom reaction with olefins deduced here from a number of observations on the *cis* and *trans*-2-butene systems can, at least in one instance, be tested. For the reaction between O and 2-methyl-2-butene, the new precursor state repre-

(6) Corresponds to 370 cal/mol.

sentation would be

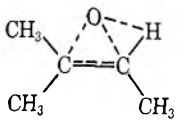

It would be predicted, therefore, that the principal carbonyl product would be dimethylpropionaldehyde. The localized triplet state model

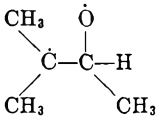

(III)

would lead to the prediction that 3-methyl-2-butanone would be the major product. The reaction between $O(^3P)$ and 2-methyl-2-butene was effected at 90°K with propane as a diluent in a ratio of 10 to 1. The products were 2,3-epoxy-2-methylbutane, dimethylpropionaldehyde, and 3-methyl-2-butanone. The ratio of dimethylpropionaldehyde to 3-methyl-2-butanone was found to be approximately 4 to 1. The results decisively verify the prediction based on the transition-state model proposed here.

Summary

The reaction of ground-state oxygen atoms with *cis*- or *trans*-2-butene at low temperatures yields *cis*- and *trans*-2,3-epoxybutane, 2-butanone, and isobutyraldehyde. These occur in different proportions depending on whether the *cis*- or the *trans*-2-butene is the reactant. The ratio of *trans*-2,3-epoxybutane to 2-butanone is constant as is that of *cis*-2,3-epoxybutane to isobutyraldehyde. A new model of the precursor or transition state for the $O(^3P)$–olefin reaction is proposed. The model correctly predicted that dimethylpropionaldehyde would be the main carbonyl product in the O atom addition to 2-methyl-2-butene.

The Influence of Micelles on Titrations of Aqueous Sodium and Potassium Soap Solutions[1a]

by Myron E. Feinstein[1b] and Henri L. Rosano

Department of Chemistry, The City College of the City University of New York, New York, New York 10031
(Received August 8, 1968)

Sodium and potassium caprate, laurate, and myristate solutions below and above the critical micelle concentration were titrated with HCl. The cationic activity (H^+, Na^+, K^+) was monitored during the titrations using a pH glass electrode and a cationic glass electrode. The curves of pH *vs.* HCl added can be theoretically calculated for these systems from equilibrium considerations. The simultaneous monitoring of H^+ and K^+ activity during the course of a titration of a micellar laurate solution leads to the conclusion that H^+ ions compete with K^+ ions at the negatively charged micelle–solution interface. The effect of charged interfaces on the ionic distribution is discussed in terms of the apparent surface concentrations of counterions.

Introduction

In a previous publication,[2] it has been shown that when a micellar potassium laurate solution is titrated with HCl the titration curve looks like a titration curve of a diacid. The interpretation of this result was based on the marked influence of molecular aggregate surfaces (*i.e.*, soap micelles) on the bulk pH. In another publication,[3] using cationic glass electrodes, it was established that the potassium ion activity is lowered in micellar soap solutions. The interpretation advanced was that the charged micelle–solution interface depletes the bulk concentration of potassium ion.

In the present study, it was decided to expand the previously advanced interpretation by simultaneously monitoring the activity of the hydrogen and potassium ions while titrating potassium soap solutions.

Lucassen has investigated the hydrolysis and precipitates in potassium carboxylate solutions.[4] We have used a similar theoretical approach to interpret our titration curves. Although this equilibrium treatment quantitatively describes the systems studied it does not provide an adequate qualitative physical description.

Experimental Section

The soap solutions were prepared by neutralizing a weighed amount of the melted fatty acid with a known

(1) (a) Submitted in partial fulfillment of the thesis requirement for the Ph.D. of M. E. F.; presented at the Symposium on Colloidal Electrolytes, 154th National Meeting of the American Chemical Society, Chicago, Ill., Sept 1967; (b) Unilever Research Laboratory, Port Sunlight, Chesire, England.

(2) (a) H. L. Rosano, K. Breindel, J. H. Schulman, and A. J. Eydt, *J. Colloid Interface Sci.*, **22**, 58 (1966); (b) H. L. Rosano and M. E. Feinstein, *Rev. Franc. Corps Gras*, **13**, 661 (1966).

(3) M. E. Feinstein and H. L. Rosano, *J. Colloid Interface Sci.*, **24**, 73 (1967).

(4) J. Lucassen, *J. Phys. Chem.*, **70**, 1824 (1966).

excess of the appropriate standardized base and diluted with distilled water. The capric (C_{10}), lauric (C_{12}), and myristic (C_{14}) acids were all highest grade purity obtained from Eastman Organic Chemicals, Rochester, N. Y. Fifty milliliters of a soap solution in a beaker (with a water jacket maintained at constant temperature, ±0.1°) placed on a magnetic stirrer were titrated with HCl. A Thomas Combination pH electrode (No. 4858 L-60, A. H. Thomas Co., Philadelphia, Pa.) and a Cationic glass electrode (Beckman No. 39137, Beckman Instruments, Inc., Fullerton, Calif.) in conjunction with a Photovolt Model 110 electronic pH meter (Photovolt Corp., New York, N. Y.; readability ±0.02 pH unit or ±1 mV) was used to determine the pH (or $-\log a_{Na}$ or $-\log a_K$) after each addition of acid.

Results

The titration curves of nonmicellar solutions of K caprate, K laurate, and K myristate are shown in Figure 1. Those for Na caprate, Na laurate, and Na

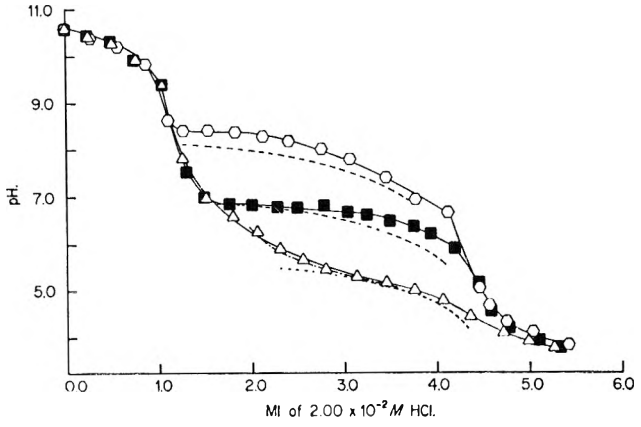

Figure 1. Titrations of nonmicellar soap solutions (excess base present) at 29.4°; pH *vs.* ml of 2.00 × 10^{-2} *M* HCl added; potassium ion concentration = 1.74 × 10^{-3} *M*; long-chain anion concentration = 1.00 × 10^{-3} *M*: △, K caprate; ■, K laurate; ◇, K myristate.

myristate were found to be identical, within the experimental error, with the potassium series and are, therefore, not shown. In all cases the concentration of the cation is 1.74 × 10^{-3} *M* and that of the long-chain anion is 1.00 × 10^{-3} *M*. Fifty milliliters of each soap solution was titrated at 29.4° with 2.00 × 10^{-2} *M* HCl.

In the titrations of the laurate and myristate soap solutions a precipitate was first noted at approximately 1.25 ml of HCl added. X-Ray analysis[5] indicated that the precipitate was fatty acid. In the titrations of the caprates the solutions remained clear until approximately 3.20 ml of HCl was added, at which point capric acid commenced precipitation.

In Figure 2 two titrations of micellar soap solutions

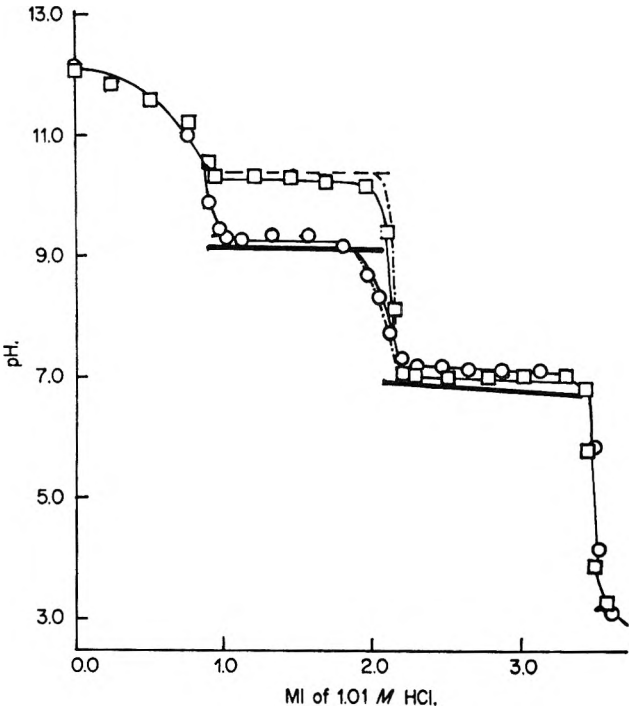

Figure 2. Titrations of 50.00 ml of micellar soap solutions (excess base present) at 29.4°; pH *vs.* ml of 1.01 *M* HCl added; potassium ion concentration = 6.97 × 10^{-2} *M*; long-chain anion concentration = 5.00 × 10^{-2} *M*: ○, K laurate; □, K myristate.

are shown. One is the titration of a potassium laurate solution (open circles) with the potassium ion concentration equal to 6.97 × 10^{-2} *M* and the laurate ion concentration equal to 5.00 × 10^{-2} *M;* the other is a titration of a potassium myristate solution (open squares) with ionic concentrations identical with those of the potassium laurate solution. In both titrations the initial solutions were clear. Upon adding HCl the pH decreased until the appearance of a precipitate in the solutions. Along this plateau of pH *vs.* HCl added the precipitates were analyzed and found to be 1:1 acid soap–potassium acid laurate

$$\left(\begin{matrix}CH_3(CH_2)_{10}COO^-K^+\\ CH_3(CH_2)_{10}COOH\end{matrix}\right)_n$$

or potassium acid myristate

$$\left(\begin{matrix}CH_3(CH_2)_{12}COO^-K^+\\ CH_3(CH_2)_{12}COOH\end{matrix}\right)_n$$

Upon further addition of acid the pH again fell and a new plateau was reached. The precipitate was analyzed along this plateau and found to be a mixture of 1:1 acid soap and free fatty acid—with the percentage of fatty acid increasing at the expense of the acid soap as more HCl was added. At the end of the titration the only precipitate present was the free acid.

Figure 3 shows a titration of a micellar K laurate solution in which the potassium ion concentration is

(5) F. Ryer, *Oil Soap*, **23**, 310 (1946).

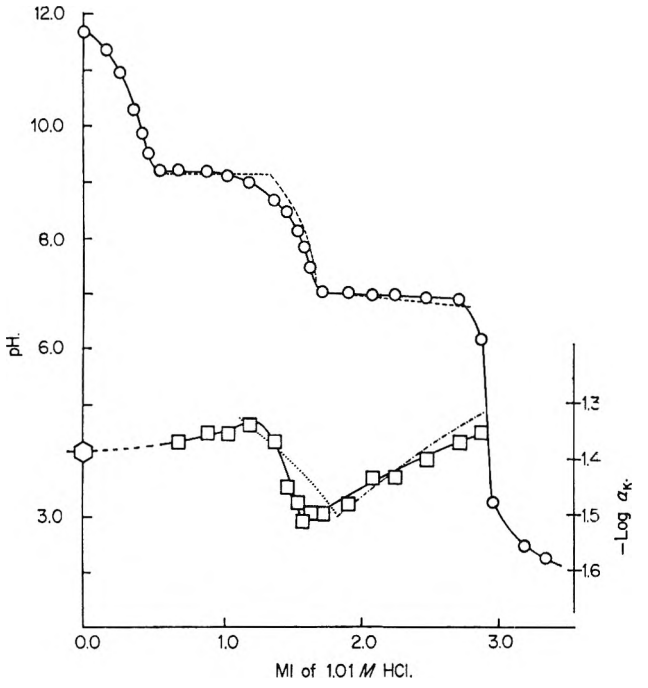

Figure 3. Titration of 50.00 ml of a micellar K laurate solution (excess base present) at 29.0°; potassium ion concentration = 6.01×10^{-2} M; laurate ion concentration = 5.00×10^{-2} M: ○, pH *vs.* ml of 1.01 M HCl added; □, $-\log a_K$ *vs.* ml of 1.01 M HCl added.

equal to 6.01×10^{-2} M and the laurate ion concentration is equal to 5.00×10^{-2} M. The description of this titration is the same as that for the one in Figure 2 (open circles) except that a cationic glass electrode was used to monitor the potassium ion activity (plotted as the negative logarithm) at the same time that a glass electrode was used to record the pH.

Theory

Recently, Lucassen[4] has presented a quantitative equilibrium interpretation of hydrolysis in fatty acid soap solutions; theoretical pH was calculated as a function of the concentration of potassium carboxylate present. It was demonstrated that pH measurements give a simple method for evaluating the composition and solubility parameters of the precipitates formed in soap solutions—fatty acid, acid soap, or neutral soap. We have adapted this treatment, here, for our solutions of potassium and sodium soaps and have, instead, calculated the theoretical pH as a function of the degree of acidification of the soap solution.

I. Nonmicellar Soap Solutions. A. Precipitate of Fatty Acid. The titrations of nonmicellar soap solutions containing excess base are shown in Figure 1. It has been previously noted that a precipitate of fatty acid is formed in each case. It is the fatty acid solubility which determines the height of the pH plateaus in the figure.[4] The less soluble the fatty acid, the lower is the hydrogen ion concentration tolerated in the solution (resulting in a higher pH plateau).

We represent the fatty acid dissociation equilibrium by

$$\frac{C_H C_Z}{C_{HZ}} = K_A \tag{1}$$

where C_H, C_Z, and C_{HZ} represent the concentration in solution of hydrogen ions, fatty acid anions, and fatty acid molecules, respectively, and K_A is the dissociation constant of the fatty acid.

The condition for electroneutrality of the solution is

$$C_M + C_H = K_w/C_H + C_Z + XC_t + G \tag{2}$$

where C_M is the concentration of alkali metal cations in solution; $K_w = C_H C_{OH}$ = ionization constant of water; C_t is the total amount of soap present in moles per unit volume; X is the molar ratio between added hydrochloric acid and total amount of soap (therefore has values from 0 to 1); XC_t, therefore, represents the concentration of chloride ions added to the solution as a consequence of acidification of the soap with HCl; and G is the concentration of chloride ions added to the solution in neutralizing the excess base present with HCl.

In all our soap solutions an excess of base was originally present. Since the fatty acid precipitate contains no metal ions, we may write

$$C_t = KC_M \tag{3}$$

where K is a constant smaller than 1. The concentration of fatty acid molecules in the solution equals the solubility of the fatty acid (S_{HZ}), and therefore

$$C_{HZ} = S_{HZ} \tag{4}$$

When eq 1, 3, and 4 are substituted in the equation for the electroneutrality of the solution (2) the result is

$$C_H = \frac{K_w + K_A S_{HZ}}{C_t(1/K - X) + C_H - G} \tag{5}$$

In Figure 1

$$C_t = 1.00 \times 10^{-3}\ M$$

$$1/K = 1.74$$

$$G = 7.4 \times 10^{-4}\ M$$

For the cases of the myristates and the laurates since $C_t(1/K - X) \geq 7.4 \times 10^{-4}$ and $C_H < 10^{-6}$ (pH is always greater than 6 for these cases—see Figure 1, and X can never be greater than 1) we can write $C_H \ll C_t(1/K - X)$, and taking negative logarithms in eq 5 we obtain

$$\text{pH} = -\log(K_w + K_A S_{HZ}) + \log[10^{-3}(1.74 - X) - 7.4 \times 10^{-4}] \tag{6}$$

When the values for K_w, K_A, and S_{HZ} are sub-

stituted in eq 6

$$K_w = 1.47 \times 10^{-14} \quad \text{(given at 30°)}^6$$
$$K_A = 1.25 \times 10^{-5}$$
$$S_{HZ} = 1.05 \times 10^{-5} \quad \text{for } C_{12} \text{ acid}$$
$$= 5.25 \times 10^{-7} \quad \text{for } C_{14} \text{ acid}$$

(where it is assumed that the values of the dissociation constant of the fatty acid, K_A, and the solubility of the fatty acid, S_{HZ}, reported by Lucassen[4] for 20° are valid in our systems containing excess base and maintained at 29.4°) K_w (1.47×10^{-14}) is seen to be $\ll K_A S_{HZ}$ (1.31×10^{-10} for C_{12}, 5.51×10^{-12} for C_{14}). Therefore, from eq 6 we obtain

$$\text{pH} = 8.18 + \log(1 - X) \quad \text{for myristate} \qquad (7)$$

$$\text{pH} = 6.88 + \log(1 - X) \quad \text{for laurate} \qquad (8)$$

Equations 7 and 8 provided theoretical values of pH as a function of the degree of acidification (X from 0 to 1) drawn in Figure 1 as a dashed line.

For the case of caprate[4] $S_{HZ} = 2.09 \times 10^{-4}$ and again $K_w \ll K_A S_{HZ}$ ($1.47 \times 10^{-14} \ll 2.61 \times 10^{-9}$); eq 5 becomes

$$C_H = \frac{(1.25 \times 10^{-5})(2.09 \times 10^{-4})}{10^{-3}(1.00 - X) + C_H} \qquad (9)$$

Equation 9 provided the theoretical values of pH as a function of acidification for the caprate case drawn in Figure 1 as a dashed line.

B. No Precipitate is Present. In the titrations of the caprates it was previously noted that a precipitate of capric acid did not form until approximately 3.20 ml of HCl was added. Consequently, to predict pH as a function of the degree of acidification up to the point where a precipitate starts to form, a different equation was used which is valid for the case when no precipitate is present.

In this case

$$C_t = C_Z + C_{HZ} \qquad (10)$$

and eq 1, 2, 3, and 10 combine to give

$$C_t = \frac{(K_w - C_H^2 + GC_H)(K_A + C_H)}{C_H[(1/K - X)C_H + K_A(1/K - X - 1)]} \qquad (11)$$

but $K_w \ll C_H^2$ (*e.g.*, at pH 6, $C_H^2 = 10^{-12}$ and $K_w = 1.47 \times 10^{-14} \ll 10^{-12}$) and $K_w \ll GC_H$ (*e.g.*, at pH 6, $GC_H = (7.4 \times 10^{-4})(10^{-6}) = 7.4 \times 10^{-10}$ and $K_w = 1.47 \times 10^{-14} \ll 7.4 \times 10^{-10}$) and substituting the values given above for the caprate cases

$$10^{-3} = \frac{(-C_H^2 + 7.4 \times 10^{-4} C_H)(1.25 \times 10^{-5} + C_H)}{C_H[(1.74 - X)C_H + 1.25 \times 10^{-5}(0.74 - X)]} \qquad (12)$$

Equation 12 provided values of pH as a function of the degree of acidification, X, when no precipitate was present (alternately dashed and dotted line in Figure 1).

In our treatment of nonmicellar soap solutions, activity coefficients have been omitted since the solutions were dilute (the order of magnitude of the concentrations was 10^{-3} M). Moreover, discrepancies between the theory and experimental results may be due, in part, to using S_{HZ} and K_A values which were given[4] at 20°.

II. Micellar Soap Solutions. The titration curves of the micellar soap solutions in Figures 2 and 3 exhibit two plateaus when pH is plotted as a function of added acid.[2b] The plateau at the higher pH is due to the coexistence of micelles and acid soap and the plateau at the lower pH results from the conversion of acid soap to free fatty acid. In the systems studied here, only 1:1 acid soap was formed, and it is therefore apparent that after half of the total number of long-chain anions in micellar form have been neutralized (along the plateau at higher pH), the conversion of micelles to acid soap is complete, and any further addition of acid results in converting the monomeric long-chain anions (the critical micelle concentration) to acid soap. At half neutralization of the soap all the carboxylate anions are in the form of acid soap and upon adding more HCl a new equilibrium is established between acid soap and free fatty acid.

A. K Laurate—Coexistence of Micelles and Acid Soap. In laurate solutions for the case where soap micelles coexist with acid soap (plateau at higher pH), the relevant equilibria are represented by

$$C_M C_H C_Z^2 = K_{MHZ_2} \qquad (13)$$

where K_{MHZ_2} is the solubility product of the 1:1 acid soap, and[7]

$$0.57 \log C_M + \log C_Z = -2.617 \qquad (14)$$

Equations 13 and 14 can be combined to give

$$-\log C_H = \text{pH} = -\log K_{MHZ_2} + \log C_M C_Z^2$$
$$= -\log K_{MHZ_2} - 5.234 - 0.14 \log C_M \qquad (15)$$

For potassium acid laurate[4] $K_{MHZ_2} = K_{KHL_2} = 6.31 \times 10^{-15}$ and eq 15, therefore, becomes

$$\text{pH} = 8.97 - 0.14 \log C_M \qquad (16)$$

Since C_M is of the order of 10^{-2} the pH is approximately 9.2, as observed (*e.g.*, Figure 2, open circles). Moreover, eq 16 shows that pH is not very sensitive to changes in C_M, indicating a pH plateau. C_M, however, is the concentration of metal cations in solution ("unbound") and is unknown. In order to calculate theoretical pH for the laurate case in Figure 2, eq 13

(6) "Handbook of Chemistry and Physics," 44th ed, The Chemical Rubber Publishing Co., Cleveland, Ohio, 1962, p 1752.

(7) M. L. Corrin and W. D. Harkins, *J. Amer. Chem. Soc.*, **69**, 683 (1947).

and 14 were combined with the equation of electroneutrality (2) to give

$$10^{-37.4}\left(\frac{C_H}{K_{MHZ_2}}\right)^{7.15} + C_H = \frac{K_w}{C_H} + 10^{18.7}\left(\frac{K_{MHZ_2}}{C_H}\right)^{4.075} + XC_t + G \quad (17)$$

Since $C_H \approx 10^{-9}$, the terms C_H and K_w/C_H can be neglected. With the value of K_{MHZ_2} given above, and $C_t = 5.00 \times 10^{-2}$ and $G = 1.97 \times 10^{-2}$, eq 17 provided the pH values (by successive approximations) plotted in Figure 2 (heavy solid line) for values of the degree of acidification, X, from 0 to 0.5.

B. K Laurate—Coexistence of Acid Soap and Fatty Acid. Along the plateau where acid soap and fatty acid coexist (plateau at lower pH), eq 1 and 13 are substituted in the equation for the condition of electroneutrality (2) and the following equation is obtained

$$K_{MHZ_2}C_H^2 = (K_A S_{HZ})^2[K_w + K_A S_{HZ} + XC_H C_t + GC_H - C_H^2] \quad (18)$$

However, $K_w(1.47 \times 10^{-14})$, $K_A S_{HZ}[(1.25 \times 10^{-5}) \times (1.05 \times 10^{-5}) = 1.31 \times 10^{-10}]$, and $C_H^2(\simeq 10^{-14})$ are all considerably smaller than $XC_H C_t[X(10^{-7}) \times (5 \times 10^{-2})]$ so that taking negative logarithms and rearranging yields

$$\text{pH} = \log K_{MHZ_2} - 2\log K_A S_{HZ} - \log (XC_t + G) \quad (19)$$

Equation 19 provided the values of pH as a function of X (from 0.5 to 1) plotted, along the plateau at lower pH, in Figure 2 as a heavy solid line.

C. K Myristate. For the case of micellar solutions of K myristate containing excess base, the pH along the plateau where micelles are converted to acid soap is calculated by combining eq 13 (with $K_{MHZ_2} = K_{KHM_2} = 1.58 \times 10^{-17}$), (2), and[4]

$$\log C_Z + 0.57 \log C_M = -3.22 \quad (20)$$

The equation which results, after neglecting negligibly small terms, provides pH values as a function of X from 0 to 0.5 (dashed line in Figure 2)

$$7.6 \times 10^{74.5}(C_H)^{7.15} - \frac{1.29 \times 10^{-44.3}}{(C_H)^{4.07}} - 0.394 = X \quad (21)$$

For the plateau corresponding to the conversion of potassium acid myristate to myristic acid, eq 19, with the appropriate values of K_{MHZ_2}, K_A, and S_{HZ} for the myristate case, gives the same values of pH for values of X from 0.5 to 1 as the laurate case (heavy solid line along lower pH plateau).

Figure 2 illustrates that the plateau at pH 7 is longer than the plateau at pH 9.2 or 10.5; this is because at the higher pH micelles are converted to acid soap and then, with the micellar phase gone and a degree of freedom thus gained, the pH decreases as the monomers are converted to acid soap. It is, therefore, not expected that micelles are converted to acid soap in the range X (degree of acidification of the soap) from 0 to 0.5, but rather in some smaller range (*viz.* all the micelles are converted to acid soap before the point $X = 0.5$ is reached). The difference between the end of the plateau at higher pH and the beginning of the one at lower pH represents the critical micelle concentration. This is much smaller in the case of K myristate than in the case of K laurate (which has a higher critical micelle concentration).

The drop in pH between the two plateaus can also be predicted from equilibrium considerations. After all the micelles have been converted to acid soap, the only other long-chain species present is ionized soap monomers. The amount of long-chain anion in the acid soap precipitate is, therefore, equal to $C_t - C_Z$. The amount of alkali metal cation in the acid soap is equal to the total analytical concentration minus the amount still in solution or, $C_t/K - C_M$. In the acid soap there are two long-chain anions for every alkali metal cation and therefore

$$2\left(\frac{C_t}{K} - C_M\right) = C_t - C_Z \quad (22)$$

Equations 2, 13, and 22 were solved by successive approximations to provide values of pH as a function of the degree of acidification, X, in the range where the pH rapidly falls ($X < 0.5$). These theoretical values have been drawn in Figure 2 as alternately dashed and dotted lines for the cases of K laurate and myristate.

Activity coefficients for the hydrogen ion were not available for solutions of the compositions and concentrations studied here, and therefore the negative logarithm of the hydrogen ion concentration was equated to pH. Despite this, and the fact that Lucassen's values of K_A, K_{MHZ_2}, and S_{HZ} (given at 20°) were used for our systems (at 29.4°), the agreement of the theory with the experimental results is, nevertheless, good.

III. Titrations Using a Cationic Glass Electrode. A. Nonmicellar Soap Solutions. Glass electrodes have been used to determine the activity of potassium and sodium ions in micellar and nonmicellar surfactant solutions.[3,8,9] Cationic glass electrodes have glass

(8) L. Shedlovsky, C. W. Jakob, and M. B. Epstein, *J. Phys. Chem.*, **67**, 2075 (1963).

(9) J. S. Stanley and J. A. Radley, *Proc. 3rd Int. Congr. Surface Activity, Cologne*, **I**, 246 (1960).

compositions which make them selective for a variety of cations other than the hydrogen ion. The theory describing the response of these specific ion glass electrodes is the same as that for the common pH responsive glass electrode.[10]

For the titrations of sodium laurate and myristate and potassium laurate and myristate (Figure 1) the use of a cationic glass electrode revealed no change in activity of the cation throughout the course of the titration (emf of the cationic electrode *vs.* an Ag–AgCl electrode did not change by more than ±1 mV). This was not done for the caprate cases because low pH prohibited the use of the cationic glass electrode (interference from hydrogen ion). A cationic glass electrode was, however, used in the titration (excess base present) of a potassium caprate solution ($[K^+] = 1.98 \times 10^{-2}$ *M*, $[\text{caprate}^-] = 1.85 \times 10^{-2}$ *M*) and a sodium caprate solution ($[Na^+] = 8.68 \times 10^{-2}$ *M*, $[\text{caprate}^-] = 7.53 \times 10^{-2}$ *M*) where X-ray analysis revealed capric acid as the only precipitate, and again the activity of the cation was found to remain constant throughout the titrations (the pH plateau of these titrations did not fall below 6).

In all the above mentioned titrations the use of a cationic glass electrode confirmed the fact that fatty acid was the only precipitate, for if acid soap or neutral soap precipitated one would have detected a decrease in the bulk cation activity.

B. Micellar Laurate Solution. Figure 3 shows a titration of a micellar K laurate solution in which the potassium and hydrogen ion activities were monitored simultaneously. The dashed curve of pH as a function of HCl added was derived from the same equations (*mutatis mutandis*) used for the titrations shown in Figure 2. It is noted that using either eq 16 (with our experimental a_K values substituted for C_M) or eq 17, the calculated value of pH at the first plateau is the same—9.16. For this titration the cationic electrode was calibrated with KCl solutions at pH 7 and was used in the soap solution between pH 5 and pH 9 where it was assumed the KCl calibration was valid.

We note that when all the long-chain anions have been converted to acid soap ($X = 0.5$, ~ 1.75 ml of HCl added), it is expected that the maximum amount of potassium ions would have been removed from the solution and indeed the potassium ion activity is seen to be at a minimum here. As potassium acid laurate is converted to lauric acid (plateau at pH ~7), the potassium ions are returned to the bulk solution and the activity increases until the maximum is reached when all the laurate is in the form of lauric acid.

The theory outlined in the foregoing text was used to predict the curve of cation activity ($-\log a_K$) *vs.* added acid. Equations 1, 13, and 2 were combined to give values of C_M ($= C_{K^+}$) as a function of X (from 0.5 to 1) as acid soap is converted to lauric acid. With the negligibly small terms omitted this equation is (with $C_t = 5.00 \times 10^{-2}$ and $G = 1.01 \times 10^{-2}$, Figure 3)

$$C_M - \frac{4.81 \times 10^{-5}}{C_M} - 1.01 \times 10^{-2} = (5 \times 10^{-2})X \qquad (23)$$

At the end of the titration in Figure 3, the concentration of potassium ions is

$$\left(\frac{50.0 \text{ ml}}{52.9 \text{ ml}}\right)(6.01 \times 10^{-2}\ M) = 5.69 \times 10^{-2}\ M$$

$\gamma_\pm$ for 5.69×10^{-2} *M* KCl is[11] 0.808, and this value was used to obtain values of $-\log a_K$ ($= -\log C_{K^+}\gamma_\pm$) from the values of C_M calculated from eq 23 (X from 0.5 to 1, pH ~7). This calculated variation of $-\log a_K$ with X is shown in Figure 3 as a dashed and dotted line.

Equations 2, 13, and 22 were solved by successive approximations to provide values of $-\log C_M$ as a function of X (dotted line) in the range where $-\log a_K$ rapidly falls ($X < 0.5$). The agreement between theory and experiment is poor here presumably because in the pH range 7–9 the approximation that $-\log C_{K^+}$(theory) $= -\log a_K$(experiment) is too gross (no $\gamma_\pm$ values are available). In any event, the theoretical equations (dotted, and dotted and dashed lines) give the same type of curve as the experimental results shown in Figure 3.

The open hexagon in Figure 3 indicates the measured activity of potassium ions in the K laurate solution with no HCl added (pH 11.70; the cationic electrode was calibrated with KOH for this measurement) and the dashed line ($-\log a_K$ *vs.* ml of HCl added) indicates how the potassium ion activity must increase as HCl is added to the solution and the hydrogen ions displace the potassium ions from the micelle–solution interface.

No experimental points are given for $-\log a_K$ *vs.* ml of HCl added for pH's between 11.7 and 9.1. In this region the cationic electrode cannot be calibrated with KOH (calibration is valid for potassium ion activity measurements made at high pH) or KCl (calibration is valid for potassium ion activity measurements made in the pH range near 7) alone. It should be mentioned that, in general, mean activity coefficients of potassium ion are larger for KOH solutions of a given concentration than for KCl solutions of the same concentration.[11] Therefore, in a solution of constant potassium ion concentration one would expect the potassium ion activity ($a = C\gamma_\pm$) to *decrease* slightly as the pH was changed from 11.7 to 9.1.

(10) G. Eisenman, "Advances in Analytical Chemistry and Instrumentation," Vol. 4, Interscience Publishers, New York, N. Y., 1965, p 213.

(11) H. S. Harned and B. B. Owen, "The Physical Chemistry of Electrolytic Solutions," 3rd ed, Reinhold Publishing Corp., New York, N. Y., 1958, p 594.

During the course of the titration shown in Figure 3, the emf of the cationic electrode *vs.* the reference electrode (Ag/AgCl) *increased* slightly in this pH range. This indicates that the bulk activity of potassium ion is increasing in this region (because $a = C\gamma_{\pm}$ and $\gamma_{\pm}$ is known to decrease in this region; since a increases, C (concentration of potassium ion) must be increasing.

This fact (slight increase in bulk potassium ion concentration in the pH region 11.7 to 9.1) and the fact that the potassium ion activity does not decrease steadily as soon as acid soap precipitate begins to form (pH 9.1) indicates that a compensating effect is operating. Potassium ions are released into the bulk of the solution from the charged interfaces as the micelles are destroyed (converted to acid soap) and potassium ions are removed from the solution by the formation of the acid soap precipitate. Consequently, $-\log a_K$ of the solution does not change drastically until most of the micelles are destroyed (see Figure 3).

Conclusions

Although a valid quantitative description of hydrolysis in potassium soap solutions has been given by Lucassen[4] (wherein the pH of a partially acidified potassium soap solution was determined from the soap concentration), little qualitative description was offered. Rosano, *et al.*,[2] on the other hand, gave a qualitative description of titrations of soap solutions but did not attempt to give a theoretical quantitative description of their systems. It has been shown, in the present work, that Lucassen's treatment (*i.e.*, equilibrium considerations) can be adapted to predict pH as a function of acidification for micellar and nonmicellar solutions containing excess base (and that, in the case of nonmicellar soap solutions, this treatment is valid for both potassium and sodium soaps).

In our titrations of micellar solutions of potassium laurate and myristate, we have found both the quantitative treatment of Lucassen and the qualitative description of Rosano, *et al.*, are valid (Figures 2 and 3). For example, as acid is added to a micellar potassium laurate solution (Figure 3), hydrogen ions displace potassium ions from around the negatively charged micelles and the bulk potassium ion activity increases. When potassium acid laurate begins to precipitate (bulk pH $\sim$10.3), it indicates that the surface hydrogen ion concentration around the micelles has reached a certain critical value at which lauric acid can form. This lauric acid formed at the micelle surface precipitates as a 1:1 acid soap. Since the micelles are converted stoichiometrically to acid soap, this is, in fact, a surface titration. As previously noted, the fact that the plateau at this pH is shorter than the one at lower pH indicates that the concentration of hydrogen ions near the micelle surface must be greater than that in the bulk solution—the monomers in the solution are precipitated as acid soap only *after all the micelles have been neutralized.* It is therefore just as natural to attribute the buffering action of a micellar soap solution to a surface effect[2] as it is to interpret it on the basis of solubilities of the precipitates present.[4]

The pH at the lower plateau in Figure 2 is determined by the solubilities of the coexisting precipitates (fatty acid and acid soap). Equation 19 predicts the same pH for a micellar potassium laurate or myristate solution of the same concentration. This is because the longer the chain length of the anion the less soluble is the acid and the corresponding acid soap. The first two logarithmic terms on the right in eq 19 change with the chain length of the anion in such a way as to just compensate each other and the resulting pH is the same whether the system is laurate or myristate.

The validity of pH measurements in colloidal solutions has been questioned[12] and the data in the present work are open to similar criticism. The presence of ionized soap micelles in solution may be expected to affect both the liquid junction potential (between solution and reference)[12] and the ionic activity coefficients. The fundamental questions raised concerning these effects are not discussed here. The authors feel, however, that the lack of quantitative information for evaulating the effects should not preclude the experimental testing of existing theory.

The technique of simultaneous monitoring of cation activities during a titration of a micellar solution affords a method of obtaining a qualitative (as well as quantitative) physical picture of what occurs at the interfaces in solution and provides an illustration of the competition of counterions at a charged interface.

Acknowledgment. The authors wish to thank Dr. E. D. Goddard and Mr. F. Ryer of Lever Brothers Company—Dr. Goddard for his helpful discussions and Mr. Ryer for his X-ray analyses. We also wish to acknowledge the financial support of the City College Research Fund.

(12) H. R. Kruyt, "Colloid Science," Vol. I, Elsevier Publishing Co., New York, N. Y., 1952, pp 184–193.

On the Second Virial Coefficient of Real Gases

by Aleksander Kreglewski

Department of Chemical Engineering, The Ohio State University, Columbus, Ohio 43210 *(Received August 12, 1968)*

The second virial coefficients of gases were evaluated by using the formerly developed principle of corresponding states.[1] The intermolecular potential energy curve was expressed by means of a two-step square-well potential with one empirical parameter. The remaining constants of the potential, assumed to be universal constants, were derived from the properties of liquid and gaseous argon or methane. Satisfactory agreement with experimental data for all elements and compounds, also in presence of weak donor–acceptor interactions, proves the usefulness of the new principle. A table of values of the energy of vaporization (E^*) and liquid molar volume (V^*) at the reduced temperature $T/T^c = 0.6$ is given for 127 elements and compounds.

Introduction

In a recent paper,[1] evidence was presented that for molecules larger than methane the configurational energy in the liquid, as well as the pair potential in the gas, is proportional to the force constant ϵ/k and to the surface of the molecules. Accordingly, for a gas composed of large molecules, the Boltzmann factor can be expressed as a function of E^*/RT or $T^c(V^*)^{1/3}/T$, where E^* and V^* are the energy of vaporization and liquid molar volume, respectively, at the reduced temperature $T/T^c = 0.6$.

According to the classical principle of corresponding states, valid for small molecules (*i.e.*, smaller than the size of methane), this factor is a function of either E^*/RT or T^c/T. Thus, the second virial coefficient β of both small and large molecules can be expressed as a function of E^*/RT.

The calculations based on the cell model[2] imply that small molecules are much "softer" than the large ones, that is, the intermolecular repulsion varies less rapidly with distance than for large molecules. However, the square-well potential fits the data on β for argon[3] better than any other potential. Also, for a correct evaluation of the effects of size differences in mixtures it is necessary to assume that small molecules are rigid spheres[4] (van der Waals approximation). An attempt was therefore made to obtain a universal expression for β based on the square-well potential. It was found earlier[1] that the "packing factor" b in the relation $\frac{2}{3}\pi N\sigma^3 = bV^*$ is not constant but varies with temperature if the remaining constants are evaluated from the properties of the liquid state (eq 5 and 6). The simplest way to eliminate the temperature dependence of b, while retaining the simplicity of the square-well potential, is to divide the well into two steps as shown in Figure 1. The width of the first deep step is $s_0\sigma_0$ and the depth of the second shallow step is $s\bar{u}/k$. It was found empirically that the two constants s_0 and s are interrelated (eq 3c) and one common constant suffices for practical purposes.

The second virial coefficient is given by

$$\beta = -2\pi N \int_0^\infty (e^{-u/kT} - 1) r^2 dr \tag{1}$$

where u/k is the pair potential and r is the intermolecular distance. For the two-step potential it becomes

$$\frac{\beta}{bV^*} = 1 - (\Re_1 - 1)(e^{-u/kT} - 1) - (\Re_2 - \Re_1) \times (e^{-su/kT} - 1) \tag{2}$$

where

$$\Re_1 = \left(1 + \frac{s_0\sigma_0}{\sigma}\right)^3 = \left[1 + \frac{s}{(V^*)^{1/3}}\right]^3 \tag{3a}$$

$$\Re_2 = \left(1 + \frac{\sigma_0}{\sigma}\right)^3 = \left[1 + \left(\frac{V_0^*}{V^*}\right)^{1/3}\right]^3 \tag{3b}$$

$$s = s_0(V_0^*)^{1/3} \tag{3c}$$

Since the pair potential is constant in the respective ranges of distances, u/k in eq 2 is identical with $\bar{u}/k$ and can be expressed by the relations

$$-\frac{u}{kT} = \frac{\rho E^*}{RT} \tag{4a}$$

or

$$-\frac{u}{kT} = \rho_c \frac{T^c}{T}\left(\frac{V^*}{V_0^*}\right)^{1/3} \tag{4b}$$

where ρ and ρ_c are constants and V^* is divided by the universal constant V_0^* to operate with dimensionless parameters.

(1) A. Kreglewski, *J. Phys. Chem.*, **72**, 1897 (1968).

(2) T. M. Reed, III, and M. D. McKinley, *J. Chem. Eng. Data*, **9**, 553 (1964).

(3) A. E. Sherwood and J. M. Prausnitz, *J. Chem. Phys.*, **41**, 429 (1964).

(4) T. W. Leland, J. S. Rowlinson, and G. A. Sather, to be published.

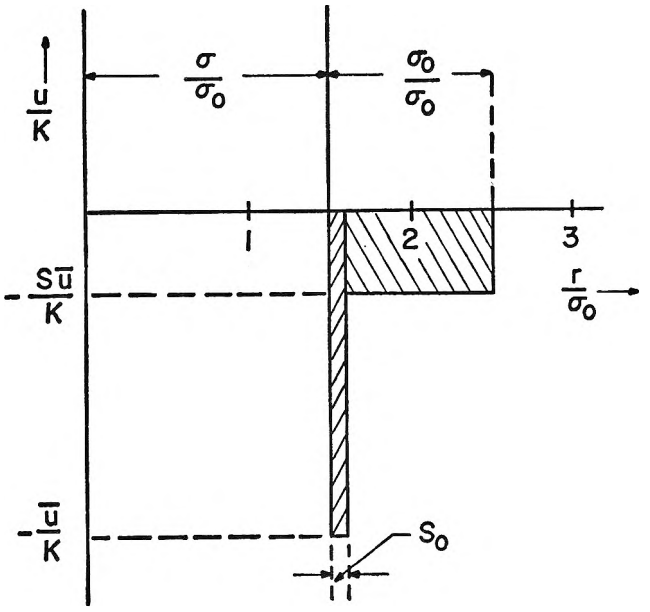

Figure 1. The two-step potential as function of normalized distance r/σ_0 (for $s = 0.21$, $s_0 = 0.21/3.373 = 0.062$, and $\sigma/\sigma_0 = 1.5$).

Determination of the Constants of Eq 2

The data on liquid state imply that the significant range of pair interaction does not exceed the diameter σ of methane.[1] Present calculations based on the data on β for methane, n-pentane, and benzene[5] confirm that this is nearly the optimum value. Therefore we set

$$(V_0^*)^{1/3} = 3.373 \text{ cm}/(\text{mol})^{1/3} \qquad (5)$$

The constant ρ was evaluated from the limiting slope of configurational energy U_0 of liquid methane (or argon) when $T \rightarrow 0°K$. The data given by Rowlinson[6] imply a linear relation of U_0/RT against E^*/RT with a slope[1] equal to 1.426; however, they extend over a limited temperature range. A more realistic value may be obtained by using Theisen's relation[7] which yields a slope equal to 1.60 for both Ar and CH_4. Guggenheim and McGlashan[8] evaluated U_0 of liquid argon near the triple point by assuming additivity of pair potentials and found that the number of nearest neighbors is $z = 10$. Hildebrand and coworkers[9] found from the radial distribution function of xenon near the normal boiling point that $z = 8.5$. This value should approach 9.5 near the triple point and a rounded value of $z = 10$ was adopted. Since in a dilute gas a molecule may have at most one nearest neighbor ($z_0 = 1$), we have $U_0/(zR) = \frac{1}{2}u/k$, that is, the coefficient relating u/k to E^*/R at low densities of the system is 1.60/5, or

$$\rho = 0.32 \qquad (6)$$

Sinanoglu[10] estimated recently that the deviations from the additivity of pair potential weaken the interaction energy in liquid, slightly in argon, but significantly in carbon tetrachloride. Linder[11] stated that in general all types of London interactions are temperature dependent and accordingly a more proper relation would be $-u/k = \rho E^*/R + \gamma T$. We retain, however, the crude approximation that $\gamma = 0$, that the pair potential is additive, as well as the above value of ρ for all molecules.

The value of $\rho_c = (\rho E^*/RT^c)[(V_0^*/V^*)^{1/3}]$ can be found from the properties of any liquid which follows the new principle of corresponding states. The data for methane, n-pentane, and benzene (Table I) yield 1.438, 1.443, and 1.410, respectively, with a mean value of

$$\rho_c = 1.430 \qquad (7)$$

The values of b and s were initially adjusted on a computer to the data for methane, n-pentane, and benzene and found to be variable. It is plausible however, that the parameter s has a common value for all substances and one may set the rounded value (obtained for CH_4)

$$s = 0.21 \qquad (8)$$

The parameter b was then related to T^c on the assumption that the degree of packing of the molecules is proportional to the force of interaction. By using the data on β for methane, pentane, and benzene, the following approximate relations were obtained[12,13]

$$b = 0.77 + 0.0595\left[\frac{E^*}{(V^*)^{1/3}}\right]^{1/3} \qquad (9)$$

$$b = 0.77 + 0.1325(T^c)^{1/3} \qquad (10)$$

Equation 10, when applied to mixtures, yields correct values of pseudocritical volumes. The rigid-sphere model requires that $\sigma_{12} = \frac{1}{2}(\sigma_{11} + \sigma_{22})$. For $T_{12}^* < (T_1^c + T_2^c)/2$ (positive deviations from an ideal mixture), V_{12}^* increases above the arithmetic mean of the molar volumes of the components at the given reduced temperature.

Comparisons with Experimental Data

The constants E^* and V^* were evaluated by the methods described previously[1] for the 127 elements and compounds listed in Table I. For any of them a value of liquid density and enthalpy of vaporization ($H^v = E^v + RT$), measured at a temperature close to $T/T^c =$

(5) All the experimental data and the values, calculated from PVT data, are given by Sherwood and Prausnitz.[3]

(6) J. S. Rowlinson, "Liquids and Liquid Mixtures," Butterworth & Co., Ltd. London, 1959.

(7) For references and application of Theisen's relation see ref 1.

(8) E. A. Guggenheim and M. L. McGlashan, *Mol. Phys.*, **3**, 571 (1960).

(9) J. H. Hildebrand and R. L. Scott, "Regular Solutions," Prentice-Hall, Inc., Englewood Cliffs, N. J., 1962.

(10) O. Sinanoglu, *Advan. Chem. Phys.*, **12**, 283 (1967).

(11) B. Linder, *ibid.*, **12**, 225 (1967).

(12) The value of the "packing factor" may depend on the shape of molecules. This effect is later discussed for neopentane as an example. For a detailed study of this effect see J. W. Leach, P. S. Chappelear, and T. W. Leland, *Proc. Amer. Petroleum Inst.*, **26**, 223 (1966); *A.I.Ch.E. J.*, **14**, 568 (1968).

(13) Neon still follows the above relations, whereas the data for ^4He and H_2 indicate that $b \rightarrow 0$ when $T^c \rightarrow 0$.

Table I: Values of Critical Temperature, Configurational Energy, and Liquid Molar Volume at Reduced Temperature $T/T^c = 0.6$[a]

	T^c, °K	E^*, J/mol	V^*, cc/mol	$(V^*)^{1/3}$
Hydrogen (normal)	33.25	750	28.3	3.046
Neon	44.45	1,510	16.61	2.551
Argon	150.72	5,640	29.14	3.077
Krypton	209.41	7,760	35.31	3.281
Xenon	289.75	10,850	43.0	3.505
Nitrogen	126.26	5,020	34.34	3.250
Oxygen	154.75	5,940	28.26	3.046
Fluorine	144.2	5,800	34.36	3.251
Chlorine	417.2	(17,810)	46.28	3.590
Carbon monoxide	132.92	5,460	35.06	3.273
Carbon dioxide	304.19	16,780	33.87	3.235
Sulfur dioxide	430.65	23,040	43.51	3.517
Nitric oxide (NO)	180.3	13,980	22.06	2.805
Nitrous oxide (N_2O)	309.58	14,950	(36.6)	3.321
Water	647.3	36,560	19.02	2.670
Methane	190.55	7,120[e]	38.38[e]	3.373
Ethane	305.43	13,240	54.87	3.800
Propane	369.81	17,390	74.54	4.208
n-Butane	425.16	21,250	93.77	4.543
n-Pentane	469.49	25,040	110.4	4.797
n-Hexane	507.30	28,670	132.8	5.102
n-Heptane	540.14	32,270	152.4	5.341
n-Octane	568.75	35,610	172.3	5.564
n-Nonane	593.5	38,990	192.1	5.770
n-Decane	617.6	42,160	212.3	5.965
2-Methylpropane	408.13	20,140	94.95	4.562
2-Methylbutane	460.39	23,790	113.4	4.840
Neopentane	433.75	21,820	114.9	4.861
2-Methylpentane	497.45	27,430	133.0	5.104
3-Methylpentane	504.4	27,590	131.5	5.085
2,2-Dimethylbutane	488.73	25,570	132.75	5.101
2,3-Dimethylbutane	499.93	26,600	131.6	5.086
2,2,4-Trimethylpentane	543.89	31,230	172.0	5.561
Cyclopentane	511.65	25,570	95.86	4.577
Methylcyclopentane	532.73	27,860	116.3	4.881
Ethylcyclopentane	569.5	31,550	135.5	5.137
Cyclohexane	553.45	28,540	113.5	4.841
Methylcyclohexane	572.12	(30,170)	135.3	5.134
Ethylcyclohexane	609.	(33,860)	154	5.361
cis-Decalin	702.15	42,340	172.8[b]	5.570
trans-Decalin	686.95	41,420	177.1[b]	5.616
Acetylene	308.33	16,410	(40.2)	3.427
Ethylene	283.1	12,110	49.31	3.667
Propylene	365.1	16,910	68.21	4.086
1-Butene	419.6	20,630	87.11	4.433
Benzene	562.09	27,750	93.97	4.546
Toluene	591.72	31,910	113.9	4.847
Ethylbenzene	617.09	34,890	133.1	5.106
n-Propylbenzene	638.30	(38,270)	153.1	5.350
o-Xylene	630.25	35,970	131.5	5.085
m-Xylene	616.97	35,620	133.1	5.106
p-Xylene	616.15	35,390	133.8	5.114
1,3,5-Trimethylbenzene	637.28	(39,420)	152.3	5.340
Naphthalene	748.35	41,650	142.7	5.226
Phenol	694.25	44,890	(97.8)	4.607
o-Cresol	697.55	44,890	(115.8)	4.874
m-Cresol	705.75	47,690	(117.2)	4.894
p-Cresol	704.55	47,790	(117.1)	4.893
Dimethyl ether	400.1	19,950	62.23	3.963
Diethyl ether	466.70	25,990	101.7	4.668
Methyl ethyl ether	437.9	23,570	81.3	4.331
p-Dioxane	587.2	34,270	(91.2)	4.502
Methyl alcohol	512.58	34,240	41.2	3.455
Ethyl alcohol	516.25	38,870	59.36	3.901
n-Propyl alcohol	536.71	42,790	77.23	4.259
n-Butyl alcohol	562.93	(46,530)	96.36	4.584
n-Pentyl alcohol	586.2	(49,740)	114.6	4.857
2-Propanol	508.32	42,420	77.55	4.264
2-Butanol	547.73	45,970	95.75	4.575
sec-Butyl alcohol	535.95	45,070	95.09	4.564
t-Butyl alcohol	506.15	43,610	95.56	4.572
Methyl formate	487.2	26,350	61.50	3.947
Ethyl formate	508.5	29,150	81.57	4.337
n-Propyl formate	538.1	31,240	101.1	4.659
Methyl acetate	506.9	30,400	80.53	4.318
Ethyl acetate	523.3	32,230	100.7	4.652
n-Propyl acetate	549.4	35,190	120.5	4.939
n-Butyl acetate	(579)	...	(140.5)	5.198
Isobutyl acetate	(565)	(37,570)	(140.4)	5.197
Methyl propionate	530.6	32,280	99.58	4.635
Acetone	508.10	28,030	74.71	4.212
Methyl ethyl ketone	535.65	30,690[c]	92.99	4.530
Diethyl ketone	560.95	...	111.4	4.812
Ammonia	405.6	21,130	25.16	2.930
Methylamine	430.2	24,180	44.09	3.533
Dimethylamine	437.8	25,380	65.21	4.025
Trimethylamine	433.3	21,700	94.95	4.562
Ethylamine	456.5	26,740	63.95	3.999
Diethylamine	496.65	28,630	104.6	4.712
Triethylamine	535.15	32,190	144.2	5.244
Aniline	698.8	42,340	102.3	4.677
N-Methylaniline	701.7	45,030	121.79	4.957
N,N-Dimethylaniline	687.6	(44,710)	141.48	5.211
Pyridine	620.0	33,000	87.73	4.443
Acetonitrile	548	30,190	55.00	3.803
Nitromethane	588.2	32,310[d]	(57.5)	3.860
Hydrogen sulfide	373.6	16,240	36.07	3.304
Methyl mercaptan	469.95	22,080	54.50	3.791
Ethyl mercaptan	499	24,750	74.73	4.212
Carbon disulfide	552	23,070	63.22	3.984
Thiophene	579.35	29,100	84.20	4.383
Perfluoromethane	227.55	11,090[e]	52.32	3.740
Perfluoroethane	293.2	15,800[e]	(81.5)[e]	4.336
Perfluoropropane	345.05	19,130[e]	109.0[e]	4.781
Perfluoro-*n*-butane	386.35	23,700[e]	137.8[e]	5.165
Perfluoro-*n*-pentane	420[f]	(28,420)[e]	164.7[e]	5.482
Perfluoro-*n*-hexane	447.65	32,500[e]	194.0[e]	5.789
Perfluoro-*n*-heptane	474.75	(35,320)	221.1	6.047
Perfluoro-*n*-octane	500[f]	...	249.1	6.292
Perfluorocyclobutane	388.37	(23,650)	115.2	4.865
Perfluoromethylcyclohexane	486.75	32,840	194.03	5.789
Trifluoroacetic acid	491.28	...	76.72	4.249
Sulfur hexafluoride	318.70	17,410	(68.3)	4.088
Hydrogen chloride	324.56	14,230	31.12	3.146
Hydrogen bromide	363.2	15,300	38.50	3.377
Hydrogen iodide	424.2	16,950	46.98	3.608
Methyl chloride	416.25	19,440	50.68	3.701
Methyl bromide	467.2	21,410	55.46	3.813

Table I (*Continued*)

	T^c, °K	E^*, J/mol	V^*, cc/mol	$(V^*)^{1/3}$		T^c, °K	E^*, J/mol	V^*, cc/mol	$(V^*)^{1/3}$
Methyl iodide	528	(25,340)	64.25	4.005	Ethyl chloride	460.4	22,880	70.18	4.125
Methylene dichloride	510	25,820	65.22	4.025	Ethyl bromide	503.8	24,530	75.56	4.228
					Monofluorobenzene	560.09	30,010	98.83	4.623
Chloroform	536.3	26,640	83.23	4.3€6	Monochlorobenzene	632.4	33,540	111.2	4.808
Carbon tetrachloride	556.4	28,010	101.6	4.6€6	Monobromobenzene	670.2	35,720	116.70	4.887

[a] Unless otherwise indicated, the following sources of experimental or smoothed data for T^c, E^*, and V^* were used: "Selected Values of Properties of Hydrocarbons and Related Compounds," American Petroleum Institute Research Project 44, Thermodynamics Research Center, Texas A & M University, College Station, Texas; ref 14; "Landolt-Börnstein Zahlenwerte und Funktionen," Vol. II, Part 2, Springer-Verlag, Berlin, 1960; J. Timmermans, "Physico-chemical Constants of Pure Organic Compounds," Vol. I (1950), Vol. II (1965), Elsevier Publishing Co., Amsterdam; R. C. Reid and T. K. Sherwood, "The Properties of Gases and Liquids," McGraw-Hill Book Co., New York, N. Y., 1966. [b] W. F. Seyer and C. H. Davenport, *J. Amer. Chem. Soc.*, **63**, 2425 (1941). [c] J. K. Nickerson, K. A. Kobe, and J. J. McKetta, *J. Phys. Chem.*, **65**, 1037 (1961). [d] J. P. McCullough, D. W. Scott, R. E. Pennington, and G. Waddington, *J. Amer. Chem. Soc.*, **76**, 4791 (1954). [e] Based on the sources given in ref 1 and calculated by using new values of T^c from ref 14. [f] Correlated value of T^c.

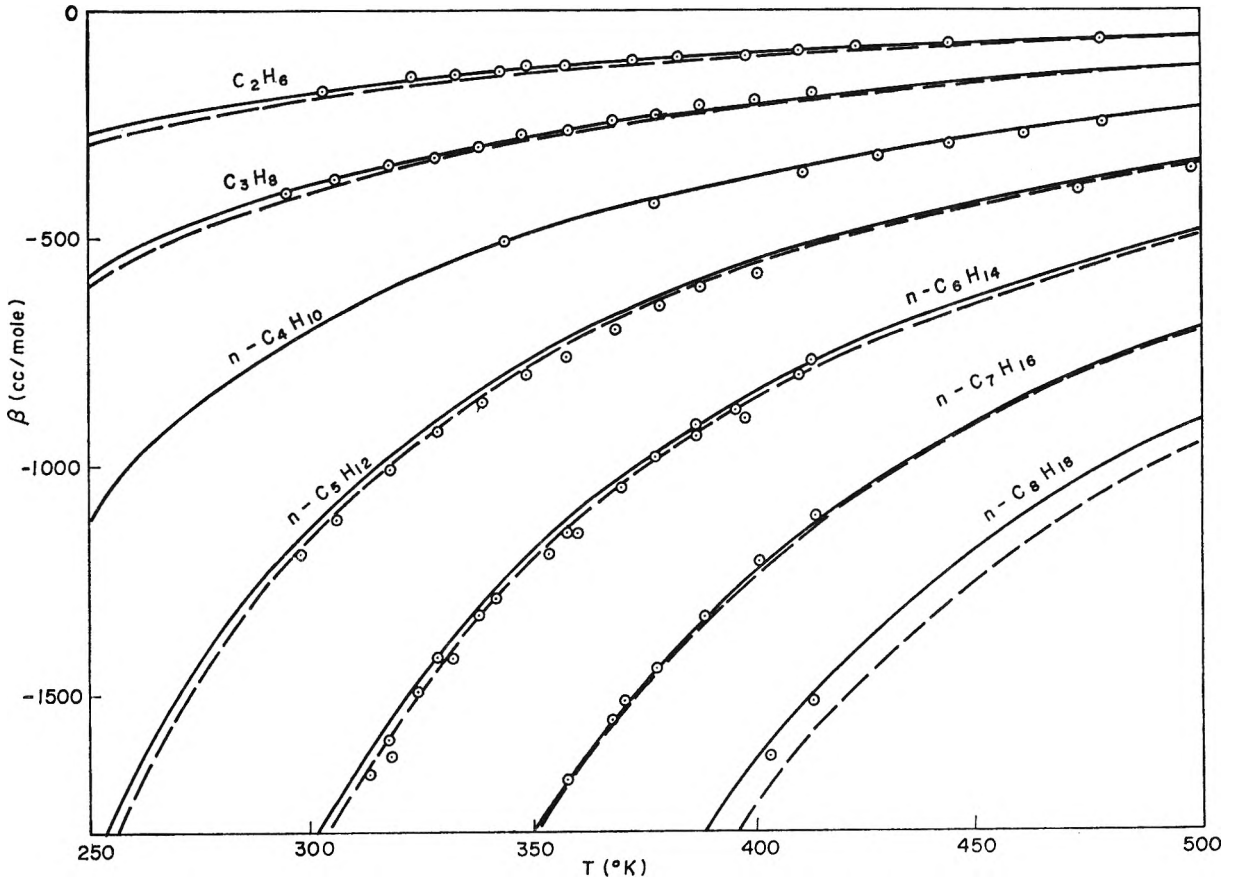

Figure 2. The second virial coefficients of *n*-alkanes. Sources of experimental data: C_2H_6: S. D. Hamann and W. J. McManamey, *Trans. Faraday Soc.*, **49**, 149 (1953); C_3H_8 through *n*-C_8H_{18}: M. L. McGlashan and D. J. B. Potter, *Proc. Roy. Soc.*, **A267**, 478 (1962); data for *n*-C_5H_{12} above 470°K: see ref 3.

0.6, was selected to diminish the errors of interpolation. Let us add here that H^v represents a value corrected for gas imperfections. When the experimental point was remote or uncertain, the respective constant is given in brackets (particularly for phenols, NO, SF_6, and *c*-C_4F_8). Four digits are given for $(V^*)^{1/3}$ (computed from nonrounded values of V^*) without regard to the true precision. The constants previously evaluated[1] for perfluoroalkanes and several other compounds were revised by using the values of T^c, selected in a recent review of critical constants,[14] and better values of density.

The calculated curves of β against temperature are compared with experimental points in Figures 2 to 7.

(14) A. P. Kudchadker, G. H. Alani, and B. J. Zwolinski, *Chem. Rev.*, **68**, 659 (1968).

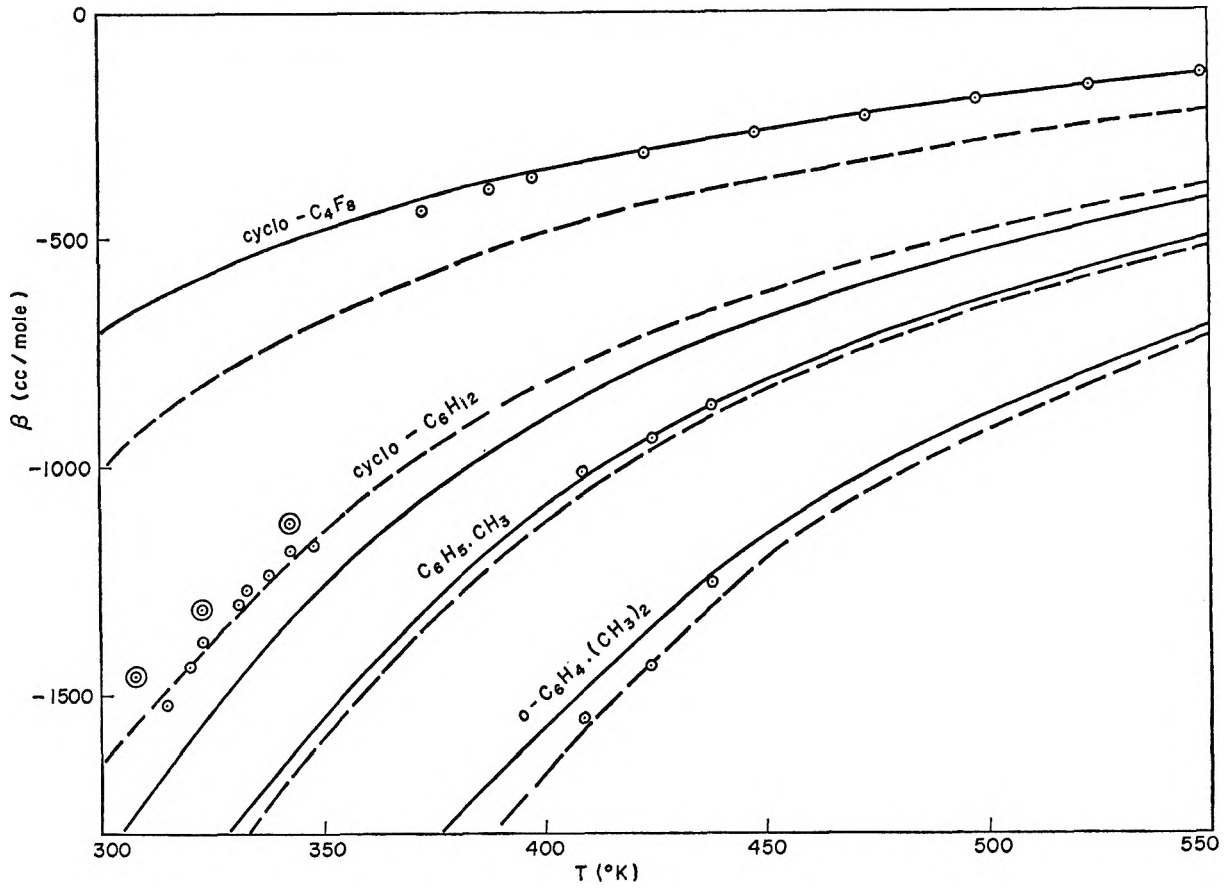

Figure 3. The second virial coefficients of cyclic compounds. Sources of experimental data: c-C_4F_8: D. R. Douslin, R. T. Moore, and G. Waddington, *J. Phys. Chem.*, **63**, 1959 (1959); c-C_6H_{12}: F. G. Waelbroeck, *J. Chem. Phys.*, **23**, 749 (1955) (circles); G. A. Bottomley and J. H. Coops, *Nature*, **193**, 268 (1962) (double circles); toluene and o-xylene: R. J. L. Andon, J. D. Cox, E. F. G. Herington, and J. F. Martin, *Trans. Faraday Soc.*, **53**, 1074 (1957).

The full lines were calculated from T^c and V^* (eq 4b and 10), *while the dashed lines were calculated from E^*/R* (eq 4a and 9). The differences between the two lines are negligible for hydrocarbons; the powers in V^* may differ slightly from $\frac{1}{3}$ or $\frac{2}{3}$, and there may be small errors in E^* (improper correction for gas imperfections) so that a coincidence of the lines such as for n-C_4H_{10} is accidental. The largest difference is noticed for neopentane (Figure 4) and may perhaps be regarded as due to difference in shape compared to that of n-alkanes, further called the "shape effect." It is supposed on the basis of data for n-alkanes (Figure 2), cyclic compounds (Figure 3), and nearly spherical molecules (Figure 4) that *shape differences affect T^c and V^* nearly to the same extent as they affect β and need not be considered in this system of variables.*

The full lines generally agree much better with experimental data (except for cyclohexane, for unclear reasons) than the dashed lines for two main reasons. (i) The shape effect is less significant at a high temperature and low (critical) density. (ii) Weak or moderate donor–acceptor interactions, if they exist at $T/T^c = 0.6$ and thus increase the value of E^* (yielding more negative values of β), largely vanish at T^c and low (critical) density.

Polarity itself does not lead to significant differences between the two curves as shown for toluene and chloroform.[15] The full curve invariably lies above the dashed curve, contrary to the shift due to the shape effect; however, the values of β along the two curves differ by not more than about 10%.

If there are donor–acceptor interactions (already known or possible in view of the charge distribution in the given molecule), the differences between the two curves exceed the limit of about 10% and the full curve lies above the dashed curve because the interactions are much stronger at $T/T^c = 0.6$ than at $T/T^c = 1$. The example of aliphatic amines is most striking. The values of ϵ/ϵ_{00}, expressed in relation to E_0^*, T_0^c, and V_0^* of methane as the reference substance by the previously

(15) We do not imply that dipole–dipole interactions are negligible. Their contribution is large in $CHCl_3$ but is partly concealed when β is expressed in terms of E^*/R or $T^c(V^*)^{1/3}$.

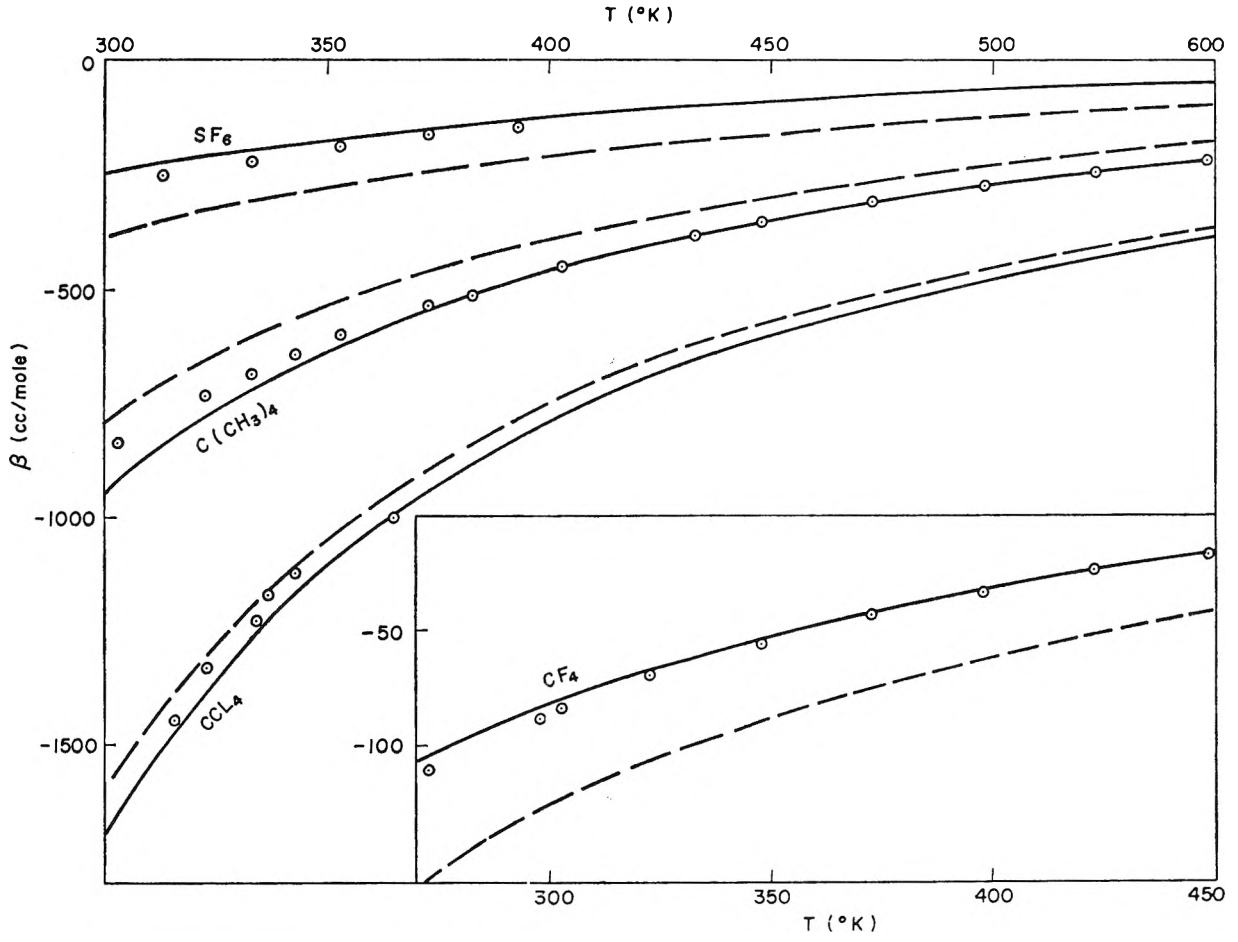

Figure 4. The second virial coefficients of nearly spherical molecules. Sources of experimental data: SF_6: S. D. Hamann, J. A. Lambert, and R. B. Thomas, *Aust. J. Chem.*, **8**, 149 (1955); $C(CH_3)_4$: S. D. Hamann and J. A. Lambert, *ibid.*, **7**, 1 (1954) (below 380°K); J. A. Beattie, D. R. Douslin, and S. W. Levine, *J. Chem. Phys.*, **20**, 1619 (1952); CCl_4: P. G. Francis and M. L. McGlashan, *Trans. Faraday Soc.*, **51**, 593 (1955); CF_4: D. R. Douslin, R. H. Harrison, R. T. Moore, and J. P. McCullough, *J. Chem. Phys.*, **35**, 1357 (1961).

given relations[1] are

	CH_3NH_2	$(CH_3)_2NH$	$(CH_3)_3N$
$\epsilon/\epsilon_{00} = 0.0177T^c/(V^*)^{1/3}$	2.16	1.93	1.68
$\epsilon/\epsilon_{00} = 0.00160E^*/(V^*)^{2/3}$	3.10	2.51	1.67

Specific NH···N interactions, moderate in CH_3NH_2 and weak in $(CH_3)_2NH$, vanish in $(CH_3)_3N$; the dashed and the full curve of $\beta(T)$ will become nearly identical in the third case.

On this basis one may suppose that all fluorocarbons and SF_6 exhibit weak specific interactions, relatively the strongest in CF_4.

Figure 6 shows the effects of specific interactions, moderate in CO_2 and strong ones in NO. The full curves cross the "best" experimental lines (not drawn) nearly exactly at $T = T^c$. Association in the gas phase persists in this case above the critical temperature.[16,17]

Figure 7 illustrates the results obtained for molecules smaller than CH_4, *i.e.*, for Ar, Kr, and N_2. The relative errors are the same as for *n*-alkanes, which conform to the new principle best of all compounds; however, the curvatures are slightly different from those of the experimental curves and point to small errors in the values of b and s.

Discussion

The above results demonstrate that the more general principle of corresponding states[1] is useful for evaluation of the second virial coefficient, particularly by using T^c and $(V^*)^{1/3}$ as the variables. The assumption that for all substances the number of nearest neighbors of a molecule in the liquid at $T/T^* = 0.6$ is $z = 10$ and the pair potential is additive, though crude, does not cause

(16) The existence of specific interactions in *gaseous* NO was proved by Guggenheim.[17] Similar behavior is exhibited by C_2H_2, N_2O, and SO_2. They appear to exist in all oxides and may correspond to the obvious schemes

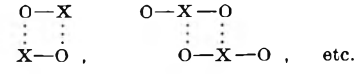

(17) E. A. Guggenheim, *Mol. Phys.*, **10**, 401 (1966).

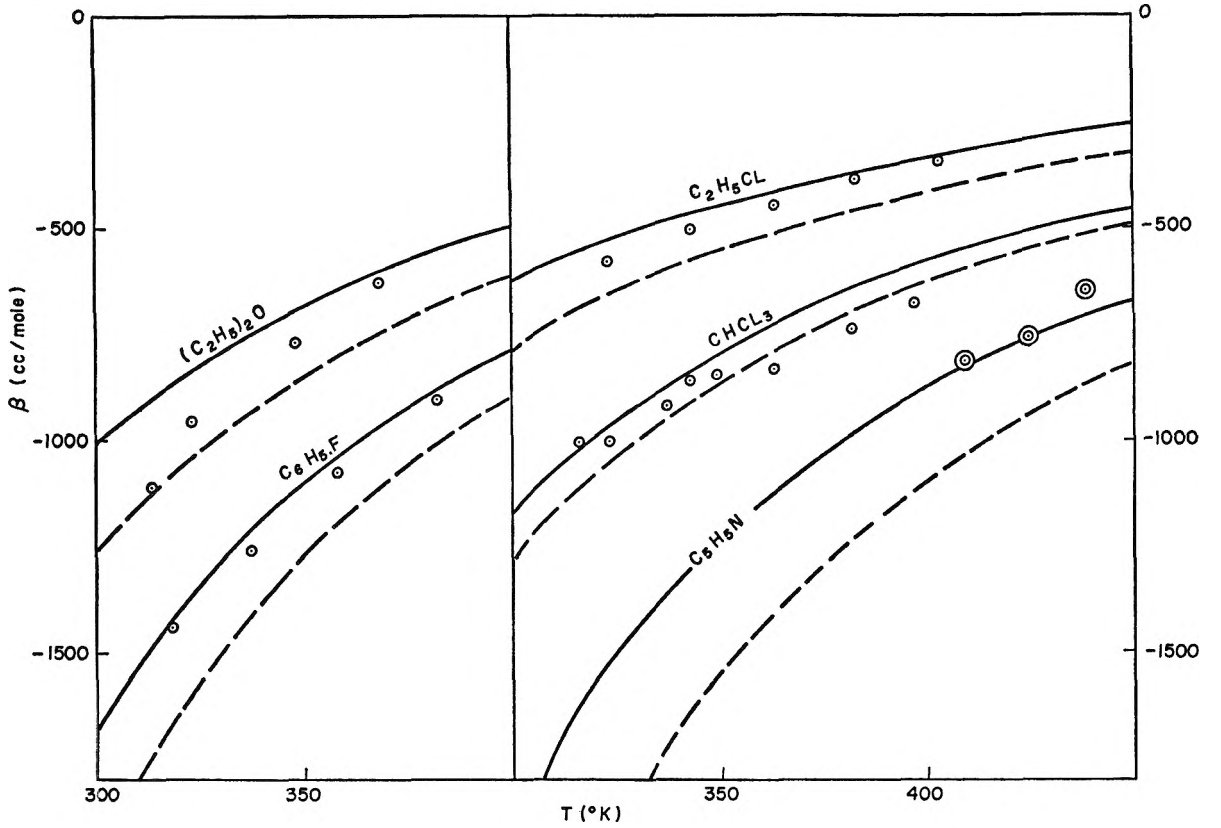

Figure 5. The second virial coefficients of polar compounds, exhibiting weak donor–acceptor interactions (except $CHCl_3$ and C_2H_5Cl). Sources of experimental data: $(C_2H_5)_2O$: R. Stryjek and A. Kreglewski, *Bull. Acad. Polon. Sci., Ser. Sci. Chim.*, **13**, 201 (1965) (circles); M. Rätzsch and H. J. Bittrich, *Z. Physik. Chem.*, **228**, 81 (1965) (double circle); C_6H_5F: D. R. Douslin, R. T. Moore, J. P. Dawson, and G. Waddington, *J. Amer. Chem. Soc.*, **80**, 2031 (1958); C_2H_5Cl: J. S. Rowlinson, *Trans. Faraday Soc.*, **45**, 974 (1949); $CHCl_3$: P. G. Francis and M. L. McGlashan, *ibid.*, **51**, 593 (1955); C_5H_5N: J. D. Cox and R. J. L. Andon, *ibid.*, **54**, 1622 (1958).

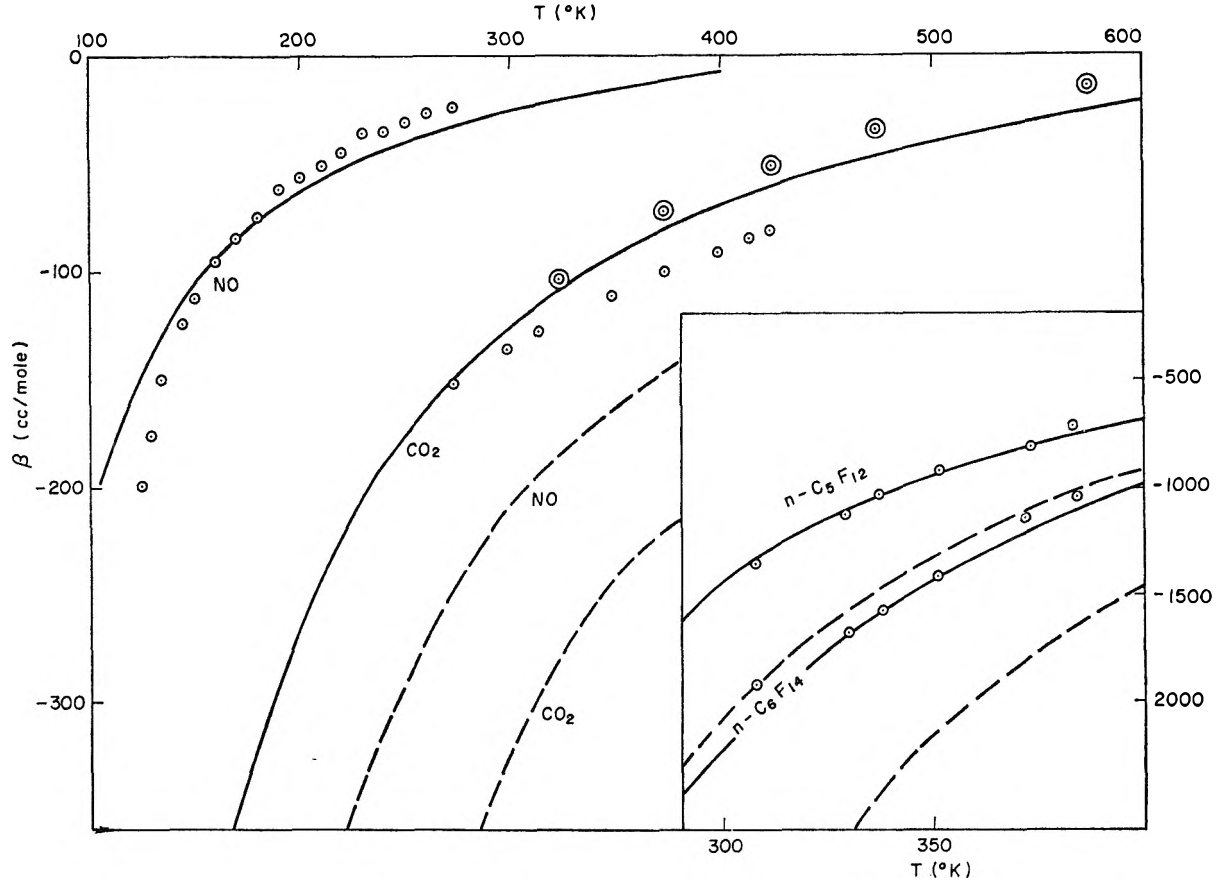

Figure 6. The second virial coefficients of NO, CO_2, and perfluoro-*n*-alkanes. Sources of experimental data: NC: H. L. Johnston and H. R. Weimer, *J. Amer. Chem. Soc.*, **56**, 625 (1934); CO_2: A. Michels and C. Michels, *Proc. Roy. Soc.*, **A153**, 201 (1935) (circles); K. E. MacCormack and W. G. Schneider, *J. Chem. Phys.*, **18**, 1269 (1950) (double circles); perfluoroalkanes: M. D. G. Garner and J. C. McCoubrey, *Trans. Faraday Soc.*, **55**, 1524 (1959).

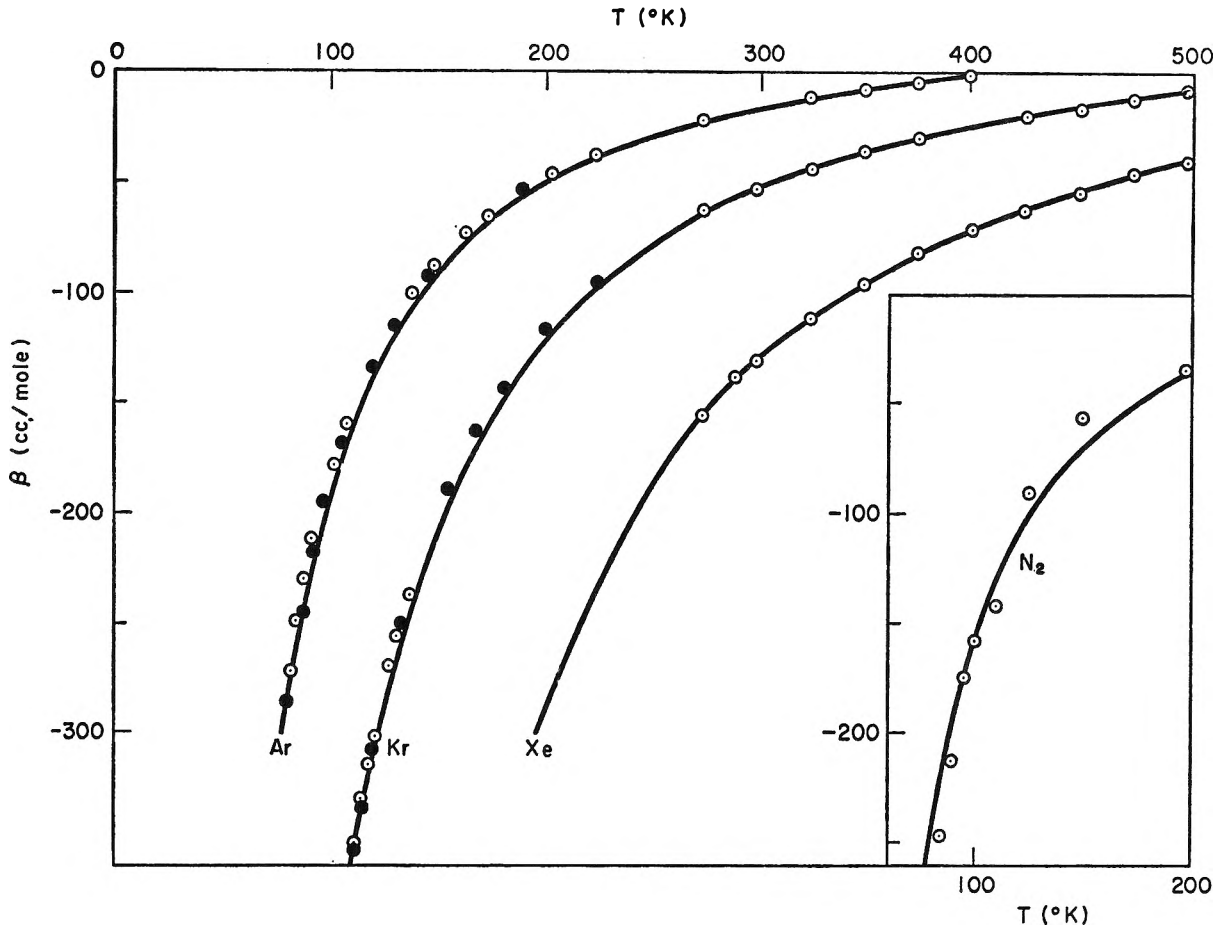

Figure 7. The second virial coefficients of Ar, Kr, N_2($V^* < V_0^*$), and Xe. Sources of experimental data: Ar: A. Michels, J. M. Levelt, and W. DeGraaff, *Physica*, **24**, 659 (1958); Ar and Kr: R. D. Weir, I. Wynn-Jones, J. S. Rowlinson, and G. Saville, *Trans. Faraday Soc.*, **63**, 1320 (1967) (filled circles); E. Whaley and W. G. Schneider, *J. Chem. Phys.*, **23**, 1644 (1955); B. E. F. Fender and G. D. Halsey Jr., *ibid.*, **36**, 1881 (1962); N_2: D. White, J. H. Hu, and H. L. Johnston, *ibid.*, **21**, 1149 (1953); Xe: J. A. Beattie, R. J. Barriault, and J. S. Brierley, *ibid.*, **19**, 1222 (1951); E. Whaley and W. G. Schneider, *ibid.*, **23**, 1644 (1955).

any serious errors. Computer calculations showed that the results could be slightly improved by taking $\rho = 0.33$ to 0.35 ($z \approx 9.5$) for large molecules; however most of the experimental data are not sufficiently precise to warrant any correction of ρ, obtained from the properties of liquid argon.

Analogous considerations apply to the value of V_0^*. A constant value of the significant distance of interaction for all molecules may imply that we are in fact employing the cell model. However, the assumption that interactions beyond a certain distance are negligible does not imply that there are cells in a liquid. Contrary to the present results, the cell model yields values of β in poor agreement with experimental data[2] even if the repulsion is assumed to vary with r^{-28}, practically equivalent to the repulsion between rigid spheres. Satisfactory results obtained with the crude, two-step potential suggest that the function is of secondary importance.

The average values of $\bar{u}/k$ in the very thin layer s_0 around a molecule, obtained from eq 4b, are larger than for the Kihara potential.[3] Let us notice that $\bar{u}/k$ of perfluoro-*n*-hexane is about the same as the value for *n*-hexane; The ratio is equal to 1.001. However, the value of ϵ/k per segment[1] (or rather per "equivalent surface") obtained by dividing $\bar{u}/k$ by the "number of segments" $(V^*/V_0^*)^{2/3}$, is smaller for the fluorocarbon and the ratio for n-C_6F_{14}/n-C_6H_{14} amounts to 0.778.

The above treatment of deviations from the classical principle of corresponding states offers some practical advantages in comparison with the acentric factor method[18] as it does not require the knowledge of critical pressure and critical volume which are often not known with sufficient precision.

Acknowledgment. The author is very much indebted to Professor Webster B. Kay for his interest in the course of the work and to the colleagues in the Department of Chemical Engineering for help in computer programming. This study was partially supported by the American Petroleum Institute, Research Project on Critical Constants of Mixtures.

(18) K. S. Pitzer, *J. Amer. Chem. Soc.*, **77**, 3427 (1955); K. S. Pitzer, D. Z. Lippmann, R. F. Curl, Jr., C. M. Huggins, and E. D. Petersen, *ibid.*, **77**, 3433 (1955); K. S. Pitzer and R. F. Curl, Jr., *ibid.*, **79**, 2369 (1957).

The Measurement of Dielectrics in the Time Domain

by Hugo Fellner-Feldegg

Hewlett-Packard Laboratories, Palo Alto, California *(Received August 15, 1968)*

The time dependence of the reflection of a step pulse from the interface between air and a dielectric medium in a coaxial line has been measured from 30 psec to 200 nsec, corresponding to a frequency range of 1 MHz to 5 GHz. The high-frequency and low-frequency dielectric constant, the relaxation time, and the dielectric loss can be obtained in a fraction of a second. Different alkyl alcohols have been measured over a wide temperature range. The results are essentially the same as obtained in the frequency domain.

Introduction

Generally, permittivity is measured by placing the substance between two plates of a capacitor (at low frequencies) or into a coaxial line and measuring the complex impedance. A number of measurements over a wide frequency range is required for complete characterization, which is time consuming and demands a considerable investment in instrumentation, particularly in the microwave region. Therefore, and in spite of its usefulness, this method found only rather limited applications in the past. However, one can obtain the same information over a wide frequency range in only a fraction of a second by making the measurement not in the frequency domain but in the time domain, using a pulse which, simultaneously, contains all the frequencies of interest. This pulse method has been applied sometimes in the past for low-frequency investigations on dielectrics. Modern tunnel diode pulse generators and wide band sampling oscilloscopes allow the extension of this method into the microwave region where savings in time and equipment are most pronounced. Such instruments have been used for years for cable testing and are known as time domain reflectometers (tdr).

Basic Relations for the Measurement of Dielectric Properties with Tdr

The time domain reflectometer consists of a pulse generator which produces a fast rise time step, a sampler which transforms a high-frequency signal into a lower frequency output, and an oscilloscope or any other display or recording device (Figure 1).

The pulse from the step generator travels along the coaxial line until it reaches point A. The sampler detects and the oscilloscope displays the voltage step (1) as it travels past point A (Figure 2). The coaxial line which transmits the pulse has a characteristic impedance $Z_0 = 50$ ohms. Whenever there is a discontinuity in this line, a fraction of the traveling wave will be reflected back into the generator. Therefore, at the interface of the 50-ohm line with any other impedance Z (point B) part of the step pulse will be reflected and will pass point A again, producing an additional signal (2) which is displayed on the oscilloscope. The time elapsed between the first and second steps is equal to the transit time of the traveling wave from A to B and back to A again.

The remainder of the wave, not reflected at B, travels to C. If we terminate the line at C with an open end then all of the wave is reflected back in phase (assuming no losses due to radiation). Part of this pulse is reflected again at B and part of it goes through past A, giving rise to another step (3). The time between steps 2 and 3 is the transit time from B to C and back to B again.

The magnitude of the first step, $V_0\rho$, is

$$V_0\rho = V_0 \frac{Z - Z_0}{Z + Z_0} \tag{1}$$

where ρ is the reflection coefficient and V_0 is the pulse height. A coaxial line with the impedance Z_0 when empty, will have a smaller impedance Z, when filled with a nonconductive dielectric of the permittivity κ^*

$$Z = \frac{Z_0}{\sqrt{\kappa^*}} \qquad (\kappa^* = \kappa' - j\kappa'') \tag{2}$$

Thus, the reflection coefficient ρ is a function of κ

$$\rho = \frac{1 - \sqrt{\kappa}}{1 + \sqrt{\kappa}} \tag{3}$$

and

$$\kappa = \left(\frac{1 - \rho}{1 + \rho}\right)^2 \tag{4}$$

For conductive dielectrics

$$Z = \sqrt{\frac{j\omega L + R}{j\omega\kappa C + G}} \tag{5}$$

where R is the series resistance, G is the parallel conductance, σ is the low-frequency conductivity in siemens/cm, and $G/C = 4\pi\sigma$. In most applications, with reasonable lengths of transmission lines, $R \approx 0$. Therefore Z becomes

$$Z = Z_0/(\kappa^* - j4\pi\sigma/\omega)^{1/2} \tag{6}$$

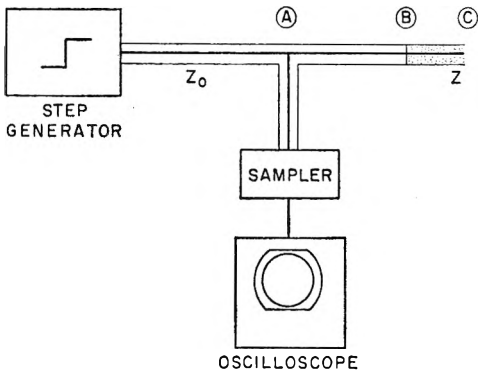

Figure 1. Time domain reflectometer system.

and for

$$\frac{4\pi\sigma}{1.1 \times 10^{-12}\omega} \ll \kappa''$$

$$Z(\omega) = \frac{Z_0}{\sqrt{\kappa^*}} \quad \text{or} \quad Z(t) = \frac{Z_0}{\sqrt{\kappa(t)}} \tag{7}$$

which was used already in eq 2.

We see now that the impedance Z, and therefore the reflection coefficient ρ, are simple functions of the permittivity κ, both in the frequency and time domain, if one can neglect the low-frequency conductivity. A time dependence of the permittivity corresponds to a time dependence of the reflection coefficient. The step at (2) in Figure 2 is modified depending on the relaxation properties of the dielectric. The measurement is made only at the interface between air and dielectric and is undisturbed as long as there are no additional reflections present from any point beyond B in Figure 1. Therefore, the time for the return trip of the wave in the line filled with the dielectric limits the maximum time available for the measurement. It is

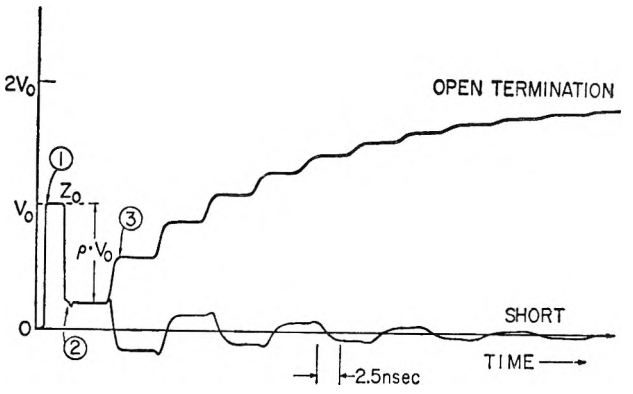

Figure 2. Typical reflection from a dielectric sample (water) in a coaxial line.

$$t[\text{nsec}] = \frac{2l\sqrt{\kappa'}}{C} = \frac{\sqrt{\kappa'}}{15} \times l[\text{cm}] \tag{8}$$

Figure 3 shows the time dependence of the reflection coefficient of amyl alcohol, recorded with an X–Y recorder from the output of the oscilloscope. After transformation of this plot, according to eq 4, we get the time dependence of the permittivity as shown in Figure 4. All the important properties of a dielectric are immediately apparent. The value κ_∞, the high-frequency permittivity, and κ_0, the static permittivity, can be read directly. The asymptotic rise of the permittivity is an indication of the orientation of dipoles in the medium with time. It is exponential for a dielectric with a single relaxation time and a plot of $\ln(\kappa_0 - \kappa(t))$ *vs.* t gives a straight line (Figure 5).

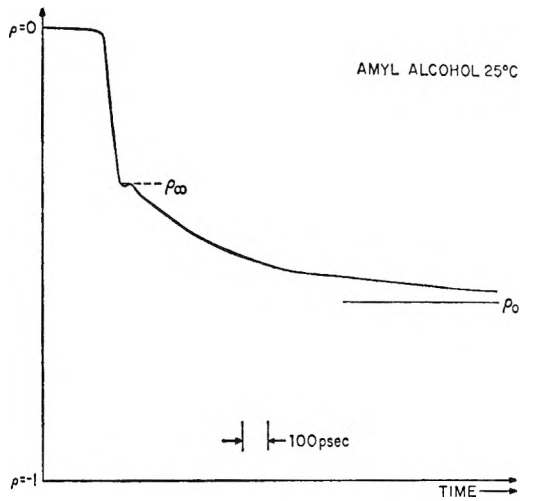

Figure 3. Reflection coefficient ρ *vs.* time from the interface air–amyl alcohol at 25°.

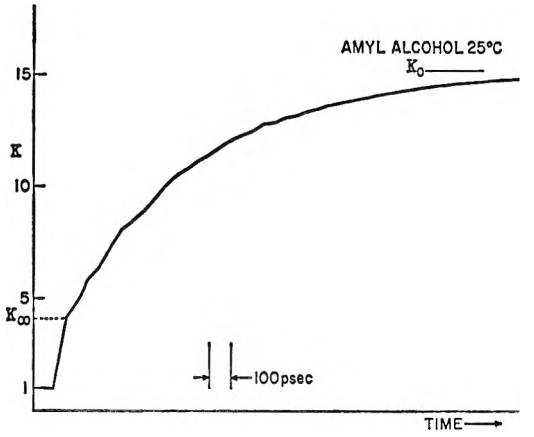

Figure 4. Permittivity κ *vs.* time for amyl alcohol at 25°.

If inter- and intramolecular interactions become important, then single relaxation times broaden into relaxation spectra. Fuoss and Kirkwood[1] and Cole[2,3] assume a relaxation spectrum which is symmetrical on a logarithmic scale about a central relaxation time τ_0.

(1) R. M. Fuoss and J. G. Kirkwood, *J. Amer. Chem. Soc.*, **63**, 385 (1941).
(2) R. H. Cole, *J. Chem. Phys.*, **23**, 493 (1955).
(3) K. S. Cole and R. H. Cole, *ibid.*, **9**, 341 (1941).

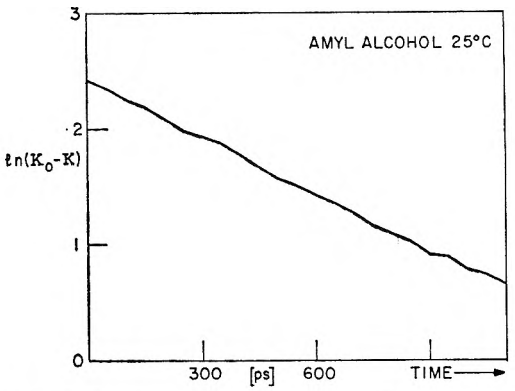

Figure 5. Plot of ln $(\kappa_0 - \kappa)$ *vs.* time for amyl alcohol at 25°.

The empirical equation of Cole fits the data to an arc of a circle in the Cole–Cole diagram and is of the form

$$\kappa(\omega) = \kappa_\infty + \frac{\kappa_0 - \kappa_\infty}{1 + (j\omega\tau_0)^{1-\alpha}} \tag{9}$$

The Laplace transform of this equation can be solved only numerically.

Finally, glycerol and other substances show a highly asymmetric Cole–Cole diagram described by Davidson and Cole[4] with

$$\kappa(\omega) = \kappa_\infty + \frac{\kappa_0 - \kappa_\infty}{(1 + j\omega\tau_0)^\beta} \tag{10}$$

The time response to a step pulse is

$$\kappa(t) = \kappa_\infty + (\kappa_0 - \kappa_\infty)\frac{1}{\tau_0^\beta \Gamma(\beta)}\int_0^t t^{\beta-1}e^{-t/\tau_0}dt$$

$$= \kappa_\infty + (\kappa_0 - \kappa_\infty)\left(\frac{t}{\tau_0}\right)^\beta \gamma^*\left(\beta, \frac{t}{\tau_0}\right) \tag{11}$$

$$\gamma^*\left(\beta, \frac{t}{\tau_0}\right) = \frac{1}{\left(\frac{t}{\tau_0}\right)^\beta \Gamma(\beta)}\int_0^{t/\tau_0} e^{-t/\tau_0}\left(\frac{t}{\tau_0}\right)^{\beta-1} \mathrm{d}\left(\frac{t}{\tau_0}\right)$$

γ^* is the incomplete gamma function which is tabulated.[5] In Figure 6 $\kappa(t)$ has been plotted for different values of β. $\kappa(t)$ for $\beta = 1$ represents a single relaxation time. Experimental values, normalized for κ and t, can easily be compared with these curves to check for deviations from the ideal behavior.

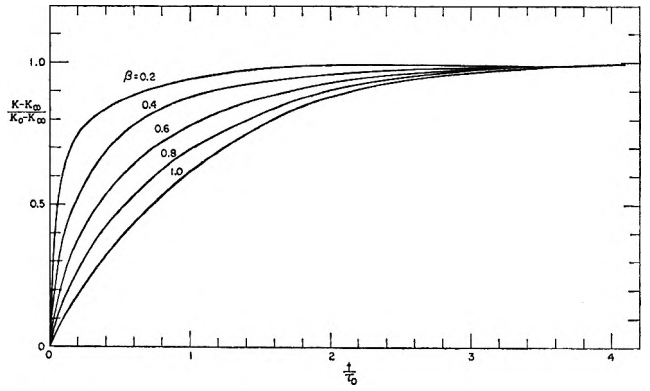

Figure 6. Step response of the normalized permittivity for different β in the Davidson–Cole equation (10).

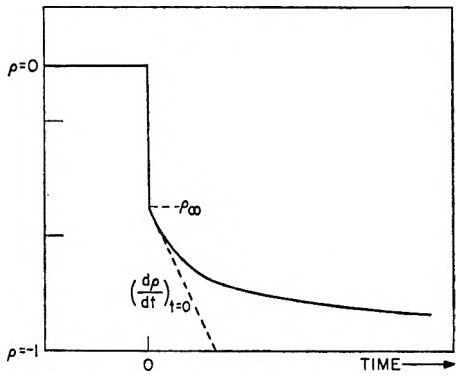

Figure 7. Step response of the permittivity for a dielectric with conductivity.

If ionic conductivity is predominant, then the reflection coefficient will not level out at a certain value, corresponding to κ_0, but will drop to zero, following the equation[6]

$$\rho(t) = (1 + \rho_\infty)(I_0(xt) + I_1(xt))e^{-xt} \tag{12}$$

with

$$x = \frac{G}{2\kappa C} = \frac{2\pi\sigma}{\kappa}$$

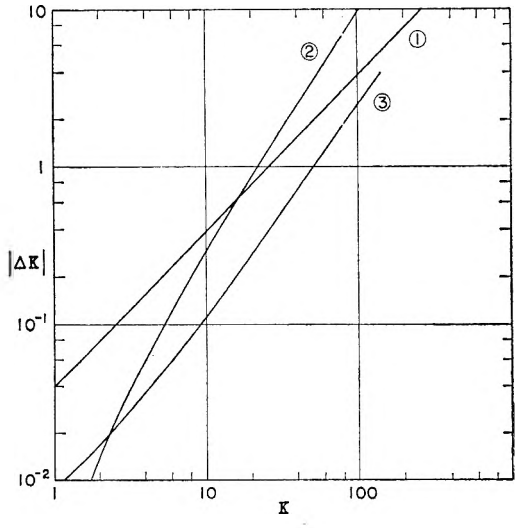

Figure 8. Absolute measurement error of the permittivity $\Delta\kappa$ for different contributions: (a) coaxial line tolerance (assumed to be ±0.2%); (2) relative measurement error of the reflection coefficient ($\Delta\rho/\rho$ assumed to be ±1%); (3) absolute measurement error of the reflection coefficient ($\Delta\rho$ assumed to be ±0.002).

(4) D. W. Davidson and R. H. Cole, *J. Chem. Phys.*, **19**, 1484 (1951).
(5) M. Abramowitz and J. A. Stegun, "Handbook of Mathematical Functions," Dover Publications, Inc., New York, N. Y. 1965.
(6) B. M. Oliver, *Hewlett-Packard J.*, **15**, No. 6 (1964).

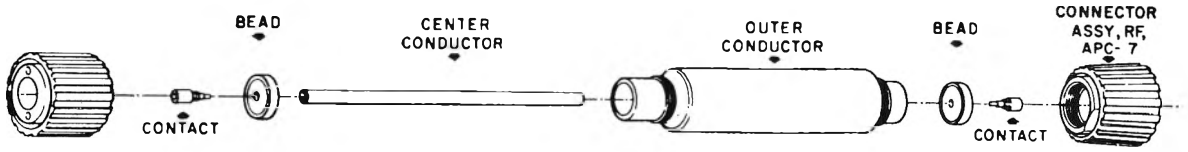

Figure 9. Precision coaxial line.

and

$$\rho_\infty = \frac{1 - \sqrt{\kappa_\infty}}{1 + \sqrt{\kappa_\infty}}$$

$\rho(t)$ is plotted in Figure 7. The first step ρ_∞ gives the dielectric constant at high frequency. The slope at $t = 0$ is

$$-\left(\frac{d\rho}{dt}\right)_{t=0} = \frac{G(1 + \rho_\infty)}{4\kappa C} = \frac{\pi\sigma(1 + \rho_\infty)}{\kappa \times 1.1 \times 10^{-12}}$$

which yields σ, under the assumption that $\kappa(t) =$ constant in the vicinity of $t = 0$. Values of $\kappa/\sigma > 100$ can be measured with tdr, corresponding to $\sigma < 0.25$ siemens/cm for $\kappa = 40$. Such a conductivity makes dielectric constant measurements with other methods at high frequencies quite difficult. With tdr, however, materials with ten times higher conductivities could be determined with ease.

A remark about the accuracy of the dielectric measurements with tdr. First, it is dependent on the mechanical accuracy of the coaxial line used. Standard 7-mm precision coaxial air lines have an impedance of 50 ± 0.1 ohms or a maximum deviation of 0.2%. Since $\kappa = (Z_0/Z)^2$, the relative error in κ can be $\pm 0.4\%$. This error can be reduced to an insignificant amount by measuring accurately the impedance or the physical dimensions of the coaxial line.

A second source of error is any inaccuracy of the measurement of the reflection coefficient ρ. It may be due to amplifier nonlinearities in the oscilloscope or the recorder, which normally is less than 1%, or due to unwanted reflections from poorly matched transmission lines, including the sampler. Arrangements shown in the next part can suppress the latter and allow, with commercial instruments, an overall measurement accuracy of the reflection coefficient $\Delta\rho/\rho \leq 0.01$ and $\Delta\rho \leq 2 \times 10^{-3}$, whichever is greater. The transformation of ρ into κ, however, multiplies this error by a factor

$$\frac{\Delta\kappa}{\Delta\rho} = -\sqrt{\kappa}(1 + \sqrt{\kappa})^2; \qquad \frac{\Delta\kappa}{\Delta\rho/\rho} = -(1 - \kappa)\sqrt{\kappa}$$

$\Delta\kappa$ is shown in Figure 8 for the different sources of error mentioned. Obviously, relative measurements, using a reference sample, can be made with much higher accuracy.

A poorly defined interface between air and the dielectric, *e.g.*, a liquid meniscus, produces another error. It reduces in effect the rise time—or high-frequency cutoff—of the system. Imagine an ideal dielectric with no relaxation reflecting a δ-function impulse, which contains all frequencies of equal amplitude. The reflected pulse will be a δ function again, if the interface air–dielectric is parallel to the electric field. If the interface extends over a certain distance in the direction of the traveling wave, however, then the reflected pulse will be spread out, corresponding to the return trip time of the wave through the interface. This reflected pulse has a limited high-frequency spectrum. The convolution in the time domain of this pulse with the reflection from any real dielectric (with relaxation) having a perfect interface gives the actual reflection obtained from the real dielectric with an extended interface. Errors thus introduced in the measurement of the high-frequency permittivity and relaxation time can be eliminated by terminating the sample cell with plastic or ceramic beads, similar to the ones shown in Figure 9. These beads have an inner and outer conductor of proper dimensions to produce a characteristic impedance of 50 ohms. They are, therefore, electrically in no way different from the remainder of the empty coaxial line but form a perfect physical interface with any liquid in contact with them.

Finally, we shall consider the influence of the finite rise time of the step pulse on the measurement of κ_∞. The pulse produced by the tunnel diode generator approximates quite well a linear voltage ramp which rises from zero to V_0 within the time t_R as shown in Figure 10. This ramp is the integral of a step pulse and the response of the dielectric becomes the integral of the step-pulse response divided by t_R

$$f(t)_{ramp} = \frac{1}{t_R}\int f(t)_{step}dt$$

Thus, the derivative of the measured time response of the reflection coefficient during the rise time of the pulse times t_R gives the response to a step pulse. The linear extrapolation of ρ to the time t_R gives ρ_∞ and, from eq 4, κ_∞.

Practical Aspects of Tdr Measurements

Sample Cells. A simple and versatile cell for measurements of liquids and granular solids is the standard 7-mm diameter precision coaxial line of 10 and 20 cm length with Amphenol APC-7 connectors (see Figure 9). As mentioned already, the maximum deviation from the 50-ohm impedance is $\pm 0.2\%$. The plastic bead on each end is machined accurately enough

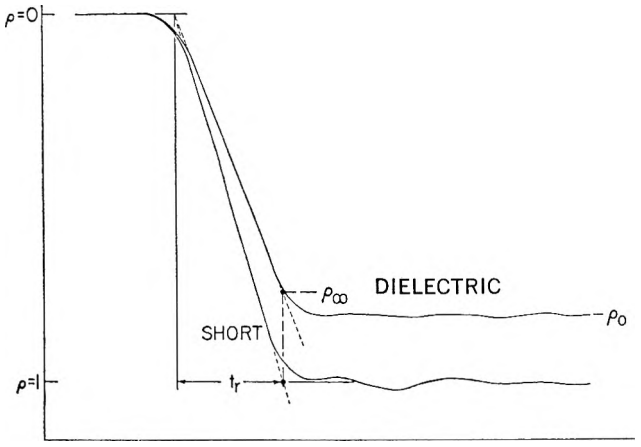

Figure 10. Reflection coefficient *vs.* time for step pulse with finite rise time.

to provide a liquid-tight seal for a few hours. The plastic may be replaced with any ceramic material, such as alumina, for operation at temperatures above 80° or to provide resistance against attack by organic solvents. The assembly on one side, including the center conductor, is held in place by the APC-7 connector, thus allowing one to fill the line from the other end. The hybrid connector itself is of high quality and does not introduce any significant reflections up to 18 GHz.

Solids can be measured in the coaxial cell by filling the line with the molten material, if possible, or by machining the substance to the dimension of the line, or by wrapping it tightly around the center conductor when available as foil, or by shredding or granulating it. Tdr measures an average value of the permittivity if the line is not completely filled with the dielectric. Therefore, for absolute measurements the fill factor has to be known. Relative measurements of the dielectric constant and exact determinations of the relaxation time can be made, however, if the fill factor is unknown but constant. A change of the packing density of the material over the length of the line will cause unwanted reflections.

The dielectric properties of large batches of liquids may be measured with a vertical coaxial line immersed into the substance. Since the characteristic impedance, Z_0, depends only on the ratio of the diameters of inner and outer conductor, the line can be made to any size for mechanical stability as long as no other modes than the TEM mode are excited. A continuous monitoring of chemical reactions by measuring the permittivity in a time interval where it is most sensitive to changes in the chemical composition is entirely feasible. In addition, the position of the surface of the liquid can be measured, thus providing a simple liquid level control. This application has been suggested long ago[7] and has found some practical use already.

The only limitation of the straight coaxial line is its length. A standard 7-mm line becomes quite unstable, if more than 30 cm long, due to vibrations and sagging of the center conductor. On the other hand, one great advantage of dielectric measurements with tdr is the freedom from multiple reflections if one measures only within the time for the return trip of the wave in the sample cell. A 40 cm long line filled with a dielectric of $\kappa = 20$ limits the range to <12 nsec.

One way to make long, compact coaxial lines is shown in Figure 11. Spiral grooves have been cut into a copper tube of 8-cm diameter. An extruded polypropylene spacer fits tightly into the grooves and supports a copper wire used as a center conductor. An outer tube fits closely over the inner one. Both tubes are sealed to a bottom plate, forming a rectangular coaxial line of 7-m length which can be filled from the top and immersed in a temperature bath. The empty line has 50-ohm impedance and a return trip time of about 50 nsec. Because of the polypropylene spacer, the line has to be calibrated with known dielectrics. Relaxation times up to 200 nsec have been measured. This corresponds to 1 MHz in the frequency domain.

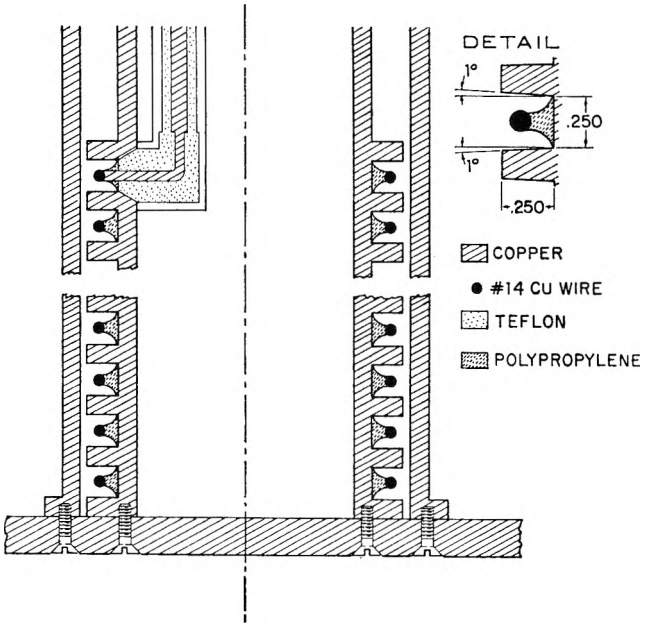

Figure 11. Helical coaxial line for the measurement of long relaxation times.

Another kind of transmission line which is well suited for many applications is the strip line. One of many possible configurations of such a line is shown in Figure 12. Two parallel, conductive strips can be prepared by etching a printed circuit board. This line can be connected to a coaxial line with a balun transformer. Placing a piece of dielectric material over the two strips reduces the characteristic impedance of the line and thus results in a dip of the oscilloscope trace. Since the test material fills only part of the field region,

(7) J. Brockmeier, *Hewlett-Packard J.*, **17**, No. 5 (1966).

Table I: Low-Frequency Permittivity, κ_0, High-Permittivity, κ_∞, and Relaxation Time τ, for Alkyl Alcohols at Different Temperatures

CH_3OH				C_2H_5OH				C_3H_7OH			
T, °C	κ_0	κ_∞	τ	T, °C	κ_0	κ_∞	τ	T, °C	κ_0	κ_∞	τ
50.2	29.0	12.5	65 psec	60.3	19	9.8	76 psec	60.3	16.2	8.5	100 psec
25	32.5	12.8	90 psec	40	21.7	9.0	110 psec	40	19.0	7.7	150 psec
−9.9	40.0	11.8	135 psec	25	24.3	8.3	130 psec	25	20.5	7.2	220 psec
−39	47.0	12.0	330 psec	1	28.0	7.1	220 psec	17.8	21.6	7.0	290 psec
−47	49.0	12.2	400 psec	−15	30.5	6.2	380 psec	−12.5	25.8	6.0	900 psec
−66	54.0	10.0	730 psec					−41.0	30.5	4.8	4.1 nsec
−75	57.0	9.5	1050 psec					−61.5	35.0	4.3	19.5 nsec
								−81.5	39.2	5.2	100 nsec

C_4H_9OH				$C_5H_{11}OH$				$C_8H_{17}OH$			
T, °C	κ_0	κ_∞	τ	T, °C	κ_0	κ_∞	τ	T, °C	κ_0	κ_∞	τ
80	11.5	6.0	90 psec	69.8	10.2	5.5	130 psec	71.5	6.4	4.2	150 psec
60.3	13.3	5.5	120 psec	50.2	11 8	5.2	230 psec	54.8	7.7	4.2	290 psec
40	15.3	5.0	210 psec	30.4	13 8	4.8	500 psec	45	8.4	3.9	500 psec
25	16.8	4.2	330 psec	11.7	15 5	3.5	1.1 nsec	35	9.0	4.0	650 psec
15.5	17.8	3.8	510 psec	−9.5	17 7	2.8	4.0 nsec	25	9.5	3.8	1.3 nsec
−3.4	20.5	2.9	1.1 nsec	−29.5	20 1	2.4	15 nsec	16.7	10.6	3.2	2.0 nsec
−17.3	22.3	2.8	2.3 nsec								
−35.5	25.0	2.9	8.2 nsec								
−50.2	27.0	3.0	25 nsec								
−61.4	28.3	3.4	61 nsec								

a calibration curve with known dielectrics has to be made. This method may be used as a simple and expedient check of dielectrics for quality control and similar applications. Also, multilayers of plastic foil, pressed against the two conductors, give rather reproducible readings.

Measurement Techniques. Some precautions are necessary to use the high sensitivity of tdr to its fullest advantage. One is the suppression of unwanted reflections, the other the correction of slight deviations of the pulse shape from an ideal step pulse with linear rise time. Interfering reflections may appear superimposed on the oscilloscope trace during the time interval in which the reflection coefficient ρ drops to its final value. They may be small bumps when originating from local discontinuities or small steps when caused by extended impedance mismatches between pulse generator and sample. They are produced by the reflected pulse from the interface air–dielectric, traveling toward the generator. They can be spaced farther apart or even suppressed by inserting a length of a transmission line between sampler and measuring cell. Also a 10-db attenuator in place of the air line dampens reflections effectively, however at the price of reduced sensitivity. Placing a short in the place of the air–dielectric interface allows one to examine these interferences most clearly. Figure 13 shows the trace of a short, 50-ohm line, and a dielectric with a deliberately produced poor connection at the sampler.

The same figure shows also the slight overshoot of the pulse at the bottom of the step due to the frequency response of the sampler and a certain slow droop to a final value. Both may cause measurement errors of the high-frequency permittivity κ_∞ and of the relaxation time τ. This interference can be eliminated by measuring the ratio ρ_m/a, which is the corrected reflection coefficient ρ, at any point in time.

Applications. The greatest assets of this method are its speed, simplicity, and ease of data evaluation. The display on the oscilloscope screen of the time domain reflectometer is easy to interpret, gives immediate information about the behavior of the material investigated, and tells at the same time whether the instrument is operating properly and whether any

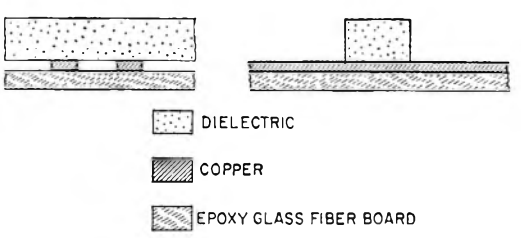

Figure 12. Material testing with a strip line.

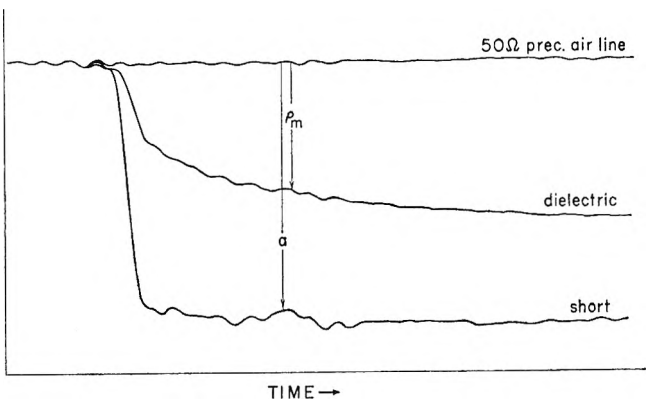

Figure 13. Correction of ρ for unwanted reflections.

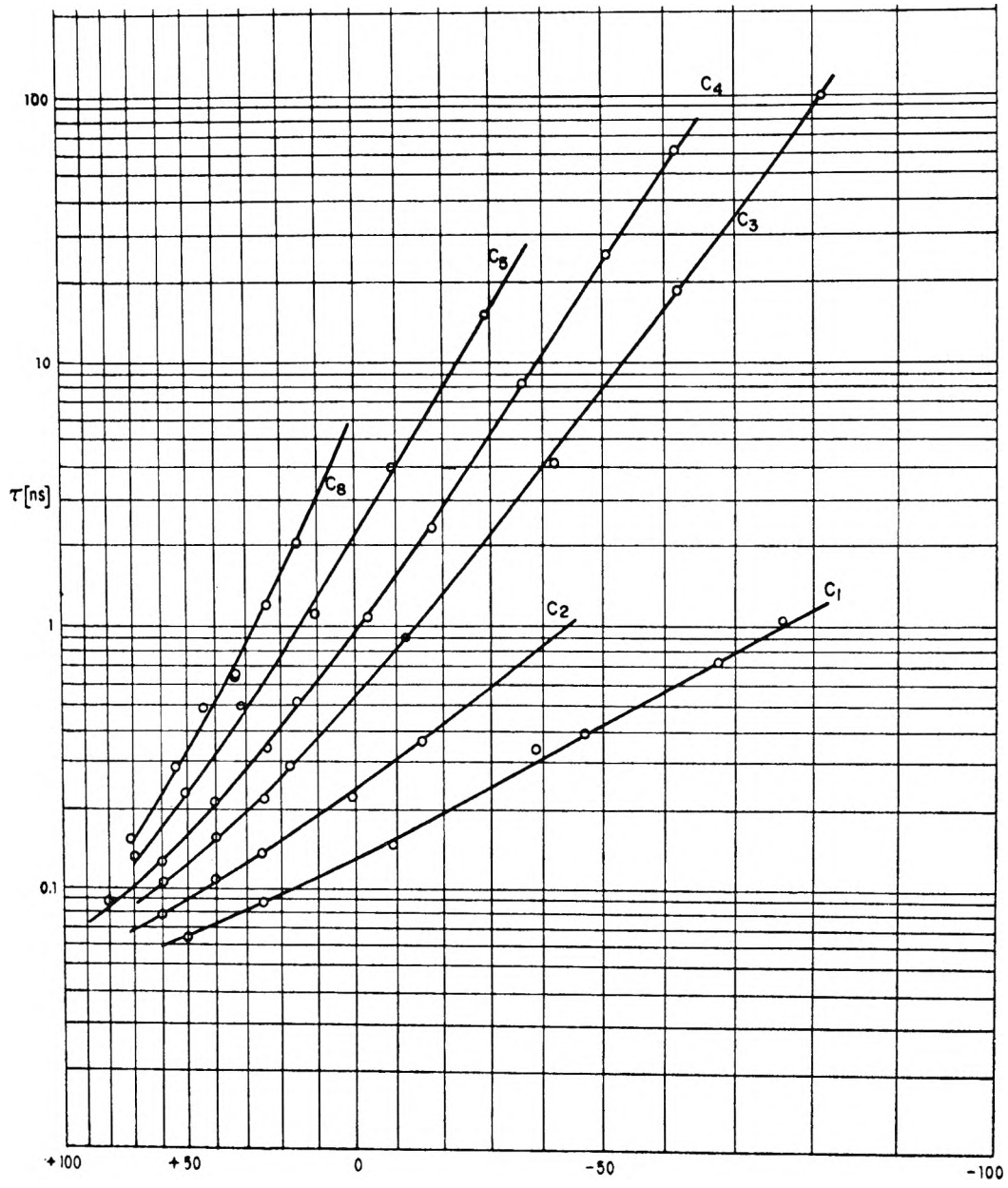

Figure 14. Relaxation times τ *vs.* temperature (°C) for different alkyl alcohols.

unwanted reflections are present. The information content is high since three parameters (κ_0, κ_∞, τ or σ) are obtainable from one measurement. In many materials the high-frequency permittivity is quite sensitive to impurities of small, free molecules, like water, monomers, etc. These impurities have very short relaxation times—sometimes below the time resolution of the time domain reflectometer—and relatively high specific permittivities. On the other hand, many host materials, like polymers, have high-frequency dielectric constants in the range of $\kappa_\infty = 2$ to 8. The high sensitivity of tdr in this range allows determination of less than 100 ppm of water in certain polymers.

The range of relaxation times which can be measured is limited by the rise time of the tdr system, which is about 30 psec today, and the practical limitations on the length of a test line, which allows return trip times of the wave of a few hundred nanoseconds. Within this range are the relaxation times of the orientation polarization of small molecules and molecular groups in liquids and the relaxation of some functional groups in liquids and solids. As an example, we have measured a number of alkyl alcohols over a wide range of temperatures. These alcohols have been investigated extensively in the past[2,4,8,9] in the frequency domain, and important information has been obtained on the structure of the liquid state. Our results, without adding much new information, are in good agreement with

(8) D. J. Denney and R. H. Cole, *J. Chem. Phys.*, **23**, 1767 (1955).
(9) S. K. Garg and C. P. Smyth, *J. Phys. Chem.*, **69**, 1294 (1965).

literature values for the static permittivity. The high-frequency permittivity measured with our method agrees well with reported values at 3–5 GHz, which corresponds with the maximum response of the tdr system used. The relaxation time measurements show, in some cases, larger deviations from literature values. It may be noted, however, that reported values of relaxation times vary considerably among different authors.

Time domain reflectometry, therefore, gives essentially the same results as measurements in the frequency domain (see Figure 14 and Table I). The measurement speed was mainly determined by the time required of the sample cell to attain thermal equilibrium. The data evaluation was done with an electronic desk top calculator in a few hours.

Since the measurement speed is essentially limited by the repetition rate of the pulse generator, which is roughly 100 kHz, very fast reactions can be monitored. Using a storage oscilloscope and adjusting the repetition rate of the pulse generator according to the reaction rate allows one to store a number of traces of the reflection coefficient *vs.* time on the oscilloscope screen and gives immediate information about the changes taking place during the reaction. The stored traces can then be photographed and evaluated in detail.

The Palladium–Bromine System. The Molecular Composition of Palladium Bromide Vapor

by Reed C. Williams and N. W. Gregory

Department of Chemistry, University of Washington, Seattle, Washington 98105 *(Received August 16, 1968)*

The reactions (a) $PdBr_2(s) = Pd(s) + Br_2(g)$, for which, in the range 760–970°K, $\ln K = -19{,}840T^{-1} - 3.02 \ln T + 40.124$; (b) $Pd(s) + Br_2(g) = PdBr_2(g)$, for which, in the range 1090–1155°K, $\ln K = -17{,}386T^{-1} - 1.006 \ln T + 13.278$; (c) $x PdBr_2(s) = (PdBr_2)_x(g)$; and (d) $x Pd(s) + x Br_2(g) = (PdBr_2)_x(g)$ have been studied by the transpiration method. A combination of monomer, tetramer, and hexamer appears to be the simplest molecular mixture consistent with all the observed equilibrium data for (d). The principal molecular forms in the saturated vapor phase above solid $PdBr_2$, equilibrium c, appear to be the tetramer and the hexamer. Thermodynamic properties of $PdBr_2(s)$ and $PdBr_2(g)$ have been evaluated.

Little information has been published about the vapor characteristics of the palladium halides. The recent work of Bell, Merten, and Tagami (BMT)[1] indicates that in the presence of chlorine, at pressures between 0.2 and 1 atm, Pd_5Cl_{10} is the dominant palladium-containing molecule in vapor in equilibrium with a liquid solution of palladium and palladium dichloride around 900°. At higher temperatures, in a direct equilibrium with metallic palladium and chlorine, monomeric $PdCl_2$ appears to be the principal molecular form. BMT account for all their observations between 700 and 1500° in terms of these two species. Although experimental difficulties caused large uncertainties in some of their data, the presence of polymeric molecules in the saturated vapor at lower temperatures is clearly indicated.

We now report a transpiration study of the palladium–bromine system; evidence for polymerization of $PdBr_2$(g) is also found. The equilibrium

$$x Pd(s) + x Br_2(g) = (PdBr_2)_x(g) \qquad (1)$$

has been studied in a quartz system between 650 and 900° and over a range of bromine pressures. Bromine pressures, in equilibrium with Pd(s) and $PdBr_2$(s) in the range 500–700°, and the total concentration of palladium in vapor molecules in equilibrium with solid palladium dibromide (550–700°) have also been determined.

Experimental Section

The transpiration apparatus used has been described previously.[2,3] Argon, or argon + bromine, or bromine alone served as carrier gases. The total pressures of gas mixtures containing significant amounts of bromine were measured with a glass diaphragm gauge; in the absence of significant amounts of bromine, argon pressures were measured manometrically. For the study of bromine equilibrium pressures above Pd(s) and $PdBr_2$(s), flow rates of 5 to 45 $cm^3\ min^{-1}$ were found to

(1) W. E. Bell, U. Merten, and M. Tagami, *J. Phys. Chem.*, **65**, 510 (1961).

(2) R. R. Richards and N. W. Gregory, *ibid.*, **68**, 3084 (1964).

(3) For full details, see the Ph.D. Thesis of R. C. Williams, University of Washington, 1968, Seattle, Wash. 98105.

Table I: Bromine Pressures for the Equilibrium: $PdBr_2(s) = Pd(s) + Br_2(g)$

T, °K	Flow rate, $cm^3\ min^{-1}$	Mol % $PdBr_2$ in Pd–$PdBr_2$ mixture	$100P_{Br_2}$, atm	T, °K	Flow rate, $cm^3\ min^{-1}$	Mol % $PdBr_2$ in Pd–$PdBr_2$ mixture	$100P_{Br_2}$, atm
765	40	~40[a]	0.282	845	40	~40	2.56
785	40	~40	0.512	943	10	~40	19.6
					5	~40	19.6
805	25	~40	0.860				
	40	~40	0.901	945	47 (2)	~40	20.7 (±0.2)
					15	~40	21.3
825	30	2	1.60[c]				
	20 (2)[b]	20	1.52 (±0.08)	959	20	2	26.9[c]
	26	23	1.51		20	20	27.0
	26	31	1.51		20	96	28.9
	20 (2)	35	1.52 (±0.01)				
	20 (2)	40	1.51 (±0.01)	967	20	~40	30.8
	40	~40	1.52				
	25 (2)	~40	1.46 (±0.05)				
	20 (2)	98	1.45 (±0.02)				

[a] ~40 is an approximate composition; the $PdBr_2$-coated Pd samples were used. Other compositions were based on actual analysis. Data for samples in the composition range 20–40 were averaged at each temperature and the averages plotted as the open circles in Figure 1. [b] (2) indicates two runs under these conditions; the deviation of the independent results from the reported average is indicated by (±). [c] Equilibrium approached from high bromine pressure (in carrier gas) side; in others, the initial carrier gas was pure argon.

give results indistinguishable within experimental uncertainty; pressures deduced from these experiments were taken as equilibrium values. In the study of the saturation vapor pressures (equilibrium with $PdBr_2(s)$) and of the formation of palladium bromide vapor from Pd(s) and bromine, flow rates between 5 and 60 $cm^3\ min^{-1}$ gave similar results as long as vapor pressures were below 2×10^{-5} atm; at higher vapor pressures it was necessary to keep flow rates below 36 $cm^3\ min^{-1}$.

Palladium (Engelhard Industries, 20 mesh, 99.95% pure), or Pd + $PdBr_2$, or pure $PdBr_2$ was initially placed in the reactor. To obtain $PbBr_2$, Pd was brominated in a preliminary experiment in the transpiration apparatus. Direct reaction of the metal with bromine around 600° without sublimination did not yield pure $PdBr_2$; at best an overall composition of $PdBr_{0.8}$ was obtained. However, this limiting composition seemed simply a kinetic effect, caused by coating of the palladium particles with the bromide which slowed further reaction. Pure $PdBr_2$ was obtained by sublimation of the product away from excess metal in a stream of bromine. The inertness of the coated metal was also demonstrated in some of the transpiration experiments. Bromine, introduced into the carrier gas at partial pressures in excess of those permitted by equilibrium between Pd(s), $Br_2(g)$, and $PbBr_2(s)$, Table I, did not react further when the $PdBr_2(g)$-coated palladium samples were used. Normal palladium dibromide vapor pressures were obtained from these experiments but the bromine pressures remained at their high values (data in part A of Table II). On the other hand, if mixtures with a large excess of palladium metal were used, the bromine pressures in such transpiration experiments fell to the expected equilibrium values.

Material indistinguishable from that sublimed away from the partially brominated Pd–$PdBr_2$ mixtures was prepared, alternatively, by dissolution of the metal in concentrated nitric acid, dilution of the solution with water, and addition of HBr to form a precipitate of $PdBr_2$. $PdBr_2$ is not hygroscopic and is not appreciably soluble in water; however, it does dissolve readily in concentrated HBr.

In the transpiration runs $PdBr_2$ condensed from the gas mixture on the walls of the inner gas-exit tube, in the temperature gradient at the end of the reactor furnace. The small amounts, 10^{-4} to 10^{-6} mol, were determined by a microquantitative colorimetric technique, using N,N-dimethyl-*p*-nitrosoaniline.[4] The absorbance of the red complex was measured and compared with standard solutions at 525 mμ with a Beckman DU spectrophotometer. The uncertainty estimated was ±2%.

At the highest temperatures (above 800°) some crystalline Pd metal was deposited as well as $PdBr_2$. The circumstances leading to this will be explained in the discussion of results. The crystalline metal deposit would not dissolve readily in HBr or in concentrated HNO_3; it was brominated by a subsequent treatment with bromine at *ca.* 600° to convert it to $PdBr_2$, which was sublimed to the end of the furnace and later dissolved in the usual fashion.

Bromine in the equilibrium gas mixture was condensed in a liquid oxygen-cooled trap. The quantity was determined by dissolving the sample in KI solution and titrating the resulting I_3^- with sodium thiosul-

(4) F. D. Snell and C. T. Snell, "Colorimetric Methods of Analysis," Vol. II, D. Van Nostrand Co., Inc., Princeton, N. J., 1949, p 530.

Table II: Experimental Data

T, °K	Flow rate, cm³ min⁻¹	$10P(Br_2)$, atm	10^5P_m(app), atm	T, °K	Flow rate, cm³ min⁻¹	$10P(Br_2)$, atm	10^5P_m(app), atm
			(A) $xPdBr_2(s) = (PdBr_2)_x(g)$				
805	30	0.85	2.58	880	15	2.17	46.1
					20	2.50	45.5
825	40	0.152[c]	0.654		10	2.59	48.5
	40	...	0.592				
	25	...	0.692	895	26 (2)	0.85	80.5 (±1.8)
	10	2.53	0.618		15	0.86	76.0
					5 (2)	0.88	76.7 (±3)
845	15	0.87	13.5		10	0.89	75.0
	15	2.37	13.4				
	20	...	13.6	943	5	1.96[c]	279
					10	1.99[c]	262
865	10	0.87	27.9		15	2.98	292
	15	0.87	27.9				
	26	0.87	27.8	945	47 (2)	2.07[c]	325 (±16)
	15 (2)[a]	2.11	25.7 (±1)[b]		15	2.13[c]	320
	20	2.42	27.0		20 (2)	2.82	304 (±0)
					20	3.00	364
880	26	0.79	48.5				
	10	0.88	47.9	967	15	3.34	599
	15	0.88	47.7		15	3.58	570
			(B) $xPd(s) - xBr_2(g) = (PdBr_2)_x(g)$				
925	55	0.871	19.3	1073	42	0.839	0.421
					45	1.60	1.08
945	30 (2)	0.864	55.8 (±0.8)		18	2.27	1.82
	20 (4)	1.31	35.1 (±2)				
	21 (3)	1.73	114 (±1)	1090	51	0.832	0.493
					53	1.57	1.13
965	32 (2)	0.867	1.53 (±0)		25	2.08	1.72
	20 (3)	1.31	9.57 (±0.12)		21	2.55	2.34
	20 (2)	1.73	37.0 (±0.5)		35	2.55	2.34
	22 (3)	2.17	99.1 (±1.5)				
	3	2.98	549	1105	52	0.832	0.624
	18 (2)	2.98	522 (±20)		50 (2)	1.56	1.22 (±0.05)
					33	2.14	1.93
985	23	0.862	0.553		31 (2)	2.54	2.58 (±0)
	36	0.862	0.551				
	20 (2)	1.31	3.06 (±0.06)	1130	54	0.798	0.825
	21	1.72	11.0		40	0.815	0.824
	22 (2)	2.16	33.6 (±0.6)		66	1.57	1.62
	6	2.97	151		33	1.57	1.60
	16 (2)	2.97	136 (±4)		15	2.17	2.32
	26 (2)	2.97	130 (±7)		33	2.20	2.30
					23 (2)	2.68	3.05 (±0)
1005	50 (2)	0.858	0.354 (±0.005)				
	21	1.72	3.66	1155	51	0.800	0.920
	22	2.16	10.1		53	1.55	2.15
1055	50 (2)	0.845	0.358 (±0.01)				
	61	1.37	0.743				
	64	1.89	1.30				

[a] The number of runs ( ) made under these conditions; the result given is then the average, with the maximum deviation indicated by (±). [b] Run started with pure $PdBr_2(s)$; other reactor mixtures, part A, were $PdBr_2$-coated Pd. [c] P_{Br_2} formed in reactor by reaction 2; in other cases, for part A, P_{Br_2} in carrier gas exceeds that produced by (2); see Discussion, Experimental Section.

fate. The thermal dissociation of Br_2 to bromine atoms need be considered only at the highest temperatues and lowest pressures of our study. Argon was collected by condensation in a liquid nitrogen-cooled trap; at the end of the experiment the argon sample was expanded into a calibrated volume and the number of moles determined from its temperature and pressure.

Temperatures were measured with chromel–alumel or Pt–Pt (10% Rh) thermocouples which were standardized periodically against the melting points of NBS

certified samples of aluminum and zinc. Temperatures were controlled within ±0.5° with Foxboro regulators.

Properties of Palladium Dibromide. Solid palladium bromide is reported to exist only in the form $PdBr_2$, and our observations are consistent with this conclusion.[5] Analysis of material sublimed in excess bromine gave a Pd:Br ratio of 1:2, within an estimated experimental uncertainty of ±1%. For analysis, a weighed sample was thermally decomposed under vacuum. The metallic residue, identified as Pd by chemical properties and X-ray powder pattern, was weighed; the bromine released was trapped and the quantity was determined iodometrically.

X-Ray powder patterns of samples of the sublimed bromide gave spacings expected for the structure reported by Broderson, Thiele and Gaedcke.[6] X-Ray powder patterns of various palladium and palladium bromide mixtures used were found to be a combination of those of Pd metal and $PdBr_2(s)$; no shift in the spacings characteristic of the pure phases could be seen. Hence it appears, under the conditions of our experiments, that Pd and $PdBr_2$ do not form solid solutions over a significant composition interval or a bromide phase with intermediate stoichiometry; this conclusion is also consistent with the results of vaporization equilibrium studies of mixtures of the two substances.

The melting point of $PdBr_2$, stabilized by the presence of bromine, 717 ± 2°, and the apparent eutectic temperature of Pd–$PdBr_2$ mixtures, 702 ± 2°, were detected by differential thermal analysis experiments. A thermal anomaly, suggestive of a phase transition, was also detected at 554 ± 2°, in both the pure $PbBr_2$ and in $PdBr_2$–Pd mixtures. No further work has been done to verify the existence of a transition; the associated enthalpy change appeared small relative to the heat of fusion.

Results and Discussion

Thermal Decomposition of $PdBr_2(s)$. Bromine pressures calculated for the equilibrium

$$PdBr_2(s) = Pd(s) + Br_2(g) \qquad (2)$$

are shown in Table I. At 825 and 959°K, mixtures of widely different compositions were used; within the experimental uncertainty (*ca.* 5%) these mixtures gave the same value (the 2% result at 825° appears slightly high; however, this is believed a result of a slow approach to equilibrium from the high bromine pressure side; a solubility effect would be expected to result in a lower bromine pressure). The sample reactor mixtures (~40) were frequently used for a series of five or six experiments, with the order of selection of temperatures random. No systematic variation in results of the successive runs could be detected. Thus the activities of Pd(s) and of $PbBr_2(s)$ appear independent of the bulk composition of the solid mixture; both have been assigned an activity of 1.

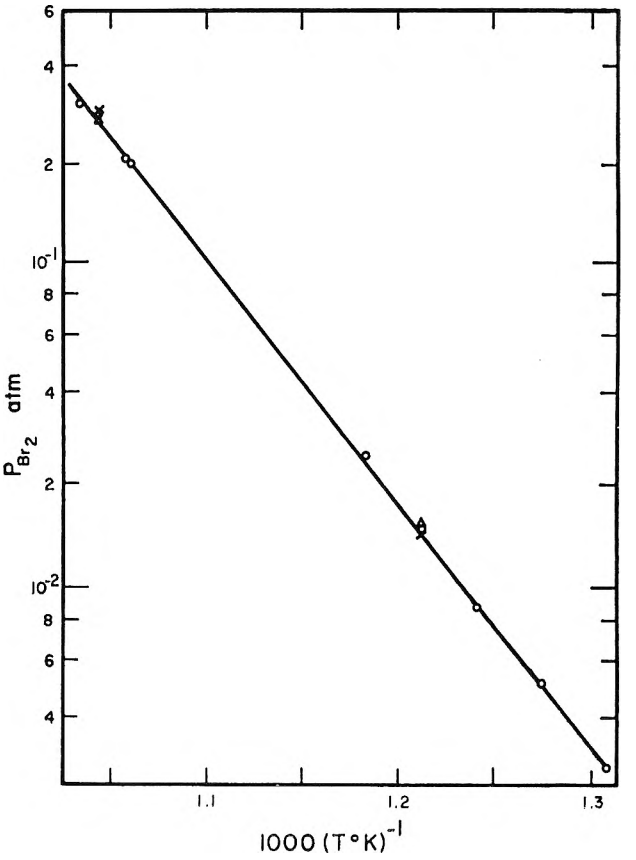

Figure 1. Bromine pressures for the equilibrium $PdBr_2(s) = Pd(s) + Br_2(g)$. Some symbols represent the average of several determinations (see Table I); mole per cent $PdBr_2$ in solid mixture: ×, 96–98; ○, 20–40; △, 2. The line indicates pressures given by eq 3.

A ΔC_P° of −6 eu (eu, entropy unit, used as an abbreviation for cal deg^{-1} mol^{-1}) was estimated for (2) by comparison with similar substances;[7] a van't Hoff treatment of the data gave the equation (P_{Br_2} in atm)

$$\ln P_{Br_2} = -19{,}840T^{-1} - 3.02 \ln T + 40.124 \qquad (3)$$

for the interval 765–970°K. This equation gives the line shown in Figure 1 and values of $\Delta H^\circ = 34.0 \pm 1$ kcal and $\Delta S^\circ = 32.8 = 1$ eu (standard state of gases taken as 1 atm) at 900°K, taken as a median temperature. Together with standard values for $Br_2(g)$[7] and Pd(s),[8] a standard entropy of 51.9 eu is derived for $PdBr_2(s)$ at 900°K.

Heat capacity data for $PdBr_2(s)$ have not been reported. With $\bar{H}^\circ_{900} - \bar{H}^\circ_{298}$ and $\bar{S}^\circ_{900} - \bar{S}^\circ_{298}$ esti-

(5) F. A. Cotton and G. Wilkinson, "Advanced Inorganic Chemistry," John Wiley and Sons, New York, N. Y., 1967, p 849.

(6) K. Broderson, G. Thiele, and H. Gaedcke, *Z. Anorg. Allg. Chem.*, **348**, 162 (1966).

(7) "JANAF Thermochemical Tables," The Dow Chemical Co., Midland, Mich.

(8) D. R. Stull and G. C. Sinke, Advances in Chemistry Series, No. 18, American Chemical Society, Washington, D. C., 1956, p 145.

mated as 12.3 kcal mol^{-1} and 21.7 eu, respectively (these values are an average of those of comparable $MBr_2(s)$ compounds),[7] values of $\Delta H°_{298}$ for formation of $PdBr_2(s)$ from liquid bromine and Pd(s) of -29.6 kcal mol^{-1} and of $S_{298}°$ of 30 eu are obtained. The former is 4.7 kcal more negative than the value based on the very early calorimetric data of Joannis,[9] derived from a study of the reaction of Pd and liquid bromine in a KBr solution. The entropy derived is less than that listed by Brewer, *et al.* (35 ± 5), but appears within the uncertainty of the estimations.[10]

The Apparent Vapor Pressure of $PdBr_2(s)$. From the total number of moles of palladium in a given volume of vapor in equilibrium with $PdBr_2(s)$, we have calculated values of P_m(app), *i.e.*, the apparent monomer pressure, the vapor pressure expected if all molecules were of the actual form $PdBr_2$ and gave perfect gas behavior. It can be seen, Table II and Figure 2, that

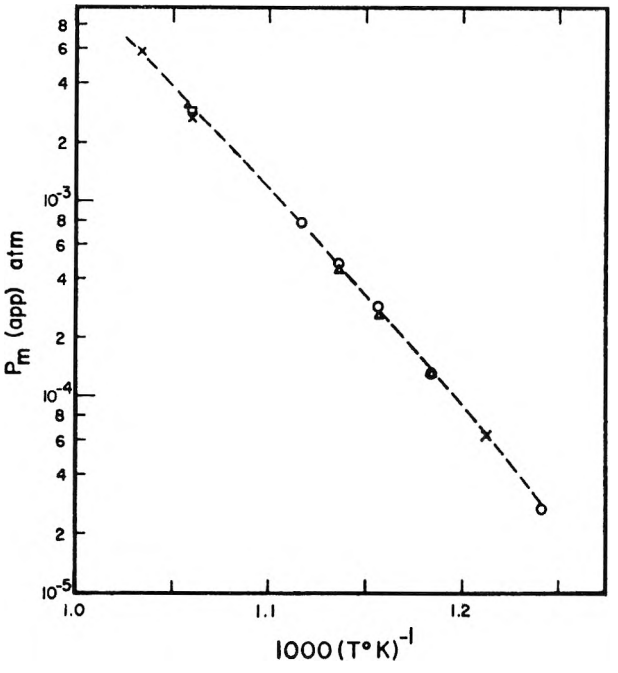

Figure 2. P_m(app) in equilibrium with $PdBr_2(s)$ at various bromine pressures. P_{Br_2}(atm): □, 0.3; △, 0.25; ×, 0.2; ○, 0.09. The line – – – was derived from eq 3, 10, and 11, *i.e.*, the monomer–tetramer–hexamer model.

the values of P_m(app) in the presence of $PdBr_2(s)$ are independent of the bromine pressure at given temperature. Hence the vaporization reaction may be represented in the general form

$$x\mathrm{PdBr_2(s)} = (\mathrm{PdBr_2})_x\mathrm{(g)} \qquad (4)$$

The values of P_m(app), when plotted as in Figure 2, show an apparent curvature greater than expected for simple vaporization of monomer. While this alone is not conclusive, the experiments to be discussed in the following section demonstrate further that the molecular composition of the vapor is not simple. Thus a van't Hoff treatment of the vapor pressure data expressed as P_m(app) has no meaning relative to the thermodynamic properties of the monomer. The dashed line shown in Figure 2 has been derived from vaporization equilibrium constants deduced in the next section.

Equilibrium between Palladium Bromide Vapor, Palladium Metal, and Bromine. When Pd(s) was the only condensed phase present, values of P_m(app) were found to be markedly dependent on the bromine pressure, see Table IIB. If x in reaction 1 has a single integral value, a plot of log P_m(app) *vs.* log P_{Br_2} will be linear with slope x. The data are graphed in this form in Figure 3; in general, curvature is evident. At the highest temperatures, the slopes approach 1; at the higher bromine pressures and lower temperatures, the slopes approach 5. This suggests that the vapor may be a mixture of pentamer and monomer, as assumed by BMT in their study of the chloride system.[1] However, it was found that the curvature in the lines in Figure 3 could not be explained adequately by a monomer–pentamer model, or, when the data at all temperatures were considered together, by any other choice of only two molecular species. On the other hand, a model consisting of a series of polymers, *i.e.*, $x = 1, 2, 3, \ldots x$ at relative concentrations predicted by a rough approximation that $\Delta H°$ and $\Delta S°$ for successive additions of a monomer unit to a chain-like polymer are constant, gives a result which also deviates widely from the curvature of the lines in Figure 3. It was concluded, therefore, that certain relatively large polymers have special stability.

An attempt to obtain mass spectrographic evidence for the composition of the vapor was not successful. The mass spectrometer available was not suitably designed to prevent interaction of the bromine in the inlet beam with metal surfaces in the source chamber (bromine pressures are from two to three orders of magnitude larger than P_m(app)). Strong peaks identified with bromides of copper, etc., dominated the spectra. Some large mass numbers were observed (range 630–800) but these could not be positively identified with palladium bromide ions by isotopic distribution. We believe, however, that some meaningful conclusions about the molecular composition of the vapor have been derived from the transpiration data.

At the highest temperature, 882°, P_m(app) was found directly proportional to P_{Br_2}, Figure 3, which suggests that the monomer is the only species of importance in these experiments; K_1, for the reaction

$$\mathrm{Pd(s) + Br_2(g) = PdBr_2(g)} \qquad (5)$$

may then be equated with $P_m(\mathrm{app})/P_{Br_2}$. At lower

(9) M. Joannis, *Compt. Rend.*, 95, 295 (1882).

(10) L. L. Quill, "Chemistry and Metallurgy of Miscellaneous Materials: Thermodynamics," McGraw-Hill, Book Co., Inc., New York, N. Y., 1950, p 97.

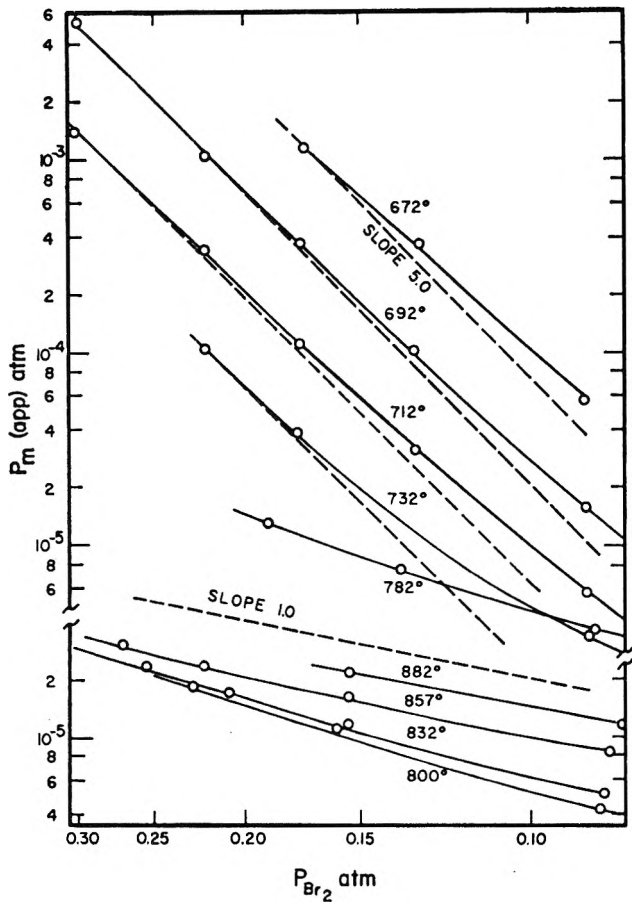

Figure 3. P_m(app) *vs.* P_{Br_2} (log–log plot). Note different scales.

temperatures this ratio was no longer independent of P_{Br_2}; an extrapolation procedure was used at 817° and above to determine K_1. In general we may write

$$P_m(\text{app}) = P_1 + 2P_2 + 3P_3 + \ldots xP_x$$
$$= K_1P_{Br_2} + 2K_2P_{Br_2}^2 + 3K_3P_{Br_2}^3 + \ldots$$
$$xK_xP_{Br_2}^x \quad (6)$$

where the subscripts designate the form of the particular species considered; 2 = dimer, 3 = trimer, etc.; P_x is the partial pressure of the x species, and K_x is the equilibrium constant for its formation from Pd(s) and Br_2(g). Data at 857, 832, and 817° could be correlated satisfactorily by using eq 6 with the monomer and only one other species. In Figure 4, which is representative, data at 832° are shown as a plot of P_m(app)/P_{Br_2} *vs.* $P_{Br_2}^{x-1}$ for choices of x of 2, 3, or 4, respectively. Within the uncertainty indicated, all three plots approach linearity and from this feature alone one cannot decide which value of x is best. It is possible, of course, that more than two species may be present. If x is set at values larger than 4, however, the lines show curvature outside experimental uncertainty.

An extrapolation of lines, of the type shown in Figure 4, to $P_{Br_2} = 0$ gives the apparent value of K_1. As

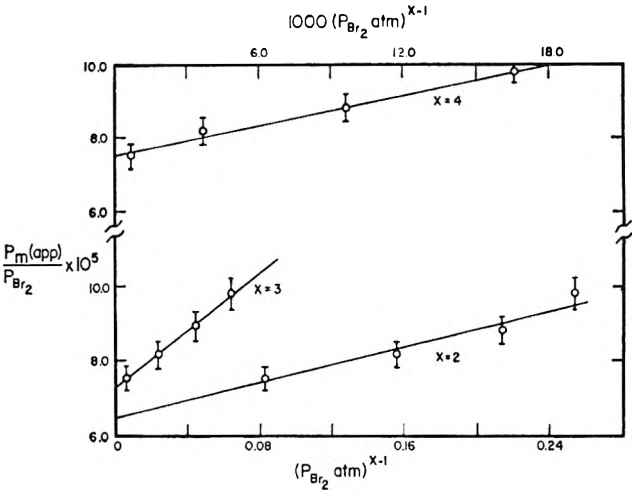

Figure 4. P_m (app)/P_{Br_2} *vs.* $P_{Br_2}^{x-1}$, for x = 2, 3, or 4, respectively, at 832°. Note different scales. Intercepts give apparent values of K_1, slopes, K_x. The range I indicates experimental uncertainty.

shown in Figure 5, the K_1 values deduced from the 1–3 and 1–4 plots are within experimental error. The values of K_1 from the 1–2 plots are significantly lower at the lower two temperatures. We have elected to use the values of K_1 given by the 1–4 model, because, as will be shown, the overall behavior of the system

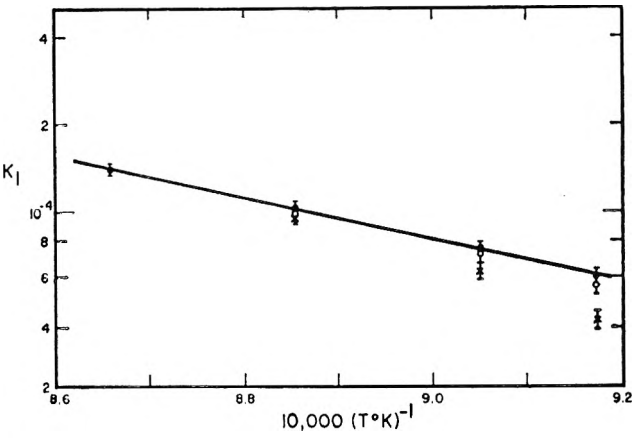

Figure 5. Values of K_1 at various temperatures: ●, 1–4 model; ○, 1–3 model; ×, 1–2 model. The line represents values given by eq 7.

can be satisfactorily explained if the vapor is assumed to be a mixture of monomer, tetramer, and hexamer (1–4–6); this model predicts that the hexamer does not contribute significantly at temperatures above 800°. Furthermore, these values of K_1 agree well with those predicted from the K_1 value at 882° and an estimated free energy function for $PdBr_2$(g) of 89 (taken as one unit larger than the value selected for $NiBr_2$(g) by Brewer, *et al.*)[11] and a $\Delta(\bar{H}°_{1155} - \bar{H}°_{298})$

(11) L. Brewer, G. R. Somayajulu, and E. Brackett, *Chem. Rev.*, **63**, 111 (1963).

value for reaction 5 of -1.1. The latter is the average of the very similar values of five similar $MBr_2(g)$ compounds.[7] The line in Figure 5 was derived from the data and, with an estimated $\Delta C_P°$ of -2 eu, corresponds to the equation (for the range 1090–1155°K)

$$\ln K_1 = -17{,}386T^{-1} - 1.006 \ln T + 13.278 \quad (7)$$

Equation 7 gives $\Delta H°$ for $PdBr_2(g)$ of 32.3 ± 2.5 kcal mol^{-1} and a standard entropy of 98.0 ± 2.5 eu at 1100°K. With the estimated relative enthalpy cited above, $\Delta H°_{298}$ becomes 26.0 kcal mol^{-1}, relative to liquid bromine as the standard state. $\Delta S°$ for (5) at 1100°K is 10.4 eu; BMT report 11.1 eu at 1573°K, for the similar reaction in the chloride system.[1]

An extrapolation of eq 7 gave values of P_1 to be expected at lower temperatures; these were significant relative to P_m(app) only at temperatures above 700° and then only at the lowest bromine pressures. Equation 6 may now be written in the form $P_m(\text{app}) - P_1 = P_m'$, with P_m' to be associated with the contributions of polymeric species. Plots of log P_m' *vs.* log P_{Br_2} at

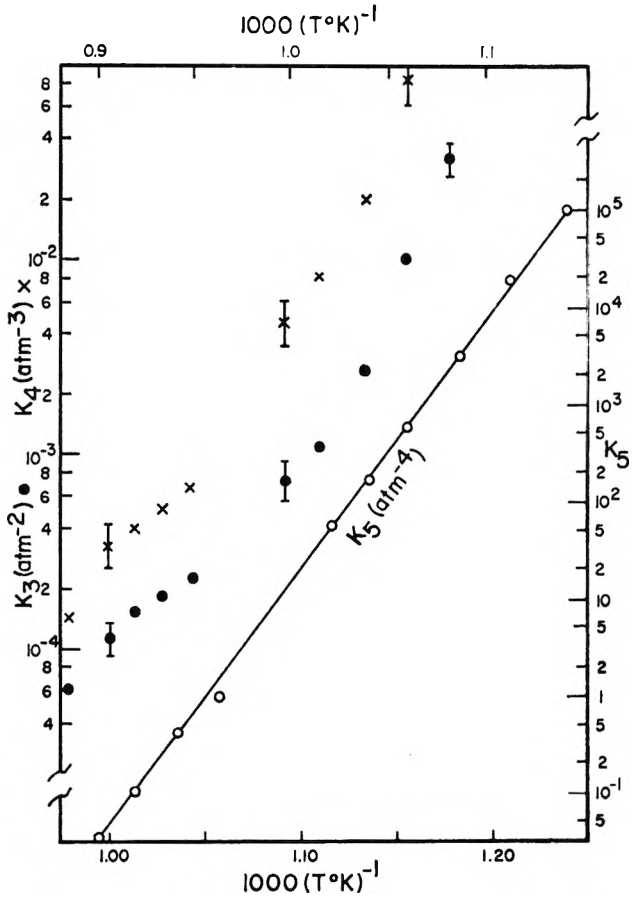

Figure 6. Apparent values of K_5, ○; K_4, ×; K_3, ●, respectively, based on trial monomer–trimer (or, alternatively, tetramer)–pentamer models. Uncertainty expected from experimental error indicated by the lengths I drawn through representative points. The curvature of K_3 and K_4 sets of points shows these models do not correlate the data satisfactorily. Note K_3 and K_4 are on a different scale than K_5.

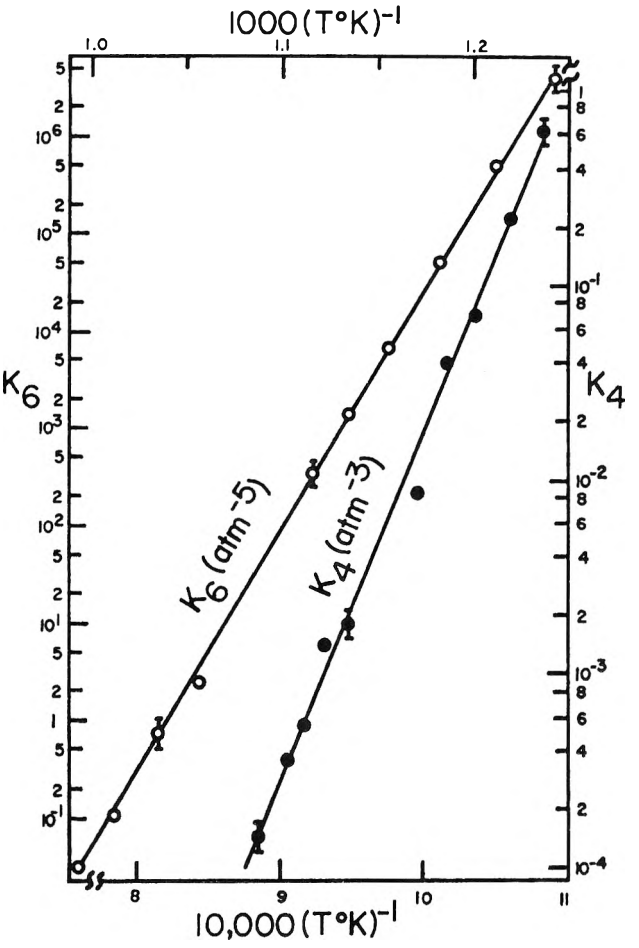

Figure 7. Apparent values of K_4, ●, and K_6, ○ (note different scales) deduced from the monomer–tetramer–hexamer model. Uncertainty expected from experimental error indicated by lengths I drawn through representative points. Note correlation is much better than in Figure 6.

732° and lower temperatures still show clearly that at least two polymeric forms must be present. Since the slopes were still near 5 at the highest bromine pressures, an attempt to fit the data was first made in the following way. The pentamer was assumed to be the major species present at the highest bromine pressure (at each temperature in the 670–732° range) and $5K_5$ approximated as $P_m'/P_{Br_2}^5$. This value was then used to calculate P_5 for the experiments at lower bromine pressures and the deviation $(P_m' - 5P_5)/P_{Br_2}^x$ examined. With $x = 3$, or alternatively $x = 4$, this ratio was found to be reasonably constant over the range of bromine pressures at each temperature; an average value was used to estimate K_3 (or alternatively K_4); *i.e.*, the mixtures were assumed to be only 1–3–5 or 1–4–5. From the estimate of K_3 (or K_4), the contribution of P_3 (or P_4) at the highest bromine pressure was calculated; a corrected $5P_5$, $P_m' - 3P_3$ (or $4P_4$), led to a revised estimate of K_5, which in turn gave a revised K_3, etc. The iteration procedure was continued until consistent values of the equilibrium constants were obtained.

The values of K_5 given by the 1–3–5 and 1–4–5 alternatives were very similar and were found to fit well with the saturation vapor pressure data (550–650°) if P_m(app) in this range was attributed entirely to pentamer. The result is shown as the K_5 plot in Figure 6. The associated values of K_3, however, when compared with the values of K_3 deduced from the 1–3 plots in the 782–857° range, did not correlate well, as may be seen by the curving set of points in Figure 6. The deviation from a linear relationship is significantly more than the uncertainty of the experimental measurements. The correlation of K_4 values, from the similar treatment of the 4–5 and 1–4 alternatives, is only slightly better, Figure 6. A further difficulty arose on linear extrapolation of the K_4 set of points to the saturation vapor pressure range; the contributions predicted from the tetramer were *ca.* 30% P_m(app), *i.e.*, the combination of P_4 and P_5 gave values of P_m(app) considerably above the observed vapor pressures. Iteration treatment of the data in this range did not produce a satisfactory general fit. Attempts to fit the data with a 1–3–4–5 model were also not successful.

Correlation of the data was found to be very satisfactory when the principal species at the lower temperatures were assumed to be the tetramer and the hexamer. Least-squares solutions of eq 6, in the form $P_m'/P_{Br_2}^4 = 4K_4 + 6K_6P_{Br_2}^2$, were first carried out at the various temperatures in the 670–732° range. The values of K_4 derived were then compared (a van't Hoff plot) with those obtained from the 1–4 model in the 782–857° range pressure range (550–650°), the contributions of P_4 evaluated and subtracted from the experimental values of P_m(app); the remainder was attributed to P_6 and used, together with the bromine pressures, to evaluate K_6 at temperatures in this range. These values were then plotted as a function of temperature, together with those deduced from the 670–732° data, and also found to give a good correlation.

The final values derived for K_4 and K_6 are shown in Figure 7. The data can be seen to correlate much better than the results in Figure 6. The predicted value of P_m(app) for the saturated vapor, *i.e.*, in the presence of Pd(s), $PdBr_2$(s), and bromine at equilibrium, is shown as the dashed line, in comparison with the experimental points, in Figure 2. The agreement is very good.

The temperature dependence derived for K_4 and K_6, which are equilibrium constants for the reactions

$$4Pd(s) + 4Br_2(g) = Pd_4Br_8(g) \quad (8)$$

and

$$6Pd(s) + 6Br_2(g) = Pd_6Br_{12}(g) \quad (9)$$

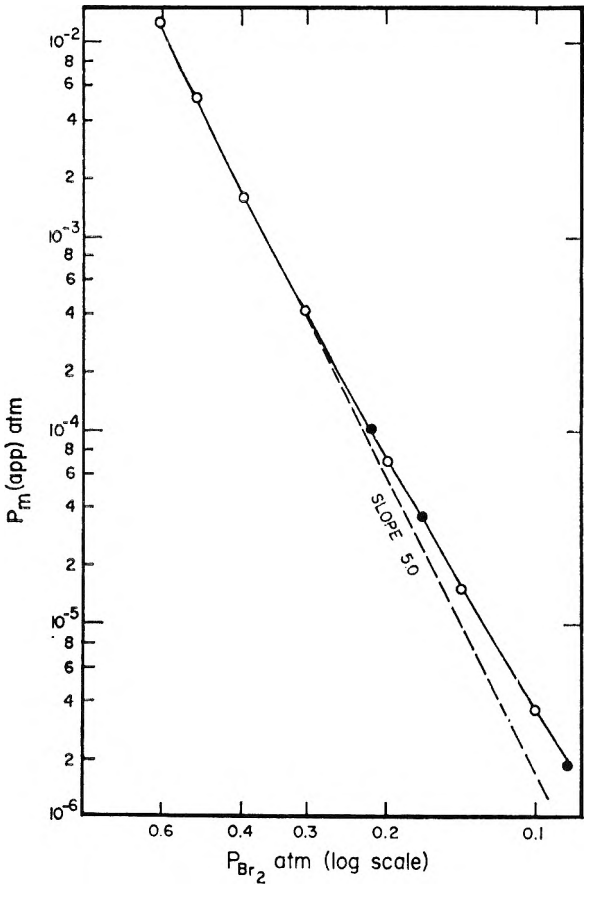

Figure 8. Calculated —○—, based on 1–4–6 model, and observed, ●, values of P_m(app) *vs.* P_{Br_2} (log–log plot) at 732°, in comparison with slope 5.

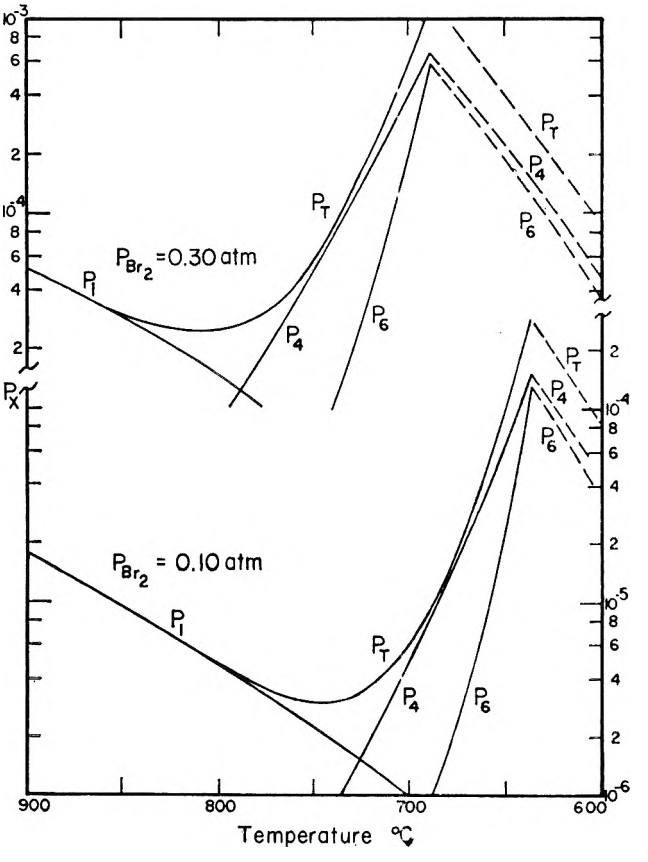

Figure 9. P_t, P_1, P_4, and P_6, at bromine pressures of 0.3 and 0.1 atm, respectively, as functions of temperature, predicted by equilibrium constants derived for the 1–4–6 model. The dashed lines characterize the vapor in equilibrium with $PdBr_2$(s); the solid lines, the vapor in equilibrium with Pd(s).

respectively, according to the 1–4–6 model may be represented by the equations

$$\ln K_4 = 42{,}210T^{-1} - 0.50 \ln T - 42.804 \quad (10)$$

$$\ln K_6 = 78{,}880T^{-1} + 2.01 \ln T - 96.055 \quad (11)$$

which give the lines shown in Figure 7. Apparent thermodynamic properties of the tetramer and hexamer may be readily evaluated from eq 10 and 11.[3] However, presentation and discussion of these quantities does not seem warranted until independent evidence is found to support the proposed vapor composition. It is clear that, in a system of this complexity, a number of alternative models of the molecular composition may fit the results equally well, particularly mixtures involving a larger number of species. However, the solution proposed is the simplest one found consistent with all the data.

Figure 8 shows a comparison of P_m(app), derived from K_4 and K_6 at 732°, with the experimental data. The figure illustrates that the combined effect of the two polymeric species on this log–log plot gives a slope closely approximating 5, even up to bromine pressures of 0.6 atm. It seems possible that a similar mixture may also form in the chloride system. BMT,[1] in their discussion, recognized that their data could be equally well explained by combinations involving a hexamer, etc., but saw nothing to suggest that this was more likely than their simpler pentamer–monomer model. The two systems may, of course, be different.

Figure 9 shows calculated values of P_1, P_4, and P_6 as functions of temperature at two representative bromine pressures; when Pd(s) is the only condensed phase present, P_1 decreases as the temperature decreases whereas P_4 and P_6 increase. This behavior is related to the conclusion, which may be drawn from eq 6, 10, and 11, that the enthalpies of formation of the polymeric species are negative whereas that of the monomer is positive. Thus when the monomer is the principal constituent of the vapor, gradual cooling at a fixed bromine pressure will lead first to deposition of palladium metal. On the other hand, when the tetramer and hexamer are dominant, cooling will result in deposition of $PdBr_2$(s) rather than Pd(s). The experimental observations are in accord with this behavior. Deposition of Pd(s) was observed only in the regions near the reactor zone and only when the latter was above 800°. It should be noted, however, that a similar behavior might also be expected for other polymeric forms and hence the deposition of palladium does not provide support for the particular polymeric composition proposed.

The apparent special stability of the tetramer and the hexamer suggests that closed structures, rings, or similarly interlocked groups, are formed rather than "linear" open-ended chains. From the structural form of the solid, one expects planar $PdBr_4$ groups to link together, with neighboring palladium atoms sharing pairs of bromine atoms. Closed structures compatible with expected bond angles can be constructed with four or six $PdBr_2$ units, although not with two or three.

Acknowledgment. This work was done with financial support from the National Science Foundation, Grant 6608x, which is acknowledged with thanks.

The Self-Diffusion of Oxygen in Magnetite. The Effect of Anion Vacancy Concentration and Cation Distribution

by J. E. Castle and P. L. Surman

Central Electricity Research Laboratories, Leatherhead, Surrey, England *(Received August 19, 1968)*

The variation of the self-diffusion coefficient of oxygen in magnetite with hydrogen/water ratio and temperature can be expressed as

$$D = 1.8 \times 10^{-13}(P_{H_2}/P_{H_2O})^{0.27} \exp(-17{,}000/RT) \text{ cm}^2 \text{ sec}^{-1}$$

The variation of D with P_{H_2}/P_{H_2O} is compared with the theoretical predictions made by Wagner and Schmalzried for ternary oxides. It is concluded that at temperatures above 500°, the distribution of cations in the magnetite lattice becomes randomized due to electron exchange.

Introduction

In an earlier paper,[1] the influence of temperature on the rate of self-diffusion of oxygen in magnetite, in a water vapor atmosphere, was described. Magnetite is stable over only a small range of composition, corresponding to 27.4 to 27.7 wt % oxygen,[2] and the initial work was carried out at the oxygen-rich end of this range, where the anion defect concentration and hence the diffusion coefficient would be expected to be smallest. The phases in equilibrium with hydrogen–water mixtures in the temperature range of interest to this study are illustrated by Dushman.[3] At 500° magnetite is stable over the range $P_{H_2}/P_{H_2O} = 10^{-5}$ to 3.8. The extension of our investigation to include the whole of this range enables us to confirm that diffusion is a function of anion vacancy concentration and also tests our assumption that the very slight degree of oxidation of the sample to produce the equilibrium atmosphere $P_{H_2}/P_{H_2O} = 10^{-5}$ will have no significant effect on the results.

Experimental Section

The exchange between 10% oxygen-18 enriched water vapor and single crystalline magnetite particles, of radius 0.15 μm, was followed by continuous sampling into a mass spectrometer, which was heated to 180°. The apparatus and experimental procedure have been described in detail previously,[1] the only modification being a device for establishing constant hydrogen–water vapor ratios. This was achieved by dosing from calibrated bulbs and calculated making allowances for the temperature variation in the diffusion cycle. When only small hydrogen/water ratios were used ($<10^{-1}$) the hydrogen partial pressure was controlled by connecting the diffusion loop to a 5-l. bulb *via* a palladium–silver thimble heated to just below dull red. Initial tests without water in the system showed that even with 10^{-3} Torr of H_2 in the reserve bulb the thimble was quite permeable to hydrogen, and that equilibrium, against a pressure of 60 Torr of krypton in the diffusion cycle, was established within 30 min. When the leak-valve into the mass spectrometer was set at 10^{-2} l. μsec^{-1} the recorded hydrogen pressure in the mass spectrometer and in the reserve bulb did not vary appreciably within the time taken by the exchange experiments. Samples of magnetite were equilibrated with isotopically normal water for 7 days under the conditions of the experiment.

Results

Plots of the dimensionless parameter Dt/a^2 *vs.* time gave straight lines with intercepts at the origin (D is the diffusion coefficient, t is the time for exchange, and a is the particle radius determined by krypton adsorption). This is good evidence that, as for previous results, the system approximates to the conditions required for the solution of the diffusion equation. Figure 1 illustrates the variation of the diffusion coefficient with hydrogen–water composition. The relationship established is

$$D_{500°} = 2.9(\pm 0.6) \times 10^{-18}(P_{H_2}/P_{H_2O})^{0.27(\pm 0.05)} \text{ cm}^2 \text{ sec}^{-1} \quad (1)$$

where the limits in brackets are obtained from the standard deviation of the individual parameters and are adjusted for 95% confidence limits.

Figure 2 compares the Arrhenius rate plot found for very low hydrogen levels with that found for $P_{H_2}/P_{H_2O} = 1.2$ (the 500° point is interpolated from the curve in Figure 1). It can be noted that the slopes of the lines are the same and hence that only the preexponential term is changed. Combining eq 1 with the relationship (2) previously reported

$$D = 3.2(\pm 1.6) \times 10^{-14} \times \exp[(-17{,}000 \pm 1650)/RT] \text{ cm}^2 \text{ sec}^{-1} \quad (2)$$

(1) J. E. Castle and P. L. Surman, *J. Phys. Chem.*, 71, 4255 (1967).

(2) N. D. Tomashov, "Theory of Corrosion and Protection of Metals," The Macmillan Co., New York, N. Y., 1966, p 82.

(3) S. Dushman, "Scientific Foundations of Vacuum Technique," 2nd ed, John Wiley and Sons, Inc., New York, N. Y., 1962, p 754.

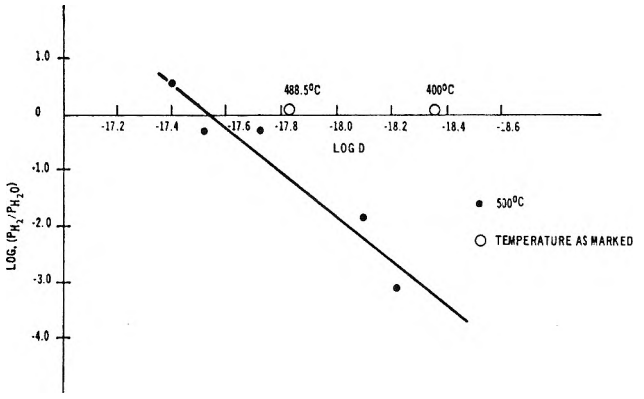

Figure 1. Plot of log diffusion coefficient *vs.* log hydrogen/water ratio.

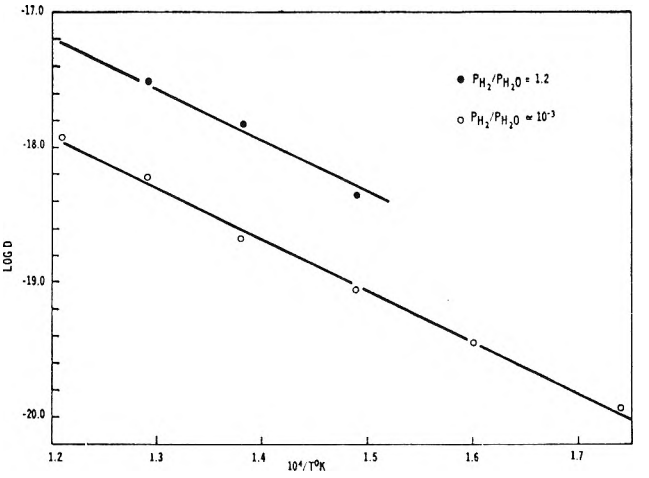

Figure 2. Arrhenius rate plot comparing two H_2/H_2O levels.

we obtain the general relationship

$$D = 1.8 \times 10^{-13}(P_{H_2}/P_{H_2O})^{0.27} \times \exp(-17{,}000/RT)\ \text{cm}^2\ \text{sec}^{-1} \quad (3)$$

for which there are insufficient experimental data to quote the statistical limits of error.

Discussion

The dependence of the diffusion coefficient on the oxygen partial pressure can be predicted on the basis of a theory of ternary oxides proposed by Wagner and Schmalzried.[4] They suggested that, in order to define the defect structure of these oxides, it is necessary to fix the activity of one of the constituent oxides, in addition to pressure temperature and thermodynamic activity of one constituent element as required for binary oxides. On this basis they treated magnetite as an inverse spinel consisting of the components FeO and Fe_2O_3, and showed that

$$C_{Fe^{2+}V} = \text{constant} \times P_{O_2}^{2/3} \quad (4)$$

and

$$C_{O^{2-}V} = \text{constant} \times P_{O_2}^{-1/2} \quad (5)$$

where (following the convention of A. B. Lidiard) C_{xV} represents the vacancy concentration of species x.

Experimentally it is convenient to define the oxygen partial pressure in terms of the CO/CO_2 or H_2/H_2O equilibrium, *i.e.*

$$P_{O_2} = K_1(P_{CO_2}/P_{CO})^2 = K_2(P_{H_2}/P_{H_2O})^{-2} \quad (6)$$

Thus, following Wagner's[4] assumption that the self-diffusion coefficient is linearly dependent on the relevant defect concentration (for a detailed discussion of this point see ref 5 and 6), we obtain

$$D_{O^{2-}} = \text{constant} \times P_{H_2}/P_{H_2O} \quad (7)$$

for the conditions of the present study and

$$D_{Fe^{2+}} = \text{constant} \times (P_{CO}/P_{CO_2})^{4/3} \quad (8)$$

for the study of iron self-diffusion in magnetite at 1115° carried out by Schmalzried[7] to test the model. These predictions are not in good accord with the experimental findings of Schmalzried (exponent = 0.8 ± 0.1) or of the present study (exponent = 0.27 ± 0.05).

The predicted values were based on the viewpoint that magnetite can be treated as a ternary oxide, *i.e.*, that the oxide has two distinct cation sublattices. At temperatures below 113°K this is undoubtedly the case[8,9] since the structure is that of a perfectly ordered inverse spinel. At higher temperatures there is electron interchange between Fe^{3+} and Fe^{2+} ions in the octahedral sites leading to random occupation of these sites.[10] Calculations of the lattice energy[11] suggest that the structure should be that of the normal spinel; *i.e.*, the ferrous ions should occupy the tetrahedal sites and ferric the octahedral sites. In fact, many 2-3 spinels including magnetite have the inverse-spinel structure at room temperature, but Dunitz and Orgel[12] have shown on the basis of crystal-field theory that the stabilization energy of the inverse spinel is only of the order of 4 kcal; this value is so small that at high temperatures electron exchange between tetrahedral Fe^{3+} ions and octahedral Fe^{2+} ions should be possible leading to randomization of the cations in the oxide.[13] Magnetite would then behave as a binary oxide with

(4) H. Schmalzried and C. Wagner, *Z. Phys. Chem.* (Frankfurt am Main), **31**, 198 (1962).
(5) H. Schmalzried, *Progr. Solid State Chem.*, **2**, 265 (1965).
(6) N. F. Mott and R. W. Gurney, "Electronic Processes in Ionic Crystals," Oxford, 1940, Chapter 2.
(7) H. Schmalzried, *Z. Phys. Chem.* (Frankfurt am Main), **31**, 184 (1962).
(8) E. J. W. Verwey, P. W. Hanyman, and F. C. Romeijn, *J. Chem. Phys.*, **15**, 181 (1947).
(9) C. D. Shull, E. O. Wollman, and W. C. Koehler, *Phys. Rev.*, **84**, 912 (1951).
(10) S. Takeuchi and K. Farukawa, *Sci. Repts. Research Inst., Tohuku Univ. Ser. A.*, **12**, 120 (1960).
(11) J. B. Goodenough and A. L. Loeb, *Phys. Rev.*, **98**, 391 (1955).
(12) J. D. Dunitz and L. E. Orgel, *J. Phys. Chem. Solids*, **3**, 20, 318 (1957).
(13) D. S. McLure, *ibid.*, **3**, 311 (1957).

the following phase boundary equilibria

$$2O_2 = Fe_3O_4 + Fe^{2+}V + 2Fe^{3+}V + 8e^- \quad (9)$$

$$\text{Null} = 2O^{2-}V + 4e^-V + O_2 \quad (10)$$

where the symbol V indicates a vacancy, e^- represents an electron, and Null denotes a stoichiometric crystal without lattice deffects.

These reactions can be expressed in terms of their equilibrium constants as

$$P^2_{O_2} = \text{constant } C_{Fe^{2+}V} \times C^2_{Fe^{3+}V} \times C^8_{e^-} \quad (11)$$

$$\text{constant} = C^2_{O^{2-}V} \times C^4_{e^-V} \times P_{O_2} \quad (12)$$

but $C_{Fe^{3+}V} = 2C_{Fe^{2+}V}$; $C_{e^-} = 8C_{Fe^{2+}V}$; $C_{e^-V} = 2C_{O^{2-}V}$

$$\therefore C_{Fe^{2+}V} = \text{constant } P_{O_2}^{2/11} \quad (13)$$

$$C_{O^{2-}V} = \text{constant } P_{O_2}^{-1/6} \quad (14)$$

Equations 13 and 14 for binary oxides can be compared directly with eq 4 and 5 which refer to the ternary oxide. Combining eq 13 and 14 with eq 6 and again assuming a linear dependence of the self-diffusion coefficient on the defect concentration, we obtain

$$D_{Fe^{2+}} = \text{constant} \times (P_{CO}/P_{CO_2})^{4/11} \quad (15)$$

$$D_{O^{2-}} = \text{constant} \times (P_{H_2}/P_{H_2O})^{1/3} \quad (16)$$

The exponents are in better agreement with the measured values than those predicted for ternary oxides. This supports the probability that the structure of magnetite is randomized within the temperature range of the studies (>500°): it is not therefore a useful oxide with which to test the Wagner–Schmalzried model.

The response of the oxygen diffusion coefficient to the oxygen partial pressure is particularly satisfactory since it shows that the oxygen sublattice remains in thermodynamic equilibrium with the atmosphere, even in an oxide in which the bulk of the stoichiometric deviations are accommodated in the cation sublattice. The change in the value of the self-diffusion coefficient over the complete composition range of magnetite is only one order of magnitude. This result, therefore, does not alter our earlier conclusion that the solid-state diffusion of oxygen is unlikely to be important in the oxidation of iron by steam or water.

Acknowledgments. The authors are grateful to the Central Electricity Generating Board for permission to publish this work, and also to Professor J. S. Anderson for valuable discussions.

A Comparison of the Proton Affinities of Neutral Oxygen and Sulfur in Chelating Ligands[1]

by Thomas L. James and Richard J. Kula

Department of Chemistry, University of Wisconsin, Madison, Wisconsin 53706 *(Received August 29, 1968)*

The nuclear magnetic resonance chemical shift behaviors of the nonexchanging carbon-bonded proton resonances of various S-alkylthioacetic acids and alkoxyacetic acids were studied in aqueous solution as a function of solvent acidity to determine the relative proton affinities of the donor atoms in such chelating ligands. The relative electron-donating abilities, ascertained from the sites and sequences of protonation, were found to be in the order

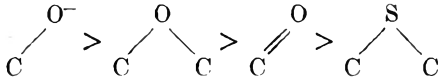

This order of proton affinity seems to reflect the relative contributions of these donor atoms to the stability of metal chelates for those metal ions with little tendency for the formation of dative π bonds. The suitability of internal references in the strongly acidic solutions used in this investigation was also studied.

Preliminary proton nuclear magnetic resonance (nmr) studies of some metal ion complexes of various S-alkylthioacetic acids (R–S–CH_2COOH) indicated little, if any, metal–sulfur interaction. Differences in metal–sulfur bond strengths for different ligands are governed by the Lewis basicity of the sulfur atom and the tendency for back-donation π bonding of sulfur. For transition metal ions, the strength of the metal–thioether sulfur bonding is apparently determined primarily by the latter mechanism—formation of dative π bonds with the empty d orbitals of sulfur.[2]

(1) This work was supported by a grant (GP4423) from the National Science Foundation and by a National Institutes of Health Predoctoral Fellowship (T. L. J.).

(2) (a) H. H. Jaffe, *J. Phys. Chem.*, **58**, 185 (1954); (b) D. P. Craig, A. Maccoll, R. S. Nyholm, L. E. Orgel, and L. E. Sutton, *J. Chem. Soc.*, 332 (1954).

In the absence of back-donation, the Lewis basicity of the sulfur is presumably the predominant factor determining the metal–sulfur bond strength.

Studies have been made of metal ion coordination with several S-alkylthioacetic acids and also with the corresponding alkoxyacetic acid ($R-O-CH_2COOH$) ligands.[3] While these studies indicate that the extent of metal thioether sulfur bonding and metal–ether oxygen bonding depends on the structure of the ligand as well as the metal ion, no definitive data are available comparing the relative basicities of thioether sulfur and ether oxygen.

One method of determining the relative Lewis basicities of oxygen and sulfur donor atoms is to compare the proton affinities of these atoms in a variety of carboxylic acid ligands containing thioether sulfur or ether oxygen. If there are no steric factors which affect the bonding, the proton affinities of the donor atoms in the ligands should in turn reflect the strength of the metal–donor bond for those metal ions which are incapable of forming dative π bonds with the donor atom. Rather than relying on comparisons of macroscopic protonation constants for analogous ligands in order to determine the relative basicities of the donor atoms, the sites and sequences of protonation have been ascertained using proton nmr. The protonation schemes of ethylenebisthioglycolic acid (ETGA), thiodiglycolic acid (TDG), (ethylthio)acetic acid (ETAA), ethoxyacetic acid (EOAA), acetic acid (HAc), dimethyl sulfide (DMS), and diethyl ether (DEE) were determined in aqueous solution.

Experimental Section

Proton nuclear magnetic resonance spectra were obtained with a Varian A-60A high-resolution spectrometer operated at a probe temperature of $25 \pm 2°$. Tetramethylammonium chloride, at a concentration of about 0.02 M, was used as an internal reference. The chemical shifts, ν, are reported in cycles per second from the central resonance of the tetramethylammonium (TMA) triplet, negative shifts corresponding to a resonance downfield from TMA. The spectrum of each sample was obtained five times and the reported chemical shift is an average of these five individual measurements.

Solution pH measurements were made at 25° using a Sargent Model DR line-operated pH meter equipped with a wide-range glass electrode. Conventional NBS buffers were employed for standardization of the pH meter.

Reagents were of the highest available commercial purity and were used without purification with the exception of ethylenebisthioglycolic acid which was recrystallized from water. Aqueous solutions of the reagents were prepared by weighing the requisite amounts of the chemicals in the case of solid reagents or by pipetting in the case of liquid reagents, and diluting to the prescribed volume. The reagent concentration was normally between 0.1 and 0.2 M, and in this limited range no concentration dependence of the nmr spectra was observed. Solutions were adjusted to the desired pH using concentrated potassium hydroxide or perchloric acid. Strongly acidic solutions were prepared with perchloric acid dihydrate (determined to be 73.5% by weight). Because the S-alkylthioacetic acids were found to be oxidized in perchloric acid at this concentration, the upper concentration limit for perchloric acid was about 60%. In some cases, additional data were obtained using concentrated hydrochloric acid for preparing the acid solutions.

To check for possible chemical degradation or alterations of the organic ligands in the concentrated acids, solutions of the ligand were neutralized and the nmr spectra were obtained. If the spectra of the neutralized solutions were identical with those of the ligands which had not been acidified, it was presumed that no alteration of the ligand had occurred. The use of concentrated sulfuric acid as a proton source was discontinued after finding that ETGA decomposed in such a solvent.

Solutions of the organic reagents ranged in acidity from pH 12 to 10 M perchloric acid in this study, but at present no adequate scale exists which will give a quantitative measure of acidity over such a range. In principle a scale based on the Hammett acidity function should be applicable. However, the Hammett acidity function may be utilized with confidence only in those cases where the compounds under observation have structural features which are similar to those of the indicator bases used in establishing the acidity scale.[4] For lack of a better scale, the acidity of the systems investigated here will be described by pH. For solutions of pH greater than 0.5, the pH signifies an activity function determined from the pH meter; for solutions of greater acidity, pH will signify the negative logarithm of the hydrogen ion molarity. This approach is justified because no absolute quantitative measurements are made in the strongly acidic region. Good correlation of the chemical shift data was obtained using both types of pH measurement in the 0 to 1 pH range.

The acid dissociation contants for the loss of a proton from the neutral carboxylic acids were calculated from nmr data. From the chemical shifts of the carbon-bonded ligand proton resonances at each pH, the concentrations of the protonated and nonprotonated forms of the compound were determined.[5] The cal-

(3) (a) M. Yasuda, K. Yamasaki, and H. Ohtaki, *Bull. Chem. Soc. Japan*, **33**, 1067 (1960); (b) K. Suzuki and K. Yamasaki, *J. Inorg. Nucl. Chem.*, **24**, 1093 (1962); (c) A. Sandell, *Acta Chem. Scand.*, **15**, 190 (1961).

(4) K. Yates and H. Wai, *J. Amer. Chem. Soc.*, **86**, 5408 (1964).

(5) E. Grunwald, A. Loewenstein, and S. Meiboom, *J. Chem. Phys.* **27**, 641 (1957).

culated dissociation constants contain the conjugate acid–base pair terms as concentrations and the hydrogen ion term as an activity function; the hydrogen ion activity was not converted to concentration because the error incurred in measuring the concentrations of the other species from the nmr spectra is greater than the magnitude of the activity correction. Also, no attempts were made to maintain a constant ionic strength by adding excess inert electrolyte, because these nmr studies necessitated the use of high concentrations of the species being studied. The experimentally determined acid dissociation constants in Table I are compared with previously determined values of these constants.

Table I: Acid Dissociation Constants for Neutral Carboxylic Acids Calculated from Nmr Data

Acid	Acid dissociation constant	Reference
ETGA	4×10^{-4} [a]	This work
	2.4×10^{-4} [a]	3b (at 25° at μ = 0.1 with $NaClO_4$)
TDG	2×10^{-4} [a]	This work
	7.1×10^{-4} [a]	3a (at 25° at μ = 0.1 with $NaClO_4$)
ETAA	1.8×10^{-4}	This work
	2.43×10^{-4}	3c (at 20° in 1.00 *M* $NaClO_4$)
EOAA	2.7×10^{-4}	This work
	3.5×10^{-4}	3c (at 20° in 1.00 *M* $NaClO_4$)

[a] $(K_1K_2)^{1/2}$.

Results

Solvent Effect on Tetramethylammonium Ion. The tetramethylammonium ion (TMA) is a useful internal reference for measuring chemical shifts in aqueous solution because of its solubility, its closely spaced triplet spectrum which enables adjustment of the magnetic field homogeneity, and its chemical shift (3.20 ppm downfield from tetramethylsilane, TMS) which is in the region of many aliphatic ligand resonances. Further, in aqueous solutions the TMA chemical shift is generally unaffected by the presence of other ions or molecules. The first indication that TMA might be subject to solution effects was the anomalous upfield chemical shifts of the ETGA resonances (Figure 1) in solutions made progressively more acidic with HCl. This behavior was not observed when the solutions were acidified with $HClO_4$ and suggested an interaction of TMA with Cl^-.

In order to determine the extent of specific ion or solvent interaction with TMA, measurements were made of the chemical shift difference between the methyl resonances of TMA and sodium 3-(trimethylsilyl)-1-propanesulfonate (TMS*) for a variety of solution conditions. In neutral aqueous solutions the methyl resonance of TMS* is 190.2 cps upfield from

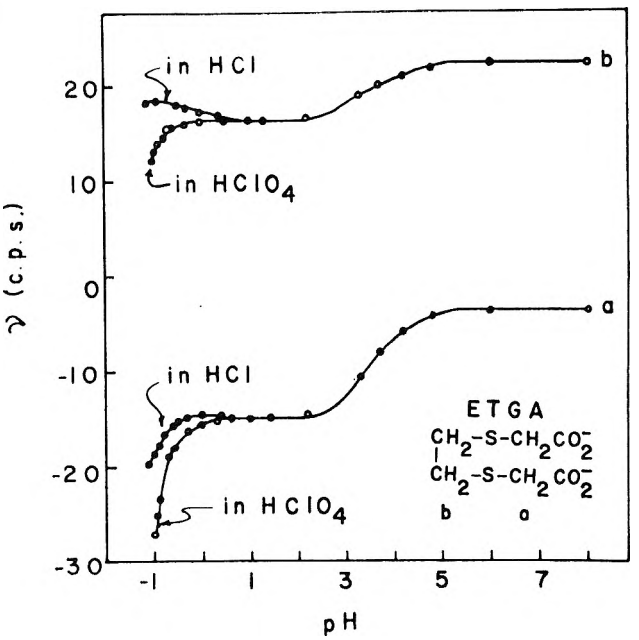

Figure 1. Chemical shifts of ethylenebisthioglycolic acid (ETGA) proton resonances as a function of pH.

TMA. The results of these studies are given in Table II. These results can be interpreted (assuming that the methyl proton resonance of TMS* is not affected by Cl^- and that the TMA resonance is not affected by H^+) in terms of an ion-pair interaction of TMA with Cl^- and a protonation of TMS*. The ion pairing of TMA with Cl^- results in a perturbation of the TMA electronic structure, a decreased shielding of the methyl protons, and consequently a downfield chemical shift of the TMA resonance,[6,7] manifested as a larger chemical shift difference between TMA and TMS*. In the strongly acidic solutions, TMS* is

Table II: Chemical Shift Differences between the Methyl Resonances of Tetramethylammonium Ion and 3-(Trimethylsilyl)-1-Propanesulfonate under Various Solution Conditions

Solution	$\Delta\nu = \nu_{TMS*} - \nu_{TMA}$
H_2O	190.2[a]
4 *M* $NaClO_4$	189.1[a]
4 *M* NaCl	192.3
4 *M* HCl	192.2
8 *M* HCl	192.6
4 *M* $HClO_4$	189.3
6 *M* $HClO_4$	188.8
10 *M* $HClO_4$	187.6

[a] The difference in chemical shifts for these two solutions may be due to association of the sulfonate group of TMS* with Na^+, ion association of TMA with ClO_4^-, or some combination of the two effects in the concentrated $NaClO_4$ solution.

(6) A. D. Buckingham, *Can. J. Chem.*, **38**, 300 (1960).

(7) A. D. Buckingham, T. Schaefer, and W. G. Schneider, *J. Chem. Phys.*, **32**, 1227 (1960).

Table III: Sequence of Protonation and Chemical Shifts of the Variously Protonated Species of Chelating Ligands Containing Neutral Oxygen and Sulfur

Symbol	Structure	Site for addition of *n*th proton: C–O⁻	C–O	C–O–C	C–S–C	Chemical shifts[a]: ν_a	ν_b	ν_c
ETGA	$^-OOCCH_2SCH_2CH_2SCH_2COO^-$	0				−3.6	22.2	
	(a) (b)	1, 2[b]				−14.8	16.4	
			3, 4[c]			−27.2[c]	12.2[c]	
TDG	$^-OOCCH_2SCH_2COO^-$	0				−4.1[d]		
	(a)	1, 2[b]				−18.3[d]		
			3, 4[e]			−22.5[d,e]		
ETAA	$CH_3CH_2SCH_2COO^-$	0				−1.8	35.2[f]	117.2[f]
	(c) (b) (a)	1				−13.2	31.0[f]	116.3[f]
			2[c]			−26.5[c]	25.3[c,f]	112.0[c,f]
EOAA	$CH_3CH_2OCH_2COO^-$	0				−43.2	−23.3[f]	118.9[f]
	(c) (b) (a)	1				−60.5	−28.0[f]	117.8[f]
				2[c]		−76.7[c]	−43.2[c,f]	110.2[c,f]
HAc	CH_3COO^-	0				75.6[d]		
	(a)	1				64.9[d]		
			2[e]			59.2[d,e]		
DMS	CH_3SCH_3	0				64.3		
	(a)				1[c]	17.6[c]		
DEE	$CH_3CH_2OCH_2CH_3$	0				−23.3[f]	120.0[f]	
	(b) (a)			1[c]		−57.1[c,f]	104.9[c,f]	

[a] Chemical shifts in cps from internal tetramethylammonium ion (TMA) at 25°. [b] Both carboxylate groups are protonated. [c] Value in 9.7 *M* $HClO_4$; protonation not complete. [d] At 38°. [e] Value in 12.1 *M* HCl; protonation not complete. [f] Denotes center of multiplet.

protonated to form the sulfonic acid resulting in a small downfield shift of the TMS* methyl resonance, manifested as a smaller chemical shift difference between TMA and TMS*. This interpretation is contrary to the conclusions of Abraham and Thomas who failed to recognize the possibility of interaction between hydrochloric acid and tetramethylammonium ion and the shift of the TMS* resonance to lower fields upon protonation.[8]

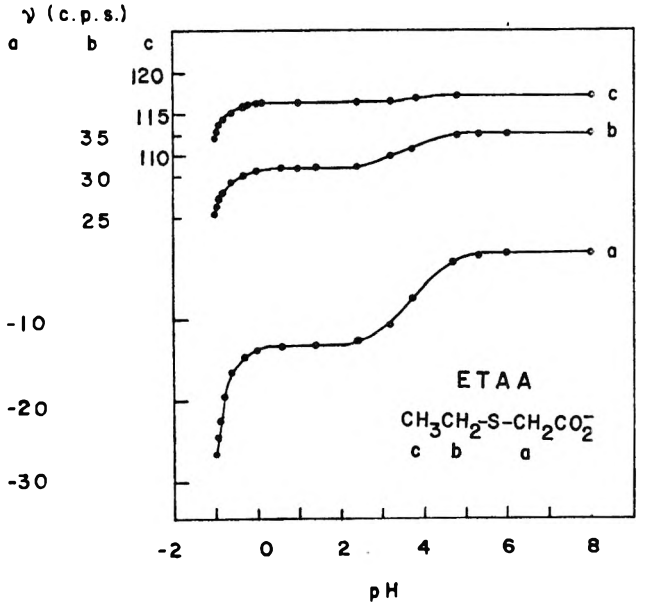

Figure 2. Chemical shifts of (ethylthio) acetic acid (ETAA) proton resonances as a function of pH.

Tetramethylsilane (TMS) and TMS* are unsuitable references for these studies. TMS is insoluble in aqueous solutions and TMS*, like a number of other common references, is itself being protonated in the region of interest. Although it could hardly be expected that TMA would remain completely adamant to the solvent change, especially in the concentrated solutions of perchloric acid, it is felt on the basis of the results observed that the use of TMA as an internal reference in perchloric acid solutions is probably superior to the use of other internal references or of an external reference, which would require corrections for bulk diamagnetic susceptibility differences for all solutions encountered because of the wide range of solvent composition: from water to concentrated perchloric acid.

Observed Spectra. The nmr parameter of interest in this investigation is the chemical shift of resonances for the nonexchanging carbon-bonded ligand protons. The chemical shifts of these protons are pH dependent as seen in Figures 1–5. The breaks in the chemical shift *vs.* pH curves correspond to protonation at one or more basic sites in the ligands. The structures and resonance assignments for the ligands are shown in the figures and in Table III.

The proton nmr spectra for ETGA have two singlets of equal intensity; the low-field resonance has been assigned to the acetate protons (labeled a in Table III) and the upfield resonance has been assigned to the b

(8) R. J. Abraham and W. A. Thomas, *J. Chem. Soc.*, 3739 (1964).

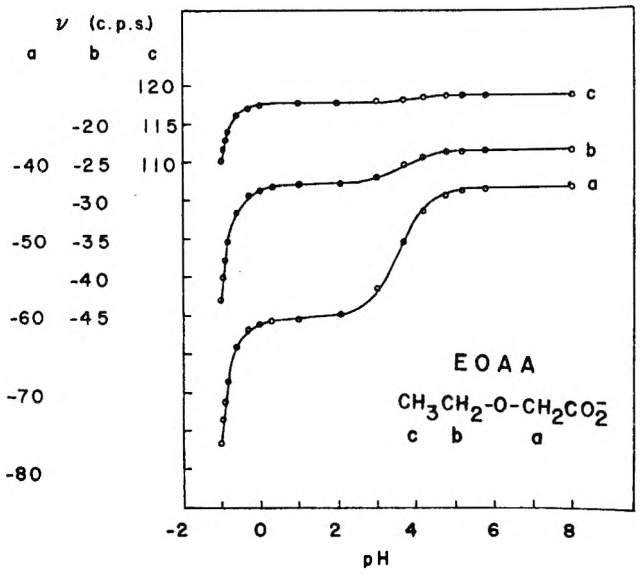

Figure 3. Chemical shifts of ethoxyacetic acid (EOAA) proton resonances as a function of pH.

protons. Potentiometric titrations revealed that two equivalents of acid were consumed by the ETGA dianion between pH 6 and 2. In this pH range the a resonance was shifted downfield by 11.2 cps and the b resonance was shifted downfield by 5.8 cps. In stronger perchloric acid solutions, the resonances are shifted still further downfield but the chemical shifts have not reached a constant value even in 9.7 *M* perchloric acid. In stronger solutions of perchloric acid, ETGA was slowly oxidized. The downfield chemical shift change between pH 1 and pH −1 is 12.4 cps for the a resonance and 4.2 cps for the b resonance.

The nmr spectrum of TDG was characterized by only a sharp singlet whose chemical shift had approximately the same pH dependence as the a proton resonance of ETGA.

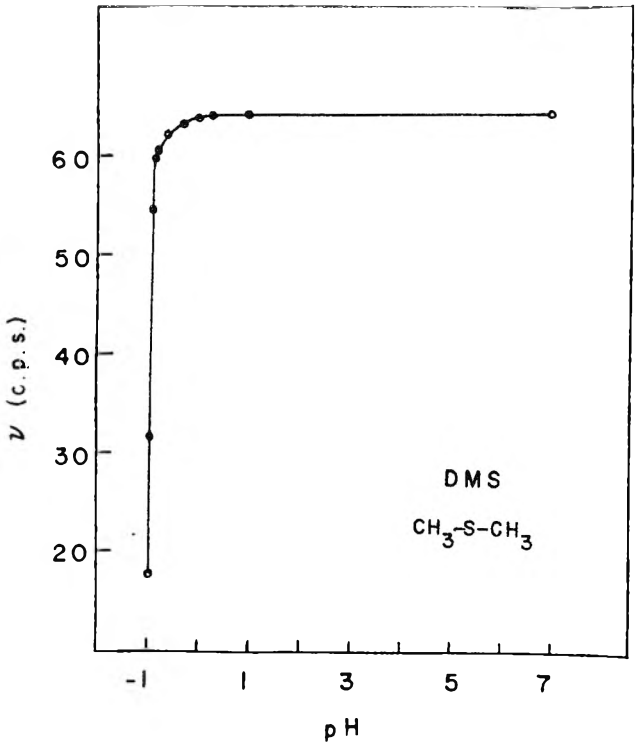

Figure 4. Chemical shift of dimethyl sulfide proton resonance as a function of pH.

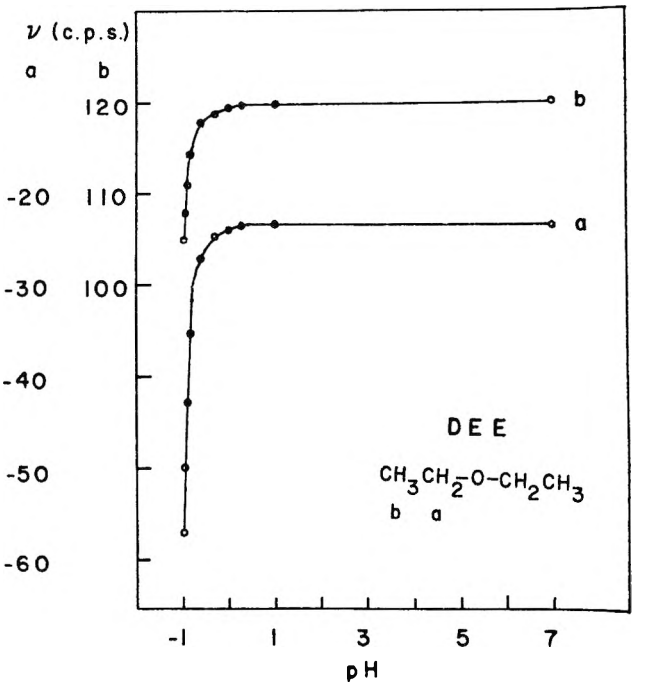

Figure 5. Chemical shifts of diethyl ether proton resonances as a function of pH.

The nmr spectra of ETAA are distinguished by three groups of resonances with integrated intensity ratios a:b:c of 2:2:3. The a proton resonance is a sharp singlet downfield from the TMA resonance. Spin–spin coupling between the b and c protons produces the typical ethyl group triplet at higher fields for the c resonances and quartet at lower fields for the b resonances. In solutions of positive pH, a small amount of second-order coupling was evident and the triplet and quartet were further split into an A_2B_3 pattern. The extent of the second-order coupling was sufficiently small that for most purposes, the center of each multiplet could be taken as its chemical shift. In strongly acidic solutions, the pattern simplified to an A_2X_3. In the positive pH region, simple protonation results in an 11.4-cps downfield shift for the a resonance, a 4.2-cps downfield shift for the b resonance, and a 0.9-cps downfield shift for the c resonance. The a resonance line shift compares with the 11.2-cps shift for the a resonance of ETGA. The b resonance shift plus the c resonance shift gives approximately the same value as the b resonance shift of ETGA. Further acidification results in downfield shifts similar to those of the ETGA resonances.

The nmr spectra of EOAA are similar to those of ETAA except that the a and b resonances of EOAA are further downfield than the corresponding resonances of ETAA. The large chemical shift between the b quartet and c triplet is maintained over the entire pH range, obviating any second-order coupling phenomena. In contrast to ETAA, the a and b resonances are shifted downfield to approximately the same extent below pH 1.

Dimethyl sulfide (DMS) gives a single resonance upfield from TMA. The spectra for diethyl ether (DEE) approximate A_2X_3 patterns. Both DMS and DEE show only one break in the chemical shift curves and in neither case has the chemical shift reached a constant value, even in the most concentrated acid solutions studied.

Discussion

The chemical shifts of the various ligand resonances depend upon the solution pH, and in all cases the resonances are shifted downfield as the solutions are made more acidic. When a proton associates with a basic site of the ligand, a deshielding effect is produced on the ligand protons which results in a downfield shift of their resonances. Because the deshielding effect attenuates with distance from the site of perturbation, the magnitudes of the downfield shifts depend on which donor site within the ligand associates with the acidic proton. The resonances for those ligand protons which are further from the site of acidic proton association will be shifted less than the resonances for the ligand protons which are closer to the protonated donor site.[9]

In the ETGA system, the downfield shifts between pH 6 and 2 must correspond to

$$^{-}OOCCH_2SCH_2CH_2SCH_2COO^{-} + 2H^{+} \longrightarrow HOOCCH_2SCH_2CH_2SCH_2COOH$$

The greater chemical shift change for the a than for the b resonance indicates that the carboxylate oxygens are the sites of protonation in this region which is in agreement with the consumption of two H^+/EGTA in this region as was determined potentiometrically.

The upfield shift of the ETGA a and b resonances below pH 1 in HCl can be attributed to ion pairing of TMA with Cl^- as discussed previously. The ETGA resonances are shifted downfield only slightly between pH 1 and 0 (*cf.* Figure 1 in $HClO_4$), but ion pairing of the reference ion, TMA, with Cl^- shifts the TMA resonance downfield, resulting in an *apparent* upfield shift for the ETGA resonances.

Further proton interaction is indicated in solutions of negative pH by additional shifts of the resonances to lower fields. The greater downfield shift of the a resonance relative to the b resonance is not commensurate with protonation of the thioether sulfur. A more reasonable explanation would involve proton interaction at the carbonyl oxygen

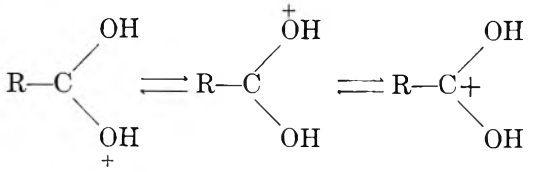

The structures depicted may be formed *via* an intermediate in which the carbonyl oxygen is hydrogen bonded to the acidic solvent.[10] For a comparison chemical shifts of the TDG resonance and the methyl proton resonance of acetic acid were found to have the same pH behavior as the a resonance of ETGA. Previous studies of acetic acid in concentrated sulfuric acid and in fluorosulfuric acid have provided evidence that the carbonyl oxygen is the site of protonation.[11,12] Deno, *et al.*,[11] obtained a change in chemical shift of 34 cps for the complete protonation of the carbonyl oxygen in sulfuric acid, which indicates that the protonation is no more than one-third complete in any of the cases considered here.

The pH dependence of the chemical shifts for the various resonances of ETAA further substantiate the carbonyl oxygen as the site of the second protonation for S-alkylthioacetic acids. Thus, for ETAA below pH 1 the a resonance is shifted more than twice as much as the b resonance which is shifted further than the c resonance.

The pH dependencies of the resonances of EOAA, the oxygen analog of ETAA, are depicted in Figure 3. The behavior upon protonation of the carboxylate group (pH 6–2) is analogous to that of the S-alkylthioacetate ligands. In more acidic solutions (from pH 1 to −1), the a resonance of EOAA shifts 16.4 cps downfield, the b resonance shifts 15.3 cps downfield, and the c resonance shifts 7.7 cps downfield. The magnitude of the shifts of these resonances is not in accord with those of the corresponding shifts of the S-alkylthioacetic acids, which have been postulated to undergo protonation of the carbonyl oxygen. Rather, these results suggest that the predominant proton interaction occurs at the ether oxygen because the b resonance shifts approximately the same amount as the a resonance. Edward, Leane, and Wang investigated the chemical shift difference between the methyl proton resonance and the methylenic proton resonance (which they designated the "internal shift") of diethyl ether as a function of acidity in sulfuric acid.[10] They interpreted the observed increase in

(9) See, for example: (a) E. Grunwald, A. Loewenstein, and S. Meiboom, *J. Chem. Phys.*, **27**, 641 (1957); (b) A. Loewenstein and J. D. Roberts, *J. Amer. Chem. Soc.*, **82**, 2705 (1960); (c) J. L. Sudmeier and C. N. Reilley, *Anal. Chem.*, **36**, 1968 (1964).

(10) J. T. Edward, J. B. Leane, and I. C. Wang, *Can. J. Chem.*, **40**, 1521 (1962).

(11) N. C. Deno, C. U. Pittman, Jr., and M. J. Wisotsky, *J. Amer. Chem. Soc.*, **86**, 4370 (1964).

(12) T. Birchall and R. J. Gillespie, *Can. J. Chem.*, **43**, 1045 (1965).

"internal shift" with increasing acidity in terms of a mechanism involving hydrogen bonding of the solvent H_2O to the ether oxygen, followed by formation of the protonated ether species. Whether the shifts observed in the present study, in which the acidity is not so great as in the study of Edward, Leane, and Wang, are attributable to a hydrogen-bonding phenomenon or to a direct protonation is not determinable. However, whichever phenomenon predominates, it is clear from the relative chemical shift changes that the basic site within the ligand, which is associated with the acidic proton, is the ether oxygen. Therefore, in the alkoxyacetic acids the ether oxygen has a greater proton affinity than the carbonyl oxygen.

These results reveal, on a qualitative basis, the differences in intrinsic Lewis basicities of neutral oxygen and sulfur. In the S-alkylthioacetic acids and the alkoxyacetic acids studied here, the donor tendencies are in the order

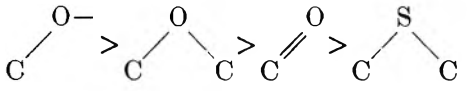

On the basis of this ordering, the ether oxygen is expected to contribute significantly more to the stability of chelates of metal ions having little capacity for back-bonding than the thioether sulfur in corresponding ligands. An investigation of the relative stability constants of some S-aryl and S-alkylthioacetic acids, including ETGA, and their oxygen analogs with the divalent ions of Zn, Cd, and Pb concurs with the conclusions reached here; *i.e.*, those ions with filled d orbitals showed greater affinity toward oxygen than sulfur.[3]

The observed basicity of the carbonyl oxygen has interesting implications concerning the

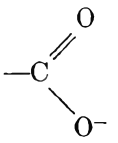

group as a possible bidentate chelating group. Bidentate carboxylate bonding has been detected from X-ray studies of

$$Na[UO_2(CH_3COO)_3],^{13}\ Zn(CH_3COO)_2\cdot 2H_2O^{14}$$

and

$$Cu[H_2N\text{–}CH(CH_2CH_2COO)\text{–}COO]\cdot 2H_2O^{15}$$

The carbonyl oxygen may also be utilized in polymeric chelates in which $-COO^-$ is an asymmetric bridging ligand; this type of structure has been detected by X-ray studies of $Zn(H_2NCH_2COO)_2\cdot H_2O$ and $Cd(H_2NCH_2COO)_2\cdot H_2O$.[16] More recently, infrared studies of several crystalline metal chelates of methionine, $CH_3SCH_2CH_2CHNH_2COOH$, have indicated that metal–carbonyl oxygen bonding is favored over metal–thioether sulfur bonding.[17] The results of the present work suggest that perhaps the carbonyl oxygen may be a factor to be considered in chelate formation in solution as well.

(13) W. H. Zachariasen and H. A. Peltinger, *Acta Cryst.*, **12**, 526 (1959).

(14) J. H. Talbot, *ibid.*, **6**, 720 (1953).

(15) H. C. Freeman in "The Biochemistry of Copper," J. Peisach, P. Aisen, and W. E. Blumberg, Ed., Academic Press, New York, N. Y., 1966, p 84.

(16) B. M. Low, F. L. Hirshfeld, and F. M. Richards, *J. Amer. Chem. Soc.*, **81**, 4412 (1959).

(17) C. A. McAuliffe, J. V. Quagliano, and L. M. Vallarino, *Inorg. Chem.*, **5**, 1996 (1966).

Dielectric Constant and Refractive Index of Weak Complexes in Solution[1a]

by M. E. Baur, D. A. Horsma, C. M. Knobler, and P. Perez

Department of Chemistry, [1b] *University of California, Los Angeles, California 90024* *(Received September 4, 1968)*

The effect on the dielectric constant and refractive index of weak complex formation between the components of a binary solution is calculated. Equations are developed which relate the deviations from additivity of the molar polarization and the molar refraction at infinite wavelength to the equilibrium constant for complex formation and the atomic polarizability and dipole moment of the complex. Dielectric constant and refractive index measurements are reported for the benzene–hexafluorobenzene system. These data are consistent with the presence of a weak complex in solution and from them the atomic polarizability increment and dipole moment of the complex are estimated. The values of these quantities indicate that charge-transfer effects are not of primary importance for stability of the complex.

I. Introduction

The measurement of the static dielectric constant, ϵ, as is well known, furnishes useful if not always unambiguous information concerning the geometrical structure of stable molecules in liquids and gases.[2] In particular, if the temperature dependence of the quantity $(\epsilon - 1)/(\epsilon + 2)$ for a fluid at a fixed density can be represented by a function of the form $A + B/T$, the dipole moment of the component molecules of the fluid can be estimated from B, and their average polarizability from A. For the case of gases or dilute solutions of polar molecules in nonpolar solvents, A and B assume, to good approximation, the simple forms

$$A = 4\pi N N_j \alpha/3 \tag{1a}$$

$$B = 4\pi N N_j \mu^2/9k \tag{1b}$$

where N_j is the molar concentration of the species of interest, α is its average polarizability, μ is the magnitude of its dipole moment, N is Avogadro's number, and k is the Boltzmann constant.

Measurement of the dielectric constant has been employed as well for the elucidation of the structure of molecular complexes in fluids in cases in which it is expected that the complex possesses electrical properties greatly distinct from the mean of its individual components. The most noteworthy such complexes are those of charge-transfer type,[3] and dielectric measurements are now well known in their application to such systems.[4,5] Indeed, dielectric measurements are frequently considered diagnostic for the presence of a meaningful degree of charge-transfer character in molecular complexes. However, certain difficulties enter in the interpretation of dielectric studies of charge-transfer systems which are not present in the case of stable polar molecules. In particular, we find the following.

(1) The constants A and B given by eq 1 involve the products $N_j\alpha$ and $N_j\mu^2$. The concentration N_j of a complex is not known unless the equilibrium constant K for formation of the complex has been determined, and it has usually been deemed necessary to adduce information on K from nondielectric measurements in order to arrive at a value of μ for the complex.

(2) K and N_j, and hence the factors A and B for a complex, are in general temperature dependent so that a simple $1/T$ dependence as indicated in eq 1 for the quantity $(\epsilon - 1)/(\epsilon + 2)$ is not to be expected. This makes it more difficult to separate polarizability and permanent dipole effects for complexes than for stable polar molecules and, in fact, it appears that no thorough study of the temperature dependence of ϵ for a charge-transfer complex in solution has been reported. Usually the presence of a complex is inferred by comparing the dielectric properties of a solution in which the complex is believed to be present with those of reference solutions of the separated components of the complex at the same temperature. Any deviation from additivity in the factor $(\epsilon - 1)/(\epsilon + 2)$ is then attributed to the presence of a complex, and it is universally assumed that the deviation is due to nonadditivity in the B factor. That is, the assumption is made that the polarizability of a complex is the sum of the polarizabilities of the individual component molecules. Although such additivity is by no means to be expected to hold rigorously, the rationale for this method of approach is that in the case of a strong complex with a large dipole moment, the effects of the B term will greatly overshadow those of the A term. This need not be the case in weak complexes, but until now no consideration has been given to the modification necessary in the interpretation of dielectric data for complexes occasioned by the nonadditivity of polarizability. In principle it is clear

(1) (a) Supported in part by the National Institutes of Health–Public Health Service under Grant No. GM 11125. (b) Contribution No. 1795.

(2) General reference: C. J. F. Böttcher, "The Theory of Electric Polarization," Elsevier Publishing Co., Amsterdam, 1952.

(3) For a general reference, G. Briegleb, "Charge-Transfer Complexes," Springer-Verlag, 1962, Section III.

(4) C. G. Le Fevre and R. J. W. Le Fevre, *J. Chem. Soc.*, 957 (1935).

(5) (a) F. Fairbrother, *Nature*, **160**, 87 (1947); *J. Chem. Soc.*, 1051 (1948); (b) F. Fairbrother, *ibid.*, 180 (1950).

what is required to introduce such a modification; measurement of the refractive index of a solution containing a charge-transfer complex gives the requisite information on the polarizability and such measurements together with appropriate dielectric measurements make possible a complete separation of polarizability and dipole moment effects. Information on the refractive index of charge-transfer complexes, however, is almost entirely lacking.[6]

The object of this article is twofold. We first present a generalized formulation of the relation between the measurable quantities, dielectric constant and refractive index of a solution containing a complex, and the polarizability, dipole moment, and equilibrium constant for the complex. Within the context of this formulation we show that: (a) the measurement of dielectric constant can be reliably used to estimate the dipole moment of the complex only if measurements of the refractive index of the systems of interest are also made; (b) in principle both the dipole moment of the complex *and* the equilibrium constant for formation of the complex can be obtained from measurements of the concentration dependence of dielectric constants and refractive indices of solutions containing such complexes; (c) certain extrapolation schemes for the determination of dipole moments from dilute solution dielectric measurements[7-9] may, if used in the discussion of systems containing complexes, lead to serious errors in the estimate of the dipole moment of the complex. Secondly, we present new data on the dielectric constant and refractive index of benzene and hexafluorobenzene mixtures, both to illustrate the use of the formalism previously developed and to shed light on the question of the presence of a weak charge-transfer complex in this system.

In section II of this article, we present the generalized development of relations for the dielectric constant and refractive index of a fluid containing a complex in terms of the dipole moment, polarizability, and equilibrium constant for formation of the complex. In section III we discuss the experimental procedure and results for the investigation of benzene–hexafluorobenzene mixtures. A discussion of these data and a critique of earlier work are presented in section IV.

II. Theoretical Formulation

We follow, in the main, the nomenclature and procedure of Böttcher.[2] The analysis is based on the Clausius–Mossotti–Debye equation for the dielectric constant ϵ of a mixture of J components

$$\frac{\epsilon - 1}{\epsilon + 2} = \frac{4\pi N}{3} \sum_{j=1}^{J} N_j(\alpha_j + \mu_j^2/3kT) \qquad (2)$$

where N_j is the concentration of species j in moles per cm^3, α_j is the average polarizability of a molecule of species j, μ_j is the magnitude of the permanent dipole moment of such a molecule, N is Avogadro's number, and k is the Boltzmann constant. Equation 2 is not exact, but for dilute solutions of a polar species in a nonpolar medium it is a reasonable approximation. In the case of a polar charge-transfer species present in low concentration in an otherwise nonpolar or weakly polar solution under consideration here, use of eq 2 is therefore appropriate. We have further

$$\alpha_j = \alpha_j^{e} + \alpha_j^{a} \qquad (3)$$

where α_j^{e} and α_j^{a} denote electronic and atomic polarizabilities, respectively. If the refractive index of a mixture is determined for several optical frequencies and extrapolated to infinite wavelength to yield n_∞, the electronic polarizabilities of the components of the mixture are related to n_∞ by the Lorenz–Lorentz equation

$$\frac{n_\infty^2 - 1}{n_\infty^2 + 2} = \frac{4\pi N}{3} \sum_{j=1}^{J} N_j \alpha_j^{e} \qquad (4)$$

Specializing now for simplicity to the case of a three-component system consisting of species A (acceptor), species D (donor), and a 1–1 complex DA, we assume that the equilibrium between these species is adequately described by

$$K_n = N_{DA}/N_D N_A \qquad (5)$$

that is, we take the ratio of activity coefficients equal to 1.

Introducing the *formal* molar concentrations N_{0A} and N_{0D}, we have

$$N_A = N_{0A} - N_{DA} \qquad (6a)$$

$$N_D = N_{0D} - N_{DA} \qquad (6b)$$

$$N_{DA} = K_n(N_{0A} - N_{DA})(N_{0D} - N_{DA}) \qquad (6c)$$

Substitution of these relations into eq 2 and 4 yields

$$\frac{\epsilon - 1}{\epsilon + 2} = \frac{4\pi N}{3} [N_{0A}\alpha_A + N_{0D}\alpha_D + N_{DA}(\alpha_{DA} - \alpha_D - \alpha_A) + N_{DA}\mu_{DA}^2/3kT] \qquad (7a)$$

$$\frac{n_\infty^2 - 1}{n_\infty^2 + 2} = \frac{4\pi N}{3} [N_{0A}\alpha_{0A}^{e} + N_{0D}\alpha_{0D}^{e} + N_{DA}(\alpha_{DA}^{e} - \alpha_A^{e} - \alpha_D^{e})] \qquad (7b)$$

Here we assume that the complex possesses a permanent dipole moment of magnitude μ_{DA} and that A and D are nonpolar. We now define the effective average molar volume $\bar{V}$ by

$$\bar{V} = \bar{M}/d = (1/d)[N_{0A}M_A + N_{0D}M_D]/(N_{0A} + N_{0D}) \qquad (8)$$

(6) The single exception to this seems to be recent work of M. G. Voronkov and A. Ya. Deich, *Latvijas PSR Zinatnu Akad. Vestis. Kim. Ser.*, 689 (1965).

(7) I. F. Halverstadt and W. D. Kumler, *J. Amer. Chem. Soc.*, **64**, 2988 (1942).

(8) E. A. Guggenheim, *Trans. Faraday Soc.*, **45**, 714 (1949).

(9) E. A. Guggenheim, *ibid.*, **47**, 573 (1951).

where M_A and M_D are the molecular weights of acceptor and donor molecules, respectively, and d is the measured density in grams per cm³ of the solution. If $\bar{V}'$ is the average molar volume calculated taking the presence of the complex as a separate species into account, it is clear that

$$\bar{V} = \bar{V}'\left[1 - \frac{N_{DA}}{N_{0A} + N_{0D}}\right] \tag{9}$$

so that the difference between $\bar{V}$ and $\bar{V}'$ is first order in the small quantity N_{DA}. We shall base our further development mainly on use of $\bar{V}$ (which is directly calculable) rather than $\bar{V}'$.

The quantity $\bar{V}$ and the measured dielectric constant and refractive index are used in the experimental definition of the effective molar polarization, P, and the effective molar refraction, R

$$P \equiv \frac{\epsilon - 1}{\epsilon + 2}\bar{V} \tag{10a}$$

$$R \equiv \frac{n_\infty^2 - 1}{n_\infty^2 + 2}\bar{V} \tag{10b}$$

As is well known,[2] P and R are additive functions of mole fraction for solutions in which the electrical properties of the component molecules are unaffected by formation of the mixture, even if the excess volume of mixing is not zero. Hence an analysis of the electrical properties of a solution is properly based on consideration of these quantities. Explicitly, from eq 7, 8, and 10

$$P = \frac{4\pi N}{3(N_{0A} + N_{0D})}[N_{0A}\alpha_A + N_{0D}\alpha_D + N_{DA}(\alpha_{DA} - \alpha_A - \alpha_D) + N_{DA}\mu_{DA}^2/3kT] \tag{11a}$$

$$R = \frac{4\pi N}{3(N_{0A} + N_{0D})}[N_{0A}\alpha_A^e + N_{0D}\alpha_D^e + N_{DA}(\alpha_{DA}^e - \alpha_A^e - \alpha_D^e)] \tag{11b}$$

We now define the increments $\Delta(P)$ and $\Delta(R)$ to be the differences between the measured P and R for a solution containing a complex and the values for P and R which would be obtained for a reference solution having the same formal mole fractions of donor and acceptor molecules but without a complex, that is, one for which strict additivity of electrical properties holds

$$\Delta(P) = \frac{4\pi N}{3}\bar{V}N_{DA}[\alpha_{DA} - \alpha_D - \alpha_A + \mu_{DA}^2/3kT] = \frac{4\pi N N_{DA}}{3(N_{0A} + N_{0D})}[\alpha_{DA} - \alpha_D - \alpha_A + \mu_{DA}^2/3kT] = \bar{V}\Delta(\epsilon) \tag{12a}$$

$$\Delta(R) = \frac{4\pi N}{3}\bar{V}N_{DA}[\alpha_{DA}^e - \alpha_D^e - \alpha_A^e] = \frac{4\pi N N_{DA}}{3(N_{0A} + N_{0D})}[\alpha_{DA}^e - \alpha_D^e - \alpha_A^e] = \bar{V}\Delta(n) \tag{12b}$$

In eq 12 we have introduced the increments $\Delta(\epsilon)$ and $\Delta(n)$. These are the differences between the measured values of $(\epsilon - 1)/(\epsilon + 2)$ and $(n_\infty^2 - 1)/(n_\infty^2 + 2)$ for a solution in which there is a complex and for a hypothetical reference solution having the same formal concentration of components but in which there is no complex. Finally, the difference between the increments in P and R can be written

$$\Delta \equiv \Delta(P) - \Delta(R) = \bar{V}[\Delta(\epsilon) - \Delta(n)] = \frac{4\pi N N_{DA}}{3(N_{0A} + N_{0D})}[\alpha_{DA}^a - \alpha_D^a - \alpha_A^a + \mu_{DA}^2/3kT] \tag{13}$$

This is the fundamental working equation in our analysis. Examination of eq 12 and 13 leads to the following conclusions concerning the effect of complex formation.

1. It is only when the sum of the atomic and electronic polarizabilities is conserved upon formation of the complex that a departure from additivity in P is directly proportional to the square of the dipole moment of the complex, μ_{DA}^2.

2. Formation of a complex may reflect itself in nonadditivity of either or both P and R. Additivity of either of these *in itself* does not constitute proof of the absence of a complex. In particular, a complex with nonvanishing dipole moment can be present even if P is additive, but only if Δ is nonadditive.

3. A clear separation between the effect of nonadditivity of atomic polarizability upon formation of a complex and the effect of a complex dipole moment is not possible within the framework of measurements of ϵ and n at a single temperature. In principle, measurement of P and R and the temperature dependence of each permits a complete separation of atomic, electronic, and permanent dipole terms. It should be noted that mixtures of nonpolar components generally exhibit a small degree of nonadditivity in R even when there is no complex formation,[10] but this effect is generally on the order of a few tenths of a per cent, with the deviation being positive. We also remark that in a complex with pronounced charge-transfer character and a dipole moment μ_{DA} having a magnitude of 1 D or greater, the term $\mu_{DA}^2/3kT$ will be on the order of 10^{-23} cm³, or about the same in magnitude as the total molecular polarizability of the components of the complex. The polarizability increment $(\alpha_{DA} - \alpha_D - \alpha_A)$ will be significantly smaller than the polarizabilities themselves, and hence

(10) See ref 2, p 265 ff.

the dipole term may be expected to dominate in eq 12. In such cases measurement of P by itself should give reasonably reliable estimates of the dipole moment of the complex. However, if μ_{DA} is significantly less than 1 D, increments in the polarizability will be relatively more important and consideration of P only may then lead to erroneous conclusions as to the character of the species present.

We now consider the determination of μ_{DA} and the equilibrium constant for complex formation from dielectric constant and refractive index data. For simplicity we neglect the atomic polarizability increment in eq 13, bearing in mind that the effective value for $\mu_{DA}^2/3kT$ obtained in this way may in fact include a contribution from this term. We introduce the mole fraction equilibrium constant K_x

$$K_x = X_{DA}/X_D X_A \tag{14}$$

where X_{DA}, X_A, and X_D are the mole fractions of complex, acceptor, and donor. It is convenient to define an effective mole fraction X_j'

$$\begin{aligned} X_j' &= N_j/(N_{0A} + N_{0D}) \\ &= X_j[1 - N_{DA}/(N_{0A} + N_{0D})] \end{aligned} \tag{15a}$$

The following relations then hold among the three sets of mole fractions, X_{0j}', X_j, and X_j'

$$X_{0D}' + X_{0A}' = 1 \tag{15b}$$

$$X_D + X_A + X_{DA} = 1 \tag{15c}$$

$$X_D' + X_A' + X_{DA}' = 1 - X_{DA}' \tag{15d}$$

$$X_j'/(1 - X_{DA}') = X_j, \qquad j = \text{A, D, DA} \tag{15e}$$

$$X_j' = X_{0j}' - X_{DA}', \qquad j = \text{A, D} \tag{15f}$$

Substitution of eq 15e and 15f into eq 14 then yields an equation connecting K_x and X_{DA}' with the observables X_{0D}' and X_{0A}'

$$K_x = \frac{X_{DA}'(1 - X_{DA}')}{X_{0A}'X_{0D}' - X_{DA}' + (X_{DA}')^2} \tag{16}$$

Rearrangement of eq 16 yields a quadratic equation in X_{DA}' whose only physical solution is

$$X_{DA}' = \tfrac{1}{2}\left[1 - \left(\frac{1 + K_x(1 - 4X_{0A}'X_{0D}')}{1 + K_x}\right)^{1/2}\right] \tag{17}$$

Expansion of the root in eq 17 then gives

$$X_{DA}' = \frac{K_x X_{0A}'X_{0D}'}{K_x + 1}\left(1 + \frac{K_x X_{0A}'X_{0D}'}{K_x + 1} + \ldots\right) \tag{18}$$

Substitution of eq 18 into eq 13 together with use of eq 15a and 15b and rearrangement then yields a relation for Δ in the limit of small acceptor concentration

$$\Delta = \frac{4\pi N}{9kT}\frac{\mu_{DA}^2 K_x}{K_x + 1}[X_{0A}' - (K_x + 1)^{-1}(X_{0A}')^2 + \ldots)] \tag{19}$$

A corresponding equation for the case of small donor concentration can of course also be written. Hence if the variable $9kT\Delta/4\pi N X_{0A}'$ is plotted against X_{0A}', the intercept of this plot with $X_{0A}' = 0$ yields $\mu_{DA}^2 K_x/(K_x + 1)$ and the limiting slope yields $-\mu_{DA}^2 K_x/(K_x + 1)^2$. In principle, therefore, both μ_{DA}^2 and K_x can be independently determined from data of this kind.

Finally, we wish to comment briefly on the general question of the accuracy of determinations of electrical properties of the complex based on the extrapolation of measurements to infinite dilution. A variety of such extrapolation schemes have been developed for the determination of the dipole moment and polarizability of stable polar molecules in nonpolar solvents,[11] and these can be applied to the case in which the polar species is a charge-transfer complex. The methods are all based on the systematic representation of P for a dilute solution as a function of the mole fraction of the polar species and the simplest form of such a representation is

$$P = (1 - X)P_s + XP_d = P_s + X(P_d - P_s) \tag{20}$$

where X is the mole fraction of the polar species and P_s and P_d are molar polarizations of the pure solvent and pure polar liquid, respectively. It is easily seen that eq 19 is a modified form of eq 20, in which the presence of equilibrium between polar and nonpolar components and the subtraction of effects associated with electronic polarizability have been taken into account. It is important to recognize, however, that whereas for a stable polar molecule, eq 20 gives a linear dependence of P on mole fraction, as a consequence of the presence of an equilibrium eq 19 contains quadratic and higher terms in mole fraction. Thus in order to apply extrapolation methods to charge-transfer equilibria, measurements must be made at much higher dilutions than are generally required for corresponding studies on stable polar molecules. Indeed it can be seen from eq 19 that forcing a linear fit on data points spread over a range of X_{0A}' from 0 to 0.1, for example, would yield a result for the limiting slope of Δ in error by 10% or more if $K_x \lesssim 1$, as expected for most weak complexes. To reduce the error in a linear fit to less than 1% it would be required that X_{0A}' be restricted to values between zero and 0.01. In addition, in order to use the particular form of extrapolation developed by Hedestrand[12] and Halverstadt and Kumler[7] it is necessary to extrapolate both the dielectric constant and the density of the solution to infinite dilution. The density of a solution containing a charge-transfer complex will show a nonlinear dependence on mole fraction in the same way as do the electrical properties, so that in the application of the Hedestrand–Halver-

(11) See ref 2, section 52.

(12) G. Hedestrand, *Z. Physik. Chem.*, **B2**, 428 (1929).

Table I: Refractive Index and Molar Polarization of Benzene–Hexafluorobenzene Mixtures

$X_{C_6F_6}$	n_∞	$a \times 10^{-6}$ Å^{-2}	$b \times 10^{-12}$ Å^{-4}	$\tilde{V}$, cm^3/mol	R^∞, cm^3/mol
0.0000	1.4786 ± 0.0012	5.57	4.1	89.39	25.32
0.2417	1.4328 ± 0.0011	5.32	2.6	96.50	25.06
0.3408	1.4161 ± 0.0014	7.10	−0.1	99.23	24.90
0.4646	1.4055 ± 0.0009	5.27	1.6	102.46	25.13
0.4839	1.4004 ± 0.0005	4.26	2.4	102.95	24.99
0.7127	1.3812 ± 0.0005	5.02	0.7	108.71	25.24
0.8608	1.3738 ± 0.0009	4.28	1.4	111.14	25.36
1.0000	1.3642 ± 0.0014	3.30	2.0	115.76	25.80

Table II: Dielectric Constant of Benzene–Hexafluorobenzene Mixtures ($\tilde{V}$ and P in cm^3/mol)

	25.0°			35.0°			45.0°			55.0°			65.0°		
$X_{C_6F_6}$	ϵ	$\tilde{V}$	P	ϵ	$\tilde{V}$	P	ϵ	$\tilde{V}$	P	ϵ	$\tilde{V}$	P	ϵ	$\tilde{V}$	P
1.0000	2.029	115.79	29.59	2.013	117.46	29.67	1.995	119.18	29.69	1.997	120.94	29.71	1.960	122.76	29.77
0.8687	2.052	112.60	29.23	2.035	114.19	29.30	2.017	115.83	29.33	2.001	117.52	29.41	1.983	119.26	29.44
0.7419	2.066	109.46	28.70	2.048	110.99	28.74	2.029	112.55	28.75	2.012	114.16	28.80	1.997	115.82	28.90
0.6167	2.091	106.36	28.37	2.074	107.81	28.42	2.056	109.30	28.46	2.037	110.84	28.47	2.021	112.42	28.55
0.4850	2.127	103.01	28.13	2.110	104.39	28.20	2.093	105.81	28.26	2.074	107.26	29.68	2.058	108.76	28.35
0.4466	2.130	102.02	27.92	2.113	103.38	27.98	2.095	104.78	28.02	2.076	106.21	28.04	2.059	107.68	28.10
0.3817	2.152	100.33	27.84	2.134	101.65	27.89	2.117	103.01	27.95	2.097	104.41	27.96	2.081	105.84	28.04
0.2522	2.187	96.82	27.45	2.170	98.07	27.51	2.152	98.85	27.57	2.134	100.67	27.61	2.116	102.02	27.66
0.0000	2.275	89.41	26.64	2.256	90.52	26.70	2.237	91.65	26.74	2.219	92.82	26.82	2.200	94.01	26.85

stadt–Kumler procedure to such systems,[13,14] the necessity of obtaining data for extremely dilute solutions is further reinforced.

III. Experimental Investigations

A number of recent measurements of the properties of benzene–hexafluorobenzene (B–HFB) mixtures strongly suggest that there is a specific interaction between these two molecules. Positive evidence for this interaction is to be found in the heats[15] and volume changes[13] on mixing and there is further support from investigations of the phase diagram[16] which show the presence in the solid of a 1:1 complex. In addition, solid mixtures of HFB with other donors such as mesitylene and *p*-xylene show similar behavior, and X-ray investigations[17] of the complexes formed in these systems indicate that the molecules are arranged in an alternating layer structure. Yet another study consistent with the hypothesis of specific interaction in these mixtures has involved the determination of heats of mixing of a large variety of systems involving partially fluorinated benzenes.[18]

Although this substantial body of evidence strongly points to the existence of a B–HFB complex, none of these experiments has uncovered any feature which can be unequivocally identified with a complex in liquid mixtures. No charge-transfer bands have been detected and neither the proton nor the fluorine nmr spectrum of a mixture shows any new features. Dielectric methods should be ideal for demonstrating the presence of a complex since both of the pure components are nonpolar and it is likely that a complex would have a permanent dipole moment. Two measurements of the dielectric constant of B–HFB liquid mixtures have been reported[13,14] from which values of the dipole moment of a complex have been derived. However, these results are at variance with each other and, as we shall see in section IV, there seems good reason to doubt the validity of this earlier work. For this reason we have undertaken the experimental investigation outlined below.

We have carried out measurements of the dielectric constant and refractive index of B–HFB solutions over the entire range of mole fraction. The details of sample preparation are given in paragraph A below, and the methods employed in the determination of ϵ and n are described in paragraphs B and C. Numerical results are presented in Tables I–III and used to calculate the molar polarization P and molar refraction R of the mixtures listed in the tables and plotted in Figure 1 of section IV. A discussion of the qualitative implications of these data in terms of the theory already given is presented in section IV.

A. Materials. The benzene used in these studies

(13) W. A. Duncan, J. P. Sheridan, and F. L. Swinton, *Trans. Faraday Soc.*, **62**, 1090 (1966).

(14) C. C. Meredith and G. F. Wright, *Can. J. Chem.*, **38**, 1177 (1960).

(15) D. V. Fenby, I. A. McLure, and R. L. Scott, *J. Phys. Chem.*, **70**, 602 (1966).

(16) W. A. Duncan and F. L. Swinton, *Trans. Faraday Soc.*, **62**, 1082 (1966).

(17) C. Knobler and R. L. Scott, private communication; J. C. A. Boeyens and F. H. Herbstein, *J. Phys. Chem.*, **69**, 2153 (1965).

(18) D. V. Fenby and R. L. Scott, *ibid.*, **71**, 4103 (1967).

Table III: Dielectric Constant of Dilute Solutions of Hexafluorobenzene in Benzene

$X_{C_6F_6}$	ϵ	d, g/cm³	P_{HFB}^0
0.00000	2.2740	0.8736	...
0.005984	2.27134	0.8790	29
0.01271	2.26834	0.8850	29.3
0.01926	2.26556	0.8909	29.4
0.02445	2.26341	0.8955	29.5

was Matheson Spectrograde. The material was purified by slow fractional crystallization, dried by refluxing with P_2O_5, and then fractionally distilled, once over K_2CO_3 and then with no drying agent. The purified material was stored in a closed container to prevent absorption of moisture. Hexafluorobenzene was obtained from the Pierce Chemical Co., Rockford, Ill., and from the Whittaker Corporation, San Diego, Calif., and was prepared in the same manner. For the benzene $n^{20}D$ was 1.5012 and for the hexafluorobenzene $n^{20}D$ was 1.3772.

B. Measurement of Refractive Index. The refractive index measurements were performed using the method of minimum deviation. A copper cell, 1 cm³ in volume, was mounted on a 7.5-in. spectrometer manufactured by the Precision Tool and Instrument Co. The divided circle can be read to 30 sec of arc so that with the 60° prism angle of the cell the refractive index can be determined with an accuracy of 0.0002. Water, circulated through the cell walls from a thermostatic bath, maintains the sample temperature constant to 0.02° as determined by temperature measurements of liquids in the cell. The prism angle was determined from measurements of the angle of minimum deviation for water and the accurately known values of its refractive index.[19]

Each of the mixtures studied was prepared by weight in tubes sealed with septum caps. The samples were immediately transferred to the cell with a hypodermic syringe and the cell was closed with a screw cap and sealed, as are the cell windows, with a Teflon gasket. In each case the initial measurements were duplicated at the end of a run to check for any composition change due to evaporative losses; none was ever observed.

Measurements were performed at seven different wavelengths: the mercury lines at 4358 and 5461 Å, the cesium lines at 6213, 6010, 5845, and 5649 Å, and the sodium line at 5893 Å. The results were fitted by the method of least squares to a dispersion relation of the form

$$n(\lambda) = n_\infty + a/\lambda^2 + b/\lambda^4$$

The values of n_∞, a, and b at 24.8° are given for each mixture in Table I. In every case the dispersion relation represents the data within the experimental error. The standard deviations listed for n_∞ have been obtained from the least-squares analysis.

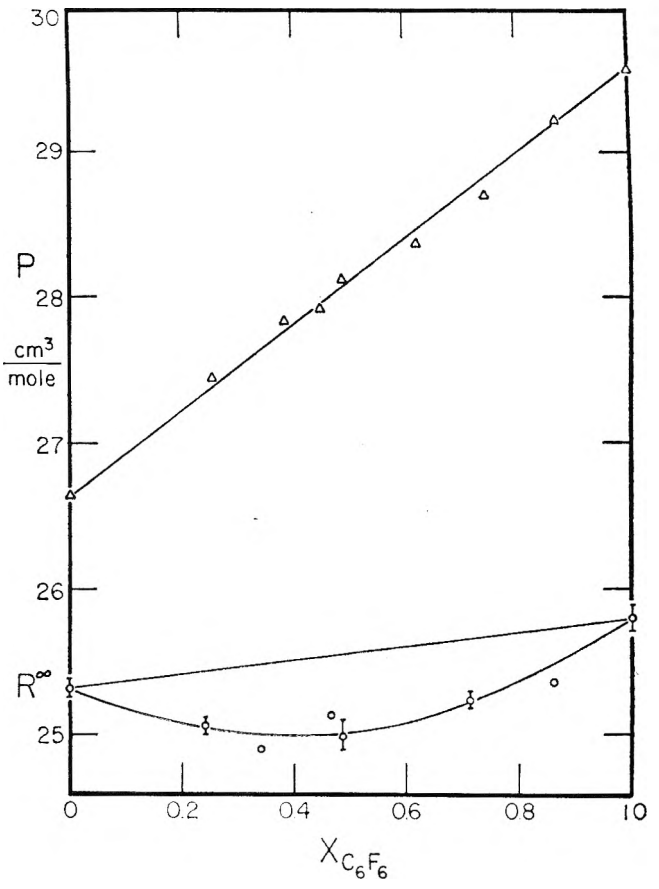

Figure 1. The molar polarization and molar refraction at infinite wavelength for benzene–hexafluorobenzene mixtures at 25°.

Molar volumes given in Table I for each mixture were calculated from the molar volumes of benzene[20] and hexafluorobenzene[21] in conjunction with the values of the excess volume reported by Duncan, *et al.*[13] Their measurements were performed at 40°, but the excess volume is generally only weakly temperature dependent and for this system it is at most less than 1% of the total molar volume. The refractive index and volume data have been used to calculate the values of R^∞, the molar refraction at infinite wavelength, listed in the table and shown in Figure 1. The error bars in the figure represent the result of the compounded uncertainties in the refractive index, molar volume, and mole fraction.

C. Measurement of Dielectric Constant. Measurement of the dielectric constant of the mixtures was carried out using the bridge method. The signal source was a General Radio 1311-A audio oscillator, operated at 1 kHz, and the bridge was a General Radio 1615-A capacitance bridge, with imbalance detection on a General Radio 1232-A null detector. The cell employed

(19) L. W. Tilton and J. K. Taylor, *J. Res. Nat. Bur. Stand.*, 20, 419 (1938).

(20) J. Timmermans, "Physico-Chemical Constants of Pure Organic Compounds," Elsevier Publishing Co., New York, N. Y., 1965.

(21) J. F. Counsell, J. H. S. Green, J. L. Hales, and J. F. Martin, *Trans. Faraday Soc.*, 61, 212 (1965).

was of the three-terminal concentric cylinder electrode type, constructed of monel (Balsbaugh Laboratories, Duxbury, Mass., Type 3HT 35 pF. The cell was calibrated using dried cyclohexane, ϵ^{25} 2.0172.[22] With this arrangement, the sensitivity of the capacitance measurements was to better than 0.001 pF (0.005%). The temperature of the cell was maintained to within 0.01° with a standard relay control bath.

In view of the large volume of solution required to fill the cell, solutions of large and moderate concentration were prepared by successive dilution with pure benzene. These solutions were made up volumetrically and the weight of the components determined on an analytical balance. The composition of solutions prepared in this way was determined to better than 0.05% in mole fraction. As a check, the dielectric constant of a freshly made up control sample with $X_{HFB} = 0.4466$ was determined and found to agree within experimental error with values obtained by the successive dilution method. For dilute solution measurements ($0.006 \leq X_{HFB} \leq 0.024$), a fresh sample was prepared from the pure components for each measurement.

The measurements at large and moderate HFB concentration were subject to a determinate error caused by a variation of the cell constant attendant upon opening the cell to empty and reload it. The magnitude of this error was established to be not greater than 0.1%. The dilute solution measurements were not subject to this error since, for these measurements, the cell was emptied and reloaded by the usual vacuum techniques. The dilute solution measurements may accordingly be considered accurate to ±0.005%, the sensitivity of the measuring apparatus.

Two independent sets of dielectric measurements on B–HFB mixtures were carried out. A series of seven solutions, with HFB formal mole fraction (X_{0F}) in the range 0.2522 to 0.8687, was studied. The dielectric constant of each of these solutions, together with those of the pure components, was determined at 10° temperature intervals from 25.0 to 65.0°. The results of this set of measurements are summarized in Table II. For each composition and temperature, we give the measured dielectric constant ϵ, the molar volume $\bar{V}$ in cm³/mol, and the experimental value of P, the molar polarization of the mixture, calculated from eq 10a. All polarizabilities are given in units of cm³/mol. The overall experimental uncertainty in P is ±0.05 cm³/mol. In addition, a set of measurements was performed on four dilute solutions of HFB in benzene, with HFB formal mole fraction in the range 0.006 to 0.024. These measurements were made only at 25.0°. The results are summarized in Table III, in which are given the formal mole fraction of HFB, d in g/cm³, and ϵ. These data were used to calculate the values of P_{HFB}^0 for HFB given in the table, where

$$P_{HFB}^0 = [P_s - (1 - X)P_B^0]/X$$

and P_s is the molar polarization of the solution, P_B^0 that of pure benzene, and X the mole fraction of HFB.

IV. Discussion of Data and Conclusions

The overall aspect of the dielectric and refractive index data for the B–HFB solutions is best seen in the plot of the molar polarization P and molar refraction R of the mixtures as a function of mole fraction at 25°, Figure 1. Inspection of this plot or of the values given in Table II shows that to within experimental error, ±0.05 cm³/mol, additivity of molar polarization holds at all concentrations. The polarization values given for other temperatures in Table II show that this additivity holds at all temperatures studied. Additional confirmation of this conclusion is obtained from the results of the dilute solution measurements at 25° summarized in Table III. Extrapolation of the values for P_{exp} given there to zero concentration yields a limiting value P_{exp}^0 of 29.8 ± 0.2 cm³/mol for the incremental molar polarization associated with HFB in dilute solution in B. This value is in agreement within experimental error with the value $P = 29.59$ cm³/mol obtained for pure HFB at 25°, and confirms the lack of any deviation from additivity in P in these systems. According to the usual criteria based only on dielectric measurements, one would have to conclude that no dipole moment associated with a B–HFB complex is present.

The conclusions which follow from the dilute solution work reported here are different from those reported in the two previous studies to which we have alluded.[13,14] Duncan, *et al.*,[13] did not report the results of their dielectric investigation in terms of molar polarization values, but stated only that their application of the Halverstadt–Kumler extrapolation procedure led to an estimated dipole moment of the complex of 0.3 D. From this value, it is easy to work backward and calculate that the limiting molar polarization P_{exp}^0 found in their work was about 3 cm³/mol greater than that found here, a difference of about 10%. Similarly, the very much larger dipole moment reported in ref 14 corresponds to a value for P_{exp}^0 about 10 cm³/mol greater than that found here. The resolution of these discrepancies lies in a careful examination of the plot of dielectric constant *vs.* mole fraction. The data in Tables II and III show curvature even at mole fractions of HFB as low as 0.02 and similar curvature is present for the same concentrations in the plot of density *vs.* composition. However, Duncan, *et al.*, made a linear fit to data in the mole fraction range 0.01 to 0.15 in HFB and such a procedure leads to a value for P_{exp}^0 in excess of our value by 10% or more. Thus the actual data of Duncan, *et al.*, are probably in agreement with those given here, the only difference being in the details of the

(22) L. Hartshorn, J. V. L. Parry, and L. Essen, *Proc. Phys. Soc.*, **68B**, 422 (1955).

analysis. It is likely that the same considerations apply to the work of ref 14, but insufficient information is given there for a deeper analysis to be performed. We thus feel that the values for the molar polarization given here are internally consistent and preferable to those reported by the earlier workers.

It is useful to estimate the maximum magnitude which a dipole moment associated with a B–HFB complex could have, if the experimentally determined additivity to within 0.05 cm³/mol in P were to be used as the sole criterion. For this it is necessary to have a value for K_x, the equilibrium constant for complex formation. In principle this could be obtained from our data using eq 19 but in the present case experimental uncertainty is too great for this to be accurate. Hence we resort to a different method. Fenby[23] has given a survey of available calorimetric data on mixtures of hydrocarbons and fluorinated benzenes and has discussed the separation of the heat of mixing $\tilde{H}^E$ for these systems into a "physical" part $\tilde{H}_P{}^E$ which is positive in all cases and a "chemical" part $\tilde{H}_C{}^E$ which reflects the presence of specific interaction and is negative.[24] According to Fenby's analysis, the observed $\tilde{H}^E$ for B–HFB at mole fraction 0.5 at 25° can be considered the resultant of an $\tilde{H}_P{}^E$ of about 360 cal/mol and an $\tilde{H}_C{}^E$ of about −490 cal/mol. Assuming that the "chemical" contribution is associated with the formation of a complex with heat of formation ΔH_f, we have for the case X(formal) = 0.5

$$\tilde{H}_C{}^E = [1 - (1 + K_x)^{-1/2}]\Delta H_f/2$$

$$K_x = (2H_C{}^E/\Delta H_f - 1)^{-2} - 1$$

We do not have an exact value for ΔH_f, but in view of the evident stability of a 1–1 B–HFB complex in the solid state[16] and in light of the fact that the B–HFB system in the liquid phase can at best exhibit a fairly weak complex, it seems reasonable to assume that ΔH_f is in the range 2000–4000 cal/mol.[24] Taking for $\tilde{H}_C{}^E$ the value reported above we find that K_x lies in the range 0.8–3 at 25°. Correspondingly, the mole fraction of complex in an equimolar mixture of B and HFB at that temperature is between 0.14 and 0.33. If we set the molar polarization deviation $\Delta(P)$ equal to the maximum positive value which it could have consistent with experimental error and use the relation

$$\Delta(P) = 0.05 \text{ cm}^3/\text{mol}$$

$$= (4\pi/3)NX_{\text{complex}}\mu^2_{\text{complex}}/3kT$$

we find that the maximum value of μ_{complex} is 0.09–0.12 D. Actually 0.05 cm³/mol is an overestimate of the probable deviation from linearity of the data as a whole, so that the upper limit for μ_{complex} can be set at no more than about 0.1 D on this criterion.

Turning to the refractive index data (lower curve in Figure 1), we note the negative deviation from additivity in R of magnitude 0.55 cm³/mol at $X = 0.5$. The curve drawn was obtained by a least-squares fit assuming a simple parabolic form for $\Delta(R)$, and typical error bars on some of the individual measurements are indicated. The probable error in the negative deviation for an equimolar mixture is less than 0.05 cm³/mol. The quantity Δ defined in eq 13 is seen to be positive. Thus the entire deviation stems from the inequality

$$\alpha^a{}_{\text{complex}} + \mu^2{}_{\text{complex}}/3kT > \alpha_B{}^a + \alpha_{HFB}{}^a \qquad (21)$$

and the data show the presence of specific B–HFB interactions, with a decrease in the electronic polarizability of the complex relative to the sum of isolated B and HFB molecules.

It is not possible rigorously to say from these experiments what portion of the deviation comes from failure of additivity in the atomic polarizability and what portion from the presence of a permanent dipole moment in the B–HFB complex. It is also not possible to determine how much of the deviation is due to departures from additivity which arise from the nonspecific electronic perturbations associated with van der Waals forces. However, the usual magnitude of such effects is much less than 1%.[10] Preliminary investigations of the model system cyclohexane–HFB, for which there is no evidence of complex formation, show that R there deviates from additivity by no more than 0.2%, about 10% of the effect observed here. It is also to be noted that in the usual nonpolar mixtures the deviations from additivity in R are paralleled by similar deviations in P and as a result there is no net contribution to Δ, in accordance with the notion that the effects in such systems arise from induced dipole–induced dipole interactions which affect mainly the electronic polarizability. In the present case the difference in behavior in P and R is striking and in this sense the B–HFB system clearly exhibits qualitative behavior consistent with our formalism and distinctly different from that observed in simple mixtures.

We can advance certain simple qualitative considerations which shed light on the relative importance of dipole and atomic polarizability contributions to the observed nonzero value of Δ. To first illustrate our approach, we consider the atomic polarizability of pure B. As seen from Figure 1, the difference $P - R$ for pure B is 1.32 cm³/mol in the liquid phase at 25°. If we associate this quantity with the atomic polarizability of B using the Clausius–Mossotti equation, we find that $\alpha_B{}^a = 5.3 \times 10^{-25}$ cm³/molecule. This polarizability may be regarded as made up of contributions from the ir active normal modes of vibration of the B molecule. Only seven of these vibrations have ir intensity sufficiently great to indicate a large transition dipole moment and hence a large contribution to the

(23) D. V. Fenby, Ph.D. Dissertation, UCLA, 1967.
(24) W. J. Gaw, Ph.D. Dissertation, University of Strathclyde, 1966.

atomic polarizability[25]: their frequencies are $\nu_4(a_{2u}) = 671\ cm^{-1}$, $\nu_{14}(e_{1u}) = 1037\ cm^{-1}$, $\nu_{13}(e_{1u}) = 1485\ cm^{-1}$ and $\nu_{12}(e_{1u}) = 3099\ cm^{-1}$. We consider the isotropic polarizability $\alpha = (\alpha_{xx} + \alpha_{yy} + \alpha_{zz})/3$ and use for the contribution of a normal vibration to the polarizability along a given principal axis of the B molecule the formula from second-order perturbation theory for a harmonic oscillator[26]

$$\alpha_j = 2\mu_j^2/D_j \qquad (22)$$

where D_j is the energy separation between the ground and first excited states of the normal vibration j and μ_j is the transition dipole matrix element between them. From the known oscillator strengths of the ir active transitions in B, we can say that μ_j is on the order of 0.1–0.2 D for the seven vibrational modes listed. Taking an approximate value 0.15 D for each mode and summing the contributions from each to the atomic polarizability, where we use the quoted frequencies to obtain D_j in the calculation of α_j according to eq 22, we find a total atomic polarizability $\alpha_B{}^a$ of about 4×10^{-25} cm³/molecule, in reasonable agreement with experiment. A similar calculation can be carried out for HFB. When a B–HFB complex is formed, six new vibrational modes arise. Assuming that the geometry of the complex in the liquid phase is like that in the solid phase[17] with the planes of the B and HFB rings parallel, these correspond to stretching of the B–HFB bond, torsional oscillation about it, and rocking and sliding motions of the B and HFB moieties with respect to each other. Each of these modes would be expected to be ir active in view of the lowered symmetry and will contribute to the atomic polarizability of the complex. Their frequencies will lie in the far-ir, giving rise to a spectrum not readily observable by standard techniques and presumably much broadened by lifetime effects. The most important of these modes from our standpoint will be the B–HFB stretch, which may be expected to have the largest transition dipole moment. Although we have no rigorous value for the frequency of this mode, it seems reasonable to take for it a figure which makes the quantum of vibrational energy for the stretch equal to about 0.1 the total B–HFB bond energy. Assuming the latter to be a few kilocalories, the frequency for the B–HFB stretch should be on the order of $200\ cm^{-1}$. It may be noted that the stretching frequency for hydrogen bonds, with similar bond energies, has been estimated at values of this order.[27] To utilize eq 22 for a calculation of the atomic polarizability associated with the B–HFB stretch, we also require a value for the transition dipole moment for this mode. The magnitude of the latter depends upon the polarity of the B–HFB bond which from symmetry considerations cannot be rigorously zero. Since the force constant for this bond is weak, excitation of a stretching vibration extends the bond by a significant fraction of its length in the ground state, and hence the transition dipole moment should not be much less than the "permanent" dipole moment associated with the bond. If m denotes the latter moment, then the contribution to the isotropic atomic polarizability associated with the stretching motion should be about $2m^2/3D$, and the total incremental contribution to the Clausius–Mossotti function arising from the bond stretch and the permanent dipole is

$$\delta\alpha^a{}_{complex} = m^2[(2/\Delta) + (1/kT)]/3 \qquad (23)$$

From our experiments, we have that Δ for the equimolar B–HFB mixture at 25° is 0.55 cm³/mol, and with our previous estimate of K_x, this means that $\delta\alpha^a{}_{complex}$ is in the range 1×10^{-24} to 2×10^{-24} cm³/molecule. On our estimate, D is nearly equal to kT at 25°, so according to eq 23 m must be in the range 0.2–0.4 D. However, two-thirds of this is then associated with the atomic polarizability term, and only one-third, or about 0.1 D, with the permanent dipole term. This conclusion that the permanent dipole term is extremely small is in agreement with work of Smyth,[28] who has found no evidence for a dielectric relaxation in the microwave spectrum of B–HFB mixtures. No observable effect would be expected in such experiments with a permanent dipole moment of the complex as small as that estimated here. Of course the numerical estimates given above are very rough, but it should be noted that even if all of Δ were to be assigned to the permanent dipole term, the magnitude of the dipole moment of the complex would still be no more than a few tenths of a debye.[29]

To summarize what has been established here: in utilizing dielectric measurements for the characterization of weak complexes, it is essential that refractive index studies also be performed on the same systems. The general formalism set out in section II in which it is shown how these two types of measurement should be combined is of general validity and not restricted to B–HFB systems. Our measurements, though more

(25) G. Herzberg, "Infrared and Raman Spectra," D. van Nostrand Co., Princeton, N. J., 1945, Chapter 3.

(26) See, for example, H. Eyring, J. Walter, and G. Kimball, "Quantum Chemistry," John Wiley and Sons, Inc., New York, N. Y., 1944, Chapter 8.

(27) G. Pimentel and A. McClellan, "The Hydrogen Bond," W. H. Freeman, San Francisco, Calif., 1960, Chapter 3.

(28) C. P. Smyth, private communication.

(29) One of the reviewers has pointed out that although the interpretation of the dilute solution B–HFB measurements reported in ref 14 may be in error for the reasons cited in section IV, similar studies of dilute solutions of HFB in cyclohexane have been made at concentrations sufficiently low for the Halverstadt–Kumler extrapolation procedure to be justified. An analysis of these results[14] leads to a dipole moment for HFB of 0.67 D, presumably the effect of excited states. However, other measurements on the same system[13] lead to a value of 0.0 ± 0.1 D for the HFB dipole moment and the small loss for pure HFB at microwave frequencies *might* be interpreted as arising from a dipole moment of no more than 0.1 D.[28] If, in fact, HFB is polar, $\mu_{DA}{}^2$ in eq 12a and all subsequent equations would have to be replaced by $\Delta\mu^2$, the difference between the squares of the dipole moments of the complex and pure HFB. The conclusions concerning the presence of a complex and the magnitude of its dipole moment would not be substantially altered.

refined than previous work in this area, are not sufficiently accurate to employ the formalism of section II in full quantitative detail. However, they allow a number of qualitative conclusions to be drawn about the B–HFB system. The nonadditivity of R shows the presence of specific B–HFB interactions which it seems reasonable to interpret in terms of formation of a complex. This complex has very little polar character, with a permanent dipole moment probably not in excess of 0.1 D, the remainder of Δ being associated with atomic polarizability effects whose magnitude seems reasonable on the basis of our rough theoretical estimates. Previous estimates of the permanent dipole moment of the complex appear to be too large.

Finally, the implications of these results for the nature of the bonding in the B–HFB complex should be noted. In the case of undoubted charge-transfer complexes, *e.g.*, I_2 with benzene, the degree of mixing of the charge-transfer state into the ground state is usually estimated to be on the order of 5–10%, leading to dipole moments of the complex on the order of 1 D or greater. The bonding energy of the complex and the dipole moment are both roughly proportional to this degree of mixing,[3] and a dipole moment of that magnitude is usually implied by energies in the kilocalorie range arising from charge transfer. The enthalpy of formation of the B–HFB complex is in this range and it seems difficult to see how a charge transfer mechanism could account for such a large effect without a greatly larger dipole moment than can be inferred from our work. We conclude that although some charge transfer may occur in the B–HFB mixtures, the formation of a complex is attributable in the main to entirely different effects.

Acknowledgment. We thank Professor R. L. Scott and Dr. D. V. Fenby for many helpful discussions on this work, and Mr. R. H. Wang for performing some preliminary refractive index measurements. Professor C. P. Smyth kindly provided us with the results of his microwave measurements.

Acidity and Association of Aluminum Ion in Dilute Aqueous Acid[1]

by Ernest Grunwald and Dodd-Wing Fong

Department of Chemistry, Brandeis University, Waltham, Massachusetts 02154 *(Received September 11, 1968)*

The acid dissociation of $Al(OH_2)_6^{3+}$ in water at 30° was examined by measuring the change of pH as HCl is added in very small increments to 0.007–0.06 vol. F $AlCl_3$. The data show clearly that dimerization of $(H_2O)_5AlOH^{2+}$ is significant. Equilibrium constants (referred to infinite dilution) were determined as follows: for acid dissociation of $Al(OH_2)_6^{3+}$, $K_A^\circ = 2.44 \times 10^{-5}$ M at 30°; for association constant $(H_2O)_5AlOH^{2+}$ to a dimer, $K^\circ = 60$ M^{-1} at 30°, $\Delta H^\circ \approx -11$ kcal, $\Delta S^\circ \approx -28$ gibbs.

In water, aluminum ion exists largely in the form of the hexahydrate, $Al(OH_2)_6^{3+}$,[2,3] which is a weak acid.[4–6] However, the pH of pure aqueous solutions of aluminum salts is consistent with a model of simple acid dissociation (eq 1) only at low aluminum concentration (<0.005 vol. F).[4–6,7]

$$Al(OH_2)_6^{3+} + H_2O \overset{K_A^\circ}{\rightleftharpoons} Al(OH_2)_5OH^{2+} + H_3O^+ \quad (1)$$

At higher concentrations, the model becomes progressively less adequate, and some form of association evidently becomes significant. In this paper we wish to show that the first species that is formed is the dimer of $Al(OH_2)_5OH^{2+}$. This dimer is surprisingly stable. The association constant, K° (referred to infinite dilution), is 60 M^{-1} at 30°; $\Delta H^\circ \approx -11$ kcal; $\Delta S^\circ \approx -28$ gibbs.

Regarding the structure of the dimer, we prefer the

(1) Work supported by the Petroleum Research Fund of the American Chemical Society. Grateful acknowledgment is made to the donors of that Fund.

(2) R. Schuster and A. Fratiello, *J. Chem. Phys.*, **47**, 1554 (1967).

(3) R. E. Connick and D. N. Fiat, *ibid.*, **39**, 1349 (1963); H. W. Baldwin and H. Taube, *ibid.*, **33**, 206 (1960).

(4) J. N. Brønsted and K. Volqvartz, *Z. Physik. Chem.*, **134**, 97 (1928).

(5) R. K. Schofield and A. W. Taylor, *J. Chem. Soc.*, 4445 (1954).

(6) C. R. Frink and M. Peech, *Inorg. Chem.*, **2**, 473 (1963). These authors find no significant deviations from the model of simple acid dissociation up to 0.01 vol. F Al^{3+}.

(7) C. Brosset, *Acta Chem. Scand.*, **6**, 910 (1952), and references cited therein.

hydrated cyclic octahedral structure (2) to that of an anhydride with octahedral or tetrahedral structure, such as (3) or (4), although such structures cannot be ruled out.

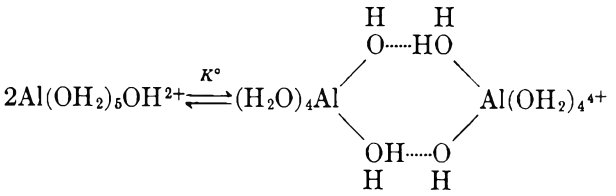

(2)

$$(H_2O)_mAl{-}O{-}Al(OH_2)_m^{4+} \qquad (m = 5, 3) \qquad (3)$$

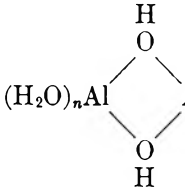

(4)

We prefer (2) because it permits the mutually repelling aluminum ions to be fairly far apart, and also because the reversible formation of an anhydride would lead to the exchange of water molecules between the solvation shell of the formal Al^{3+} species and bulk water. Such exchange is known to be quite slow, with a half-life greater than 0.02 sec, even under conditions where $(H_2O)_5AlOH^{2+}$ and its dimer are present at significant concentrations.[2,8] We prefer a cyclic structure involving two hydroxide bridges to a linear structure with one bridge because of the high stability of the dimer relative to that of the complex formed between $(H_2O)_5AlOH^{2+}$ and $Al(OH_2)_6^{3+}$, in which there can be only one hydroxide bridge. The *upper limit* to the association constant for the formation of the latter is found by us to be 10 M^{-1} at 30°.

Results

We used a differential potentiometric method[9] to measure the apparent K_A of aluminum ion as a function of the Al^{3+} concentration. The relationship can then be analyzed theoretically to elucidate the chemical equilibria.

Beginning with a "pure solution" of $AlCl_3$ in water, we added HCl in very small increments and measured the pH as a function of HCl added. Following previous practice,[9] we defined a titration function, ϵ, such that $\epsilon = 1 +$ (equivalents of HCl)/(formula wts of $AlCl_3$). That is, $\epsilon = 1$ for pure $AlCl_3$ in pure water. The increments of HCl added were so small that the total decrease in pH below that of the "pure solution" was less than about 0.4 unit. Under those conditions, pH was an almost exactly linear function of ϵ, and dpH/dϵ at $\epsilon = 1$ could be determined experimentally with good precision. An apparent K_A was then calculated for the formal acid, aluminum ion in the given "pure solution," as described previously. Results, obtained at 30°, are summarized in Table I.

Table I: Apparent K_A of $Al(OH_2)_6^{3+}$ in Water at 30° by Differential Potentiometry near pH 3

$[Al^{3+}]$	K_A (apparent), $M \times 10^5$	y[a]	x[a]	$K_A^\circ K^\circ \times 10^3$
0.00070	1.95	0.763	6.07	(1.62)[b]
0.00100	1.90	0.729	7.38	(1.78)[b]
0.00400	1.62	0.576	16.3	1.38
0.0100	1.60	0.460	27.2	1.79
0.0201	1.54	0.379	40.6	1.52
0.0401	1.63	0.310	58.5	1.48
0.0587	1.71	0.277	71.0	1.43
				Av 1.46[c]

[a] Calculated from eq 18 and 22; $K_A^\circ = 2.44 \times 10^{-5}$. [b] Omitted from average. Formation of $(ALOH)_2^{4+}$ is quite insignificant at these low concentrations. [c] Weighted average. $K^\circ = 60$.

This experimental arrangement avoids several sources of potentially serious error. Measurements are made well below the pH range in which a hydrous aluminum gel precipitates out of solution.[7] Small amounts of basic hydrolysis products, commonly present in the $AlCl_3 \cdot 6H_2O$ reagent,[4] cause little or no error in the measurement of dpH/dϵ since the linear relationship of pH to $\epsilon = 1$ extends, without change in slope, to $\epsilon < 1$. The amount of HCl added is so small that measurements are made at virtually constant ionic strength and composition. Thus in pH-measuring cells with liquid junctions, the junction potentials are virtually constant.

An experimental arrangement similar to ours, in which, however, the pH was measured by a kinetic method, was used by Brønsted and Volqvartz[4] in their classical work on the acidity of aquo-ions. Their results at 15° for $Al(OH_2)_6^{3+}$ and for the structurally and electrostatically similar roseo-ion, $Co(NH_3)_5OH_2^{3+}$, are cited in Table II.

Tables I and II permit the following conclusions. The variation of K_A with ionic strength for roseo-ion, our model substance, is perfectly normal for an acid of charge number +3 and can be brought into quantitative agreement with Debye–Hückel theory. To show this, we express K_A in terms of K_A° (at infinite dilution) and molar activity coefficients y_z, as in (5).

$$K_A = K_A^\circ y_{+3}/y_{+2}y_{+1} \qquad (5)$$

Activity coefficients in turn are expressed according to Debye–Hückel theory, as in (6), where z is the charge number

$$\log y_z = -z^2 S\sqrt{\mu}/(1 + A\mathring{a}\sqrt{\mu}) \qquad (6)$$

μ is the ionic strength, S (the limiting slope) and A are

(8) H. W. Baldwin and H. Taube, *J. Chem. Phys.*, **33**, 206 (1960); J. A. Jackson, J. F. Lemons, and H. Taube, *ibid.*, **32**, 553 (1960); J. P. Hunt and H. Taube, *ibid.*, **19**, 602 (1951).

(9) E. Grunwald, *J. Amer. Chem. Soc.*, **73**, 4934 (1951).

Table II: Interpretation of K_A Values in Water at 15° [a]

ϵ [b]	$10^6 K_A$, M Obsd	$10^6 K_A$, M Calcd
Data for $(H_3N)_5CoOH_2^{3+}$ (Roseo-Ion)		
0	...	1.549[c]
0.010	0.700	0.711
0.015	0.648	0.637
0.025	0.552	0.550
0.035	0.498	0.498
0.050	0.442	0.447
Data for $Al(OH_2)_6^{3+}$		
0	...	7.70[d]
0.005	5.48	5.46
0.01	5.53	5.39
0.02	5.50	5.61

[a] Data of Brønsted and Volqvartz.[4] [b] Volume formal concentration of roseo-ion or aluminum ion. [c] $K_A = K_A^\circ y^4$; eq 7, $\mathring{a} = 6$ Å. [d] Calculated on the basis of eq 7, 18, and 22; $K^\circ K_A^\circ = 1.20 \times 10^{-3}$.

known functions, and $\mathring{a}$ is an adjustable parameter.[10] In water, $S = 0.5161$ at 30° and 0.5028 at 15°; $A = 0.3301$ at 30° and 0.3273 at 15°.[10] For $\mathring{a}$ we adopt a single, as yet unspecified, value for all ion species to be considered, all of which are strongly hydrated cations. On that basis we may express all activity coefficients in terms of a single variable, y, as shown in eq 7 and 8.

$$\log y = -S\sqrt{\mu}/(1 + A\mathring{a}\sqrt{\mu}) \quad (7)$$

$$\log y_z = z^2 \log y \quad (8)$$

It then follows that $K_A = K_A^\circ y^4$. The treatment still requires that we specify the value of $\mathring{a}$. This was done by fitting the K_A data for roseo-ion. As the trial value of $\mathring{a}$ was varied from 5 to 9 Å, the fit went through a sharp optimum at $\mathring{a} = 6$ Å. The close agreement with observation is demonstrated in Table II. The 6 Å value for $\mathring{a}$ is consistent with measured activity coefficients for a variety of metal chlorides.[11] An $\mathring{a}$ value of 9 Å, suggested by some authors,[6,12] is decidedly unsatisfactory.

While the ionic strength effect on K_A for roseo-ion is normal, that for aluminum ion is not. Instead of showing the expected systematic decrease, K_A is nearly stationary between 0.005 and 0.06 M, going through a very shallow minimum. Figure 1 shows that attempts to reproduce this relationship by an extended form of the Debye–Hückel theory are unsuccessful even when implausible values are used for the adjustable parameters. We shall see in the next section that the deviation from normal behavior can be ascribed to ionic association according to (2).

Equilibrium Constants. We shall consider the following species: $ALOH_2^{3+}$, $ALOH^{2+}$, H^+, $H_2OAL_2OH^{5+}$, and $(ALOH)_2^{4+}$, where AL $\equiv Al(OH_2)_5$. The stoichiometry is then expressed by eq 9 and 10, where c

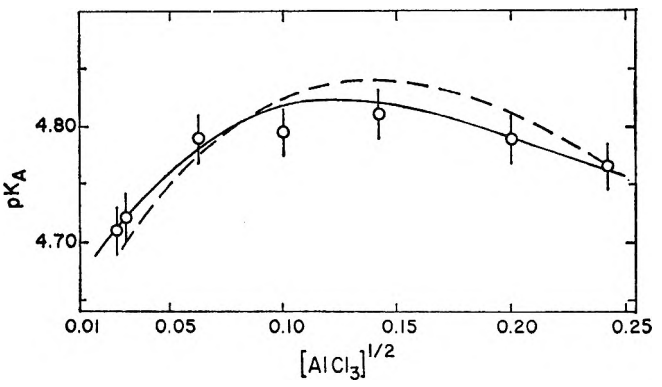

Figure 1. Apparent pK_A of aluminum ion at 30° in water as a function of the volume formal concentration of $AlCl_3$. The dashed curve represents the equation, $pK_A = 4.578 + [2.046\mu^{1/2}/(1 + 3\mu^{1/2})] - 0.706\mu$, where $\mu = 6[AlCl_3]$. The solid curve is calculated on the basis of two simultaneous equilibria, (1) and (2), as described in Case 3 in the text.

is the vol. formal concentration of Al^{3+}, and c_A, c_B, c_{BB}, and c_{AB} denote, respectively, the molar concentrations of $ALOH_2^{3+}$, $ALOH^{2+}$, $(ALOH)_2^{4+}$, and $H_2OAL_2OH^{5+}$.

$$c = c_A + c_B + 2c_{BB} + 2c_{AB} \quad (9)$$

$$(\epsilon - 1)c = [H^+] - c_B - 2c_{BB} - c_{AB} \quad (10)$$

$$[H^+]c_B/c_A = K_A = K_A^\circ y^4 \quad (11)$$

$$c_{BB}/c_B^2 = K = K^\circ y^{-8} \quad (12)$$

$$c_{AB}/c_A c_B = K^* = K^{*\circ} y^{-12} \quad (13)$$

In addition, we shall make the justified assumptions that $c_A \approx c$, and the amount of HCl added in any given measurement of $dpH/d\epsilon$ is so small that c and μ may be regarded as constant. On that basis, we shall derive expressions for $d \ln [H^+]/d\epsilon = -2.303 dpH/d\epsilon$, as follows.

Case 1: c_{BB}, $c_{AB} \ll c_B$. Then, on neglecting c_{BB} and c_{AB} in (10), we find that $K_A = [H^+][H^+ - (\epsilon - 1)c]/c$, and that $d \ln [H^+]/d\epsilon$ at $\epsilon = 1$ is related to K_A by (14).

$$2\left(\frac{d \ln [H^+]}{d\epsilon}\right)_{\epsilon=1} = \left(\frac{c}{K_A}\right)^{1/2} \quad (14)$$

Case 2: $c_{BB} \ll c_{AB}$, c_b. Then, on neglecting c_{BB} in (10) and making use of (13), we find that $K_A = [H^+][H^+ - (\epsilon - 1)c]/c(1 + K^*c)$ and that $d \ln [H^+]/d\epsilon$ at $\epsilon = 1$ is related to K_A by (15).

$$2\left(\frac{d \ln [H^+]}{d\epsilon}\right)_{\epsilon=1} = \left(\frac{c}{K_A(1 + K^*c)}\right)^{1/2} \quad (15)$$

(10) See, for example, R. A. Robinson and R. H. Stokes, "Electrolyte Solutions," 2nd ed, Butterworth and Co. Ltd., London, 1959, p 468.

(11) F. H. Spedding, P. E. Porter, and J. M. Wright, *J. Amer. Chem. Soc.*, **74**, 2781 (1952).

(12) J. Kielland, *J. Amer. Chem. Soc.*, **59**, 1675 (1937).

Case 3: $c_{AB} \ll c_{BB}, c_B$. Then, on neglecting c_{AB} in (10) and making use of (12), we find that K_A is given by (16) and that $d \ln [H^+]/d\epsilon$ at $\epsilon = 1$ is related to K_A by (17)

$$K_A = [H^+]^2[H^+ - (\epsilon - 1)c]/c[H^+ + 2KK_Ac] \quad (16)$$

$$2\left(\frac{d \ln [H^+]}{d\epsilon}\right)_{\epsilon=1} = \frac{x(1 + 2KK_Ax)}{(1 + 3KK_Ax)};$$

$$x = \left(\frac{c}{[H^+]}\right)_{\epsilon=1} \quad (17)$$

where $x = c/[H^+]$ at $\epsilon = 1$. On solving (16) for $\epsilon = 1$, we obtain (18), and on substituting this result in (17), we arrive finally at (19).

$$x = [c/K_A(1 + 2KK_Ax)]^{1/2} \quad (18)$$

$$2\left(\frac{d \ln [H^+]}{d\epsilon}\right)_{\epsilon=1} = \left(\frac{c(1 + 2KK_Ax)}{K_A(1 + 3KK_Ax)^2}\right)^{1/2} \quad (19)$$

The experimental quantity, K_A(apparent), is always calculated on the assumption of normal behavior (Case 1).[13] Thus, on comparing (14) with (15) and (19), we obtain the following relationships between K_A (apparent) and K_A, depending on which Case corresponds to reality.

In Case 1

$$K_A(\text{apparent}) = K_A = K_A^\circ y^4 \quad (20)$$

In Case 2

$$K_A(\text{apparent}) = K_A(1 + K^*c) \quad (21a)$$

$$y^{-4}K_A(\text{apparent}) = K_A^\circ(1 + K^{*\circ}cy^{-12}) \quad (21b)$$

In Case 3

$$K_A(\text{apparent}) = K_A(1 + 3KK_Ax)^2/(1 + 2KK_Ax) \quad (22)$$

Case 1 has already been disposed of, since K_A(apparent) does not vary as y^4. In Case 2, we expect from (21b) that the relationship of $y^{-4}K_A$(apparent) to cy^{-12} is linear. In fact, this relationship is strongly and unmistakably curved, showing that the formation of $H_2O \cdot AL_2OH^{5+}$ is not the dominant source of the deviation from normal behavior. From the result obtained at the highest concentration we estimate that $K^* < 10\ M^{-1}$. In testing for Case 3, we proceeded as follows: (i) calculate y for each experimental point; neglect the effect of reactions 1 and 2 on μ; (ii) obtain K_A° by extrapolation of log $[y^{-4} \cdot K_A(\text{apparent})]$ to infinite dilution; (iii) calculate KK_Ax from (22), using $K_A = K_A^\circ y^4$; (iv) calculate x from (18), using the result obtained in (iii); (v) calculate K_AK and $K_A^\circ K^\circ = K_AKy^4$.

Results of the test are shown in Table I. It can be seen that $K_A^\circ K^\circ$ is quite constant over the entire concentration range. Final average values are, at 30°: $K_A^\circ = 2.44 \times 10^{-5}$; $K_A^\circ K^\circ = 1.46 \times 10^{-3}$; $K^\circ = 60\ M^{-1}$. The success of the treatment in reproducing K_A(apparent) is shown by the solid curve in Figure 1.

Analogous treatment of the data of Brønsted and Volqvartz[4] leads to these values at 15°: $K_A^\circ = 0.77 \times 10^{-5}$; $K^\circ = 156$. Although the fit of the data is satisfactory, the test is not decisive because there are only three data points. From the temperature coefficient of K° we calculate that $\Delta H^\circ = -11.0$ kcal and $\Delta S^\circ = -28$ gibbs. These values are tentative and need further checking before they can be accepted.

Experimental Section

Materials. Aluminum chloride hexahydrate, hydrochloric acid, and water were reagent grade chemicals and have been described elsewhere.[14]

Differential Potentiometric Measurement of K_A. Measurements and calculations were made substantially as recommended by Grunwald.[9] The pH measurements were made with a Beckman research pH meter and a Beckman No. 39030 glass and reference "combination electrode." pH readings were precise to better than 0.01 unit and ranged about an average value just above pH 3. The values of $dpH/d\epsilon$ at a given $AlCl_3$ concentration were reproducible to about ±1%, except in the case of 0.06 M $AlCl_3$ where the precision was ±3%.

(13) In the actual calculations we used the more exact equations given in ref 9, which do not involve the approximations that $c_A = c$ = constant as ϵ is varied. The main difference between these equations and those stated in the text is that they allow for the slight dilution as HCl is added. The difference amounts to a few per cent and is nearly constant in all three cases.

(14) D.-W. Fong and E. Grunwald, *J. Amer. Chem. Soc.*, in press.

Effect of Pressure on the Rate of Hydrolysis of Methyl and Isopropyl Bromides

by B. T. Baliga and E. Whalley

Division of Applied Chemistry, National Research Council, Ottawa *(Received May 6, 1968)*

The rate constants for the spontaneous hydrolysis of methyl and isopropyl bromides in water have been measured to an accuracy of about 0.2% up to 3 kbars at three temperatures. The shape of the rate-constant–pressure curve for methyl bromide shows clearly that a second mechanism occurs at high pressures. The high-pressure mechanism has perhaps more covalent attachment of water in the transition state, *i.e.*, is more SN2-like, than the low-pressure mechanism. The results for isopropyl bromide are consistent with, but do not prove, a similar but more reluctant change of mechanism with pressure. The activation volume for both reactions becomes less negative with increasing temperature at 1 bar, but this trend reverses at about 500 bars. The activation enthalpy and entropy vary with pressure in a complicated fashion, partly although not entirely connected with the change of mechanism. The constant-volume heat capacity of activation is about −93 cal deg^{-1} mol^{-1} for both reactions, which is about twice the constant-pressure heat capacity. It varies much less with pressure but much more with temperature than the constant-pressure heat capacity. A detailed interpretation of this unexpected behavior is premature at present.

1. Introduction

The temperature dependence of the constant-pressure activation enthalpy $\Delta H_p^{\ddagger}$ is usually described by an activation heat capacity at constant pressure $\Delta C_p^{\ddagger}$ defined by

$$\Delta C_p^{\ddagger} = (\partial \Delta H_p^{\ddagger}/\partial T)_p \qquad (1)$$

In recent years many measurements of this quantity have been made[1] with a view to correlating it with mechanism. All these attempts, however, suffer from a disadvantage common to all attempts to interpret heat capacities of condensed phases at constant pressure, namely that part of the energy required to increase the temperature goes to expanding the system against its own internal forces. Unless the magnitude of this energy can be estimated, it is not possible to discuss the various contributions to the heat capacity of activation with any accuracy. The heat capacity of activation at constant volume $\Delta C_V^{\ddagger}$

$$\Delta C_V^{\ddagger} = (\partial \Delta U_V^{\ddagger}/\partial T)_V \qquad (2)$$

where $\Delta U_V^{\ddagger}$ is the internal energy of activation at constant volume, ought to be more informative than $\Delta C_p^{\ddagger}$, but no previous attempt to measure it has been reported. The relationship between the two heat capacities of activation is[2]

$$\Delta C_p^{\ddagger} - \Delta C_V^{\ddagger} = \frac{T\alpha\Delta V^{\ddagger}}{\kappa}\left\{\left(\frac{\partial}{\partial T}\ln\frac{\alpha\Delta V^{\ddagger 2}}{\kappa^2}\right)_p + \frac{\alpha}{\kappa}\left(\frac{\partial}{\partial p}\ln\frac{\Delta V^{\ddagger}}{\kappa}\right)_T\right\} \qquad (3)$$

where T is the temperature, p is the pressure, α and κ are the thermal expansivity and compressibility of the mixture, and $\Delta V^{\ddagger}$ is the activation volume. An estimate of the magnitude of the difference between the two heat capacities for the neutral hydrolysis of ethylene oxide in water[3] gave[4] roughly −30 cal deg^{-1} mol^{-1}. This is of the magnitude of $\Delta C_p^{\ddagger}$ for many reactions, and it shows that the two heat capacities can differ significantly.

This paper describes the measurement of the quantities required to determine $\Delta C_p^{\ddagger} - \Delta C_V^{\ddagger}$ for the hydrolysis of methyl and isopropyl bromides in water. These reactions were chosen because there is already a large amount of accurate information about them,[5-8] including several measurements of the heat capacity of activation at constant pressure, and they typify an important class of solvolyses. Furthermore, to measure $\Delta C_p^{\ddagger} - \Delta C_V^{\ddagger}$ by means of eq 3, the activation volume and its temperature and pressure coefficients are required. To determine these coefficients, accurate rate constants are required and these reactions can conveniently and accurately be followed by conductance measurements.

Unfortunately, for a present understanding of these reactions the measurements have revealed unexpected complexities, and emphasize our ignorance more than our understanding. The most significant information is probably a sigmoid variation of ln k in the pressure for methyl bromide, which is interpreted as due to a change of mechanism.

(1) For reviews, see G. Kohnstam, "The Transition State," Chemical Society Special Publication No. 16, 1962, p 179; J. R. Hulett, *Quart. Rev.*, **18**, 227 (1964); G. Kohnstam, *Advan. Phys. Org. Chem.*, **5**, 121 (1967); R. E. Robertson, *Progr. Phys. Org. Chem.*, **4**, 213 (1966).

(2) E. Whalley, *Adv. Phys. Org. Chem.*, **2**, 93 (1964).

(3) J. Koskikallio and E. Whalley, *Can. J. Chem.*, **37**, 783 (1959).

(4) B. T. Baliga, R. J. Withey, D. Poulton, and E. Whalley, *Trans. Faraday Soc.*, **61**, 517 (1965).

(5) E. A. Moelwyn-Hughes, *Proc. Roy. Soc.*, **A164**, 295 (1938).

(6) E. A. Moelwyn-Hughes, *ibid.*, **A220**, 386 (1953).

(7) R. L. Heppolette and R. E. Robertson, *ibid.*, **A252**, 273 (1959).

(8) R. L. Heppolette and R. E. Robertson, *Can. J. Chem.*, **44**, 677 (1966).

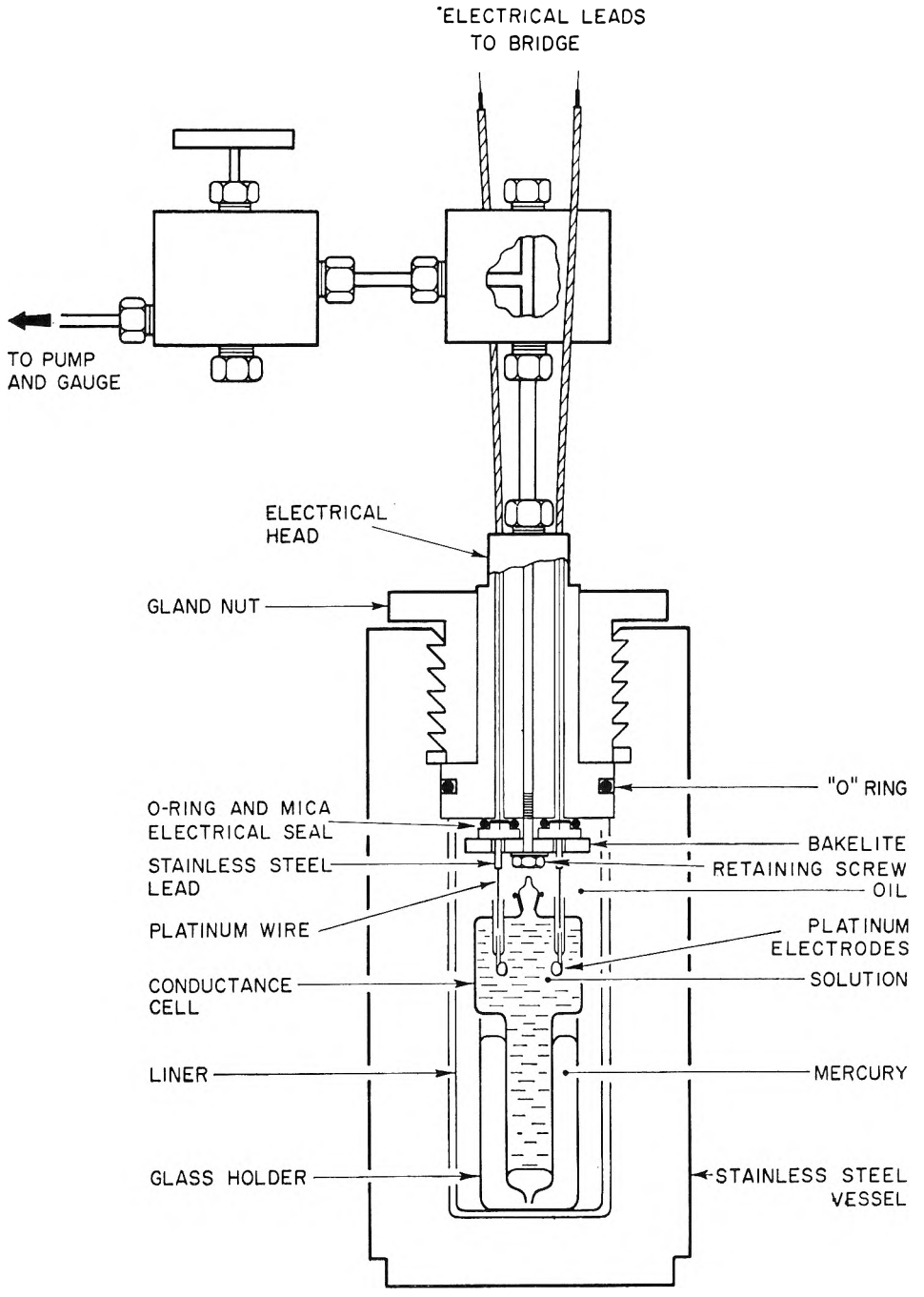

Figure 1. Sketch of conductance cell and pressure vessel.

2. Experimental Methods

Materials. Methyl bromide from a Matheson of Canada lecture bottle analyzed 99.9% by gas chromatography, and was used directly. Eastman Kodak White Label isopropyl bromide was refluxed over anhydrous sodium sulfate and distilled, and the middle fraction boiling at 59.5–60.0° was collected. It analyzed 99.7% by gas chromatography. Distilled water was freed of carbon dioxide by boiling and was stored out of contact with carbon dioxide. The conductance in the cell used was <0.8 μmho.

Pressure Techniques. The pressure equipment is shown in Figure 1. The pressure vessel is of the kind used previously,[9] with the head modified for electrical seals. The electrical seals were made with mica and Viton O-rings as described elsewhere[10] and were held in place by a Bakelite retaining plate. The resistance between leads and between a lead and the head was >100 megohms at all pressures and temperatures.

The pressure-transmitting fluid was medium grade Stanolax, and pressure was generated by an air-driven oil pump and adjusted by a screw injector. The rate constants obtained in this work are reproducible to 0.1

(9) J. Koskikallio and E. Whalley, *Trans. Faraday Soc.*, **55**, 809 (1959).
(10) R. J. Withey and E. Whalley, *ibid.*, **59**, 895 (1963).

Table I: Rate Constants $10^6k/sec^{-1}$ for the Hydrolysis of Methyl Bromide in Water

	p, bars												
t, °C	50	249	496	741	987	1234	1480	1727	1973	2221	2472	2712	2955
60.00	35.67	39.97	45.40	49.92	53.27		60.52		68.74	75.44	81.59	87.48	92.05
	35.59[a]	40.00	45.29	50.11	53.41		60.35		69.04	75.49	81.26	87.10	92.03
	35.64												
70.00	103.9	114.8	127.6	140.0	154.6	165.8	176.9	187.9	197.4	218.1	238.3	255.7	271.7
	103.8[a]	115.0	128.0	140.2	154.8	166.0	176.9	187.8	197.7	217.8	237.9	255.3	271.7
													271.9
80.00	274.5	296.4	327.4	365.1	399.9								
	274.4	296.4	327.5	364.9	400.2								
	274.9[a]												
	274.5[a]												

[a] Rates measured at 10 kcps. All others at 5 kcps.

Table II: Rate Constants $10^6k/sec^{-1}$ for the Hydrolysis of Isopropyl Bromide in Water[a]

	p, bars										
t, °C	50	100	249	398	496	741	987	1480	1973	2472	2955
40.00	32.63	33.44	36.33	38.59	40.12	43.79	47.36	54.86	62.97	71.90	81.36
	32.53										
50.00	115.7	118.5	126.8	134.4	138.9	151.8	163.6	192.4	222.4	256.3	289.4
	115.8										
60.00	362.5		390.0		426.4	466.8	509.3				

[a] All rates measured at 5 kcps.

or 0.2%, and so the pressure must be measured to a corresponding accuracy. If the volume of activation is 20 $cm^2\ mol^{-1}$, a change of rate constant of 0.1% corresponds to a change of pressure of about 2 bars. The pressure was measured by a 3-kbar Heise Bourdon gauge that was calibrated before and after each run against a pressure balance. The construction of the pressure balances and their calibration against a 17-m differential mercury column have been described.[11] The Bourdon gauge was reproducible to ±1 bar when calibrated in this way, and all pressures have this accuracy.

The thermostat was a well insulated 15-gallon stainless steel tank filled with light transformer oil and controlled to ±0.005°.

Conductance Measurements. A Leeds and Northrup Catalog 1554-A2 ac bridge with a Hewlett-Packard Model 202B oscillator, a Rohde and Schwartz or General Radio tunable amplifier, and an oscilloscope were used. The system was thoroughly tested and was calibrated against standard resistors. In the experimental range, the bridge errors were <0.01%.

The conductance cell is shown in Figure 1. It was made of Pyrex and was about 15 cm long and 4 cm in diameter at the upper end. Pressure was transmitted to the reaction mixture by mercury that was held in a glass cup to insulate it electrically from the vessel. The electrodes were of platinum about 6 mm in diameter. The electrical seal through the glass was made with 0.5 mm diameter, 0.05 mm wall, 1 cm long, platinum tubes. The tube seals had much longer life under pressure than rod seals, presumably because the tube can conform to the compression of the glass better than a rod can. The life of the seal at pressures up to 3 kbars was several tens of runs. The cell was supported by a stainless steel holder which was suspended from the head of the pressure vessel by wire attached to hooks screwed into the head.

The cells were conditioned before use by refluxing with 0.1 *M* aqueous hydrogen bromide for many days until the conductance of millimolar hydrogen bromide in the cell at 80° remained constant to 1 in 10^4 for 50 hr. They were stored in aqueous hydrogen bromide at 80°. Electrode polarization was tested for by measuring the conductance of millimolar hydrogen bromide in the cell between 0.5 and 10 kcps. When the electrodes were slightly platinized,[5] the conductance differed by about 0.02% at room temperature and pressure between 0.5 and 5 kcps but at 70° and 500 bars the difference was about 0.4%. The difference was about 0.03% in the frequency range 5–10 kcps, and this was at least partly due to losses from the high-potential lead to the head of the vessel though the insulators

(11) G. S. Kell and E. Whalley, *Phil. Trans. Roy. Soc.*, A258, 565 (1965).

Table III: Comparison of Rate Constants and Activation Parameters with Previous Values

Methyl bromide						Isopropyl bromide					
10^6 k/sec^{-1} extrapolated to p = 0			Activation parameters at 70°			10^6 k/sec^{-1} extrapolated to p = 0			Activation parameters at 50°		
60.00°	70.00°	80.00°	$\Delta H_p^{\ddagger}$, cal mol^{-1}	$\Delta S_p^{\ddagger}$, cal deg^{-1} mol^{-1}	Ref	40.00°	50.00°	60.00°	$\Delta H_p^{\ddagger}$, cal mol^{-1}	$\Delta S_p^{\ddagger}$, cal deg^{-1} mol^{-1}	Ref
34.59	101.2	269.2	23,177 ± ~50	−9.5 ± ~0.2 (50 bar)	This work	31.70	112.7	355.6	24,300 ± ~50	−1.5 ± ~0.2 (50 bar)	This work
35.12	101.4	271.3	23,220	−9.4	7	31.32	110.1	349.8	24,360	−1.4	8
35.2	105	271.5			6[a]						

[a] The temperatures used were 333.11, 343.66, and 353.38°K, respectively.

such as the Viton O-ring, Bakelite, mica, Stanolax, etc. Losses of this kind have no effect on the rate constant if they stay constant throughout a run, and so 5 kcps was used throughout this work. Some runs were followed at both 5 and 10 kcps and gave rate constants agreeing to 0.2%.

Kinetics. Stock 0.1 *M* aqueous methyl bromide was made by bubbling the gas into deaerated water. Both this and stock 0.03 *M* aqueous isopropyl bromide were stored at 0°; 1.5 m*M* solutions for kinetic runs were made by dilution. The cells were well rinsed with distilled water and the kinetic solution and were filled and placed in the pressure vessel. The vessel was pressurized to 50 bars to prevent loss of reactant when the solution was heated and was placed in the thermostat which was preheated about 4° higher than the experimental temperature to facilitate thermal equilibrium. The first readings were taken after at least 1 hr, and the reaction was followed for at least 4 to 5 half-lives. In the slower runs, the reaction was followed for 2 days, leaving a gap overnight.

Calculation of Rate Constants. The equivalent conductance Λ ($= 10^3\ KG/c$ where K is the cell constant expressed in cm^{-1}, G the conductance expressed in mhos, c the concentration expressed in mol l.$^{-1}$, and Λ is expressed in mhos cm^2 mol^{-1}) of hydrogen bromide changes by about 1.8% over the concentration range 0.2 to 1.5 m*M*, and so to obtain accurate rate constants an allowance must be made. This can be done using the limiting law

$$\Lambda = \Lambda_0 - (A\Lambda_0 + B)c^{1/2} \qquad (4)$$

where Λ_0 is the equivalent conductivity extrapolated to infinite dilution

$$A = 8.20 \times 10^5/(\epsilon T)^{3/2};\ B = 82.4/(\epsilon T)^{1/2}\eta \qquad (5)$$

ϵ is the dielectric constant, T is the Celsius temperature, and η is the viscosity in poises. By rearrangement, we find for the adjusted conductance G° that is proportional to the concentration

$$G^\circ = G(1 + \beta G^{1/2}) \qquad (6)$$

where

$$\beta = (10^3 K/\Lambda^3)^{1/2}(A\Lambda + B) \qquad (7)$$

and since $\beta << 1$, Λ has been substituted for Λ_0 to sufficient accuracy. The dielectric constant of water was obtained from ref 12 and 13 and the viscosity was interpolated from ref 14. The equivalent conductance of hydrogen bromide was measured at concentrations of 0.5, 1.0, and 2.0 m*M* at several temperatures and pressures. To sufficient accuracy, the mean value for the three concentrations was used in eq 7.

The first-order rate constants were calculated by the Guggenheim method using least squares with a digital computer. The deviations were always apparently nonsystematic.

3. Results

The first-order rate constants for methyl and isopropyl bromides are summarized in Tables I and II and are plotted against pressure in Figure 2. The curves for methyl bromide at 60 and 70° are sigmoid—an unusual and probably unique observation. Because of this unexpected complexity, all points were duplicated to verify their accuracy. The standard error of the rate constants from the internal consistency of the least-squares fit was about 0.1%, and the reproducibility of duplicate runs (see Tables I and II) was 0.1 to 0.2%. The standard error is probably about 0.15%. The rate constants extrapolated to zero pressure and the activation enthalpies and entropies obtained by least-squares from the measured rate constants at 50 bars are compared with those from other workers at 1 bar in Table III. The agreement is good. The activation enthalpy and entropy ($T\Delta S^{\ddagger}$) at 1 and 50 bars differ by only several tens cal mol^{-1} (see later, Figures 4 and 5).

To calculate the heat capacity of activation at constant volume, it is necessary to know the activation volume and its pressure and temperature coefficients. The rate-constant–pressure curves are too complicated for any numerical analysis to be accurate, particularly for methyl bromide, and a graphical analysis is necessary. The best method is probably to plot mean ac-

(12) B. B. Owen and S. R. Brinkley, *Phys. Rev.*, 64, 32 (1943).
(13) B. B. Owen, R. C. Miller, C. E. Milner, and H. L. Cogan, *J. Phys. Chem.*, 65, 2065 (1961).
(14) K. E. Bett and J. B. Cappi, *Nature*, 207, 620 (1965).

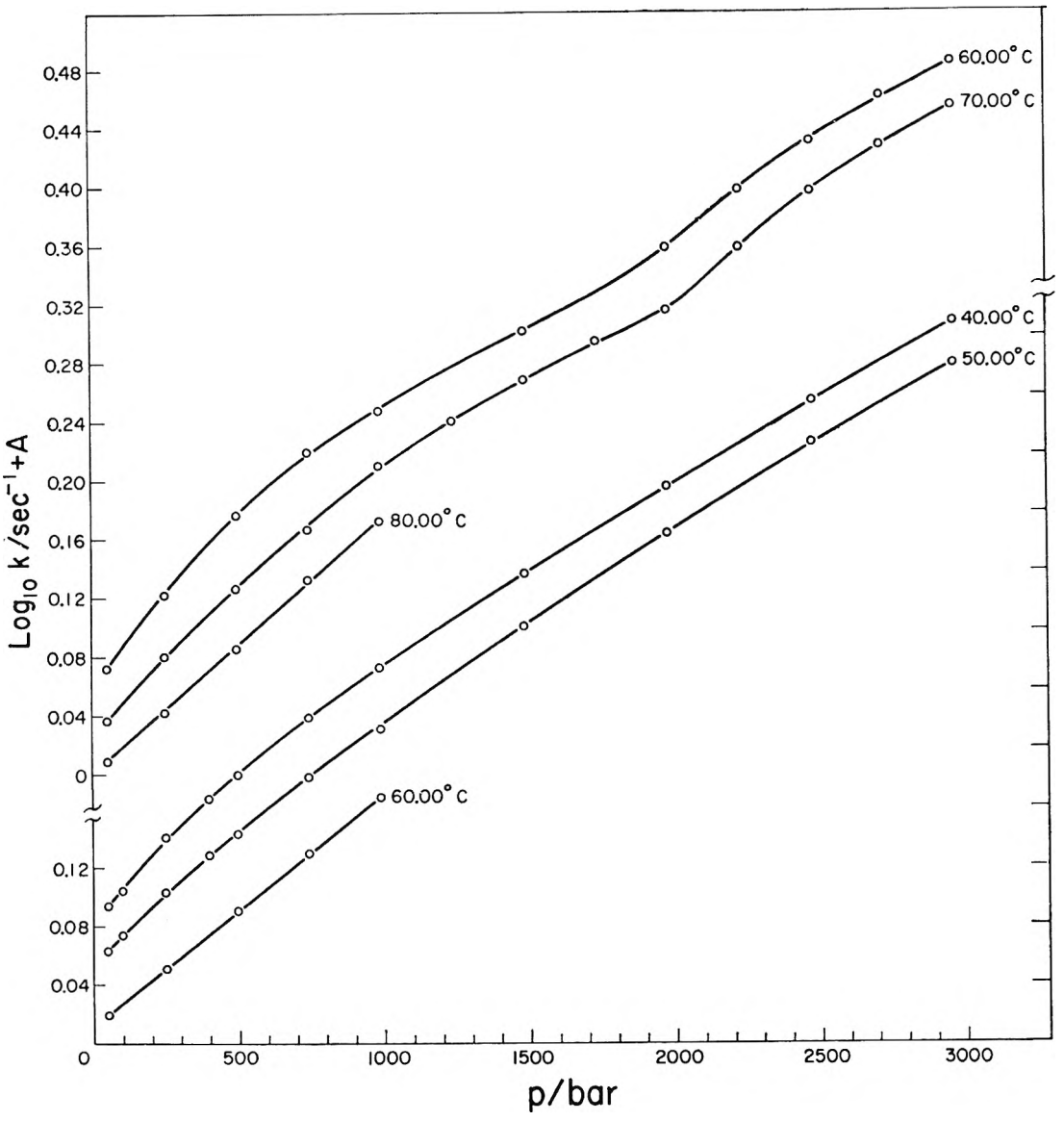

Figure 2. Rate constants for the hydrolysis of methyl bromide (upper three curves) and isopropyl bromide (lower three curves) in water. The numbers attached to the curves are the temperatures.

tivation volumes between adjacent pressures

$$\Delta V_{\text{mean}}^{\ddagger} = -[RT \ln k(p_2)/k(p_1)]/(p_2 - p_1) \quad (8)$$

against the mean pressure $\frac{1}{2}(p_2 + p_1)$. This is done in Figure 3. Because of the sigmoid rate-constant–pressure curve for methyl bromide, the volume of activation is also sigmoid in the pressure at 60 and 70°. The zero-pressure activation volumes were obtained by extrapolation and are listed in Table IV, together with estimated standard errors. The volumes were chosen to be consistent both with the curves of Figure 3 and the difference of activation volumes at different temperatures obtained as described in the next paragraph.

The first derivatives of the activation volume with respect to pressure and temperature, or the second derivatives of the Gibbs energy of activation $\Delta G^{\ddagger}$, were obtained at zero pressure as follows. The pressure coefficient of the activation volume is the slope of the curves in Figure 3 at zero pressure. The values obtained are listed in Table IV. They depend strongly on the temperature, changing over each 10° interval by about 5 cm^3 mol^{-1} kbar^{-1} for methyl bromide and about 6 cm^3 mol^{-1} kbar^{-1} for isopropyl bromide. They appear to reach zero at the high end of the temperature range for both substances.

The temperature coefficient of the activation volume is best obtained by plotting $T_1 \log k_1 - T_2 \log k_2$ where k_1 and k_2 are the rate constants at temperatures T_1 and T_2 and the same pressure, against pressure. The slope of the curve is related to the difference of activation volumes at the two temperatures according to the relation

$$R\frac{\partial}{\partial p}(T_1 \log k_1 - T_2 \log k_2) = -(\Delta V_1^{\ddagger} - \Delta V_2^{\ddagger}) \quad (9)$$

The curves are shown in Figure 4, and yield the values

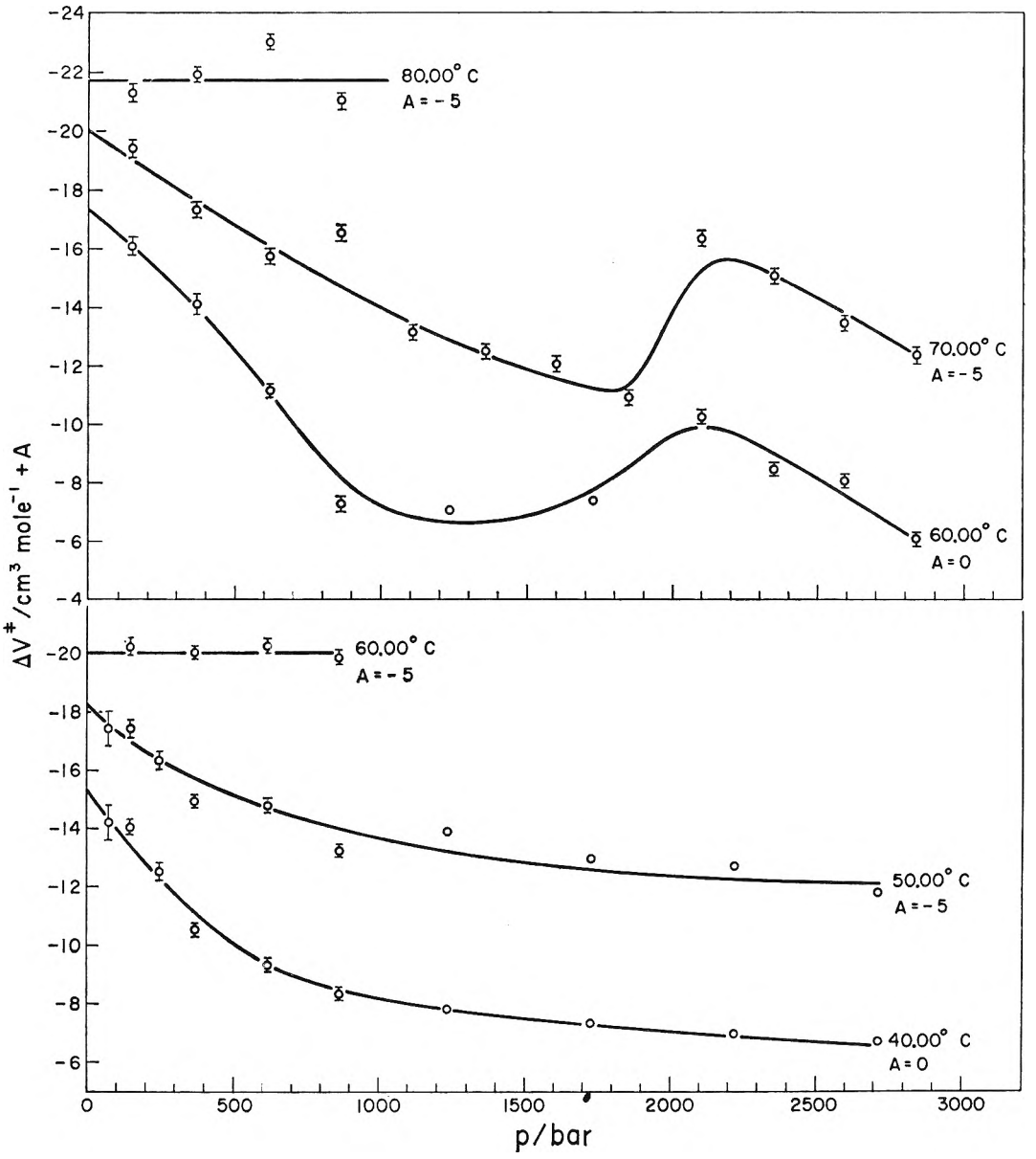

Figure 3. Mean activation volumes between adjacent pressures for the hydrolysis of methyl bromide (upper three curves) and isopropyl bromide (lower three curves).

at 1 bar for methyl bromide

$$\Delta V^{\ddagger}_{70} - \Delta V^{\ddagger}_{60} = 2.14 \pm \sim 0.15 \text{ cm}^3 \text{ mol}^{-1}$$

$$\Delta V^{\ddagger}_{80} - \Delta V^{\ddagger}_{70} = 3.20 \pm \sim 0.15 \text{ cm}^3 \text{ mol}^{-1}$$

$$\Delta V^{\ddagger}_{80} - \Delta V^{\ddagger}_{60} = 5.38 \pm \sim 0.25 \text{ cm}^3 \text{ mol}^{-1}$$

and for isopropyl bromide

$$\Delta V^{\ddagger}_{50} - \Delta V^{\ddagger}_{40} = 2.14 \pm \sim 0.2 \text{ cm}^3 \text{ mol}^{-1}$$

$$\Delta V^{\ddagger}_{60} - \Delta V^{\ddagger}_{50} = 3.06 \pm \sim 0.2 \text{ cm}^3 \text{ mol}^{-1}$$

$$\Delta V^{\ddagger}_{60} - \Delta V^{\ddagger}_{40} = 5.4 \pm \sim 0.3 \text{ cm}^3 \text{ mol}^{-1}$$

The last value in each set is included as a check. The temperature coefficients of the activation volumes obtained from these results are listed in Table IV. The difference between the activation volumes at two temperatures is of course more accurate than the activation volumes themselves. The temperature coefficient of the activation volume is about 50% higher in the higher than in the lower temperature range for both reactants.

Because of the thermodynamic relations

$$(\partial S/\partial p)_T = -(\partial V/\partial T)_p$$

$$(\partial H/\partial p)_T = V - T(\partial V/\partial T)_p$$

where S is the entropy, H the enthalpy, and V the volume, the effect of temperature on the activation volume and the effect of pressure on the activation entropy $\Delta S^{\ddagger}$ and enthalpy $\Delta H^{\ddagger}$ are closely related. The values of $(\partial \Delta S^{\ddagger}/\partial p)_T$ at zero pressure are the negative of the values of $(\partial \Delta V^{\ddagger}/\partial T)_p$ listed in Table IV. The points in Figure 4 are actually $(T_1 - T_2) \log A$ where A is the Arrhenius preexponential factor (ekT/h)

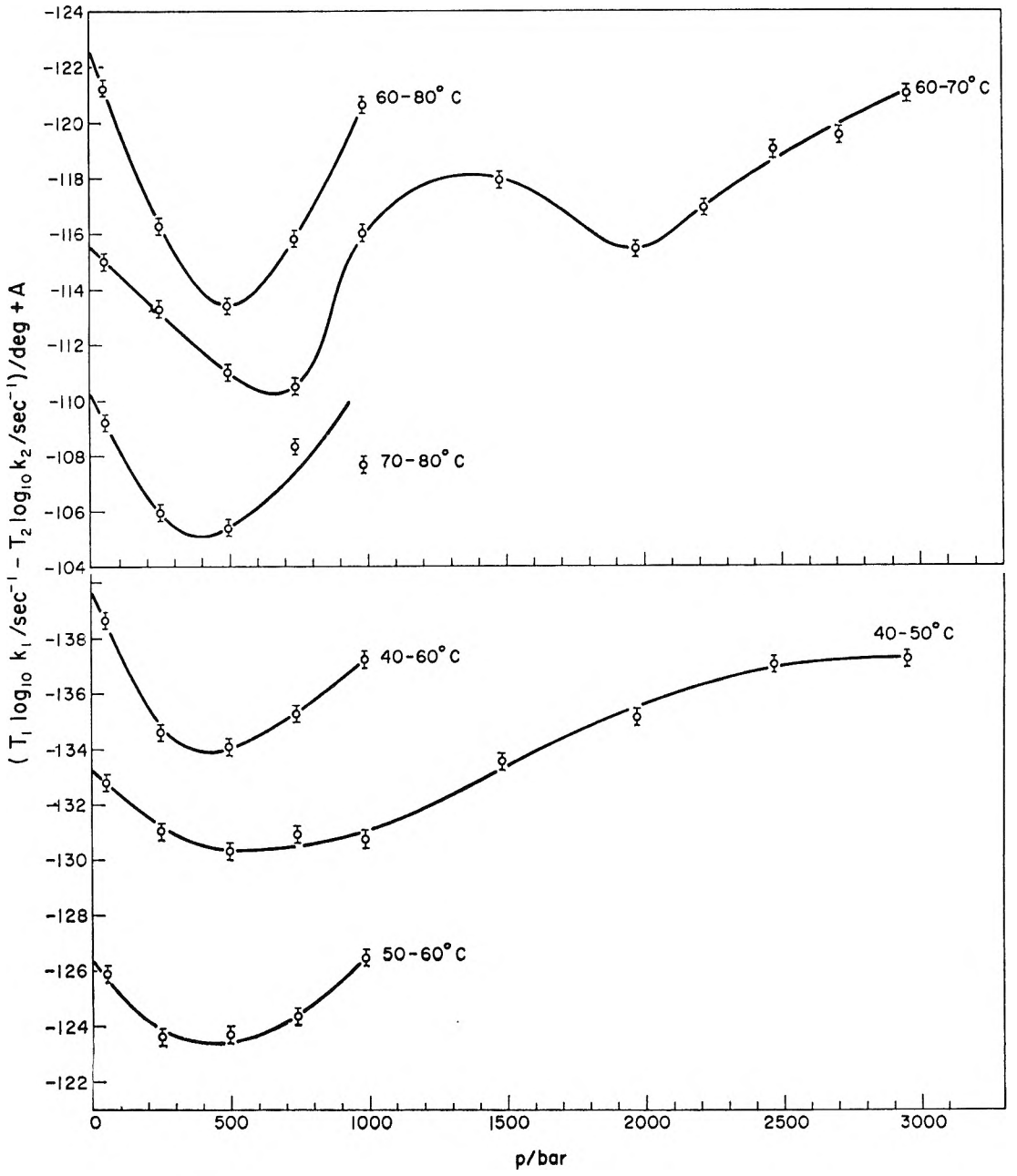

Figure 4. Plot of $T_1 \log k_1 - T_2 \log k_2$ against pressure according to eq 9. The upper three curves are for methyl bromide and the lower three curves for isopropyl bromide. The numbers attached to the curves are temperatures for that curve.

Table IV: Activation Volumes for the Hydrolysis of Methyl and Isopropyl Bromides in Water

Methyl bromide				Isopropyl bromide			
Temp, °C	$\Delta V^{\ddagger}$, cm³ mol⁻¹	$(\partial \Delta V^{\ddagger}/\partial p)_T$, cm³ mol⁻¹ kbar⁻¹	$(\partial \Delta V^{\ddagger}/\partial T)_p$, cm³ mol⁻¹ deg⁻¹	Temp, °C	$\Delta V^{\ddagger}$, cm³ mol⁻¹	$(\partial \Delta V^{\ddagger}/\partial p)_T$, cm³ mol⁻¹ kbar⁻¹	$(\partial \Delta V^{\ddagger}/\partial T)_p$, cm³ mol⁻¹ deg⁻¹
60.0	−17.0[a]	11.0 ± ~2	0.21 ± 0.01	40.0	−15.2[a]	~12	0.21
70.0	−14.9	5.5 ± ~1		50.0	−13.1	~6	
80.0	−11.7	−0.5 ± ~0.5	0.32 ± 0.01	60.0	−10.0	0	0.31

[a] The standard error of these volumes is about 0.3 cm³ mol⁻¹, all values being in error by the same amount within 0.1 cm³ mol⁻¹.

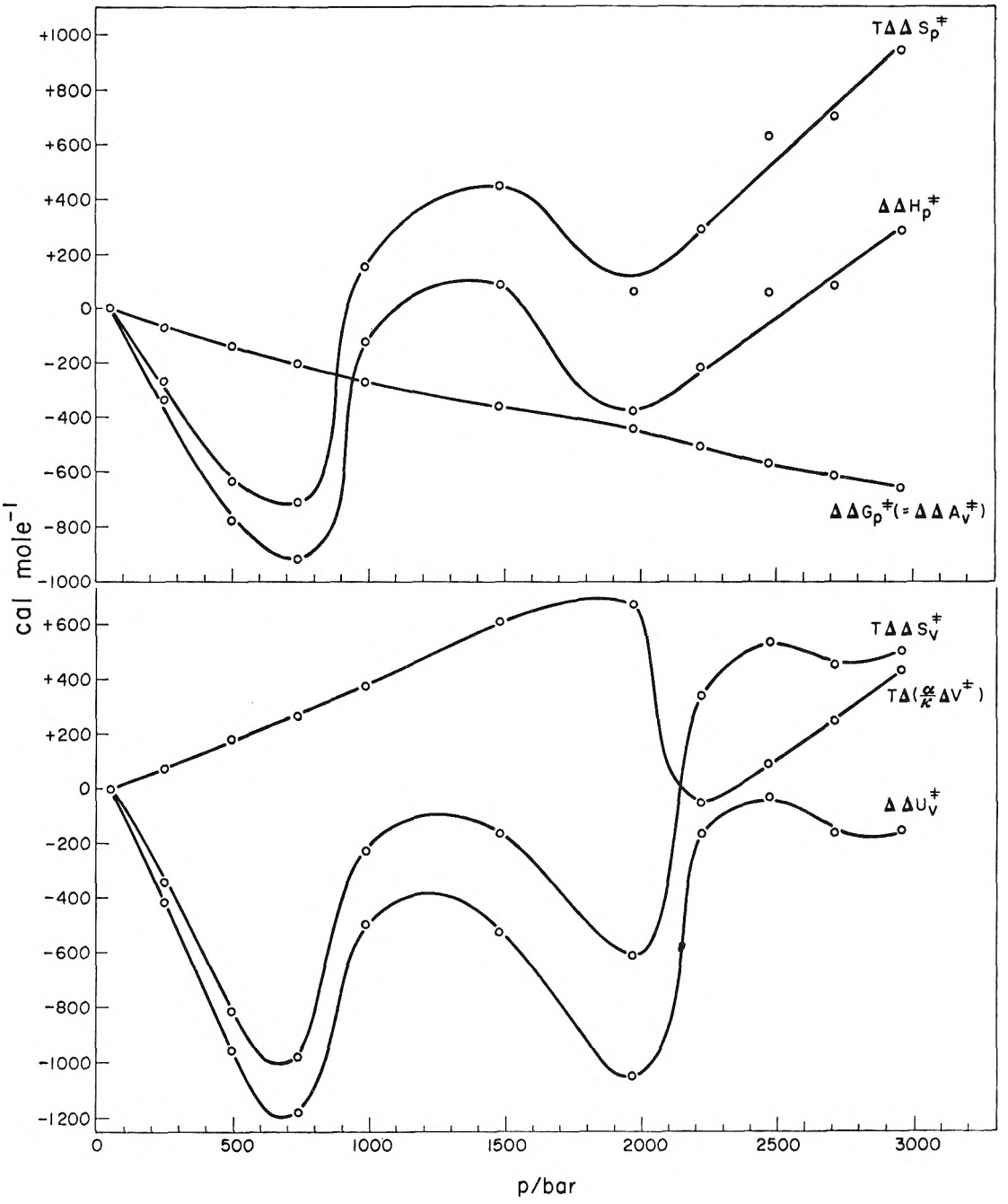

Figure 5. Effect of pressure on the free energy, enthalpy or internal energy, and entropy of activation at constant pressure (upper frame), and at constant volume (lower frame), for the hydrolysis of methyl bromide.

$\exp\Delta S^{\ddagger}/R$, e is the base of natural logarithms, k and h Boltzmann's and Planck's constants, and R the gas constant, and the slopes of the curves at any pressure are $(\partial\Delta S^{\ddagger}/\partial p)/2.303R$. Up to about 500 bars the activation entropy increases with increasing pressure for both methyl and isopropyl bromides, but decreases at higher pressures. By direct analysis of the rate constants under pressure, or by use of the curves of Figure 4, the enthalpy and entropy of activation at constant pressure can be obtained as a function of pressure. The values ($T\Delta S^{\ddagger}$ is plotted for the entropy) are given in the upper frames of Figures 5 and 6. The values for methyl bromide oscillate strongly with an amplitude well over 1 kcal mol^{-1}. The accuracy of the rate constants is such that the strong variation must be real.

The constant-volume parameters of activation $\Delta U_V^{\ddagger}$ (U = internal energy) and $\Delta S_V^{\ddagger}$ are sometimes simpler functions of an independent variable (usually solvent composition) than the constant-pressure parameters,[4,15,16] and so they have been examined for the present reactions. They were calculated as functions of

(15) B. T. Baliga and E. Whalley, *Can. J. Chem.*, 42, 1835 (1964).
(16) B. T. Baliga and E. Whalley, *J. Phys. Chem.*, 71, 1166 (1967).

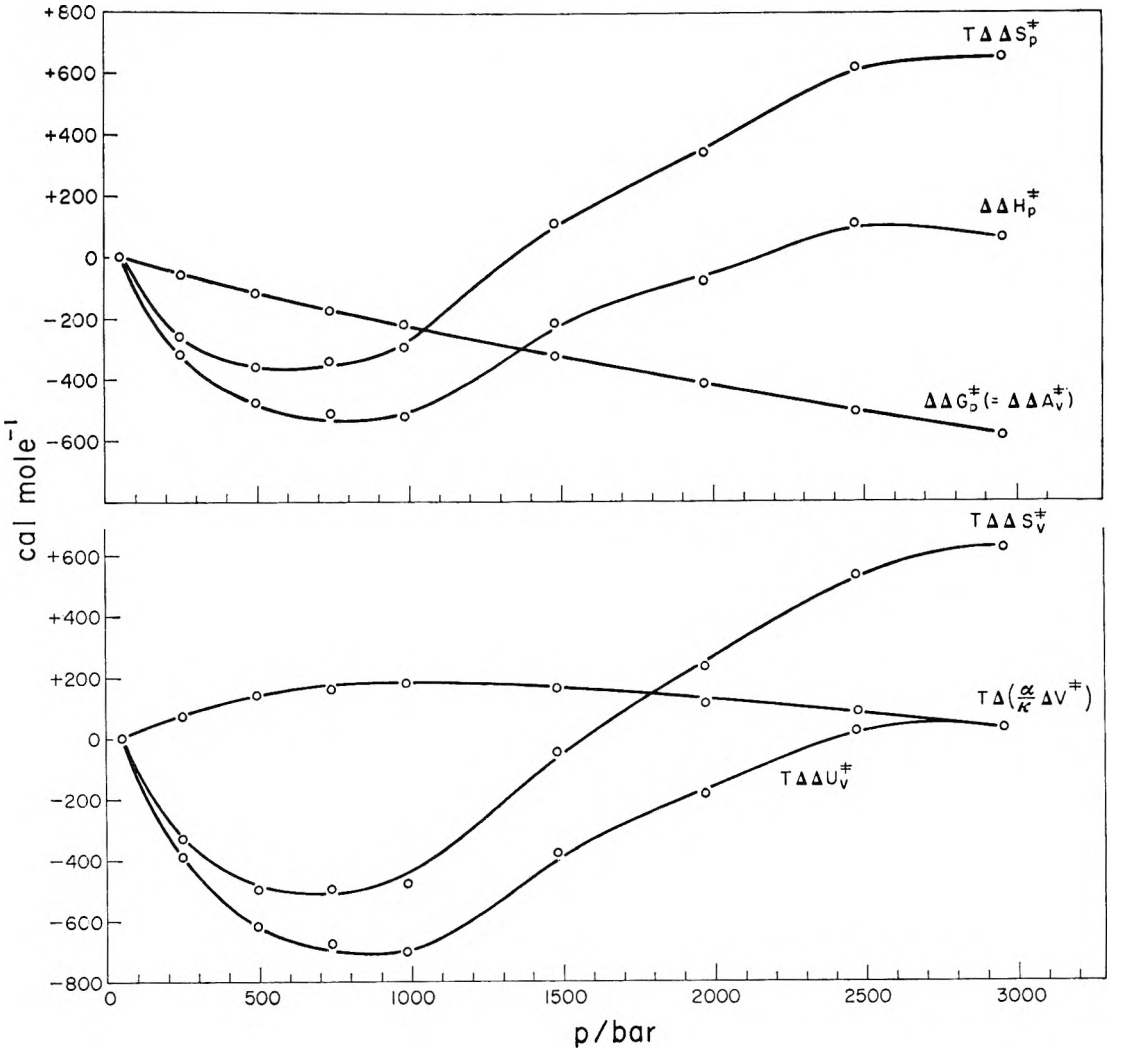

Figure 6. Effect of pressure on the free energy, enthalpy or internal energy, and entropy of activation at constant pressure (upper frame) and at constant volume (lower frame) for the hydrolysis of isopropyl bromide.

pressure for methyl and isopropyl bromides from the usual relations

$$\Delta U_V^{\ddagger} = \Delta H_p^{\ddagger} - T\alpha\Delta V^{\ddagger}/\kappa$$

$$\Delta S_V^{\ddagger} = \Delta S_p^{\ddagger} - \alpha\Delta V^{\ddagger}/\kappa$$

The thermal expansivity and compressibility of water were kindly provided by Dr. G. S. Kell from a fit to the data of ref 11 which was extrapolated to 3 kbars. The values so obtained are probably at least as reliable as published measurements. The results are plotted in the lower frame of Figures 5 and 6. They vary with pressure in much the same way as the constant-pressure parameters.

There are four third derivatives of the Gibbs energy with respect to temperature and pressure. The effects of $\partial^3\Delta G^{\ddagger}/\partial p^3 = \partial^2\Delta V^{\ddagger}/\partial p^2$ can be seen in the curvature of mean activation volume against pressure in Figure 3 but no accurate value can be obtained.

$$\partial^3\Delta G^{\ddagger}/\partial p\partial T^2 = \partial^2\Delta V^{\ddagger}/\partial T^2 =$$

$$-\partial^2\Delta S^{\ddagger}/\partial p\partial T = -T^{-1}\partial\Delta C_p^{\ddagger}/\partial p$$

is probably finite and of the magnitude 0.01 cm^3 mol^{-1} deg^{-2} for both methyl and isopropyl bromides, which corresponds to $\partial\Delta C_p^{\ddagger}/\partial p = \sim -80$ cal deg^{-1} mol^{-1} kbar^{-1}. The effect of temperature on the activation volume depends strongly on the pressure, and according to Figure 4 $\partial\Delta V^{\ddagger}/\partial T$ changes sign for both reactions at about 500 bars. The value of $\partial^3\Delta G^{\ddagger}/\partial^2 p\partial T = \partial^2\Delta V^{\ddagger}/\partial p\partial T = -\partial^2\Delta S^{\ddagger}/\partial p^2$ appears therefore to be about 0.54 cm^3 mol^{-1} deg^{-1} kbar^{-1} for both reactions, which agrees well, as it should, with the value 0.57 cm^3 mol^{-1} deg^{-1} kbar^{-1} obtained from the effect of temperature on the pressure coefficient of the activation volume.

The values of the various terms in eq 3 going to make the value of $\Delta C_p^{\ddagger} - \Delta C_V^{\ddagger}$ at 1 bar are given in Table V. The properties of water required were obtained from recent measurements in this laboratory[11] and a reanalysis of the density of water at 1 atm.[17]

From the value of $\Delta C_p^{\ddagger}$ reported by Heppolette and

(17) G. S. Kell, *J. Chem. Eng. Data*, 12, 66 (1967).

Table V: Differences of Heat Capacities of Activation at Constant Pressure and Constant Volume

	$\frac{T\alpha\Delta V^{\ddagger}}{\kappa}\left\{\frac{\partial}{\partial T}\ln\alpha\right.$	$-2\frac{\partial}{\partial T}\ln\kappa$	$-\frac{\alpha}{\kappa}\frac{\partial}{\partial p}\ln\kappa$	$+2\frac{\partial}{\partial T}\ln\Delta V^{\ddagger}$	$\left.+\frac{\alpha}{\kappa}\frac{\partial}{\partial p}\ln\Delta V^{\ddagger}\right\} =$	$\Delta C_p^{\ddagger} - \Delta C_v^{\ddagger}$
Methyl bromide, 70°, 1 bar	−15.8	5.7	−5.4	57	7.5	49 cal deg^{-1} mol^{-1}
Isopropyl bromide 50°, 1 bar	−18.2	0.8	−3.0	47.8	5.7	33 cal deg^{-1} mol^{-1}

Robertson,[7,8] $\Delta C_V^{\ddagger}$ is for methyl bromide

$$\Delta C_V^{\ddagger} = -95 \pm \sim 10 \text{ cal deg}^{-1} \text{ mol}^{-1}$$

and for isopropyl bromide

$$\Delta C_V^{\ddagger} = -92 \pm \sim 10 \text{ cal deg}^{-1} \text{ mol}^{-1}$$

By far the largest contribution to $\Delta C_p^{\ddagger} - \Delta C_V^{\ddagger}$ comes from the temperature coefficient of the activation volume. As pointed out in the preceding paragraph, however, this value changes sign at about 500 bars, and has about the same magnitude but opposite signs at 0 and 1000 bars. $\partial(\Delta C_p^{\ddagger} - \Delta C_V^{\ddagger})/\partial p$ is therefore of the magnitude of −100 cal deg^{-1} mol^{-1} kbar^{-1} for both substrates. But $\partial\Delta C_p^{\ddagger}/\partial p$ is ∼−80 cal deg^{-1} mol^{-1} kbar^{-1}, so that $\Delta C_V^{\ddagger}$ is much less dependent on the pressure than $\Delta C_p^{\ddagger}$, and its dependence is probably zero within experimental error. The value of $\Delta C_p^{\ddagger} - \Delta C_V^{\ddagger}$ is largely determined by the term

$$2(T\alpha\Delta V^{\ddagger}/\kappa)(\partial \ln \Delta V^{\ddagger}/\partial T) = 2(T\alpha/\kappa)(\partial\Delta V^{\ddagger}/\partial T)$$

which changes in magnitude by about 50% in a 10° interval, due mainly to the change in $\partial\Delta V^{\ddagger}/\partial T$. This implies an appreciable temperature dependence of $\Delta C_p^{\ddagger} - \Delta C_V^{\ddagger}$ at 1 bar. There is, however, no evidence[7,8] that $\Delta C_p^{\ddagger}$ varies with temperature, so that a variation of $\Delta C_V^{\ddagger}$ is implied that is much greater than the variation of $\Delta C_p^{\ddagger}$.

Furthermore, since the thermal expansivity of water is zero at 4°, $\Delta C_p^{\ddagger} - \Delta C_V^{\ddagger}$ is also zero there; it follows then that $\Delta C_p^{\ddagger} - \Delta C_V^{\ddagger}$ for methyl bromide changes by 49 cal deg^{-1} mol^{-1} in 66° at 1 bar, and for isopropyl bromide by 39 cal deg^{-1} mol^{-1} in 46°. The temperature variations discussed in this paragraph are of course at constant pressure. It is worth enquiring what happens to $\Delta C_p^{\ddagger} - \Delta C_V^{\ddagger}$ as the temperature is varied at constant density. At 4° and 1 bar, $\Delta C_p^{\ddagger} - \Delta C_V^{\ddagger}$ is zero because α is zero. The same density as at these conditions is obtained under a pressure of about 300 bars at 50° and about 500 bars at 70°. Then $\Delta C_p^{\ddagger} - \Delta C_V^{\ddagger}$ is not far from zero because $\partial\Delta V^{\ddagger}/\partial T$ is small, and it seems that perhaps $\Delta C_p^{\ddagger} - \Delta C_V^{\ddagger}$ is much less temperature dependent if the volume is kept constant as the temperature is varied. However, the reason why $\Delta C_p^{\ddagger} - \Delta C_V^{\ddagger}$ is small changes with temperature, from a small thermal expansivity at 4° to a small temperature coefficient of the activation volume at the temperatures of the experiments.

4. Discussion

1. A Second Mechanism of Hydrolysis of Methyl Bromide. The complexity of the graph of log k against pressure for methyl bromide in Figure 2 is very striking. The activation volume, which is plotted as a function of pressure in the upper frame of Figure 3, at first becomes less negative with increasing pressure, then becomes more negative, and finally less negative again. There is no doubt that this complexity is real because each point was duplicated and reproduced to 0.2% or better (see Table I for the individual values). If the same mechanism occurred throughout the pressure range, the transition state would be less compressible than the initial state at low pressures, more compressible near 1.6 kbars, and again less compressible at higher pressures. While nothing prohibits such behavior, it seems preferable to assume that there are two different transition states arising from two competing mechanisms, one of which dominates at low pressures and the other at high pressures. The high-pressure mechanism must of course have the more negative volume of activation.

This view assumes that the two transition states are separated by a high free-energy barrier. It is, however, possible to explain the observed effects by assuming that the transition state occupies a broad col in configuration–free-energy space, the different parts of which have different molar volumes. The effect of pressure would then be to depress one part of the col faster than the rest. The place at which most of the reaction crosses the col would then change gradually with pressure. It is difficult if not impossible to distinguish between these possibilities by experiment. For definiteness, however, two distinct mechanisms will be discussed, one of which replaces the other as the pressure changes. It is easy, if preferred, to translate into a description in which a transition state gradually changes character.

An accurate estimate of the relative rate constants of the two mechanisms at atmospheric pressure is quite impossible, but by a very rough extrapolation from Figure 2 it appears to be of the magnitude of 10 rather than 1 or 100. If the activation energies of the two mechanisms were different, then that with the lower value would tend to dominate at low temperatures and that with the higher at high temperatures.

Moelwyn-Hughes,[6] following the reaction titri-

metrically, found that while the heat capacity of activation at constant pressure was negative below about 60 or 70°, it was positive above. Heppolette and Robertson,[7] on the other hand, who followed the reaction by the more accurate conductivity method, reported that $\Delta C_p^{\ddagger}$ is -46.5 cal deg^{-1} mol^{-1}, essentially independent of temperature in the range 35 to 100°. The incursion of a new mechanism at high temperatures would contribute a positive term to the heat capacity of activation, and so there is no evidence in these results of a change of mechanism.

Heppolette and Robertson's[7] results do not, however, exclude a change of mechanism. The constant-pressure activation heat capacity of methyl bromide is about 10 cal deg^{-1} mol^{-1} less negative than those of the other methyl halides, so a positive contribution of 10 cal deg^{-1} mol^{-1} or more from a changing mechanism could easily occur. It is easily shown that the contribution $\Delta C_p^{\ddagger}$(mech) to the constant-pressure activation heat capacity of a change from mechanism 1 to mechanism 2 is

$$\Delta C_p^{\ddagger}(\text{mech}) = f(1 - f)(\Delta E_A)^2/RT^2$$

where

$$f = k_1/(k_1 + k_2)$$

k_1 and k_2 are the rate constants for the two mechanisms, and ΔE_A is the difference in Arrhenius energy. If, for purposes of calculation, $f = 0.1$ and $\Delta C_p^{\ddagger}$ from this cause is 10 cal deg^{-1} mol^{-1}, then ΔE is 1.6 kcal mol^{-1}, df/dT is 0.6×10^{-6} deg^{-1}, and $\Delta C_p^{\ddagger}$ changes by 2 cal deg^{-1} mol^{-1} over the range 35–100°. These are not inconsistent with Heppolette and Robertson's[7] measurements, and indeed appreciably greater differences of activation energy could be tolerated. There is therefore no inconsistency between the present evidence for a change of mechanism under pressure at 70° and existing rate constants at 1 bar if the two mechanisms do not differ in activation energy by more than a few kcal mol^{-1}. Although it is not possible to determine activation energies of the two mechanisms because their rates cannot be well separated, the activation enthalpy and entropy under pressure, given in Figure 5, suggest that the mechanisms have similar values.

What are the two mechanisms? The only information at present about the high-pressure mechanism is that its activation volume is much more negative than that for the low-pressure mechanism, but its activation enthalpy and entropy are nearly the same, and this is hardly sufficient to base much speculation on. The most obvious interpretation is that one mechanism approximates the SN1 mechanism with a transition state resembling

$$\overset{\delta+}{\text{CH}_3}\cdots\overset{\delta-}{\text{Br}}$$

interacting with the solvent by essentially dipole–dipole and other electrostatic forces, and the other approximates the SN2 mechanism with a transition state resembling

$$\overset{\delta+}{\text{H}_2\text{O}}\cdots\text{CH}_3\cdots\overset{\delta-}{\text{Br}}$$

also interacting with the solvent by essentially dipole–dipole etc. forces.

It seems likely that the SN2 mechanism will have a more negative volume of activation than the SN1 mechanism. The reasons for this are as follows. If the dipoles are spherical and the solvent is represented by a dielectric, the interaction free energy[18] is proportional to μ^2/v where μ is the dipole moment and v is the volume of a molecule. The molar volume of liquid methyl bromide is 54 cm^3 mol^{-1}, and the volume of a mole of methyl bromide plus a mole of water is 72 cm^3. There is undoubtedly a contraction when the SN2 transition state is formed due to the formation of the partial O···C bond, and there are expansions of both transition states due to the lengthening of the C···Br bond. In addition, both transition states are contracted by the dipole–solvent interaction,[19] so it seems that their molar volumes are the same to perhaps 10 to 15%. If the same charges are separated in both transition states, the dipole moments are in the ratio of the charge separations. On the most naive view of the structure of the transition states, the separation of the charges in the SN2 is roughly double that in the SN1. The dipole moment of the SN2 is therefore probably appreciably greater than that of the SN1. Hence, both the increased electrostatic interaction, which cause both the transition state and the solvent to contract, and the formation of a new O···C bond will probably cause the SN2 transition state to have a smaller volume than the SN1. Hence, the present results could be readily understood if methyl bromide hydrolyzed by a mechanism approximating to SN1 at low pressure and tended to become approximately SN2 at higher pressure. The terms SN1 and SN2 should not of course be interpreted too literally: perhaps the terms "less and more covalent attachment of water in the transition state" would be more accurate.

The results for isopropyl bromide are not inconsistent with this suggestion. If methyl bromide adopts the "SN1-like" mechanism at low pressures, then so would isopropyl bromide. It would be expected to transfer to the "SN2-like" mechanism less readily than methyl bromide, and as expected the results show no clear evidence of a change of mechanism. However, the volume of activation is strongly dependent on the pressure at low pressure, but becomes almost independent of pressure above about 1 kbar. This unusual behavior can be explained by supposing that at the higher pressures the "SN2-like" mechanism begins to intrude enough to compensate the fall in the volume of activa-

(18) J. G. Kirkwood, *J. Chem. Phys.*, **2**, 351 (1934).
(19) E. Whalley, *ibid.*, **38**, 1400 (1963).

tion of the "SN1-like" mechanism. To verify this, the reactions will have to be followed to yet higher pressures.

2. Temperature Coefficient of the Activation Volume. For most reactions so far studied, the modulus $|\Delta V^{\ddagger}|$ of the activation volume increases as the temperature increases. For example, for the spontaneous hydrolysis of ethylene oxide in water[3]

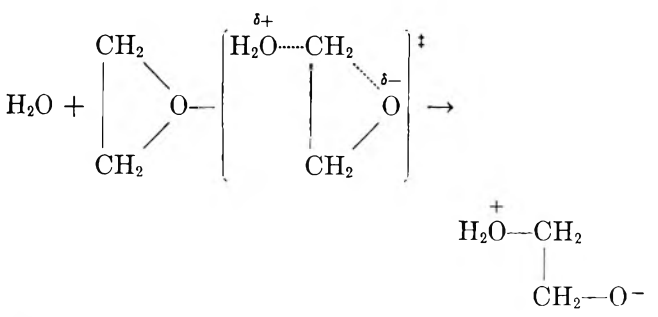

the activation volume decreases (becomes more negative) at about the rate 0.1 $cm^3\ mol^{-1}\ deg^{-1}$. This is the direction of change expected on simple grounds, because the lower the density the lower usually the intermolecular forces and so the higher the thermal expansion. For the hydrolysis of both methyl and isopropyl bromides at 1 bar, on the other hand, the transition states have a smaller volume than the initial states, but have a higher thermal expansion. Furthermore, the difference of thermal expansion increases with increasing temperature. The situation is quite different under pressure, however. At about 500 bars for both reactions the activation volume is independent of temperature, and at about 1000 bars it varies at about the same rate as at 1 bar but with opposite sign.

The decrease of $|\Delta V^{\ddagger}|$ with increasing temperature is not entirely without precedent. The ionization volume of carbonic acid[20]

$$2H_2O + CO_2 \rightleftharpoons HCO_3^- + H_3O^+$$

in the range 25 to 65° increases (becomes less negative) at about the rate 0.070 $cm^3\ mol^{-1}\ deg^{-1}$ at 1 bar and about the rate 0.10 $cm^3\ mol^{-1}\ deg^{-1}$ at 3000 atm. There appears, however, to be no precedent for the reversal of sign of the temperature coefficient of the activation volume as the pressure is increased.

The unusual temperature coefficient of the activation volume is unlikely to be connected with there being two parallel mechanisms. The contribution to $\partial\Delta V^{\ddagger}/\partial T$ of the changing mechanism, $(\partial\Delta V/\partial T)(\text{mech})$, is

$$(\partial\Delta V^{\ddagger}/\partial T)(\text{mech}) = f(1-f)(\Delta E_A/RT^2)\Delta\Delta V^{\ddagger}$$

where $\Delta\Delta V^{\ddagger}$ is the difference in activation volume for the two mechanisms. It is unlikely that $(\partial\Delta V^{\ddagger}/\partial T)(\text{mech})$ can reach several tenths $cm^3\ mol^{-1}\ deg^{-1}$ for either methyl or isopropyl bromides. However, some of the peculiarities of methyl bromide under pressure, that are not so evident in isopropyl bromide, might be linked with the changing mechanism under pressure.

It is also unlikely that the effect can be explained on the basis of the simple model of the solvation of the transition state in which the transition state is represented as a spherical dipole in a spherical cavity in the solvent. On this model, the electrostatic volume of solvation of the transition state $\Delta V_{es}^{\ddagger}$ is[19]

$$\Delta V_{es}^{\ddagger} = \tfrac{3}{2}N(\mu^{\ddagger 2}/a^{\ddagger 3}) \times \{\tfrac{1}{2}(\partial\epsilon/\partial p) + [1 - (3/2\epsilon)](\partial \ln a^{\ddagger}/\partial p)\}$$

where $\mu^{\ddagger}$ is the dipole moment of the transition state, $a^{\ddagger}$ is the radius of the cavity in the solvent, ϵ is the dielectric constant of the solvent, and N is Avogadro's number. $\partial\epsilon/\partial p$ is negative and becomes more so as the temperature increases, and if the cavity expands thermally like either the solvent or methyl bromide, so also does $\partial \ln a^{\ddagger}/\partial p$. Only the activation volume above 500 bars can be accommodated in this theory.

The peculiar behavior at low pressures can of course be rationalized by introducing specific hypotheses, but this has little value at present. These observations emphasize once again the contention[4] that things are often quite different under pressure, and an understanding of chemical kinetics gleaned from studies at 1 bar only may be very incomplete.

3. Activation Enthalpy and Entropy under Pressure. The effect of pressure on the activation enthalpy and entropy is of course closely related to the effect of temperature on the activation volume

$$(\partial\Delta H_p^{\ddagger}/\partial p)_T = \Delta V^{\ddagger} - (\partial\Delta V^{\ddagger}/\partial T)_p$$

$$(\partial\Delta S_p^{\ddagger}/\partial p)_T = -(\partial\Delta V^{\ddagger}/\partial T)_p$$

Nevertheless, they are worth mentioning separately. The variations of $\Delta H_p^{\ddagger}$ and $T\Delta S_p^{\ddagger}$ are shown graphically in the upper frames of Figures 5 and 6. For isopropyl bromide (Figure 6) both have minima as functions of pressure several hundred calories per mole deep at about 500 to 1000 bars, and then rise steadily by about 1 kcal mol^{-1}. For methyl bromide (Figure 5) they oscillate as a function of pressure with an amplitude of over 1 kcal mol^{-1}.

The cause of these variations is quite as obscure as the cause of the variation in the temperature coefficient of the activation volume. No doubt part of the complexity, for methyl bromide at least, is connected with the changing mechanism that occurs at high pressures.

The constant-volume energy and entropy of activation, which are plotted in the lower frames of Figures 5 and 6, are as complex functions of pressure as the constant-pressure parameters. Clearly, the variation of both sets of parameters with pressure is fundamental to an understanding of the mechanisms. In this sense, the reactions under study contrast with the dimerization of cyclopentadiene, for which the con-

(20) A. J. Ellis, *J. Chem. Soc.*, 3689 (1959).

stant-pressure parameters[21] are reported to vary with pressure in a strongly compensatory way, but the constant-volume parameters do not. For the dimerization of cyclopentadiene, the compensation in the constant-pressure parameters is presumably trivial; if the constant-volume parameters do not compensate then the constant-pressure parameters must do so simply because $T\alpha\Delta V^{\ddagger}/\kappa$ varies with pressure.

4. Constant-Volume Heat Capacity of Activation. The constant-volume heat capacity of activation is about -93 cal deg^{-1} mol^{-1} for both methyl and isopropyl bromides. It appears to vary much less with pressure than the constant-pressure heat capacity of activation but much more with temperature. Some of the pressure variation is probably connected with the change of mechanism discussed in section 4.1, but not all of it is.

A detailed understanding of these effects implies a detailed understanding of the effect of temperature on the volume of activation (see section 4.2). Any detailed discussion is at present premature. Clearly, however, discussions which ignore the difference between $\Delta C_p^{\ddagger}$ and $\Delta C_V^{\ddagger}$ must be far from the truth. The contributions to $\Delta C_V^{\ddagger}$ are the changes, when the transition state is formed, of the excitation of the internal and external degrees of freedom of the molecules going to make the transition state, including all the solvent molecules affected by the initial and transition states, and of the effect of temperature on the configurational energy. There is at the present time no sound evidence about the relative importance of changes in the kinetic and potential energies.

Summary

The thermodynamic activation parameters for the solvolysis of methyl and isopropyl bromides are now better known than those of any other reaction. The first and second derivatives with respect to temperature and pressure of the Gibbs energy are known well, and something is known about three of the four third derivatives. Unfortunately, the additional measurements serve to illuminate our ignorance more than our understanding.

It seems clear that the mechanism of hydrolysis of methyl bromide changes significantly with pressure, probably in the direction of a tighter binding of water molecules in the transition state at higher pressure. Perhaps a similar change tends to occur with isopropyl bromide, but the evidence is less dramatic.

The heat capacities of activation at constant pressure and at constant volume differ by about a factor of 2 at the temperature investigated (70° for methyl bromide and 50° for isopropyl bromide). Discussions that ignore the large contribution of thermal expansion to $\Delta C_p^{\ddagger}$ must be far from the truth. Unfortunately, it is not yet possible to divide $\Delta C_V^{\ddagger}$ into its components—that arising from the excitation of the degrees of freedom of the system and that from the configurational energy.

It seems clear that the spontaneous hydrolysis of these simple halides is not to be understood without much more experimental work. What is required are critical experiments that answer specific questions about the mechanism: unfortunately, it is not easy to devise such experiments. In the meantime, it seems that simpler systems should be sought that might be more readily understandable.

Acknowledgments. We are greatly indebted to A. Lavergne for help with the high-pressure apparatus and to Dr. G. S. Kell for providing data on water.

(21) D. M. Newitt and A. Wasserman, *J. Chem. Soc.*, 735 (1940).

Nuclear Magnetic Resonance Investigation of Conformations of Isotactic Polyelectrolytes in Aqueous Solution

by Yoshio Muroga, Ichiro Noda, and Mitsuru Nagasawa

Department of Synthetic Chemistry, Nagoya University, Chikusa-ku, Nagoya, Japan *(Received June 7, 1968)*

Nuclear magnetic resonance spectra of isotactic poly(acrylic acid) and its sodium salt, as well as those of its model compound, show no significant change in the vicinal coupling constants between α and β protons with neutralization. From this experimental result, it is concluded that the polyion and its model compound have practically fixed local conformations independent of their degrees of neutralization and, consequently, that expansion of the polyion with increasing degree of neutralization (of the polyion) may reasonably be interpreted by the long-range interaction, *i.e.*, by the interactions between charged groups at long intervals, assuming that the change in the short-range interaction, *i.e.*, the change in the size of the segment with degree of neutralization, is negligible. Moreover, detailed analysis shows that the isotactic polyacrylate ion has the local conformation of a 3_1 helical structure. It has also been shown that the relative chemical shifts of the characteristic peaks of stereoregular polymers are markedly changed by exchanging the substituents and, consequently, that the typical nmr patterns of isotactic polymers disappear by hydrolysis or by neutralization.

Introduction

The macroscopic dimension of a linear polymer in solution changes with solvent and temperature. The following two factors are believed to be responsible for this change of polymer dimension: the long-range interaction between the constituents of the polymer chain at long intervals and the short-range interaction between adjacent elements. In particular, it is well known that the radii of gyration of polyelectrolytes markedly change with degree of neutralization and ionic strength. However, the change in the radius of gyration of polyelectrolytes is, in general, a consequence of the long-range interaction only, assuming that the size of the segment, *i.e.*, the short-range interaction, is not affected by the presence of charge.[1-6] The assumption appears to be valid in interpreting the experimental results of intrinsic viscosity of polyelectrolytes. Strictly speaking, however, we have had no experimental or theoretical foundation for the assumption.

It has been often pointed out that isotactic polymers may have locally helical conformations in solution. Considering the strong electrostatic repulsive force between charged groups, it may be more probable that isotactic polyelectrolytes have the locally helical conformations in solution. Although the possibility was pointed out in a previous paper[7] on the potentiometric titration of stereoregular poly(methacrylic acid), the speculation has not yet been supported by independent experiments.

To determine the local conformation of a polymer, nmr spectroscopy may be most promising, since it can reveal the geometric relationship between the positions of hydrogen atoms on the adjacent carbon atoms through the vicinal coupling constants between them, so that the probabilities of *trans*, *gauche*, and *gauche'* forms (see Figure 1) can be estimated. In practice, the nmr method has been used to determine not only the configurations of nonionic polymers but also their conformations in solutions.[8,9] The main purpose of the present work is to determine the local conformations of isotactic polyelectrolytes from their nmr spectra and to acquire information about the short-range interaction in polyelectrolyte coils. Our supplementary purpose is to find out why, in nmr spectra of isotactic poly(methyl methacrylate), the quartet of methylene protons aggregates into a singlet when this polymer is hydrolyzed into the acid form.[7]

Even though stereoregular polymers, such as isotactic poly(acrylic acid), are adopted as samples, the nmr spectra of linear polymers generally show broad and very complicated patterns, where the intuitive assignment of peaks is quite difficult. Of the few techniques available for obtaining accurate values of nmr parameters from such complicated spectra, the method using a model compound (*meso*-α,α'-dimethylglutaric acid) is used in this work.

Experimental Section

Samples. (1) The α,α'-dimethylglutaric acid (*meso*-DMGA) was prepared from diethyl methylmalonate and methyl β-bromoisobutylate by the method of Auw-

(1) J. Hermans and J. Overbeek, *Rec. Trav. Chim.*, **67**, 761 (1948).
(2) A. Katchalsky and S. Lifson, *J. Polymer Sci.*, **11**, 409 (1953).
(3) P. J. Flory and J. E. Osterheld, *J. Phys. Chem.*, **58**, 653 (1954).
(4) M. Nagasawa, *J. Am. Chem. Soc.*, **83**, 300 (1961).
(5) A. Takahashi and M. Nagasawa, *ibid.*, **86**, 543 (1964).
(6) M. Fixman, *J. Chem. Phys.*, **41**, 3772 (1964).
(7) M. Nagasawa, T. Murase, and K. Kondo, *J. Phys. Chem.*, **69**, 4005 (1965).
(8) T. Yoshino, Y. Kikuchi, and J. Komiyama, *ibid.*, **70**, 1059 (1966).
(9) F. A. Bovey, F. P. Hood, III, E. W. Anderson, and L. C. Snyder, *J. Chem. Phys.*, **42**, 3900 (1965).

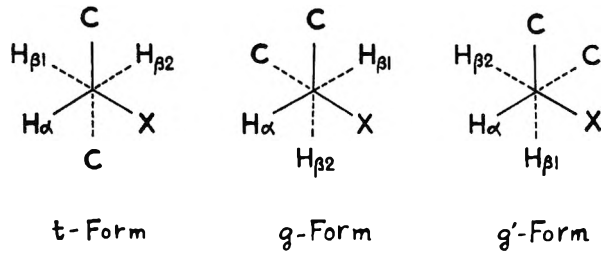

Figure 1. Three conformers of poly(sodium acrylate) and its model compound.

ers and Thorpe.[10] Separation of the *meso* diacid from the mixture of *dl* and *meso* compounds was carried out by making use of a great difference between solubilities of both corresponding anhydrides, as reported by Allinger.[11] We found the melting point of the *meso* anhydride to be 91.5–92.5°, whereas Allinger[11] reported a melting point of 91.4–92.8°.

(2) The polymerization of isotactic poly(methyl acrylate), P(MA), was carried out with lithium aluminum hydride in toluene at −78° for 20 hr. The degree of tacticity is $I = 0.96$ when calculated from the methylene peaks in its nmr spectrum (Figure 3a),[12] which was run on a JNM4H-100 spectrometer (Japan Electron Optics Laboratory, Tokyo, Japan). The isotactic poly(methyl acrylate) thus prepared was hydrolyzed with sodium hydroxide in acetone at room temperature. Then the isotactic poly(sodium acrylate), P(NaAA), was purified by repeated precipitation from its aqueous solution with methanol. The degree of hydrolysis was 100%, when estimated from the dry weight and the acid-group content of the sample.

(3) Isotactic poly(methyl methacrylate), P(MMA), was prepared by polymerization of methyl methacrylate with phenylmagnesium bromide in toluene at 20° for 6 hr. The nmr spectrum of P(MMA) (Figure 4a) recorded by a JNMC-60 spectrometer showed the α-methyl triplet with a microtacticity of $I = 0.68$.[13] The isotactic P(MMA) thus prepared was dissolved in 98% sulfuric acid and hydrolyzed in an atmosphere of N_2 gas at 60° for about 4 hr, as reported previously.[7] The degree of hydrolysis of the sample was 70%, but the incomplete hydrolysis has no effect on the final conclusion in the present paper. The low degree of hydrolysis seemed to arise from the low content of isotactic sequence in the sample.

Measurements of Nmr Spectra. Varian HA-100 and JNM4H-100 spectrometers were employed to record the spectra of the polymers and the model compound. The concentrations of the sample solutions were 0.05 and 0.1 g/ml for the polymers and 0.2 g/ml for the model compound. The temperature of the measurements is indicated in each figure caption.

Nmr Spectra and Their Interpretation

The degrees of neutralization, DN, of the above three samples in D_2O solution were adjusted to the desired values by adding NaOD–D_2O solutions. An internal reference was used only in measurements for Figures 3a and 4a, and therefore the absolute positions of the peaks were not well assigned, because only their relative positions are required for the present purpose.

In Figure 2 are shown the spectra of the methylene protons of *meso*-α,α′-dimethylglutaric acid and its sodium salts. The measurements were carried out at room temperature, but comparison between the nmr pattern of a sample (DN = 50%) taken at room temperature and one taken at 100° revealed no temperature effect on the nmr pattern except for a narrowing of the peaks and an increase of relative chemical shift between geminal β protons, *i.e.*, no significant change in the conformation of the sample due to temperature. According to the results for dimethyl *meso*-α,α′-dimethylglutarate reported by Yoshino, *et al.*,[14] it is assumed that the lower and the higher field parts of the two methylene signals correspond to the protons $H_{\beta 2}$ (oriented *trans* to the α protons H_α for the planar *trans* conformation) and the protons $H_{\beta 1}$, respectively (see Figure 1). To obtain accurate values of the nmr parameters from spectra of the methylene parts, the parameters were first estimated using the first-order approximation, as illustrated in Figure 2b. The expected spectrum (to be compared with the observed spectrum) was then reproduced with the parameters thus estimated using the method of Fujiwara and Fujiwara,[15] in which the methylene part spectrum is assumed to be the KL part in the ABKL system. The parameters were slightly adjusted once to obtain satisfactory agreement between both spectra. Two examples for comparison of the calculated and observed spectra are shown in Figures 2a, a′, d, and d′. The values of the nmr parameters for the model compound thus determined are listed in Table I.

The observed proton multiplets of isotactic P(MA) were assigned to the methylene and methine groups, as

Table I: Relative Chemical Shifts and Spin-Coupling Constants (in cps) of β Protons of Sodium *meso*-α,α′-Dimethylglutarate

DN, %	$\langle J_{\beta 1\beta 2}\rangle$	$\langle J_{\alpha\beta 1}\rangle$	$\langle J_{\alpha\beta 2}\rangle$	$\langle \delta_{\beta 1\beta 2}\rangle$
100	13.5	7.3	7.1	45.4
50	13.5	7.0	7.4	46.3
25	13.6	7.0	7.4	47.0
0	13.6	6.9	7.4	50.7
		Mean 7.1	Mean 7.3	

(10) K. Auwers and J. F. Thorpe, *Ann.*, **285**, 310 (1895).
(11) N. L. Allinger, *J. Am. Chem. Soc.*, **81**, 232 (1959).
(12) K. Matsuzaki, T. Uryu, A. Ishida, T. Ohki, and M. Takeuchi, *J. Polymer Sci., Part A-1*, **5**, 2167 (1967).
(13) F. A. Bovey and G. V. D. Tiers, *Fortschr. Hochpolymer. Forsch.*, **3**, 139 (1963).
(14) T. Yoshino, M. Shinomiya, and J. Komiyama, *J. Am. Chem. Soc.*, **87**, 387 (1965).
(15) Y. Fujiwara and S. Fujiwara, *Bull. Chem. Soc. Japan*, **37**, 1005 (1964).

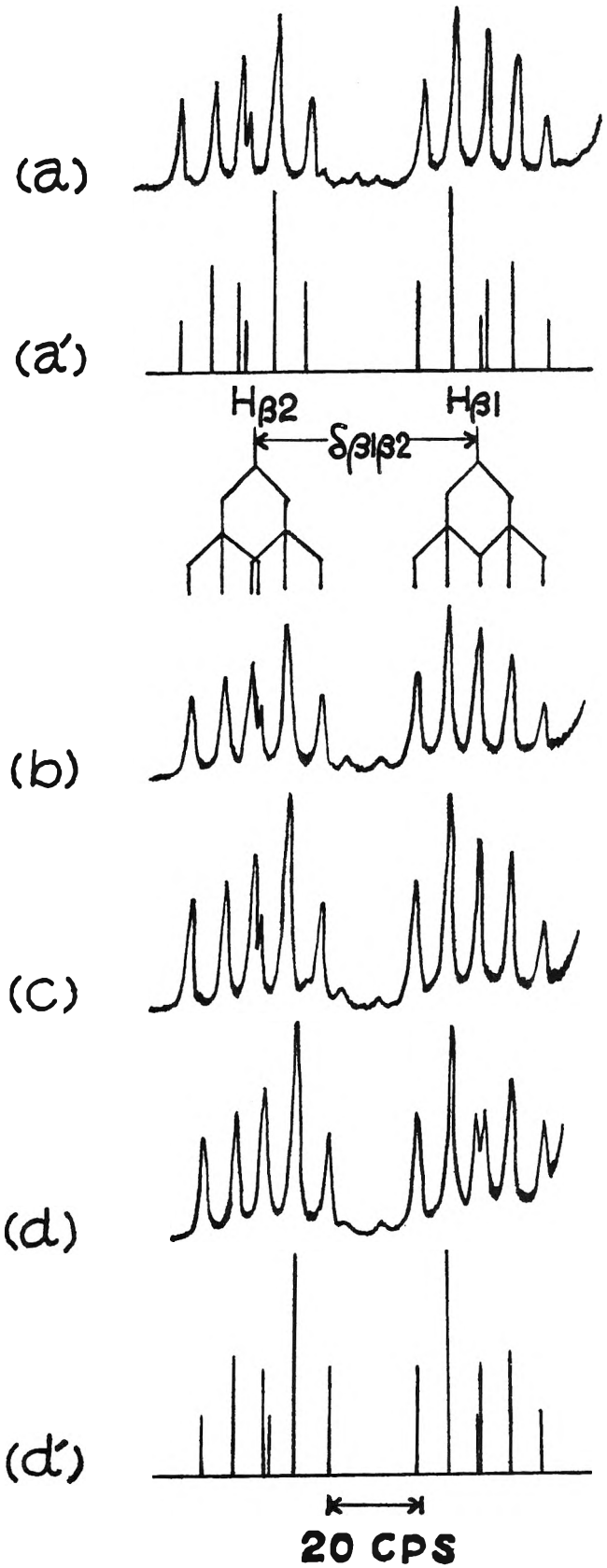

Figure 2. Methylene spectra of model compounds of isotactic poly(acrylic acid) and its sodium salts: (a) observed spectrum of *meso*-DMGA (*i.e.*, DN = 0) in octadeuteriodioxane–D_2O at room temperature; (b)–(d) observed spectra of *meso*-NaDMGA with DN of (b) 25%, (c) 50%, and (d) 100% in D_2O at room temperature; (a'), (d') calculated spectra obtained with parameters for (a) and (d) in Table I, respectively.

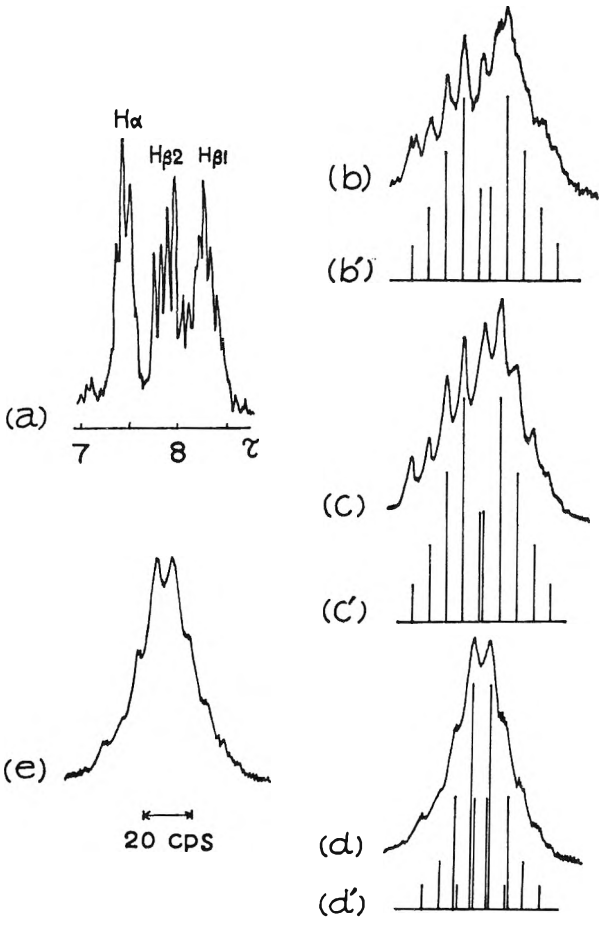

Figure 3. Nmr spectra of isotactic poly(methyl acrylate) and isotactic poly(sodium acrylate): (a) observed methylene and methine spectrum of isotactic P(MA) in *o*-dichlorobenzene at 115°; (b)–(d) observed methylene spectra of isotactic P(NaAA) with DN of (b) 20%, (c) 50%, and (d) 100% in D_2O at 100°; (e) observed methylene spectrum of isotactic P(NaAA) with DN of 100% in D_2O–0.5 *M* NaCl at 100°; (b')–(d') calculated methylene spectra obtained with parameters for (b)–(d) in Table II, respectively. Concentrations are 10% (w/v) for all samples.

shown in Figure 3a, where the notation for the methylene parts is the same as in Figure 2b, taking into account the results obtained by Yoshino, *et al.*[14] In Figures 3b–d are shown typical spectra of the methylene parts of the isotactic P(AA) partially neutralized with NaOD. It is noticed that two methylene quintets collapse into a singlet as the degree of neutralization is increased. The calculated methylene spectra in Figures 3b'–d' and the parameters listed in Table II were obtained by the same method as used for the model compound. The agreement between the calculated and observed spectra is satisfactory. The asymmetry of the methylene peaks (appearing at intermediate values of the degree of neutralization) is believed to arise from the imperfection of isotacticity ($I = 0.96$) since the analogous asymmetry is observed in the methylene spectra of P(MA) as shown in Figure 3a. The spectrum of the methylene part of P(NaAA) with 100% degree of neutralization in the presence of 0.5

Table II: Relative Chemical Shifts and Spin-Coupling Constants (in cps) of β Protons of Isotactic Poly(sodium acrylate)

DN, %	Concn, %	$<J_{\beta_1\beta_2}>$	$<J_{\alpha\beta_1}>$	$<J_{\alpha\beta_2}>$	$<\delta_{\beta_1\beta_2}>$
100	10	13.5	7.0	7.0	16.0
50	10	13.8	7.0	7.0	25.3
40	5	14.0	7.0	7.0	25.3
30	5	14.0	7.0	7.0	27.0
20	10	14.0	7.0	7.0	28.7
20	5	14.0	7.0	7.0	29.0
			Mean 7.0	Mean 7.0	

M NaCl, which is shown in Figure 3e, is the same as the spectrum in the absence of the salt. The uncertainty in the vicinal coupling constants in Tables I and II is estimated to be ±0.2 cps.

The nmr spectrum of isotactic P(MMA) is shown with assignments of peaks in Figure 4a while the spectra of the methylene part of the partially neutralized poly(methacrylic acid), P(MAA), are shown in Figures 4b–d. A marked tendency for the methylene quartet (peaks a, b, c, d) to gather and change into a singlet with an increasing degree of neutralization of the sample is observed. The change in the appearance of the spectrum is similar to that which would be observed if the isotactic molecule were isomerized into a syndiotactic one. Peak e in Figures 4a and d seems to be due to the presence of sequences other than isotactic ones. The nmr spectra were analyzed by regarding the methylene part as AB type.[16] A comparison between the observed methylene spectra and calculated ones with parameters listed in Table III is shown in Figures 4b and c.

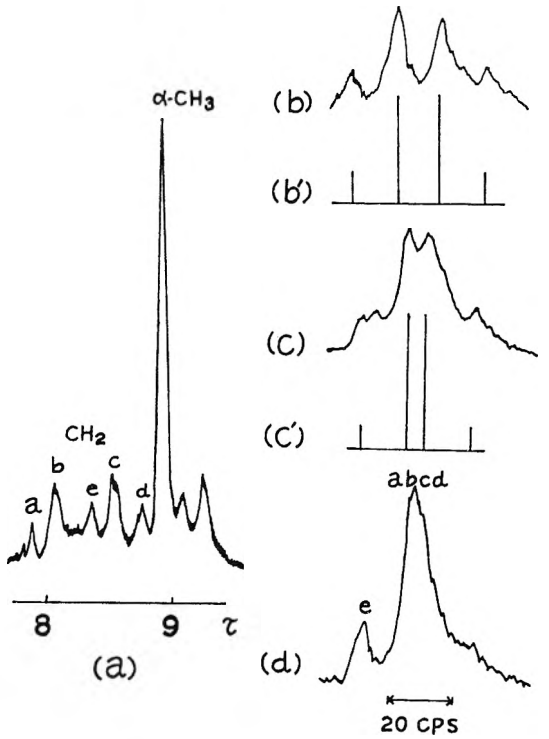

Figure 4. Nmr spectra of isotactic poly(methyl methacrylate) and isotactic poly(sodium methacrylate): (a) observed methylene and α-methyl spectrum of isotactic P(MMA) in chloroform at 50°; (b)–(d) observed methylene spectra of isotactic P(NaMA) with DN of (b) 50%, (c) 100%, and (d) 150% in D_2O at 100°; (b'), (c') calculated methylene spectra obtained with parameters for (b) and (c) in Table III, respectively. Concentrations were 10% (w/v) for all samples.

Table III: Relative Chemical Shifts and Spin-Coupling Constants (in cps) of β Protons of Isotactic Poly(sodium methacrylate)

DN, %	Concn, %	$<J_{\beta_1\beta_2}>$	$<\delta_{\beta_1\beta_2}>$
150	5	...	...
100	10	15.0	14.7
75	5	15.0	26.0
50	10	15.0	23.6
40	5	15.0	34.5
30	5	15.0	37.1
20	5	15.0	37.3

Discussion

In Tables I and II, it is observed that the vicinal coupling constants $<J_{\alpha\beta_1}>$ and $<J_{\alpha\beta_2}>$, as well as the geminal coupling constants $<J_{\beta_1\beta_2}>$, are independent of the degree of neutralization of isotactic P(NaAA) and *meso*-DMGA. While the independence of $<J_{\beta_1\beta_2}>$ simply means that the steric relationship between H_{β_1} and H_{β_2} protons belonging to the same carbon is independent of the degree of neutralization, here it is worthwhile noticing the independence of $<J_{\alpha\beta_1}>$ and $<J_{\alpha\beta_2}>$, since it provides interesting information on the local conformations of isotactic P(NaAA) and sodium *meso*-α,α'-dimethylglutarate (*meso*-NaDMGA), as discussed below. In Tables II and III, it is noticed that the concentration of the sample solution has no effect on the values of $<J_{\beta_1\beta_2}>$, $<J_{\alpha\beta_1}>$, and $<J_{\alpha\beta_2}>$ but does influence the difference between the chemical shifts of the H_{β_1} and H_{β_2} protons, $<\delta_{\beta_1\beta_2}>$. These experimental results imply that vicinal coupling constants derived in the present paper, $<J_{\alpha\beta_1}>$ and $<J_{\alpha\beta_2}>$, can be utilized in estimating the conformation of the isotactic P(NaAA) without correction for concentration.

Vicinal coupling constants observed, $<J_{\alpha\beta_1}>$ and $<J_{\alpha\beta_2}>$, can be related to the conformations of the chain by the general relationships

$$<J_{\alpha\beta_2}> = P_t J_t + P_g J_g + P_{g'} J_g \quad (1)$$

$$<J_{\alpha\beta_1}> = P_t J_g + P_g J_t + P_{g'} J_g \quad (2)$$

$$P_t + P_g + P_{g'} = 1 \quad (3)$$

(16) J. A. Pople, W. G. Schneider, and H. J. Bernstein, "High-Resolution Nuclear Magnetic Resonance," McGraw-Hill Book Co., Inc., New York, N. Y., 1959, p 119.

where P_t, P_g, and $P_{g'}$ are the probabilities that the chain has the *trans*, *gauche*, and *gauche'* forms, respectively, and J_t and J_g are the vicinal coupling constants between the α and β protons in *trans* and *gauche* arrangements. According to eq 1–3, the constant values of $<J_{\alpha\beta1}>$ and $<J_{\alpha\beta2}>$ imply that the values of P_t, P_g, and $P_{g'}$, as well as of J_t and J_g, do not change with neutralization, if we may neglect the very small chance that every parameter on the right side of eq 1 and 2 might change considerably and still give the observed values on the left side, $<J_{\alpha\beta1}>$ and $<J_{\alpha\beta2}>$, for all degrees of neutralization. That is to say, the present experimental results indicate that the samples have fixed local conformations independent of degree of neutralization.

The detailed calculation of probabilities P_t, P_g, and $P_{g'}$ can be performed as follows. The values of $<J_{\alpha\beta1}>$ and $<J_{\alpha\beta2}>$ in *meso*-α,α'-dimethylglutaric acid and its sodium salt are found to agree with the values for dimethyl *meso*-α,α'-dimethylglutarate (7.0 and 7.4 cps, respectively) reported by Matsuzaki, *et al.*[17] We may conclude that the values of P_t, P_g, and $P_{g'}$, as well as those of J_t and J_g, are little affected not only by solvents but also by the species of the substituent X (*i.e.*, COOH, COONa, and $COOCH_3$). This conclusion is supported by many works on *meso*-α,α'-disubstituted pentanes, where the values of $<J_{\alpha\beta1}>$ and $<J_{\alpha\beta2}>$ are known to be fixed between 6.5 and 7.5 cps, independent of the nature of substituent X (Cl,[18] CN,[12] and C_6H_5[19]). Thus, J_t and J_g may reasonably be estimated to be 12.1 and 3.2 cps, respectively, which were determined by using trimethyl *cis*-hexahydrotrimesate by Yoshino, *et al.*[7] The probabilities P_t, P_g, and $P_{g'}$ for isotactic P(NaAA) and *meso*-NaDMGA can be calculated from eq 1–3 by substituting the observed values into $<J_{\alpha\beta1}>$ and $<J_{\alpha\beta2}>$ together with J_t = 12.1 and J_g = 3.2 cps. The probabilities thus obtained are listed in Table IV.

Table IV: Conformations of Sodium *meso*-α,α'-Dimethylglutarate and Isotactic Poly(sodium acrylate)

	P_t	P_g	$P_{g'}$
meso-NaDMGA	0.46	0.44	0.10
Isotactic P(NaAA)	0.43	0.43	0.14

From the values in Table IV, it is possible to calculate the probabilities of possible conformations caused by the internal rotation about two adjacent skeletal bonds. If we neglect the probabilities of tt, gg, and g'g' forms because of the steric hindrance between side groups and take into account the presence of mirror image conformations, the conformation of isotactic poly(acrylic acid) is expressed by 72% tg, 14% tg', and 14% g'g. (t = *trans*, g = *gauche*, and g' = *gauche'*.) This result indicates that the isotactic P(NaAA) has a 72% local conformation of 3_1 helical structure. Although we cannot observe the vicinal coupling constants in isotactic P(MAA), it is highly probable that isotactic P(MAA) has a more helical structure in solution than isotactic P(AA) since the α-methyl group is favorable for the helical structure. This conclusion is supported by the difference observed between the potentiometric titration data for isotactic and syndiotactic polyelectrolytes.[7,20]

The vicinal coupling constants for *meso*-DMGA as shown in Table I are not absolutely constant but change with degree of neutralization slightly. If the variation is assumed to be beyond the present experimental error, however, the probabilities of the conformers would deviate from the average values reported in Table IV, at most by ±2%.

As discussed in the Introduction, the radius of gyration of a polyelectrolyte, *i.e.*, the intrinsic viscosity of a polyion in solutions, markedly increases with increasing degree of neutralization. The change in the intrinsic viscosity, *i.e.*, in the radius of gyration of a polyion with neutralization, is, in general, explained by long-range interaction between charged segments, assuming that the short-range interaction is almost independent of the degree of neutralization. It is not possible to estimate the radius of gyration from the local conformations determined by the nmr method.[9] At least, however, the present experimental result that the local conformation is independent of degree of neutralization is not in disagreement with the above assumption. Moreover, if we take into account the fact that the unperturbed dimension of a polyion determined from intrinsic viscosity studies is not changed much with degree of neutralization,[21] in addition to the present result, we may safely accept the assumption that the long-range interaction between charged segments is predominant for the expansion of a polyion. This conclusion is confirmed by the fact that nmr spectra of P(NaAA) are not affected by addition of sodium chloride in spite of the great change in the viscosity of the solution (see Figure 3e).

In contrast to the behavior of the coupling constants, the relative chemical shift between geminal β protons, $<\delta_{\beta1\beta2}>$, is markedly changed with hydrolysis and neutralization, as seen in Tables I–III. The change is, in general, caused by two factors: the change in the conformation of the polymer and the change in the substituents or solvents. In the case of isotactic P(NaAA)

(17) K. Matsuzaki, T. Uryu, K. Tameda, and M. Takeuchi, *Kogyo Kagaku Zasshi*, **68**, 1466 (1965).

(18) D. Doskočilová and B. Schneider, *Collection Czech. Chem. Commun.*, **29**, 2290 (1964).

(19) D. Doskočilová and B. Schneider, *J. Polymer Sci., Part B*, **3**, 213 (1965).

(20) Y. Kawaguchi and M. Nagasawa, to be submitted for publication.

(21) I. Noda, T. Tsuge, and M. Nagasawa, Preprints of the International Symposium on Macromolecular Chemistry, IUPAC, Tokyo and Kyoto, Japan, pp VI-207

and *meso*-NaDMGA, the change is caused only by the effect of substituents (or by the effect of solvents), since the conformation is found to be fixed over all degrees of neutralization. In the case of isotactic P(NaMA), however, we were unable to decide between the two possibilities, since the vicinal coupling constants are not known. It is at least probable, however, that the effect of the substituent should be most important for the change in $<\delta_{\beta 1 \beta 2}>$. In any case, it is certain that the effect of the substituent or the solvent should be carefully examined when assigning the nmr peaks or calculating the tacticity of polymers.

Acknowledgment. Most of the measurements were carried out by a Varian HA-100 spectrometer of Toyo Rayon Co. We wish to thank this company for its aid and particularly Dr. Kenkichi Nukada for his interest and advice in this work. We also wish to thank Mr. Y. Kawaguchi, who prepared the sample of isotactic P(AA).

Phase Transformations and Electrical Properties of Bismuth Sesquioxide

by C. N. R. Rao,[1] G. V. Subba Rao, and S. Ramdas

Department of Chemistry, Indian Institute of Technology, Kanpur, India *(Received June 10, 1968)*

Phase transformations of Bi_2O_3 have been studied by differential thermal analysis. The enthalpy and activation energy of the monoclinic–cubic transformation are 8.8 and 110 kcal mol^{-1}, respectively. The enthalpies of the cubic–tetragonal and tetragonal–monoclinic transformations are estimated to be 6.7 and 2.1 kcal mol^{-1}. The electrical conductivity of Bi_2O_3 shows marked changes in conductivity at temperatures where the phase transformations occur. In addition, Bi_2O_3 shows a change in slope in the $\log \sigma - 1/T$ curve due to a change from p-type to n-type behavior; this observation is supported by the change in sign of the Seebeck coefficient, β, around the same temperature. β changes sign at lower temperatures as the oxygen partial pressure is reduced. The band model seems to be applicable in the case of Bi_2O_3.

Introduction

Bismuth sesquioxide, Bi_2O_3, is an important solid-state material which finds uses in glass technology and electronics. The phase transformations of Bi_2O_3 have been examined by X-ray diffraction[2] and differential thermal analysis[3] and it appears certain that there is structural hysteresis in the reversible crystal structure transformation. Bi_2O_3 changes from a monoclinic (pseudoorthorhombic) structure to a cubic structure on heating to ~730° (and then melts at ~825°); on cooling, the cubic form reverts back to the monoclinic form through a metastable tetragonal phase. There seems to be some uncertainty in the enthalpy of the monoclinic–cubic transformation[3,4] and there are no data in the literature on the enthalpies of the reverse transformations.

Electrical properties of Bi_2O_3 have been studied by a few workers.[5-7] Bi_2O_3 behaves like a p-type semiconductor up to ~650° at moderate pressures of oxygen and there are some indications that it changes over to n-type behavior at relatively low temperatures (<600°) at low pressures of oxygen ($\leq 10^{-3}$ mm). We have presently carried out a systematic investigation of the phase transformations and electrical properties of spectroscopically pure Bi_2O_3 with a view to obtaining better insight into the mechanism of conduction.

Experimental Section

Spectroscopically pure Bi_2O_3 (Johnson and Matthey, London) was used for the study. The sample had 3 ppm of Al and Fe and less than 1 ppm of Na, Ca, Cu, Mg, Si, Ag, and other impurities.

Differential thermal analysis curves were recorded employing an Aminco thermoanalyzer fitted with a temperature programmer and an automatic voltage stabilizer. A constant heating rate of 16°/min was employed for the heating curves. While recording the cooling curves it was not possible to control the rate. The enthalpy, ΔH, of the monoclinic–cubic transforma-

(1) To whom all the correspondence should be addressed.

(2) E. M. Levin and R. S. Roth, *J. Res. Natl. Bur. Std.*, **A68**, 189 (1964).

(3) E. M. Levin and C. L. McDaniel, *ibid.*, **A69**, 237 (1965).

(4) G. Gattow and D. Schütze, *Z. Anorg. Allgem. Chem.*, **328**, 45 (1964).

(5) R. Mansfield, *Proc. Phys. Soc.* (London), **B62**, 476 (1949).

(6) K. Hauffe and H. Peters, *Z. Physik. Chem.*, **201**, 121 (1952).

(7) O. K. Fidrya, *Nauk Zap. Vinnit's K. Derzh.*, **17**, 125 (1960); *Chem Abstr.*, **56**, 6755*h* (1962).

tion was estimated from the peak area employing the phase transformations of K_2SO_4 and quartz as external standards.[8] Reliable ΔH values for phase transformations have been obtained in this laboratory by this procedure.[8] It may be noted that the use of internal standards by Levin and McDaniel[3] gave ΔH values for the monoclinic–cubic transformation which differed slightly with the standard employed. The activation energy for the monoclinic–cubic transformation was calculated by employing the procedure of Borchardt and Daniels.[8,9] Although the activation energy obtained by this procedure could have large uncertainties (±15%), a linear log k–$1/T$ plot seems to indicate that the transformation follows the exponential rate law. Thermogravimetric analysis of Bi_2O_3 was carried out with an Aminco unit at an oxygen partial pressure of 157 mm.

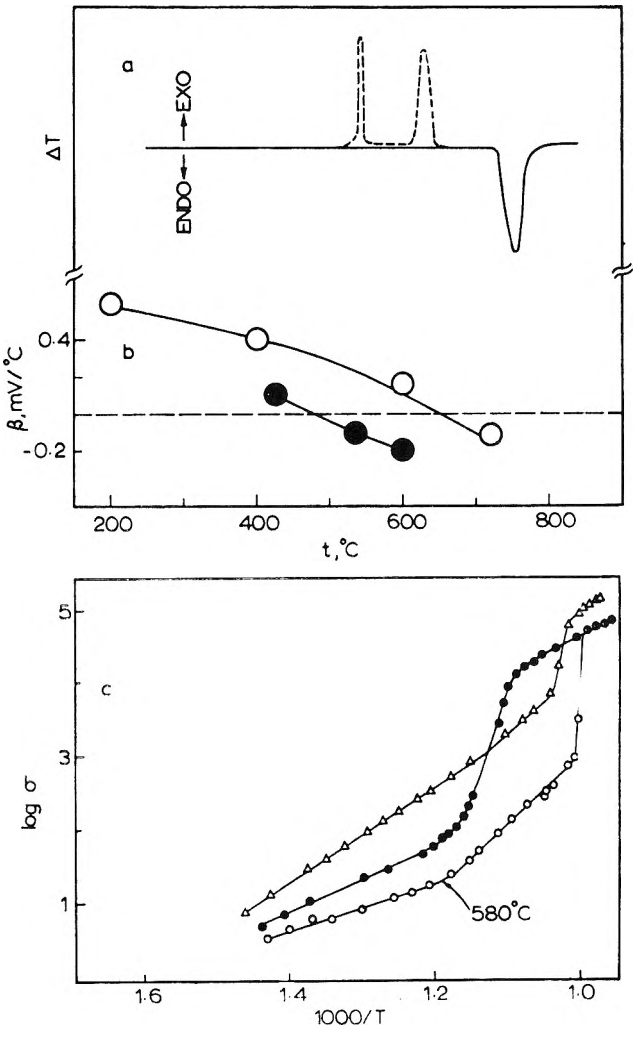

Figure 1. (a) Differential thermal analysis curves of Bi_2O_3 in air: heating curve (rate 16°/min), full line; cooling curve (rate not known), dotted line. (b) Seebeck coefficient of Bi_2O_3 as a function of temperature: open circles, at 160 mm of oxygen; closed circles, at 10^{-4} mm of oxygen. (c) Plots of the logarithm of electrical conductivity of Bi_2O_3 against the reciprocal of absolute temperature: open circles, at 0.2 mm of oxygen (while heating); closed circles, at 0.2 mm of oxygen (while cooling); triangles, p_{O_2} = 157 mm (while heating). The cooling curve at 157 mm of oxygen is similar in appearance to that at 0.2 mm. The conductivities are all in micromhos per centimeter.

The electrical conductivity and thermoelectric power measurements were made on pellets prepared from fused Bi_2O_3. A pressure of 20,000 psi was employed for pressing the pellets. The measurements were repeated several times on freshly prepared samples in order to be certain of the various features of the conductivity and Seebeck coefficient data (Figure 1). The conductivity cell employed for the study has been described elsewhere;[10] the conductivity measurements were made (at 1 Kc) employing a GR-1608A impedance bridge using a GR-1232A tuned amplifier and null detector. Thermoelectric power measurements were made employing a cell similar to that described by Honig and coworkers.[11]

The dielectric constant of Bi_2O_3 was measured as a function of frequency (20 cps to 15 Mc) employing a GR-716C capacitance bridge and a Boonton Type 260 AP Q-meter. The ϵ_∞ and ϵ_0 obtained by extrapolation were 12 and 25, respectively.

Results and Discussion

Phase Transformations of Bi_2O_3. Differential thermal analysis (dta) of Bi_2O_3 from room temperature to 800° showed (Figure 1a) the monoclinic–cubic transformation to begin at ~727° with the peak at 752°. By employing external standards, the ΔH of the transformation was estimated to be 8.8 ± 0.4 kcal mol^{-1}. This value is intermediate to the values reported earlier by Levin and McDaniel[3] and Gattow and Schütze.[4] The energy of activation of the monoclinic–cubic transformation was found to be 110 ± 15 kcal mol^{-1}, typical of a reconstructive transformation.[12] Such large activation energies are found in the reconstructive transformation involving changes in primary coordination as in the transformations of CsCl[13] or $CaCO_3$[14] or changes in secondary coordination as in the transformations of the anatase and brookite forms of TiO_2.[15]

The differential thermal analysis curves in Figure 1a show that the cubic form of Bi_2O_3 comes back to the monoclinic form in two stages (peaks at ~630 and 543°). Assuming that the peak at 630° is due to the

(8) K. J. Rao and C. N. R. Rao, *J. Mater. Sci.*, **1**, 238 (1966).
(9) H. J. Borchardt and F. Daniels, *J. Am. Chem. Soc.*, **79**, 41 (1957).
(10)(a) P. N. Mehrotra, G. V. Chandrashekhar, E. C. Subbarao, and C. N. R. Rao, *Trans. Faraday Soc.*, **62**, 3586 (1966); (b) G. V. Chandrashekhar, P. N. Mehrotra, G. V. Subba Rao, E. C. Subbarao, and C. N. R. Rao, *ibid.*, **63**, 1295 (1967).
(11) J. M. Honig, A. A. Cella, and J. C. Cornwell, "Rare Earth Research," Vol. 2, Gordon and Breach, New York, N. Y., 1964.
(12) C. N. R. Rao and K. J. Rao, *Prog. Solid State Chem.*, **4**, 131 (1967).
(13) K. J. Rao, G. V. Subba Rao, and C. N. R. Rao, *Trans. Faraday Soc.*, **63**, 1013 (1967).
(14) G. V. Subba Rao, M. Natarajan, and C. N. R. Rao, *J. Am. Ceram. Soc.*, **51**, 179 (1968).
(15)(a) C. N. R. Rao, *Can. J. Chem.*, **39**, 498 (1961); (b) C. N. R. Rao, S. R. Yoganarasimhan, and P. A. Faeth, *Trans. Faraday Soc.*, **57**, 504 (1961).

cubic-(metastable) tetragonal phase transformation[16] and that the 543° peak is due to the tetragonal–monoclinic transformation, it can be readily seen that the latter is a very sharp transition compared to the former. This observation further substantiates the metastable nature of the tetragonal phase.[2] The ΔH values of the cubic–tetragonal and tetragonal–monoclinic transformations are estimated to be 6.7 and 2.1 kcal mol^{-1} on the basis of the relative peak areas.

Electrical Conductivity and Thermoelectric Power Measurements. The electrical conductivity of Bi_2O_3 was measured as a function of temperature up to ~820° at oxygen partial pressures of 157 and 0.2 mm while both heating and cooling the sample. The log σ–$1/T$ plots (Figure 1c) show breaks which can be attributed to phase transformations or changes in the mechanism of conduction.[10,17] Thus, the heating curves in Figure 1c show marked changes in conductivity around 730° which are most likely due to the phase transformation from the monoclinic to the cubic structure. In addition, the heating curve at a p_{O_2} of 0.2 mm shows a distinct change in slope at ~580°; the curve at a p_{O_2} of 157 mm shows a change in slope at ~650°, though not as distinctly.

The conductivity in the temperature range 300–580° showed an increase with the oxygen pressure and the data obtained at several oxygen partial pressures (0.2–157 mm of p_{O_2}) could be fitted into the equation

$$\sigma = k p_{O_2}^{1/4} \qquad (1)$$

Bi_2O_3 is undoubtedly a p-type semiconductor up to ~580° in this range of oxygen partial pressures. The energy of activation, E_i, for the conduction process at a p_{O_2} of 157 mm (300–580°) was found to be 1.4 eV, which differs from the value of 0.9 eV reported by Mansfield.[5] The $p_{O_2}^{1/4}$ dependence of the conductivity can be understood in terms of the defect equilibria involving metal ion vacancies rather than oxygen interstitials.[18] Oxygen interstitials should give rise to a $p_{O_2}^{1/6}$ dependence of the conductivity.

The change in slope in the conductivity curve at 580° at 0.2 mm of oxygen (or at ~650° at 157 mm) can be ascribed to a change in the mechanism of conduction from p type to n type on the basis of thermoelectric power measurements. The Seebeck coefficient, β, changes sign around 650° at a p_{O_2} of 160 mm (Figure 1b). When the oxygen pressure was 2×10^{-4} mm, β changed sign around 550°; at 10^{-4} mm of oxygen, the change of sign was at ~490°. These results are consistent with the observation of the break in the conductivity curve (due to the change from p-type to n-type behavior) at a lower temperature (~580°) at 0.2 mm rather than at 157 mm of oxygen (~650°).

The conductivity curve of Bi_2O_3 obtained while cooling at 0.2 mm of oxygen (Figure 1c) shows changes in slope around 636, 585, and 540°. The change in conductivity at 636° is not sharp as in the case of the monoclinic–cubic transformation and probably arises from the cubic–tetragonal transformation (dta peak at ~630°). The break at 540° may similarly be due to the tetragonal–monoclinic transformation (dta peak at ~540°). The break around 585° is likely to be due to the change from n type to p type.[19] The cooling curve at 157 mm of oxygen was similar to that at 0.2 mm in that it showed the same features.

Mechanism of Conduction. We shall now briefly examine the mechanism of conduction in Bi_2O_3 on the basis of the experimental observations discussed till now. The activation energy, E_i, as measured from the electrical conductivity data in the 300–580° range is quite large (1.4 eV). Thus, $E_i > E_g \gg kT_{max}$. Further, there appears to be negligible interaction between the charge carriers and the phonons[20] as indicated by the small value ($\ll 1$) of the Frölich coupling constant, α_F

$$\alpha_F = \pi e^2 (2m^*/\hbar^3 \nu_L)^{1/2} (\epsilon_\infty^{-1} - \epsilon_0^{-1}) \qquad (2)$$

where m^* is the effective mass[21,22] of the charge carriers, ν_L is the longitudinal mode frequency, and ϵ_0 and ϵ_∞ are the static and high-frequency dielectric constants, respectively. The low values of m^* and α_F rule out the applicability of the Polaron or the hopping model to Bi_2O_3. The dependence of the Seebeck coefficient on oxygen partial pressure also provides further justification to this conclusion. If the hopping model were applicable, β should vary discontinuously through zero; instead, it shows a gradual change with oxygen pressure, becoming zero at progressively lower temperatures as the oxygen pressure is decreased.

On the basis of the above arguments, it is felt that the band model is applicable in the case of Bi_2O_3. Initially, at lower temperatures, Bi_2O_3 has an anion excess and shows p-type behavior; the Fermi level will then be in the lower half of the energy gap. At a constant p_{O_2}, the Fermi level moves upward with increase in temperature accompanying the loss of oxygen from the lattice. The Fermi level also moves upward with the decrease in p_{O_2} at a constant temperature (Figure 2). The Seebeck coefficient changes sign at lower tempera-

(16) For convenience, we shall call the metastable intermediate phase tetragonal in this paper.

(17) J. L. Bates, C. A. Hinman, and T. Kawada, *J. Am. Ceram. Soc.*, **50**, 652 (1967).

(18) G. G. Libowitz, *Prog. Solid State Chem.* **2**, 216 (1965).

(19) Both electrons and holes act as carriers even at lower temperatures, but electrons become the majority carriers around 585°. Thermogravimetric analysis curves showed that Bi_2O_3 starts losing oxygen above ~300° at a P_{O_2} of 157 mm; the creation of anion vacancies is thus responsible for producing the carrier electrons.

(20) H. Fröhlich, in "Polarons and Excitons," C. G. Kuper and G. D. Whitefeld, Ed., Plenum Press, New York, N. Y., 1963.

(21) The effective mass m^* was calculated to be $\sim 10^{-2}\ m$ from the concentration of charge carriers[5] and the Seebeck coefficients. The value of ν_L was calculated from the Resltrahlen frequency.[22] The values of ϵ_0 and ϵ_∞ were obtained experimentally. It may be noted that such estimations of m^* are only approximate since carrier concentrations have not been measured at this time.

(22) D. M. Mattox and L. Gildart, *J. Phys. Chem. Solids*, **18**, 215 (1961).

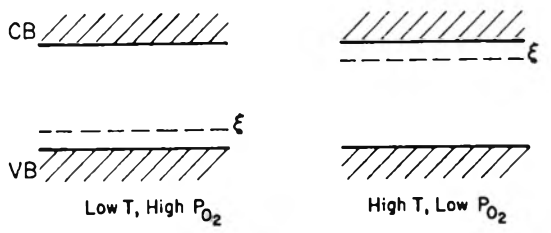

Figure 2. Position of the Fermi level in Bi_2O_3.

tures when p_{O_2} is decreased since there will be fewer holes under these conditions. The changes in the Seebeck coefficient with Fermi level, ξ, can be rationalized by the relation[23]

$$e\beta T = -(\sigma_n/\sigma)[R_n - (\xi - E_c)] + (\sigma_p/\sigma) \times [R_p + (\xi - E_v)] \quad (3)$$

where σ_n and σ_p are the contributions to conductivity from electrons and holes, respectively, and R_n and R_p are determined by the transport integrals.

The large change in conductivity accompanying the monoclinic–cubic transformation is readily understandable on the basis of the band model. Since the change over to the higher symmetry cubic structure will be accompanied by the broadening of bands, the conductivity would be expected to show a marked increase.

Acknowledgment. The authors are thankful to the U. S. National Bureau of Standards for a research grant (G-51) through their Special International Program.

(23) T. C. Harman and J. M. Honig, "Thermoelectric and Thermomagnetic Effects and Applications," McGraw-Hill Book Co., New York, N. Y., 1967.

Extraction of $HClO_4$ and $HReO_4$ by Dilute Solutions of Tributyl Phosphate in Carbon Tetrachloride, Isooctane, and 1,2-Dichloroethane[1]

by J. J. Bucher and R. M. Diamond

Lawrence Radiation Laboratory, University of California, Berkeley, California *(Received June 25, 1968)*

The extraction of $HReO_4$ or $HClO_4$ into dilute solutions of tributyl phosphate (TBP) in CCl_4, isooctane, and 1,2-dichloroethane has been studied, and the extracting species have been determined. A previous study of TBP in CCl_4, where the TBP concentrations were 0.03 to 0.3 *M* and the stoichiometric ratio TBP/H^+ was >3, indicated the only extracting species were the molecular adduct $TBP\cdot H_2O$ and the hydronium ion species $3TBP\cdot H_3O^+\cdot pH_2O \cdots ClO_4^-$, an ion pair, where $0 \leq p \leq 1.5$. In this study even more dilute TBP solutions in CCl_4 were examined, and a two-TBP acid complex, in addition to the three-TBP complex, was found. In the isooctane system either a two- or three-TBP acid complex, depending upon TBP concentration, was found to predominate. With 1,2-dichloroethane–TBP and at the organic-phase acid concentrations examined, only a dissociated three-TBP complex was found. In addition to an anion effect, it is suggested solvent effects upon both TBP and the extraction complex are changing, to a greater or lesser extent, the TBP coordination number of the extracted hydronium ion from three to two.

Introduction

A previous study of $HClO_4$ extraction by dilute solutions of tributyl phosphate (TBP) in CCl_4 indicated that the proton was coordinated with three TBP molecules in the organic phase.[2] This study also showed that at least one water molecule was always coextracted. From these two results a model for the extracted species was suggested; the complex has a hydronium ion core to which the three TBP molecules are coordinated. It was also suggested that this model could have general application as a guide for understanding acid extraction by dilute solutions of other weakly basic organic extractants as well as by other TBP–diluent systems.

To test the validity of this proposed model the extraction of $HClO_4$ by TBP in other diluents was investigated. In this paper, the first of a two-part study, the use of isooctane and of 1,2-dichloroethane as diluents was investigated. Isooctane was chosen to illustrate the extraction process in a solvent which possesses relatively weak solvating properties and so can be considered relatively "inert." This system will be used as a reference against which the other TBP–diluent systems can be compared. The solvent 1,2-di-

(1) This work was done under the auspices of the U. S. Atomic Energy Commission.

(2) D. C. Whitney and R. M. Diamond, *J. Phys. Chem.*, **67**, 209 (1963).

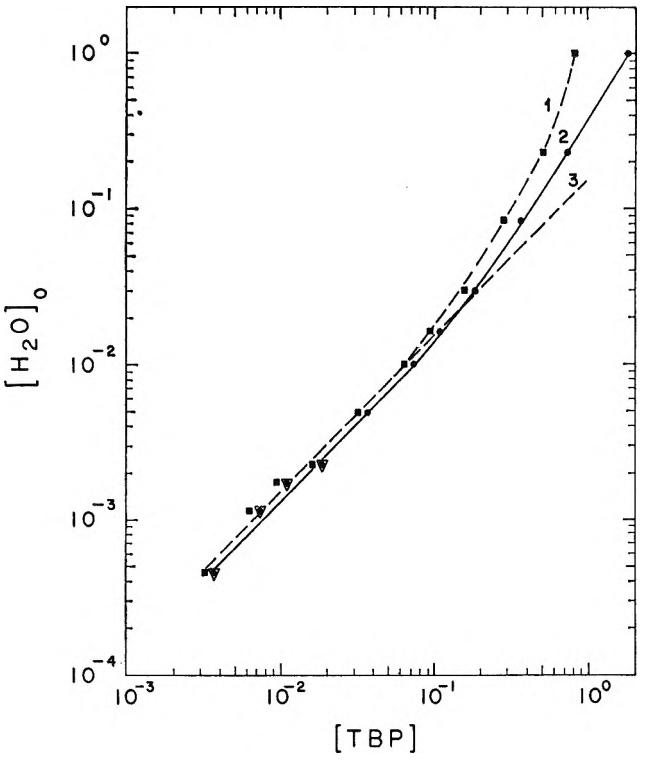

Figure 1. Variation of water content of organic phase with TBP concentration in isooctane ($[H_2O]_0$ = total H_2O − H_2O dissolved by diluent): line 1, ■, is $[H_2O]_0$ *vs.* equilibrium TBP ($[TBP]_0$ = total TBP − $[H_2O]_0$); line 2, ●, is $[H_2O]_0$ *vs.* initial TBP concentration. The symbol ● denotes averaged measurements by both Karl Fischer titrations and the tritium tracer method; ▽ denotes measurements using tritiated water alone. Line 3 is a continuation of the line of unit slope.

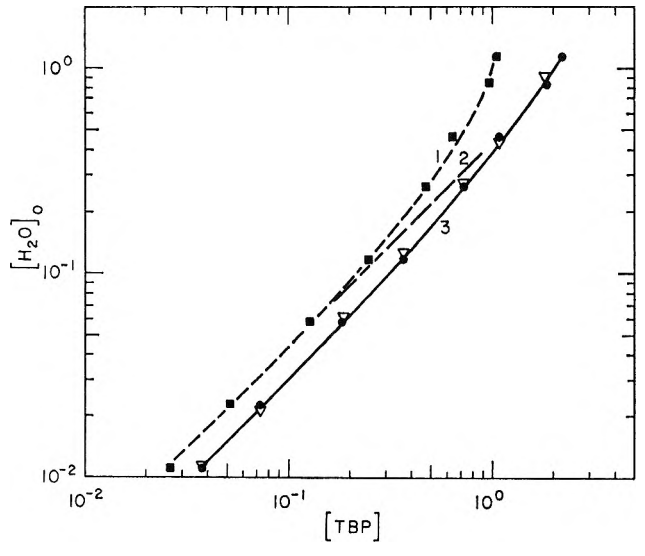

Figure 2. Variation of water content of organic phase with TBP concentration in 1,2-dichloroethane ($[H_2O]_0$ = total H_2O − H_2O dissolved by diluent): line 1, ■, is $[H_2O]_0$ *vs.* equilibrium TBP ($[TBP]_0$ = total TBP − $[H_2O]_0$); line 2 is a continuation of the line of unit slope; line 3, ●, ▽, is $[H_2O]_0$ *vs.* initial TBP concentration. The symbol ● denotes Karl Fischer titration values; ▽ denotes values using tritiated water.

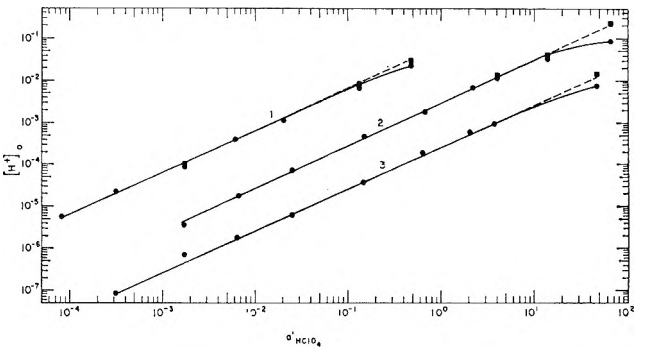

Figure 3. Variation of acid content of organic phase with aqueous $HClO_4$ activity for 0.074 *M* TBP in isooctane (line 3) and for 0.367 *M* TBP in isooctane (line 1), as measured by ReO_4^- tracer out of $HClO_4$ acid, and for 0.367 *M* TBP in CCl_4 (line 2), as measured by ReO_4^- tracer out of $HClO_4$ acid; ●, uncorrected data; ■, data corrected for used-up TBP. Dashed lines drawn with slope unity.

chloroethane was chosen for its relatively high dielectric constant; this property may allow dissociation of the extraction complexes into independent ions, thus freeing the cation from any close interaction with the anion. Instead of using acid–base titration methods for determining the amount of extracted acid, as was mainly done in the previous TBP–CCl_4 investigation,[2] radioactive perrhenate (ReO_4^-) tracer was employed. Since the molecular structure and charge of ReO_4^- is similar to ClO_4^- it is found that this tracer anion can be used successfully as a marker for ClO_4^- although it is not identical in behavior. Because this radioactive tracer technique allows accurate determination of much lower organic-phase acid concentrations than those previously obtained, the TBP–$HClO_4$ ($HReO_4$)–CCl_4 system was also reexamined over a greater range of dilute TBP concentrations.

Experimental Section

Reagents. The $HClO_4$ solutions were prepared by dilution with distilled water of G. F. Smith reagent grade $HClO_4$, 70 to 72%. The stock 70–72% solution was standardized by titration with sodium hydroxide to the bromothymol blue end point. $HReO_4$ solutions were made by dilution from a stock solution, standardized in the same way, and prepared by dissolving Re_2O_7 in water. The $^{186}ReO_4^-$ tracer solution was prepared by irradiating $KReO_4$ with neutrons in the Vallecitos reactor and dissolving the product in distilled water. The CCl_4 was Baker and Adamson reagent grade; the isooctane was Spectrograde obtained from Matheson Coleman and Bell, and the 1,2-dichloroethane was Matheson Coleman and Bell reagent grade.

Procedure. Procedures for sample preparation, measurements, and data analysis are essentially the same as already noted elsewhere.[2,3] Additions or changes

(3) T. J. Conocchioli, M. I. Tocher, and R. M. Diamond, *J. Phys. Chem.*, **69**, 1106 (1965).

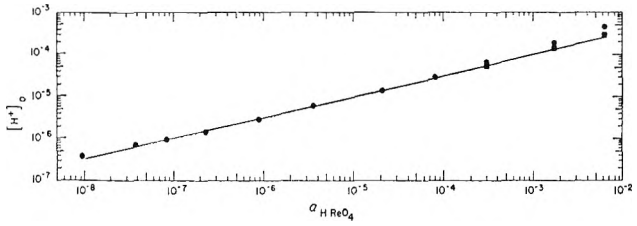

Figure 4. Variation of acid content of organic phase with aqueous $HReO_4$ activity for 0.367 M TBP in 1,2-dichloroethane: ●, uncorrected data; ■, data corrected for activity coefficients.

are as follows. (1) When using 1,2-dichloroethane as a diluent, shaking times of 5–6 hr were necessary to obtain reproducible results. (2) The volume ratios of organic to aqueous phases were not always kept one-to-one as before. (3) End-point determination in the Karl Fischer water titrations was by the dead-stop instead of a visual end-point technique. (4) To supplement the Karl Fischer titration and to extend the lower range of water determinations, tritium, in the form of tritiated water, was used as a tracer in the studies of water extraction by TBP. Transfer of the equilibrated solutions from one piece of glassware to another was not possible in the isooctane diluent system, as when this was done, nonreproducible errors as large as 50% occurred, probably due to wall absorption of tritium-labeled water. Consequently, ground-glass-stoppered round-bottom centrifuge cones were used to equilibrate the water samples, and pipets preequilibrated with nonactive water-saturated isooctane or

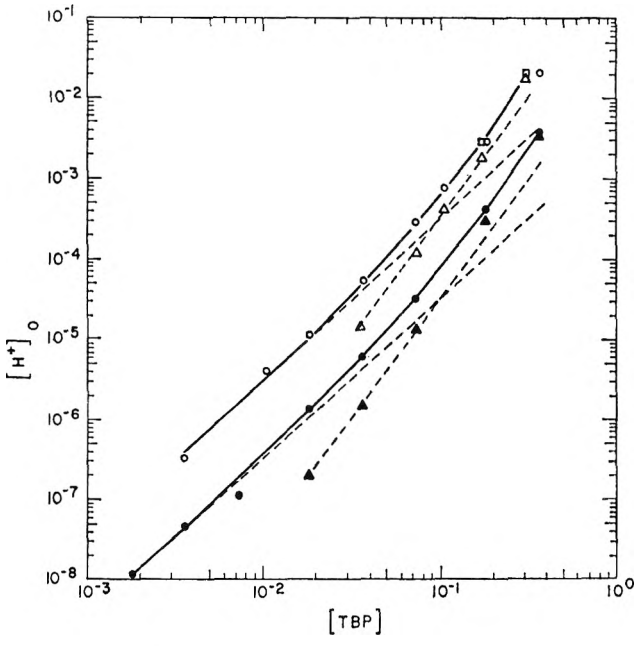

Figure 5. Variation of acid content of organic phase with TBP concentration in CCl_4 for aqueous $HReO_4$ concentrations of 1.60 M (●) and of 2.91 M (○); ▲, △, resolved $n = 3$ line; other dashed line, $n = 2$; □, data corrected for used-up TBP.

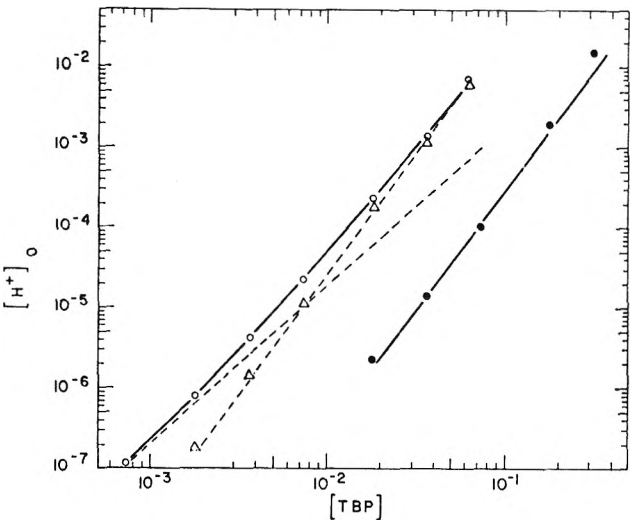

Figure 6. Variation of acid content of organic phase with TBP concentration in isooctane for aqueous $HReO_4$ concentration of 0.870 M (●), and for aqueous $HClO_4$ concentration of 4.00 M (○); △, resolved $n = 3$ line; other dashed line, $n = 2$.

1,2-dichloroethane solutions were employed to separate them. Aliquots from both the organic and aqueous phases were counted in a room-temperature liquid scintillation apparatus. Quenching and counting efficiency were held constant to 1–2% and were checked by the "channel ratio" method. All extractions were performed at 23 ± 2°.

Results

The experimental results are shown as log–log plots in Figures 1–7. The raw data are indicated by circles and are connected by solid lines. Corrections made to the experimental points, as described below, are indicated in each of the plots by square symbols and are connected by dashed lines.

The log–log plots of organic-phase water concentration *vs.* TBP concentration are shown in Figures 1 and

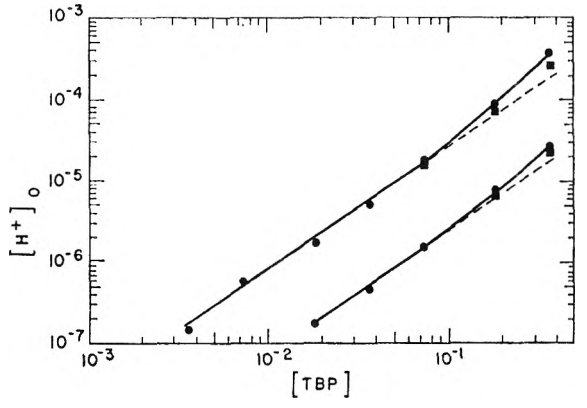

Figure 7. Variation of acid content of organic phase with TBP concentration in 1,2-dichloroethane for aqueous $HReO_4$ concentrations of 0.0100 M and of 0.100 M (●); ■, data corrected for activity coefficients.

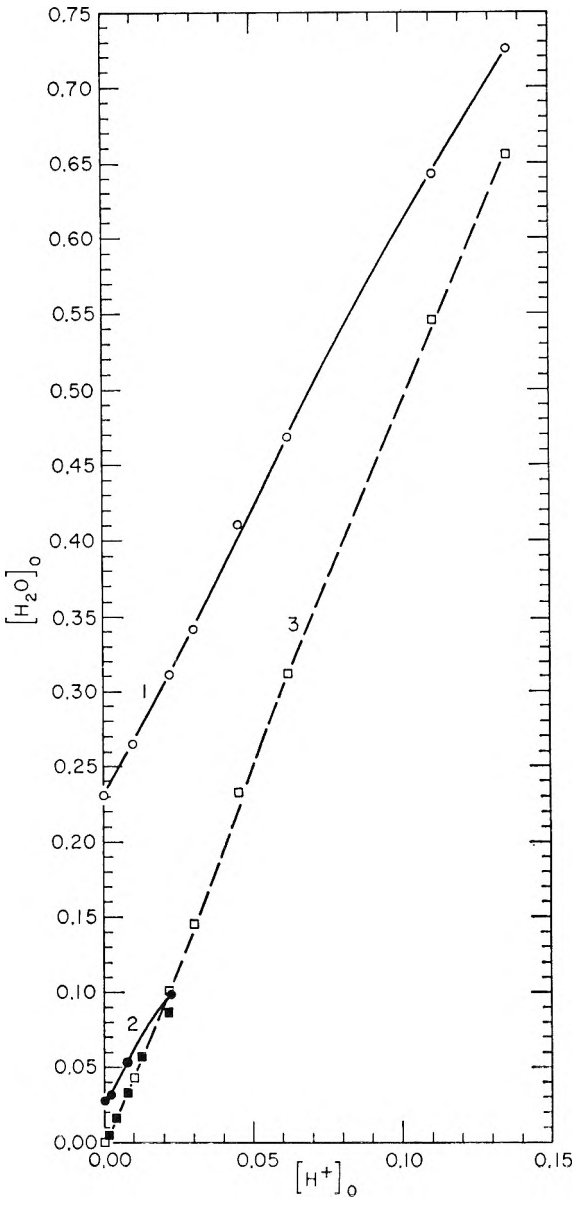

Figure 8. Water content *vs.* $HClO_4$ concentration in the organic phase (as the aqueous $HClO_4$ concentration increases) for total TBP concentrations of 0.183 *M* and 0.73 *M* in isooctane. Lines 1 and 2, ○, and ●, are the total organic-phase water less the solvent water; line 3, ■, □, is the total organic-phase less both the solvent water and the water bound to TBP.

2 for the TBP–isooctane and TBP–1,2-dichloroethane systems at a water activity of unity ($a_w = 1$). The amount of water extracted by the diluent alone, calculated as the product of the molar solubility in the diluent, times the volume fraction of diluent, has already been subtracted from the water concentrations plotted (water solubility in isooctane, 0.0035 *M*; literature values, 0.002 *M*[4] to 0.006 *M*[5] at 25°; water solubility in 1,2-dichloroethane, 0.125 *M*; literature value, 0.129 *M*[6] at 25°).

The log–log plots in Figures 3 and 4 are of organic-phase acid concentration *vs.* aqueous activity of acid times the water activity to the appropriate power (described below) for 0.073 *M* and 0.367 *M* TBP in isooctane; for 0.367 *M* TBP in CCl_4; and for 0.367 *M* TBP in 1,2-dichloroethane. Perrhenate tracer out of perchloric acid was used to determine the concentrations in both the isooctane and CCl_4 systems shown in Figure 3; ReO_4^- tracer out of perrhenic acid was used for the 1,2-dichloroethane system, Figure 4.

Figures 5, 6, and 7 show the log–log dependence of organic-phase acid concentration *vs.* concentration of TBP in CCl_4, isooctane, and 1,2-dichloroethane, respectively. Perrhenate tracer out of perrhenic acid was used in both the CCl_4 and 1,2-dichloroethane systems and for one set of data in the isooctane system; for the other set of data in isooctane, perrhenate tracer out of perchloric acid was employed.

The relationship between coextracted water and the organic-phase acid concentration is shown in Figure 8 for isooctane. The total amount of water extracted, exclusive of that in the diluent itself, is shown by line 1 for (initial) 0.73 *M* TBP and by line 2 for 0.183 *M* TBP. The difference between organic-phase water concentration when the acid is present and that which extracts into equivalent solutions of TBP alone (but corrected to the appropriate water activity) is indicated by line 3.

In those systems where ReO_4^- tracer was used as a marker for ClO_4^-, the plotted organic-phase acid concentrations, $[H^+]_0$, may be up to a factor of 2 higher than the actual $HClO_4$ concentrations, as ReO_4^- extracts somewhat better than ClO_4^- out of $HClO_4$. As long as the correction for the amount of TBP complexed with extracted acid is small, this causes no error in the slope analyses used in this paper, as it produces only a parallel displacement of the curves and no change in slope. But at high concentrations of extracted acid, where corrections for that fraction of the TBP complexed to the acid become important, a knowledge of the actual concentrations of organic-phase $HClO_4$ is needed, and these were obtained by direct two-phase titrations. In those systems where data were obtained using ReO_4^- tracer out of macro-perrhenic acid, no problem arises, and the values of $[H^+]_0$ plotted are the correct ones.

Discussion

TBP–H_2O. The equilibrium for the distribution of water into a solution of TBP in an organic diluent is maintained independently of any other extraction equilibria, and may be written

$$n\text{TBP(org.)} + m\text{H}_2\text{O} = m\text{H}_2\text{O}\cdot n\text{TBP(org.)} \quad (1)$$

(4) T. I. Berkengeim, *Zavodskaya Lab.*, **10**, 592 (1941); *Chem. Abstr.*, **40**, 6961 (1946).

(5) B. A. Englin, A. F. Plate, V. M. Tugolukov, and M. A. Pryanishnikova, *Khim. i Teknol. Topliv i Masel*, **10**, 42 (1965); *Chem Abstr.*, **63**, 14608*f* (1965).

(6) A. J. Staverman, *Rec. Trav. Chim.*, **60**, 836 (1941).

The corresponding equilibrium constant is

$$K_{H_2O} = \frac{(mH_2O \cdot nTBP)_0}{(H_2O)^m(TBP)_0^n} = \frac{[mH_2O \cdot nTBP]_0 y_{H_2O}}{(H_2O)^m[TBP]_0^n y_{TBP}^n} \quad (2)$$

where parentheses signify activity, brackets denote molar concentrations, and y is a molar activity coefficient. With the assumption that the ratio y_{H_2O}/y_{TBP}^n is a constant in these dilute solutions, eq 2 suggests a log–log plot of the organic-phase water concentration (corrected for water uptake of the diluent), $[H_2O]_0$, *vs.* the equilibrium TBP concentration, $[TBP]_0$, should generate a line of slope n, where n is the number of TBP molecules bound to each extracted water complex. Such plots are shown in Figures 1 and 2 for isooctane and 1,2-dichloroethane, respectively. In these figures, the data connected by a solid line result from plotting $[H_2O]_0$ *vs.* the initial TBP concentration. It can be seen that for values below 0.2 *M* in dichloroethane and below 0.07 *M* in isooctane a line of slope 1 can be drawn through the points. This suggests that a water complex containing only one TBP molecule occurs at these (and lower) TBP concentrations, at least when $a_w \cong 1$; the majority of the TBP molecules, however, remain unhydrated. Without determining $[H_2O]_0$ as a function of a_w it cannot be definitely asserted how many water molecules are involved in the complex. However, from published[2,7,8] and unpublished studies[9] made upon similar extractant–solvent systems, it is clear that the assumption of only one water molecule being involved is reasonable. That is, at or below 0.2 *M* in dichloroethane and 0.07 *M* TBP in isooctane, the TBP–water species present is a predominantly 1:1 ($n = m = 1$) complex. Correcting the TBP concentrations to equilibrium values, $[TBP]_0$, on this basis of as many TBP molecules complexed as there are extracted waters, leads to the dashed curves in Figures 1 and 2, and values of K_{H_2O} for the dichloroethane and isooctane systems of 0.44 and 0.12 $(mol/l.)^{-1}$, respectively.

For higher concentrations of TBP, the experimental points deviate from the line of unit slope. This result probably indicates a higher TBP–water complex is being formed, but we must also consider how the activity coefficients of the TBP and of the complex are varying. At some point, as the TBP concentration is increased, the properties of the solution begin to deviate significantly from those of the pure diluent. The individual activity coefficients of the TBP and TBP·H_2O species change from their infinitely dilute solution values.[10,11] But experience indicates that the coefficients of such similar species change in the same direction, that the assumption of a constant activity coefficient ratio is still valid. Such "compensation" of activity coefficient effects in extraction systems has been described by other authors.[12,13] However, at some higher concentration of TBP, even the ratio of coefficients may no longer remain constant, and then deviations from the straight line determined at lower concentration may occur even though no new species is formed. Experience with a number of extraction systems seems to indicate that such behavior does not occur much below about 5 volume % TBP (0.2 *M*). Thus the deviations observed in isooctane starting below 0.07 *M* probably do indicate a new species. Definite corroboration of the existence of at least one additional water complex (in more concentrated solutions) has been obtained from nmr studies[8,9] made on TBP–CCl_4 systems. But over most of the range of TBP concentrations in isooctane used in this work, and for all the 1,2-dichloroethane solutions, the 1:1 TBP–H_2O complex is the dominant hydrated species.

A study of $[H_2O]_0$ for the TBP–CCl_4 system, using both Karl Fischer titrations and normalized infrared intensities, has been published previously.[2] The data presented are quite similar in form to those found in Figure 1. A 1:1 TBP–H_2O complex occurs up to a TBP concentration of 0.1 *M*. Beyond this concentration the water extraction curve again indicates the formation of an additional water–TBP complex. The K_{H_2O} for the 1:1 complex was 0.15 $(mol/l.)^{-1}$.

TBP–H_2O–$HClO_4$ or –$HReO_4$. The extraction of $HClO_4$ or $HReO_4$ by solutions of TBP in a diluent may be expressed as

$$H^+ + X^- + xH_2O + n\text{TBP(org.)} =$$

$$H^+ \cdot n\text{TBP} \cdot xH_2O \cdots X^-\text{(org.)} \quad (3)$$

$$= H^+ \cdot n\text{TBP} \cdot xH_2O\text{(org.)} + X^-\text{(org.)} \quad (3')$$

with the corresponding equilibrium constants

$$K^a = [H^+ \cdot n\text{TBP} \cdot xH_2O \cdots X^-]_0 y_{HX} / [TBP]_0^n y_{TBP}^n (H_2O)^x (HX) \quad (4)$$

$$K^d = [H^+ \cdot n\text{TBP} \cdot xH_2O]_0 [X^-]_0 y_\pm^2 / [TBP]_0^n y_{TBP}^n (H_2O)^x (HX) \quad (4')$$

From log–log plots of the organic-phase acid concentration, $[H^+]_0$ *vs.* the aqueous-phase activity product $(HClO_4)(H_2O)^x \equiv a_{HClO_4}'$, with the TBP concentration held constant, it can be determined whether the extracting species is an ion pair (eq 4) or a pair of dissociated ions (eq 4'). Such log–log plots are shown in Figure 3 for 0.367 *M* and 0.073 *M* solutions in isooctane and for

(7) C. J. Hardy, D. Fairhurst, H. A. C. McKay, and A. M. Willson, *Trans. Faraday Soc.*, **60**, 1626 (1964).

(8) S. Nishimura, C. H. Ke, and N. C. Li, *J. Amer. Chem. Soc.*, **90**, 234 (1968).

(9) J. J. Bucher, A. Beck, and R. M. Diamond, unpublished work.

(10) A. M. Rozen, L. P. Khorkhorina, V. G. Yurkin, and N. M. Novikova, *Dokl. Akad. Nauk SSSR*, **153**, 1387 (1963).

(11) D. Dyrssen and Dj. Petković, *J. Inorg. Nucl. Chem.*, **27**, 1381 (1965).

(12) S. Sierkierski, *ibid.*, **24**, 205 (1962).

(13) A. M. Rozen, "Physical Chemistry of Solvent Extraction," in "Solvent Extraction Chemistry," D. Dyrssen, J. Liljenzin, and J. Rydberg, Ed., North-Holland Publishing Co., Amsterdam, 1967, pp 195–235.

0.367 M TBP solutions in CCl_4. (Experimentally, x has values near 3 and 5 for TBP–CCl_4 and TBP–isooctane, respectively, as described below.) At low concentrations of extracted acid all the points lie on lines of unit slope, suggesting that the extraction complex is associated as ion pairs. At higher concentrations, where curvature of the plot becomes pronounced, an increasingly large fraction of TBP is complexed with the extracted acid. Since such TBP is no longer free, this represents a serious departure from the required condition of a fixed equilibrium concentration of extractant. The value of $[H^+]_0$ can be corrected to a fixed concentration of TBP by means of eq 5.

$$[H^+]_0' = [H^+]_0[TBP]_0'^n/[TBP]_0^n \quad (5)$$

Here primed quantities refer to the condition of a fixed (initial) equilibrium concentration, and unprimed quantities denote the experimental values, among which $[TBP]_0$ can be obtained from the relationship

$$[TBP]_0 = [TBP]_{initial} - [TBP\cdot H_2O]_0 - n[H^+]_0 \quad (6)$$

By using the value $n = 3$ (whose origin is justified later) in applying eq 5 and 6 to correct the data in Figure 3, it can be seen that the points on the curved portions of the plots are brought onto the straight line of unit slope extended from the dilute solution regions where corrections are not necessary.

A similar plot for the system TBP–1,2-dichloroethane is given in Figure 4. With this diluent the slope observed is closer to 0.5 than to unity, suggesting the presence of a dissociated species (eq 1′). If so, the value of $[H^+]_0$ should be corrected by an electrostatic, or Debye–Hückel, mean ion activity coefficient. An estimate of these coefficients, perhaps a tenuous one for a solvent with a dielectric constant of only 10.5, was made by using the Mayer–Poirier expression.[14] The computed values of $y_\pm$ were applied to the raw extraction data and gave the results indicated by the square symbols plotted in Figure 4. Clearly the application of the calculated $y_\pm$ values to the higher $[H^+]_0$ concentrations lowers these data onto the line of slope 0.5. This line has already been determined by the points at lower concentrations where activity coefficients are negligibly different from unity. Thus, it may be concluded that over the entire range of extracted acid concentrations studied, the extraction complex in 1,2-dichloroethane is principally dissociated into two independent ions. This result is not unreasonable; Fuoss's equation for ion-pairing would predict approximately 70% free ions at the highest $[H^+]_0$ in Figure 4, for an $\mathring{a} = 7$ A.[15] At yet higher organic-phase acid concentrations, however, the above conclusions may not still be true.

It is possible to determine the value of n, the number of TBP molecules coordinated in the extracted complex, for each diluent–TBP system. From log–log plots of the extracted acid *vs.* TBP concentration at a constant a_{HClO_4}' or a_{HReO_4}', the slopes of the curves directly equal n for ion-paired complexes or $0.5n$ for dissociated complexes. The TBP concentrations so used in Figures 5, 6, and 7 are not equilibrium TBP but initial TBP concentrations corrected for the amount of TBP bound in the acid complex. Except for the case where an appreciable amount of TBP is involved in the acid complex, correcting the data for the amount of TBP bound by water would only result in a parallel displacement of the curve and would not change the values of the slopes found in the slope analysis techniques employed in this paper.

The above outlined procedure is shown in Figure 5 for TBP–CCl_4 at two fixed concentrations of perrhenic acid, 1.60 M and 2.91 M. The plots of the raw data (solid lines) do not have a unique slope over the range of TBP concentrations used. It is evident, however, that a limiting slope equal to two ($n = 2$) can be obtained at the lower end. Extension of this line of slope two (dashed line) to higher TBP concentrations and subsequent subtraction from the raw data yields a line whose slope is three ($n = 3$). It thus appears, for TBP concentrations in CCl_4 less than 0.1 M, a two-TBP one-$HReO_4$ complex predominates, and that above 0.1 M a three-TBP complex takes over. But above about 0.2 M TBP it may become questionable to use this type of slope analysis; activity coefficient ratios may not remain constant, as already mentioned in the TBP·H_2O discussion, and such behavior would lead to (unknown) curvature in the lines.

In a previous study of $HClO_4$ extraction by TBP–CCl_4,[2] only a three-TBP coordinated complex was found, in disagreement with the present finding of a 2TBP complex, as well as a 3TBP species. The previous result, however, is due to the experimental limitation of using TBP concentrations ≥ 0.0367 M. With that restriction the present data would also yield a good fit to a value of $n = 3$ alone. It is only when more dilute TBP solutions are examined by means of ReO_4^- tracer that the existence of a 2TBP complex is clearly evident.

Another example of this behavior is shown in Figure 6. The lower curve is a log–log plot of $[H^+]_0$ *vs.* TBP in isooctane for 0.874 M $HReO_4$, and shows only a slope of 3 for the range of TBP concentrations studied, namely 0.3–0.02 M. But when a higher acid concentration is used so as to be able to carry the study to smaller TBP concentrations, evidence for a lower complex appears. The curve for 4.00 M $HClO_4$ shown in Figure 6 covers the range of TBP concentrations from 7×10^{-4} to 7×10^{-2} M and clearly can be resolved into two components; predominantly a 3:1 complex above

(14) J. C. Poirier, *J. Chem. Phys.*, **21**, 965 (1953).
(15) R. M. Fuoss, *J. Amer. Chem. Soc.*, **80**, 5059 (1958).

7×10^{-3} M TBP and a 2:1 complex below that concentration. It may be noted that this cross-over point is at an order of magnitude lower concentration in isooctane than in CCl_4, as will be discussed later.

In Figure 7 the TBP dependence data are shown for TBP–1,2-dichloroethane. In this case the extracted species is dissociated into two ions; the value of the slope in the log–log plot is $0.5n$ and the raw data must be corrected by Debye–Hückel type activity coefficients.[14] At the higher organic-phase acid concentrations where these activity coefficient corrections become noticeable, the corrected points are shown as open squares. A slope of 1.5 is obtained at both acid concentrations, so that over the range of TBP concentrations from 3×10^{-3} M to 3×10^{-1} M a dissociated 3TBP complex is extracted. There is no evidence for a 2TBP complex in the range of TBP concentrations employed.

The amount of water associated with the extracted acid complex in TBP–isooctane is shown in Figure 8. The slope of line 3 in this figure indicates that four-to-five water molecules are coordinated to the ion-paired 3TBP complexes formed at the TBP concentrations investigated. A previous study of the TBP–CCl_4–$HClO_4$–H_2O system[2] found a smaller number ($\sim$2.5) of water molecules coordinated to the acid complex. While the different amounts of water coextracted in these two solvent systems probably has significance, it will only be noted now that both systems have more than one water per acid. That is, both systems have sufficient coextracted water to allow the formation of a hydronium ion. It is this last fact, in addition to the finding of a 3TBP complex in CCl_4, which led to the previously suggested model for interpreting acid extraction data in these moderately basic organic systems.

However, with the observation in this study of a 2TBP complex in addition to the 3TBP complex, the question arises whether the previously suggested extraction model is appropriate. Unfortunately, we cannot determine the water coextracted by the 2TBP complex so as to prove that at least one water molecule is still involved with it; the concentrations where this species predominates are too low for satisfactory Karl Fischer determinations. But we believe the hydronium core model is still necessary to explain the present data. In each of the three diluent systems, over some range of TBP concentrations, a 3TBP complex is found. Without the existence of a hydronium ion, with its three positive charge sites, it is difficult to conceive how TBP coordination numbers of three could be obtained. It is suggested that the appearance of a 2TBP species at lower TBP concentrations is a natural consequence of the stepwise formation of coordination complexes, rather than an indication of the breakdown of the proposed model. This is analogous to the behavior found with metal complexes, where lower complexes appear in the more dilute solutions of the complexing reagent and the (higher) saturated complex occurs in more concentrated solutions.

Another interesting result of this study is the difference in TBP concentration at which a 2TBP complex becomes dominant. In isooctane, the lower complex predominates only up to TBP concentrations of 0.007 M, while it is the major species to almost 0.1 M in CCl_4. Clearly in the CCl_4 system one or more factors are operating to stabilize the 2TBP complex over the 3TBP complex with respect to the situation in isooctane. It is probable that the main factor is the CCl_4 molecule itself, providing solvation for both the TBP molecule and the extracted 2TBP–acid complex by means of dispersion force interactions *via* its chlorine atoms. Interaction of CCl_4 with the TBP molecules is confirmed by activity coefficient measurements on TBP in both TBP–CCl_4,[10,16] and TBP–CCl_4–H_2O[11] systems. These show that the value of γ_{TBP} initially decreases and then becomes constant at a reduced value as the amount of CCl_4 in the solution increases; there is a marked negative deviation from ideal behavior. The result of this interaction between CCl_4 and TBP corresponds to a reduction in the effective concentration of the latter ($\gamma_{TBP} < 1$), leading to reduced extraction of the acid (see Table I) and a higher range of (stoichiometric) TBP concentration for which the 2:1 acid complex dominates. But we must also consider the interaction of CCl_4 with the extracted acid complexes. Although the situation is not exactly the same, it can be pointed out that the $UO_2(NO_3)_2 \cdot 2TBP$ complex has also been shown to have attractive interactions with CCl_4[13,16,17] as diluent; we think it is most reasonable that the hydronium ion–TBP complex should behave in a similar manner. This should be particularly true for the 2:1 complex, with its exposed site, the third hydronium hydrogen, and so would reduce the need of that complex for a third TBP molecule. The result is to again help increase the range of existence of the 2:1 complex. Thus the interactions of CCl_4 with TBP and with the acid complex both tend to favor the lower complex, and the former interaction decreases all acid extraction while the latter helps extraction of the 2:1 complex mainly.

The situation is just the opposite with isooctane as the diluent. Activity coefficient data for TBP (and for the $UO_2(NO_3)_2 \cdot 2TBP$ complex) in hexane indicate that the hydrocarbons are not very effective in solvating these species.[10,17] The coefficients of TBP (and $UO_2(NO_3)_2 \cdot 2TBP$) increase in magnitude with increasing proportion of hexane. This time the deviations from ideality are positive. The effective concentration of TBP in isooctane is greater than that indicated by the stoichiometric value ($\gamma_{TBP} > 1$), and at any given

(16) A. Apelblat and A. Hornik., *Trans. Faraday Soc.*, **63**, 183 (1967).
(17) M. F. Pushlenkov, E. V. Komarov, and O. N. Shuvalov, *Radiokyimiya*, **4**, 543 (1963).

TBP concentration the higher TBP–acid complex should be favored over the 2:1 species compared to CCl_4 as a diluent. This trend is reinforced by the relatively poorer ability of isooctane to solvate the 2:1 acid complex and displace a TBP molecule. The differences in behavior of 2:1 and 3:1 acid complexes in CCl_4 and isooctane thus can be reasonably explained.

A comparison of the extraction data with 1,2-dichloroethane and with isooctane points to still another factor which may be important in the extraction process. It is noted that only a 3TBP–acid complex is found in 1,2-dichloroethane at TBP concentrations equal to or lower than those which in isooctane show evidence for a 2TBP complex. It would surely be expected that 1,2-dichloroethane would provide free TBP and the extracted complex with "chemical solvation" at least equal to that of isooctane. An estimate of the direction of change for the TBP activity coefficient in 1,2-dichloroethane can be obtained from a distribution experiment into water from 0.183 *M* TBP in 1,2-dibromoethane, where rather strong negative nonideality is indicated.[12] It might then be expected that the interaction of 1,2-dichloroethane with TBP and with the extraction complex should yield behavior along the lines already found for the TBP–CCl_4 system. The existence of a lower (2:1) complex might therefore be expected to be observed with 1,2-dichloroethane at an equal or higher TBP concentration than with isooctane. The two systems, however, have a major difference. In 1,2-dichloroethane, the extracted acid is dissociated; the ReO_4^- anion is free of the cation complex, while in isooctane the anion is electrostatically bound to it. It may be that in isooctane and CCl_4 the oppositely charged anion gives sufficient electrostatic solvation to the hydronium complex to help displace one of the coordinating TBP molecules, to help stabilize the lower coordination complex. But in dichloroethane, the lack of interaction of the dissociated anion with the hydronium cation reinforces the latter's need for more complete coordination with TBP. Hence the 3:1 complex would be favored down to still lower TBP concentrations than in isooctane, as is observed experimentally.

It is evident that the resolved lines of slope two or three in Figures 5–7 only fit the data up to concentrations of about 0.2 *M*, and have fallen below the experimental points at 0.3 *M* and higher TBP concentrations. From slope analysis this would indicate a still higher TBP complex. But the coordination of additional TBP molecules to the hydrated hydronium cation should be more difficult, though it is conceivable. It is unlikely that TBP could coordinate to ClO_4^- or ReO_4^-. We believe the enhanced extraction of acid at TBP concentrations above 0.2 *M* is due mainly to the change in the nature of the diluent. It is no longer isooctane or CCl_4 or 1,2-dichloroethane, but an isooctane–TBP or CCl_4–TBP, etc., mixture with a significant proportion of TBP. The consequent changes in the physical and chemical properties of the diluent mixture naturally affect its extraction properties, and these changes probably are reflected in the breakdown of the assumption of a constant activity coefficient ratio y_{HX}/y_{TBP}^n. This would mean that in CCl_4, y_{HX} increases less rapidly with increasing TBP concentration than does y_{TBP}^n, and in isooctane, y_{HX} decreases more rapidly than y_{TBP}^n. In the more concentrated TBP solutions, the extracted acid complex(es) obtain better solvation, relative to the TBP molecules themselves, than in the dilute solutions.

The equilibrium constants for the extraction of $HReO_4$ tracer by TBP dissolved in isooctane, CCl_4, and 1,2-dichloroethane as found in this study are listed in Table I. They are not true equilibrium constants, as concentrations, rather than activities, have been used for the organic-phase species. But since the ratio of organic-phase activity coefficients appears to be constant in dilute solutions of TBP, the substitution of concentrations for activities in dilute solution should not lead to serious error. However, we shall use a different symbol, $K_m^{a,d}$, instead of K. The superscript indicates whether the species in question is associated (a) or dissociated (d) and the subscript indicates whether a 2:1 or 3:1 complex is involved. The TBP concentrations used in evaluating the K's are equilibrium values, corrected for the TBP bound in the acid complex and to water. Finally, for calculating the aqueous activity of perrhenic acid, the activity coefficient of perchloric acid[18] at the same concentration was used.

Table I: Constants for the Extraction of $HReO_4$

Diluent	Macro-acid	K_2^a	K_3^a
Isooctane	$HClO_4$	5.0×10^{-3}	8.3×10^{-1}
	$HReO_4$	...	7.6×10^{-1}
CCl_4	$HReO_4$	1.7×10^{-3}	2.0×10^{-2}
			K_3^d
1,2-Dichloroethane	$HReO_4$	...	2.4×10^{-4}

Several points can be made from this table. It can be seen that the value of K_3^a in isooctane is ~40 times larger than that in CCl_4. We believe that this is mainly due to the stronger interaction of CCl_4 with TBP, effectively decreasing the concentration of TBP available to the acid complex and so indirectly hindering complex formation in CCl_4. The 3:1 acid complex is essentially coordinatively saturated by the TBP, and so is not greatly influenced directly by the nature of the diluent. But this is not true for the 2:1 complex which

(18) M. Gazith, Israel Atomic Energy Commission Report IA-1004, (Oct 1964).

has an open hydronium hydrogen, and so CCl_4 can solvate this complex better than can isooctane. This enhanced solvation by CCl_4 just about compensates for the effect of the enhanced interaction of CCl_4 with TBP itself, and so the values of K_2^a are almost alike in the two diluents. The diluent 1,2-dichloroethane also must interact with TBP more strongly than does isooctane, thus hindering formation of the acid complex,[17] but its most important property is its relatively high dielectric constant, which favors extraction and leads to dissociated ions in the extracted species. No evidence for a 2:1 species was found in this system in the concentration range studied, and we believe that the loss of interaction with the anion in the dissociated species requires a more complete solvation of the cation by the TBP, thus favoring the 3:1 complex.

In this paper we have shown that the hydronium ion–TBP complex can have lower complexes than the saturated 3:1 species, and that the nature of the diluent employed affects both the magnitude of the extraction and the nature of the extracted complex in a reasonable way. Several other studies of $HClO_4$[19,20] or $HReO_4$[21] extraction by TBP or TBP–diluent systems have been made. These studies, however, are either at higher concentrations of TBP than used in this study or use a different diluent, so that comparisons with the present work are difficult. In the next paper, this type of study will be extended to chloroform and to aromatic diluents.

(19) See ref 1–9 in D. C. Whitney and R. M. Diamond, *J. Phys. Chem.*, 67, 209 (1963).
(20) K. Naito and T. Suzuki, *ibid.*, 66, 983 (1962).
(21) R. Colton, U.K.A.E.A. Report AERE-R3823 (Sept 1961).

Thermodynamic Properties in the Systems Vanadium–Hydrogen, Niobium–Hydrogen, and Tantalum–Hydrogen[1]

by Ewald Veleckis[2] and Russell K. Edwards

Department of Chemistry, Illinois Institute of Technology, Chicago, Illinois 60616 *(Received July 29, 1968)*

Comprehensive thermodynamic studies have been conducted for the systems V–H (246–554°), Nb–H (352–671°), and Ta–H (350–631°) in the pressure range 1–800 Torr by measuring the equilibrium hydrogen pressure as a function of composition. Each of these systems is comprised of a single solid phase in the temperature and pressure ranges studied. For each system a semiempirical equation, based on the statistical formulation of the simple interstitial solid solution model, is presented. The equations not only adequately reproduce the *P–C–T* data within the ranges of study but appear to be reliable to much lower temperatures. For example, they have been used to predict the *T–C* boundaries of immiscibility regions; for one system (Nb–H), for which comparison with an experimentally derived diagram is possible, agreement is very good. Calculated critical compositions, temperatures, and pressures are given. The partial and integral entropies and enthalpies of formation were calculated for the single-phase regions at 1 atom % intervals up to the maximum compositions of 34 (V–H), 39 (Nb–H), and 27 (Ta–H) atom % H. The results are compared in detail with those of other work.

Introduction

Like palladium, the group Vb transition metals, vanadium, niobium, and tantalum, form with hydrogen wide ranges of solid solutions which, at lower temperatures, are interrupted by miscibility gaps. For the palladium–hydrogen system the pressure–composition–temperature (*P–C–T*) data have been obtained both above and below the critical temperature. For the V–H, Nb–H, and Ta–H systems such data below the critical temperature are difficult to obtain because of the slowness of achieving equilibrium; nonetheless, these systems afford the opportunity of obtaining extensive *P–C–T* data above the critical temperatures to contribute to the advance of theoretical models.

The reported *P–C–T* work from which useful thermodynamic data have been or may be calculated consists principally of the following studies.[3] Kofstad and Wallace[4] obtained data for the system V–H in the range 165 to 456°. The Nb–H system, which received considerable attention because of the use of niobium in nuclear reactors, was investigated by Albrecht,

(1) Abstracted from the Ph.D. Thesis of E. Veleckis, Illinois Institute of Technology, 1960.
(2) Address correspondence to the authors at Argonne National Laboratory, Chemical Engineering Division, Argonne, Ill. 60439.
(3) For more complete literature references refer to H. J. Goldschmidt, "Interstitial Alloys," Butterworth and Co., Ltd., London, 1967, Chapter 9.
(4) P. Kofstad and W. E. Wallace, *J. Amer. Chem Soc.*, 81, 5019 (1959).

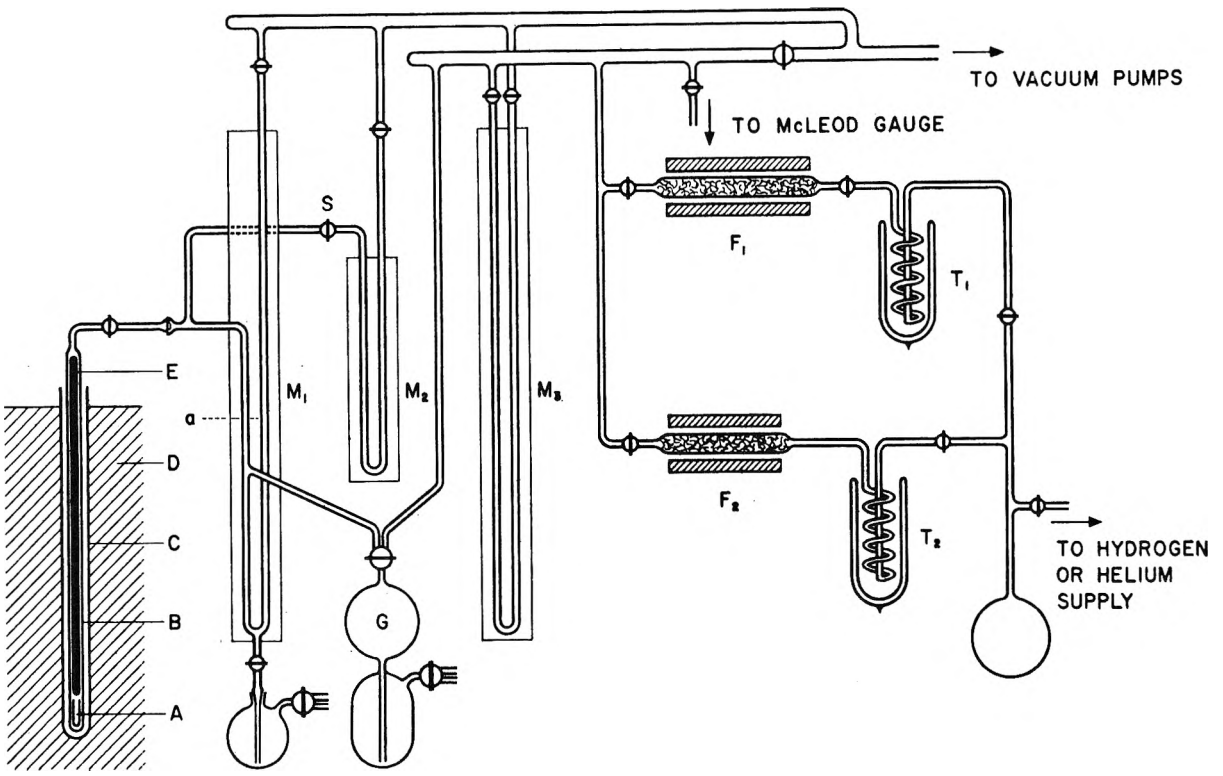

Figure 1. Schematic diagram of hydrogen–metal equilibration apparatus: A, porcelain specimen container; B, Vycor tube; C, porcelain protection tube; D, liquid metal bath; E, gas displacement rod; F_1, purification and storage furnace for hydrogen; F_2, gettering furnace for helium purification; G, calibrated bulb for gas measurements; M_1, mercury manometer; M_2, M_3, oil manometers; T_1, T_2, cold traps.

et al.[5] (100–900°), Komjathy[6] (300–1500°), and Katz and Gulbransen[7] (225–513°, by the microbalance technique). The Ta–H system was studied by Kofstad, *et al.*[8] (300–400°) and by Mallett and Koehl[9] (300–700°).

The present work was undertaken to establish for these systems more comprehensive and reliable *P–C–T* data suitable for detailed thermodynamic evaluation and for testing theoretical models.

Experimental Section

Apparatus. Figure 1 shows a schematic diagram of the apparatus. The metal specimen was placed in a small porcelain crucible, A, which, in turn, was introduced into a long Vycor tube, B. The tube was situated within the porcelain protection tube, C, which was submerged in the liquid metal bath, D. A Vycor rod, E, was placed within the tube to minimize the gas volume. The gas pressure in the tube was measured with one of the two manometers: manometer M_1 filled with mercury was used to measure pressures above 20 Torr; manometer M_2 filled with octoil was used for pressures in the range 1–20 Torr. In either case, during measurement, the mercury level was adjusted to mark *a* in the left arm of manometer M_1 to maintain a fixed residual gas volume. The number of moles of gas to be introduced into this residual volume was quantitatively measured in a calibrated bulb, G, having a volume of 509.8 cm³. Fluctuations in the temperature of the bulb were reduced by covering it with several wrappings of aluminum foil. Temperatures of the bulb were measured with two thermocouples attached directly to the glass; pressures of the gas in the bulb were read on manometer M_3 filled with octoil. To provide parallax-free readings the manometers were attached to etched scales backed by mirrors.

Hydrogen was admitted to the system through a liquid nitrogen trap, T_1, to rid the gas of condensible impurities. It next was passed over zirconium turnings contained in furnace F_1 for further purification from gaseous impurities by the gettering action of zirconium. The turnings also served as a reservoir for storage of the large quantities of purified hydrogen needed for the experiments. Purification of helium, used for calibration, was accomplished in a parallel purification train consisting also of a trap, T_2, and a furnace, F_2. Furnaces F_1 and F_2 were operated at 800° whenever

(5) W. M. Albrecht, M. W. Mallett, and W. D. Goode, *J. Electrochem. Soc.*, **105**, 219 (1958); **106**, 981 (1959).

(6) S. Komjathy, *J. Less-Common Metals*, 2, 466 (1960).

(7) O. M. Katz and E. A. Gulbransen, "Columbium Metallurgy," D. L. Douglass and F. W. Kunz, Ed., Interscience Publishers, New York, N. Y., 1961, pp 523–537.

(8) P. Kofstad, W. E. Wallace, and L. J. Hyvönen, *J. Amer. Chem. Soc.*, **81**, 5015 (1959).

(9) M. W. Mallett and B. G. Koehl, *J. Electrochem. Soc.*, **109**, 611 (1962).

purification of either of the gases by gettering action was desired.

The system was evacuated by means of a mechanical forepump and a mercury diffusion pump. The vacuum obtained was generally 5×10^{-6} Torr as read with the aid of a McLeod gauge.

An electric pot furnace was used for heating the liquid bath in which tube C (containing the hydrogen equilibration zone) was submerged. Above 350° lead was used for the bath; for lower temperatures Wood's metal was employed. Pot capacity was about 20 l. The temperature of the bath was controlled so that the temperature of the metal sample was held constant to within 0.5°. A calibrated chromel–alumel thermocouple was used for temperature measurements. It rested against the Vycor tube in the immediate vicinity of the specimen. The thermocouple was frequently recalibrated against tin, lead, zinc, antimony, and silver freezing point standards.

Procedure. A typical run was made as follows. A specimen of metal in foil form was accurately weighed and placed in a small porcelain crucible. The latter, along with the gas displacement rod, E, was enclosed within the Vycor tube, B, which was then attached to an auxiliary apparatus (not shown) and degassed at 800–900° until a vacuum of 10^{-5} Torr was established. Following degassing, the specimen was saturated with hydrogen several times by repeated sorption and desorption. After the final desorption it was quenched *in vacuo* to room temperature by immersion of the Vycor tube in cold water. Pretreated in this manner the metals exhibited distinctly increased absorption rates.

The evacuated reaction tube was then attached to the main apparatus as shown in Figure 1 after the furnace had been heated to the desired temperature. The effective residual volume surrounding the sample (extending to mark *a* of manometer M_1 and stopcock S for the higher pressure measurements or to mark *a* and the variable meniscus level of the left arm of manometer M_2 for the low-pressure measurements) was determined by calibration with helium at each furnace temperature anticipated for the subsequent hydrogen *P–C–T* measurements. For this purpose purified helium was first admitted to the volume G where its pressure and temperature were measured. The gas was then transferred to the residual volume by simultaneously raising the mercury levels in the gas bulb G and in manometer M_1 up to mark *a* in the left arm thus using the apparatus essentially as a Toepler pump.

After the helium was removed, hydrogen (obtained by heating the turnings in furnace F_1) was admitted to the residual volume in a manner similar to that performed in the helium calibration. Equilibrium pressures were measured following each successive addition of hydrogen.

The uptake of hydrogen by the metal specimen was generally quite rapid, but an equilibration interval was allowed before taking pressure readings. The attainment of equilibrium was judged to be complete when the pressure remained constant to within the error of observation for a period of at least 20 min. Tests with longer equilibration times established that this was a reliable criterion. The equilibration periods were, of course, temperature dependent. Thus, for temperatures above 400° equilibrium was achieved within 20 min; at 300°, however, an interval of 2 hr was necessary.

Immediately after the equilibration and measurements following the final hydrogen addition, a "desorption" measurement was carried out as a test of thermodynamic reversibility. This was accomplished by removing a measured amount of hydrogen from the specimen by Toepler pumping and measuring the pressure after the reestablishment of equilibrium.

At the end of the determination of a given pressure *vs.* composition isotherm the Vycor tube was closed off and disconnected from the apparatus by separation at the ball–socket joint. The metal specimen was then completely degassed in the auxiliary apparatus, quenched *in vacuo* to room temperature, and stored in preparation for the determination of another isotherm.

The composition of the solid solution after each successive equilibration (and pressure measurement) could be calculated from the net amount of hydrogen absorbed (or desorbed) and the weight of the metal specimen. Appropriate corrections were made for the gas remaining in the residual volume.

Materials. Niobium (99.8% pure) and tantalum (99.9% pure) were obtained from Fansteel Metallurgical Corp. in the form of cold-rolled foil. The thickness of the niobium foil was 10 mils and of the tantalum foil 5 mils. Vanadium (99.5% pure), refined by the electron-gun process, was supplied in pellet form by the Vanadium Corp. of America; the pellets were flattened to 5–10 mils.

Since, for a given system, a single metal specimen was used for all absorption experiments, accumulation of contaminants from gaseous impurities was a possibility. Therefore, the impurity content was assayed (by means of vacuum fusion analysis) in both the degassed specimens remaining from the experiments and in representative portions of the as-received metals. The results of these analyses, shown in Table I, indicate that the accumulation of impurities was not large.

Before use the metal foils were cut in strips approximately $\frac{1}{8}$ in. wide. Specimen sizes were approximately 2.5 g for vanadium, 5 g for niobium, and 7 g for tantalum.

Results

Presentation of Data. The basic data for each of the three studies are sets of pressure–temperature–com-

Table I: Gas Analysis Results for As-Received (a) and Used (b) Specimens of Vanadium, Niobium, and Tantalum[a]

Sample	Gas content, ppm O_2	N_2	H_2
Vanadium (a)	1360	43	4
(b)	1460	39	2
Niobium (a)	233	0.5	23
(b)	487	5	4
Tantalum (a)	101	6	9
(b)	228	8	9

[a] Vacuum fusion analyses performed by the Chemical Research Services, Inc., Addison, Ill.

position values. Because of the great bulk of data, they are only presented here graphically; however, they are also available in tabular form in a report.[10] The graphs (Figures 2, 3, and 4) consist of families of isotherms projected on the square root[11] of hydrogen pressure *vs.* composition planes. The lines in Figures 2, 3, and 4 result from drawing smooth curves connecting the data points for each set of isothermal measurements. In the temperature ranges studied, all isotherms show monotonic increases of the hydrogen pressure with composition. This indicates that each of the condensed hydrogen–metal systems has only a single homogeneous

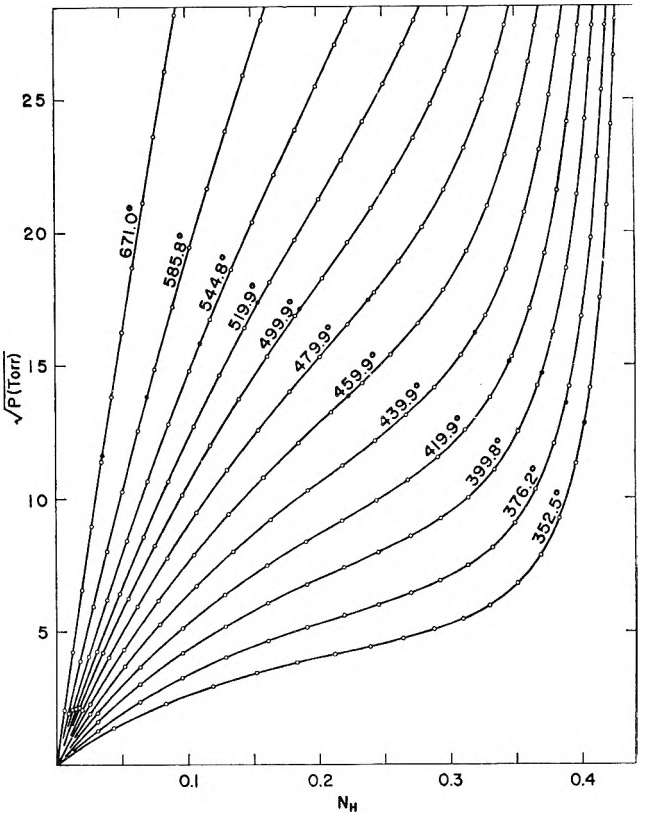

Figure 3. Pressure isotherms for the system Nb–H: O, absorption measurements; ●, desorption measurements.

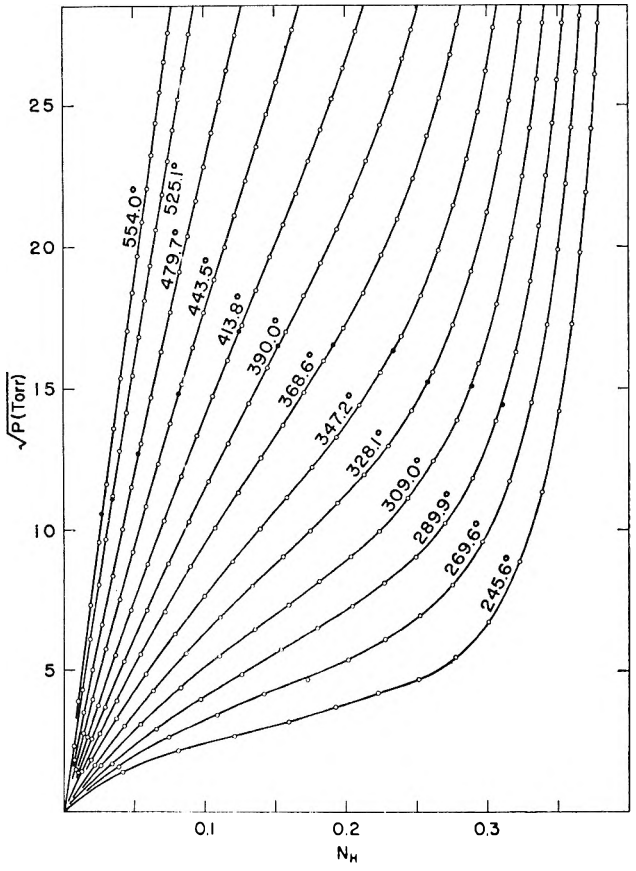

Figure 2. Pressure isotherms for the system V–H: O, absorption measurements; ●, desorption measurements.

phase region. It is evident that with increasing temperatures and the consequent lower solubilities of hydrogen in the metal, the isotherms progressively approach linearity as is expected according to Sieverts' law. On the other hand, the isotherms become progressively more curved with decreasing temperatures in a manner which suggests that at still lower temperatures a miscibility gap would exist in the condensed systems.

The desorption data are also shown in the graphs. No evidence of hysteresis was observed in any case; thus the hydrogen–metal reactions appear to be reversible. Because of the particular apparatus used, the hydrogen pressures were limited within the range 1–800 Torr. The error in the individual pressure measurements was estimated to be ±0.2 Torr.

The relative partial molal entropies and enthalpies were derived from sets of data taken from the smooth curves of Figures 2, 3, and 4 at selected compositions (1 atom % intervals). A least-squares treatment of $\ln \sqrt{P(\text{Torr})} = A + BT^{-1}$ was performed to evaluate for each composition the parameters A and B which

(10) E. Veleckis and R. K. Edwards, Report AFOSR-1107 (available through the Clearinghouse for Federal Scientific and Technical Information, U. S. Department of Commerce, Springfield, Va., as AD-282433). This report is essentially identical with ref 1.

(11) At lower hydrogen concentrations it is generally expected that Sieverts' law is obeyed *i.e.*, $\sqrt{P}/N_H$ = constant, where P is the hydrogen pressure and N_H is the atom fraction of hydrogen. This form of plotting is convenient since any nonlinearity of the plots provides a ready measure of the extent to which the solution deviates from Sieverts' law.

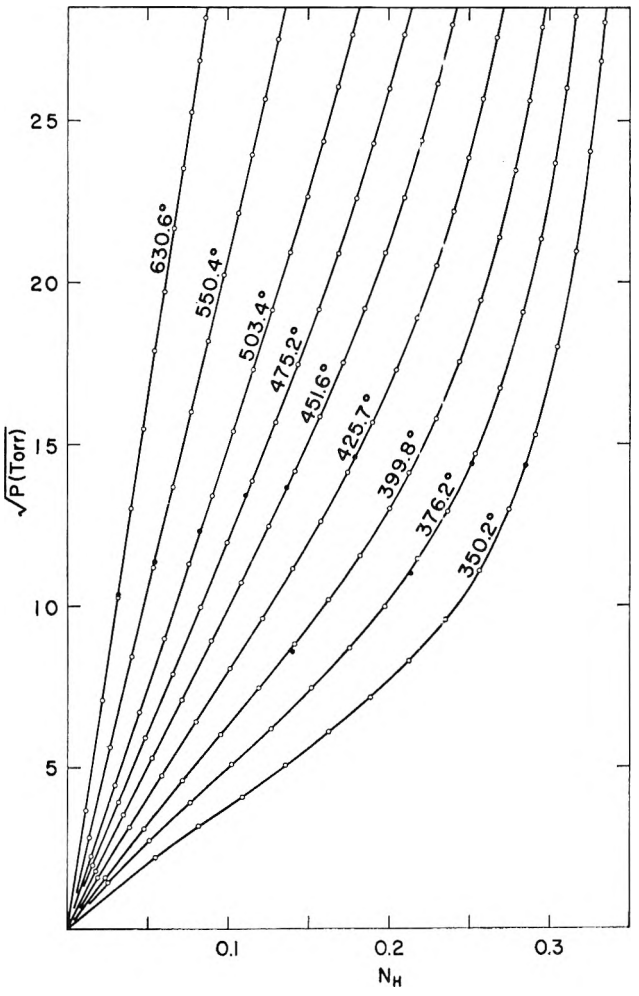

Figure 4. Pressure isotherms for the system Ta–H: ○, absorption measurements; ●, desorption measurements.

yield, respectively, the relative partial molal entropy $(\bar{S}_H - {}^1/_2S^\circ_{H_2}) = R(\ln\sqrt{760} - A)$ and enthalpy $(\bar{H}_H - {}^1/_2H^\circ_{H_2}) = RB$ for atomic hydrogen. The corresponding integral quantities were derived, *via* the Gibbs–Duhem relation, from the relative partial molal quantities for hydrogen by a graphical evaluation of the integral[12]

$$\Delta X_f = N_M \int_0^{N_H/N_M} (\bar{X}_H - \tfrac{1}{2}X^\circ_{H_2})\mathrm{d}(N_H/N_M) \quad (1)$$

Here, ΔX_f (X = S, H) is the entropy (or enthalpy) of formation of one gram-atom of solid solution at atom fraction N_H from the solid metal and gaseous diatomic hydrogen (as an ideal gas) at a pressure of 1 atm; likewise $(\bar{X}_H - {}^1/_2X^\circ_{H_2})$ is the partial molal entropy (or enthalpy) of hydrogen atoms relative to gaseous diatomic hydrogen at 1 atm.

To handle the familiar problem of integration of the entropy from the infinite dilution limit, Sieverts' law for hydrogen (and consequently Raoult's law for metal) was assumed to be applicable for the composition interval $N_H \leq 0.01$. Therefore, the contribution to the entropy of formation in the interval $N_H = 0$ to $N_H = 0.01$ was taken to be $z(\bar{S}_H - {}^1/_2S^\circ_{H_2})_z + R \ln (1 + z)$, where z is the value of N_H/N_M at $N_H = 0.01$, and $(\bar{S}_H - {}^1/_2S^\circ_{H_2})_z$ is the particular value of the relative partial molal entropy of hydrogen at the concentration represented by z.

The use of Sieverts' law at compositions $N_H \leq 0.01$ is subject to some question since more detailed plots than those shown in Figures 2, 3, and 4 indicate that at the lower temperatures appreciable deviations from Sieverts' law occur even in this composition range.[13] To assess the possible error resulting from the Sieverts' law assumption, an alternative evaluation of $(\bar{S}_M - S^\circ_M)_z$ was carried out using data derived from a linear extrapolation to $N_H = 0$ (with the slope corresponding to that at the last observed point) of $\sqrt{P}/N$ *vs.* N_{HH} plots. The discrepancy between the results for the two cases was <5%, *i.e.*, well within the experimental error. Thus, barring extraordinary deviations in the region of extrapolation, the Sieverts' law assumption seems to be adequate.

The relative partial and integral entropies and enthalpies for the three systems are listed as a function of composition at 1 atom % intervals in Tables II and III. The assigned errors are the 95% confidence limits.

The partial molal entropy and enthalpy of the metal relative to pure solid metal $(\bar{X}_M - X^\circ_M)$ are not listed since they can be readily calculated from the corresponding partial quantities for hydrogen and the derived (eq 1) integral quantities by use of eq 2

$$\Delta X_f = N_H(\bar{X}_H - {}^1/_2X^\circ_{H_2}) + N_M(\bar{X}_M - X^\circ_M) \quad (2)$$

The results from this study are discussed below along with other work in the literature. The quality of experimentation in metal–hydrogen systems has improved in recent years to a level which merits a detailed comparison among related investigations. For the three systems studied comparisons are made in Figure 5 where the relative partial molal entropies, enthalpies (both taken as invariant with temperature), and free energies (calculated from the first two quantities for the arbitrary temperature, 400°) are plotted against composition. Only those studies which are readily amenable to the extraction of thermodynamic results were used in the comparison.

V–H System. The data for the 13 isotherms (246–554°) measured in the V–H system are shown in Figure 2. The thermodynamic data are summarized in Tables IIa and IIIa. The results are in good agreement (see Figure 5a) with those obtained by Kofstad and Wallace,[4] whose experiments were performed using vanadium of comparable purity. The free energy

(12) See, *e.g.* (a) O. Kubaschewski, E. L. Evans, and C. B. Alcock, "Metallurgical Thermochemistry," Pergamon Press, Oxford, 4th ed, 1967, p 43 or (b) G. G. Libowitz, "The Solid-State Chemistry of Binary Metal Hydrides," W. A. Benjamin, Inc., New York, N. Y., 1965, Chapter 4.

(13) This observation supports the earlier findings of "complex behavior in dilute solutions" by Kofstad, *et al.*, for the Ta–H[8] and V–H[4] systems.

Table II: Entropy Data in the Systems V–H, Nb–H, and Ta–H

	(a) V–H		(b) Nb–H		(c) Ta–H	
$100N_H$	$-[\bar{S}_H - \frac{1}{2}S°_{H_2}]$, cal/deg g-atom of H	$-\Delta S_f$, cal/deg g-atom	$-[\bar{S}_H - \frac{1}{2}S°_{H_2}]$, cal/deg g-atom of H	$-\Delta S_f$, cal/deg g-atom	$-[S_H - \frac{1}{2}S°_{H_2}]$, cal/deg g-atom of H	$-\Delta S_f$, cal/deg g-atom
0	$-\infty$	0	$-\infty$	0	$-\infty$	0
1	4.33 ± 0.22	0.023 ± 0.002	4.91 ± 0.21	0.030 ± 0.001	4.74 ± 0.26	0.030 ± 0.003
2	5.94 ± 0.16	0.074 ± 0.003	6.36 ± 0.09	0.086 ± 0.002	6.16 ± 0.20	0.082 ± 0.005
3	6.89 ± 0.15	0.139 ± 0.004	7.18 ± 0.05	0.154 ± 0.003	7.08 ± 0.26	0.149 ± 0.007
4	7.54 ± 0.13	0.211 ± 0.005	7.77 ± 0.06	0.229 ± 0.004	7.70 ± 0.24	0.224 ± 0.009
5	8.07 ± 0.08	0.291 ± 0.006	8.23 ± 0.06	0.311 ± 0.005	8.20 ± 0.22	0.304 ± 0.010
6	8.50 ± 0.06	0.375 ± 0.007	8.61 ± 0.07	0.396 ± 0.005	8.62 ± 0.19	0.389 ± 0.011
7	8.89 ± 0.05	0.463 ± 0.007	8.99 ± 0.07	0.485 ± 0.006	8.99 ± 0.18	0.479 ± 0.013
8	9.21 ± 0.05	0.556 ± 0.008	9.30 ± 0.07	0.579 ± 0.006	9.31 ± 0.16	0.572 ± 0.015
9	9.51 ± 0.05	0.652 ± 0.009	9.60 ± 0.07	0.675 ± 0.007	9.62 ± 0.12	0.669 ± 0.016
10	9.77 ± 0.06	0.751 ± 0.010	9.92 ± 0.07	0.775 ± 0.008	9.93 ± 0.14	0.769 ± 0.018
11	10.00 ± 0.07	0.852 ± 0.011	10.17 ± 0.07	0.878 ± 0.008	10.21 ± 0.12	0.872 ± 0.020
12	10.25 ± 0.07	0.956 ± 0.011	10.38 ± 0.06	0.984 ± 0.009	10.43 ± 0.11	0.978 ± 0.021
13	10.45 ± 0.08	1.06 ± 0.01	10.59 ± 0.05	1.09 ± 0.01	10.64 ± 0.13	1.09 ± 0.02
14	10.67 ± 0.08	1.17 ± 0.01	10.79 ± 0.05	1.20 ± 0.01	10.81 ± 0.14	1.20 ± 0.03
15	10.88 ± 0.08	1.28 ± 0.01	10.99 ± 0.05	1.31 ± 0.01	10.98 ± 0.17	1.31 ± 0.03
16	11.10 ± 0.08	1.40 ± 0.01	11.16 ± 0.05	1.43 ± 0.01	11.17 ± 0.17	1.42 ± 0.03
17	11.26 ± 0.11	1.51 ± 0.02	11.34 ± 0.06	1.55 ± 0.01	11.36 ± 0.18	1.54 ± 0.03
18	11.43 ± 0.12	1.63 ± 0.02	11.53 ± 0.07	1.66 ± 0.01	11.57 ± 0.18	1.66 ± 0.03
19	11.59 ± 0.13	1.75 ± 0.02	11.69 ± 0.07	1.79 ± 0.01	11.74 ± 0.26	1.78 ± 0.04
20	11.77 ± 0.13	1.88 ± 0.02	11.84 ± 0.05	1.91 ± 0.01	11.94 ± 0.25	1.91 ± 0.04
21	11.94 ± 0.12	2.00 ± 0.02	12.02 ± 0.05	2.04 ± 0.01	12.13 ± 0.17	2.04 ± 0.04
22	12.14 ± 0.19	2.13 ± 0.02	12.18 ± 0.05	2.16 ± 0.02	12.32 ± 0.23	2.16 ± 0.05
23	12.31 ± 0.14	2.26 ± 0.02	12.37 ± 0.06	2.29 ± 0.02	12.56 ± 0.21	2.30 ± 0.05
24	12.55 ± 0.15	2.39 ± 0.03	12.53 ± 0.07	2.42 ± 0.02	12.84 ± 0.14	2.43 ± 0.05
25	12.78 ± 0.18	2.52 ± 0.03	12.68 ± 0.09	2.56 ± 0.02	13.05 ± 0.18	2.57 ± 0.08
26	13.02 ± 0.30	2.66 ± 0.03	12.83 ± 0.09	2.69 ± 0.02	13.24 ± 0.27	2.71 ± 0.08
27	13.28 ± 0.34	2.80 ± 0.04	12.99 ± 0.09	2.83 ± 0.02	13.42 ± 0.36	2.85 ± 0.08
28	13.47 ± 0.30	2.95 ± 0.04	13.13 ± 0.10	2.97 ± 0.02	...	...
29	13.64 ± 0.39	3.10 ± 0.05	13.32 ± 0.12	3.11 ± 0.02	...	...
30	13.80 ± 0.39	3.24 ± 0.06	13.51 ± 0.12	3.26 ± 0.02	...	...
31	13.90 ± 0.34	3.40 ± 0.06	13.70 ± 0.11	3.41 ± 0.02	...	...
32	14.05 ± 0.34	3.55 ± 0.07	13.92 ± 0.15	3.56 ± 0.03	...	...
33	14.17 ± 0.68	3.70 ± 0.10	14.13 ± 0.15	3.71 ± 0.03	...	...
34	14.44 ± 0.39	3.86 ± 0.11	14.36 ± 0.20	3.87 ± 0.03	...	...
35	...	...	14.56 ± 0.26	4.03 ± 0.04	...	...
36	...	...	14.80 ± 0.19	4.19 ± 0.04	...	...
37	...	...	15.03 ± 0.22	4.36 ± 0.05	...	...
38	...	...	15.28 ± 0.15	4.53 ± 0.05	...	...
39	...	...	15.58 ± 0.23	4.71 ± 0.07	...	...

curves of both studies superimpose throughout the entire composition range although the entropy and enthalpy curves diverge beyond the experimental error below $N_H \cong 0.15$.

Nb–H System. The twelve isotherms obtained for the niobium–hydrogen system in the temperature range 352–671° are represented in Figure 3. The thermodynamic data are listed in Tables IIb and IIIb.

The detailed comparison of the thermodynamic results of this study with other work reported[5–7] is made in Figure 5b. The free energy data are in excellent agreement with those of Katz and Gulbransen[7] and the generally good agreement with the data of Albrecht, *et al.*,[5] over most of the composition range becomes excellent at the more dilute concentrations.

The agreement in the entropies and enthalpies among these three studies is also quite satisfactory although the values obtained by Albrecht, *et al.*, do not quite fall within the combined error limits. The results of Katz and Gulbransen, which are in excellent agreement with this work over most of the composition range, show divergence at compositions $N_H \leq 0.07$. For instance, in this range, their $(\bar{H}_H - \frac{1}{2}H°_{H_2})$ *vs.* N_H plot shows an abrupt change in slope. No such change was observed either by us or by Albrecht, *et al.*,

Table III: Enthalpy Data in the Systems V–H, Nb–H, and Ta–H

	(a) V–H		(b) Nb–H		(c) Ta–H	
$100N_H$	$-[\bar{H}_H - \frac{1}{2}H^\circ_{H_2}]$, kcal/g-atom of H	$-\Delta H_f$, kcal/g-atom	$-[\bar{H}_H - \frac{1}{2}H^\circ_{H_2}]$, kcal/g-atom of H	$-\Delta H_f$, kcal/g-atom	$-[\bar{H}_H - \frac{1}{2}H^\circ_{H_2}]$, kcal/g-atom of H	$-\Delta H_f$, kcal/g atom
0	6.93 ± 0.13	0	8.44 ± 0.14	0	8.05 ± 0.19	0
1	7.00 ± 0.14	0.070 ± 0.001	8.57 ± 0.15	0.085 ± 0.001	8.11 ± 0.18	0.081 ± 0.001
2	7.03 ± 0.10	0.140 ± 0.002	8.65 ± 0.06	0.171 ± 0.002	8.15 ± 0.14	0.162 ± 0.002
3	7.15 ± 0.10	0.211 ± 0.003	8.69 ± 0.04	0.258 ± 0.002	8.25 ± 0.18	0.244 ± 0.004
4	7.23 ± 0.08	0.283 ± 0.004	8.73 ± 0.04	0.345 ± 0.003	8.30 ± 0.18	0.327 ± 0.006
5	7.32 ± 0.05	0.356 ± 0 004	8.78 ± 0.04	0.432 ± 0.003	8.36 ± 0.16	0.410 ± 0.008
6	7.38 ± 0.04	0.429 ± 0 005	8.81 ± 0.05	0.520 ± 0.003	8.41 ± 0.14	0.494 ± 0.009
7	7.46 ± 0.03	0.504 ± 0.005	8.90 ± 0.05	0.609 ± 0.004	8.47 ± 0.13	0.579 ± 0.010
8	7.52 ± 0.04	0.579 ± 0.006	8.97 ± 0.05	0.699 ± 0.005	8.52 ± 0.12	0.664 ± 0.012
9	7.58 ± 0.03	0.654 ± 0.006	9.04 ± 0.05	0.789 ± 0.005	8.58 ± 0.09	0.750 ± 0.013
10	7.61 ± 0.05	0.731 ± 0.006	9.15 ± 0.05	0.880 ± 0.006	8.66 ± 0.10	0.836 ± 0.014
11	7.68 ± 0.05	0.807 ± 0.007	9.22 ± 0.05	0.973 ± 0.006	8.72 ± 0.08	0.924 ± 0.016
12	7.75 ± 0.04	0.885 ± 0.006	9.28 ± 0.04	1.06 ± 0.007	8.76 ± 0.08	1.01 ± 0.02
13	7.79 ± 0.05	0.963 ± 0.009	9.34 ± 0.04	1.16 ± 0.01	8.80 ± 0.09	1.10 ± 0.02
14	7.85 ± 0.05	1.04 ± 0.01	9.41 ± 0.04	1.25 ± 0.01	8.81 ± 0.09	1.19 ± 0.02
15	7.91 ± 0.05	1.12 ± 0.01	9.48 ± 0.04	1.35 ± 0.01	8.82 ± 0.12	1.28 ± 0.02
16	7.98 ± 0.05	1.20 ± 0.01	9.54 ± 0.04	1.44 ± 0.01	8.86 ± 0.12	1.36 ± 0.02
17	8.02 ± 0.06	1.28 ± 0.01	9.61 ± 0.04	1.54 ± 0.01	8.90 ± 0.13	1.45 ± 0.02
18	8.06 ± 0.08	1.36 ± 0.01	9.69 ± 0.05	1.64 ± 0.01	8.96 ± 0.13	1.54 ± 0.02
19	8.10 ± 0.07	1.45 ± 0.01	9.74 ± 0.05	1.74 ± 0.01	8.99 ± 0.18	1.64 ± 0.03
20	8.14 ± 0.08	1.53 ± 0.01	9.80 ± 0.04	1.84 ± 0.01	9.03 ± 0.17	1.73 ± 0.03
21	8.19 ± 0.07	1.61 ± 0.01	9.88 ± 0.04	1.94 ± 0.01	9.07 ± 0.12	1.82 ± 0.03
22	8.25 ± 0.11	1.70 ± 0.01	9.95 ± 0.04	2.04 ± 0.01	9.11 ± 0.16	1.91 ± 0.04
23	8.30 ± 0.09	1.78 ± 0.02	10.04 ± 0.04	2.14 ± 0.01	9.18 ± 0.14	2.00 ± 0.04
24	8.38 ± 0.09	1.86 ± 0.02	10.11 ± 0.05	2.24 ± 0.01	9.28 ± 0.09	2.10 ± 0.04
25	8.45 ± 0.10	1.95 ± 0.02	10.18 ± 0.06	2.35 ± 0.01	9.32 ± 0.11	2.19 ± 0.05
26	8.52 ± 0.18	2.04 ± 0.02	10.23 ± 0.06	2.45 ± 0.01	9.34 ± 0.18	2.29 ± 0.05
27	8.59 ± 0.19	2.13 ± 0.02	10.30 ± 0.06	2.56 ± 0.01	9.34 ± 0.24	2.38 ± 0.06
28	8.62 ± 0.17	2.22 ± 0.02	10.35 ± 0.07	2.66 ± 0.02	...	...
29	8.62 ± 0.22	2.30 ± 0.03	10.44 ± 0.08	2.77 ± 0.02	...	...
30	8.61 ± 0.22	2.39 ± 0.03	10.52 ± 0.08	2.88 ± 0.02	...	...
31	8.64 ± 0.19	2.48 ± 0.04	10.59 ± 0.08	2.99 ± 0.02	...	...
32	8.49 ± 0.19	2.57 ± 0.04	10.68 ± 0.11	3.10 ± 0.02	...	...
33	8.40 ± 0.38	2.66 ± 0.06	10.75 ± 0.11	3.21 ± 0.02	...	...
34	8.39 ± 0.22	2.74 ± 0.06	10.83 ± 0.14	3.32 ± 0.02	...	...
35	...	...	10.87 ± 0.18	3.44 ± 0.03	...	...
36	...	...	10.92 ± 0.12	3.55 ± 0.03	...	...
37	...	...	10.95 ± 0.15	3.67 ± 0.04	...	...
38	...	...	10.97 ± 0.10	3.78 ± 0.04	...	...
39	...	...	10.98 ± 0.15	3.90 ± 0.05	...	...

and the conclusion of Katz and Gulbransen that the change in M–H bond strength is "larger for the first small additions of hydrogen" does not seem to be warranted.

Ta–H System. The nine isotherms obtained for the tantalum–hydrogen system in the temperature range 350–631° are represented in Figure 4. The thermodynamic data are listed in Tables IIc and IIIc.

Comparison of the thermodynamic results of this study with those of other work is made in Figure 5c. The free energy data of Kofstad, *et al.*,[8] and of Mallett and Koehl[9] are in excellent agreement with ours. The entropy and enthalpy data of the twc studies diverge from ours beyond the experimental error. Since the divergence is in opposite directions, our values are probably to be preferred.

Discussion

In the simplest of the several theoretical models[14] which have been used to describe metal–hydrogen systems, it is assumed that hydrogen atoms form solutions by entering interstitial positions within a perfect metal lattice.[15] This assumption may be adequate for the systems V–H, Nb–H, and Ta–H (as well as Pd–H) since in these cases the hydrided materials have the

(14) See, *e.g.*, G. G. Libowitz, *J. Nucl. Mat.*, **2**, 1 (1960).
(15) A. L. G. Rees, *Trans. Faraday Soc.*, **50**, 335 (1954).

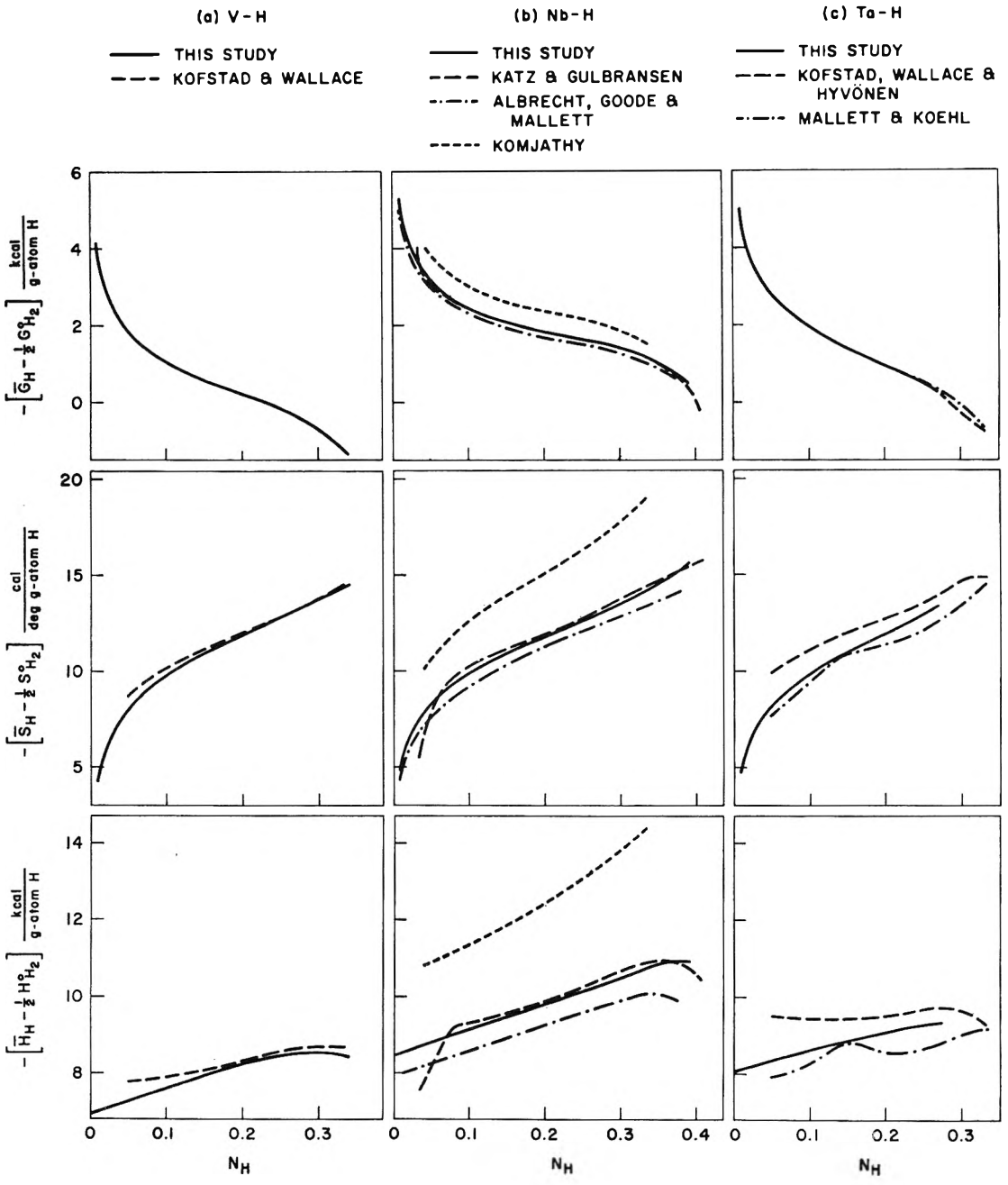

Figure 5. Comparison of thermodynamic data with literature values for the systems V–H, Nb–H, and Ta–H. The free energies are calculated for 400°.

same crystal structures as their parent metals. Nmr studies[16] of tantalum and vanadium hydrides have been interpreted[17] as indicating that hydrogen atoms are quite mobile within the lattice as would be appropriate for solution behavior. Thus this simple model was chosen to provide a mathematical framework for extrapolation of data toward lower temperatures where phase diagram features might be revealed.

According to the model chosen, the P–C–T relationships can be represented by eq 3[15,18]

$$\sqrt{P} = K[r/(s - r)]\exp[(1/RT) \times (\partial/\partial r)(W + \tfrac{1}{2}rD_0)] \quad (3)$$

where P is the hydrogen pressure, r is the H/M atom ratio, s is the number of sites available for hydrogen atoms in the metal lattice per metal atom, W is the energy of hydrogen atoms dissolved in 1 gram-atom of metal with the reference state taken as that of free hydrogen atoms at rest, D_0 is the dissociation energy of the hydrogen molecule in the ground state, and K is a

(16) R. A. Oriani, E. McCliment, and J. F. Youngblood, *J. Chem. Phys.*, 27, 330 (1957).

(17) K. M. Mackay, "Hydrogen Compounds of the Metallic Elements," E. and F. N. Spon, Ltd., London, 1966, p 48.

(18) R. H. Fowler and E. A. Guggenheim, "Statistical Thermodynamics," The University Press, Cambridge, 1956, Chapter XIII.

slowly varying function of temperature generally assumed to be constant over the temperature ranges involved.

Equation 3 being an equivalent form of the expression for the relative partial molal free energy of hydrogen, $(\bar{G}_H - {}^1/_2 G^\circ_{H_2}) = RT \ln \sqrt{P}$, can be conveniently separated into its entropy and enthalpy components

$$(\bar{S}_H - \tfrac{1}{2}S^\circ_{H_2}) = -R\{\ln K + \ln [r/(s-r)]\} \quad (4)$$

$$(\bar{H}_H - \tfrac{1}{2}H^\circ_{H_2}) = (\partial/\partial r)(W + (r/2)D_0) \quad (5)$$

From the observed entropy data (Table II), the values of parameters K and s were computed by the Newton–Raphson successive approximation method[19] in which assumed values were statistically adjusted to provide the best fit to eq 4. For the analysis of the relative partial molal enthalpy, eq 5 was expressed as

$$(\bar{H}_H - \tfrac{1}{2}H^\circ_{H_2}) = \sum_{i=0}^{i=4} A_i r^i \quad (6)$$

where A_i's are the interaction energy parameters. A quartic polynomial was required to fit the enthalpy data (Table III) adequately, although, in the case of the Pd–H system polynomials of only two[20] or three[21] terms have proven to be satisfactory. Calculated values of the parameters K, s, and A_i are listed in Table IV.

Table IV: Parameters of Eq 7 and Critical Constants in the Systems V–H, Nb–H, and Ta–H

	V–H	Nb–H	Ta–H
K, atm$^{1/2}$	801	1024	760
s	0.779	0.904	0.702
A_0, cal/g-atom of H	-6.93×10^3	-8.43×10^3	-8.05×10^3
A_1, cal/g-atom of H	-6.50×10^3	-7.95×10^3	-6.62×10^3
A_2, cal/g-atom of H	5.09×10^3	1.76×10^4	1.66×10^4
A_3, cal/g-atom of H	-1.51×10^3	-3.84×10^4	-3.39×10^4
A_4, cal/g-atom of H	9.57×10^3	3.22×10^4	3.37×10^4
r_c	0.21	0.37	0.20
t_c, °C	51	183	−59
P_c, Torr	9.0×10^{-4}	5.2×10^{-2}	4.2×10^{-11}

Combination of eq 3, 5, and 6 gives the semiempirical equation

$$\sqrt{P} = K[r/(s-r)] \exp\left[\frac{1}{RT}\sum_{i=0}^{i=4} A_i r^i\right] \quad (7)$$

where P is the hydrogen pressure in atmospheres and R, the gas constant, is 1.987 cal/deg g-atom of H. With the listed parameters it permits the calculation of the P–C–T relationships for the systems V–H, Nb–H, and Ta–H for the temperature and composition range of the experiments. The families of isotherms in Figures 2, 3, and 4 can be reproduced generally within ~3% and with a maximum discrepancy of ~10% in P except for the steepest portions of the two lowest temperature isotherms in the V–H system where the error reaches ~20%. It seems reasonable that eq 7 will retain its validity to both higher and lower temperatures.

The equation was therefore used to extend the P–C–T relations to lower temperatures where hydrogen pressure measurements are impractical. The critical compositions, temperatures, and pressures were calculated (also listed in Table IV) from eq 7 and from the two additional equations that characterize the critical

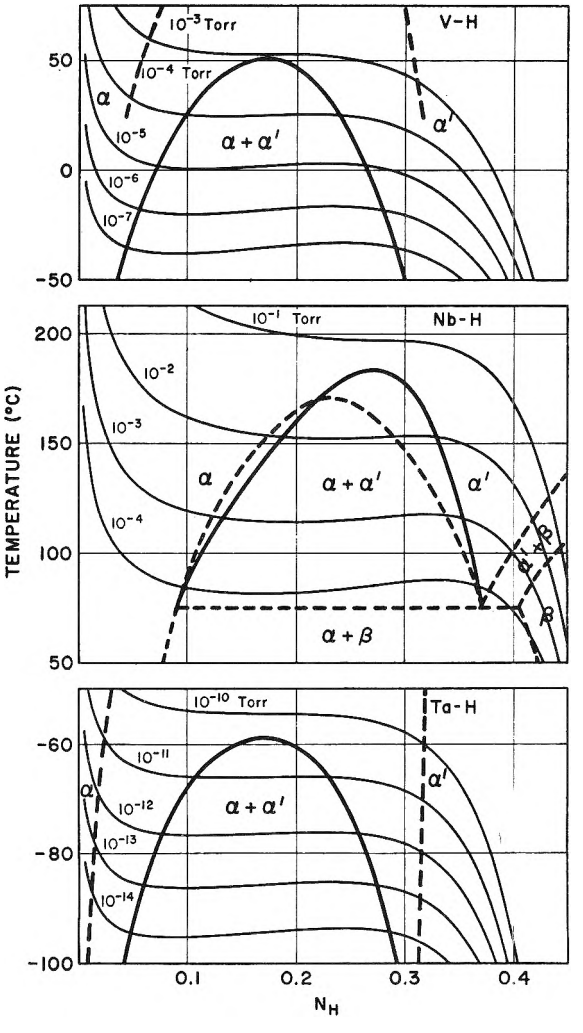

Figure 6. Phase diagrams and isobars for the systems V–H, Nb–H, and Ta–H: ——, calculated from eq 7; — — —, from 25, 24, and 26, respectively.

(19) J. B. Scarborough, "Numerical Mathematical Analysis," 4th ed, The Johns Hopkins Press, Baltimore, Md., 1958.

(20) J. R. Lacher, *Proc. Roy. Soc.*, A161, 525 (1937). Lacher used $W = -E_H r - (E_{HH}/s)r^2$, where E_H is the molal energy of hydrogen atoms and E_{HH} is the nearest-neighbor molal interaction energy. Substitution of this expression into eq 3 gives what is widely known as Lacher's formula.

(21) A Harasima, T. Tanaka, and K. Sakaoku, *J. Phys. Soc. Jap.*, **3**, 208 (1948).

point, *i.e.*

$$[(\partial \ln \sqrt{P})/\partial r]_{T_c} = 0; \quad [(\partial^2 \ln \sqrt{P}/\partial r^2)]_{T_c} = 0 \quad (8)$$

Comparison of these critical constants with those from another evaluation (Albrecht, *et al.*[5]) can be made for the case of Nb–H systems. These investigators used both X-ray and hydrogen pressure data to obtain $r_c = 0.3$, $t_c = 140°$, and $P_c = 0.01$ Torr with which our results are in good agreement.

Equation 7 was also used to estimate the boundaries of the region in which the metal phase, α, coexists at equilibrium with the hydride phase, α'. Throughout this region the hydrogen pressure isotherms derived from eq 7 assume sigmoidal shapes characteristic[22] of phase instability. For the systems at equilibrium the sigmoid regions must, of course, be replaced by horizontal lines. These were evaluated by making use of the equal area rule.[23] The terminal intersections of the horizontal lines with the derived isotherms define the boundaries of the $(\alpha + \alpha')$ coexistence regions. The conventional temperature *vs.* composition diagrams (*i.e.*, projections of the boundary points on the t *vs.* N_H plane) constructed by this method are shown in Figure 6. Also shown are some representative isobars as calculated from eq 7.

For the Nb–H system a complete phase diagram was recently determined by Walter and Chandler[24] by hot-stage X-ray diffraction and differential thermal analysis. Their diagram is shown for comparison in Figure 6 (dashed lines). Except for minor discrepancies at the higher temperatures, there is exceptionally good agreement between our calculated and their experimental boundaries in the $(\alpha + \alpha')$ region. A more complicated theoretical model, such as that proposed by Rees,[15] subdividing the sites available for hydrogen occupancy into statistical classes, would have been required to have provided an adequate framework for an equation capable of predicting the second two-phase field $(\alpha' + \beta)$. The isobars sketched in Figure 6 in the $(\alpha + \beta)$, $(\alpha' + \beta)$, and β-phase regions are invalid since the existence of the β phase was not recognized by the model used.

Directly determined phase diagrams for the V–H and Ta–H systems are not well defined, but those available are shown in Figure 6 (dashed lines) for comparison. The tentative diagram obtained from X-ray diffraction studies at temperature has been presented by Maeland[25] for the V–H system. The two-phase region predicted by our calculations is confirmed by Maeland's diagram although the agreement of the boundary compositions is not good. For the Ta–H system Waite, Wallace, and Craig[26] have constructed a composite phase diagram using the heat capacity data of Kelley[27] and their own X-ray diffraction and electrical resistance results. Here again the two-phase field which we predict is confirmed but the agreement of the boundary compositions is poor.

A comment is in order on the magnitude of the parameter s. The values listed in Table IV do not necessarily represent actual solubility limits as might be inferred from eq 7. Higher hydrogen concentrations have been obtained by use of more severe hydriding conditions.[28] The implication in eq 7 results from the simplicity of the model used.

Acknowledgments. Financial support of the ONR and AFOSR during the course of this study is gratefully acknowledged. The authors wish to thank the Chemical Engineering Division of Argonne National Laboratory for the support during the preparation of the manuscript.

(22) Reference 18, p 558.

(23) Reference 18, p 315.

(24) R. J. Walter and W. T. Chandler, *Trans. Met. Soc. AIME*, **233**, 762 (1965).

(25) A. J. Maeland, *J. Phys. Chem.*, **68**, 2197 (1964).

(26) T. R. Waite, W. E. Wallace, and R. S. Craig, *J. Chem. Phys.*, **24**, 634 (1956).

(27) K. K. Kelley, *ibid.*, **8**, 316 (1940).

(28) A. J. Maeland, T R. Gibb, Jr., and D. P. Schumacher, *J. Amer. Chem. Soc.*, **83**, 3728 (1961).

Radiative and Radiationless Processes in Aromatic Molecules. Coronene and Benzcoronene[1]

by William R. Dawson and John L. Kropp

Chemical Sciences Department, TRW Systems, Redondo Beach, California *(Received August 2, 1968)*

The lifetimes of fluorescence and phosphorescence as well as the quantum yields of fluorescence, phosphorescence, and triplet formation have been measured at temperatures between −196 and 23° for samples of coronene-h_{12}, coronene-d_{12}, and benzcoronene in poly(methyl methacrylate). The rate constants for radiationless and radiative deactivation of the lowest excited singlet and triplet states S_1 and T_1 have been calculated from the lifetimes and quantum yields. The rate constants for radiative deactivation of both S_1 and T_1 are constant between −196 and 23° for coronene-h_{12}, coronene-d_{12}, and benzcoronene. Rates of intersystem crossing from S_1 to T_1 are also insensitive to variation of temperature. The radiative rate constants for depopulation of T_1 are the same for coronene-h_{12} and coronene-d_{12} but the radiative rate constant for depopulation of S_1 is 7% higher for coronene-h_{12} than for coronene-d_{12}. No significant radiationless deactivation of S_1 directly to the ground state has been found for coronene-h_{12} or coronene-d_{12} between −196 and 23°. However, in the case of benzcoronene direct radiationless deactivation of S_1 to the ground level does occur at 23° but not at −196°. This is associated with the decrease of the fluorescence lifetime of benzocoronene with increasing temperature. An activation energy of 514 cm^{-1} for radiationless deactivation of S_1 can be obtained from the fluorescence lifetimes.

Introduction

Processes by which molecules relax from their excited states are of great interest. Models and theories to explain the radiative and radiationless internal conversion processes in aromatic molecules have been postulated.[2-4] Accurate specific rates of the various processes may be useful in testing these various theories of radiationless transitions. What are needed to calculate the various specific rates are measurements of the fluorescence yield, Φ_F, the phosphorescence yield, Φ_P, the triplet yield, Φ_T, the fluorescence lifetime, τ_F, and the phosphorescence lifetime, τ_P.

We have developed techniques for measuring these parameters as a function of temperature and thus determining the variation of specific rates as temperature is varied. Initially, coronene-h_{12}, coronene-d_{12}, and benzcoronene dissolved in poly(methyl methacrylate) (PMM) have been studied. We had originally studied delayed fluorescence in coronene-h_{12} and coronene-d_{12}.[5] In that work we assumed that Φ_F was constant with temperature. It was desirable to check this assumption experimentally. We were also interested in studying radiationless processes as a function of temperature. Coronene has a long singlet and triplet lifetime and a large phosphorescence yield, hence it is a convenient compound for these studies also. Benzcoronene was also studied to compare results with those obtained for coronene. PMM was chosen as a matrix since it has no first-order phase transitions between −196 and 100°. Thus it presents a relatively stable environment to the aromatic hydrocarbon.

Determination of Rate Constants

Figure 1 shows the energy level diagram for a typical hydrocarbon. The paths of radiative and radiationless deactivation of the lowest excited singlet S_1 and the lowest triplet T_1 are given together with the rate constants. In Figure 1, k_1 is the rate constant for fluorescence, k_2 that for deactivation of S_1 directly to ground, and k_3 that for intersystem crossing from S_1 to T_1; k_4 is the rate constant for triplet emission and k_5 the rate constant for radiationless deactivation of the triplet. The following equations give the relation of the measured parameters to the rate constants determined.

$$\Phi_F = (k_1 + k_2 + k_3)^{-1}; \quad \tau_P = (k_4 + k_5)^{-1}$$

$$\Phi_F = k_1\tau_F; \quad \Phi_T = k_3\tau_F; \quad \Phi_P = k_4\Phi_T\tau_P$$

The individual rate constants can be separated from the above relations so that they can be evaluated from measured parameters.[6]

$$k_1 = \Phi_F\tau_F^{-1} = 1/\tau_{F,0} \tag{1}$$

$$k_2 = (1 - \Phi_F - \Phi_T)\tau_F^{-1} \tag{2}$$

$$k_3 = \tau_F\Phi_T^{-1} \tag{3}$$

$$k_4 = \Phi_P\Phi_T^{-1}\tau_P^{-1} = 1/\tau_{P,0} \tag{4}$$

$$k_5 = (1 - \Phi_P\Phi_T^{-1})\tau_P^{-1} \tag{5}$$

where $\tau_{F,0}$ and $\tau_{P,0}$ are the radiative lifetimes, respectively, of phosphorescence and fluorescence.

By using these equations together with the observed

(1) Supported by the Office of Naval Research under Contract NOOO14-67-CO327.

(2)(a) G. W. Robinson and R. P. Frosch, *J. Chem. Phys.*, **38**, 1187 (1963); (b) M. Gouterman, *ibid.*, **36**, 2846 (1952).

(3) E. F. McCoy and I. G. Ross, *Aust. J. Chem.*, **15**, 573 (1962); G. R. Hunt, E. F. McCoy, and I. G. Ross, *ibid.*, **15**, 591(1962).

(4) S. H. Lin, *J. Chem. Phys.*, **44**, 3759 (1966).

(5) J. L. Kropp and W. R. Dawson, *J. Phys. Chem.*, **71**, 4499 (1967).

(6) M. W. Windsor and W. R. Dawson, *Mol. Cryst.* **4**, 253 (1968).

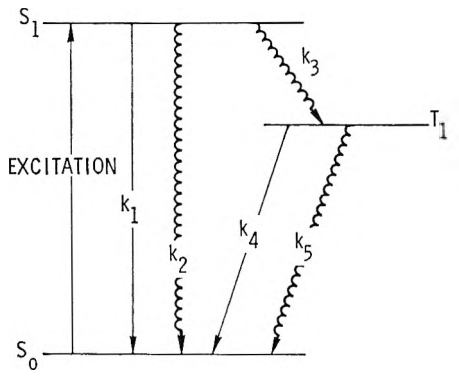

Figure 1. State diagram of aromatic molecules and the first-order rate constants for deactivation of the lowest excited singlet and triplet states, S_1 and T_1.

values for the parameters, the various rate constants can be determined.

Experimental Section

Materials and Sample Preparation. The purity of coronene-h_{12} and of coronene-d_{12} used were the same as before.[5] Benzocoronene was used as received from Rutgerswerke. PMM samples were prepared as previously described.[5]

Measurement of Φ_F, Φ_P, τ_P, *and* τ_F. The method used for determining the fluorescence yield Φ_F and phosphorescence yield Φ_P between -196 and 23° is a modification of the technique used for measuring Φ_F and Φ_P, of aromatic compounds in PMM at room temperature and described in detail elsewhere.[5] The essential features of this method are summarized here. Luminescence, emitted from the front face of a PMM sample upon which the excitation light impinges, is detected with an EMI 9558B multiplier phototube. Φ_F and Φ_P are determined from two measurements: (1) the equilibrium phototube output due to fluorescence and phosphorescence detected together with the excitation light on, and (2) the output due to phosphorescence detected immediately after the excitation is shut off. A PMM sample containing 1.0×10^{-3} *M* pyrene is used as a luminescence standard at 23°; Melhuish determined that Φ_F for pyrene in PMM has a value of 0.61.[7]

The above method must be modified to permit measurements below room temperature. Figure 2 shows the cell used. The outer cell consists of a Pyrex top, B, and a square-section quartz bottom, A, 1.5 in. on a side. Tube J is joined to part B at the top and to a copper block E, at the bottom by a Pyrex–Kovar seal D. Tube J serves as a reservoir for liquid nitrogen or other coolant. The copper block contains a hole with a 0.50-in. aperture F in the front face. The PMM sample G is placed in the copper block and a back plate, M, is screwed on to hold it in place. The copper block is then put reproducibly into the bottom section A by mating B and A. The two sections are mated at a flat, ground seal and are clamped together reproducibly

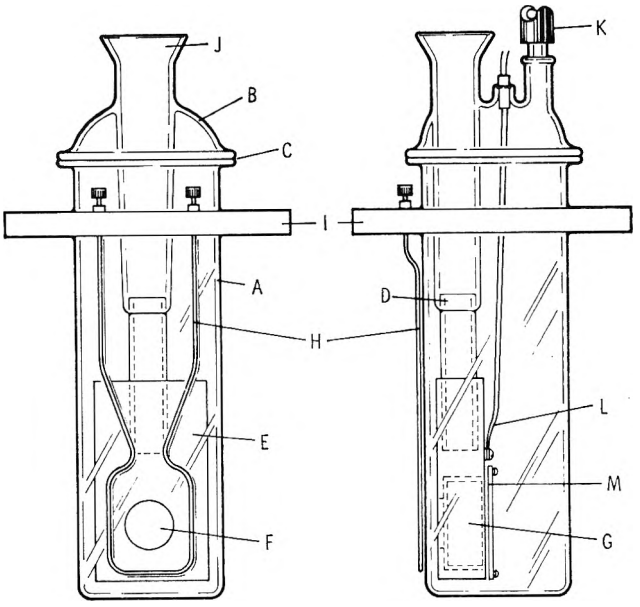

Figure 2. Front and side views of the cell for measurement of fluorescence and phosphorescence yields between -196 and 23°.

with a yoke. The copper block is positioned so that the front edge of the PMM sample is less than 2 mm from the quartz surface. This arrangement eliminates scattering of excitation and fluorescence or phosphorescence light by the corners of the quartz tube.

The PMM sample is cooled by pouring liquid nitrogen through the tube J into the reservoir in the copper block. The temperature of the sample is determined by using a copper–constantan thermocouple wire L whose junction is in the copper block. The entire apparatus is evacuated through K to maintain a low temperature. A nichrome heating wire H attached to the outside of the quartz bottom prevents frosting of A.

The cell in Figure 2 was made to be compatible with the apparatus for measuring luminescence yields. Care was taken that the PMM samples were not exposed to oxygen from the time they were being prepared until the measurements were completed. The PMM samples in their original evacuated tube and all cell components were put into a nitrogen-filled glove bag. The PMM samples were then broken from the tube and quickly ground and polished. They were put into the copper block and the entire cell assembled in the glove box. This prevented absorption of atmospheric oxygen by the PMM samples. Oxygen results in triplet quenching and reduced phosphorescence yield. The cell was constantly evacuated during the measurement by attaching it to a vacuum pump at K.

Values of Φ_F and Φ_P are determined from comparison of the luminescence signals from the pyrene standard at 23° to those of PMM samples containing coronene or benzcoronene at temperatures between -196 and 23°.

(7) W. H. Melhuish, *J. Opt. Soc. Amer.*, **54**, 183 (1964).

These luminescence signals are corrected for the variation of the EMI 9558B phototube sensitivity with wavelength. The method used for calibrating the relative response of the phototube between 3000 and 7000 Å has been described elsewhere.[8] The experimentally determined response curve decreased more rapidly beyond 4000 Å than is reported for the S-20 photo surface.[9] The wavelengths of phosphorescence and fluorescence is also needed to assign detector response factors. The fluorescence and phosphorescence spectra of coronene have been published.[5] The fluorescence of benzcoronene in PMM is between 4300 and 5000 Å and the phosphorescence is between 6000 and 6500 Å.

Values of the triplet lifetime τ_P were obtained from oscilloscope traces showing the decay of phosphorescence after the excitation light is shut off.

Values of τ_F were determined using a TRW nanosecond spectral source.[10] Lifetimes were determined from oscilloscope traces using a Tetronix Model Type 564 storage oscilloscope. The sample was placed in a square-section quartz dewar surrounded by a liquid temperature bath. For temperatures between −196 and 23°, 3-methylpentane was used as a thermal bath. Above room temperature water was used.

Measurement of Φ_T. A method has been described for measuring the triplet yield, Φ_T, of compounds in EPA at −196° from separate measurements of the excitation coefficient of triplet absorption ϵ_T and of $\epsilon_T\Phi_T$.[11] The ϵ_T spectrum is obtained from a detailed correlation of the measured spectrum between 3200 and 7000 Å of the extinction coefficient of singlet absorption, ϵ_S, with the measured spectrum of the change in absorbance, ΔA, arising from T–T absorption associated with the excitation of molecules to the triplet state. The value of $\epsilon_T\Phi_T$ for a wavelength, λ, is obtained from measurement of the initial rate of increase of ΔA at λ resulting from absorption of excitation photons using eq 6.

$$\Delta A/I = 1000\epsilon_T\Phi_T\tau_P[1 - \exp(-t/\tau_P)] \qquad (6)$$

where I is the excitation intensity and t is the time after turning on the excitation beam.

The method of measuring Φ_T must be modified for measurements of compounds in PMM for two reasons. First, PMM absorbs below 3400 Å and care must be taken that this absorption does not give rise to large error in determination of Φ_T. Second, the PMM is a solid throughout the entire temperature range. EPA is liquid at 23° and could be poured into the cell for measurement of ϵ_T and $\epsilon_T\Phi_T$. Thus, for the measurements of $\epsilon_T\Phi_T$ and ϵ_T in EPA the same cell can be filled with EPA and ferrioxalate actinomer solutions. However, for solid PMM samples a new holder shown in Figure 3 had to be designed.

The modified cell and sample holder, C, are shown in Figure 3. The quartz cell, B, has 4 cm long evacuated end sections which protrude from the ends of a urethane foam box, A. One end of the cell is cemented to the box; the other end is fitted to the box with a sliding seal of silicone casting resin. The 0.5 cm long cylindrical PMM sample, E, with parallel faces is cut, ground, and polished under nitrogen in a glove bag and inserted into C which has a 0.50-cm² aperture D. The holder is connected to a quartz tube, F, with a 19/38 ⅋ inner joint. This assembly is inserted into the quartz cell in the nitrogen atmosphere. The joint on the mouth of the cell allows reproducible positioning of the aperture in the center of the cell. The cell was connected to a vacuum pump and evacuated before the temperature of the PMM sample was lowered to −196° by filling the urethane foam box with liquid nitrogen.

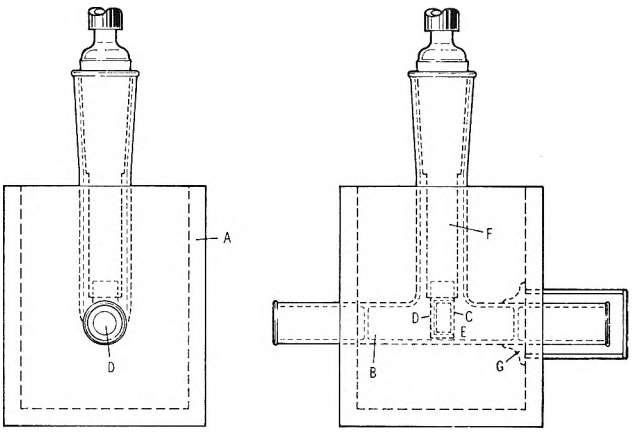

Figure 3. Front and side views of cell and sample holder used for measurement of the triplet yield at −196 and 23°.

Samples of 3.5×10^{-5} *M* coronene and 7.0×10^{-5} *M* benzcoronene in PMM were used for measurement of ϵ_T. The 20% contraction that occurs during polymerization of methyl methacrylate was accounted for in calculating concentrations. No further correction is necessary at low temperatures since PMM contracts less than 3% upon cooling. The absorption spectra of the specimens kept under vacuum in the cell were measured at −196 and 23° using a Cary 14 spectrophotometer. The absorption spectra of a 0.50-cm sample of pure PMM was also measured at these temperatures as a background reference. The ϵ_S spectrum at each temperature was determined from the absorption spectra of the samples.

The ΔA spectra of these samples were then measured between 3300 and 7000 Å with the same PMM specimens at temperatures of −196 and 23° using the cell shown in Figure 3, and the optical assembly described elsewhere.[11] These measurements did not have to be corrected for light absorption by the PMM since the attenuation by a 0.50-cm path of PMM of light wavelengths longer than 3300 Å is less than 2%, but in other

(8) W. R. Dawson and J. L. Kropp, *J. Opt. Soc. Amer.*, **55**, 822 (1965).
(9) J. Sharpe, *IRE Trans. Nuclear Sci.*, NS-7, 44 (1960).
(10) TRW Instruments (Model 31A Manosecond Spectral Source).
(11) W. R. Dawson, *J. Opt. Soc. Amer.*, **58**, 222 (1968).

cases where it may be necessary to measure ΔA spectra below 3200 Å, the sample must be shortened and the concentration of the aromatic compound increased sufficiently so that light absorption by the PMM is negligible at wavelengths studied below 3200 Å.

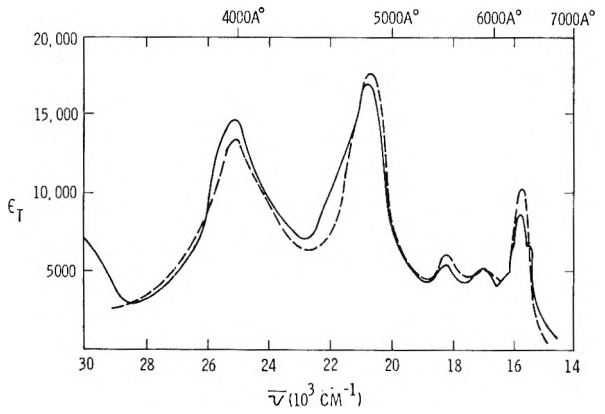

Figure 4. Triplet absorption of coronene-d_{12} in PMM: solid line, 23°; dotted line, −196°.

The ϵ_T spectra of benzcoronene and coronene-d_{12} in PMM are shown in Figures 4 and 5. The ϵ_T spectra of coronene-d_{12} and coronene-h_{12} are identical to within the experimental error. There is also little change in the ϵ_T spectra of coronene-h_{12}, coronene-d_{12}, and benzcoronene between 23 and −196°. This contrasts with the behavior of the singlet absorption spectra in PMM samples, which become sharper and usually shift to the red as the result of a decrease of temperature.

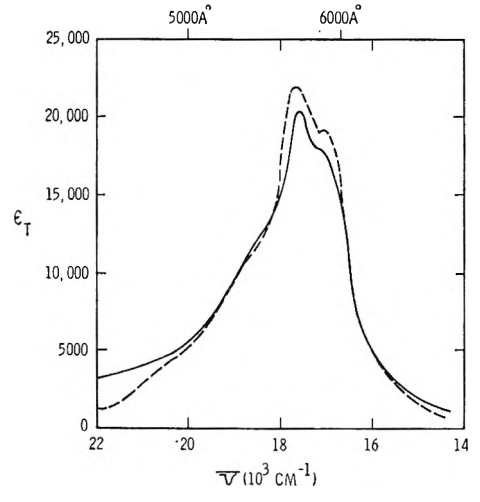

Figure 5. Triplet absorption of benzcoronene in PMM; solid line, 23°; dotted line, −196°.

Values of $\epsilon_T\Phi_T$ were also measured at −196 and 23° with PMM samples in the Dewar cell shown in Figure 3. The rate of buildup of triplet absorption upon turning on a beam of 3130-Å excitation light was measured. The wavelengths of T–T absorption monitored were 4813 Å for coronene and 5680 Å for benzcoronene samples. The concentrations of the benzcoronene and coronene in the samples used in these measurements were 3×10^{-4} and 1.0×10^{-3} M, respectively, which was sufficient to absorb the 3131-Å excitation light completely.

Deterioration of samples containing coronene-h_{12} and coronene-d_{12} in PMM at 23° by the 3131-Å excitation light was indicated by the decreasing rates of triplet buildup occurring during successive intervals of excitation. However, an accurate value of $\epsilon_T\Phi_T$ could be obtained if the rate of buildup of the triplet absorption of a coronene sample is measured during the initial exposure to excitation light before appreciable deterioration occurs. The intensity of the excitation light I was measured by ferrioxalate actinometry.[12] The actinometer solution (0.15 M ferrioxalate) in a 1 mm thick quartz absorption cell was placed in a separate holder similar to C, also having a 0.50-cm² aperture and a 19/38 ⅋ joint. This holder was positioned in the cell in Figure 3 so that the aperture was centered in the same place as that of the PMM sample. Consequently, the same flux of light which excited triplet absorption was absorbed by the actinometer solution.

Estimates of Error. Values of τ_P are accurate to within 5% as determined from the linearity of the semilog plot of the decay of OD with time and the reproducibility of values of the lifetime from sample to sample. Using the same criteria to determine the errors in τ_F gives an accuracy of about 5% for those fluorescence lifetimes which are much longer than 100 nsec, as in this work.

Values of Φ_F and Φ_P depend upon the value of Φ_F used for the reference pyrene sample of 0.61. Assuming this value to be correct the values of Φ_F are reproducible to within 10% and those of Φ_P to within 20%. The larger errors in Φ_P arise because the signal due to phosphorescence is smaller.

Errors in values of Φ_T have been detailed elsewhere.[11] There is an additional source of error in plastic samples in that at room temperature there is deterioration under uv excitation. However, this can be counteracted by using fresh samples. We estimate that errors in Φ_T are about 10%.

As a consequence of these precision limits, the errors in k_1, k_2, and k_3, are less than 12% while uncertainty in values of k_4 and k_5 are about 20%. However, the accuracy of the ratio of values of any of these rate constants for a compound taken at two temperatures will be greater than the accuracy of the value of the rate constant itself.

Results

The fluorescence lifetimes of coronene-h_{12} and coronene-d_{12} in PMM as a function of temperature are given

(12) C. G. Hatchard and C. A. Parker, *Proc. Roy. Soc.*, **A235**, 518 (1956).

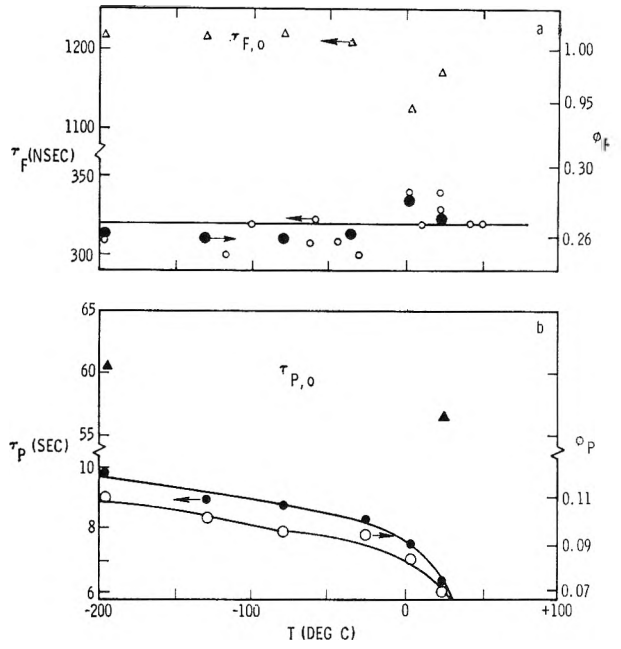

Figure 6. Variation of luminescence lifetimes and yields with temperature for coronene-h_{12} in PMM: a. O, fluorescence lifetime, τ_F, and △, radiative lifetime of fluorescence, $\tau_{F,O}$, left-hand ordinate; ●, fluorescence yield, Φ_F, right-hand ordinate. b. ●, phosphorescence lifetime, τ_P, and ▲, radiative lifetime of phosphorescence, $\tau_{P,O}$, left-hand ordinate; O, phosporescence yield, Φ_P, right-hand ordinate.

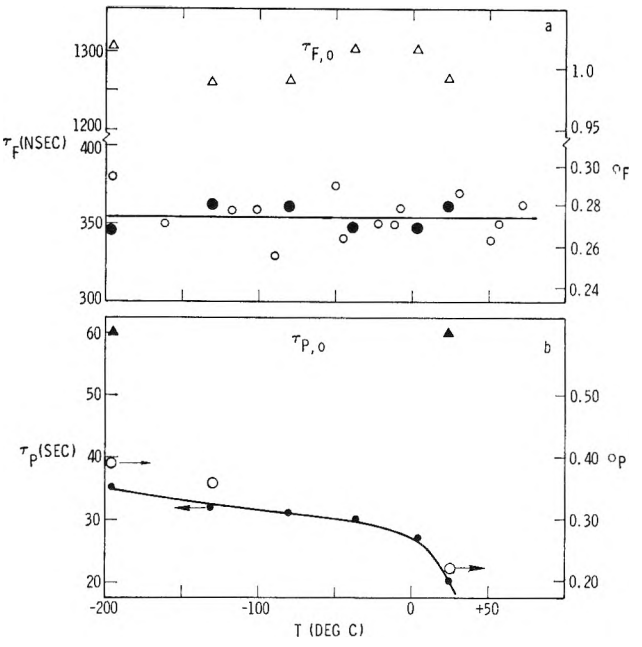

Figure 7. Variation of luminescence lifetimes and yields with temperature for coronene-d_{12} in PMM: a. O, fluorescence lifetime, τ_F, and △, radiative lifetime of fluorescence, $\tau_{F,O}$, left-hand ordinate; ●, fluorescence yield, Φ_F, right-hand ordinate. b. ●, phosphorescence lifetime, τ_P, and ▲, radiative lifetime of phosphorescence, $\tau_{P,O}$, left-hand ordinate; O, phosphorescence yield, Φ_P, right-hand ordinate.

in Figures 6a and 7a, respectively. The lifetime of coronene-h_{12} in PMM is constant from 77 to 340°K with a value of 320 ± 15 nsec. The lifetime of coronene-d_{12} is also constant over the same temperature range with a value of 355 ± 15 nsec. The solid lines in Figures 6a and 7a represent the averaged values of the lifetime data. The fluorescence yields of these two compounds are likewise shown in Figures 6a and 7a and are constant with temperature with average values of 0.27 for coronene-h_{12} and 0.28 for coronene-d_{12}. There is no change of Φ_T with concentration between 3×10^{-4} and 1×10^{-3} M.

The phosphorescence yields and phosphorescence lifetimes are shown for coronene-h_{12} and coronene-d_{12} in Figure 6b and 7b, respectively. Again, there is no change in Φ_P as the concentration is varied from 3×10^{-3} to 1×10^{-4} M. The triplet yield was determined at −196 and 23° and is 0.68 and 0.64, respectively, for coronene-h_{12}. The values of Φ_T for coronene-d_{12} are 0.67 and 0.66 for these same temperatures.

The results for benzcoronene differ from coronene in that the values of the fluorescence yield Φ_F and τ_F, as well as the phosphorescence yield and τ_P vary with temperature. The variations of τ_F and Φ_F with temperature are shown in Figure 8a. The curve drawn in Figure 8a is given by eq 7. The parameters given in eq 7 represent a least-square fit of the fluorescence lifetime data. The corresponding data for Φ_P and τ_P are shown in Figure 8b. The value of Φ_T at room temperature for benzcoronene is 0.58. At 77°K the value of Φ_T has

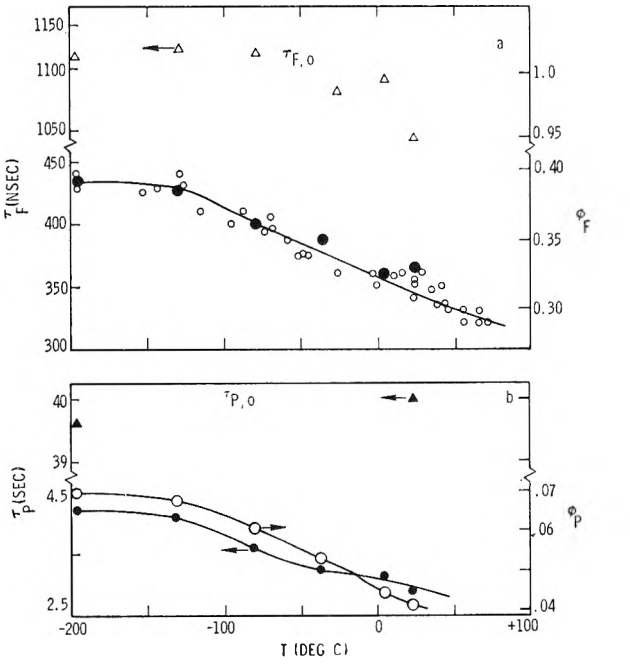

Figure 8. Variation of luminescence lifetimes and yields with temperature for benzcoronene in PMM: a. O, fluorescence lifetime, τ_F, and △, radiative lifetime of fluorescence, $\tau_{F,O}$, left-hand ordinate; ●, fluorescence yield, Φ_F, right-hand ordinate. b. ●, phosphorescence lifetime, τ_P, and ▲, radiative lifetime of phosphorescence, $\tau_{P,O}$, left-hand ordinate; O, phosphorescence yield, Φ_P, right-hand ordinate.

Table I: Rate Constants for Depopulation of S_1 and T_1 in Coronene and Benzcoronene

	Coronene-h_{12}		Coronene-d_{12}		Benzcoronene	
Process, sec^{-1}	77°K	296°K	77°K	296°K	77°K	296°
k_1	8.4×10^5	8.4×10^5	7.8×10^5	7.8×10^5	9.0×10^6	9.6×10^5
k_2	1.6×10^5	2.8×10^5	1.4×10^5	1.7×10^5	[a]	2.6×10^5
k_3	2.1×10^6	2.0×10^6	1.9×10^6	1.9×10^6	1.5×10^6	1.7×10^6
k_4	0.017	0.018	0.017	0.017	0.025	0.025
k_5	0.086	0.141	0.012	0.033	0.21	0.32

[a] Since $\Phi_F + \Phi_T = 1.05$, k_2 is considered to be zero.

increased to 0.66. The value of Φ_T of benzcoronene in EPA glass at −196° is 0.64, which is very similar to that in PMM. Thus the triplet yield of benzcoronene is more sensitive to change of temperature than to change of solvent.

Discussion

Using eq 1–5 we can calculate the rate constants for the various processes that depopulate singlet and triplet states in coronene-h_{12}, coronene-d_{12}, and benzcoronene. The rate constants for these compounds at −196 and 23° are tabulated in Table I. The values of k_1 were calculated at −196, −130, 80, −37, 2, and 23° using eq 1 and values of τ_F taken from curves fitted to τ_F values in Figures 6a, 7a, and 8a and the values Φ_F measured at each temperature. The reciprocal of values of k_1 are presented as $\tau_{F,0}$ in Figures 6a, 7a, and 8a for the compounds studied. As can be seen, there is no change in k_1 at any temperature for any compound.

Some of the values determined for coronene and for coronene-d_{12} were estimated earlier.[5] The values of Φ_F and τ_F at 23° are slightly revised from our earlier work. The values of Φ_F for coronene-h_{12} and coronene-d_{12} have been increased by 20% from the earlier values. The reason for this difference is the use in this work of a better phototube calibration factor. In earlier calculations the published wavelength sensitivity curve for the EMI 9558B multiplier phototube (S-20 response) was used. The present values of luminescence yields were calculated using a phototube that has been calibrated in these laboratories. As described in the experimental section this calibration curve is different than the published one. This results in the increase in the present values of fluorescence and phosphorescence yields. Similarly, the previous value of Φ_F for benzcoronene at 23° of 0.28[11] is now determined to be 0.33. The present value of τ_F of coronene-h_{12} in PMM is also 6% higher than the previous value of 300 nsec.[5] We believe these latter values to be more accurate. The value of τ_F for coronene-d_{12} has not previously been measured. In our previous work it was assumed that τ_F was the same for coronene-h_{12} and coronene-d_{12}. Using these values k_1 is now measured to be 8.4×10^5 sec^{-1} for coronene-d_{12} compared to 7×10^5 sec^{-1} previously.

Average values for τ_F between −196 and 60° for coronene-h_{12} and coronene-d_{12} of 320 and 355 nsec, respectively, differ slightly from each other. This difference is outside the 90% confidence limits established for each value by taking the average of values at all temperatures. Values of Φ_F of coronene-d_{12} are 4% larger than those of coronene-h_{12} and k_1 of coronene-h_{12} is approximately 7% larger than k_1 of coronene-d_{12}. Similarly, values of k_3 for coronene-h_{12} are approximately 7% higher than corresponding values for coronene-d_{12}. This indicates that the rates of both fluorescence and intersystem crossing are decreased in coronene-h_{12} compared to coronene-d_{12}. The value of k_2 is always less than 10% of the total decay rate from S_1 for coronene-h_{12} and coronene-d_{12}. In view of the experimental errors and the indirect method of determining k_2 as a small difference between large numbers, the probable error in our values of k_2 is such that we cannot rule out the possibility that k_2 may actually be zero. This is in agreement with previous results. Lim[13] reported that k_2 is zero within experimental error for benzene in an EPA glass at −196°. Similarly, Medinger and Wilkinson[14] and Parker and Joyce[15] found that k_2 is zero for several aromatic compounds in fluid solvents at room temperature. However, in PMM at 23°, it appears that k_2 is not zero for many aromatic compounds such as benzcoronene.

The rate constants derived for 1,2-benzcoronene show a different behavior with changing temperature than do those of coronene. The fluorescence lifetime and fluorescence yield of this compound are temperature dependent and decrease by about 20% from 77°K to room temperature. It can be seen from Figure 8a that values of τ_F and Φ_F can be normalized to nearly fit the same curve indicating that k_1 for benzcoronene is temperature independent; k_1 has a constant value of 9.1×10^5 sec^{-1} within 7% from −196 to 23°. This is shown by values of $\tau_{F,0}$ shown in Figure 8a. The decrease in Φ_T from −196 to 23° is only 12%. However, k_3 is still constant at these two temperatures to within 12%. The value of $\Phi_F + \Phi_F = 1.05$ at 77°K. This gives a negative value for k_2. The best we can do is assume that k_2 is 0 at −196°, but the fact that values of τ_F, Φ_F, and Φ_T

(13) E. C. Lim, *J. Chem. Phys.*, **36**, 3497 (1962).
(14) T. Medinger and F. Wilkinson, *Trans. Faraday Soc.*, **61**, 620 (1965).
(15) C. A. Parker and T. A. Joyce, *ibid.*, **62**, 2785 (1966).

all *decrease* between 12 and 20% as the temperature increases from −196 to 23°, besides showing that the rate constants for fluorescence and triplet formation remain nearly constant with temperatures, implies that the temperature sensitive process observed is the S_1–S_0 quenching of the excited singlet to ground. At room temperature the value of k_2 is estimated to be 2.6×10^5 sec^{-1}. As in the case of coronene, this is not a reliable value due to experimental uncertainty and it is still quite small. However, with benzcoronene the parallel temperature dependence of the measured parameters is strong evidence that some radiationless deactivation of S_1 to S_0 occurs at 23° and that k_2 increases with increasing temperature.

The phosphorescence lifetime and yields all vary with temperature as shown in Figures 6b, 7b, and 8b. However, the value of k_4 (Table I) is independent of temperature for both coronene-h_{12}, and benzcoronene. Values of k_4 are the same within our experimental error for coronene-h_{12} and coronene-d_{12}, but the value of k_4 for benzcoronene is 50% greater than that for coronene. Siebrand[16] in his theoretical treatment has concluded that most hydrocarbons (including coronene) should have values of $\tau_{P,0}$ = 20–40 sec (k_P = 0.050–0.025 sec^{-1}), but experimental data here show that the value of k_P can be much less than 0.025 sec^{-1} and is only 0.017 sec^{-1} for coronene.

The value of k_5, is reduced upon deuteration in coronene-d_{12} compared to coronene-h_{12}. At −196° k_5 for coronene-h_{12} is 7 times that of coronene-d_{12}. However, at room temperature this factor has decreased to 4. The value of k_5 increases between −196 and 23° by a factor of 1.6 in coronene-h_{12}, but by a factor of 2.2 in coronene-d_{12}. These results indicate a greater temperature sensitivity for radiationless depopulation of triplet coronene-d_{12} than coronene-h_{12}. This has been qualitatively noted previously.[5] It is interesting that even for coronene-d_{12} at −196° the radiationless quenching of the triplet plays an important role in deactivation of the triplet state. Radiationless quenching of the triplet still accounts for 40% of the energy loss in coronene-d_{12} where H vibrations are removed.

Benzcoronene fluorescence lifetime and yield are temperature dependent. The lifetime data can be fitted to eq 7. The best fit of the τ_F data to the plot is given

$$(1/\tau_F) - (1/\tau_0) = A \exp(-\Delta E/RT) \qquad (7)$$

in Figure 8a. The parameters that best fit the data are $A = 7.6 \times 10^6$ sec^{-1} and ΔE = 514 cm^{-1}. This is a low activation energy. It is important to determine whether these temperature-dependent activation energies are intermolecular effects or dependent upon solvent properties. However, more work is needed in other plastic hosts to determine this. Such work is now in progress and will be reported elsewhere.[17]

(16) W. Siebrand, *J. Chem. Phys.*, **46**, 440 (1967).
(17) J. L. Kropp and W. R. Dawson, to be published.

Concurrent Solution and Adsorption Phenomena in Chromatography. I. General Considerations

by J. R. Conder,[1a] D. C. Locke,[1b] and J. H. Purnell

Department of Chemistry, University College of Swansea, Swansea, Glamorgan, Great Britain *(Received August 13, 1968)*

The dependence of the several sources of solute retention in chromatography—bulk liquid partition, liquid interfacial adsorption, and solid support adsorption—on solvent volume and on surface areas is considered for a variety of practical situations. The relative magnitudes of the individual contributions may then be qualitatively predicted over a wide range of stationary phase loadings, for the situations of (a) constant sample size and (b) constant concentration of solute in the mobile phase. The individual contributions are finally summed to show qualitatively the various forms of variation of the net retention volume with liquid loading which may be met with in practice. The results are presented in graphical form. Certain features are found in these curves which are useful for diagnosis of interfacial adsorption effects in chromatography. The predicted curves are in formal agreement with published experimental plots. Means for the recognition of and correction for interfacial adsorption effects in experimental data are suggested. For chromatographic systems in which all three mechanisms occur, only bulk liquid partition coefficients can be determined unequivocally by chromatography alone. The range of application of chromatography to the measurement of physicochemical data is considerably broadened by these conclusions.

The quantitative interpretation of chromatographic data is often complicated by the occurrence of solute adsorption at one or more of the interfaces present in the system. Solid supports for the stationary phase have long been known to interact with some types of solutes and preventative measures are widely taken. Interactions at the other interfaces, on the other hand, have received little theoretical and no practical consideration. Martin[2] was the first to demonstrate that solute adsorption on the surface of the bulk liquid (Gibbs adsorption) could markedly affect experimental retention volumes in some gas–liquid partition chromatographic (glpc) systems. This finding was reproduced and extended by Pecsok, *et al.*,[3] and directly substantiated by the static measurements of Martire, Pecsok, and Purnell.[4,5] In each case, a "polar" stationary phase was used. The suggestion was originally made[2a] that an appreciable Gibbs adsorption effect would be observed only with such solvents. Later,[5,6] this statement was generalized to include not only polar solvents, but any system in which the solute activity coefficient, f, exceeded about 5. Martire[7] has lately shown this to be a sufficient condition, but has further demonstrated that liquid surface excess effects may also be observed with certain polar solute–polar solvent systems in which the solute activity coefficients are only around unity.

Pecsok and Gump[8] have recently measured, by a static method, the relevant solution and surface tension data for a variety of polar solutes in the nonpolar liquid, squalane, and concluded that a considerable retention volume contribution from Gibbs adsorption should be found in the corresponding glpc system. In direct conflict with this, the study of the same systems by Urone and Parcher[9] appeared to reveal only the occurrence of substantial adsorption on the surface of the solid support. Thus the general basis of the hypothesis of liquid surface adsorption in glpc is to some extent challenged and, certainly, doubt is cast on occurrence of the phenomenon with nonpolar solvents.

It is the purpose of this paper to define as quantitatively as possible all sources of solute retention in chromatography and thus to test the practice of detecting and measuring liquid surface adsorption by chromatographic means. In so doing we are able to offer a reconciliation of the conflicting data and to propose better procedures for the chromatographic measurement of surface phenomena. While all quantitative investigations have so far been restricted to glpc systems, the results of this paper are equally applicable to liquid–liquid chromatographic (llc) systems, where the phenomena described have also been tentatively detected.[10]

(1)(a) Department of Chemical Engineering, University College of Swansea. (b) Department of Chemistry, Queens College of the City University of New York, Flushing, N. Y. 11367.

(2)(a) R. L. Martin, *Anal. Chem.*, **33**, 347 (1961); (b) R. L. Martin, *ibid.*, **35**, 116 (1963).

(3) R. L. Pecsok, A. de Yllana, and A. Abdul-Karim, *ibid.*, **36**, 542 (1964).

(4) D. E. Martire, R. L. Pecsok, and J. H. Purnell, *Nature*, **203**, 1279 (1964).

(5) D. E. Martire, R. L. Pecsok, and J. H. Purnell, *Trans. Faraday Soc.*, **61**, 2496 (1965).

(6) D. E. Martire and L. Z. Pollara in "Advances in Chromatography," Vol. 1, J. C. Giddings and R. A. Keller, Ed., Marcel Dekker, New York, N. Y., 1966, p 335.

(7) D. E. Martire, *Anal. Chem.*, **38**, 244 (1966).

(8) R. L. Pecsok and B. H. Gump, *J. Phys. Chem.*, **71**, 2202 (1967).

(9) P. Urone and J. F. Parcher, *Anal. Chem.*, **38**, 270 (1966).

(10) D. C. Locke in "Advances in Chromatography," Vol. 7, J. C. Giddings and R. A. Keller, Ed., Marcel Dekker, New York, N. Y., 1968.

Theory

I. Sources of Solute Retention in Glpc and Llc. Partitioning of solutes between the mobile phase and the liquid stationary phase is the predominant mechanism of solute retention in most, but not all, practical glpc and llc systems. Perhaps more often than is generally recognized, the solute may also be retained in the column by adsorption (i) at the gas–liquid interface (or liquid–liquid interface in llc) and/or (ii) as a result of the presence of the solid support. Except as discussed below, these retention mechanisms operate essentially independently. Consequently, the number of moles of solute held stationary within a length dl of the column of total length l, in equilibrium with a concentration c in the gas phase, is ndl/l where

$$n = q_L V_L + q_I A_I + q_S A_S = \sum_i q_i \phi_i \qquad (1)$$

Here q_L, q_I, and q_S are the solute concentrations (mole cc^{-1}, mole cm^{-1}, and mole cm^{-1}) in the bulk liquid, gas–liquid (or eluent–liquid) interface and support-adsorbed phase, respectively; V_L is the total volume of liquid phase in the column; A_I and A_S are the active surface areas of the liquid and support, respectively; and ϕ_i represents V_L, A_I, or A_S.

For each of these retention mechanisms, the contribution to the net retention volume of an eluted zone whose concentration in the gas phase (assumed ideal) is c is given[11,12] by the equation

$$V_{N,i} = (1 - jy_0)K_i'\phi_i \qquad (2)$$

where

$$K_i' = dq_i/dc \qquad (3)$$

j is the usual James–Martin gas compressibility factor and y_0 is the mole fraction of solute, corresponding to c, at the column outlet. K_i' is the gradient of the distribution isotherm for retention mechanism i and is to be distinguished from the distribution coefficient, given by

$$K_i = q_i/c \qquad (4)$$

In the limit of infinite dilution, $K_i' = K_i$. From eq 1, 2, and 3, the total retention volume, as observed experimentally, is given by

$$V_N = \sum_i V_{N,i} = (1 - jy_0)dn/dc \qquad (5)$$

We propose to consider only conventional elution chromatography in which solute concentrations are very small (sample size ~0–1 μmol). Here it is a good approximation to set

$$jy_0 \ll 1 \qquad (6)$$

but curvature of the distribution isotherm for mechanisms (i) and (ii) is often still sufficiently marked at these low concentrations to render the further possible approximation, $K_i' = K_i$, grossly inaccurate. Using relation 6, eq 5 can be written in the form

$$V_N = K'_{obs}V_L \qquad (7)$$

where K'_{obs}, the experimentally observed partition coefficient calculated from the experimental V_N and V_L, is given by

$$K'_{obs} = (1/V_L)(dn/dc) \qquad (8)$$

Combination of eq 1, 7, and 8 now gives

$$(V_N/V_L) = K'_{obs} = K_L' + (K_I'A_I/V_L) + (K_S'A_S/V_L) \qquad (9)$$

At true infinite dilution, eq 8 becomes

$$K_{obs} = n/V_L c \qquad (10)$$

and eq 9 is

$$V_N/V_L = K_{obs} = K_L + (K_I A_I/V_L) + (K_S A_S/V_L) \qquad (11)$$

Equation 11 is applicable when symmetrical peaks are observed. The occurrence of asymmetrical peaks clearly indicates that effective infinite dilution is not attained, and the more general eq 9 must then be used instead of eq 11. Asymmetry resulting from kinetic or extra-column factors cannot readily be considered and is therefore to be experimentally avoided, for example by operation at low flow velocities. In consequence, the discussion of this paper assumes these effects are absent.

The several retention mechanisms can be treated as essentially independent if sufficient solvent is present on the solid support to act as a bulk liquid with a depth much greater than that of the gas–liquid and liquid–solid interfacial layers. The precise required depth has not been defined in this context, since the definition of "surface layer" is arbitrary.[13] The surface layer can be considered to be the distance from the surface to the point to which the influence of that surface extends.[14–16] A simple calculation[5] gives an indication of typical liquid film thicknesses; at 1% solvent/support weight ratio (w/w), the average film thickness is about 50 Å if the liquid is spread on Chromosorb P, and about 150 Å on Chromosorb W,[5] whereas at 10% loading, the average thicknesses are roughly 1000 Å and 3000 Å, respectively. While these values are only guides, since they represent averages of layer thicknesses ranging from perhaps a monolayer to relatively thick droplets or

(11) J. R. Conder in "Progress in Gas Chromatography," J. H. Purnell, Ed., John Wiley and Sons Inc., New York, N. Y., 1968, p 209.

(12) J. R. Conder and J. H. Purnell, *Trans. Faraday Soc.*, **64**, 3100 (1968); **65**, 824, 839 (1969).

(13) E. A. Guggenheim, "Mixtures," Oxford University Press, London, 1952, Chapter 9.

(14) D. E. Martire in "Progress in Gas Chromatography," J. H. Purnell, Ed., John Wiley and Sons Inc., New York, N. Y., 1968, p 93.

(15) R. A. Keller and G. H. Stewart, *Anal. Chem.*, **34**, 1834 (1962).

(16) W. D. Harkins and G. Jura, *J. Amer. Chem. Soc.*, **66**, 919 (1944).

layers, it is clear that true bulk solvent may not exist at low loadings. Discussion of interfacial effects thus becomes meaningless because of the absence of the required reference state, the bulk liquid. For most systems, it is unlikely that the essential independence of liquid interfacial and bulk liquid effects is maintained at solvent/support ratios of less than 5–10% by weight.

II. Choice of Experimental Approach. The standard chromatographic procedure for study of liquid surface adsorption[2-5,7,8,14] assumes that the solutions involved are at effectively infinite dilution[5,6,11] (*i.e.*, constant, zero sample concentration), and that no solid support interactions can occur. In such circumstances

$$V_N = K_L V_L + K_I A_I \qquad (12)$$

The solvent/support ratio may then be varied at constant temperature, and K_L and K_I evaluated from a plot of V_N/A_I against V_L/A_I. If $K_I > 0$, the plot will have a nonzero intercept, K_I, and a positive slope, K_L. A plot of V_N/V_L against A_I/V_L gives the same information but the roles of K_I and K_L are reversed.

These procedures give no useful information if solid support effects occur and cannot be applied at all unless A_I is known as a function of V_L. A preferable procedure, which avoids both these shortcomings, is to plot V_N/V_L against $1/V_L$. According to eq 11, this allows K_L to be determined whether A_I is known or not. If A_I is known, both K_I and $K_S A_S$ can be obtained from the plot, as described by Conder.[17]

If, in addition, the solutions involved are not truly at infinite dilution, K'_{obs} and thus V_N become dependent on concentration. In this case, experiments in which the solvent/support ratio is varied can be carried out in either of two ways: (a) maintaining constant sample size so that concentration varies, or (b) adjusting sample size to maintain constant concentration. Experimental mode (a) is exemplified in the work of Urone and Parcher,[9] who varied liquid loading while using a fixed amount of sample. Analytical treatment of the results in terms of eq 8 gives no useful information in this case since there are too many variables, *viz.* both the distribution coefficients and the area/volume ratios. Experimental mode (b), however, is much more useful since it eliminates variation of the distribution coefficients and permits their evaluation, as described previously.[17]

In conducting experiments in either modes (a) or (b), the possibility is evident that variations in the relative contributions of two or more of the effects can yield some compensation among them, so that retention behavior may appear simpler than is actually the case. It is important, therefore, to examine in detail what the concentration dependences of the individual terms in eq 8 might be. Each individual retention mechanism will be considered in turn, and finally the contributions will be summed to predict complex retention volume relationships which might be met in practice.

III. Effects of Constant Sample Size. A. Bulk Solution. The three most common types of partition isotherms encountered in chromatographic systems are depicted in Figures 1 A(i), (ii), and (iii). By definition,

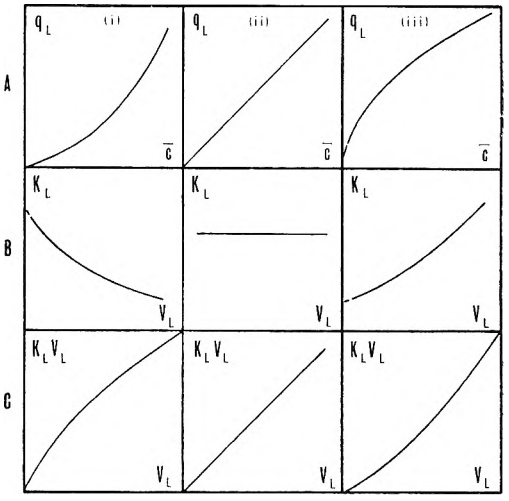

Figure 1. A, Bulk liquid partition isotherms: (i) anti-Langmuir; (ii) linear; and (iii) Langmuir. B, Variation of K_L with liquid loading for (i) anti-Langmuir, (ii) linear, and (iii) Langmuir partition isotherms. C, Dependence of $K_L V_L$ on V_L for (i) anti-Langmuir; (ii) linear; and (iii) langmuir partition isotherms.

K_L is equal to $q_L/\bar{c}$ and is calculable from the isotherm by construction of chords from the origin to any point on the curve.[11] The corresponding variations of K_L with V_L and of $K_L V_L$ with V_L are, respectively, shown in Figures 1B and 1C. In each case, (a) represents an anti-Langmuir isotherm, (b) a linear isotherm, and (c) a Langmuir isotherm. As V_L is increased at constant sample size, the liquid phase becomes more dilute in solute and this can be represented as moving along the isotherm to a different point. Since V_L increases linearly, and proportionally more rapidly than K_L changes, the variation of $K_L V_L$ with V_L is as shown in Figures 1C. In glpc, case (a) is by far the most common; cases (b) and (c) are observed only in the presence of very strong negative deviations from Raoult's law, such as might be caused by complexing, hydrogen bonding, or other form of association. Insofar as peak shape is determined by the partitioning process, case (a) leads to peaks with trailing edges steeper than their leading edges (skew ratio, $\eta > 1$).[11,18,19]

B. Liquid Surface Adsorption. The relationship between the liquid surface partition coefficient, K_I, and the Gibbs adsorption isotherm has been reviewed re-

(17) J. R. Conder, *J. Chromatogr.*, **39**, 273 (1969).

(18) G. F. Freeguard and R. Stock in "Gas Chromatography 1962," M. van Swaay, Ed., Butterworth and Co. Ltd., London, 1962, p 102.

(19) A. J. B. Cruickshank and D. H. Everett, *J. Chromatogr.*, **11**, 289 (1963).

cently.[5,14] The surface excess concentration, $\Gamma_2^{(1)}$, which is proportional to the variation of solution surface tension with solute mole fraction, $(d\gamma/dx_2)$, is by definition related to K_I according to

$$K_I = \Gamma_2^{(1)}/c \qquad (13)$$

Figure 2A(i) presents a typical γ–x_2 plot; the initial rapid decrease in γ usually occurs over a quite narrow range of x_2. For example,[8] in the methanol–squalane system at 30°, γ decreases from 27 dyn cm^{-1} at $x_2 = 0$ to its minimum value of 22 dyn cm^{-1} at $x_2 = 0.02$. In Figure 2A(ii) is shown the resulting variation of K_I with x_2 and, in Figure 2A(iii), that of K_I with V_L.

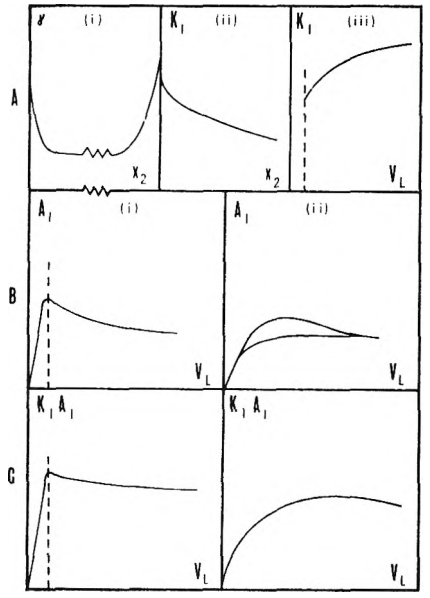

Figure 2. A, (i) Change in solution surface tension, γ, with solute concentration, x_2; (ii) variation of K_I with solute concentration, x_2; (iii) change in K_I with liquid loading, V_L, at constant sample size. B, Liquid surface area, A_I, as a function of liquid loading, V_L, for (i) support wetted by stationary phase and (ii) support not wetted by stationary phase. In (i), vertical broken line: corresponds to V_L of formation of an ideal uniform monomolecular liquid film. In (ii), upper and lower curves: expected extremes of anticipated A_I–V_L plots. C, Variation of $K_I A_I$ with V_L for (i) wetted and (ii) nonwetted solid supports, at constant sample size. Vertical broken line: point of monolayer formation.

The liquid surface adsorption isotherm is Langmuir in form (K_I decreasing with increasing concentration), which produces skew ratios, $\eta < 1$. Since the curvature of this isotherm can be more pronounced than that of the bulk partition isotherm, the effect on peak shape can be greater. Consequently, tailed peaks can be anticipated when sufficient liquid interfacial adsorption occurs, unless solutes are introduced in quantities small enough to produce solutions at infinite dilution.

C. Liquid Surface Area. Martin[2a] and Pecsok, *et al.*,[3] have presented experimental plots of liquid surface area *vs.* V_L. Martire, *et al.*,[5] have independently confirmed the form of these plots as presented in Figure 2B(i). The broken vertical lines in the figures indicate the point of monolayer formation for an ideally uniform liquid film. Such a film would reach monolayer solvent/support ratio in the vicinity of 0.1 wt %. (For clarity, the V_L scales are expanded at low V_L to the left of the broken lines.)

Experimental techniques used for measurement of A_I have been either the continuous flow method of Nelsen and Eggertsen[20] (used by Martin[22]) or a modified BET technique using nitrogen as the adsorbate.[3] In either case, what is in fact being measured is a gross area (liquid surface plus any exposed solid surface), since all exposed surfaces are equally accessible to adsorbable vapors. It is also noteworthy that the cross section for adsorption of nitrogen differs substantially from that for most gc solutes.

Martire, *et al.*,[4,5] determined A_I by first determining in a static system the K_I value for cyclohexane in β,β'-thiodipropionitrile. Using glpc-measured $K_I A_I$ values[2,3] for the same system, they then calculated A_I values and thus constructed a "corrected" A_I–V_L plot. The value of A_I extrapolated to 0.1% solvent loading (*i.e.*, the approximate monolayer point for a uniform film), ~2 m^2 g^{-1}, is quite close to that found for uncoated Chromosorb using a BET–organic vapor technique.[21] This is to be expected if the liquid is distributed upon the solid in a monolayer, and, insofar as such extrapolation is valid, provides some evidence for the smooth distribution of this stationary phase on this support.[4,5] At high V_L values, A_I asymptotically approaches a limiting value. Clearly, this limiting area is that of the support less the area of its narrow pores and channels. These two area limits are analogous to the comparison of the true length of a coastline ($V_L = 0$) with that of the 3 mile limit ($V_L >> 0$) which ignores estuaries, inlets, etc.

One feasible independent method for estimating A_I is applicable only to low surface energy solid supports such as Teflon. The total surface could be measured by a BET–organic vapor technique. Subsequent examination of the same wetted packing by electron microscopy should allow calculation of the average size and geometrical distribution of liquid droplets on the surface. The total surface area could then be apportioned to the exposed solid surface and the liquid surface areas.

There is no reason to believe that the form of the A_I–V_L plots for the systems previously studied[2–5] apply to all chromatographic solid support–solvent combinations. Smooth liquid distributions (such as described by Figure 2B(i) can be achieved only if the liquid wets the solid support surface. The consequence of nonwetting of the support upon the resulting A_I is

(20) F. M. Nelsen and F. T. Eggertsen, *Anal. Chem.*, **30**, 1387 (1958).
(21) R. H. Perrett and J. H. Purnell, *J. Chromatogr.*, **7**, 455 (1962).

pictured in Figure 2B(ii). Instead of a sharp rise up to the monolayer point followed by a gradual tailing off, the liquid can now only form isolated droplets which at small V_L have only a small total surface area. As more liquid is added, the combined droplet area increases until sufficient solvent is present to cause the drops to coalesce. A_I must then level off or fall off, again to the same limiting values as found for the wetted support.

A_I–V_L plots of the type shown in Figure 2B(i) are expected for most solvent–support systems. Figure 2B(ii) should better describe the cases of solvents on Teflon supports and perhaps strongly polar liquids on silanized firebrick.

D. Contribution of Liquid Surface Adsorption to Retention. The contribution of liquid surface adsorption to retention is given by the product K_IA_I. For each of the expected A_I–V_L relationships, K_IA_I is plotted as a function of V_L in Figures 2C(i) and 2C(ii). The variations of K_I and of A_I with V_L are opposed and the relative sizes of the variation determine the overall form of K_IA_I. For the unwetted support, comparison of Figures 2C(i) and 1C immediately shows that no compensation, in terms of slopes of opposite sign, is possible between K_IA_I and K_LV_L, so that the net retention volume must increase with V_L. However, in the case of a wetted support, if A_I decreases with V_L faster than K_I increases, the product can decrease with V_L. This behavior would allow compensation, but only if the relative contribution of K_IA_I to V_N was significant compared with that of K_LV_L. Evidently, an observed lack of dependence of V_N on V_L by no means indicates the absence of liquid surface adsorption. This point assumes critical importance since it has hitherto been axiomatic that the converse is true.

E. Solid Support Adsorption. It is generally supposed that adsorption induced by the support takes place only at the uncoated solid surface, but account should be taken also of the possibility of adsorption at the liquid–solid interface where solute and solvent compete for the support surface.[22] The existence of the latter has been conclusively demonstrated recently by Urone, *et al.*,[23] for the system acetone–tri-*o*-tolyl phosphate–Chromosorb P or W. If the surface is completely covered, all apparent support effects must clearly stem from this type of adsorption. On the other hand, at less than monolayer coverage, or if the solvent does not wet the support, adsorption can occur at both the liquid–solid and exposed interfaces. Both types are taken into account here, as well as the effect of wetting and nonwetting of the support.

If the support is wetted, the total area available for adsorption varies with V_L as shown in Figure 3A(i). The upper curve relates to adsorption at both types of location, and the lower to adsorption on exposed solid only. These two types of behavior are characteristic of nonpolar and polar stationary phases, respectively,

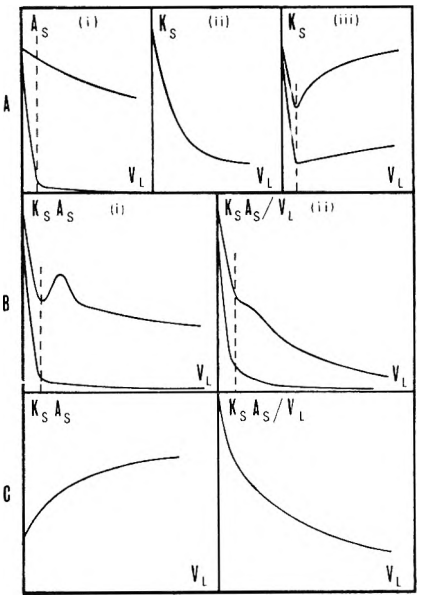

Figure 3. A, (i) Change in area, A_S, of solid support accessible to polar solute, with V_L. Upper and lower curves: nonpolar and very polar stationary phases, respectively. Vertical broken line: point of monolayer formation. (ii) Solute adsorption coefficient on solid support, K_S, as a function of solute concentration in the stationary phase, c, for Langmuir adsorption isotherm. (iii) Dependence of K_S of a polar solute on V_L, at constant sample size. Upper and lower curves: stationary phases which are, respectively, nonpolar and more polar than the solute. Vertical broken line: liquid monolayer point. B, Variation of (i) K_SA_S and (ii) K_SA_S/V_L with V_L, for a polar solute, at constant sample size. Upper and lower curves: stationary phases which are nonpolar and more polar than the solute, respectively. C, Variation of (i) K_SA_S and (ii) K_SA_S/V_L, on nonwetted support, for constant sample size.

on adsorptive solid supports. The variation in the apparent K_S associated with either A_S curve is shown in Figure 3A(iii). The initial rapid fall in K_S is due to blocking of pores and other active sites by solvent, and is most marked for polar solvents. Beyond the point of monolayer coverage a region of negative curvature reveals the influence of the strongly curved isotherm, which is expected to be most frequently of the Langmuir type, as indicated by the K_L–$\bar{c}$ plot shown in Figure 3A(ii). The sharp minima arising in the K_S–V_L curves at the point of monolayer formation are notable. The resulting dependences of K_SA_S and of K_SA_S/V_L on V_L are shown in Figures 3B(i) and (ii). A remarkable feature which emerges for nonpolar stationary phases is that if the solute is sufficiently polar, a strong hump may develop in such plots. This effect is unique to nonpolar liquids which wet the support and is a useful diagnostic feature.

The alternative situation, in which the solvent does not wet the support, is summarized by the plots of K_SA_S and K_SA_S/V_L against V_L in Figures 3C(i) and (ii).

(22) J. C. Giddings, *Anal. Chem.*, **35**, 440 (1963).

(23) P. Urone, Y. Takahashi, and G. H. Kennedy, *ibid.*, **40**, 1130 (1968).

In this case, there can be no marked changes associated with a point of monolayer formation. No hump is observed and behavior is similar for polar and nonpolar solvents. Since nonwetted supports (*e.g.*, Teflon) are likely to be only very weakly adsorptive toward most solutes, the contribution of $K_S A_S$ to the net retention volume may in this case be insignificant.[24]

F. Combined Contribution to Retention. Different systems may display gross retention effects which reflect the combined contributions of several or all of the physical processes discussed. A number of possibilities arise which we consider in turn.

Suppose, first, that the contribution of $K_S A_S$ to V_N can be neglected. We then have three possible situations: (a) $K_L V_L >> K_I A_I$; (b) $K_I A_I >> K_L V_L$; and (c) $K_L V_L \simeq K_I A_I$. Cases (a) and (b) need not be discussed since the dependence of V_N upon V_L, etc., is as shown earlier in Figures 1C and 2C, respectively.

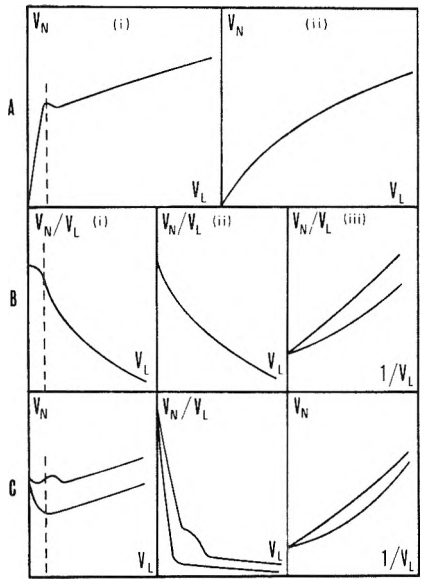

Figure 4. A, Variation of net retention volume, V_N, with V_L for the case where $K_L V_L \simeq K_I A_I >> K_S A_S$, for (i) wetted and (ii) nonwetted solid supports, at constant sample size. Vertical broken line: corresponds to V_L at which monolayer formation is complete. B, Variation of V_N/V_L with V_L for (i) wetted and (ii) nonwetted solid supports, and (iii) variation of V_N/V_L with $1/V_L$, all at constant sample size. Upper and lower curves in (iii): smaller and larger sample sizes, respectively. C, Net retention volume of a polar solute for $K_L V_L \simeq K_I A_I \simeq K_S A_S$, at constant sample size, for wetted support. Upper curve: nonpolar stationary phase; lower curve: stationary phase more polar than the solute. Vertical broken line: point of monolayer formation.

Case (c), however, is of considerable interest. V_N is the sum of separate bulk and surface liquid contributions, and is plotted in Figures 4A(i) and (ii), for wetted and nonwetted supports, respectively. The derivative plots of V_N/V_L against V_L are drawn in Figures 4B(i) and (ii), corresponding to Figures 4A(i) and (ii), respectively. The most important plot for purposes of measurement and calculation, however, is that of V_N/V_L against $1/V_L$, shown in Figure 4B(iii). According to eq 9, the intercept on the ordinate axis gives K_L at infinite dilution, so that plots for different sample sizes all extrapolate to the same point. The positive curvature of the plot is determined mainly by A_I, but is reduced somewhat by the variation of K_I with concentration. The latter factor also causes the plot for a small sample size to lie above that for a larger sample size. Variation of K_L with concentration has a much smaller influence on the curvature of these plots, since the liquid surface absorption isotherm is of greater curvature than the bulk liquid partition isotherm.

The second situation of relevance is where $K_L V_L \simeq K_I A_I \simeq K_S A_S$. Figures 4C are derived from compounding the earlier plots for wetted supports. The upper and lower curves refer to the extreme cases of solvent polarity, *i.e.*, nonpolar and strongly polar, respectively. Again, when solute is adsorbed at the nonpolar liquid–solid interface, a hump is observed in the plots, as in Figures 4C(i) and (ii), but is less pronounced than when $K_S A_S$ predominates; if $K_S A_S$ is sufficiently small compared with $K_L V_L$ and $K_I A_I$, this hump may not be observed.

Finally, when $K_I A_I >> (K_L V_L + K_I A_I)$, we again have behavior which is distinctive enough to be useful diagnostically (Figures 3B). An example of such behavior is to be found in the work of Urone and Parcher.[9] These authors represented their data in the form of retention volume per gram of column packing against percentage loading of solvent on the support. This method of presentation, first adopted by Martin,[2a] is less basic than a plot of V_N against V_L, since the weight of solid support is included among the variables. In consequence, the data can be readily interpreted only if the packing density is independent of liquid loading. Since this assumption was apparently met for the packings used by Urone and Parcher, their data show exactly the same behavior as that of the upper curves in Figure 3B.

IV. Effects of Constant Mobile Phase Concentration. Constant mobile phase concentration can be achieved either by operation at infinite dilution or by one of several available finite concentration techniques, described elsewhere.[11,12,17]

If $\bar{c}$ is maintained constant while V_L is varied, then since a point has been fixed on each of the three relevant distribution isotherms, each of the q_i, and consequently K_i', of eq 9 must be constant. Only V_L, A_I, and A_S can vary. It is then a straightforward matter to construct the appropriate plots. Since K_L is constant, the variations of K_L and $K_L V_L$ with V_L are the same as that shown in Figures 1B(ii) and IC(ii), respectively. The $K_I A_I$ plot differs from Figures 2C in that the curve follows the A_I–V_L plot because K_I is also constant.

(24) J. J. Kirkland, *Anal. Chem.*, 35, 2003 (1963).

Likewise, plots of $K_S A_S$ against V_L follow those of Figure 3A(i).

Two compound cases are considered for the condition of constant sample concentration. In the first, when $(K_L V_L + K_I A_I >> K_S A_S$, V_N will vary with V_L according to Figure 5A(i). In this figure, differences in

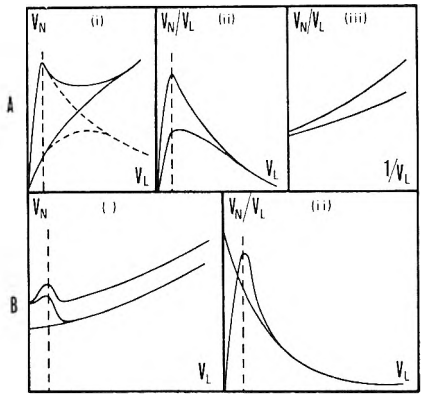

Figure 5. A, Net retention volume at constant solute concentration in the mobile phase, for the case where $K_L V_L \simeq K_I A_I >> K_S A_S$. In (i) and (ii): upper curves: wetted support; lower curves: nonwetted support; broken curves: $K_I A_I > K_L V_L$; solid curves: $K_L V_L > K_I A_I$; vertical broken line: point of monolayer formation. Upper curves in (iii) smaller and larger sample sizes; curves do not intersect at $V_L = \infty$. B, Net retention volume at constant solute concentration in the mobile phase, where $K_L V_L \simeq K_I A_I \simeq K_S A_S$. (i) Variation of V_N with V_L. Upper curve: nonpolar stationary phase which wets the support; middle curve: polar stationary phase which wets the support; lower curve: nonpolar stationary phase which does not wet the support. Vertical broken line: point of monolayer formation. (ii) Variation of V_N/V_L with V_L. Upper curve: nonpolar stationary phase which wets the support; curve for polar, wetting stationary phase is similar. Lower curve: nonpolar stationary phase which does not wet the support. Vertical broken line: point of monolayer formation.

relative importance of $K_L V_L$ and $K_I A_I$ are taken into account; the pair of broken curves apply to systems in which liquid surface adsorption predominates over bulk partition, and the pair of full curves to the reverse situation. The upper curves of each pair refer to wetted supports, and the lower curves to nonwetted supports. It is of interest that Kirkland[24] found precisely the behavior shown in the lower solid curve of Figure 5A(i) for butanol solute on squalane coated onto Kel-F, which is not wet by the squalane. The $V_N/V_L - V_L$ and the $V_N/V_L - 1/V_L$ plots are formally quite similar for the cases of constant concentration and constant sample size, as is made clear by comparison of Figures 5A(ii) and (iii) with 4B(ii) and (iii). The main differences are twofold. First, K_L, still given by the intercept on the ordinate axis, now varies with solute concentration, but to no great extent, since curvature of the bulk partition isotherm is less pronounced than that of the adsorption isotherm. Secondly, curvature in the plot for a given concentration now reflects only the variation of A_I, since both K_L and K_I are constant. Thus if A_I is known as a function of V_L, K_I, as well as K_L, can be determined.

Secondly, we consider the case where $K_L V_L \simeq K_I A_I \simeq K_S A_S$. The resulting plots of V_N and of V_N/V_L are as illustrated in Figure 5B and the behavior is not always formally distinguishable from the situation of constant sample size (Figure 4C). The solid support adsorption-dominated situation, as may be expected, is describable by Figure 3A(i).

Discussion

The results of most importance are obviously those describing overall net retention volume for each of the various combination cases considered above. Some experimental results are available from the literature for comparison. It should be pointed out, however, that Figures 4 and 5, which involve sums of contributions, can only be illustrative in that their exact form is determined by the extent to which each individual retention mechanism contributes. For any particular situation, the figures describing these individual sources of retention should be consulted before drawing conclusions from the overall retention diagrams.

In most fundamental chromatographic work, an attempt is made to reach infinite dilution by the use of the smallest convenient detectable sample size consistent with an acceptable signal to noise ratio. Martin,[2a] for example, used 0.02 μl (*ca.* 0.2 μmol) of each component over the whole range of liquid loadings studied. This sample size produces chromatographic solutions of mean solute mole fractions of the order of 10^{-3}. According to the solution tension measurements of Martire, *et al.*,[5] at these concentrations ($d\gamma/dx$), and therefore $\Gamma_2^{(1)}$ is almost constant, so that K_I will not vary with V_L. This is clearly a case where infinite dilution is effectively achieved. Martin[2a] proved that in his systems $K_S A_S = 0$, so his results should be described by a plot in the form of Figure 5A, *i.e.*, by the sum of Figures 1C and 2B(i). Some calculations based on his data are of interest here. For solution in β,β'-thiodipropionitrile at 25°, the $K_I A_I$ contribution for isooctane at low loadings (1.5% w/w) is about 90% of V_N, while at 25% loading, it is 48%. For cyclopentane, at 1.5% w/w of solvent, the liquid surface contribution is 77% of the total, while at 25% w/w, it is only 6% of V_N. Thus for isooctane, the V_N–V_L plot should be similar to the broken portion of the upper curve in Figure 5A(i), while that for cyclopentane should be closer to the solid upper curve of the same figure. This is, in fact, what is evident in Figure 3 of Martin's paper.[2a]

The more interesting systems to compare are those squalane systems studied by Urone and Parcher[9] and by Pecsok and Gump.[8] Constant sample size was used in the glpc study,[9] and for methanol was 10 μmol in 1 cc of helium carrier gas. For untreated firebrick,

strong solid support interaction can be anticipated and the result should appear as the upper curve in Figure 3B(i). Such a maximum is in fact found in Figure 1 of ref 9. A replot of Urone and Parcher's data as V_N/V_L *vs.* V_L is formally similar to our Figure 3B(ii), showing a well-developed hump at low solvent/support ratios. The magnitude of the solid support adsorption swamps out the other retention mechanisms. If pure partition was observed, methanol should elute before acetone, since its activity coefficient–vapor pressure product is about 5 times that of acetone. The relative support adsorption coefficients for this firebrick must therefore be in the ratio of about 15/1 [K_S(methanol)/K_S(acetone) to match the published data.[9]

Urone and Parcher's data for tri-*o*-tolyl phosphate stationary phase are dominated at low liquid loadings by support adsorption also. However, as more liquid is added, interfacial adsorption and partition become dominant, resulting in a plot similar to the lower curve of Figure 4C(i) for support coated by a polar solvent. Data are also given for silanized firebrick.[9] The most obvious result of the support treatment is a reduction in the observed retention volume of methanol by a factor of 20 to 40. Clearly the majority of adsorbing sites have been eliminated. According to the static measurements of Pecsok and Gump,[8] the infinite dilution values of K_L and K_I, extrapolated to 75°, are for methanol 2.92 and 80 $\times$ 10^{-6} cm, respectively. Assuming that Urone and Parcher's 1 m $\times$ 4 mm i.d. columns contained 10 g of packing, values of K_LV_L can be calculated. Subtracting this K_LV_L from the V_N values determined from a redrawn plot of the published figure,[9] the remainder is ($K_IA_I + K_SA_S$). Using values of A_I taken from Martire, *et al.*,[5] we can then calculate values of ($K_I + K_SA_S/A_I$) for columns containing 0.5 to 16% w/w of squalane. These values range from 34 $\times$ 10^{-6} cm at 0.5% w/w to 109 $\times$ 10^{-6} cm at 16% w/w squalane. K_SA_S/A_I can now be calculated since values of K_I as a function of the solute mole fraction in solution can be calculated from Pecsok and Gump's data as follows. Values of the solute mole fraction in solution at the column inlet are calculated from the known sample size, sample volume, and V_L, and vary from 0.06 at 0.5% w/w to 0.04 at 16% w/w. (It is interesting that over the range of liquid loadings from 0.5 to 16% w/w, the maximum solute mole fraction varies only by a factor of 1.5.) If the reasonable assumption is made that the center of the solute band undergoes dilution by a factor of about 50 in moving to the outlet end of the column, the mole fraction is about 10^{-3} at the outlet. At this concentration, calculation from Pecsok and Gump's extrapolated data gives a value of K_I for the methanol–squalane system of about 20 $\times$ 10^{-6} cm for all the liquid loading used. Thus K_SA_S/A_I goes from about 10 $\times$ 10^{-6} cm at 0.5% w/w to about 90 $\times$ 10^{-6} cm at 16% w/w. Solid support adsorption must therefore provide a very significant contribution to the overall solute retention in this system even after careful silanization. The exact relative magnitude of the contribution cannot be deduced, since computation of precise values of K_I would require more exact information than is available as to the solute concentration profile and the dependence of the solution surface tension on concentration in this system. The important conclusion is that these three contributions—partition, liquid surface, and solid surface adsorption—are all participating to roughly the same extent and add up to an apparent linear variation of V_N with V_L. Because support adsorption masks liquid interfacial adsorption in the system studied by Urone and Parcher,[9] no inconsistency exists between their experimental results and the known occurrence[8] of liquid interfacial adsorption in the system.

Conclusions

The glpc systems so far chosen for study of the Gibbs effect have been largely free of complicating support effects and so have provided valuable information. If the technique is to be extended beyond the relatively limited range of suitable systems of this type—and there may well be great need for this, for example, to allow study of complexing reactions by glpc—certain practical and theoretical criteria must clearly be met.

First, we see from earlier argument that the use of columns of much less than about 5% w/w loading is undesirable since no theory exists for the liquid surface situation in the absence of a bulk phase. It is also advantageous to use a sensitive detector which permits recording of peaks small enough to approach symmetry in profile. If asymmetrical peaks cannot be avoided, a procedure is available for dealing with the situation, but is longer and involves some loss of accuracy.[17]

Treatment of data is best effected by plotting V_N/V_L against $1/V_L$ at constant concentration which may, of course, be infinite dilution. This gives K_L without need for any ancillary data, and can also yield K_I and K_SA_S if A_I is independently determined. Values of K_L are given by the intercept on the ordinate axis and, since K_L varies more slowly with concentration than K_IA_I or K_SA_S, the plots for different, but small, concentrations should all extrapolate to the same point.

Operation at constant sample size, as opposed to constant concentration, does not lead to evaluation of thermodynamic parameters but is useful for one particular purpose: the appearance of a hump, such as that shown in Figures 3B(i) and (ii), in a plot of V_N or V_N/V_L against V_L, is a diagnostic test for support adsorption in the presence of a nonpolar solvent wetting the support. More generally, the diagrams previously given can be used to draw conclusions about the types of interaction involved in a given chromatographic system, operated at either constant concentration or constant sample size. Finally, because of the possibility of compensa-

tion between two or more mechanisms, it is incorrect to draw conclusions about surface effects on the basis of measurements at only two different loadings. Use of a wide range of loadings is mandatory.

Acknowledgments. J. R. C. thanks the University of Wales for an I.C.I. Research Fellowship. D. C. L. thanks the National Science Foundation for a Postdoctoral Fellowship.

Concurrent Solution and Adsorption Phenomena in Chromatography. II. System Alcohols–Squalane

by D. F. Cadogan, J. R. Conder,[1a] D. C. Locke,[1b] and J. H. Purnell

Department of Chemistry, University College of Swansea, Swansea, Glamorgan, Great Britain *(Received August 13, 1968)*

Gas–liquid partition chromatography has been used for the first time to determine accurate values of the limiting activity coefficients of C_3–C_5 alcohols in squalane over the temperature range 50–70°. A newly devised data-treatment procedure was used to circumvent the problems of liquid and solid support interfacial adsorption which occur in these systems, and which have plagued previous chromatographic investigations. The results validate the corrective procedure used, thus allowing the extension of chromatographic techniques to the study of the thermodynamics of such systems.

In part I,[2a] we considered in qualitative detail the problems of interpretation which arise when chromatographic retention arises from the simultaneous occurrence of bulk solution, liquid interface adsorption, and solid interface adsorption. Comparison of the alternative procedures of evaluating retention data corresponding to constant sample size or to constant sample concentration clearly showed the latter to be preferable. It was then shown that true bulk partition coefficients could always be obtained if the appropriate data treatment methods were adopted.[2] This work describes an experimental glpc test of the methods devised. Alcohol–squalane systems have been chosen for study because they show complex retention characteristics in high degree. In a previous study of such systems[3] the influence of surface retention was not correctly allowed for and it is of interest to determine the extent of the error introduced.

Experimental Section

Columns of stainless steel tube of about 50 cm length, 1/4 in. o.d., and 0.028 in. wall thickness were packed with squalane supported on carefully HMDS-silanized 100–120 mesh Sil-O-Cel. Four such columns were prepared, the percentage of squalane in the coated packing varying from 7.3 to 32.5 by weight. Squalane was deposited on the solid support from solution in ether. The exact amount of squalane deposited was determined by careful weighing. The results were checked by refluxing weighed portions of the packing with acetone in a Soxhlet extraction apparatus until the packing was reduced to a constant weight. In all cases the weights of squalane on each column deduced from several extractions were within 0.3% of each other and in agreement with the expected weight on the column to at worst 3% and usually much better. The percentage loading was taken as the mean of the two values so obtained.

The columns were contained in a forced air thermostat electronically controlled to within ±0.01° and with a total temperature difference between the ends of the oven of less than 0.1°. Hydrogen carrier gas, dried by passage through 5A molecular sieve and silica gel, was flow controlled to better than 1%, the flow being frequently checked by use of a thermostated soap bubble flow meter.

Liquid samples were injected from a 0–1 μl Hamilton microsyringe through a silicone rubber septum contained in an injection block heated to 102°. The solutes were injected separately and in mixtures with no noticeable effect on their retention volumes. The retention volume of the peak maximum for each solute was measured for a series of sample injection sizes ranging from less than 0.01 to 0.07 μl and found to

(1) (a) Department of Chemical Engineering, University College of Swansea. (b) Department of Chemistry, Queens College of the City University of New York, Flushing, N. Y. 11367.

(2) (a) J. R. Conder, D. C. Locke, and J. H. Purnell, *J. Phys. Chem.*, **73**, 700 (1969); (b) J. R. Conder, *J. Chromatogr.*, **39**, 273 (1969).

(3) A. B. Littlewood and F. W. Willmott, *Anal. Chem.*, **38**, 1031 (1966).

decrease with increase in sample size. The proportional change in retention over this range of sample size varied from 7 to 70%, depending on the liquid loading, temperature, and nature of the solute. With markedly asymmetrical peaks, such as were observed in all cases in this study, the peak maximum of a sample of a given size is found to be almost coincident with a point of the same height on the diffuse edge of a peak of larger size. A plot of peak height against retention volume was thus constructed, effectively reproducing the diffuse boundary of a large, asymmetrical peak. As retention volume, V_N, increases with changing liquid loading, the height of a zone of given solute concentration on the boundary also increases. In accordance with the procedure of Conder,[2b] the heights chosen on the plots at each liquid loading were therefore proportionated to V_N by a process of successive approximation to give a series of values of V_N at different liquid loadings but constant concentration. This was done for four different concentrations.

A twin-channel katharometer was situated in the thermostat in close proximity to the column, one channel being situated at the column outlet and the other at the inlet to enable the injection peak to be recorded. The time constant of the read-out system did not exceed 2 sec, the resulting contribution to recorded peak asymmetry being negligible. Retention volumes were measured from the injection peak and corrected for column dead volume by subtracting the retention volume of a separately injected air sample.

Squalane used was May and Baker "Embaphase" brand for gas chromatography and the alcohols were all B.D.H. laboratory reagents.

Results

It was shown in part I[2a] that the general retention equation

$$V_N = K_L'V_L + K_I'A_I + K_S'A_S \qquad (1)$$

described the retention behavior of a solute subject to solution and the several forms of adsorption possible in a chromatographic system (see part I for definition of symbols). The K values in eq 1 are primed since each is sample size (concentration) dependent. Only at true infinite dilution can we write

$$V_N = K_LV_L + K_IA_I + K_SA_S \qquad (2)$$

with truly constant distribution coefficients.

Since V_N of eq 1 is deduced from an experimental datum *via*

$$V_N = K_{obsd}V_L \qquad (3)$$

it follows that we may write

$$(V_N/V_L) = K_{obsd} = K_L' + (K_I'A_I + K_S'A_S)/V_L \qquad (4)$$

and hence a plot of K_{obsd}, the apparent (experimental) distribution coefficient, against $1/V_L$, even at constant solute concentration, should be a curve since both A_I and A_S are functions of V_L. The intercept at $1/V_L = 0$ is K_L. Since K_L' varies much less with concentration than K_I' or K_S' and since only low concentrations can be used if eq 1 and 4 are to remain valid, K_L' is essentially constant and equal to the infinite dilution value K_L. Thus, if K_{obs} is determined as a function of V_L, plots of the data at a variety of (constant) solute concentrations should take the form of a family of curves with a common intercept. The procedure adopted for analyzing the chromatograms so as to maintain constant concentration as V_L varies is described in ref 2.

Figure 1 illustrates the families of curves obtained as

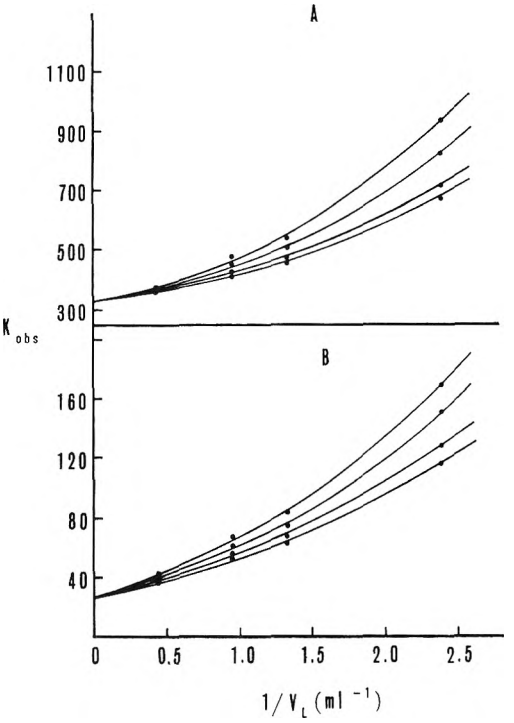

Figure 1. Plot of V_R/V_L against $1/V_L$ at four different solute concentrations (arbitrary concentration units) for (A) 1,1-dimethyl-1-propanol and (B) 2-propanol, at 50°.

described for elution at 50° of 2-propanol and of 3-methyl-1-butanol, representing the extremes of the molecular weight range of solutes used and of distribution coefficients measured. These are typical of all the others. The fact that in all cases the curves for different solute concentrations extrapolate so closely to a common point is encouraging confirmation of our procedure and the theory on which it is based. The derived values of K_L for all solutes at the three temperatures used are listed in Table I.

The data of Table I may be converted to specific retention volumes (V_g) for bulk solution at infinite dilution *via* the expression

$$V_g = 273K_L/T\rho_L \qquad (5)$$

where T is absolute temperature and ρ_L is solvent den-

Table I: Values of K_L Derived for Alcohols in Squalane from Plots of K_{obs} against $1/V_L$

Alcohol	K_L 50°	60°	70°
2-Propanol	26	...	14
1-Butanol	148	98	72
2-Butanol	94	63	50
2-Methyl-1-propanol	109	70	57
2-Methyl-2-propanol	46	32	26
2-Pentanol	264	173	125
3-Methyl-1-butanol	330	200	146
1,1-Dimethyl-1-propanol	169	112	83

sity. The latter was measured at the relevant temperatures by dilatometry and the results are listed in Table II.

In order to convert V_g data to activity coefficients, saturation vapor pressure data are required. Data for 2-propanol were taken from Parks and Barton,[4] while those for the butanols and pentanols, except for 3-methyl-1-butanol, were calculated from the equations

Table II: Density of Squalane (g ml^{-1})

	Temp, °C 50	60	70
ρ_L	0.7900	0.7834	0.7770

of Butler, Ramchandani, and Thomson.[4] The published equation[5] for 3-methyl-1-butanol is erroneous and so the vapor pressure data were plotted and interpolated for this compound. Table III lists the values employed.

Table III: Saturation Vapor Pressures (mm) of Alcohols in the Range 50–70°

Alcohol	p_2°, mm 50°	60°	70°
2-Propanol	176.8	288.5	454.8
1-Butanol	35.22	61.86	104.0
2-Butanol	79.38	135.0	219.5
2-Methyl-1-propanol	54.80	94.65	156.4
2-Methyl-2-propanol	175.8	287.7	452.0
2-Pentanol	31.81	56.56	95.90
3-Methyl-1-butanol	18.00	33.45	58.75
1,1-Dimethyl-1-propanol	75.84	128.2	207.2

Values of γ_p^0 were derived through the usual infinite dilution equation

$$\gamma_p^0 = 273R/p_2^\circ M_S V_g \qquad (6)$$

and are listed in Table IV. Since K_L' was observed to be virtually independent of concentration at the very low concentrations used, the data relate essentially to infinite dilution, so that the possibility of alcohol polymerization in these solutions is precluded.

Table IV: Values of γ_p° for Alcohols in Squalane over the Temperature Range 50–70°

No.	Alcohol	γ_p° 50°	60°	70°
1	2-Propanol	8.19	...	6.17
2	1-Butanol	7.22	6.35	5.25
3	2-Butanol	5.04	4.52	3.58
4	2-Methyl-1-propanol	6.28	5.83	4.44
5	2-Methyl-2-propanol	4.65	4.18	3.34
6	2-Pentanol	4.48	3.93	3.28
7	3-Methyl-1-butanol	6.34	5.75	4.58
8	1,1-Dimethyl-1-propanol	2.94	2.68	2.29

Excess partial molar Gibbs free energies, $\bar{g}_2^e$ (kcal mol^{-1}), were calculated from the γ_p° values interpolated to 333.3°K. Partial molar enthalpies, $\bar{h}_2^e$ (kcal mol^{-1}), were derived from the slopes of the lines in Figure 2, and excess partial molar entropies, $\bar{s}_2^e$ (eu), determined from the difference. The values are all presented in Table V.

Table V: Derived Thermodynamic Quantities for Alcohols in Squalane

Alcohol	$\bar{g}_2^e$ kcal mol^{-1}	$\bar{h}_2^e$ kcal mol^{-1}	$\bar{s}_2^e$ cal mol^{-1} deg^{-1}
2-Propanol	1.29	3.36	6.2
1-Butanol	1.22	3.62	7.2
2-Butanol	0.959	3.79	8.5
2-Methyl-1-propanol	1.11	3.58	7.4
2-Methyl-2-propanol	0.916	3.56	7.9
2-Pentanol	0.876	3.47	7.8
3-Methyl-1-butanol	1.12	3.52	7.2
1,1-Dimethyl-1-propanol	0.622	2.90	6.8

In principle, fugacity corrections should be applied to γ_p° to yield the more meaningful γ_f°. For the alcohols of interest here the literature offers no help since no second virial coefficients, B_{22}, for the temperature range of this study have been quoted. We have, therefore, adopted a corresponding states approach in which all available B_{22} data[6-11] have been plotted in reduced form as B_{22}/V_c against T/T_c where the critical

(4) G. S. Parks and D. Barton, *J. Amer. Chem. Soc.*, **50**, 24 (1928).
(5) J. A. V. Butler, C. N. Ramchandani, and D. W. Thomson, *J. Chem. Soc.*, **138**, 280 (1935).
(6) J. D. Cox, *Trans. Faraday Soc.*, **57**, 1674 (1961).
(7) C. B. Kretschmer and R. Wiebe, *J. Amer. Chem. Soc.*, **76**, 2579 (1954).
(8) J. D. Lambert, G. A. H. Roberts, J. S. Rowlinson, and V. J. Wilkinson, *Proc. Roy. Soc.*, **A196**, 113 (1949).
(9) J. D. Lambert, *Discussions Faraday Soc.*, **15**, 226 (1953).
(10) M. P. Moreland, J. J. McKetta, and I. H. Silberberg, *J. Chem. Eng. Data*, **12**, 329 (1967).
(11) R. L. Pecsok and B. H. Gump, *J. Phys. Chem.*, **71**, 2202 (1967); (they cite unpublished data of Dymond).

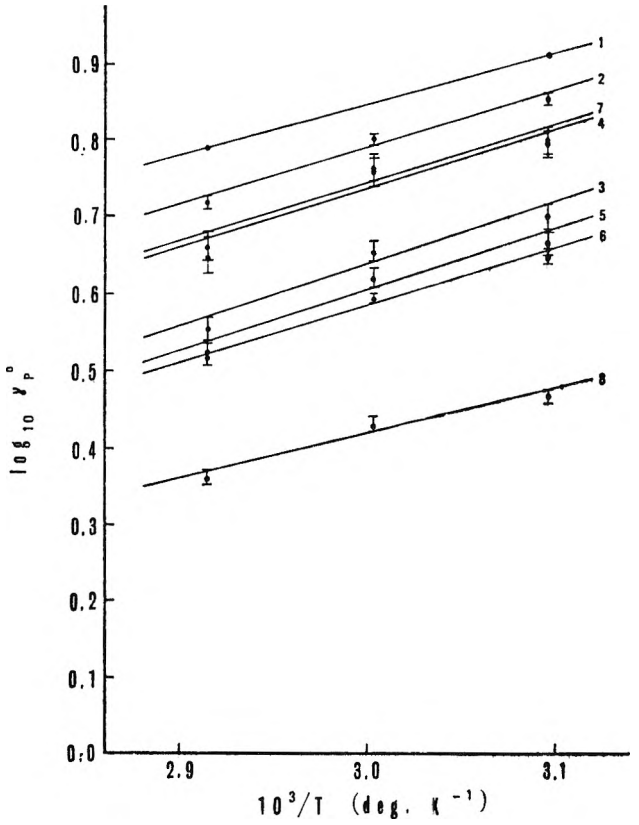

Figure 2. Temperature dependence of log γ_p^0 for alcohols in squalane. Solutes are numbered as in Table IV. Estimated experimental errors in γ_p^0 are indicated.

volumes V_c and temperatures T_c are those of Ambrose and Townsend.[12] The lack of even these data for the pentanols restricts the calculations to the lower alcohols. With the exception of the data for methanol[7,8,11] and ethanol,[7,9,11] all the available data were obtained at reduced temperatures greater than 0.68. Since the reduced temperature range of interest here is 0.57–0.68, a best curve was drawn through the data and extrapolated. The values of B_{22} derived are listed in Table VI.

Table VI: Second Virial Coefficients (cc mol^{-1}) for Alcohols in the Temperature Range 50–70°

Alcohols	$-B_{22}$, cc mol^{-1} 50°	60°	70°
Methanol	1800	1400	1100
Ethanol	2600	2100	1600
1-Propanol	4600	3700	3000
2-Propanol	3100	2400	1900
1-Butanol	7400	6200	5400
2-Butanol	5800	4500	3600
2-Methyl-1-propanol	6600	5500	4400
2-Methyl-2-propanol	3800	2900	2300

The values listed are liable to error on a number of counts but the overall correction to γ_p° is only in the order of a few per cent. Thus, this matter is of secondary importance. The equation

$$\ln \gamma_f^0 = \ln \gamma_p^0 - (p_2^0/RT)(B_{22} - v_2^0) - (\bar{p}v_2^0/RT) \quad (7)$$

was then used for computation, where $\bar{p}$ is the mean column pressure and v_2° the molar volume of solute. The term in $\bar{p}\ B_{12}/RT$ was dropped since no data for interaction in hydrogen–alcohol vapor mixtures exist and no satisfactory method for calculation of B_{12} is known. In any case, the value is small for hydrogen carrier gas and the overall result is negligible. Table VII lists values of γ_f° calculated as above.

Table VII: γ_f° Values for Some Alcohols in Squalane in the Temperature Range 50–70°

Alcohol	γ_f° 50°	60°	70°
2-Propanol	8.39	...	6.31
1-Butanol	7.46	6.57	5.43
2-Butanol	5.06	4.54	3.68
2-Methyl-1-propanol	6.37	5.96	4.57
2-Methyl-2-propanol	4.78	4.30	3.48

Although B_{22} increases with increasing molecular weight, it is seen that the extent of the fugacity correction diminishes. This results from the functional dependence of ln γ_f° on the product p_2°/B_{22}. The validity of the approximations made is established by comparison of the data of Table IV and VII. The fugacity correction is small in all cases, never exceeding 3%.

Discussion

Figure 2 illustrates plots of log γ_p° against $1/T$ for all the alcohols studied. Experimental errors are indicated in the figure. The procedure used to subtract adsorption contributions from measured retention data is expected to introduce an uncertainty of a few per cent into the derived solution activity coefficients. Errors of this order in retention data are to be expected whenever adsorption phenomena accompany solution in chromatographic systems. High precision of the order of a few tenths of one per cent is attainable only when adsorption phenomena are absent and no correction procedures are required. Although the points plotted in Figure 2 appear to be best represented by curves of negative curvature for all solutes, it is perhaps more realistic, in view of the indicated precision of the data, to adopt straight line plots. As shown in Table V, the excess enthalpy of mixing varies little from one solute to another and averages 3.5 kcal mol^{-1}. Savini, Winterhalter, and van Ness[13] present heat of mixing

(12) D. Ambrose and R. Townsend, *J. Chem. Soc.*, 3614 (1963).
(13) C. G. Savini, D. R. Winterhalter, and H. C. Van Ness, *J. Chem. Eng. Data*, **10**, 168 (1965).

data for some C_3–C_5 alcohols in C_5–C_9 paraffins, extrapolated with some misgivings to infinite dilution to give values of the order of 5.4 kcal mol^{-1}. Little variation is expected and found between solutes since $\bar{h}_2^e$ is essentially the enthalpy of hydrogen-bond breaking. These two sets of values are not inconsistent in view of the relatively large expected uncertainties (20–40%) in the derived chromatographic values. As expected, the excess partial molar entropies of mixing are large and positive, ranging from 6–8 cal mol^{-1} deg^{-1}.

The dependence of the activity coefficient on solute structure may be seen by reference to Figure 2. The dominant features determining solubility are (a) carbon number and (b) the position of the –OH group. Thus, solubility increases with increasing carbon number and increases in the series: primary < secondary < tertiary alcohol, *i.e.*, as the screening of the –OH group increases. In contrast, chain branching at points remote from the position of the functional group has little effect on solubility.

Support for the validity and accuracy of our activity coefficient data is provided by measurements on methanol and ethanol in a static apparatus by Pecsok and Gump.[11] These data correlate well with ours when plotted in the form of log γ_p° against carbon number.

This agreement between the chromatographically and statically measured data would seem to be excellent confirmation of the general hypothesis and procedures discussed in part I[2a] and clearly allows the extension of the glpc technique to the study of polar–nonpolar systems. The advantages of glpc may thus be brought into a new area of study.

It is appropriate now to consider the errors which are introduced when remedial procedures for accounting for surface effects are not adopted. Comparison of our data with those of Littlewood and Willmott[3] shows that at 70° the agreement between the γ_p° values is remarkably good, but that as the temperature is diminished, disagreement increases. At 50°, our values are about 10% greater than theirs. While this may not appear to be a significant absolute difference, there are considerable relative differences in the general temperature dependences observed. Thus, for example, in the data of these authors[3] there are curious inversions in the relative magnitudes of γ_p° within the homologous series. In contrast, there is a regularity evident in our data at all temperatures and the relative values of γ_p° change little; the heats of mixing are sensibly constant for all the alcohols studied. We conclude that failure to correct for surface effects can lead to very misleading information, even though the absolute error involved may not be very great.

Consideration of eq 1 and the probable temperature dependences of the individual terms leads us to an interesting conclusion of wide relevance. Significant surface effects are most likely to occur where bulk solubility is low, *i.e.*, where a strong positive deviation from Raoult's law obtains. In consequence, the bulk heat of solution will be expected to be considerably less than the heat of condensation of the solute. On the other hand, the heats of adsorption at the interfaces will equal or exceed the heat of condensation. Thus, the contribution of the surface terms relative to the bulk solution will diminish with increasing temperature and at some limiting temperature will become negligible for every system.

This proposition offers an explanation for the discrepant temperature dependences recorded by Littlewood and Willmott[3] and also allows correlation of their work with ours. Since they ignored the surface contribution and in effect attributed the whole of retention to bulk solubility, at low temperatures the solubility will appear to be enhanced and γ_p° will apparently be smaller than the true value, in accord with our comparison.

Although in this work we have chosen to evaluate only bulk solution data, it is apparent that our method[2a] can be further employed to determine at least one of the surface partition coefficients if either A_I or A_S is known. Having evaluated K_L as described, we may now rewrite eq 1 in the form

$$V_N - K_L V_L = K_I A_I + K_S A_S \qquad (8)$$

and a plot of the left-hand side against A_I or A_S will yield a curve, the limiting slope of which will correspond to K_I or K_S, respectively. An alternative procedure has been suggested by Conder.[2b] Data can be obtained for A_I as a function of V_L for glpc systems[2a] and so in principle one of these procedures may be followed. We have not chosen to do so here since our primary objective has been to establish the glpc method as a viable technique for the study of solutions in which adsorption effects are also present.

Further discussion of the values of γ_p° deduced is hindered by lack of an adequate theory for alcohol solutions. Considerably more experimental studies are required. In addition, as has been explicitly pointed out by Van Ness, *et al.*,[14] direct measurement of appropriate thermodynamic parameters is the fastest and most accurate means available. To this end, we believe that the advantages offered by glpc make it most important to establish its role in this context.

Acknowledgment. J. R. C. thanks the University of Wales for an I.C.I. Research Fellowship, D. C. L. thanks the National Science Foundation for a Postdoctoral Fellowship, and D. F. C. thanks the Foxboro Company, Foxboro, Massachusetts, for a Studentship and an equipment grant.

(14) H. C. Van Ness, J. Van Winkle, H. H. Richtol, and H. B. Hollinger, *J. Phys. Chem.*, **71**, 1483 (1967).

Hydrolysis Kinetics of Dilute Aqueous Chromium(III) Perchlorate[1]

by Larry D. Rich, David L. Cole, and Edward M. Eyring[2]

Department of Chemistry, University of Utah, Salt Lake City, Utah 84112 *(Received August 22, 1968)*

Dissociation field effect relaxation times in dilute aqueous chromium(III) perchlorate solutions have been measured and attributed to the hydrolysis equilibrium

$$Cr^{3+} + H_2O \underset{k_{-1}}{\overset{k_1}{\rightleftharpoons}} CrOH^{2+} + H^+$$

At 25° the specific rate $k_{-1} \cong 7.8 \times 10^8\ M^{-1}\ sec^{-1}$ at an ionic strength $\mu \cong 5 \times 10^{-4}\ M$. This k_{-1} is approximately six times smaller than that measured previously for reaction between a proton and $AlOH^{2+}$.

Introduction

The aqueous solution chemistry of chromium(III) has been summarized by Earley and Cannon.[3] Dilute aqueous solutions of chromium(III) perchlorate reportedly contain the hydrolysis products $CrOH^{2+}$ and $Cr(OH)_2^+$ as well as polymeric species such as $Cr_2(OH)_2^{4+}$. The water molecules in the first coordination spheres of these species have been omitted in this notation simply for convenience. In the absence of evidence for complexing of aquated chromium(III) species by perchlorate, we expect that the major equilibria in acidic, dilute aqueous chromium(III) perchlorate solutions will be

$$Cr^{3+} + H_2O \underset{}{\overset{k_1}{\rightleftharpoons}} CrOH^{2+} + H^+ \quad (1)$$

$$CrOH^{2+} + H_2O \underset{}{\overset{k_2}{\rightleftharpoons}} Cr(OH)_2^+ + H^+ \quad (2)$$

$$2CrOH^{2+} \underset{}{\overset{k_3}{\rightleftharpoons}} Cr_2(OH)_2^{4+} \quad (3)$$

Two of the corresponding equilibrium constants

$$K_1 = \frac{k_1}{k_{-1}} = [H^+][CrOH^{2+}]/[Cr^{3+}] = 1.05 \times 10^{-4}\ M \quad (4)$$

$$K_2 = \frac{k_2}{k_{-2}} = [H^+][Cr(OH)_2^+]/[CrOH^{2+}] = 10^{-5.55}\ M \quad (5)$$

were determined spectroscopically by Emerson and Graven[4] for chromium(III) perchlorate solutions at 25° and ionic strengths μ ranging from 0.01 to 0.05 M. Tsuchiya and Umayahara[5] have obtained a conductometric value of $K_1 = 1.1 \times 10^{-4}\ M$ for aqueous chromium(III) sulfate at 25° extrapolated to $\mu = 0$ in excellent agreement with the K_1 of Emerson and Graven.[4] A dimerization equilibrium constant

$$K_3 = \frac{k_3}{k_{-3}} = [Cr_2(OH)_2^{4+}]/[CrOH^{2+}]^2 \cong 10^4\ M^{-1} \quad (6)$$

can be deduced[3,6] from the data of Bjerrum[7] and Finholt.[8]

In 10^{-3} M chromium(III) perchlorate solutions maintained at 30° and ranging in pH from 2 to 3, Postmus and King[9] found no evidence of polymerization after 1.5 years. The very slow polymerization and depolymerization reactions of aqueous chromium(III) have also been noted by other workers.[3,10,11] True equilibrium can only be achieved by aging for very long periods or by heating aqueous chromium(III) solutions well above room temperature. We chose to explore the kinetics of chromium(III) perchlorate hydrolysis in freshly prepared acidic solutions kept at 25° or below. Thus the system is clearly out of true equilibrium and the concentration of $Cr_2(OH)_2^{4+}$ and higher polymers can be assumed to be negligible.

Our immediate goal is to determine the rate constants k_1 and k_{-1}. We wish eventually to correlate values of k_1 *vs.* reciprocal metal ion radii for a large number of isovalent ions. For the present we must content ourselves with a comparison of k_{-1} for chromium(III) with a value $k_{-1} = 4.4 \times 10^9\ M^{-1}\ sec^{-1}$ found[12] for the reaction

$$AlOH^{2+} + H^+ \xrightarrow{k_{-1}} Al^{3+} + H_2O$$

(1) This research was supported by the Directorate of Chemical Sciences, Air Force Office of Scientific Research, Grant AF-AFOSR-476-66.

(2) To whom communications should be addressed.

(3) J. E. Earley and R. D. Cannon, "Transition Metal Chemistry," Vol. 1, R. L. Carlin, Ed., Marcel Dekker, Inc., New York, N. Y., 1965, p 34 ff.

(4) K. Emerson and W. M. Graven, *J. Inorg. Nucl. Chem.*, **11**, 309 (1959).

(5) R. Tsuchiya and A. Umayahara, *Bull. Chem. Soc. Jap.* **36**, 554 (1963).

(6) J. I. Morrow and J. Levy, *J. Phys. Chem.*, **72**, 885 (1968).

(7) N. Bjerrum, "Studier over Basiske Kromiformbindelser," Inaugural Dissertation, Copenhagen, 1908.

(8) J. Finholt, Thesis, Berkeley, UCRL Report No. 8879 (1960).

(9) C. Postmus and E. L. King, *J. Phys. Chem.*, **59**, 1208 (1955).

(10) J. N. Bronsted and K. Volquartz, *Z. Phys. Chem.*, **134**, 97 (1928).

(11) H. T. Hall and H. Eyring, *J. Amer. Chem. Soc.*, **72**, 782 (1950).

(12) L. P. Holmes, D. L. Cole, and E. M. Eyring, *J. Phys. Chem.*, **72**, 301 (1968).

Table I: Calculated Molar Concentrations and Experimental Dissociation Field Effect Relaxation Times in Dilute Aqueous Chromium(III) Perchlorate at 25°

c_0,[a] 10^{-5} M	pH[b]	μ,[c] 10^{-4} M	γ_{H^+}[d]	$[H^+]$,[e] 10^{-5} M	$[Cr^{3+}]$,[f] 10^{-5} M	$[CrOH^{2+}]$,[f] 10^{-5} M	$[Cr(OH)_2^+]$,[f] 10^{-6} M	$\bar{\tau}$,[g] μsec	n[h]
14.86	3.98_4	7.52	0.969	10.72	7.42	7.28	1.92	3.74 ± 0.41	8
11.14	3.97_8	5.77	0.972	10.80	5.58	5.43	1.44	4.59 ± 0.17	8
9.20	3.82_8	5.30	0.967	15.35	5.42	3.70	0.68	3.03 ± 0.17	9
7.43	4.21_6	3.54	0.979	6.22	2.68	4.52	2.05	4.03 ± 0.18	7
5.58	4.31_0	2.59	0.981	4.99	1.73	3.64	2.06	4.69 ± 0.32	6
3.71	4.24_0	1.89	0.984	5.84	1.28	2.31	1.12	5.26 ± 0.41	5
2.23	4.63_8	0.956	0.989	2.33	0.368	1.66	2.01	5.77 ± 0.31	10

[a] Total molar concentration of chromium(III) perchlorate. [b] Glass electrode pH of the sample solution. [c] Ionic strength of the sample solution. [d] Activity coefficient of hydrogen ion calculated from the limiting form of the Debye–Hückel relation. [e] Molar concentration of hydrogen ion, $[H^+] = 10^{-pH}/\gamma_{H^+}$. [f] Molar ionic concentrations calculated from eq 4, 5, and 7 through 10 of the text. [g] Average experimental dissociation field effect relaxation time with standard deviation calculated from the range. [h] Number of independent determinations of the relaxation time.

in aqueous aluminum(III) chloride at 25° and ionic strength $\mu \cong 10^{-3}$ M.

Eigen's relaxation methods are well suited to kinetic studies of protolytic equilibria such as that in eq 1. The dissociation field effect or electric field jump (E-jump) relaxation method[13] permits the ready determination of chemical relaxation times of 10^{-5} to 10^{-7} sec that we would anticipate for such a monomeric hydrolysis step in $\sim 10^{-4}$ M aqueous chromium(III) solutions.

Experimental Section

G. F. Smith Co. reagent grade chromium(III) perchlorate, $Cr(ClO_4)_3 \cdot 3H_2O$, was dissolved in distilled, deeminized, boiled water to yield an approximately 5×10^{-3} M stock solution. The exact chromium concentration was determined volumetrically: oxidation to dichromate using ammonium persulfate was followed by a titration of the dichromate with ferrous ion, the latter solution having been previously standardized with a primary standard potassium dichromate solution.[14] Sample solutions for the E-jump experiments were prepared by adding small aliquots of this stock solution under a Linde high-purity dry nitrogen atmosphere to 10^{-7} ohm^{-1} cm^{-1} conductivity water prepared by an electrophoretic ion-exclusion technique.[15] The pH of each sample solution was determined with a Beckman 1019 pH meter fitted with 41263 glass and 39071 calomel electrodes.

Our E-jump apparatus for conductometric determination of chemical relaxation times resulting from the application of a square, high-voltage wave has been described previously.[16,17] Our experimental results are summarized in Table I. The concentrations shown were calculated from the measured pH, known total concentration of chromium(III) denoted hereafter by c_0, eq 4 and 5, and the additional equations

$$c_0 = [Cr^{3+}] + [CrOH^{2+}] + [Cr(OH)_2^+] \quad (7)$$

$$\mu = \tfrac{1}{2}(9[Cr^{3+}] + 4[CrOH^{2+}] + [Cr(OH)_2^+] + 3c_0) \quad (8)$$

$$-\log \gamma_{H^+} = 0.509\sqrt{\mu} \quad (9)$$

$$[H^+] = 10^{-pH}/\gamma_{H^+} \quad (10)$$

The relaxation times τ were obtained from the oscilloscope traces by plotting the relative voltage (ordinate) *vs.* time (abscissa) on semilog paper and drawing a single straight line through the data. In no case did a photographed oscilloscope trace give rise to multiple slopes in the corresponding semilog plot.

Results

The available equilibrium data, eq 1–6, and the Smoluchowsky–Debye–Eigen phenomenological equation[18] for the limiting values of diffusion-controlled ionic reactions led us to anticipate observing two E-jump relaxation times each of the order of a few microseconds and caused by the coupled monomeric hydrolyses, eq 1 and 2. For instance, let us assume that $k_{-1} = 9 \times 10^8$ M^{-1} sec^{-1} and $k_{-2} = 4 \times 10^9$ M^{-1} sec^{-1}. These specific rates are plausible since they are considerably smaller than the upper limit for the diffusion-controlled reaction rate constants calculated from the Smoluchowsky–Debye–Eigen equation for the general reactions

$$H^+ + B^{2+} \xrightarrow{k_{-1}} \quad \text{and} \quad H^+ + B^+ \xrightarrow{k_{-2}}$$

in water at 25°, and since this phenomenological equation would also predict that $k_{-2} > k_{-1}$. Using the equilibrium concentrations calculated for the first

(13) M. Eigen and L. De Maeyer, "Technique of Organic Chemistry," Vol. VIII, Part II, S. L. Friess, E. S. Lewis, and A. Weissberger, Ed., Interscience Publishers, Inc., New York, N. Y., 1963, p 988 ff.

(14) D. A. Skoog and D. M. West, "Fundamentals of Analytical Chemistry," Holt, Rinehart and Winston, Inc., New York, N. Y., 1963, p 457.

(15) W. Haller and H. C. Duecker, *J. Res. Nat. Bur. Stand.*, **A64**, 527 (1960).

(16) D. T. Rampton, L. P. Holmes, D. L. Cole, R. P. Jensen, and E. M. Eyring, *Rev. Sci. Instrum.*, **38**,, 1637 (1967).

(17) D. L. Cole, E. M. Eyring, D. T. Rampton, A. Silzars, and R. P. Jensen, *J. Phys. Chem.*, **71**, 2771 (1967).

(18) Reference 13, p 1032.

experiment of Table I (*i.e.*, $[H^+] = 1.07 \times 10^{-4}\ M$, $[CrOH^{2+}] = 7.28 \times 10^{-5}\ M$, $[Cr(OH)_2^+] = 1.92 \times 10^{-6}\ M$), $k_1 = K_1k_{-1} = 9.45 \times 10^4\ sec^{-1}$ and $k_2 = K_2k_{-2} = 1.13 \times 10^4\ sec^{-1}$, we may calculate from the appropriate expression for the relaxation times

$$\tau_{1,2}^{-1} = \frac{\alpha_{11} + \alpha_{22}}{2}\left[1 \pm \sqrt{1 - \frac{4(\alpha_{11}\alpha_{22} - \alpha_{12}\alpha_{21})}{(\alpha_{11} + \alpha_{22})^2}}\right] \quad (11)$$

where

$$\alpha_{11} = k_1 + k_{-1}([H^+] + [CrOH^{2+}]) \quad (12)$$

$$\alpha_{12} = k_{-1}([H^+] + [CrOH^{2+}]) \quad (13)$$

$$\alpha_{21} = (k_2 - k_{-2}[Cr(OH)_2^+]) \quad (14)$$

$$\alpha_{22} = k_2 + k_{-2}([H^+] + [Cr(OH)_2^+]) \quad (15)$$

that $\tau_1 = 3.93\ \mu sec$ and $\tau_2 = 2.22\ \mu sec$. There is no serious obstacle to resolving two relaxation times this widely spaced as is evident, for example, from a rate study[19] of nickel(II) diglycine and imidazole complex formation. Thus, the simplest inference to draw from our observation of a single microsecond time range relaxation is that only one protolytic equilibrium is present in these aqueous chromium(III) perchlorate sample solutions. We can easily provide a tentative identification of this equilibrium by plotting the data of Table I first in terms of the equation

$$\tau_1^{-1} = k_1 + k_{-1}([H^+] + [CrOH^{2+}]) \quad (16)$$

and then in terms of the equation

$$\tau_2^{-1} = k_2 + k_{-2}([H^+] + [Cr(OH)_2^+]) \quad (17)$$

The least-squares straight line through the data plotted in terms of eq 16 has a slope $k_{-1} = 7.8 \times 10^8\ M^{-1}\ sec^{-1}$ and an intercept $k_1 = 1.4 \times 10^5$. The quotient $k_1/k_{-1} = 1.8 \times 10^{-4}\ M$ is in quite good agreement with $K_1 = 1.1 \times 10^{-4}\ M$ of eq 4. Equation 17 also gives a good straight line fit of the data with a slope $k_{-2} = 1.1 \times 10^9\ M^{-1}\ sec^{-1}$ and intercept $k_2 = 1.5 \times 10^5\ sec^{-1}$. However, the quotient $k_2/k_{-2} = 2.4 \times 10^{-4}\ M$ is in very poor agreement with $K_2 = 2.8 \times 10^{-6}\ M$ of eq 5. Thus we have evidently observed the first monomeric hydrolysis step, eq 1.

Discussion

There are actually at least two plausible explanations for our failure to observe a second relaxation time attributable to the second monomeric hydrolysis step of eq 2. It may indeed by true that K_2 is much smaller than $10^{-5.55}$ in freshly prepared, dilute aqueous chromium(III) perchlorate solutions. In this case the correct calculation of k_1 and k_{-1} from the experimental relaxation times requires the iterative solution of

$$K_1 = [H^+][CrOH^{2+}]/[Cr^{3+}] \quad (18)$$

$$c_0 = [Cr^{3+}] + [CrOH^{2+}] \quad (19)$$

$$\mu = {}^1/_2(9[Cr^{3+}] + 4[CrOH^{2+}] + 3c_0) \quad (20)$$

and eq 9, 10, and 16 starting from $K_1 = 1.05 \times 10^{-4}\ M$ and rapidly attaining a different, constant value of $K_1 = k_1/k_{-1}$. Since the dominant term in eq 16 is $[H^+]$ and not $[CrOH^{2+}]$, the constant values $k_1 = 1.4 \times 10^5\ sec^{-1}$, $k_{-1} = 6.7 \times 10^8\ M^{-1}\ sec^{-1}$, and $K_1 = k_1/k_{-1} = 2.1 \times 10^{-4}\ M$ obtained from eq 18–20, 9, 10, and 16 in four iterations do not differ significantly from those reported in the preceding paragraph.

The other plausible explanation for our observation of one rather than two relaxations in the microsecond time region was suggested by Hammes and Steinfeld.[19,20] For a coupled system of two equilibria, such as eq 1 and 2, one of the two normal concentration variables, y_i,[21] proportional to the amplitude of the observed voltage change, is a sum of two large terms in the concentrations, rate constants, reciprocal relaxation times, etc., whereas the other normal concentration variable is equal to a difference of two such terms. Thus the amplitude of the latter relaxation effect could be too small for detection even though both of the coupled chemical equilibria were present in the sample system.

Returning now to a discussion of the kinetics of eq 1, it is interesting to compare the previously found[12] $k_{-1} = 4.4 \times 10^9\ M^{-1}\ sec^{-1}$ and $k_1 = 4.2 \times 10^4\ sec^{-1}$ for aluminum(III) with the present $k_{-1} = 7.8 \times 10^8\ M^{-1}\ sec^{-1}$ and $k_1 = 1.4 \times 10^5\ sec^{-1}$ for chromium(III). Taking the dielectric constant ϵ to be that of bulk solvent, 78.5 for water at 25°, and assuming an interionic reaction distance $\sigma = 7.5$ Å previously found suitable for diffusion-controlled reactions in water,[22] we calculate from the Smoluchowsky–Debye–Eigen equation[18] that the upper limit of k_{-1} for the reaction $H^+ + MOH^{2+} \rightarrow M^{3+} + H_2O$ is $\sim 2 \times 10^{10}\ M^{-1}\ sec^{-1}$. Our experimental k_{-1} values for aluminum(III) and chromium(III) both lie comfortably below this limit for diffusion-controlled reaction, but why is k_{-1} for Cr(III) only one-sixth that for Al(III)? An explanation might involve either differences in dielectric constant near $CrOH^{2+}$ compared to $AlOH^{2+}$ or differences in the distances to which solvent water molecules are highly structured away from these two ions. Differences in both properties for these two ions would arise from differences in ionic radii (for Al^{3+} $r = 0.50$ Å and for Cr^{3+} $r = 0.69$ Å)[23] that in turn yield differences in electrostatic potential gradient near the surfaces of these isovalent ions.

Since the reverse reaction

$$Cr(H_2O)_6^{3+} \xrightarrow{k_1} Cr(H_2O)_5OH^{2+} + H^+$$

(19) G. G. Hammes and J. I. Steinfeld, *J. Amer. Chem. Soc.*, **84**, 4639 (1962).

(20) J. I. Steinfeld, B. S. Thesis, M.I.T., 1962, pp 51-54.

(21) See ref 13, p 908 ff.

(22) M. Eigen and L. De Maeyer, *Proc. Roy. Soc.*, **A247**, 505 (1958).

(23) L. Pauling, "The Nature of the Chemical Bond and the Structure of Molecules and Crystals," 3rd ed, Cornell University Press, Ithaca, N. Y., 1960.

involves the separation of repulsive charges as well as the migration of a very mobile proton, we are not surprised that $k_1 = 1.4 \times 10^5$ sec^{-1} for this reaction is a great deal larger than the 25° first-order rate constant $k_1^* \sim 10^{-5}$ to 10^{-6} sec^{-1} reported[24] for the much studied reaction

$$Cr(H_2O)_6^{3+} \xrightarrow{k_1^*} Cr(H_2O)_5^{3+} + H_2O$$

that bears it a superficial resemblance. The ion–dipole attractive interaction in this latter reaction as well as the lower mobility of H_2O than H^+ could account for a markedly lower k_1^* than k_1.

(24) M. Eigen and R. G. Wilkins in "Mechanisms of Inorganic Reactions," Advances in Chemistry Series, No. 49, R. F. Gould, Ed., American Chemical Society, Washington, D. C., 1965, p 64.

An Infrared Study of the Adsorption and Mechanism of Surface Reactions of 1-Propanol on γ-Alumina and γ-Alumina Doped with Sodium Hydroxide and Chromium Oxide

by A. V. Deo and I. G. Dalla Lana

Department of Chemical and Petroleum Engineering, University of Alberta, Edmonton, Alberta, Canada
(Received September 9, 1968)

Infrared studies of the adsorption of 1-propanol on γ-alumina and the effect of doping the γ-alumina with sodium hydroxide and/or chromium oxide in the temperature range from room temperature to 400° are described. Four different types of surface species were observed: (i) strongly physically hydrogen-bonded propanol to the surface hydroxyl groups; (ii) an aluminum propoxide type structure chemisorbed on Al^{3+} ions; (iii) a carboxylate structure in which both surface hydroxyl and Al^{3+} ions are involved; and (iv) a conjugated hydrocarbon species bonded probably to the Al^{3+} ions. Dehydration mainly occurred on the pure γ-alumina surface, particularly on the high-frequency hydroxyl groups. On the addition of sodium hydroxide, the dehydration reaction was suppressed and the dehydrogenation reaction became dominant. The addition of chromium oxide apparently creates more dehydrogenating sites. The dehydrogenation possibly proceeds *via* a mechanism involving both carbonium and carbanion ions. The results are correlated by both infrared spectra and mass spectral analysis of the gaseous products.

Introduction

One of the earliest studies of the catalytic dehydrogenation of primary alcohols was reported by Ipatieff[1] in 1936. Komarewsky[2] used this method to prepare symmetrical ketones. In a similar study, with 1-propanol as the feed to a fixed-bed reactor using a sodium hydroxide-treated chromia–Alundum catalyst, Dalla Lana,[3] *et al.*, proposed a chemical model for the multiple reaction sequence. By isolating and identifying chemical intermediates and by examining the chemical reactions of several intermediates under identical conditions, they showed the chemical sequence involved dehydrogenation of the 1-propanol to propionaldehyde followed by parallel condensation of the aldehyde to either its aldol or to propyl propionate under the elevated temperature at 400°. They also encountered some thermal reactions.[4] The present paper discusses some mechanistic aspects of this reaction system, obtained by studying the infrared spectra of 1-propanol adsorbed on the catalyst and of the intermediate surface species formed thereof. Some attention is also devoted to the catalytic influence of γ-alumina on 1-propanol.

Infrared spectral studies of the adsorption of primary alcohols on alumina have been previously reported. Babushkin and Uvarov[5] studied the adsorption of ethanol on alumina at 20° and found that the alcohol was adsorbed in fragments such as OH, $-CH_2-CH_2-$, and also as an ethoxy group bound directly to an aluminum atom on the surface, $Al-O-CH_2-CH_3$.

(1) V. N. Ipatieff, "Catalytic Reactions at High Pressures and Temperatures," The Macmillan Co., New York, N. Y., 1936, pp 411–451.

(2) V. I. Komarewsky and J. R. Coley, *J. Amer. Chem. Soc.*, **63**, 700, 3269 (1941); *Advan. Catal.*, **8**, 207 (1956).

(3) I. G. Dalla Lana, K. Vasudeva, and D. B. Robinson, *J. Catalysis*, **6**, 100 (1966).

(4) I. G. Dalla Lana, S. E. Wanke, and A. V. Deo, paper presented at the Second Symposium on Catalysis, Hamilton, Ontario, Canada, June 16, 1967.

(5) A. A. Babushkin and A. V. Uvarov, *Dokl. Akad. Nauk SSSR*, **110**, 581 (1956).

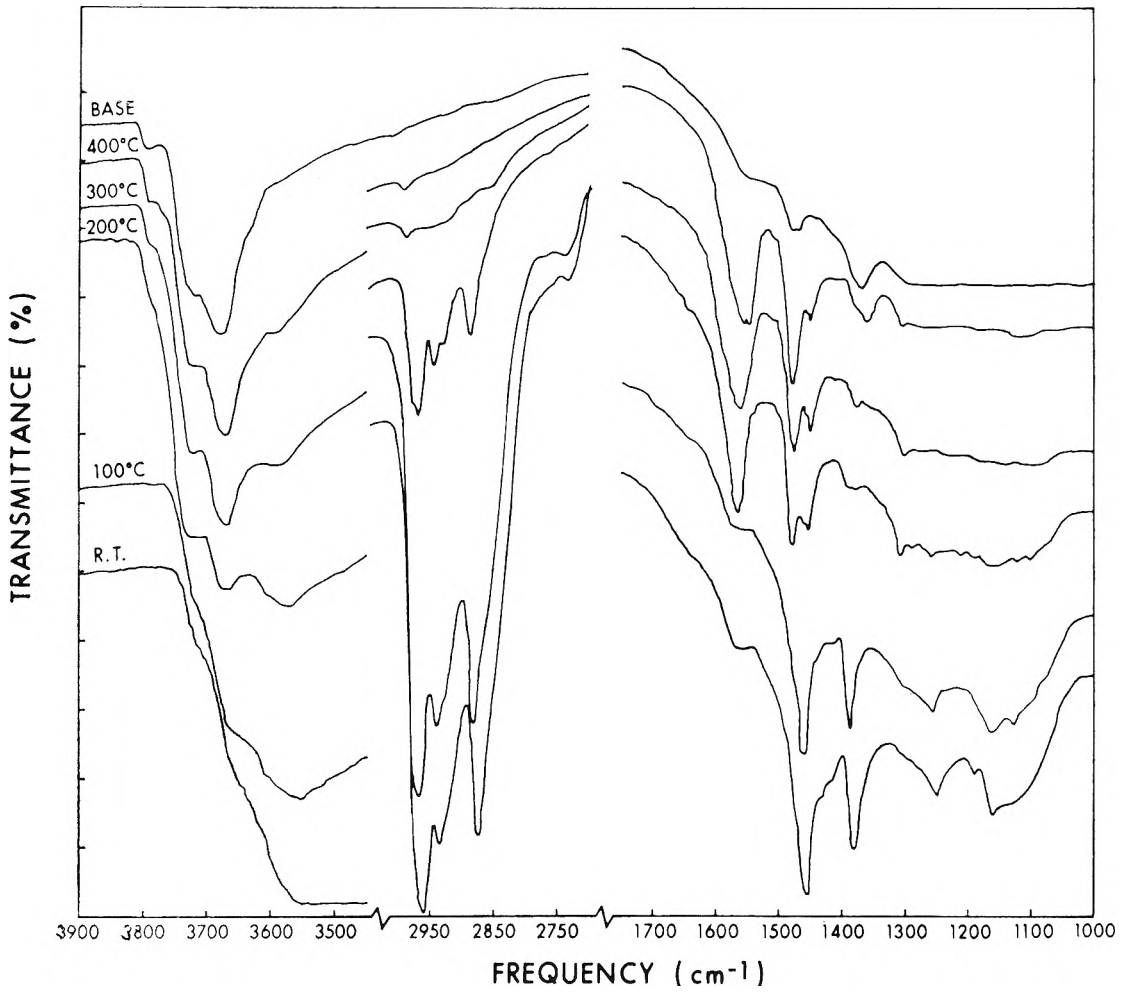

Figure 1. 1-Propanol on γ-alumina. Heated in 1 cm of PrOH at $T°$ for 1 hr and pumped off at $T°$ for 1 hr.

Roev and Terenin[6] studied the mechanism of decomposition of methanol and ethanol on chromium oxide catalyst at 20 and 150° and observed that water molecules and hydroxyl groups split off from the alcohols with the formation of unsaturated compounds. The elimination of an H atom also resulted in the formation of surface components of the type Cr–O–R. Greenler[7] studied the adsorption of methanol and ethanol on γ-alumina in the temperature range from 35 to 430° and identified three surface species, *viz.*, an easily removed liquid phase, a surface alkoxide structure, and an ester-like surface structure. More recently, Kagel[8] studied the adsorption and surface mechanism of C_1 to C_4 normal alcohols on γ-alumina in the temperature range from 25 to 500° and observed the same three species as reported by Greenler. He proposed a mechanism for these adsorption processes. The present work restricts the study to 1-propanol but investigates the effect of doping γ-alumina with sodium hydroxide and chromium oxide, in the temperature range from room temperature to 400°. Sodium hydroxide is generally believed to suppress the catalytic dehydration activity of γ-alumina, and chromium oxide itself behaves as a dehydrogenation catalyst. Their use as doping agents in this work parallels the earlier studies reported by Dalla Lana, *et al.*[3]

Experimental Section

A γ-Alumina powder, Alon-C,[9] was used to prepare thin infrared-transparent wafers by pressing the fine powder in a 2-in. diameter die at a pressure of 12 tons/in.^{2}. To dope the γ-alumina catalyst with sodium hydroxide and/or chromium oxide, 2% aqueous solutions were mixed with alumina into a thick slurry using a minimum amount of water. The excess water was removed by evaporation from the slurry at 110° and the resulting cake was crushed into fine powder, which could then be pressed into thin wafers. The catalyst wafer was then placed in an *in situ* infrared cell[10] with sodium chloride windows. The pretreatment of the pure γ-alumina and the one doped with sodium hydroxide involved degassing at 450° for 2 hr, heating

(6) L. M. Roev and A. N. Terenin, *Dokl. Akad. Nauk SSSR*, 124, 373 (1954).
(7) R. G. Greenler, *J. Chem. Phys.*, 37, 2094 (1962).
(8) R. O. Kagel, *J. Phys. Chem.*, 71, 844 (1967).
(9) Cabot Corporation, Boston, Mass.
(10) J. B. Peri and R. B. Hannan, *J. Phys. Chem.*, 64, 1526 (1960).

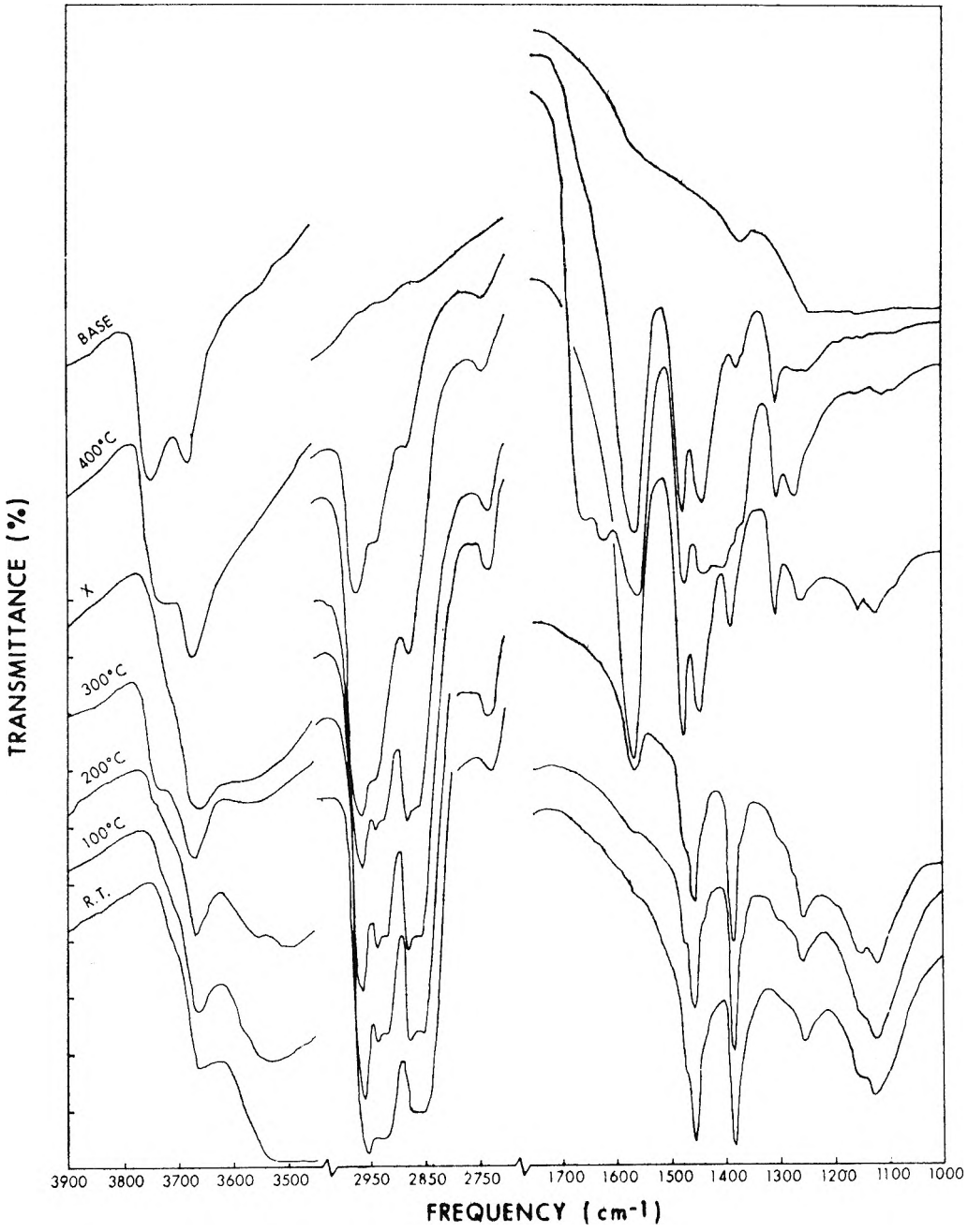

Figure 2. 1-Propanol on NaOH treated γ-alumina. Heated in 1 cm of PrOH at $T°$ for 1 hr and pumped off at $T°$ for 1 hr. ($\times$: heated at 400° for 1 hr and pumped off at 300° for 1 hr.)

in oxygen at 10 cm pressure for 2 hr at 450°, and again degassing at this temperature overnight. In the case of chromia-doped catalyst, the oxygen treatment was followed by heating in hydrogen at 10 cm pressure for 2 hr at the same temperature to ensure that the chromium was in a reduced state.

After cooling to room temperature, the base line spectrum of the catalyst was recorded on a Perkin-Elmer Model 621 infrared spectrophotometer, using a similar evacuated cell without a catalyst wafer in the reference beam. Because of the low transmission of the catalyst wafers, the reference beam had to be attenuated and the slits opened to compensate for the loss in energy, the slit opening being directly proportional to the square root of the reciprocal of transmittance.

The 1-propanol (Fisher Co.) was purified by distillation followed by repeated freezing and thawing on the vacuum rack. One centimeter of absolute pressure of propanol vapor was introduced in both cells and the spectrum was recorded differentially to eliminate interference from spectrum of gaseous propanol. To check that the spectrum of the adsorbed species alone was obtained, the procedure was repeated but with removal

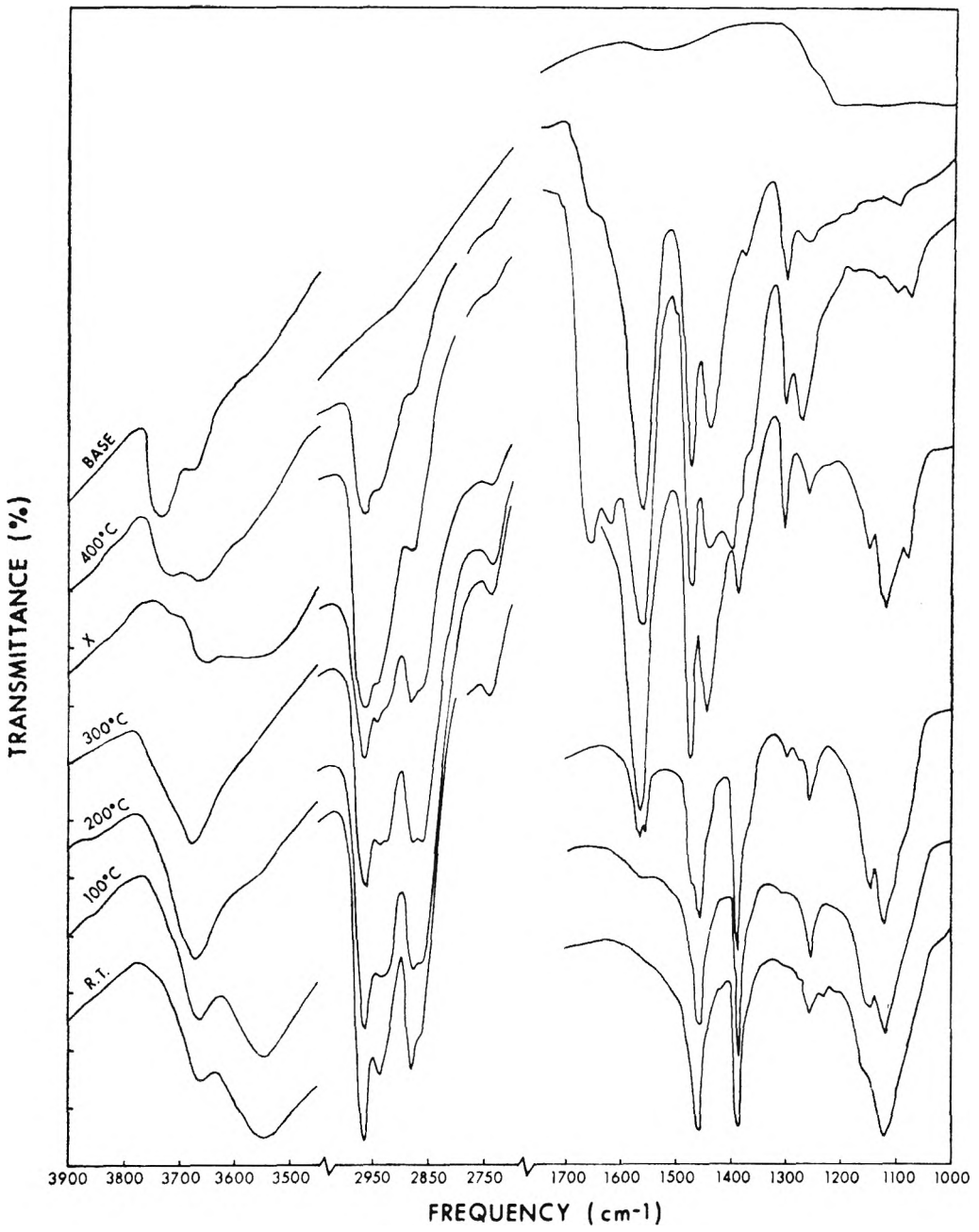

Figure 3. 1-Propanol on NaOH treated γ-alumina doped with chromium oxide. Heated in 1 cm of PrOH at $T°$ and pumped off at $T°$ for 1 hr. (×: heated at 400° for 1 hr and pumped off at 300° for 1 hr.)

of the catalyst from the sample beam and again recording the spectrum with vapor alone in both cells. After recording the spectrum of the adsorbed substance, excess alcohol was pumped off at room temperature for 1 hr. Physically adsorbed alcohol was removed by degassing at 100° for 1 hr. High-temperature heating up to 400° was maintained for a further 1 hr with the vapor of propanol at 1 cm pressure in the cell. The subsequent degassing was completed in steps of 100°, the spectrum being recorded after each step.

The spectra so obtained are shown in Figures 1 to 3. They show selected spectra for each set of experiments and the spectra are shifted along the transmission scale for convenience and clarity in reading. Although Figures 1 to 3 appear rather crowded in detail, the presentation of all related spectra in a single figure (rather than in several figures) facilitates the observation and comparison of changes in infrared spectra. The region between 1300 and 1000 cm^{-1}, where the transmission of the catalyst drops sharply, is shown as a difference between the base line and the spectrum in the adsorbed state, whereas in the region at higher frequencies, the spectra are shown as recorded.

After heating the propanol in the presence of the catalyst wafer, the infrared spectrum of the vapor was recorded to study the products formed. These results

were checked against the related mass spectra, for the same vapor phase as well as for the species removed by pumping. The mass spectra were obtained with an AEI(MS2) mass spectrometer.

Results and Discussion

I. 1-Propanol on Pure γ-Alumina. Figure 1 shows the results of adsorption of propanol on alumina at different temperatures, along with the base line. The base line shows three broad bands at 3785, 3720, and 3680 cm^{-1} which are attributed to the three different types of surface hydroxyl groups as reported by Peri.[10] The model put forward by Peri[11] for the surface sites on γ-alumina will be used in the discussion of the results. The model assumes that even after sufficient dehydration, when the water molecules physically adsorbed are largely eliminated, the surface of alumina still retains hydroxyl groups with neighboring sites of oxide and aluminum ions. Moreover, the number of oxide ions surrounding the hydroxyl groups differentiates them from one another and imparts different acidity to them.

Spectra obtained at room temperature and 100° (and up to ≃170°) are more or less similar to the propanol spectrum in the vapor phase except for a few distinct changes and sharper bands. The high-frequency 3758 cm^{-1} band disappears completely while the other two hydroxyl bands are still evident. The large broad band around 3500 cm^{-1} is due to hydrogen bonding of the alcohol molecules to the surface hydroxyl groups. Because of the possibility of hydrogen bonding between the alcohol molecules themselves, though normally negligible in the gas phase at low pressures, as well as with the surface groups, the hydroxyl group interactions are difficult to interpret but may be used as an indirect evidence of hydrogen bonding with the surface.

There are no changes in the C–H stretching and bending regions; however, the OH in-plane bending band at 1220 cm^{-1} shifts to a higher frequency of 1250 cm^{-1}. More pronouncedly, the –C–OH stretching band also shifts upwards from 1060 to around 1150 cm^{-1}. These shifts to higher frequencies and the presence of the OH in-plane bending band suggest that the H of the hydroxyl group in the alcohol is free and that the alcohol molecules are hydrogen bonded to the surface hydroxyl through the oxygen in the alcohol. Moreover, this band structure corresponds almost exactly to that reported[7,8] for an aluminum alkoxide (in the present case aluminum propoxide). Although the 1150 and 1250-cm^{-1} bands might mask one another, additional supporting evidence was observed. The large broad band at roughly 3500 cm^{-1} is characteristic of hydrogen bonding. Furthermore, pumping at higher temperatures after room temperature adsorption of alcohol resulted in rather easy desorption of the hydrogen-bonded alcohol molecules. The minor differences are due to the number of hydrocarbon chains, aluminum propoxide with three hydrocarbon chains, while the surface structure will have only one. From these results, one may surmise that, up to 170°, two types of adsorbed species (I and II) are formed, with their structures as follows.

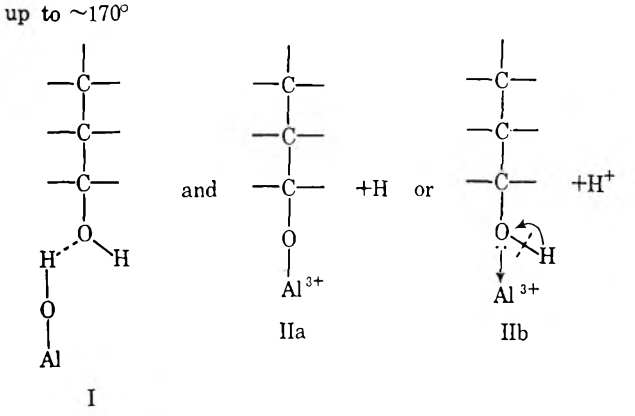

I IIa IIb

Structure I is the strongly hydrogen-bonded physically adsorbed species. Considering either IIa where the H atom is dissociated as such, or IIb where the hydrogen ion H^+ is removed, structure IIb seems to be the more plausible one. The H^+ ion thus removed is free to migrate to oxide surface sites and form H_2.

Significant changes occur in the spectra of adsorbed species on heating above 170°. The broad band around 3500 cm^{-1} attributed to the hydrogen bonding with the surface now increases to a larger extent than that encountered at room temperature and up to ≃170°. Correspondingly, a new band at around 1650 cm^{-1} (not shown in figure) appears due to H–O–H bending of adsorbed water. This water band and also the increased broad band around 3500 cm^{-1} are easily removed on pumping at room temperature.

Four new bands are observed at 1565, 1480, 1450, and 1303 cm^{-1}. These are stable up to 400° with degassing. The bands at 1565 and 1480 cm^{-1} correspond to asymmetric and symmetric stretching vibrations of the carboxylate ion; the bands at 1450 and 1303 cm^{-1}, which decrease in intensity on pumping at higher temperatures, seem to be either characteristic of the propionate structure or associated with the carboxylate structure. The sources of these two bands were not confirmed. Now, since the alkoxide structure is not observed above 200° but the carboxylate structure is, it may be expected that the alkoxide must have formed the carboxylate. Greenler[7] has shown by studying the adsorption of CH_3OD and CD_3OH on γ-alumina that the hydrogen removed from the surface carboxylate (formate) comes from the methyl group, and taking into consideration the bridge structure proposed by Eischens and Pliskin[12] for chemisorbed formic acid on nickel, one can write the carboxylate structure

(11) J. B. Peri, *J. Phys. Chem.*, **69**, 220 (1965).

(12) R. P. Eischens and W. A. Pliskin, *Actes Congr. Intern. Catalyse, Paris* (1960).

of the adsorbed species (III) as

above ~170° to 400°

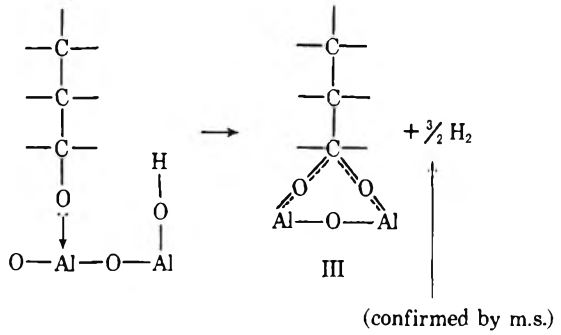

The hydrogen evolved in this reaction was detected by mass spectrometer. The shift to the lower frequency side of 1565-cm^{-1} band on degassing at higher temperatures may be due to a change in Al–Al distance with the corresponding change in the carboxylate bond angle.

The infrared spectrum of the gaseous products formed above 200° shows that propylene is the major reaction product. The band at 1650 cm^{-1} for the adsorbed species suggests that water is also formed during the reaction above 200°. This was confirmed by mass spectral analysis of the gaseous product formed at 400°, which was found to consist mainly of propylene, water, and less than 1% hydrogen. This reaction, occurring above 200°, is explained on the basis that structure I, hydrogen-bonded propanol, dehydrates giving propylene.

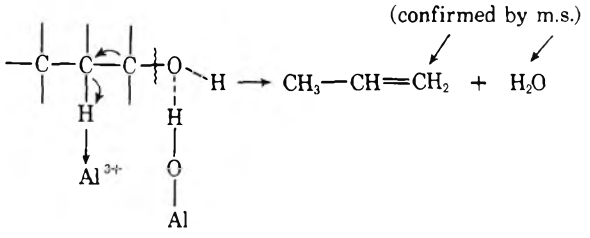

II. 1-Propanol on Sodium Hydroxide Treated γ-Alumina. Figure 2 shows results from a similar set of studies of adsorption of propanol on sodium hydroxide treated γ-alumina at different temperatures, along with the corresponding base line. The base line shows only two well-separated hydroxyl bands at 3740 and 3680 cm^{-1} instead of the three encountered in the case of pure alumina. Peri[10] has reported that the band at the lower frequency of 3680 cm^{-1} appears to be the more acidic of the three hydroxyl groups, shown by the greater ease with which it exchanges hydrogen. As a result, the disappearance of the high-frequency 3785-cm^{-1} band and not the low-frequency more acidic 3680-cm^{-1} band is rather unexpected. The results from the adsorption of propanol on γ-alumina (Figure 1) show that the high-frequency 3785 cm^{-1} hydroxyl band disappears completely while the other two remain more or less separated, and on desorption at high temperatures, this high-frequency band reappears last. The disappearance suggests that sodium hydroxide reacts with the high-frequency surface hydroxyl to form Al–O–Na.

Adsorption spectra at room temperature, 100°, and 200° are more or less similar to the one on pure alumina. The following three differences were noted: (i) the hydroxyl region is more distinctly outlined suggesting a lesser degree of hydrogen bonding; (ii) in the C–H stretching region, 2940 and 2880-cm^{-1} bands are resolved into doublets. In conjunction with this, the fact that the 1380-cm^{-1} band, which is always smaller in intensity than the 1455-cm^{-1} band as is the case on pure alumina, has reversed the intensity relation, suggesting an O–R bonding;[13] and (iii) the small band at 1562 cm^{-1} gives an indication of the beginning of formation of carboxylate species. From this, one can conclude that up to 200° the major surface species formed is the alkoxide (II) with very little of the hydrogen-bonded species (I).

At 300°, the asymmetric and symmetric stretching bands of the carboxylate ion become more pronounced but the bands due to the alkoxide species still exist, suggesting an abundance of this latter species. Up to this high temperature, the spectrum of the gaseous phase does not change from that of propanol showing that no reaction has taken place.

The spectrum marked X was taken after heating the catalyst with 1 cm of propanol at 400° for 1 hr and then pumping off at room temperature, 100, 200, and 300° for 1 hr each. Two new bands are observed at 1650 and 1617 cm^{-1}, while the other bands due to the alkoxide species were much reduced. These new bands show the presence of conjugated double bonds; however, these bands disappear after pumping at 400° and then only the carboxylate bands remain. The spectrum of the gaseous product shows the band structure is similar to unsaturated compounds. This was confirmed by a mass spectral analysis of the gaseous product, which showed the presence of propylene and mainly conjugated hydrocarbons with the molecular formulas C_6H_{10} (confirmed by exact mass measurements) and 7% hydrogen. Water was not formed in this reaction, indicated by the fact that the hydroxyl region did not increase in intensity and the absence of the 1650-cm^{-1} band which disappears on pumping at room temperature.

From studies by other workers on silica and alumina, both having surface hydroxyl groups, the greater reactivity of alumina is attributed to the electron-abstracting Lewis acid centers present on the alumina surface as aluminum ions. The results of adsorption of propanol on γ-alumina and the mechanism proposed here suggest that the surface hydroxyl groups more than compete with the aluminum ions resulting in dehydra-

(13) K. Nakanishi, "Infrared Adsorption Spectroscopy," Holden-Day, Inc., San Fransisco, Calif., 1962, p 22.

tion of the alcohol. Once this tendency is suppressed by doping with sodium hydroxide, the main reaction involves aluminum ions and thus the dehydrogenation reaction becomes dominant. Sodium hydroxide, it seems, does not take part in the reaction but essentially suppresses one type of active site and leaves the other unaffected. The following mechanism for the formation of unsaturated hydrocarbon then seems plausible.

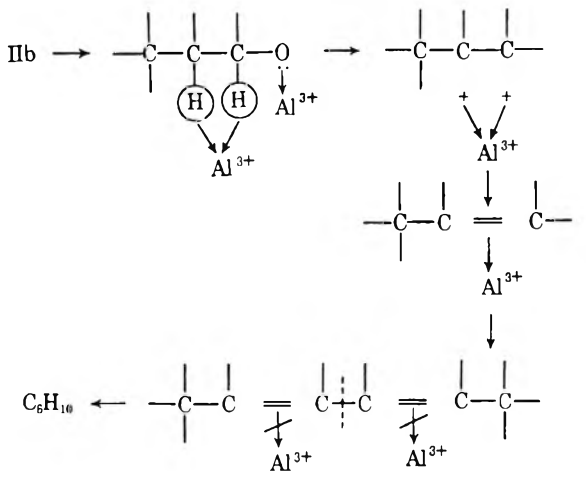

From two alkoxide groups, two carbonium ions will be formed, in which either one of two neighboring Al^{3+} ions will be involved to give the unsaturated hydrocarbon and hydrogen. This result was confirmed with mass spectral analysis.

III. 1-Propanol on Sodium Hydroxide Treated Chromia–Alumina. Figure 3 shows the result of adsorption of propanol on sodium hydroxide treated chromia–alumina at different temperatures. The spectra are similar to those of the propanol adsorbed on sodium hydroxide-treated γ-alumina except, (i) the hydrogen-bonded hydroxyl region is less intense and, (ii) the band structure below 1300 cm^{-1} is more pronounced. This suggests an increase in the number of alkoxide species formed on the surface. It may be mentioned that the alkoxide species may form equally well on chromium ions. The infrared spectrum of the gaseous product is unchanged from that of propanol up to 300°. At 400°, the presence of unsaturated bonds, especially C_5H_8, and carbon monoxide is indicated and confirmed by mass spectral analysis, along with 2% hydrogen. The decrease in the percentage of hydrogen found compared with that from sodium hydroxide-treated γ-alumina may be attributed to chemisorption of hydrogen on chromium ions, which did not desorb when pumped at room temperature.

Burwell, *et al.*,[14] and Van Reijen, *et al.*,[15] have shown that surface chromium ions, on catalyst reduction, are in divalent state, Cr^{2+}, surrounded by oxygen neighbors, and are responsible for the dehydrogenation character of such a catalyst. So, in effect, by adding chromia, one increases the number of surface sites available for dehydrogenation reaction. The decarboxylation reaction and the formation of conjugated hydrocarbons may be explained by considering the carbanion ion mechanism suggested by earlier workers.

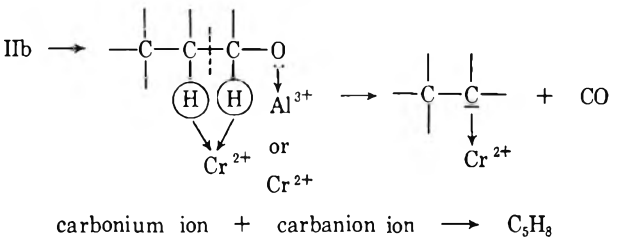

carbonium ion + carbanion ion → C_5H_8

Such a carbanion ion will then react with another carbonium ion, as was shown to form on the sodium hydroxide-treated γ-alumina surface, resulting in the formation of C_5H_8.

Conclusions

The above results show that, under the conditions studied, four types of surface species are mainly formed: (i) hydrogen-bonded propanol (I) strongly physically adsorbed to the high-frequency surface hydroxyl groups; (ii) the aluminum propoxide (II) chemisorbed on the electron-abstracting Lewis-acid aluminum ion, Al^{3+}; (iii) the carboxylate with the bridge structure (III) in which a hydroxyl group is involved; and (iv) the conjugated hydrocarbon species. These observations concur with the results reported by earlier workers, though no single prior study has reported all of these species.

The appearance of and extent of formation of each species varies with temperature and the composition of the catalyst. The formation of the fourth species with the conjugated olefinic structure, formed only on sodium hydroxide-doped catalyst, is tentatively explained through a carbonium ion and carbanion ion mechanism.

The formation of water during the dehydration is amply confirmed by both mass spectra and infrared analysis. In the latter, the hydrogen-bonded hydroxyl region increases in intensity and the 1650-cm^{-1} band due to H–O–H bending appears, both of which disappeared upon pumping at room temperature. In the case of hydrogen, the only evidence obtained for its presence is the mass spectral analysis. The stoichiometric amounts of hydrogen suggested by the proposed mechanism were not quantitatively established. Very recently, Shimizu and Gesser,[16] while studying the esr spectra of hydrogen adsorbed on porous glass, observed signals due to hydrogen on the surface, and have suggested that the hydrogen atom becomes attached to the aluminum atom of the porous glass. This may be one

(14) R. L. Burwell, A. B. Littlewood, M. Cardew, G. Pass, and C. T. H. Stoddart, *J. Amer. Chem. Soc.*, 82, 6272 (1960).

(15) L. L. Van Reijen, W. M. H. Sachtler, P. Cossee, and D. N. Brouwer, Third Congress on Catalysis, North Holland Publishing Co., Amsterdam, 1965, p 829.

(16) M. Shimizu and H. D. Gesser, private discussion.

of the reasons accounting for the variation in the amount of hydrogen observed in the products *via* mass spectral analysis of products desorbed from sodium hydroxide-doped and chromium oxide-doped catalysts. Chromium ions themselves may also present a strong adsorption site for hydrogen.

Thus it appears that the main reaction of propanol on γ-alumina is that of dehydration, involving primarily one type, the least acidic, of surface hydroxyl groups. Once these high-frequency surface sites have been removed by doping with sodium hydroxide, the hydrogenation reaction involving the Al^{3+} becomes dominant. The addition of chromium oxide to the catalyst creates more sites for dehydrogenation. Adsorption of propanol on chromia–alumina catalyst, without sodium hydroxide treatment, gave similar results to those obtained on pure γ-alumina. This suggested that for dehydrogenation to occur, the activity of the dehydrating sites must be first suppressed.

Further studies using the intermediates observed in propanol dehydrogenation[3] and the effect of preadsorbed hydrogen, water, and carbon monoxide will be reported later.

Acknowledgment. This work was supported by funds provided by the National Research Council of Canada and by the University of Alberta.

Electrical Conductances of Aqueous Sodium Iodide and the Comparative Thermodynamic Behavior of Aqueous Sodium Halide Solutions to 800° and 4000 Bars[1]

by Lawrence A. Dunn[2] and William L. Marshall

Reactor Chemistry Division, Oak Ridge National Laboratory, Oak Ridge, Tennessee 37830 *(Received September 9, 1968)*

From electrical conductance measurements on dilute (0.001–0.10 *m*) aqueous solutions, the ionization behavior of NaI was studied in the temperature range 0–800° and at pressures to 4000 bars. Both the conventional (K) and complete (K^0) ionization constants were calculated for comparison with published values for NaCl and NaBr. As expected, NaI ionized to a greater extent than either NaBr or NaCl, the order being directly proportional to the anion size. The net change (k) in waters of solvation on ionization decreased from 10.2 for NaCl to 9.7 for NaI. For the temperature range 400–800°, the van't Hoff isochore yielded standard thermodynamic functions for the complete equilibrium, $NaX(solvated) + kH_2O \rightleftharpoons Na^+(solvated) + X^-(solvated)$. The $\Delta H°$ obtained, approximately constant with temperature, was essentially the same as found for NaBr and NaCl. With the calculated values of $\Delta G°$ and an average value for $\Delta H°$ of -7.0 kcal mol^{-1}, standard entropy changes of -88.3, -86.2, and -82.9 cal mol^{-1} deg^{-1} for the complete reactions were obtained for NaCl, NaBr, and NaI, respectively. The negative values of $\Delta S°$ show that order is increased by additional solvation on ionization of the electrolyte. Thus, at high temperatures, inclusion of the solvent as a reactant provides a simple description whereby each equilibrium can be described by only three values (k, $\Delta H°$, and $\Delta S°$) which are essentially independent both of temperature and pressure. The closeness in values of k and $\Delta S°$ for the three halides suggests that averaged values from these salts may be used to estimate the equilibrium properties of most 1–1 salts between 400 and 800°.

Introduction

The properties of aqueous electrolyte solutions at high temperatures and pressures, particularly in the supercritical region, are amenable to investigation by conductance techniques. This method has been applied in several recent publications from this laboratory to the study of the behavior of dilute aqueous solutions of $KHSO_4$,[3] NaCl,[4] NaBr,[5] and HBr[6] to 800° and to pressures of 4000 bars. The results from these studies have indicated that, at high temperatures and pressures, aqueous electrolyte solutions exhibit a simplified behavior not evident at lower temperatures. It was found that the isothermal limiting equivalent conductances of these salts in the temperature range 100–800°

(1) Research sponsored by the U. S. Atomic Energy Commission under contract with Union Carbide Corp. Presented before the Division of Physical Chemistry at the 156th National Meeting of the American Chemical Society, Atlantic City, N. J., Sept 8–13, 1968.

(2) Mellon Institute, Carnegie-Mellon University, Pittsburgh, Pa. 15213.

(3) A. S. Quist and W. L. Marshall, *J. Phys. Chem.*, **70**, 3714 (1966).

(4) A. S. Quist and W. L. Marshall, *ibid.*, **72**, 684 (1968).

(5) A. S. Quist and W. L. Marshall, *ibid.*, **72**, 2100 (1968).

(6) A. S. Quist and W. L. Marshall, *ibid.*, **72**, 1545 (1968).

are linear functions of the solvent density.[3-6] Moreover, at temperatures from 400 to 800°, the limiting equivalent conductances for a particular electrolyte were found to be independent of the temperature at constant solvent density.[3-6]

This paper presents conductance measurements of dilute (0.001–0.10 *m*) aqueous NaI solutions at temperatures from 0 to 800° and at pressures to 4000 bars. From these measurements limiting equivalent conductances of NaI were obtained at integral temperatures and densities. Ionization constants (K) for the conventional equilibrium, $NaI \rightleftarrows Na^+ + I^-$, were also obtained where NaI behaves as a weak electrolyte. From these values the complete ionization constants (K^0) for NaI were calculated at each temperature.[7,8] These results were used for calculation of thermodynamic quantities for NaI for comparison with the previously published results for NaCl and NaBr.

For NaCl, NaBr, and NaI a unified behavior has been observed between 400 and 800° in the attainment of an essentially constant value of $\Delta H°$, independent both of pressure and temperature, that describes the behavior of all three electrolytes. Similarly constant values of $\Delta S°$ and of the net change in waters of solvation (k) for each electrolyte have also been calculated.

Experimental Section

A detailed description of the high-pressure conductance equipment and procedures used has been given previously.[4] The conductance cell with no pressure seals in the high-temperature region was used exclusively in this work. All solutions were prepared by weight from reagent grade NaI (Mallinckrodt Chemical Works) and conductivity water. The salt was dried for 24 hr at 120° before use. The conductivity water was obtained by passing distilled water through an ion-exchange column and then redistilling it twice from a fused quartz distillation unit. Conductivity measurements were made to 800° and 4000 bars on four solutions of NaI: 0.0009996, 0.005001, 0.05000, and 0.1000 *m*. Previous data of Quist and Marshall[9] for 0.01000 *m* NaI solutions under the same conditions have been included in the calculations. Four different inner electrodes were used for the conductance measurements. Their cell constants ranged from 0.495 to 2.104 cm^{-1}, as determined fron 0.01 and 0.10 demal KCl solutions at 25.00 ± 0.01°.

Results and Discussion

Specific conductances and equivalent conductances were calculated from the experimental data in the manner described previously.[4] An example of isothermal specific conductances of NaI solutions as a function of pressure at the temperatures of the measurements is shown in Figure 1. From comparable figures for all five molalities of NaI, specific conductances at integral pressures were obtained by interpolation. Isobaric

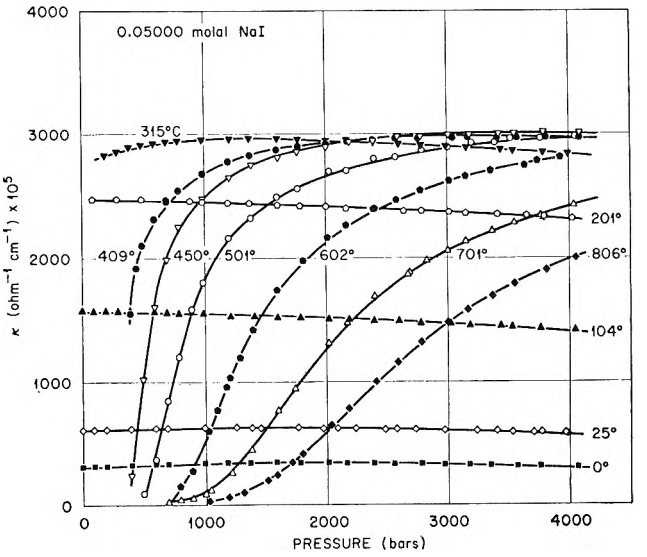

Figure 1. Specific conductances of 0.05000 *m* NaI solutions as a function of pressure at several temperatures.

specific conductances for 0.05000 *m* NaI solutions *vs.* temperature are shown in Figure 2, and isothermal equivalent conductances *vs.* solvent density in Figure 3. The other solutions of NaI exhibit similar behavior except that the density at which the equivalent conductance maximum occurs increases with increasing electrolyte molality. For 0.0009996 *m* NaI the maximum occurs near 0.50 g cm^{-3}, while it occurs at about 0.70 g cm^{-3} for 0.1000 *m* NaI solutions. Similar behavior has been observed for NaCl[4] and NaBr[5] solutions.

From plots like Figure 3 equivalent conductances at integral densities were obtained for each molality of NaI at the experimental temperatures. These values were then plotted against temperature at constant solvent density, and from smoothed curves through the data, equivalent conductances at various temperatures and densities were obtained. These are presented in Table I for temperatures from 100 to 800°, and include equivalent conductances for 0.01000 *m* NaI calculated from the specific conductances given elsewhere.[9] Data obtained at 0 and 25° have been used only for comparative purposes as shown in Figures 1–3, and have not been included in Table I. The values in parentheses represent equivalent conductances at saturation vapor pressure at that temperature.

Calculation of Limiting Equivalent Conductances. From the conductance values in Table I limiting equivalent conductances were calculated by the several methods described previously,[4] and with the computer programs developed earlier.[3-6] At low temperatures and high densities the Robinson–Stokes equation,[10] the

(7) W. L. Marshall and A. S. Quist, *Proc. Natl. Acad. Sci., U. S.*, **58**, 901 (1967).

(8) A. S. Quist and W. L. Marshall, *J. Phys. Chem.*, **72**, 1536 (1968).

(9) A. S. Quist and W. L. Marshall, *ibid.*, in press.

(10) R. A. Robinson and R. H. Stokes, *J. Amer. Chem. Soc.*, **76**, 1991 (1954).

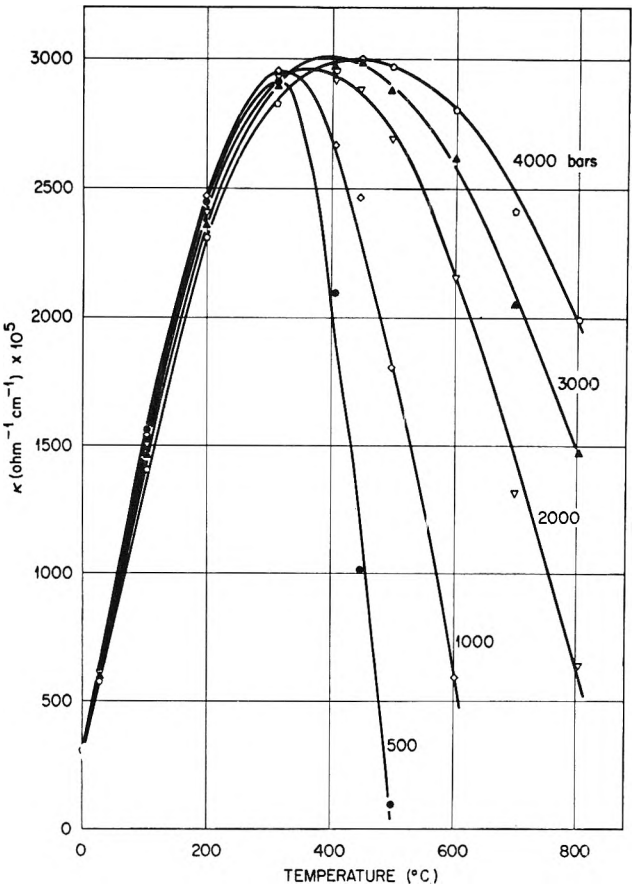

Figure 2. Isobaric variation of the specific conductances of 0.05000 *m* NaI solutions as a function of temperature at pressures from 500 to 4000 bars.

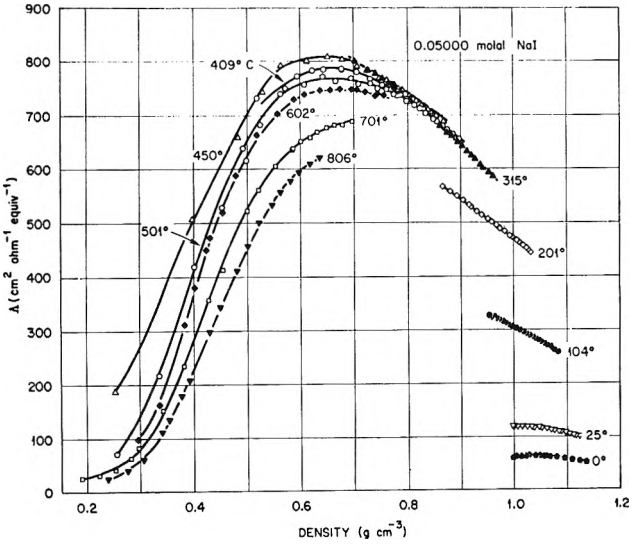

Figure 3. Equivalent conductances of 0.05000 *m* NaI solutions as a function of density at several temperatures.

Fuoss–Onsager–Skinner equation,[11] and the Shedlovsky equation (including an ionization constant)[12] gave essentially identical limiting equivalent conductances. As found previously for NaCl[4] and NaBr,[5] at densities below 0.70 g cm^{-3} the Robinson–Stokes equation did not represent the data as well as the other equations, while below about 0.60 g cm^{-3} only the Shedlovsky equation, which includes an ionization constant, fitted the data satisfactorily.

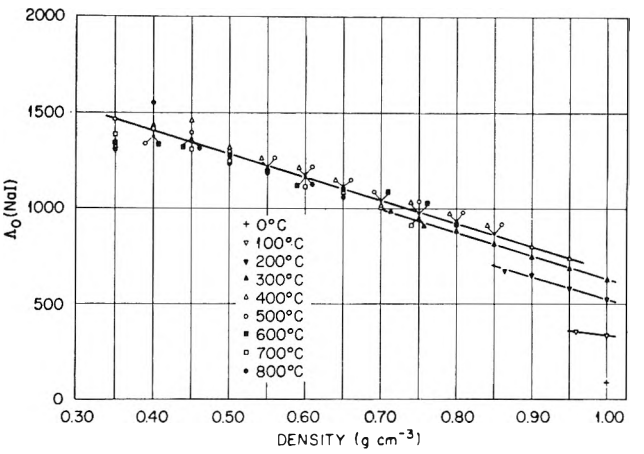

Figure 4. Limiting equivalent conductances of NaI as a function of density at temperatures to 800°.

Limiting equivalent conductances calculated for NaI at the various temperatures and densities are included in Table I, where the (limiting) molality of NaI is set equal to zero. At densities of 0.65 g cm^{-3} and above, the standard errors associated with the Λ_0(NaI) values of Table I are less than 1%. Below this density the uncertainty in the limiting equivalent conductances increases with increasing temperature and decreasing density. Figure 4 shows the linear relationship observed when isothermal values of Λ_0(NaI) from Table I are plotted against the density of the solvent. As found previously with NaCl[4] and NaBr,[5] the limiting equivalent conductance of NaI at constant density increases steadily with temperature, reaching a maximum, constant value at about 400° and above. The deviations from linearity (Figure 4) at high temperatures and at densities below 0.45 g cm^{-3} may be due to difficulty in making accurate experimental measurements at sufficiently low electrolyte concentrations for reliable extrapolation to infinite dilution. The limitation under these conditions is the relatively high solvent conductance.[3]

A linear equation describing the variation of the limiting equivalent conductance of NaI with solvent density (d) in the temperature range 400–800° is given as

$$\Lambda_0(\text{NaI}) = 1897 - 1210d \quad (1)$$

Similar relationships were found previously for $KHSO_4$ (considered as a 1–1 electrolyte),[3] NaCl,[4] NaBr,[5] and HBr.[6]

$$\Lambda_0(KHSO_4) = 1740 - 1100d \quad (2)$$

$$\Lambda_0(\text{NaCl}) = 1876 - 1160d \quad (3)$$

$$\Lambda_0(\text{NaBr}) = 1880 - 1180d \quad (4)$$

$$\Lambda_0(\text{HBr}) = 1840 - 560d \quad (5)$$

(11) R. M. Fuoss, L. Onsager, and J. F. Skinner, *J. Phys. Chem.*, **69**, 2581 (1965).

(12) T. Shedlovsky, *J. Franklin Institute*, **225**, 739 (1938); R. M. Fuoss and T. Shedlovsky, *J. Amer. Chem. Soc.*, **71**, 1496 (1949).

Table I: Equivalent Conductances (cm^2 ohm^{-1} $equiv^{-1}$) of Dilute Aqueous NaI Solutions at Various Temperatures and Densities

		Density, g cm^{-3}													
T(°C)	Molality	0.35	0.40	0.45	0.50	0.55	0.60	0.65	0.70	0.75	0.80	0.85	0.90	0.95	1.00
	0.00000													(356)	336
	0.0009996													(345)	329
100	0.005001													(340)	320
	0.01000													(336)	315
	0.05000													(322)	309
	0.1000													(315)	301
	0.00000													496	444
	0.0009996													481	434
150	0.005001													472	424
	0.01000													457	414
	0.05000													438	402
	0.1000													432	391
	0.00000											(670)	653	583	526
	0.0009996											(655)	645	563	512
200	0.005001											(630)	602	534	502
	0.01000											(595)	589	545	488
	0.05000											(570)	548	512	469
	0.1000											(540)	540	507	458
	0.00000											780	708	644	586
	0.0009996											770	698	621	569
250	0.005001											720	656	610	559
	0.01000											694	640	602	544
	0.05000											640	605	562	516
	0.1000											629	596	556	505
	0.00000								(986)	955	888	815	750	687	632
	0.0009996								(970)	950	868	805	738	666	611
300	0.005001								(920)	884	822	747	694	645	600
	0.01000								(860)	840	780	730	677	638	586
	0.05000								(810)	768	722	678	641	593	550
	0.1000								(760)	742	707	665	631	585	538
	0.00000								1013	964	910	860	780	718	
	0.0009996								1002	960	888	830	767	701	
350	0.005001								930	888	838	772	721	666	
	0.01000								890	850	802	754	702	659	
	0.05000								798	771	733	700	661	609	
	0.1000								773	748	717	687	650	599	
	0.00000	1320	1430	1460	1310	1220	1180	1115	1030	970	934	867	799	739	
	0.0009996	1076	1175	1190	1200	1180	1155	1102	1015	968	907	847	785	724	
400	0.005001	825	1000	1045	1030	1025	1070	990	940	890	846	790	735	679	
	0.01000	695	820	920	925	940	965	945	900	858	814	766	716	669	
	0.05000	495	655	645	705	760	792	798	795	770	738	710	668	613	
	0.1000	475	600	590	655	720	755	765	767	749	724	697	658	604	
	0.00000	1440	1420	1440	1300	1220	1170	1110	1040	975	936	869	806		
	0.0009996	935	1100	1145	1185	1175	1152	1097	1020	970	908	848	790		
450	0.005001	695	875	980	1005	1015	1010	988	945	890	846	789	738		
	0.01000	575	715	860	900	930	955	940	905	860	817	770	719		
	0.05000	400	550	590	680	745	780	790	788	768	740	712	666		
	0.1000	380	500	545	630	705	741	758	758	746	726	698	658		
	0.00000	1430	1380	1400	1290	1220	1170	1110	1040	975	934	863			
	0.0009996	825	1010	1100	1165	1170	1150	1092	1025	971	906	838			
500	0.005001	590	780	925	980	1005	1000	980	945	890	844	784			
	0.01000	480	630	800	880	920	942	930	900	856	811	764			
	0.05000	320	465	550	655	725	762	778	775	762	738	706			
	0.1000	305	425	500	610	685	722	743	742	738	724	694			
	0.00000	1390	1370	1380	1290	1220	1179	1105	1040	975	927				
	0.0009996	730	945	1060	1150	1160	1145	1088	1023	968	899				
550	0.005001	510	710	870	960	990	987	968	940	886	836				
	0.01000	410	565	755	855	905	920	918	888	851	804				
	0.05000	265	400	505	630	705	745	760	760	751	732				
	0.1000	250	365	460	585	665	701	722	728	726	718				
	0.00000	1340	1370	1360	1280	1210	1160	1095	1040	970	917				
	0.0009996	660	895	1025	1130	1150	1140	1080	1020	964	888				
600	0.005001	450	655	825	930	970	972	955	938	880	824				
	0.01000	350	520	705	830	885	908	903	878	844	790				
	0.05000	220	355	465	605	680	720	735	743	735	721				
	0.1000	205	315	425	555	640	675	700	710	710	707				
	0.00000	1330	1390	1340	1270	1210	1170	1090	1020	960					
	0.0009996	610	855	1000	1105	1135	1130	1071	1008	956					
650	0.005001	405	610	780	900	950	955	935	912	870					
	0.01000	310	480	665	795	865	890	885	862	834					
	0.05000	190	315	435	570	650	692	710	722	717					
	0.1000	175	280	395	520	605	640	672	688	693					
	0.00000	1390	1420	1360	1250	1200	1160	1080	1010	955					
	0.0009996	570	825	980	1075	1115	1120	1061	992	944					
700	0.005001	370	575	740	860	920	935	915	892	858					
	0.01000	285	445	630	760	835	870	865	843	824					
	0.05000	165	280	400	535	610	665	688	700	698					
	0.10000	150	250	360	485	570	612	638	663	674					
	0.00000	1200	1460	1360	1240	1190	1160	1070							
	0.0009996	535	775	950	1045	1090	1110	1048							
750	0.005001	340	545	705	820	885	915	897							
	0.01000	245	415	595	720	800	848	845							
	0.05000	140	250	370	490	570	632	653							
	0.1000	125	220	330	445	525	577	612							
	0.00000	1310	1550	1370	1240	1190	1160	1060							
	0.0009996	505	750	935	1010	1060	1095	1032							
800	0.005001	310	520	670	775	850	892	875							
	0.01000	220	390	560	680	765	825	820							
	0.05000	122	225	345	445	525	595	620							
	0.1000	110	195	305	400	480	540	578							

The significance of this similarity in behavior of 1–1 electrolytes has already been discussed.[4-6]

Calculation of the Complete Ionization Constant of NaI. The ionization of NaI in aqueous solutions can be represented by the equations[7,8]

$$NaI(H_2O)_j + kH_2O \overset{K^0}{\rightleftharpoons} Na(H_2O)_m^+ + I(H_2O)_n^- \quad (6)$$

$$K^0 = a_{Na(H_2O)_m^+} a_{I(H_2O)_n^-} / a_{NaI(H_2O)_j} a_{H_2O}^k \quad (7a)$$

$$= K/a_{H_2O}^k \quad (7b)$$

$$\log K = \log K^0 + k \log a_{H_2O} \quad (8)$$

where K^0 is the complete ionization constant including the hydration reaction and K is the conventional constant. The integers j, m, and n represent hydration

Table II: Negative Logarithm of the Conventional Ionization Constant, K, for the Dissociation of NaI into Na^+ and I^-. Standard State Is the Hypothetical 1 M Solution

	Density, g cm^{-3}								
T, °C	0.35	0.40	0.45	0.50	0.55	0.60	0.65	0.70	0.75
400	3.24	2.68	2.39	2.01	1.54	1.23	0.85	0.67	0.16
450	3.46	2.93	2.54	2.11	1.63	1.32	0.92	0.63	0.43
500	3.63	3.10	2.66	2.19	1.73	1.33	1.04	0.75	0.53
550	3.76	3.23	2.77	2.27	1.81	1.45	1.19	0.85	0.64
600	3.88	3.33	2.86	2.34	1.91	1.54	1.22	0.99	0.70
650	3.97	3.42	2.93	2.44	2.02	1.68	1.34	1.02	0.83
700	4.06	3.50	3.01	2.52	2.13	1.79	1.48	1.18	0.83
750	4.16	3.58	3.08	2.62	2.24	1.89	1.60		
800	4.25	3.65	3.14	2.73	2.36	2.00	1.72		

numbers of NaI, Na^+, and I^-, respectively, while k denotes the net change in waters of solvation resulting from the ionization of one mole of NaI. Over the complete density range from 400 to 800°, values of the conventional ionization constant (K) were obtained from the experimental data using the Shedlovsky equation,[12] with Λ_0(NaI) values calculated from eq 1. With this procedure the Shedlovsky equation contains only one parameter, the conventional ionization constant. Table II gives the calculated negative logarithms of the conventional constants at temperatures from 400 to 800° and densities from 0.35 to 0.75 g cm^{-3}. These ionization constants are based on the standard state of unit molarity at each temperature and density. The average uncertainty associated with the values in Table II is approximately 0.03 pK unit, with the greatest uncertainties occurring at the highest densities at all temperatures.

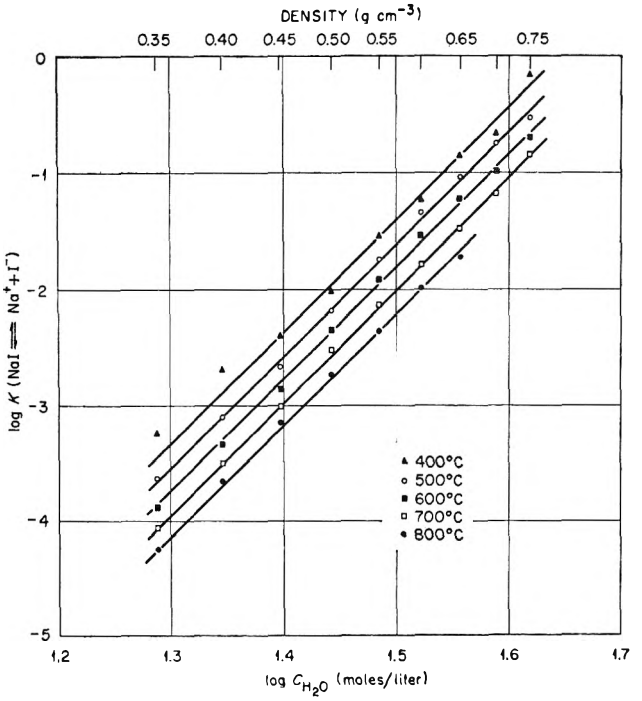

Figure 5. Log K(molar units) for the equilibrium NaI ⇌ $Na^+ + I^-$ as a function of the logarithm of the molar concentration of water at temperatures from 400 to 800°.

With the concept of the complete ionization constant (including hydration),[7,8] where a_{H_2O} is replaced by the molar concentration of water (C_{H_2O}) with a hypothetical standard state of unit molarity at the particular density (or pressure), isothermal plots of log K against log C_{H_2O} provided linear relationships at the several temperatures as shown in Figure 5. The slope k for NaI was independent of temperature in the range 400 to 800°, having an average least-squared value of 9.67 ± 0.08. Corresponding least-squared values for NaCl and NaBr are included in Table IV. These values have been proposed to represent the net changes in waters of solvation on ionization of one mole of each electrolyte. From the value of k = 9.67 for NaI (Figure 5), together with the data of Table II, values of log K^0(NaI) have been calculated and are given in Table III. Cor-

Table III: Values of the Logarithm of the Complete Ionization Constants (K^0) and the Complete Free Energy Changes (ΔG°, kcal mol^{-1}) for the NaCl, NaBr, and NaI Equilibria

	NaCl		NaBr		NaI	
T, °C	log K^0	ΔG°	log K^0	ΔG°	log K^0	ΔG°
400	−17.10	52.7	−16.49	50.8	−15.87	48.9
450	−17.23	57.0	−16.58	54.9	−16.01	53.0
500	−17.31	61.2	−16.73	59.2	−16.12	57.0
550	−17.42	65.6	−16.90	63.7	−16.23	61.1
600	−17.52	70.0	−17.04	68.1	−16.32	65.2
650	−17.62	74.4	−17.16	72.5	−16.43	69.4
700	−17.70	78.8	−17.27	76.9	−16.52	73.6
750	−17.77	83.2	−17.35	81.2	−16.61	77.8
800	−17.83	87.6	−17.38	85.3	−16.71	82.1

responding values for NaCl[4] and NaBr[5] have also been included for comparison.

Comparative Thermodynamic Behavior of the Alkali Halides. Over the entire range of temperature (T) and density (d) studied, the order of association at constant T and d, is NaCl > NaBr > NaI. This behavior can be observed from a comparison of both the conventional ionization constants, presented in Table II for NaI and previously for the other two halides,[4,5] and the complete constants, presented in Table III for the

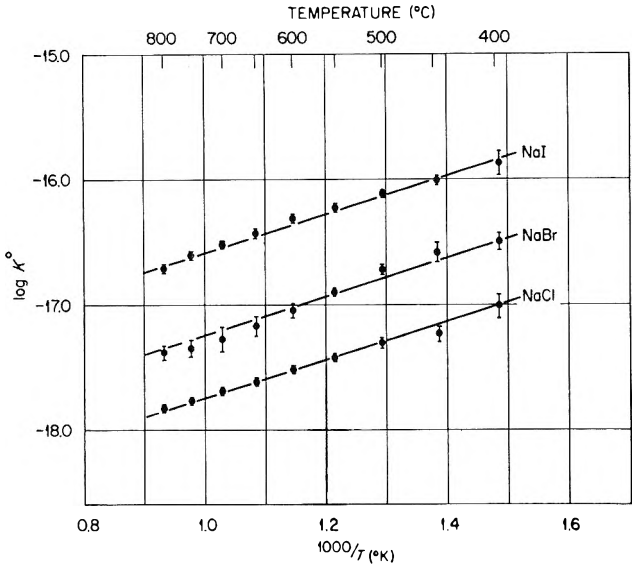

Figure 6. Log K^0 (molar units) for the equilibrium $NaX(H_2O)_j + kH_2O \rightleftharpoons Na(H_2O)_m^+ + X(H_2O)_n^-$ as a function of T^{-1}(°K) for NaCl, NaBr, and NaI.

three alkali halides. Thus, NaI is the most highly ionized electrolyte, while NaCl is the most highly associated electrolyte, with NaBr occupying an intermediate position. This pattern observed over an extreme range of temperature and density implies strongly that the halogen ion sizes, independent of the degree of hydration, remain in the order, $I^- > Br^- > Cl^-$, where the extent of association is expected to be inversely proportional to the ion sizes. The comparative values of $\Delta G°$ for the complete equilibria, tabulated in Table III at 400–800°, show the relatively small differences in standard free energy changes among the three halides.

The approximate constancy of k (the net change in waters of solvation) between 400 and 800° allows a simple comparison of the thermodynamic functions over this range of temperature, since for each electrolyte the respective equilibrium does not change in stoichiometry. Plots of the log K^0 data in Table III against T^{-1} (°K) are shown in Figure 6 for the three sodium halides. Least-squares analysis of the data indicated an average slope of 1540 ± 160 for each of the electrolytes, within the precision of the measurements. This value of the slope yielded a single value of −7.0 kcal mol^{-1} for $\Delta H°$ for the complete equilibrium for each of the three electrolytes. With this value of $\Delta H°$ and the $\Delta G°$ values in Table III, values for $\Delta S°$ for the complete reactions were calculated, and were found, within the precision of the measurements, to be independent of both density and temperature (400–800°). Comparative values for k, $\Delta H°$, and $\Delta S°$ are given in Table IV for the three electrolytes. For the complete equilibria

$$(\partial \ln K^0/\partial P)_T = -\Delta V°/RT = 0 \qquad (9)$$

Thus $\Delta H° = \Delta E° + P\Delta V° = \Delta E°$. The negative values of $\Delta S°$, approximately proportional to k, show

Table IV: Thermodynamic Values ($\Delta H°$, $\Delta S°$) and k for the NaCl, NaBr, and NaI Equilibria, 400–800°

Electrolyte	k	$\Delta H°$, kcal mol^{-1}	$\Delta S°$, cal mol^{-1} deg^{-1}
NaCl	10.20 ± 0.15	−7.0 ± 0.7	−88.3 ± 0.1
NaBr	9.94 ± 0.48	−7.0 ± 0.7	−86.2 ± 0.3
NaI	9.67 ± 0.08	−7.0 ± 0.7	−82.9 ± 0.1

that increase in solvation upon ionization of the ion pairs provides greater order in the respective systems.

Simple Description of Alkali Halide Behavior. By obtaining complete ionization constants, it has been found that at high temperatures not only does k become constant with temperature and density, but also $\Delta H°$ and $\Delta S°$. Since $\Delta H°$ is a constant, independent of density and temperature (400–800°) within the precision of the measurements for all three 1–1 salts, only $\Delta S°$ needs to be known for the particular salt in order to specify K^0 or $\Delta G°$. To specify the fraction ionized at a particular temperature and pressure, we must know the additional single value for k.

The closeness in values of k and $\Delta S°$ and the essentially identical value of $\Delta H°$ for these three alkali halides suggest that the degrees of ionization for most 1–1 salts are similar in this high-temperature range, and can be specified approximately by the above relationships and averaged values of $\Delta S°$ and k from those in Table IV. This similar behavior has been observed from a conductance study of many 1–1 electrolytes,[9] and also in the observed linear relationships of Λ_0 *vs.* density, where the intercept and slope of eq 1–4 are approximately the same for the several 1–1 electrolytes studied.[3-5]

Franck and Roth[13] have observed some apparent simplicity in the spectroscopic study of hydrogen bonding in water at temperatures to 400°. At constant density, they observe an approach to constancy (above 400°) in ν(max) of an absorption band considered to support a continuum model for water. The observed electrolyte equilibrium behavior in water from the conductance studies and this approach to constancy of ν(max) in supercritical water perhaps may be related.

The thermodynamic relationships presented herein might well be expected to exist at pressures approaching zero. With this assumption the fraction of ionization can easily be calculated for cases of immediate, applied interest, for example, in geochemistry or pressurized water technology where pressures of 200–400 bars might be the range to be considered. Thus at 200 bars and at 400°, sodium iodide (and the other 1–1 electrolytes investigated) is an extremely weak electrolyte, showing about the same extent of dissociation as water at 25°.

(13) E. U. Franck and K. Roth, *Discussions Faraday Soc.*, **43**, 108 (1967).

Ultraviolet Studies for the Adsorption of 8-Quinolinol on Evaporated Metal Films

by Kosaku Kishi and Shigero Ikeda

Department of Chemistry, Faculty of Science, Osaka University, Toyonaka, Osaka, Japan *(Received September 16, 1968)*

Ultraviolet spectra were obtained for 8-quinolinol adsorption on evaporated Ti, Mn, Fe, Ni, and Cu films. Each film exposed to 8-quinolinol vapor gave two bands due to adsorbed species near 240 and 265 mμ. These bands were assigned to the $\pi-\pi^*$ transitions of the quinolinol and the quinolinolate, respectively. The relative intensities of these two bands varied considerably according to the metal used, and were markedly affected by admission of air. These effects are discussed in terms of reaction properties of the metal surfaces. The spectra of the adsorbed quinolinol and quinolinolate were changed by addition of acetic acid vapor. These spectral changes were explained by considering complex formation of the adsorbed quinolinol with acetic acid by hydrogen bonding and the effect on the adsorbed quinolinolate of partial oxidation of the metal films during acetic acid adsorption.

Introduction

In previous reports,[1] an ultraviolet technique was applied for adsorption of β-diketones on evaporated metal films in order to investigate the chemical bonding of chemisorbed species and electronic properties of the metal surfaces. Exposure of the films to β-diketone vapor gave peaks assigned to the $\pi-\pi^*$ transition of adsorbed β-diketonate, and in some cases, a band corresponding to charge transfer from the adsorbent to the adsorbed species. These spectra were compared with those of the corresponding metal complexes and discussed on the basis of the degree of π interaction between the metal $d\pi$ orbitals and the π orbitals of the β-diketonates.

Very little is known about the electronic states of metal surfaces, so that adsorption studies for various adsorbates by an ultraviolet technique are very useful in gaining additional information about reactions and electronic properties of metal surfaces. In the present paper 8-quinolinol was used as an adsorbate, which has been the subject of considerable study as a typical nitrogen–oxygen chelating agent of metal ions.[2] Absorption by quinolinol vapor in the ultraviolet region was quite weak at room temperature due to its very low vapor pressure (path length of 1 cm). However, the quinolinol was concentrated rapidly on metal surfaces by adsorption, and even the spectra of weakly adsorbed species could be observed without evacuating or trapping the free quinolinol before recording. Spectral changes were examined for preadsorbed or coexisting chemical species.

Experimental Section

The ultraviolet cell used was described in the previous paper.[1] Thin iron foil, nickel wire, or small blocks of the other metals were set on a tungsten filament. The cell was evacuated for 5 hr at a pressure less than 10^{-5} mm and the filament was preheated electrically for 20 min in order to remove dissolved species in the metal. The path length of the windows was 1 cm. The resultant films were exposed to 8-quinolinol vapor at a constant pressure by opening a stopcock from a vessel containing the solid quinolinol. The vessel was evacuated beforehand and attached to the cell by a taper joint when the cell was pumped out. Spectra were recorded before and after admission of the gas investigated. Spectral changes were measured as a function of exposure time and for effects such as introduction of other gases or evacuation of the cell. All of the adsorptions were carried out at room temperature.

Spectra were recorded on a Hitachi EPS-2 spectrophotometer. A wire gauge was used to reduce a reference transmission and raise the apparent transmission of the sample beam, because there was a large decrease of the transmission in the sample beam due to scattering of light by metal films. The scanning speed was 10 min from 220 to 340 mμ.

The 8-quinolinol used was G.R. grade obtained from Nakarai Chemicals. Acetic acid was G.R. grade, distilled under vacuum for use. The samples of titanium, manganese, iron, nickel, and copper had purities of 99.8, 99.9, 99.99, 99.5, and 99.8%, respectively.

Results

Adsorption of 8-Quinolinol. Figure 1 shows ultraviolet spectra of adsorbed species resulting from the exposure of Ti, Mn, Fe, Ni, and Cu films to 8-quinolinol vapor. The spectra were obtained for the following exposure times; Ti: (1) 1 min, (2) 15 min, (3) 30 min, (4) 16 hr; Mn: (1) 20 min, (2) 16 hr; Fe: (1) 1 min, (2) 1 hr, (3) 20 hr, (4) 40 hr; Ni: (1) 1 min, (2) 10 min, (3) 17 hr; Cu: (1) 1 min, (2) 30 min, (3) 15 hr. Each spectrum in the figure was obtained by subtracting the absorbance of a background spectrum of the metal film from that of the apparent spectrum observed. Two

(1) (a) K. Kishi, S. Ikeda, and K. Hirota, *J. Phys. Chem.*, **71**, 4384 (1967); (b) K. Kishi and S. Ikeda, *ibid.*, **73**, 15 (1969).

(2) The reactions of 8-quinolinol have been reviewed by J. P. Phillips, *Chem. Rev.*, **52**, 459 (1953).

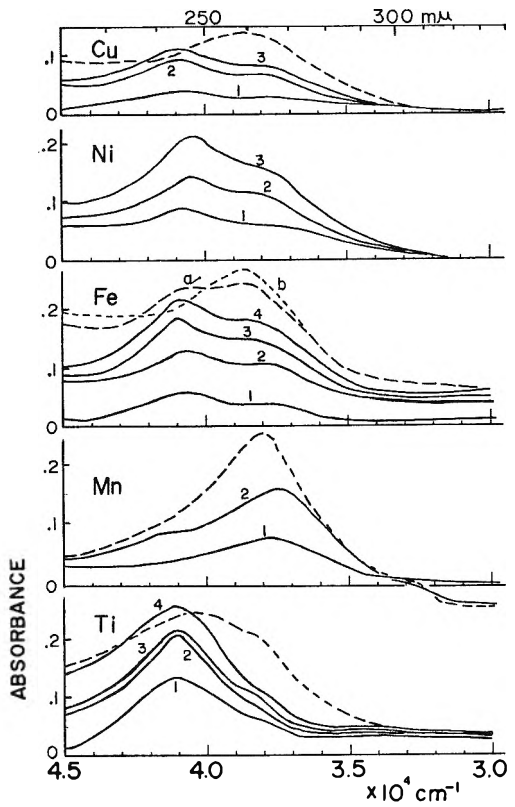

Figure 1. Ultraviolet spectra for 8-quinolinol adsorption on Ti, Mn, Fe, Ni, and Cu, for the following exposure times; Ti: (1) 1 min, (2) 15 min, (3) 30 min, (4) 16 hr; Mn: (1) 1 min, (2) 1 hr, (2) 16 hr; Fe: (1) 1 min, (2) 1 hr, (3) 20 hr, (4) 40 hr; Ni: (1) 1 min, (2) 10 min, (3) 17 hr; Cu: (1) 1 min, (2) 30 min, (3) 15 hr; ---, following elapsed times from subsequent admission of air; Ti: 5 min; Mn: 2 min; Fe: a, 15 min; b, 30 min; Cu: 30 min.

Table I: Ultraviolet Data for 8-Quinolinol and Quinolinolate in Various States

	Wavelength, mμ	Solvent
Free Species		
Molecule	239.5	H_2O
	242	CH_3OH
Anion	253	NaOH aq solution
Cation	251.5	CH_3COOH aq solution
Metal Complex		
FeQ_3	250.5	CH_3OH
NiQ_2	259	CH_3OH
CuQ_2	257	CH_3OH

	Adsorbed State		
	A	B	After admission of air
Ti	244 ≫ ~265		248 > ~262
Mn	~239 ≪ 267		263
Fe	244 > 265 → 261		259
Ni	246 > ~265		260
Cu	244 > ~265		260

peaks were observed for each metal at about 240 and 265 mμ, whose precise values are listed in Table I. These bands in the present paper are designated A and B bands, respectively. The intensities of these bands initially increased rapidly (exposure times less than about 1 hr), but afterward quite slowly for all the metals used. The intensity of the A band was larger than that of the B band for Cu, Ni, and Fe. The B band dominated the A band for Mn, while the reverse was obtained for Ti.

Dotted curves show the effect of admission of air into the cell. These curves were recorded after the following times elapsed from the admission; Ti (5 min), Mn (2 min), Fe (a, 15 min, b, 30 min). The admission strengthened the B band and shifted it to shorter wavelength, while the A band was weakened. These shifts are summarized in Table I. Only the B band was observed for Mn, Fe, and Cu after 30 min of exposure, but the rates of the spectral changes were slow, as can be seen in cases a and b of iron.

After adsorption of the quinolinol on Ni, Fe, and Ti for 2 hr, 1 hr, and 40 min, respectively, the cell was evacuated for 40 min. The resulting spectral changes were recorded as indicated by Figure 2. The letters a

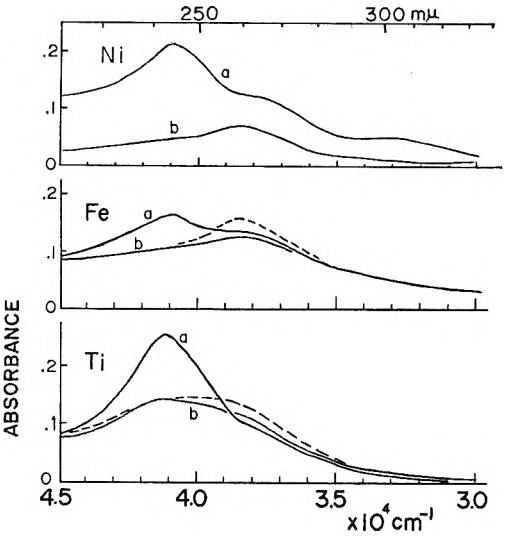

Figure 2. Spectral changes of 40 min of evacuation after the following exposure (to 8-quinolinol) times; Ni: 2 hr, Fe: 1 hr, Ti: 40 min. a and b correspond to spectra recorded before and after evacuation; ---, after 1 hr (Ti) and 10 hr (Fe) of evacuation.

and b indicate here the corresponding spectra recorded before and after the evacuation. Dotted curves indicate the changes after 1 hr (Ti) and 10 hr (Fe) of evacuation. The A band almost disappeared on Ni and Fe, but the B band still remained with considerable intensity on evacuation. In the case of Ti, however, the A band was more intense than the B band even after evacuation, although an appreciable decrease was observed in the former. The B band remained after evacuation, and increased for these metals by aging.

Figure 3 shows spectra of adsorbed species on Cu and Fe exposed to air. For cases Cu and Fe-a, the metal films were exposed to air for 10 min. In case Fe-b the film was heated in air at 100° for 40 min and the cell was cooled to room temperature. Then the cell was evacuated for 1 hr and the quinolinol vapor was introduced on these films. Spectra were recorded after

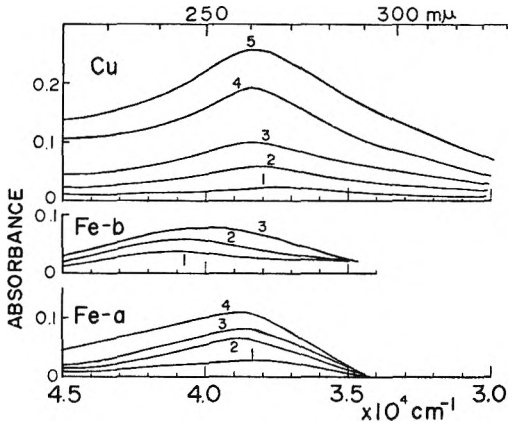

Figure 3. Spectra for 8-quinolinol adsorption on Cu and Fe treated by air. Cu, Fe-a: exposed to air for 10 min, evacuated for 1 hr. Fe-b: heated in air at 100° for 40 min, evacuated for 1 hr. Exposure times were as follows; Cu: (1) 2 min, (2) 10 min, (3) 20 min, (4) 1.5 hr, (5) 2.5 hr; Fe-a: (1) 15 min, (2) 1 hr, (3) 3 hr, (4) 19 hr; Fe-b: (1) 2 hr, (2) 18 hr, (3) after 5 min from subsequent addition of air.

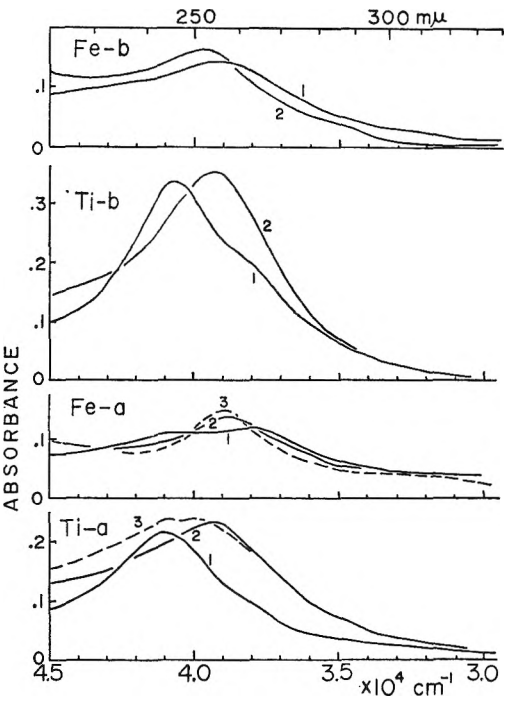

Figure 4. Effect of addition of acetic acid. a: (1) exposed to 8-quinolinol for 40 min (Ti), 2 hr (Fe), evacuated for 20 min; (2) subsequently exposed to acetic acid (30 mm) for 15 min (Ti), 1 min (Fe); (3) evacuated for 1 hr. b: (1) exposed to acetic acid (30 mm) for 30 min (Ti), 5 min (Fe), evacuated for 1 hr on introducing 8-quinolinol vapor; (2) subsequently exposed to acetic acid.

the following exposure times; Cu: (1) 2 min, (2) 10 min, (3) 20 min, (4) 1.5 hr, (5) 2.5 hr; Fe-a: (1) 15 min, (2) 1 hr, (3) 3 hr, (4) 19 hr; Fe-b: (1) 2 hr, (2) 18 hr. Only the B band was observed for modified Cu and Fe-a, with peaks at 262 and 258 mμ, respectively. On the other hand, the A band alone was obtained on Fe-b with low intensity, at 245 mμ. However, successive admission of air for 5 min shifted the band to 250 mμ as shown by case 3.

Effect of Admission of Acetic Acid. Addition of acetic acid vapor changed the spectra of adsorbed 8-quinolinol on Ti and Fe as shown in Figure 4 and Table II. The a-cases of Ti and Fe will be discussed first. After exposure of the quinolinol for 40 min (Ti) or 2 hr (Fe), the cell was evacuated for 20 min after closing the stopcock from the quinolinol vessel, in order to remove quinolinol vapor to some extent; spectrum 1 was then recorded. Absorption peaks were found at 244 and 265 mμ for Ti (the former was much more intense than the latter), and at 244 and 261 mμ for Fe (roughly equal intensities). Acetic acid vapor (30 mm) was then introduced into the cell and spectral changes were measured after 15 min (Ti) or 1 min (Fe), following the removal of free gases with a liquid nitrogen trap. Both the A and the B bands disappeared and a new band was obtained at 254 mμ (Ti) and 257 mμ (Fe), which is indicated in spectrum 2. The cell was subsequently evacuated for 1 hr. For Ti the 254-mμ band shifted to 251 mμ with a shoulder at 246 mμ. However, the 257-mμ band for Fe became sharp without any shift of the band peak. This is shown in spectrum 3.

The b-cases indicate the effect of exposure to acetic acid on the subsequent adsorption of the quinolinol. Titanium or iron was exposed to the acid vapor (30 mm) for 30 min and 5 min, respectively, and the cell was evacuated for 1 hr. A spectrum was then recorded as background. Next the quinolinol vapor was introduced on evacuating the cell and adsorbed for 1 hr. Without the evacuation the quinolinol vapor at very low pressure could not diffuse to the film due to continuous desorption acetic acid gas from the glass wall. Spectrum 1 was then recorded. An absorption peak was observed at 255 mμ for Fe. For Ti the intensive A band was observed with the B band as a shoulder and

Table II: Effect of Addition of Acetic Acid

M →	8-Quinolinil →	CH_3COOH →	evacuation
Ti	244 ≫ 265 (mμ)	254	251, 246
Fe	244 > 261	257	257

M →	CH_3COOH →	8-Quinolinil →	CH_3COOH
Ti		245 ≫ 265	254.5
Fe		255	253.5

no new band was detected. The successive addition of acetic acid, however, gave a new band at 254.5 mμ.

Discussion

Adsorption of 8-Quinolinol. The relative intensities of the A and the B bands differed considerably depending on the metal used. Evacuation of the cell showed different decreasing rates of the intensities for the two bands. Upon addition of air, the A band decreased and the B band increased. These facts indicate that the two bands originate from different molecular species.

Absorption bands of 8-quinolinolate anion have been assigned by Perkampus and Kortüm.[3] The anion gave an intensive ^1B_b band around 255 mμ as listed in Table I. The protonated 8-quinolinol cation gave a band at 251 mμ. The protonated species could not be expected in the adsorption of the quinolinol alone. Therefore, the A and the B bands were asigned to π–π^* transitions of adsorbed molecular 8-quinolinol and 8-quinolinolate anion on these metal surfaces, respectively.

In 8-quinolinol–metal complexes, the existence of various types of coordination has been proposed, especially for the cobalt complexes by Lenzer[4] as indicated by types (I)–(IV) in Figure 5. The quinolinol and the

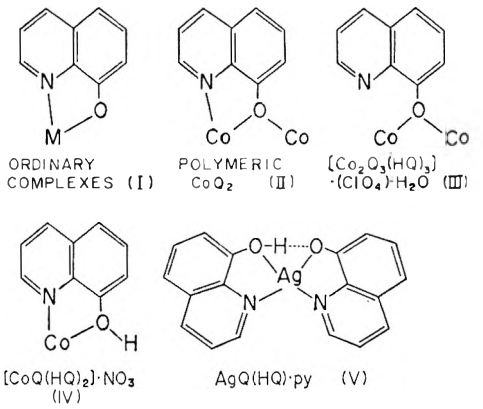

Figure 5. Various types of coordination in 8-quinolinol–metal complexes.

quinolinolate are abbreviated as HQ and Q, respectively. In the case of AgQ(HQ)·py, hydrogen bonding of the (V) type was proposed as a result of X-ray analysis of the complexes.[5] Bonding similar to that of types (I) to (V) can be expected also for the adsorbed quinolinol and quinolinolate on the metal surfaces. However, there are no means yet to determine which type does really predominate.

The intensity ratios of the A band to the B band increase along the series Mn < Fe < Ni < Cu < Ti, for about 20 hr of exposure time. In aqueous solution, the quinolinolate anion has almost the same molar extinction coefficient as molecular quinolinol. Hence the respective intensities of the A and the B bands can be considered to correspond to the numbers of these adsorbed species. Consequently, the titanium surface is characterized as favoring coordination (adsorption) of the quinolinol molecule and not causing dissociation of the OH proton. In metallic titanium, the 3d bands are only partially occupied[6] and the surface of such a metal is expected to have a tendency to draw electrons from other chemical species, in this case the lone pair electrons of nitrogen and oxygen in the quinolinol.

Manganese and iron favor the proton-dissociated chemisorption for β-diketones and adsorb a larger number of β-diketonates than other first transition metals.[1] Manganese and iron are easily dissolved in liquid β-diketones as diketonate complexes.[7] The present results for quinolinol adsorption also indicate the predominant tendency of Mn for OH proton-dissociative chemisorption. In the case of acetic acid, to be mentioned below, proton-dissociated adsorption was favored on Fe but not on Ti. From these data it can be said that in the first transition metals manganese and iron generally dissociate the OH proton of adsorbates easily, and titanium, nickel, and copper favor molecular adsorption by accepting lone pair electrons from the adsorbates. However, titanium and nickel would make use of different types of orbitals for such an adsorption, for example the 3d orbitals in titanium and the outer sp^3 hybrid orbitals in nickel. Pyridine was considerably adsorbed on Ti and Ni but absorption bands of adsorbed pyridine were quite different for the two metals.[8]

Such tendencies were, however, modified by exposure of the metal films to air. On weakly oxidized metal surfaces, the quinolinol was easily dissociated into the quinolinolate, but for bulk oxides this is not true, as shown by the cases in Figure 3. The same behavior was observed for β-diketone. These results suggest that a very reactive form of oxygen exists on the weakly oxidized metal surfaces and may generally facilitate the dissociation of the OH protons of adsorbates.

From spectral data of metal-8-quinolinolate complexes, Popovych and Rogers[9] have suggested that large bathochromic shifts of the complexes (relative to the ligand as a free anion) are characteristic of a strong metal–nitrogen (covalent) bond and on the other hand, that the absence of such a shift indicates a strong metal–oxygen (ionic) bond. The oxidization of the metal surfaces by subsequently admitted air and, as mentioned below, by acetic acid (for iron) shifted the B band to shorter wave length, namely near the band position of

(3) H. H. Perkampus and K. Kortüm, *Z. Anal. Chem.*, **190**, 111 (1962).

(4) S. Lenzer, *J. Chem. Soc.*, 5768 (1964).

(5) J. E. Fleming and H. Lynton, *Can. J. Chem.*, **46**, 471 (1968).

(6) J. B. Goodenough, *Phys. Rev.*, **120**, 67 (1960).

(7) O. Kammori, K. Sato, K. Takimoto, and K. Arakawa, *Japan Analyst*, **15**, 561 (1966).

(8) K. Kishi and S. Ikeda, "Ultraviolet Studies for the Pyridine and 2,2′-Bipyridyl Adsorbed on Evaporated Metal Films," in preparation.

(9) O. Popovych and L. B. Rogers, *Spectrochim. Acta*, **21**, 1229 (1965).

the metal complexes with ionic bond character. This may indicate that the adsorbent–adsorbate bond becomes more ionic (more attractive to the oxygen of the quinolinol) with partial oxidation of the metal surfaces.

Effects of Acetic Acid. For titanium quinolinol was adsorbed molecularly as mentioned above. Two explanations can be considered for the band shift of the adsorbed quinolinol after addition of acetic acid vapor. The first of these is that the metal surface was oxidized by the acid, accompanied by dissociation of the quinolinol, and that therefore the spectra of adsorbed quinolinolate became similar to those of metal complexes.

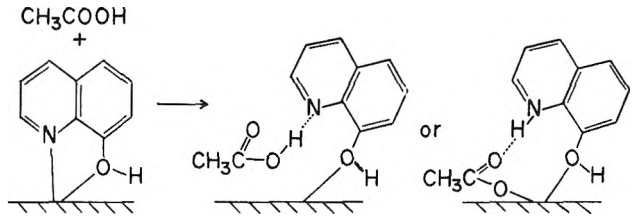

Figure 6. Reaction scheme of adsorbed 8-quinolinol with acetic acid on a titanium surface.

The second is the formation of the protonated quinolinol cation or a similar species. The protonated cation gives a band peak at 251.5 mμ in aqueous solution, as listed in Table I. The first assumption, however, was given up by considering that the spectra changed by the acid addition were partially reversed on subsequent evacuation and that the admission of the acid to fresh titanium film could scarcely affect the spectral features of the subsequently adsorbed quinolinol. Hydrogen chloride and bromide were absorbed by Cr(III)- and Fe(III)-quinolinolate complexes and the observed changes in color, infrared spectra, and X-ray diffraction patterns, etc., all favored a chemical process for the absorption.[10] The Cr–N bond disruption was proposed for an initial reaction which placed a proton on the nitrogen and a chloride ion on the chromium. About 6 moles of HCl or HBr were absorbed in one mole of the complex. Therefore, the oxygen may be also attached to the hydrogen halide by hydrogen bonding. From a consideration of these data, the second assumption was supported and the reaction scheme of Figure 6 was proposed for the adsorption system. The spectral changes upon evacuation can be explained by considering that acetic acid was gradually desorbed from such molecular complexes.

For iron the band observed after addition of acetic acid probably differed in origin from the band for titanium, since subsequent evacuation brought no shift in the band position, but only a sharpening of the band itself. For the iron modified by the acid preadsorption, only one peak was observed at 255 mμ, unlike the case of titanium. Therefore, the partial oxidization of the iron surface by acetic acid can shed light on the above results as follows: The acid dissociates on iron into adsorbed acetate and proton; such protons tend to draw electrons from the iron surface and partly combine with each other accompanied by the evolution of hydrogen gas; the partial oxidization of the surface as a result of this behavior makes the dissociation of preadsorbed or subsequently admitted quinolinol easier; hence the band peak of adsorbed quinolinolate approaches a position similar to the iron complex. Moreover, this is the reason why the band shift was not detected after evacuation. Such oxidization is supported by the fact that the iron surface was partly oxidized after proton-dissociative adsorption of β-diketones.[1]

The above examples suggest that on metal surfaces preadsorbed or coexisting gases will play an important role in determining the adsorbed forms and states of other species. This behavior is probably very useful for describing various phenomena about catalytic reactions by metals.

(10) M. M. Jones, K. V. Dandh, and G. T. Fisher, *J. Inorg. Nucl. Chem.*, 26, 773 (1964).

NOTES

The Carbon–Hydrogen Bond Dissociation Energy in Methanol[1a]

by F. R. Cruickshank[1b] and S. W. Benson

Department of Thermochemistry and Chemical Kinetics, Stanford Research Institute, Menlo Park, California 94025
(Received May 13, 1968)

The carbon–hydrogen bond dissociation energy in methanol (MeOH) has been previously obtained[2] only as an upper limit. In the present work a lower limit is obtained thus yielding a relatively accurate value whence the π bond strength of formaldehyde, D_π^0(HCHO), may be calculated.

(1) (a) This work was supported in part by Grant No. AP00353-03, Air Pollution Division of the Public Health Service; (b) Postdoctoral Research Associate.

(2) E. Buckley and E. Whittle, *Trans. Faraday Soc.*, 58, 536 (1962).

Table I: Kinetic Data

RUN NO.	INITIAL PRESSURES MeOH (torr)	INITIAL PRESSURES I_2 (torr)	CH_4 (torr)	CO (torr)	ΔI_2[b] (torr)	TIME (sec)	Δp[d] (torr)	T(°K)	$10^{11} \times K_{c_{I_2}}$ (mole/l)	$\log (k_1/l\ mole^{-1}\ sec^{-1})$
8	40.71	10.75	0	~11.1	10.75	2845	11.58	628.7	107.2	2.490
9	79.36	10.24	--	--	10.2	1600	10.6	630.0	113.7	2.450
10	42.47	21.02	1.1	12.9	21.0	5095	21.50	630.0	113.7	2.524
11	694.4	10.49	0	4.47	10.26	5771	10.0	573.7	7.220	1.49
12	10.64	11.04	1.37	2.97	3.95	84608	5.7	574.2	7.417	1.550
13	11.1	11.08	0.88	3.77	4.2	86220	6.1	572.0	6.59	1.537
14	12.72	12.25	1.75	3.73	5.7	84191	7.5	567.7	5.21	1.477
15	775.8	11.22	0	d	5.8	2546	18.0	550.8	2.00	1.263
16	638.6	4.08	0	d	3.48	4450	7.3	550.8	2.00	1.220
17	313.3	22.7	1.3	9.2	18.9	20745	21.0	546.8	1.578	1.184
18	149.1	4.56	0	1.87	4.56	800	1.3	628.0	104.0	2.468
*19	98.8	3.85	12.9	14.3	0.85	6298	--	628.0	104.0	1.277
*20	100.8	3.79	12.7	8.2	2.27	6375	15.2	629.4	110.7	1.723
†21[c]	--	--	0.6	15.7	-0.68	6300	1.0	629.4	110.7	--
§22[c]	98	0.7	13.8	8.1	-0.75	7078	14.0	629.5	110.7	--
*23	101	3.87	0	0.92	1.56	390	trace	628.9	108.2	1.744
*24	94	3.87	0.7	4.42	2.19	1637	3.5	628.9	108.2	1.688
25[a]	650.4	4.1	trace	trace	4.1	4670	--	549.9	1.894	1.940
26[a]	311.5	23.37	1.65	7.95	23.4	20800	18.3	552	2.14	2.004
27[a]	378.9	22.1	1.60	9.1	22.1	20950	19.0	551.6	2.09	1.898
28[a,c]	302.4	28.7	--	--	--	--	--	551.1	2.03	2.033
29[a,c]	61.5	14.5	13.9	10.7	c	3050	--	625.5	92.9	3.167
30[a]	38.84	9.16	7.0	12.5	c	2516	14.7	625.5	92.9	3.210
31[a]	31.24	7.36	--	--	--	2860	11.6	626.8	98.5	--
32[e]	595.1	2.79	0.	0.85	2.74	4038	trace	559	3.20	1.456
33[e]	316.7	3.23	0	1.4	3.13	7000	trace	557.6	2.96	1.502

* HI added initially to runs, 19, 20, 23, 24 was 344.6, 192.2, 192.1, 194.6 torr, respectively.

† 16.8 torr CO and 147.2 torr HI only.

§ 158 torr HI added initially.

[a] Runs in the packed vessel.

[b] ΔI_2 is the amount of I_2 consumed. Negative numbers are thus the amounts produced in excess of the initial pressure.

[c] These runs discussed in the text.

[d] Non-condensibles merely sampled and no CH_4 present.

[e] Performed in unseasoned vessel.

Experimental Section

Iodine (Mallinkrodt) was resublimed and degassed at liquid nitrogen temperatures before use. Methanol (Matheson Coleman and Bell, Spectroquality) was found pure within the sensitivity of an F and M Model 810 gas chromatograph and was merely degassed before use.

The Cary 15 spectrophotometer modified for use with a heated reaction cell has been described previously.[3]

Methanol was expanded into the reactor containing the desired pressure of iodine and the optical density monitored, as a function of time, at 445 mμ. When sufficient length of trace had been obtained, so that the initial gradient could be accurately determined, the optical density was monitored sequentially at 445, 280, and 260 mμ.

At the end of a run, the pressure change was measured on an oil or mercury manometer, nulled through a Pace pressure transducer. The products were then condensed in a trap cooled by liquid nitrogen and the noncondensable fraction was transferred by Toepler pump into a calibrated gas buret for estimation. A sample of this gas was analyzed for CH_4 and CO on a 2 m × ¼ in. o.d. Porapak Q column at 90°, using 5 ml/min He carrier gas. Occasional confirmatory analyses were performed on a mass spectrometer.

(3) S. W. Benson, F. R. Cruickshank, and R. Shaw, *Int. J. Chem. Kinetics*, in press.

Results and Discussion

The results are listed in Table I. The error in ΔP is ± 1–2% of the total pressure. The error in gas analyses is $\pm 5\%$ of the total pressure in each component, the error in the $[CH_4]/[CO]$ ratio being $\pm 5\%$. Methyl iodide was also detected and spot analyses were performed on the spectrophotometer. By analogy with previously studied[4] iodine systems, the expected mechanism is

$$I_2 \rightleftharpoons 2I\cdot; \quad K_{I_2}$$

$$I\cdot + CH_3OH \xrightarrow{1} CH_2OH + HI$$

$$CH_2OH + I_2 \xrightarrow{2} CH_2IOH + I\cdot$$

$$CH_2IOH \xrightarrow{3} HI + CH_2O$$

$$CH_2O + I\cdot \xrightarrow{4} HI + CHO$$

$$CHO + I_2 \xrightarrow{5} ICHO + I\cdot$$

$$ICHO \xrightarrow{6} CO + HI$$

Of reactions 4 through 6, reaction 4 is the slowest,[5] but it is faster than the rate-controlling step, since the observed activation energy is much larger than that of the formaldehyde reaction.[5] The activation energy for reaction -3 may be calculated,[6] for the four-center process and is 17 kcal/mol. Estimating thermodynamic parameters for CH_2IOH by bond additivity methods,[7] we may estimate the rate constant, k_3, as $10^{13.3-26.2/\theta}$ ($\theta = 2.303RT$ in kcal/mol). The concentration of CH_2IOH which would be present in equilibrium with 100 Torr of MeOH and 5 Torr of I_2 is $\sim 2 \times 10^{-5}$ mol/l., giving the value $\sim 10^{3.8}$ to the ratio, rate of reaction 3/rate of reaction 1. Reaction 3 is, therefore, not the rate-determining step.

The overall stoichiometry required by the above mechanism is

$$CH_3OH + 2I_2 \longrightarrow 4HI - CO$$

whence the rate of reaction 1 is $-\frac{1}{2}d[I_2]/dt$. By the initial rate method, k_1 has been calculated for all runs on this basis and the resulting Arrhenius plot (Figure 1) gives, for the least-squares line through all k_1 values obtained in the low surface-to-volume ratio (s/v) vessel

$$\log k_1/(1.\ mol^{-1}\ sec^{-1}) = 11.5 \pm 0.7 - (26 \pm 1.8)/\theta$$

(errors quoted are the 95% confidence limits).

The above mechanism does not explain the formation of CH_4 or CH_3I although this was only significant in the later stages of reaction. From Figure 1 it is seen that runs in which CH_4 is produced have rate constants equal, within experimental error, to those

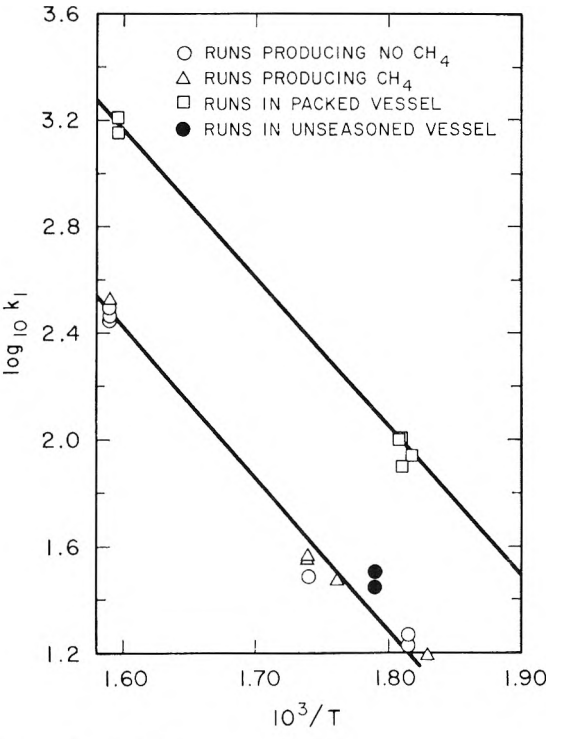

Figure 1. Arrhenius plot.

calculated for runs in which no CH_4 was produced. Such results are consistent with the production of CH_4 from CH_3I by the reactions

$$CH_3I + I\cdot \xrightarrow{8} CH_3\cdot + I_2$$

$$CH_3\cdot + HI \xrightarrow{9} CH_4 + I\cdot$$

if CH_3I production is negligible in the initial stages of reaction. No possible homogeneous path exists for the production of CH_3I at an observable rate in this system, so that it is presumably produced by a surface-sensitized reaction, possibly $CH_3OH + HI \rightarrow CH_3I + H_2O$. The effect on the initial rate measurements of an increase in the s/v ratio by a factor of 8 was tested by performing several runs in a packed vessel. As shown in Figure 1, the rate constant was increased by a factor of about 5, although the activation energy was unchanged. The activation energy of the surface-sensitive reaction, if it was not the rate-determining step in the low s/v vessel, must be the same as that of the homogeneous step. If, however, the surface reaction was the rate-controlling step in the low s/v vessel, the Arrhenius parameters are remarkably close to those expected for the homogeneous process. The

(4) D. B. Hartley and S. W. Benson, *J. Chem. Phys.*, **39**, 132 (1963); M. Teranishi and S. W. Benson, *J. Amer. Chem. Soc.*, **85**, 2887 (1963); P. S. Nangia and S. W. Benson, *ibid.*, **86**, 2773 (1964), and subsequent papers.

(5) R. Walsh and S. W. Benson, *ibid.*, **88**, 4570 (1966).

(6) S. W. Benson and G. R. Haugen, *ibid.*, **87**, 4036 (1965).

(7) S. W. Benson, "Foundations of Chemical Kinetics," McGraw-Hill Book Co. Inc., New York, N. Y., 1966, p 666.

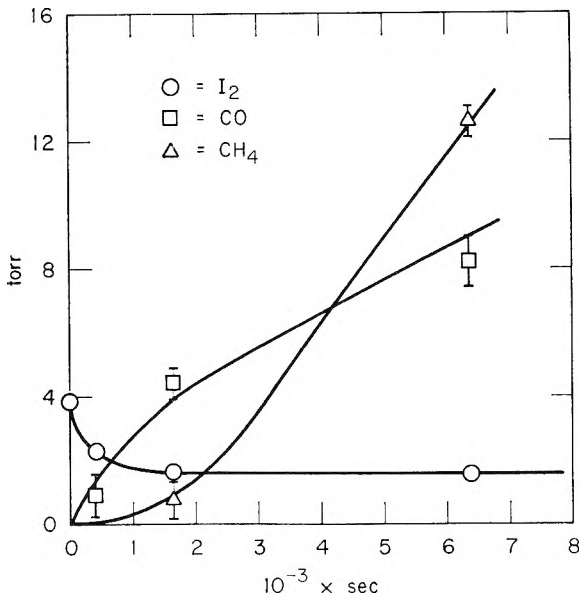

Figure 2. Product–time curves for runs 20, 23, and 24. The errors shown are estimated experimental errors and the curves shown are those discussed in the text.

A factor, $10^{11.5}$ l. mol^{-1} sec^{-1}, is close to that expected by analogy with the I· + CH_4 reaction,[8] so that the activation energy of 26 ± 1.8 kcal/mol must be a *lower* limit if the rate-determining step is the heterogeneous reaction. Comparing runs 17 and 26 (Table I), we see that CH_4 production for the same run was essentially the same in packed and unpacked vessels, whereas the initial rate of iodine consumption was five times as great. The difference in k_1 in the two reactors cannot, therefore, be attributed totally to an increased rate of CH_3I production in the packed vessel. The nature of possible surface-sensitized reactions was tested in the low s/v vessel. In run 21 (Table I), CO and HI yielded CH_4 and I_2. Run 22 shows that HI, itself, decomposes to produce I_2 (and presumably H_2). Addition of MeOH to this mixture resulted in the production of a further quantity of iodine and a considerable quantity of CH_4, as well as CO. If CH_4 is produced by reactions 8 and 9, and CO by reactions 1 through 6, 16.2 Torr of I_2 would have been consumed and 13.8 Torr produced. A net decrease of 2.4 Torr of I_2 would be expected, but production of 0.75 Torr was observed. The difference may be significant and could be due to some surface reaction, such as

$$2HI \rightleftharpoons I_2 + H_2$$

The influence on our initial rate measurements of these heterogeneous reactions will be negligible since they are very slow.

If CH_3I production was significant in the initial stages of the reaction, the assumed stoichiometry, and therefore k_1, would be in error. Analyses showed, however, that in runs 8, 9, and 10, for example, at reaction times of up to 1000 sec, no MeI was present, ±0.3 Torr and the HI produced was equal, within these limits, to twice the iodine consumed. A more sensitive measure of the initial value of [MeI] was the CH_4 produced in runs containing a large excess of HI. These runs would also indicate the significance of such reactions as

$$HI + MeOH \rightleftharpoons MeI + H_2O \text{ (surface)}$$

Comparison of runs 10 and 30 suggests although the errors involved are large by comparison with the concentrations measured, that the increased rate of CH_4 production in the packed vessel could be totally due to the higher concentration of HI arising from the acceleration in rate of step 1. Runs 20, 23, and 24 were essentially the same run, quenched at different times, and Figure 2 shows the product–time curves. Initial rate measurements were, in this case, made over the first 400 sec, and it is seen from Table I that the initial rate was inhibited by HI, as expected. Methane, and therefore CH_3I, production was insignificant over the first 400–600 sec and, from the shape of its formation curve, CH_4 is clearly a secondary product of the reaction. In the initial stages also, $[CO] \approx \frac{1}{2}(\Delta I_2)$, as required by the proposed mechanism.

After 3000 sec, the curves of Figure 2 are consistent with the relation $d[CO]/dt = \frac{1}{2}d[CH_4]/dt$, required by the observed steady state in I_2. From the observed $d[CO]/dt$, $k_1 = 10^{1.79}$ l. mol^{-1} sec^{-1}, in agreement with the value ($10^{1.723}$ l. mol^{-1} sec^{-1}), calculated from $-\frac{1}{2}(d[I_2]/dt)$ initial.

From the proposed reaction scheme

$$d[CH_4]/dt = \frac{k_8 k_9 K_{I_2}[I_2][HI][MeI]}{k_{-8}[I_2] + k_9[HI]}$$

The rate constants are well known,[9] $k_8 = 10^{11.4-20.5/\theta}$, $k_{-8} = 10^{10-1.5/\theta}$, and $k_9 = 10^{9.5-2.3/\theta}$, so that the value of $[MeI]_{ss}$ is only ≈0.7 Torr, from the observed rate of CH_4 production. This quantity is virtually undetectable spectrophotometrically in view of the large excess of HI present.

HI (162 Torr) was added to run 28 after 8288 sec, and the iodine rose from 1.04 to a maximum of 15.1 Torr. Equilibrium was not established at this point, however, and the iodine disappeared at a slower rate than initially. The added HI was not merely reversing step 1, therefore, but also reacted with MeI present, making measurements of the inhibition ratios pointless.

The rate of reaction of I_2 with MeOH is thus surface dependent and this seems to be due only partly, if at all, to an increased rate of CH_3I production, and partly

(8) C. A. Goy and H. O. Pritchard, *J. Phys. Chem.*, **69**, 3040 (1965).
(9) M. C. Flowers and S. W. Benson, *J. Chem. Phys.*, **38**, 882 (1963).

to an increased rate of

$$2I_2 + CH_3OH \longrightarrow 4HI + CO \text{ (surface)}$$

Because of the surface sensitivity of the rate, no attempt was made to measure k_{-1}/k_2, and we conclude that 26.0 kcal/mol is at least a lower limit to the activation energy of the homogeneous part of step 1, in view of the observed A factor.

This value of E_1 leads[4] to a C–H strength of 95.5 ± 2 kcal/mol for MeOH, which is greater than the limits (≤ 92 kcal/mol) set by the study[2] of the photobromination of MeOH. Recent work by Loucks and Laidler[10] yields the value of ~91 kcal/mol for the C–H bond strength in dimethyl ether which may be expected to be similar to that in methanol.

The O–H bond strength in MeOH is 103.6 kcal/mol[11] and the π-bond strength in formaldehyde is defined as ΔH for the reaction

$$CH_2O \longrightarrow \dot{C}H_2 - \dot{O}$$

i.e., the difference in ΔH for the reactions

$$CH_3OH \longrightarrow CH_3O\cdot + H\cdot$$

$$\dot{C}H_2OH \longrightarrow CH_2O + H\cdot \quad (\gamma)$$

which is 103.6[11] − 29[12,13] (±2) = 74.6 ± 2 kcal/mol. This is exactly the same as D_π^0(acetone)[14] (74.6 kcal/mol) and substituents seem, therefore, to have little or no effect on the value of D_π^0, in contrast to the situation for olefins

$$D_\pi^0(CH_2{=}CH_2) = 59.1 \text{ kcal/mol}$$

$$D_\pi^0[(Me)_2C{=}CH_2] = 55.8 \text{ kcal/mol}$$

A possible reason for the invariance of D_π^0 in the ketones is that in the carbonyl π bond, the electrons are as far removed from the C atom as they are in the biradical formed, when the π bond is broken. There will, therefore, be no change in the stabilizing effect of substituents such as methyl groups as the π bond is broken. This would imply that the sp^2 C atoms in propylene and in the butenes are probably slightly more polar in the biradical than in the ground-state olefins, so that there is decreased energy in π bond formation. This is not an unreasonable conclusion.

Acknowledgments. The authors wish to thank Drs. D. M. Golden and G. R. Haugen for helpful discussions.

(10) L. F. Loucks and K. J. Laidler, *Can. J. Chem.*, **45**, 2785 (1967).

(11) S. W. Benson and R. Shaw, Advances in Chemistry Series, No. 75, American Chemical Society, Washington, D. C., 1968, p 288.

(12) The figure 29 kcal/mol is derived from the experimental data as follows: ΔH_f° (CH_3OH) = −48.0 kcal/mol[11] and ΔH_f° (H·) = 52.1 kcal/mol, whence ΔH_f° (·CH_2OH) = D(H–CH_2OH) + ΔH_f° (CH_3OH) − ΔH_f° (H·) = −4.6. ΔH_f° (CH_2O) = −27.7 kcal/mol,[14] so that ΔH = −27.7 + 52.1 + 4.6 = 29 kcal/mol.

(13) S. W. Benson, "Thermochemical Kinetics," John Wiley and Sons, Inc., New York, N. Y., 1968.

(14) R. Walsh and S. W. Benson, *J. Amer. Chem. Soc.*, **88**, 3480 (1966).

Methyl Red Dissociation Kinetics in Dilute Aqueous Solution[1]

by L. P. Holmes, A. Silzars, D. L. Cole, L. D. Rich, and E. M. Eyring

Department of Chemistry, University of Utah, Salt Lake City, Utah 84112 *(Received August 15, 1968)*

Methyl red is a frequently used acid–base indicator in temperature-jump relaxation method[2] kinetic studies, and a knowledge of the specific rates in eq 1 is unnecessary if the sample system equilibrium has a relaxation time τ

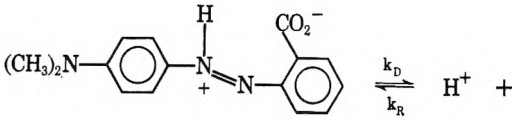

methyl red anion (1)

long compared to that of this methyl red equilibrium. However, in studying diffusion-controlled reactions, such as $AlOH^{2+} + H^+ \rightleftharpoons Al^{3+} + H_2O$ characterized by relaxation times of the order of 4 μsec,[3] known values of k_D and k_R are needed for a reliable interpretation of spectrophotometric temperature-jump relaxation data. Values of k_D and k_R have been determined by an electric field-jump (E-jump) relaxation method[2] and are reported here to meet this need.

Experimental Section

Dilute aqueous solutions of National Aniline Division methyl red recrystallized from water, mp 183–185° (lit.[4] 181–182°), were subjected to an electric field jump of 2 × 10^5 V/cm in the form of a single, square, high-voltage pulse of 2 to 3 μsec duration. A block diagram of the E-jump apparatus is shown in Figure 1. The sample cell was fashioned from Plexiglas with stainless steel electrodes spaced 2 mm apart. White light from a 300-W zirconium arc passed through a 520-nm interference filter and through 1 cm of solution in the sample cell before striking the photocathode of a 1P21 photomultiplier tube. The photomultiplier tube was operated below 500 V to avoid saturation. The distance from the sample cell to the photomultiplier tube was made large (4.5 m) to minimize the need for shielding from stray electromagnetic fields. The exponential decay in per cent light transmitted as a function of time was observed through a Tektronix Type W preamplifier on a Type 545 oscilloscope. The

(1) Supported by Grant AM 06231 from the National Institute of Arthritis and Metabolic Diseases.

(2) M. Eigen and L. DeMaeyer, "Technique of Organic Chemistry," Vol. VIII, Part II, S. L. Friess, E. S. Lewis, and A. Weissberger, Ed., Interscience Publishers, New York, N. Y., 1963, Chapter 18.

(3) L. P. Holmes, D. L. Cole, and E. M. Eyring, *J. Phys. Chem.*, **72**, 301 (1968).

(4) H. T. Clarke and W. R. Kirner, *Org. Syn.*, **2**, 47 (1922).

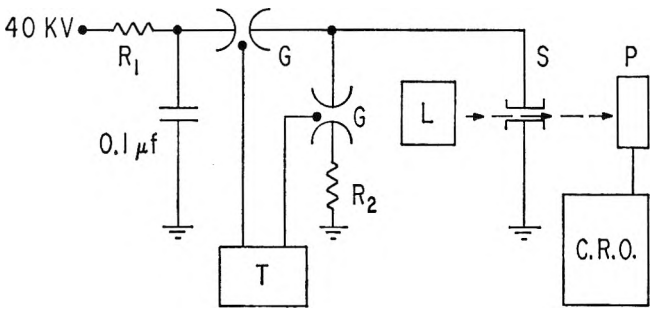

Figure 1. Block diagram of the electric field-jump relaxation method apparatus. $R_1 = 10^7$ ohms, $R_2 = 200$ ohms. The triggered spark gaps G are both E, G, and G.
Model GP-15; T, trigger pulse generator and time delay;
L, zirconium arc and interference filter;
S, sample cell; P, photomultiplier.

Table I: Electric Field-Jump Relaxation Data for Aqueous Methyl Red at 25°

C_0,[a] 10^{-6} M	pH[b]	τ,[c] μsec	n[d]
41.9	5.145	0.62 ± 0.10	4
31.4	5.163	0.73 ± 0.16	3
23.5	5.164	0.83 ± 0.11	3
7.51	5.600	1.16 ± 0.10	4
3.59	5.145	1.24 ± 0.04	3
3.27	5.805	1.67 ± 0.58	5

[a] Total methyl red molarity of sample solution calculated from the measured molar absorbance at the 460-nm isobestic point assuming a molar extinction coefficient of 15,300 l. mol^{-1} cm^{-1}. [b] Glass electrode pH of the sample solution. [c] Average electric field-jump relaxation time with standard deviation calculated from the range of n independent measurements. [d] Number of independent determinations of τ.

resulting relaxation times are given in Table I. The estimated experimental error in the individual measurements of τ is ±15%.

The electrical resistance of the sample cell in all cases exceeded 10^4 ohms so that the jump in temperature incident to the E-jump was negligible. The reliability of the apparatus was verified by reproducing the kinetic results of Ilgenfritz[5] for aqueous bromocresol purple.

Since the ionic strength of our sample solutions never exceeded 2×10^{-5} M, we were able to approximate the hydrogen ion molarity by the relation $[H^+] = 10^{-pH}$ where the glass electrode pH was determined with a Beckman 1019 meter.

Results and Discussion

The relaxation time τ attributable to equilibrium 1 is given by[2]

$$\tau^{-1} = k_R([H^+] + [A^-]) + k_D \qquad (2)$$

The least-squares straight line drawn through a τ^{-1} *vs.* $([H^+] + [A^-])$ plot of the data of Table I has a slope $k_R = 3.5 \times 10^{10}$ M^{-1} sec^{-1} and an intercept $k_D = 4.8 \times 10^5$ sec^{-1}. The quotient $K_a = k_D/k_R = 10^{-4.86}$ is in good agreement with the literature value[6,7] of $10^{-5.00}$ at zero ionic strength and 25°.

This value of k_R is approximately a third of that calculated from the Smoluchowsky–Debye–Eigen phenomenological equation[2] for diffusion-controlled reaction between H^+ and a spherical monoanion in water at 25°. Very similar differences between experimental and theoretical values of k_R have been observed[2] for such acids as p-nitrophenol, carbonic acid, and acetic acid and attributed largely to steric factors. The k_R for methyl red is also significantly smaller than values of 8×10^{10} M^{-1} sec^{-1} and 7.2×10^{10} M^{-1} sec^{-1} reported[5] for the indicators bromocresol purple and phenol red, respectively, in water at 15° from similar E-jump relaxation method experiment. This difference can be ascribed almost entirely to the greater attraction of a dianion for a proton in the equilibrium

$$HA^- \underset{k_R}{\overset{k_D}{\rightleftharpoons}} H^+ + A^{2-} \qquad (3)$$

which is under observation in the case of these two sulfonephthaleins.

The value $k_D = 4.8 \times 10^5$ sec^{-1} for methyl red is much larger than the corresponding constants 2.4×10^4 sec^{-1} and 4.9×10^2 sec^{-1} found[5] for aqueous bromocresol purple and phenol red, respectively. However, methyl red proton dissociation is from a resonance stabilized, zwitterionic acid,[7] whereas, in the sulfonephthaleins a phenolic proton dissociates. Thus, a more instructive comparison is that between methyl red and benzoic acid ($k_D = 2.3 \times 10^6$ sec^{-1})[8] as well as the three isomeric aminobenzoic acids. The values[8] $k_D = 6.4 \times 10^5$, 7.4×10^5, and 4.4×10^5 sec^{-1} for o-, m-, and p-amino benzoic acids, respectively, indicate that the difference between k_D for benzoic acid and methyl red can be accounted for entirely in terms of zwitterionic forms of protonated methyl red that do not involve significant intramolecular hydrogen bonding. Where intramolecular hydrogen bonding is important as in N,N-dimethyl-o-aminobenzoic acid, k_D drops to[8] $\sim 1 \times 10^2$ sec^{-1}.

Successful measurements of τ as short as 0.2 μsec with this spectrophotometric E-jump device suggest the feasibility of measuring the rate of the helix–random coil transition in aqueous poly-L-glutamic acid and poly-L-tyrosine. Previous studies[9] have shown that the relaxation time for this transition in these polyanions lies between 0.05 and 2.0 μsec, which is too fast for measurement by the more common Joule heating temperature-jump relaxation method.

(5) G. Ilgenfritz, Doctoral Dissertation, George August University, Goettingen, Germany, 1966.
(6) I. M. Kolthoff, *J. Phys. Chem.*, **34**, 1466 (1930).
(7) S. W. Tobey, *J. Chem. Educ.*, **35**, 514 (1958).
(8) M. Eigen and E. M. Eyring, *J. Amer. Chem. Soc.*, **84**, 3254 (1962).
(9) G. Schwarz, *J. Mol. Biol.*, **11**, 64 (1965); R. Lumry, R. Legare, and W. G. Miller, *Biopolymers*, **2**, 489 (1964); and E. Hamori and H. A. Scheraga, *J. Phys. Chem.*, **71**, 4147 (1967).

Crystal Field Activation Energies of Hexaaquo Transition Metal Complexes

by Audrey L. Companion

Department of Chemistry, Illinois Institute of Technology, Chicago, Illinois 60616 *(Received July 17, 1968)*

In recent years the concept of crystal field activation energy (CFAE) has been employed by several investigators[1-7] in attempts to rationalize trends in kinetic data for ligand replacement reactions involving transition metal complexes. The CFAE for an SN1 dissociation of a hexacoordinated species, for example, may be easily computed in terms of the relative crystal field stabilization energy (CFSE) of an octahedron (O_h) and square pyramid (C_{4v}) of ligands with the one-electron formulas as presented by Basolo and Pearson.[1] Generally, CFAE's computed this way have been in only rough agreement with experiment. In this note we examine the possibility of improving these calculations by using many-electron methods and crystal field parameters in better accord with observed spectra of transition metal ions.

For d^2 and d^7 configurations (for which one-electron formulas may be in considerable error) we computed ground state CFSE's with the matrices given in the Appendix in terms of parameters *Dq*, *Ds*, and *Dt*, in turn expressed as functions of radial integrals α_2 and α_4. While in the octahedral species only the parameter α_4 is significant in determining the CFSE, in the lower symmetry C_{4v} species knowledge of both α_2 and α_4 is necessary. Purely theoretical calculations yield values of the ratio $\rho = \alpha_2/\alpha_4$ from 2 to 6, results believed to be gross exaggerations of the importance of the α_2 contribution. While spectroscopic studies of noncubic complexes have not yet yielded definitive evidence favoring any specific ρ, several investigations[8-11] have indicated that a reduction of ρ to a value of 1 or less is necessary for compatibility of theory with experiment. The one-electron CFSE's employed thus far in CFAE considerations[1] are based on $\rho = 2$.

The weak-field one-electron and many-electron CFAE's computed for bivalent and trivalent aquo ions and the original spectroscopic data used are summarized in Table I. The only ions for which nephelauxetic relaxation influenced the CFAE over the parameter range investigated were V^{3+} and Co^{2+}, for which the F–P separations 13,200 and 12,800 cm^{-1} were used. Comparison of the results of the one-electron and many-electron treatments with $\rho = 2$ indicate that except for a small increase (about 1 kcal/mol) in the CFAE for d^2 and d^7 ions the many-electron treatment makes no appreciable correction in the computed CFAE's, at least for SN1 processes.

Note in Table I that in all cases the CFAE's of both d^3 and d^8 ions are independent of ρ, since the ground state in O_h, A_{2g}, becomes under the ρ values considered, the ground state B_1 in C_{4v}, which has no dependence on *Ds* (see Appendix). This fact, along with the known zero CFSE of d^0, d^5, and d^{10} ions in any weak field, was used in positioning what we call a "classical" activation energy curve (without crystal field effects) for a series, on which computed CFAE's were superimposed. As an illustration, consider the free energies of activation[12] determined by Swift and Connick[3] by nmr methods for the exchange of ligand and solvent water molecules in hexaaquo bivalent complexes, shown as open circles in Figure 1. Comparison of the difference between the experimental activation energies of Mn^{2+} and Ni^{2+}

Table I: SN1 Crystal Field Activation Energies for Hexaaquo Transition Metal Complexes

Ion	*Dq*, cm^{-1}	Many electron C_{4v} CFAE, kcal/mol			One-electron CFAE
		$\rho = 0$	$\rho = 1$	$\rho = 2$	$\rho = 2$
$V^{2+}(d^3)$	1180[a]	6.8	6.8	6.8	6.8
$Cr^{2+}(d^4)$	1400[a]	1.1	−5.7	−12.6	−12.6
$Mn^{2+}(d^5)$	...	0.0	0.0	0.0	0.0
$Fe^{2+}(d^6)$	1040[b]	0.9	0.9	−1.7	−1.7
$Co^{2+}(d^7)$	950[a]	1.8	1.9	−2.1	−3.1
$Ni^{2+}(d^8)$	850[a]	4.8	4.8	4.8	4.8
$Cu^{2+}(d^9)$	1300[c]	1.1	−5.6	−11.7	−11.7
$Zn^{2+}(d^{10})$	...	0.0	0.0	0.0	0.0
$Sc^{3+}(d^0)$	...	0.0	0.0	0.0	0.0
$Ti^{3+}(d^1)$	2030[a]	−1.7	1.7	−3.3	−3.3
$V^{3+}(d^2)$	1785[a]	4.1	3.3	−4.9	−5.8
$Cr^{3+}(d^3)$	1740[a]	10.0	10.0	10.0	10.0
$Mn^{3+}(d^4)$	2100[b]	1.7	−8.6	−18.9	−18.9
$Fe^{3+}(d^5)$	...	0.0	0.0	0.0	0.0

[a] C. J. Ballhausen, "Introduction to Ligand Field Theory," McGraw-Hill Book Co., Inc., New York, N. Y., 1962. [b] L. E. Orgel, "Transition Metal Chemistry," Methuen and Co., London, 1960. [c] D. S. McClure, ref 2, p 82.

(1) F. Basolo and R. G. Pearson, "Mechanisms of Inorganic Reactions," 2nd ed, John Wiley and Sons, Inc., New York, N. Y., 1967, Chapters 2 and 3.

(2) R. G. Pearson in "Some Aspects of Crystal Field Theory," T. Dunn, D. S. McClure, and R. G. Pearson, Harper and Row, New York, N. Y., 1965.

(3) T. J. Swift and R. E. Connick, *J. Chem. Phys.*, **37**, 307 (1962); **41**, 2553 (1964).

(4) M. Eigen in "Advances of the Chemistry of Coordination Compounds," The Macmillan Co., New York, N. Y., 1961, p 371.

(5) R. Hogg, G. A. Melson, and R. G. Wilkins, ref 4 p 39.

(6) D. Fiat and R. E. Connick, *J. Amer. Chem. Soc.*, **90**, 608 (1968).

(7) W. Kruse and D. Thusius, *Inorg. Chem.*, **7**, 464 (1968).

(8) J. A. Anysas and A. Companion, *J. Chem. Phys.*, **40**, 1205 (1964).

(9) D. S. McClure, *ibid.*, **36**, 2757 (1962).

(10) C. K. Jorgensen, "Absorption Spectra and Chemical Bonding in Complexes," Pergamon Press, New York, N. Y., 1962, p 55.

(11) R. A. D. Wentworth and T. S. Piper, *Inorg. Chem.*, **4**, 709 (1965).

(12) Association of CFAE with free energies of activation rather than with the less accurately known enthalpies is a common procedure, although of questionable validity. The implicit assumption of regularly varying entropy changes within a series, although logically appealing, is not well founded. At worst the crystal field model used in this way may be regarded as a heavily empiricized method with which one may make reasonably good first guesses about trends in rate constants.

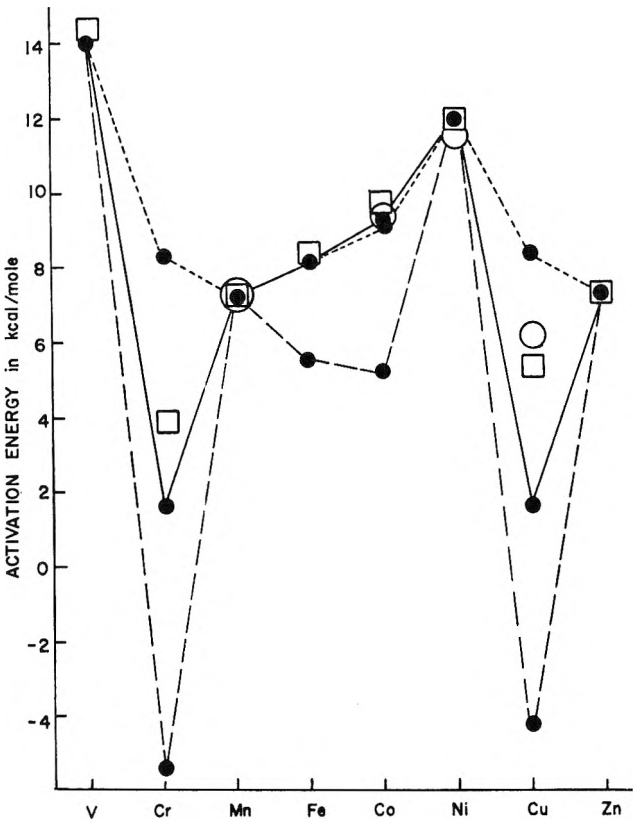

Figure 1. Activation energies for SN1 dissociations of bivalent transition metal ions: $\rho = 0$, – – –; $\rho = 1$, ——; $\rho = 2$, — —. Open circles represent experimental points of Swift and Connick;[3] open squares, experimental points of Eigen.[13]

(4.2 kcal/mol) with the computed difference in CFAE's for these ions (4.8 kcal/mol) makes it reasonable to assume that the classical activation energy is essentially constant across the series. This near-constancy is again illustrated by Eigen's data[13] for dissociation of a ligand water molecule from a hydrated ion involved in an ion pair, $[M(H_2O)_n^{2+}, SO_4^{2-}]$. The theoretical total activation energies for bivalent ions computed under the assumption of a constant classical activation energy across the series [7.2 kcal/mol, the Swift and Connick result for Mn^{2+}] are plotted in Figure 1 for ρ values of 0, 1, and 2. The open squares represent Eigen's rate constants corrected for classical contributions and with the scale adjusted such that $-\log k$ values for Mn^{2+} and Ni^{2+} correspond to the computed activation energies (both independent of ρ).

For both sets of experimental data, agreement between theory and experiment is obviously better for the lower ρ values over the whole range of ions from V^{2+} to Zn^{2+}; in particular, the lower ρ values correctly predict the observed trend from Mn^{2+} to Ni^{2+}, for which the usual $\rho = 2$ fails completely. The largest deviations between theory and experiment occur for Cr^{2+} and Cu^{2+} ions, both of which undergo strong Jahn–Teller distortions in six coordination, an effect not included in our calculations.

No rate studies by a given group of investigators using a consistent method have yet been reported for the whole series of *trivalent* transition metal ions. However, Fiat and Connick[6] and Kruse and Thusius[7] have summarized available substitution rate data indicating that for aquo complexes rate constants for Ti^{3+}, Fe^{3+}, and V^{3+} are of the same order of magnitude, ordering approximately as $k(\mathrm{Ti}) > k(\mathrm{Fe}) > k(\mathrm{V})$. Hexaaquo Cr^{3+} ion is considerably less labile than these three. Assuming that reactions of these ions do proceed through an SN1 elimination of water (a fact not yet definitively established) one may see from the CFAE's in Table I that ρ values of 1 or less describe the trend much more properly than the ratio commonly used. (For example, $\rho = 2$ predicts that V^{3+} should be *considerably* more labile than Fe^{3+}.)

Based primarily on improved agreement between theoretical and experimental activation energies for SN1 processes of hexaaquo transition metal ions, the suggestion is made that radial parameter ratios of 1 or less, rather than 2, be used in calculations of crystal field activation energies. One-electron formulas comparable to those of Basolo and Pearson[1] may be easily derived for any geometry chosen for an intermediate (including complexes with mixed ligands) with the simple approach presented earlier by Companion and Komarynsky.[14] In addition, Spees, Perumareddi, and Adamson[15] have recently recalculated one-electron energy levels for some of the Basolo–Pearson intermediates.

Acknowledgment. The author is grateful to the donors of the American Chemical Society Petroleum Research Fund for support of this work.

Appendix: C_{4v} Crystal Field Energy Matrices

$d^{1,6}$ Configurations

$$E(A_1, z^2) = 6Dq - 2Ds - 6Dt$$

$$E(B_1, x^2 - y^2) = 6Dq + 2Ds - Dt$$

$$E(B_2, xy) = -4Dq + 2Ds - Dt$$

$$E(E, xy, yz) = -4Dq - Ds + 4Dt$$

$d^{2,7}$ Configurations

$$E[B_1(A_{2g})] = 12Dq - 7Dt$$

$$E[B_2(T_{2g})] = 2Dq - 7Dt$$

(13) M. Eigen, *Ber. Bunsenges. Physik. Chem.*, **67**, 753 (1963); see also G. Geier, *ibid.*, **69**, 615 (1965).

(14) A. Companion and M. Komarynsky, *J. Chem. Educ.*, **41**, 257 (1964).

(15) S. T. Spees, Jr., J. R. Perumareddi, and A. W. Adamson, *J. Phys. Chem.*, **72**, 1822 (1968).

A_2	$F(T_{1g})$	$P(T_{1g})$
$F(T_{1g})$	$[-30Dq - 4Ds + 30Dt]/5$	$[20Dq - 12Ds - 20Dt]/5$
$P(T_{1g})$		$[14Ds + 5(P - F)]/5$

E	$F(T_{1g})$	$F(T_{2g})$	$P(T_{1g})$
$F(T_{1g})$	$[-120Dq + 8Ds + 45Dt]/20$	$[4Ds + 5Dt](15)^{1/2}/20$	$[40Dq - 12Ds - 15Dt]/10$
$F(T_{2g})$		$[8Dq + 7Dt]/4$	$[4Ds + 5Dt](15)^{1/2}/10$
$P(T_{1g})$			$[-7Ds + 5(P - F)]/5$

$Dq = \alpha_4/6$; $Ds = \alpha_2/7$; $Dt = \alpha_4/21$; $\alpha_2 = qe^2\langle r^2\rangle/R^3$; $\alpha_4 = qe^2\langle r^4\rangle/R^5$; where qe is the ligand charge, R the ligand–metal distance and $\langle r^n\rangle$ the expectation value of the nth power of the d-electron distance from the metal nucleus. The above formulas also describe d^4,[9] and d^3,[8] configurations if the signs of Dq, Ds, and Dt are changed everywhere.

Transference Numbers and Ionic Solvation of Lithium Chloride in Dimethylformamide

by Ram Chand Paul, Jai Parkash Singla, and Suraj Prakash Narula

Department of Chemistry, Panjab University, Chandigarh-14, India
(Received August 20, 1968)

In a number of publications, the potentialities of dimethylformamide[1–4] as a protonic solvent have been highlighted. Sherrington and Prue[5] have briefly mentioned the measurement of cation transference number of potassium thiocyanate in DMF. However, no attempt has been made to calculate the solvation of the ions on the basis of transference data. Gopal and Hussain[6] have calculated the solvation number of many alkali ions in different solvents from the available conductance data. In the absence of transference data of various ions, they have claimed only a limited accuracy of their results.

Lithium ion being small in size is generally solvated in solutions. Lithium chloride is appreciably soluble in DMF and accurate conductance data for it are available in the literature.[5] It has, therefore, been selected as the electrolyte for the present investigations. The ionic conductance and the solvation number of lithium ion as calculated on the basis of transference data are reported here.

Experimental Section

Materials. Lithium chloride (BDH AnalaR) was fused in a platinum crucible under a stream of dry hydrogen chloride, cooled in a desiccator, and lumps of the fused salt were powdered and reheated in a weighing bottle to 300° for ½ hr, cooled, and kept in a vacuum desiccator for use. Silver nitrate and potassium thiocyanate (both BDH AnalaR) were used as received. Silver (commercial) was purified by electrolysis in the laboratory and converted into wire for use.

Solvent. Dimethylformamide (Baker Analyzed) was purified by keeping it over anhydrous sodium carbonate (BDH AnalaR) for about 48 hr with occasional shaking. It was fractionally distilled. The middle fraction (bp 148.5–149.5°, sp. cond. $< 2 \times 10^{-7}$ ohm^{-1} cm^{-1}) was taken for use. As far as possible all transference of materials was carried out in a drybox and solutions were protected from moisture by silica gel guard tubes.

Determination of Transference Numbers. A weighed amount of lithium chloride was dissolved in DMF (250 ml). A modified Hittorf transference cell with three compartments separated with well-greased stopcocks was used. The experimental technique for the measurement of transference number is exactly the same as described by Amis and coworkers.[7,8]

There was no evolution of gas at the cathode when a current of 3–10 mA was employed. A current stabilizer (Gelman Instrument Co.) was used along with a Richard coulometer to measure the amount of current passed. Each experiment was continued for about 12–24 hr depending upon the concentration of the solution. The time of experiment was increased with the dilute solutions.

Because of the solubility of the silver chloride (formed at the anode during electrolysis) in DMF, the solutions of cathode and middle compartments were analyzed. The chloride ion concentrations of the solutions were estimated by Volhard's method. Two

(1) R. C. Paul, P. S. Guraya, and B. R. Sreenathan, *Indian J. Chem.*, **1**, 335 (1963).
(2) R. C. Paul, S. Sharda, and B. R. Sreenathan, *ibid.*, **2**, 97 (1964).
(3) R. C. Paul, S. C. Ahluwalia, and S. S. Pahil, *ibid.*, **3**, 300, 305 (1965).
(4) R. C. Paul and B. R. Sreenathan, *ibid.*, **4**, 348, 382 (1966).
(5) J. E. Prue and P. J. Sherrington, *Trans. Faraday Soc.*, **57**, 1795 (1961).
(6) R. Gopal and M. M. Hussain, *J. Indian Chem. Soc.*, **40**, 981 (1963).
(7) W. Ves Childs and E. S. Amis, *J. Inorg. Nucl. Chem.*, **16**, 114 (1960).
(8) J. O. Wear, C. V. McNully, and E. S. Amis, *ibid.*, **18**, 48 (1961).

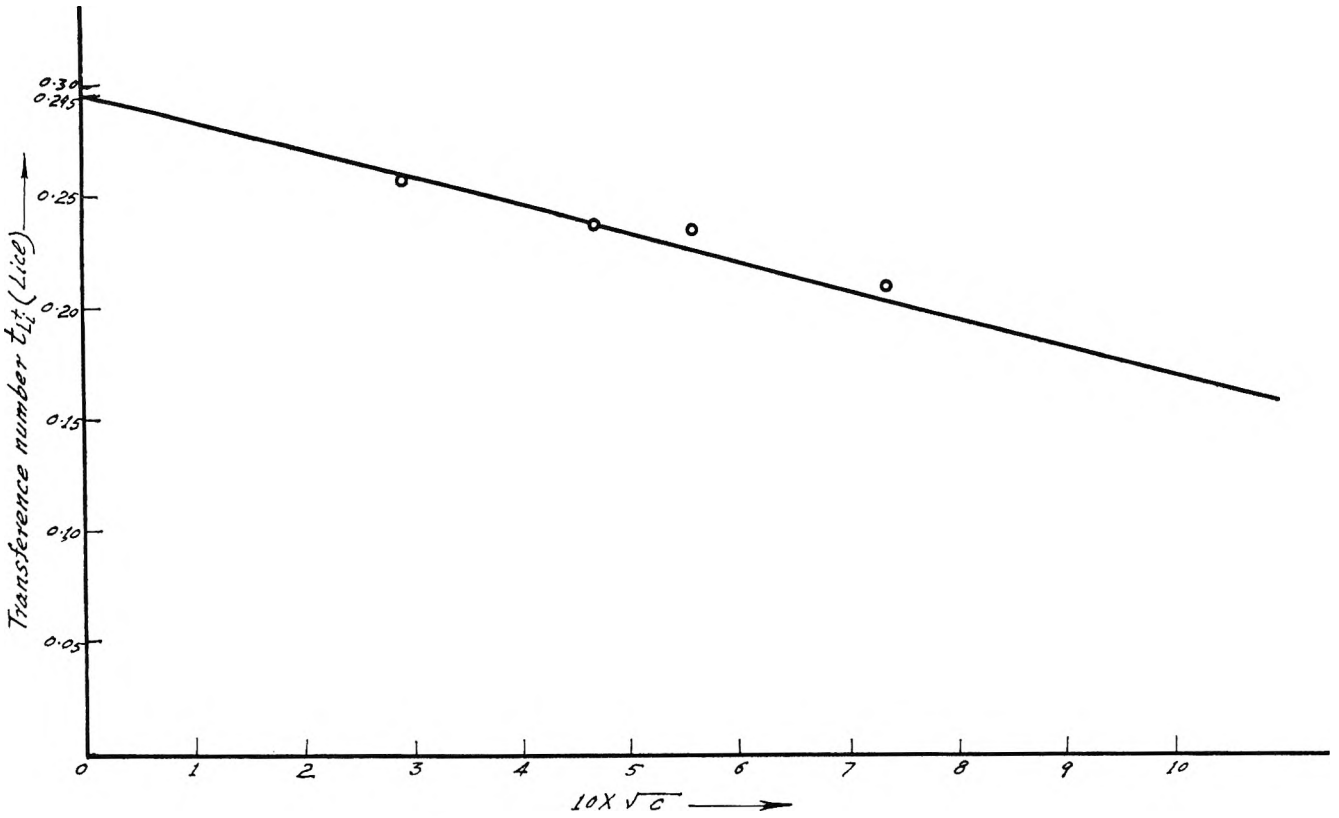

Figure 1. Plot of transference number *vs.* $\sqrt{c}$. The limiting transference number of the lithium ion, $t_+^0 = 0.295$.

to three sets of experiment for each concentration were performed to check the accuracy of the results. The equation for the calculation of transference number is the same as employed by Amis and coworkers.[7,8]

Results and Discussion

In view of the very high resistance offered by the cell as well as difficulties of accurate estimation, the investigations regarding transference numbers were carried out in the concentration range 0.08–0.55 *N* at 25°. The transference numbers have been found to vary linearly with the square root of the concentration.

On extrapolation, the limiting transference number of lithium ion was found to be 0.295 (Figure 1). The equivalent conductance was combined with the limiting transference number to give the individual ionic mobility. The ionic mobility of lithium ion in DMF was calculated to be 23.62 (int ohms)$^{-1}$ cm^2 mol^{-1}. All the relevant data are recorded in Table I.

The radius of the solvated ions (r_s) was calculated from the Stokes equation

$$r_s = F^2/6\pi\eta\lambda_+^0 N$$

The crystallographic radius ($r_c = 0.60$ Å) was obtained from the literature.[5] The Robinson–Stokes correction factor (r_{cor}/r_s) was read from the plot of r_{cor}/r_s *vs.* r_s for tetraalkylammonium ions in water solution.[9] The volume of the solvent sheath was obtained from the equation[10]

$$V = 4\pi(r_{cor}^3 - r_c^3)/3$$

The solvation number was thus obtained by dividing the above volume by the average volume of a DMF molecule (128.4 Å^3).[10] The solvation number of lithium ions in the concentration range discussed was found to be 3.24.

The cation transference number of lithium chloride in nonaqueous mixed solvents has been found to decrease with the increase in concentration.[8] In formamide, the cation transference numbers of alkali halides decrease with an increase in concentration.[10–12] In water also the cation transference numbers of lithium and sodium ions decrease with increase in their concentration though the transference numbers of K^+, Rb^+,

(9) R. A. Robinson and R. H. Stokes, "Electrolyte Solutions," Butterworth and Co. Ltd., London, 1955, p 120.

(10) J. M. Notley and M. Spiro, *J. Phys. Chem.*, **70**, 1502 (1966).

(11) L. R. Dawson and C. Berger, *J. Amer. Chem. Soc.*, **79**, 4267 (1957).

(12) G. P. Johari and P. H. Tewari, *J. Phys. Chem.*, **70**, 197 (1966).

Table I: Hittorf Transference Numbers for the Ions of Lithium Chloride in Dimethylformamide at 25° [a]

Concn, mol/l. of solvent	W_{Ag}	$F \times 10^3$	t_c (±1 %)	t_a (±1 %)	W_{sol}, g
0.0858	0.1570	1.45	0.257	0.743	45.185
0.2233	0.3434	3.69	0.237	0.763	55.935
0.3149	0.2975	2.75	0.235	0.765	55.563
0.5466	0.4397	4.05	0.208	0.792	45.04

t_c^0	λ_+^0	r_c, Å	r_s, Å	r_{cor}, Å	Solvation no.
0.295	23.62	0.60	4.37	4.66	3.24

[a] W_{Ag} is the weight of silver deposited in the coulometer; F is the Faraday (quantity of electricity); t_c is the cation transport number; t_a is the anion transport number; W_{sol} is the weight of the solution in the cathode compartment; t_c^0 is the transport number of the cation at infinite dilution; λ_+^0 is the ionic conductance at infinite dilution; r_c is the crystallographic radius of the cation; r_s is the Stokes radius of the solvated cation; and r_{cor} is the corrected value of the radius of the solvated cation.

Cs^+, Cl^-, Br^-, and I^- ions remain almost constant with an increase in their concentration.[13] This difference in behavior has been explained on the basis of ion–solvent interaction.[14]

The cation transference number of lithium chloride in DMF also decreases with an increase in concentration and shows a linear relationship. This behavior of lithium chloride is the same as in other solvents including water. DMF has a high dielectric constant and dipole moment. Thus the ion–dipole interaction between lithium ion and the solvent may result in the solvation of the cation.

The ionic mobilities of different alkali ions have been calculated from conductance data in various nonaqueous solvents.[5] The ionic conductance of lithium ion (λ_+^0) in DMF has been reported as 25.0 (int ohms)$^{-1}$ cm^2 mol^{-1}. Using this value, Gopal and Hussain[6] have calculated the solvation number of lithium ion in DMF as 3. However, they have pointed out the limited accuracy of this value particularly because of the absence of transference data of lithium chloride in this solvent. Now the ionic conductance of the Li^+ ion (λ_+^0) has been obtained from the relation

$$\lambda_+^0 = \Lambda_0 \times t_+^0$$

and has been found to be 23.62 (int ohms)$^{-1}$ cm^2 mol^{-1}. The solvation number of lithium ion calculated on the basis of the above value of ionic conductance has been found to be 3.24.

Acknowledgment. The authors thankfully acknowledge the financial assistance from National Bureau of Standards, Washington, D. C.

(13) L. G. Longsworth, *J. Amer. Chem. Soc.*, 54, 2741 (1932).

(14) R. Gopal and O. N. Bhatnagar, *J. Phys. Chem.*, 68, 3892 (1964).

Intensity Contour Maps in Molecular Beam Scattering Experiments[1]

by R. Wolfgang and R. J. Cross, Jr.

Chemistry Department, Yale University, New Haven, Connecticut 06520 *(Received September 12, 1968)*

Molecular beam experiments are now yielding information on the combined velocity and angular distributions of reaction products. The representation of such data in easily interpretable yet unambiguous graphical form has, however, posed unnecessarily vexing problems. We propose here the adoption of a simple convention which, despite its usefulness, does not seem to have been described in the literature.

Data are usually presented as relative differential cross sections $I_L(v, \Theta, \Phi)$[2] for a given range of laboratory velocity dv and solid angle $d\Omega = \sin\Theta d\Theta d\Phi$. They may be presented as an intensity or flux contour map on a standard Newton diagram[3] (see Figure 1). This representation is unambiguous but its phase space is symmetric only with respect to the laboratory (LAB) origin, the volume elements varying as v^2. A system symmetric with respect to the center of mass is, however, more useful. It enables one to check that the product distribution is symmetric around the collision axis (relative velocity vector) as is required of all randomly oriented systems, and to ascertain if the forward–backward symmetry identifying a long-lived intermediate is present.

The common solution to this problem has been to transform the LAB cross sections to similar cross sections $I_{CM}(u, \theta, \phi)$ referred to an origin at the center of mass (CM system). The above symmetry considerations can then be readily demonstrated. The transformation relationship is (see Appendix)

$$I_{CM}(u, \theta, \phi) = I_L(v, \Theta, \Phi)(u^2/v^2) \qquad (1)$$

(Note, however, that most published results to date have used the incorrect factor $(u^2/v^2)\cos\delta$, where δ is the angle between **u** and **v**.)[4]

Serious difficulties arise with the transformation to the CM system as there are normally velocity and angular spreads in one or both of the colliding beams. Thus there is no unique center of mass. Commonly an

(1) Financial support for this work from the National Aeronautics and Space Administration and from the National Science Foundation is gratefully acknowledged.

(2) $I_L(v,\Theta,\Phi)dvd\Omega$ is the intensity of product molecules between v and $v+dv$ in the solid angle $d\Omega$ divided by $(I_A n_B)$, where I_A is the beam flux of A (molecules/cm^2 sec) and n_B is the number density of B (molecules/cm^3).

(3) D. R. Herschbach, *Advan. Chem. Phys.*, 10, 319 (1966).

(4) The correct transformation has been given by Z. Herman, J. Kerstetter, T. Rose, and R. Wolfgang, *Discussions Faraday Soc.*, 44, 123 (1967); W. Miller, S. A. Safron, and D. R. Herschbach, *ibid.*, 44, 108 (1967).

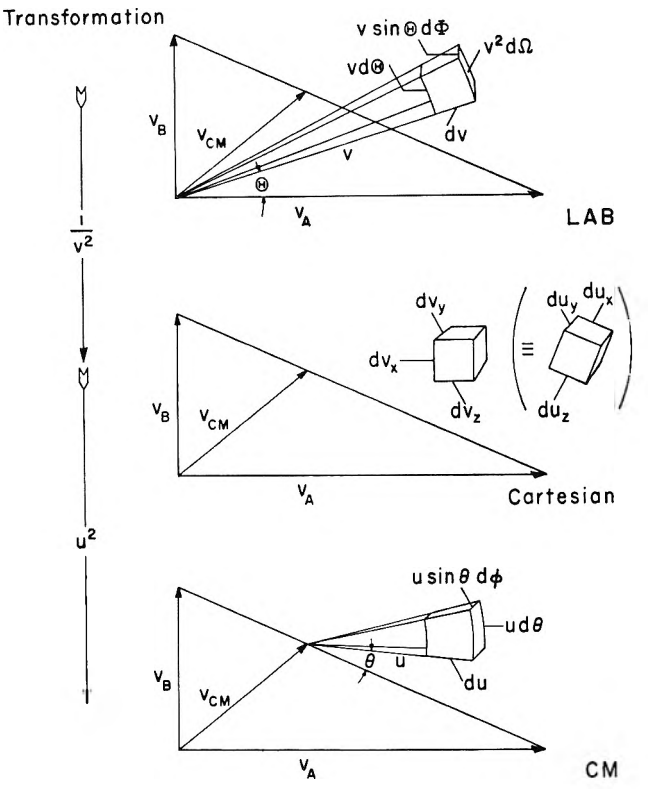

Figure 1. The Newton diagrams, coordinates, and volume elements are shown for the three-coordinate systems used. The transformations from I_L to P_C to I_{CM} are given at the left. Note that the Cartesian volume element is unaffected by rotation or translation.

approximate transformation is made, assuming some sort of average or most probable center of mass. The representation of the data has thus been adulterated by an arbitrary assumption. The result of this is particularly unrealistic near the center of mass, where there will be a "hole" in the intensity distribution due to the factor (u^2/v^2) becoming zero.

An exact treatment actually requires prior knowledge of I_{CM}, the goal of the experiment. A complicated recursive procedure is therefore required to unfold the averaging due to the range of initial conditions.[5]

These difficulties may be largely overcome by using a probability function in Cartesian coordinates

$$P_C(v_x, v_y, v_z) = P'_C(u_x, u_y, u_z) = I_L/v^2 = I_{CM}/u^2 \quad (2)$$

Like I_L it is unambiguous. As the choice of origin is arbitrary, it is independent of any assumption as to the center of mass. The asymmetry due to unequal size of volume elements in the LAB system has been removed, though obviously that introduced by the initial beam distributions remains. Hence P_C possesses all the symmetry properties of I_{CM} about any chosen center of mass. It follows that the tests for axial and forward–backward symmetry described above can be made as well with the Cartesian as with the CM system. Furthermore, since Cartesian volume elements are constant in size, the "hole" around the center of mass is absent.

Acknowledgment. A proposal made by us to adopt the Cartesian coordinate system was accepted by an informal group attending the Gordon Conference on Molecular Collisions, June 1968, and we are grateful to these colleagues. Some of them, particularly R. B. Bernstein, B. H. Mahan, and D. R. Herschbach, have already used this system privately. Earlier discussions with Z. Herman and J. Ross following the Fifth International Conference on Electronic and Atomic Collisions, Leningrad, July 1967, were most stimulating to us in developing this convention.

Appendix: Derivation of the LAB–Cartesian–CM Transformations

To prove (1) it is convenient to transform first from the intensity per solid laboratory angle as measured by a detector of constant area, $I_L(v, \Theta, \Phi)$ to the relative probability of finding a product molecule between v and $v + dv$, Θ and $\Theta + d\Theta$, and Φ and $\Phi + d\Phi$, $P_L(v, \Theta, \Phi)dvd\Theta d\Phi$. This relation is

$$P_L = I_L \sin \Theta \quad (A1)$$

We may write a similar transformation between the analogous intensity as measured by a detector in the CM system $I_{CM}(u, \theta, \phi)$ and $P_{CM}(u, \theta, \phi)$

$$P_{CM} = I_{CM} \sin \theta \quad (A2)$$

Now

$$P_L(v, \Theta, \Phi)dvd\Theta d\Phi = P_{CM}(u, \theta, \phi)dud\theta d\phi \quad (A3)$$

where P_L and P_{CM} are related by the Jacobian of the LAB–CM transformation, $J = \partial(v, \Theta, \Phi)/\partial(u, \theta, \phi)$[6] (*i.e.*, the ratio of volume elements). This Jacobian is the product of the Jacobians for three transformations: first, transform P_L to a LAB Cartesian probability, $P_C(v_x, v_y, v_z)$; next, transform P_C to the analogous CM probability $P'_C(u_x, u_y, u_z)$; finally, transform P'_C to P_{CM}. These are, respectively $(v^2 \sin \Theta)^{-1}$, 1, $(u^2 \sin \theta)$.[7] Thus

$$J = (u^2 \sin \theta)/(v^2 \sin \Theta) \quad (A4)$$

Expressing I_L and I_{CM} in terms of P_L and P_{CM} gives (1). Similarly

$$P_C = I_L/v^2 = P'_C = I_{CM}/u^2 \quad (A5)$$

(5) E. A. Entemann, Ph.D. Thesis, Harvard University, 1968; R. K. B. Helbing, *J. Chem. Phys.*, 48, 472 (1968); P. T. Warnock and R. B. Bernstein, WIS-TCI-283 (University of Wisconsin, Jan 1968).

(6) For a discussion of Jacobians, see H. Margenau and G. M. Murphy, "Mathematics of Physics and Chemistry," D. Van Nostrand Co. Inc., New York, N. Y., 1956, p 18; W. Kaplan, "Advanced Calculus," Addison-Wesley, Reading, Mass., 1959, p 90.

(7) The first and third Jacobians are simply those for the transformation between Cartesian and spherical coordinate systems, and the second is for the translation and rotation of a Cartesian coordinate system.

On the Existence of the Complex $AgSO_4^-$ in Aqueous Solutions[1a]

by M. H. Lietzke and R. W. Stoughton

Chemistry Division, Oak Ridge National Laboratory, Oak Ridge, Tennessee *(Received September 20, 1968)*

In a series of previous communications, the solubility of silver sulfate in aqueous potassium nitrate, potassium sulfate, magnesium sulfate, and silver nitrate solutions over wide temperature ranges[1b] was described. In all of these systems we were able to explain our data with a single equation

$$\ln S = \ln S_0 + \mathbb{S}\left[\frac{\sqrt{I}}{1 + A\sqrt{I}} - \frac{\sqrt{I_0}}{1 + A\sqrt{I_0}}\right] \quad (1)$$

and the assumption of complete dissociation of all electrolytes. Here S is the stoichiometric solubility product; I is the ionic strength; $\mathbb{S}$ is the appropriate Debye–Hückel slope; and the subscript 0 represents zero concentration of the supporting electrolyte. The values of the parameter A were essentially temperature independent but ionic strength dependent.

By contrast, we found it necessary to take into account the presence of HSO_4^- and the presence of $UO_2SO_4(aq)$, respectively, in interpreting the solubility of silver sulfate in sulfuric and nitric acids[2a,b,c] and in UO_2SO_4 solutions.[2d] This behavior implies a qualitative difference between the complexes HSO_4^- and $UO_2SO_4(aq)$ on the one hand and the various other possible ion pairs in the above media on the other.

Davies[3] and coworkers have interpreted their conductance measurements on silver, potassium, and magnesium sulfate solutions at 25° in terms of the species $AgSO_4^-$, KSO_4^- and $MgSO_4(aq)$, respectively, for which they reported dissociation constants of 0.05, 0.1, and 0.006. There is some question,[4] however, as to the meaning of dissociation constants so obtained, especially when relatively large, as far as actual species in solution is concerned.

Recently, Hopkins and Wulff[5] reported good agreement between the values of the heat of solution for silver sulfate obtained by direct measurement and the value estimated on the assumption of a "weak" second ionization step. They take this as evidence and cite additional evidence for the existence of $AgSO_4^-$ ions in aqueous solutions of Ag_2SO_4. They[5] cite four values for the standard Gibbs free energy of solution $\Delta G_1°$ of silver sulfate (including ours[1b] of 6595 cal/mol) which average to 6550 ± 30 cal/mol—all based on complete dissociation at finite concentrations. They then present three values averaging 6740 ± 25 cal/mol which they feel have been corrected for the presence of $AgSO_4^-$: (1) a correction of 140 cal/mol on our value[1b] of 6595 giving 6735 cal/mol; (2) a value of 6707 cal/mol reported by Pan and Lin[6] from a study with the $Ag(s)/Ag_2SO_4(s)$ electrode; and (3) a value based on the data of Righellato and Davies[3] at two concentrations.

Regarding item 1 Hopkins and Wulff[5] suggested that our value of the logarithm of the thermodynamic solubility product $K_s°$ obtained in Ag_2SO_4–KNO_3 mixtures should be the best one since this mixtures probably involved the least complications due to ion association. Actually, our value in this medium at 25° was 140 cal/mol smaller than (not larger than) our average of 6595. Thus our $\Delta G_1° = 6455$, not 6735 cal/mol. We had rejected the results in Ag_2SO_4–KNO_3 media[1b] because they were inconsistent with those in the four other media and because there appeared to be a greater tendency toward hydrolysis to Ag_2O, particularly at the higher temperatures.

We are uncertain as to the limit of error in the value of Pan and Lin.[6] In the calculation involving the use of the two data of Righellato and Davies,[3] Hopkins and Wulff[5] assumed that "the concentration dependence" of "the extent" of the second ionization step "(but not its numerical value)" was "the same as that for Tl_2SO_4 and K_2SO_4." With this assumption and by using a Debye–Hückel expression for the activity coefficient of the two ions, $-\log \gamma_1 = \mathbb{S}_i\sqrt{I}/(1 + A\sqrt{I})$ with $A \equiv 1$, they obtained a value of $\Delta G_1° = 6770$ cal/mol. While their value of A is not unreasonable, as far as we know it is not known and could vary by as much as about 0.4 to 2.0. Accordingly, we recalculated $\Delta G_1°$ using $A = 0.4$, 1.0, 1.5, and 2.0 on the assumption that the concentrations calculated by Hopkins and Wulff[5] were correct. We obtained 6875, 6770, 6680, and 6610 cal/mol, respectively. Thus we feel that their value could be off by at least as much as 100 cal/mol due solely to the unknown value of A. We do not know how to estimate the other uncertainties.

Hopkins and Wulff[5] point out that our value for the enthalpy of solution at 25° was 4.47 kcal/mol compared to two literature values of 4207 and 4215 cal/mol. They imply that this discrepancy may result from our not taking into account the presence of $AgSO_4^-$. Actually, we made no explicit claim[1b] for the accuracy of our value of $\Delta H_1°$ and would not be surprised if it were in error by some 200 to 300 cal/mol. Further, our values would be expected to be poorer at the extremes (25 and 200°) than at some of the intermediate temperatures.

(1) (a) Research sponsored by the U. S. Atomic Energy Commission under contract with the Union Carbide Corporation. (b) M. H. Lietzke and R. W. Stoughton, *J. Phys. Chem.*, **63**, 1183, 1186, 1984, (1959); **64**, 133 (1960); *J. Inorg. Nucl. Chem.*, **28**, 1877 (1966).

(2) (a) M. H. Lietzke and R. W. Stoughton, *J. Phys. Chem.*, **63**, 1188 (1959); (b) **63**, 1190 (1959); (c) **65**, 2247 (1961); (d) **64**, 816 (1960).

(3) C. W. Davies, "Ion Association," Butterworth, Inc., Washington, D. C., 1962.

(4) G. Scatchard, *Ann. Rev. Phys. Chem.*, **14**, 163 (1963).

(5) H. P. Hopkins, Jr., and C. A. Wulff, *J. Phys. Chem.*, **69**, 9 (1965).

(6) K. Pan and J-L. Lin, *J. Chinese Chem. Soc.* (Taiwan), **6**, 1 (1959).

We tried using the value of K obtained by Righellato and Davies[3] (model A below) to see whether this would improve our calculated solubilities in Ag_2SO_4–$AgNO_3$ media at 25°.

A. In this model, s in eq 1 has the value for a 1–1 electrolyte and $S = (m_{Ag^+})(m_{AgSO_4^-})$. In addition, we have the following equations

$$AgSO_4^- = Ag^+ + SO_4^{2-} \quad (2)$$

$$Q = (m_{Ag^+})(m_{SO_4^{2-}})/(m_{AgSO_4^-}) \quad (3)$$

$$\ln Q = \ln K + s\sqrt{I}/(1 + A_q(I)) \quad (4)$$

where A_q (eq 4) and A and $\ln S_0$ (eq 1) are adjustable parameters of fit and where s has twice the value it has for a 1–1 electrolyte. We attempted to evaluate the three parameters with a least-squares procedure with the criterion that $\sum_i(s_{obsd} - s_{calcd})^2$ be made a minimum. However, we encountered mathematical convergence difficulties; hence we evaluated A_q and A by permuting over ranges of values with $\ln S_0$ being the only parameter adjusted by the mathematical program. The results which gave the lowest variance of fit were selected. We then fitted our data[1b] at all temperatures by the method of least squares to each of the following models using eq 1.

B. The value of A is assumed to be temperature independent but ionic strength dependent.

C. The value of A is assumed to be constant at all temperatures and ionic strengths. A term BI is added to eq 1, where B is a function of temperature only.

D. This model is similar to model C except that both A and B were assumed to be constant at all temperatures and ionic strengths.

In order to determine whether one model fitted the Ag_2SO_4–$AgNO_3$ solubility data better than the others the F-ratio test was applied to all possible comparisons between pairs of models. At the 95% confidence level taking the $AgSO_4^-$ complex into account did not provide a significantly better fit of the data than did models B, C, or D. However, on the 90% confidence level taking into account the $AgSO_4^-$ ion did provide a significantly better fit of the solubility data. In this connection it is to be noted that since the model based on the presence of $AgSO_4^-$ contains three adjustable parameters (A, A_q, and $\ln S_0$) for four 25° data points while the other models have at the most three adjustable parameters for 24 data points from 25 to 150°, the significantly better fit on the 90% confidence level may be just apparent.

If the complex $AgSO_4^-$ exists it should also be of significance in the solutions with a common sulfate ion. However, if we assume the existence of $AgSO_4^-$ on the basis of the work of Davies and coworkers,[3] we are obliged to assume also the existence of KSO_4^- in Ag_2SO_4–K_2SO_4 mixtures and of $MgSO_4(aq)$ in Ag_2SO_4–$MgSO_4$ mixtures. Because of the mathematical convergence difficulties encountered in the Ag_2SO_4–$AgNO_3$ solutions with only the single complex $AgSO_4^-$, we have not attempted the more elaborate calculations with two complexes in the same solutions.

In summary, we do not say that the complex $AgSO_4^-$ is not present in our solutions. We say that we did not have to take it into account nor did we have to take into account the existence of the species KSO_4^- and $MgSO_4(aq)$ in order satisfactorily to explain our data. We feel that there is some question as to the physical meaning of the three complexes or ion pairs mentioned here.

Photolysis of 1,1,1-Trifluoromethylazocyclopropane. The Fate of the N.N-*c*-C_3H_5 Radical

by K. Chakravorty, J. M. Pearson, and M. Szwarc

Department of Chemistry, State University College of Forestry at Syracuse University, Syracuse, New York 13210

(Received September 23, 1968)

The reactions of neutral CH_3 radicals and electrophilic CF_3 radicals were extensively studied in this laboratory.[1-3] The extension of this work to nucleophilic radicals was highly desirable, and cyclopropyl seemed an appropriate choice. In searching for a convenient source for generating cyclopropyl radicals we synthesized 1,1,1-trifluoromethylazocyclopropane and investigated its photolysis. Although the system was found to be unsuitable for our purpose, it exhibited some intriguing features which are reported here.

Experimental Section

1,1,1-Trifluoromethylazocyclopropane (I), a compound not reported in the literature, was synthesized by a procedure similar to that used in the preparation of 1,1,1-trifluoromethylazomethane.[4] Equivalent amounts of cyclopropylamine and trifluoronitrosomethane were condensed at liquid air temperature and sealed under vacuum in a 700-ml Pyrex ampoule. As the contents were slowly warmed from −196° to room temperature, the amine liquefied and a vigorous reaction ensued. The ampoule was maintained at 40° for 1 hr to ensure completion of the condensation and thereafter the resulting pale yellow liquid was purified by bulb-to-bulb distillation. The azo compound (I) was stored in

(1) (a) J. H. Binks and M. Szwarc, *J. Chem. Phys.*, **30**, 1494 (1959); (b) M. Szwarc and J. H. Binks, "Theoretical Organic Chemistry," Kekule Symposium, Butterworth and Co. Ltd., London, 1959, p 262; (c) for details of technique: M. Gazith and M. Szwarc, *J. Amer. Chem. Soc.*, **79**, 3339 (1957).

(2) (a) J. M. Pearson and M. Szwarc, *Trans. Faraday Soc.*, **60**, 553 (1964); (b) G. E. Owen, J. M. Pearson, and M. Szwarc, *ibid.*, **61**, 1722 (1965).

(3) G. E. Owen, J. M. Pearson, and M. Szwarc, *ibid.*, **60**, 564 (1964).

(4) A. H. Dinwoodie and R. N. Haszeldine, *J. Chem. Soc.*, 2266 (1965).

Table I: Photolysis of CF_3NN-*c*-(C_3H_5) in the Gas Phase [Azo Concentration, 10^{-6} to 10^{-6} *M*; Diluent, 2,3-Dimethylbutane ($p \sim 700$ mm)][a]

T, °C	CF_3H/N_2	$CF_3CH_2CH{=}CH_2/N_2$	$CH_3CH{=}CH_2/N_2$	2-Pyrazoline/N_2	*c*-C_3H_6/N_2
65	1.0	0.25	0.25	0.15	Very small
120	1.0	0.25	0.25	0.20	Very small

[a] The results are given as mole ratios and are accurate to ±0.05.

Table II: Photolysis of CF_3NN-*c*-(C_3H_5) in Solution (Azo Concentration, 10^{-4} to 10^{-5} *M*; Temperature, 32°)[a]

Solvent	CF_3H/N_2	*c*-$C_3H_6CF_3/N_2$	$CH_3CH{=}CH_2/N_2$	*c*-C_3H_6/N_2
2,3-Dimethylbutane	1.0	0.15	0.1	Very small
2,3-Dimethylbutane + 5 mol % α-methylstyrene	0.0	0.15	0.0	...
CCl_4 + 5 mol % α-methylstyrene	0.0	0.2	0.0	...

[a] The results are given as mole ratios and are accurate to ±0.05.

a blackened ampoule at room temperature. It is stable in the dark and no decomposition was observed even at 120°.

(I) was characterized by its uv, ir, nmr, and mass spectrum: bp 60° (760 mm); uv max (CH_3OH) 337 mμ (ε 32); ir 3.29 μ (*c*-C_3H_5), 6.45 μ (—N=N—) and 7.6–8.6 μ (CF_3); nmr (CCl_4) δ = 3.81 (septet, 1, *J* = 3.5 cps) and 1.54 ppm (m, 4); mass spectrum (70 eV) *m/e* 138 (parent peak), 110 ($C_3H_5 \cdot CF_3$), 69 (CF_3), 41 (C_3H_5) and 28 (N_2).

The photolysis was investigated in the gas phase with 2,3-dimethylbutane as diluent and in the liquid phase in 2,3-dimethylbutane and in CCl_4. Pyrex reaction vessels were used and a G.E. AH-6 high-pressure mercury lamp served as the light source. The appropriate experimental details are given in ref 2 (gas phase) and in ref 3 and 2 (liquid phase). Photolysis times were of the order of 30–50 hr.

The techniques of product analyses by glpc are described elsewhere.[1] Gaseous products were analyzed on a silica gel column and the liquid products on a 30% silicone G.E. SF96 column and also a 15% carbowax column. Synthetic samples were used for identification of the products (by comparison of retention times) and for calibration.

The gas-phase photolysis of (I), performed in the presence of 2,3-dimethylbutane, yielded the following gaseous products: N_2, CF_3H, $CF_3CH_2CH{=}CH_2$ (or its isomers) and $CH_3CH{=}CH_2$. Only a trace of cyclopropane was observed and no combination product

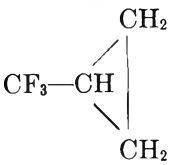

was detected. In addition, 2-pyrazoline was isolated from the liquid residue of the photolysis. The analytical results are summarized in Table I.

In contradistinction to the gas-phase photolysis, the liquid-phase irradiation produced the expected combination product

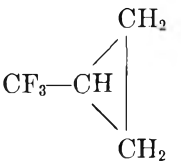

Its identity was established by comparing it with a synthetic sample prepared according to the method of Dorer and Rabinovitch.[5] The results for the liquid-phase photolysis are summarized in Table II.

Discussion

The dissociation energy of the R—N=N· radical is usually negative[6] and therefore the decomposition of azo compounds, $R_1N_2R_2$, often proceeds by simultaneous rupture of two bonds yielding a molecule of N_2 and two radicals R_1 and R_2. Exceptions are possible[7] and (I) appears to be in this category. The photolysis undoubtedly forms CF_3 radicals as demonstrated by the results. However, the findings presented in Tables I and II also show that the sum of the products involving CF_3 moieties exceeds the total amount of N_2 formed in the reaction. Therefore, at least some of the intermediate radical species, *c*-C_3H_5—N=N·, or the product of their rearrangement, do not decompose with evolution of N_2. Indeed, a nitrogen-containing material was

(5) F. H. Dorer and B. S. Rabinovitch, *J. Phys. Chem.*, **69**, 1964 (1965). We thank Dr. Rabinovitch for the details of preparation and purification of CF_3-*c*-C_3H_5.

(6) M. Szwarc, "Peroxide Reaction Mechanism," Interscience Publishers, Inc., New York, N. Y., 1961, p 153.

(7) (a) W. A. Pryor and K. Smith, *J. Amer. Chem. Soc.*, **89**, 1741 (1967); (b) S. Seltzer and F. T. Dunnel, *ibid.*, **87**, 2628 (1965); (c) S. Seltzer and S. G. Mylonakis, *ibid.*, **89**, 6584 (1967).

formed and it was identified as 2-pyrazoline by its retention time on a carbowax and on a silicone oil column. Calibration was performed with a synthetic sample prepared from acrolein and hydrazine hydrate.[8] The presence of some 1-pyrazoline cannot be excluded. However, under the conditions of the experiments the 1-pyrazoline (λ_{max} = 315 mμ, ϵ 446)[9] would be expected to decompose into N_2 and cyclopropane, whereas the 2-pyrazoline (λ_{max} 224 mμ, ϵ ?) probably is stable. Quantitative analysis showed that 2-pyrazoline/$N_2 \simeq$ 0.15–0.20 and this value is consistent with the anomalous CF_3 material balance (see Table I).

Undoubtedly, the

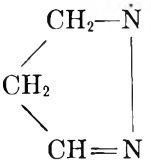

radicals are the precursors of pyrazoline, abstraction of hydrogen from 2,3-dimethylbutane leading to the final product. The question arises whether the cyclic radical is produced directly from the decomposition of the excited azo molecule, reaction 1, or by rearrangement of the intermediate diazonium radical, c-C_3H_5—N=N, reaction 2.

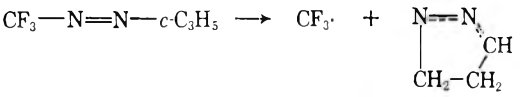

(1)

or a scission of the C—N bond followed by

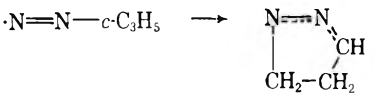

(2)

The data reported here do not permit us to resolve the question. The hypothesis of rearrangement preceding the decomposition is plausible and supported by other observations which deal with cyclopropane derivatives. Photolysis of methylcyclopropyl ketone yields methyl propenyl ketone,[10] that of dicyclopropyl ketone gives cyclopropylpropenyl ketone,[11] and of cyclopropane carboxaldehyde forms CO and propylene.[12] In all these examples the absorption of energy by the molecular chromophore leads to rupture of the cyclopropane ring. The formation of $CF_3CH_2CH{=}CH_2$ observed by us in the gas-phase photolysis may be also attributed to an intramolecular rearrangement. Under our experimental conditions any CF_3 radicals formed should react with diluent to produce CF_3H and the probability of CF_3 combination with allyl radicals (formed from the cyclopropyl moiety) is, therefore, negligible.[2] The rearrangement may involve the *syn* form of the azo compound as shown by

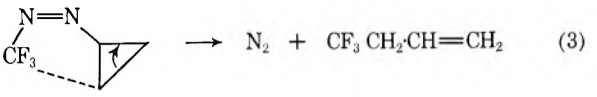

(3)

This form could be favored by the attraction between the electrophilic CF_3 and the nucleophilic c-C_3H_5.

The virtual absence of cyclopropane in the products is significant. Free cyclopropyl radicals should readily abstract hydrogen from 2,3-dimethylbutane.[13] The isolation of CF_3-c-C_3H_5 from the products of liquid-phase photolysis could be interpreted as evidence for the formation of c-C_3H_5, *i.e.*, the rearrangement of the diazonium radical might compete with its decomposition into N_2 + ·⟨|. However, an alternative interpretation is possible; *i.e.*, the combination of ·N_2—⟨| and CF_3 might give N_2 + CF_3—⟨|. Since cyclopropane is not formed in the gas-phase photolysis the decomposition apparently is slow. The radical rearranges (see reaction 2) in the gas phase, although in liquid phase its cage combination with CF_3, coupled with ejection of N_2, is quite feasible.

Acknowledgment. The financial support of this investigation by the National Science Foundation and by the Petroleum Research Fund administered by the American Chemical Society is gratefully acknowledged.

(8) K. V. Auwers and E. Caner, *Ann.*, **470**, 284 (1929).

(9) R. J. Crawford, R. J. Dummel, and A. Mishra, *J. Amer. Chem. Soc.*, **87**, 3023 (1965).

(10) J. N. Pitts and I. Norman, *ibid.*, **76**, 4815 (1954).

(11) Unpublished results of L. D. Hess and J. N. Pitts, quoted on p 405 of "Photochemistry," by J. G. Calvert and J. N. Pitts, John Wiley and Sons Inc., New York, N. Y., 1966.

(12) J. J. I. Overwater, H. J. Hofman, and H. Cerfontain, *Rec. Trav. Chim.*, **83**, 637 (1964).

(13) G. Greig and J. C. J. Thynne, *Trans Faraday Soc.*, **63**, 2196 (1967).

COMMUNICATIONS TO THE EDITOR

The Configurational Entropy of Titanium Monoxide

Sir: Recent discussions of the thermodynamic properties of TiO[1-3] suggest possible inaccuracies in entropy data[4] resulting from the failure to take into account a zero-point entropy owing to frozen-in disorder. Similar proposals were advanced by Hoch, Iyer, and Nelken[5] to explain the discrepancies between their equilibrium measurements with a galvanic cell and the tabulated data[6] derived from the calorimetric measurements of Shomate[7] and Naylor.[4] The purpose of the present letter is to show that the 0°K entropy of equiatomic TiO is zero and that the previous calculation of the configurational entropy for a disordered form of equiatomic TiO is incorrect.

Titanium monoxide may exist in either one of two modifications according to temperature. The high-temperature form (TiO_β) has the NaCl structure with 15% of both titanium and oxygen sites vacant[8,9] and randomly dispersed. Below 1264°K, TiO_β transforms to a low-temperature modification (TiO_α) with a transformation enthalpy of 820 cal/mol.[4] Recently,[10,11] the crystal structure of TiO_α was shown to be monoclinic. The structure is similar to that of NaCl but has an ordered array of vacant lattice sites, so that in every third (110) plane of the parent cubic form half of the titanium and half of the oxygen atoms are missing alternately. From the lattice parameters of the monoclinic unit cell and the pycnometric density[12] it was also deduced[11] that the ordered material had $\frac{1}{6}$ of both titanium and oxygen sites vacant. Therefore, the 0°K configurational entropy of ordered TiO_α is zero.

The 0°K entropy correction of Hoch, *et al.*,[5] was intended to allow for the configurational entropy of TiO_β with random vacancies but an incorrect number of moles was used in their calculation. Since the tabulated thermodynamic data refer to 1 mol of TiO (63.97 g), the entropy calculations are based on N titanium atoms and N oxygen atoms (N is Avogadro's number). The total number of titanium sites in 1 mol of TiO_β is, therefore, $1.177N$ since in this defect structure the N titanium atoms represent only 85% of the total available lattice sites. Similar reasoning applies to the oxygen sites and hence the configurational entropy of 1 mol of TiO_β with random vacancies is given by

$$Sp = 2k \ln \frac{(1.177N)!}{(0.177N)!\,N!} = 1.97 \text{ eu}$$

where k is the Boltzmann constant.

On this basis, the expected entropy change on ordering is 1.97 eu compared with 0.65 eu derived from the calorimetric measurements of Naylor.[4] A number of factors may account for this discrepancy. As the nature of the transformation was not previously understood, the specimen used by Naylor may not have been at equilibrium and consequently possessed a low degree of order below the transformation temperature. On the other hand, short range order of vacancies above the transformation temperature would decrease the calculated entropy change. Considerable pretransition effects were observed by Naylor during his measurements and, therefore, the accuracy of the calorimetric measurements is low. New measurements on fully ordered specimens are required.

The above considerations are strictly applicable only to TiO_α of equiatomic composition. The ordered TiO_α structure, however, is stable over a range of composition.[9,11,13] Since the amount and relative proportions of titanium and oxygen vacancies varies with composition,[9] a small degree of disorder is inherent in TiO_α of other than the equiatomic composition. This disorder, which can be deduced from X-ray and electron diffraction observations[11] and from the variation of vacancy concentration with composition,[9] can be described in terms of randomly arranged excess atoms of one species in the ordered vacant sites and random vacancies of the other atomic species in the normally occupied sites of the equiatomic ordered TiO_α structure. Consequently, a small configurational entropy term at 0°K is expected on both sides of the equiatomic composition in specimens having the ordered TiO_α structure.

(1) P. G. Wahlbeck and P. W. Gilles, *J. Chem. Phys.*, **46**, 2465 (1967).

(2) O. Kubaschewski, Proceedings of the I.A.E.A. Symposium on Thermodynamics, Vienna, Austria, Vol. 11, 1966, p 583.

(3) P. W. Gilles, *J. Chem. Phys.*, **46**, 4987 (1967).

(4) B. F. Naylor, *J. Amer. Chem. Soc.*, **68**, 1077 (1946).

(5) M. Hoch, A. S. Iyer, and J. Nelken, *J. Phys. Chem. Solids*, **23**, 1463 (1962).

(6) J. F. Elliott and M. Gleiser, "Thermochemistry for Steelmaking," Addison-Wesley Press, Reading, Mass., 1960.

(7) C. H. Shomate, *J. Amer. Chem. Soc.*, **68**, 310 (1946).

(8) P. Ehrlich, *Z. Anorg. Chem.*, **247**, 53 (1941).

(9) S. Andersson, B. Collen, U. Kuylenstierna, and A. Magnéli, *Acta Chem. Scand.*, **11**, 1641 (1957).

(10) D. Watanabe, J. R. Castles, A. Jostsons, and A. S. Malin, *Nature*, **210**, 934 (1966).

(11) D. Watanabe, J. R. Castles, A. Jostsons, and A. S. Malin, *Acta Cryst.*, **23**, 307 (1967).

(12) U. Kuylenstierna and A. Magnéli, *Acta Chem. Scand.*, **10**, 1195 (1956).

(13) A. Jostsons and P. McDougall, paper presented at the Institute of Metals International Conference on Titanium, London, 1968.

Materials Division — A. Jostsons
A.A.E.C. Research Establishment
Lucas Heights, New South Wales, Australia
School of Metallurgy — A. E. Jenkins
University of New South Wales
Kensington, New South Wales, Australia

Received July 22, 1968

A Spatial Periodic Homogeneous Chemical Reaction

Sir: Especially coupled chemical reactions, which are far from chemical equilibrium, show phenomena which are not observed near chemical equilibrium. One of these is the occurrence of oscillations during the reaction course.[1,2] This communication deals with a similar phenomenon: the periodic variation of the course of a reaction along a space coordinate (so-called "steady chemical waves"). Such a phenomenon is predicted by the theory of thermodynamics of irreversible processes.[3] A brief derivation, in which we consider only the diffusion process and the chemical reaction, may show the main features.

The equation of continuity for a chemical component of a homogeneous mixture is given by

$$\frac{\partial c}{\partial t} + \operatorname{div} J = \gamma \tag{1}$$

where c is the concentration of the chemical component, J is the space flux, and γ is its rate of production.

$$J = -D\frac{\partial c}{\partial x} \tag{2}$$

where D is the diffusion coefficient

$$\gamma = \frac{\partial \xi}{\partial t} = \vec{k}ac \tag{3}$$

which is the rate equation for a chemical reaction of autocatalytic type $A + C \rightarrow C + C$, in which the rate of product production is positive (a is the concentration of A). Let us assume further that there is in eq 1 no space dependence in y and z as well as no time dependence. Then one obtains from (1), (2), and (3)

$$-D\frac{\partial^2 c}{\partial x^2} = \vec{k}ac$$

for which

$$c = c_0 \sin\left(\frac{2\pi x}{\lambda} + \varphi\right)$$

is a solution, if the wavelength λ is

$$\lambda = 2\pi\sqrt{\frac{D}{\vec{k}a}}$$

Thus, periodic variations in space may be possible, if the reaction mechanism contains an autocatalytic step. The bromate–cerous ion reaction[1,4] is of such a type, and although the detailed reaction mechanism is not known, it represents a good example for examining the phenomenon discussed above. The spatial oscillations in this chemical system are detected by using a solution of ferroin as an indicator (Figure 1); it changes from red to blue as the redox potential increases. This technique also allows one to see very small deviations from the mean reaction course, if the reaction course changes within a fraction of a millimeter. A configuration as shown in Figure 1 is stable for hours. Its wavelength is about 0.5 mm and the first-order rate constant $\vec{k}a \sim 0.4\ \text{sec}^{-1}$. This pattern is produced in the following way: the indicator is added to the system bromate–malonic acid–cerous ions (approximate concentrations: $7 \times 10^{-2}\ M$, $0.3\ M$, $10^{-3}\ M$, respectively). Then a drop of the indicator is put on the surface, producing a gradient which propagates toward the interior by forming the periodic configuration.[5] This phenomenon occurs in a homogeneous solution. Perhaps one can use phenomena of this type to store information by chemical reactions. The cybernetic implications of these phenomena might be useful in interpreting certain aspects in biology.

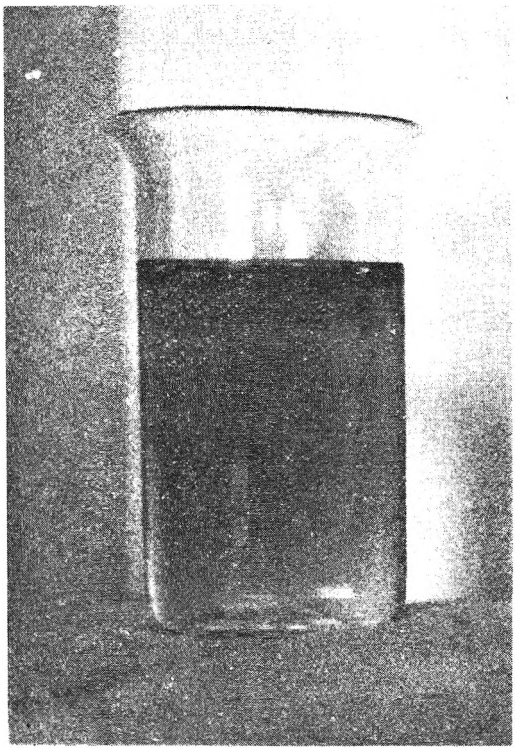

Figure 1. Alternating layers show the spatial periodic chemical reaction. The wavelength is approximately 0.5 mm.

(1) A. M. Zhabotinskij, *Dokl. Akad. Nauk SSSR*, **157**, 392 (1964).
(2) B. Chance, B. Hess, and A. Betz, *Biochem. Biophys. Res. Commun.* **16**, 182 (1964).
(3) I. Prigogine and G. Nicolis, *J. Chem. Phys.*, **46**, 3542 (1967).
(4) H. Degn, *Nature*, **213**, 589 (1967).
(5) A more detailed report will follow as more experimental data are gathered.

INSTITUT FÜR MOLEKULARE BIOLOGIE, BIOCHEMIE, UND BIOPHYSIK
STÖCKHEIM, BRAUNSCHWEIG, GERMANY
HEINRICH G. BUSSE

RECEIVED OCTOBER 28, 1968

Interpretation of the Kinetics of Thermogravimetric Analysis

Sir: Thermogravimetric analysis has now become accepted as a means of evaluating kinetic parameters of solid-state decompositions of the type

$$aA(s) \longrightarrow bB(s) + cC(g)$$

Reactions of this type are exemplified in polymer degradation and the decomposition of inorganic complexes.

One of the most commonly used methods of analysis of thermogravimetric data is that proposed by Freeman and Carroll.[1] Using a rate expression

$$-dn_a/dt = k(n_a)^x \qquad (1)$$

in which n_a is the number of moles of reactant A, k is the rate constant for the reaction, x is the order of the reaction, and t is the time parameter, they deduce the equation

$$\frac{(-E/2.3R)\Delta(1/T)}{\Delta \log W_a} = -x + \frac{\Delta \log (-dW_a/dt)}{\Delta \log W_a} \qquad (2)$$

in which E is the activation energy for the decomposition reaction, T is the temperature in degrees Kelvin, and W_a is the weight of reactive constituent remaining in the sample.

The point of this communication is to show that eq 2 is incorrect. The error arises from the use of eq 1, which, as written, is dimensionally incorrect. The rate constant for a reaction of order x has the dimensions $(\text{moles})^{(1-x)} \times (\text{volume})^{(x-1)} \times (\text{time})^{-1}$ and therefore (1) should be written as

$$-dn_a/dt = k(n_a)^x/V^{(x-1)} \qquad (3)$$

V is the total volume of the sample at time t. Using the "difference–differential" approach suggested by Freeman and Carroll, we deduce

$$-E/2.3R\Delta(1/T) = -x\Delta \log W_a + \Delta \log (-dW_a/dt) + (x - 1)\,\Delta \log (W) \qquad (4)$$

in which W is the total weight of the sample at time t. It is convenient to rewrite (4) in terms of the percentage decomposition (C) which we define as

$$C = (W_a^0 - W_a)/W_a^0$$

W_a^0 is the initial weight of active constituent in the sample

$$-E/2.3R\Delta(1/T) = -x[\Delta \log (1 - C) - \Delta \log (A^{-1} - C)] + \Delta \log [-d(1 - C)/dt] - \Delta \log (A^{-1} - C) \qquad (5)$$

A is defined as the fraction of active component initially present in the sample ($A = W_a^0/W_0$). Equation 5 can be rewritten

$$\frac{-E/2.3R\Delta(1/T)}{[\Delta \log (1 - C) - \Delta \log (A^{-1} - C)]} = -x + \frac{\Delta \log [-d(1 - C)/dt] - \Delta \log (A^{-1} - C)}{[\Delta \log (1 - C) - \Delta \log (A^{-1} - C)]} \qquad (6)$$

Equation 6 contains an extra term compared with Freeman and Carroll's equation. The extra term disappears for $x = 1$, but for all other values this modified equation should be used for analyzing thermogravimetric data by the "difference–differential" type of approach.

Acknowledgment. J. T. gratefully acknowledges the award of a maintenance grant by the Science Research Council.

(1) E. S. Freeman and B. Carroll, *J. Phys. Chem.*, **62**, 394 (1958).

DEPARTMENT OF CHEMISTRY
UNIVERSITY OF ST. ANDREWS
ST. ANDREWS, FIFE, SCOTLAND

J. R. MACCALLUM
J. TANNER

RECEIVED NOVEMBER 5, 1968

Reply to "Interpretation of the Kinetics of Thermogravimetric Analysis"

Sir: We do not agree with the authors' statement[1] that our equation (their eq 2) is dimensionally incorrect. Rate constants are endowed with dimensions that make a postulated differential rate equation dimensionally homogeneous. In the case of chemical reactions in the solid state of the type considered by MacCallum and Tanner, rate equations in terms of concentration (*i.e.*, moles/volume) are usually inapplicable.

The reaction is usually initiated at active sites provided by defects in the solid reactant. Nuclei grow in a manner that is not microscopically uniform throughout the reacting system. The solid product is generally insoluble in the reactant. It is at the interface of the solid reactant and product that the reaction proceeds.

It is interesting to note that even in apparently homogeneous solid systems as in the case for the thermal decomposition of organic polymers the rates frequently depend upon particle size and shape.[2,3]

The MacCallum and Tanner eq 4 does not follow from their eq 3 unless the assumption is made that W, the total weight at time t, is a linear function of the total volume of the reacting system. Although this may be the case macroscopically in some solid-state reactions, the mechanism of the reaction makes the use

(1) J. R. MacCallum and J. Tanner, *J. Phys. Chem.*, **73**, 751 (1969).
(2) H. L. Friedman, *J. Macromol. Sci.*, **A1**(1), 57 (1967).
(3) E. S. Freeman and A. J. Becker, *J. Polymer Sci., Part A-1*, **6**, 28, 29 (1968).

of concentrations in the kinetic equations rather meaningless.

The Freeman–Carroll method consists of inserting a temperature-dependent relationship for the rate constant directly into the selected differential rate expression. In the case of homogeneous reactions, rate equations in terms of concentrations are undoubtedly preferred. The appearance then of the term V^{x-1} will appear as given in our eq 14 or as indicated in our case 2.[4]

(4) E. S. Freeman and B. Carroll, *J. Phys. Chem.*, **62**, 394 (1958).

IIT RESEARCH INSTITUTE
CHICAGO, ILLINOIS 60616
E. S. FREEMAN
CHEMISTRY DEPARTMENT
RUTGERS UNIVERSITY
NEWARK, NEW JERSEY 07102
B. CARROLL

RECEIVED DECEMBER 30, 1968

Reevaluation of Frictional Coefficients in the System Benzene–Cyclohexane at 25°

Sir: In a recent paper, Mills[1] has presented the measurements of the intradiffusion coefficients in the system labeled benzene (1), benzene (2), labeled cyclohexane (3), and cyclohexane (4) at 25°. In combination with the mutual-diffusion coefficients,[2] these values lead to the evaluation of the frictional coefficients,[3,4] which in this case show rather unexpected bumps when plotted as a function of the mole fraction.[1] The view has been advanced[1,5] that this unusual concentration dependence may be due to an error in the calculation of the activity term ($\mathrm{d} \ln a/\mathrm{d}c$). We have therefore recalculated the frictional coefficients and have found a concentration dependence without bumps. Because of this difference we present our equations and numerical values in some detail.

The frictional coefficients R_{ik} are given by[3,4]

$$\frac{R_{42}}{RT} = \frac{c_4 V_2 (\partial \ln a_4/\partial c_4)_{T,P}}{D_v}$$

$$\frac{R_{34}}{RT} = \frac{1}{D_3^+ c_4} - \frac{c_2 V_2 (\partial \ln a_4/\partial c_4)_{T,P}}{D_v} \qquad (1)$$

$$\frac{R_{12}}{RT} = \frac{1}{D_1^+ c_2} - \frac{c_4 V_4 (\partial \ln a_2/\partial c_2)_{T,P}}{D_v}$$

The subscripts are those given by Mills.[1] D_v is the mutual-diffusion coefficient; D_3^+ and D_1^+ are the intradiffusion coefficients of cyclohexane and benzene; the other symbols have their usual meaning.[1] The R_{ik}'s are defined so as to be positive.

The equation[6]

$$c_4(\partial \ln a_4/\partial c_4)_{T,P} = [1 + m_4(\partial \ln \gamma_4/\partial m_4)_{T,P}] \times \frac{1}{c_2 V_2}$$

and a similar one for $(\partial \ln a_2/\partial c_2)_{T,P}$ may be used to transform the activity term from molarity c_i to molality m_i

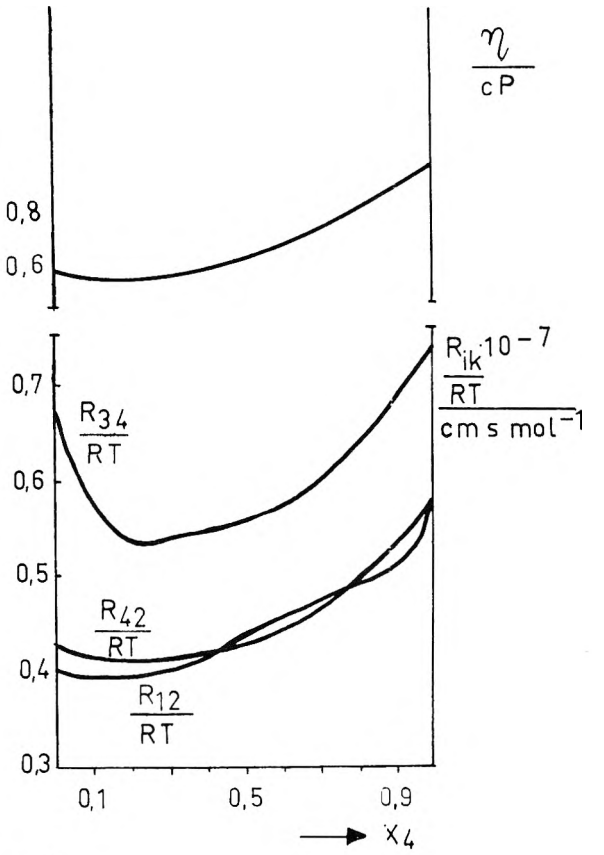

Figure 1.

$$\frac{R_{42}}{RT} = \frac{1 + m_4(\partial \ln \gamma_4/\partial m_4)_{T,P}}{D_v c_2}$$

$$\frac{R_{34}}{RT} = \frac{1}{c_4}\left[\frac{1}{D_3^+} - \frac{1 + m_4(\partial \ln \gamma_4/\partial m_4)_{T,P}}{D_v}\right] \qquad (2)$$

$$\frac{R_{12}}{RT} = \frac{1}{c_2}\left[\frac{1}{D_1^+} - \frac{1 + m_2(\partial \ln \gamma_2/\partial m_2)_{T,P}}{D_v}\right]$$

The activity terms can be derived from the equations of Scatchard, *et al.*,[7] if one takes into account that the excess chemical potentials μ_i^E given by these authors are based on the use of mole fractions x_i and activity coefficients f_i ($x_i f_i = a_i$), even if given as a function of the volume fractions z_i.

$$\mu_2^E = \mu_2 - \mu_{20} - RT \ln x_2 = RT \ln f_2$$
$$= A V_2 z_4^2 (1 - 0.168 z_4 + 0.252 z_4^2)$$
$$\mu_4^E = \mu_4 - \mu_{40} - RT \ln x_4 = RT \ln f_4$$
$$= A V_4 z_2^2 (1 + 0.252 z_4^2) \qquad (3)$$

(1) R. Mills, *J. Phys. Chem.*, **69**, 3116 (1965).
(2) H. S. Harned, *Discussions Faraday Soc.*, **24**, 7 (1947).
(3) J. G. Albright and R. Mills, *J. Phys. Chem.*, **69**, 3120 (1965).
(4) P. J. Dunlop, *ibid.*, **68**, 26 (1964).
(5) R. Mills, private communication.
(6) P. J. Dunlop and L. J. Gosting, *J. Phys. Chem.*, **63**, 86 (1959).
(7) G. Scatchard, S. E. Wood, and J. M. Mochel, *ibid.*, **43**, 119 (1939).

Let us first consider benzene (2) as the solvent; then we find

$$z_2 = \frac{n_2V_2}{n_2V_2 + n_4V_4} = \frac{V_2/M_2}{V_2/M_2 + m_4V_4}$$

and

$$z_4 = 1 - z_2 = \frac{m_4V_4}{V_2/M_2 + m_4V_4} \quad (4)$$

Here the n_i is the amount of substance of component i and M_i the molar mass of component i.

Introducing these relations into (3), the excess chemical potential $RT \ln f_4$ will be a function of the molality m_4. Furthermore, the activity coefficients f_4 and $\gamma_4 (m_4\gamma_4 = a_4)$ are connected by

$$\ln \gamma_4 = \ln f_4 + \ln 1/(1 + m_4M_2) \quad (5)$$

Equations 3 through 5 finally give

$$1 + m_4(\partial \ln \gamma_4/\partial m_4)_{T,P} = \frac{1}{1 + m_4M_2} - \frac{AV_4 2z_2^2 z_4}{RT}(1 - 0.252z_4 + 0.504z_4^2) \quad (6)$$

In a like manner one may derive

$$1 + m_2(\partial \ln \gamma_2/\partial m_2)_{T,P} = \frac{1}{1 + m_2M_4} - \frac{AV_2 2z_2 z_4^2}{RT}(1 - 0.252z_4 + 0.504z_4^2) \quad (7)$$

The partial molar volumes V_i can be considered to be independent of concentration[8]

$$V_2 = 89.3960 \text{ cm}^3 \text{ mol}^{-1}$$

$$V_4 = 108.7674 \text{ cm}^3 \text{ mol}^{-1}$$

The molarities c_i, which have to be known in eq 2, are calculated from

$$c_i = \frac{x_i}{x_2V_2 + x_4V_4} \quad (8)$$

The relations (2) through (8) allow the evaluation of the frictional coefficients. The results are given in Table I, along with c_i, $[1 + m_i(\partial \ln \gamma_i/\partial m_i)]$ and D_v, D_3^+ and D_1^+. The latter values have been extracted from a large scale plot. It may be seen from Figure 1 that the frictional coefficients form a family of smooth curves which correlate well with the viscosity[9] of the mixture.

Table I

x_2	z_2	$c_2 \times 10^3$, mol cm^{-3}	$c_4 \times 10^3$, mol cm^{-3}	$[1 + m_4(\partial \ln \gamma_4/\partial m_4)_{T,P}]$	$[1 + m_2(\partial \ln \gamma_2/\partial m_2)_{T,P}]$	$D_v \times 10^5$, cm^2 sec^{-1}	$D_3^+ \times 10^5$, cm^2 sec^{-1}	$D_1^+ \times 10^5$, cm^2 sec^{-1}	$R_{42}/RT \times 10^{-7}$, cm sec mol^{-1}	$R_{34}/RT \times 10^{-7}$, cm sec mol^{-1}	$R_{12}/RT \times 10^{-7}$, cm sec mol^{-1}
0.995	0.99392	11.1182	0.055870	0.98840	0.0049698	2.096	2.104	2.249	0.4241	0.6658	0.3978
0.990	0.98786	11.0504	0.111620	0.97700	0.009806	2.090	2.106	2.252	0.4230	0.6603	0.3976
0.98	0.97577	10.9151	0.222758	0.95705	0.019532	2.079	2.107	2.258	0.4217	0.6406	0.3971
0.97	0.96374	10.8021	0.334086	0.93659	0.028967	2.067	2.110	2.264	0.4195	0.6232	0.3959
0.95	0.93982	10.5126	0.55329	0.89753	0.047238	2.045	2.115	2.277	0.4175	0.6130	0.3958
0.925	0.91020	10.1817	0.82555	0.85195	0.069077	2.015	2.119	2.292	0.4152	0.5950	0.3948
0.9	0.88091	9.8562	1.09489	0.80965	0.089062	1.987	2.124	2.308	0.4134	0.5785	0.3937
0.8	0.76677	8.5772	2.1443	0.66654	0.16678	1.890	2.142	2.357	0.4112	0.5325	0.3918
0.7	0.65727	7.3524	3.1510	0.55589	0.23824	1.842	2.117	2.365	0.4104	0.5414	0.3992
0.6	0.55214	6.1763	4.1176	0.46501	0.31001	1.812	2.073	2.347	0.4155	0.5483	0.4128
0.5	0.45112	5.0463	5.0463	0.38673	0.38673	1.798	2.010	2.310	0.4162	0.5596	0.4316
0.4	0.35308	3.9600	5.9401	0.31516	0.47275	1.795	1.937	2.265	0.4434	0.5735	0.4498
0.3	0.26049	2.9139	6.7990	0.24531	0.57240	1.809	1.847	2.202	0.4654	0.5969	0.4726
0.2	0.17045	1.9067	7.6268	0.17256	0.69026	1.834	1.721	1.125	0.4935	0.6385	0.4941
0.1	0.08368	0.93645	8.4281	0.092346	0.83112	1.857	1.598	2.020	0.5310	0.6835	0.5074
0.075	0.06248	0.69888	8.6195	0.070581	0.87051	1.860	1.568	1.988	0.5376	0.6959	0.5008
0.050	0.04146	0.46383	8.8127	0.047986	0.91174	1.868	1.537	1.952	0.5538	0.7091	0.5219
0.030	0.02479	0.27730	8.9660	0.029960	0.94609	1.873	1.513	1.922	0.5634	0.7197	0.5471
0.020	0.01650	0.18453	9.0423	0.019668	0.96373	1.875	1.501	1.908	0.5684	0.7252	0.5484
0.010	0.00823	0.092107	9.1186	0.0099163	0.98171	1.877	1.487	1.893	0.5736	0.7317	0.5689
0.005	0.00411	0.046011	9.1561	0.0049789	0.99081	1.880	1.482	1.887	0.5756	0.7340	0.6324

(8) S. E. Wood and A. E. Austin, *J. Amer. Chem. Soc.*, **67**, 480 (1945).
(9) D. A. Collins and H. Watts, *Aust. J. Chem.*, **17**, 516 (1964).

INSTITUT FÜR PHYSIKALISCHE CHEMIE DER RHEINISCH-WESTFÄLISCHEN TECHNISCHEN HOCHSCHULE
AACHEN, GERMANY

HANSJÜRGEN SCHÖNERT

RECEIVED DECEMBER 16, 1968

Comment on Complex Ion Equilibria in Molten Salt Mixtures[1]

Sir: Bloom and Hastie[2] recently interpreted transpiration vapor pressure data to indicate the formation of complex ions in the molten salt systems $PbCl_2 + CsCl$ and $CdCl_2 + CsCl$. They claimed that their experimental activity and activity coefficient data were fitted by a model whereby a complex species, $PbCl_3^-$ in the molten mixture $PbCl_2 + CsCl$, is formed and mixes ideally with the ions from CsCl and $PbCl_2$. A test of this model requires the calculation of the Temkin activities.[3] Although the authors claim to have made this test, the equation (eq 7) which they use (without derivation or reference) to calculate the activity of $PbCl_2$ corresponds to the Dolezalek model of association in nonelectrolyte mixtures rather than to the Temkin activities in molten salts.[4] Their calculated activities and activity coefficients for $PbCl_2$ thus correspond to the association of $PbCl_2$ and CsCl to form $CsPbCl_3$, with random mixing of the hypothetical "particles" $PbCl_2$, $CsPbCl_3$, and CsCl. These do not correspond to the Temkin model of random mixing of cations on a cation "sublattice" and random mixing of anions on an interpenetrating "anion sublattice."

Writing the "equilibrium constant" in terms of the neutral components is not objectionable and avoids difficulties, related to "self-association"[5] in the pure component $PbCl_2$, which would arise if the equilibrium were written[6]

$$Pb^{2+} + 3Cl^- \rightleftharpoons PbCl_3^-$$

However, if the ionic constituents of the mixture are those designated by the authors, Cs^+, Pb^{2+}, Cl^-, and $PbCl_3^-$, the Temkin activities of CsCl and $PbCl_2$ in the mixture must be written

$$a_{CsCl} = N_{Cs}N_{Cl} = \left(\frac{n_{Cs}}{n_{Cs} + n_{Pb}}\right)\left(\frac{n_{Cl}}{n_{Cl} + n_{PbCl_3}}\right)$$

$$a_{PbCl_2} = N_{Pb}N_{Cl}^2 = \left(\frac{n_{Pb}}{n_{Cs} + n_{Pb}}\right)\left(\frac{n_{Cl}}{n_{Cl} + n_{PbCl_3}}\right)^2$$

In terms of the hypothetical constituents CsCl, $PbCl_2$, and $CsPbCl_3$, which are the only ones consistent with the authors' use of the Dolezalek equation, the activity of $PbCl_2$ is[4]

$$a_{PbCl_2} = N_{PbCl_2} = \frac{n_{PbCl_2}}{n_{PbCl_2} + n_{CsCl} + n_{CsPbCl_3}}$$

The Temkin activities defined by Bloom and Hastie's eq 5 and 6, and their equilibrium expression, however, lead to

$$a_{PbCl_2} = N_{Pb}N_{Cl}^2 = \left(\frac{n_{PbCl_2}}{n_{PbCl_2} + n_{CsCl} + n_{CsPbCl_3}}\right) \times \left(\frac{n_{CsCl} + 2n_{PbCl_2}}{n_{CsCl} + 2n_{PbCl_2} + n_{CsPbCl_3}}\right)^2$$

The two expressions for the activity of $PbCl_2$ are clearly not identical and clearly result from two different assumptions as to the nature of the species which are mixing [CsCl with $PbCl_2$ and with $CsPbCl_3$; or, Cs^+ with Pb^{2+}, and Cl^- with $PbCl_3^-$], which cannot be consistent with one another. The authors' conclusion that the results indicate $PbCl_3^-$ and $CdCl_3^-$ as the principal species rests, therefore, on the combination of two mutually inconsistent equations in the application of the Temkin model, which is itself of questionable validity for ions of such different size and charge as Cl^-, $PbCl_3^-$, Pb^{2+}, and Cs^+. The data do not justify these conclusions, particularly since they indicate (Figures 1 and 3 of ref 2) finite rather than zero limiting slopes for the plots of γ_{PbCl_2} (or γ_{CdCl_2}) as X_{PbCl_2} (or X_{CdCl_2}) $\rightarrow 1$ (and hence, by the Gibbs–Duhem relations, infinite limiting slopes for γ_{CsCl}). For mixtures of nonelectrolytes with considerably different molecular sizes, volume fractions replace mole fractions as the concentration units for estimating the entropy of mixing. While a similar approach may prove useful for electrolyte mixtures, there is an added difficulty because of the presence of ions of opposite charge. Replacing an ion by a larger one not only reduces the volume available to the other ions of that charge, but also further distorts the "quasi-lattice" of ions of opposite charge.

(1) Research sponsored by the U. S. Atomic Energy Commission under contract with the Union Carbide Corporation.

(2) H. Bloom and J. W. Hastie, *J. Phys. Chem.*, **72**, 2361 (1968).

(3) M. Temkin, *Acta Physiochim. URSS*, **20**, 411 (1945).

(4) F. Dolezalek, *Z. Phys. Chem.*, **64**, 727 (1908). See also eq 5a and 5b in J. H. Hildebrand and R. L. Scott, "The Solubility of Nonelectrolytes," 3rd ed, Dover Publications, New York, N. Y., 1950, p 177.

(5) I. Prigogine and M. Defay, "Chemical Thermodynamics," Longmans Green and Co., London, 1954, pp 432–434.

(6) J. Braunstein, *J. Chem. Phys.*, **49**, 3508 (1968).

REACTOR CHEMISTRY DIVISION
OAK RIDGE NATIONAL LABORATORY
OAK RIDGE, TENNESSEE 37830
JERRY BRAUNSTEIN

RECEIVED OCTOBER 9, 1968